

Complementary Use of Computer Simulations and Molecular-Thermodynamic Theory to Model Surfactant and Solubilize Self-Assembly

by

Brian C. Stephenson

B.S., Brigham Young University (2000)
M.S.CEP, Massachusetts Institute of Technology (2004)

Submitted to the Department of Chemical Engineering
in partial fulfillment of the requirements for the degree of

Doctor of Philosophy

at the

MASSACHUSETTS INSTITUTE OF TECHNOLOGY

November 2006

© Massachusetts Institute of Technology 2006. All rights reserved.

The author hereby grants to Massachusetts Institute of Technology permission to
reproduce and
to distribute copies of this thesis document in whole or in part.

Signature of Author
Department of Chemical Engineering
27 November 2006

Certified by
Kenneth Beers
Visiting Assistant Professor
Thesis Supervisor

Certified by
Daniel Blankschtein
Professor
Thesis Supervisor

Accepted by
William Deen
Chairperson, Committee for Graduate Students

Complementary Use of Computer Simulations and Molecular-Thermodynamic Theory to Model Surfactant and Solubilizate Self-Assembly

by

Brian C. Stephenson

Submitted to the Department of Chemical Engineering
on 27 November 2006, in partial fulfillment of the
requirements for the degree of
Doctor of Philosophy

Abstract

Surfactants, or surface active agents, are used in many pharmaceutical, industrial, and environmental applications. Selection of the appropriate surfactant or mixture of surfactants for any given application is driven by the need to control bulk solution micellization and solubilization characteristics. The goal of this thesis has been to develop computer simulations and molecular-thermodynamic modeling approaches to predict these solution characteristics based on knowledge of surfactant and solubilizate chemical structure. The ability to make such predictions would give formulators in industry the ability to design and optimize surfactant formulations with a minimum of effort and expense.

This thesis has explored the application of three theoretical approaches to model surfactant micellization and micellar solubilization. The first theoretical approach involves the use of computer simulations (CS) to obtain input parameters for molecular-thermodynamic (MT) modeling of surfactant micellization and micellar solubilization. This approach was motivated by the limitations inherent in computer simulations (the high computational expense of modeling self-assembly) and in MT modeling approaches (their restriction to structurally and chemically simple surfactants and solubilizates). A key input required for traditional MT modeling is the identification of the hydrated and the unhydrated portions (head and tail) of surfactants and solubilizates in a self-assembled micellar aggregate. By conducting simulations of surfactants and solubilizates at an oil/water interface (modeling the micelle core/water interface) or in a micellar environment, I have determined head and tail input parameters for simple and complex surfactants and solubilizates. This information has been successfully used as an input to MT modeling, and has been shown to extend the applicability of the traditional MT modeling approach to more complex surfactant and solubilizate systems than had been possible to date. A wide range of surfactant and solubilizate systems have been modeled with this approach, including ionic, zwitterionic, and nonionic surfactant/solubilizate systems. For each of the systems modeled, theoretical predictions were in reasonable agreement with the experimental data. A novel, alternative approach has also been developed to more accurately quantify the hydrophobic driving force for micelle formation by using atomistic molecular dynamics (MD) simulations to quantify the hydration changes that take place during micelle self-assembly. This new approach is referred to as the computer simulation/molecular-thermodynamic (CS-MT) model. In the

CS-MT model, hydration information determined through computer simulation is used in a new MT model to quantify the hydrophobic effect, which is decomposed into two components: g_{dehydr} , the free-energy change associated with the dehydration of hydrophobic groups that accompanies aggregate self-assembly, and g_{hydr} , the change in hydration free energy experienced during aggregate self-assembly. The CS-MT model is formulated to allow the prediction of the free-energy change associated with the formation of aggregates of any shape and size after performing only two computer simulations — one of the surfactant/solubilizate in bulk water and the second of the surfactant/solubilizate in an aggregate of arbitrary shape and size. The CS-MT modeling approach has been validated by using it to model the formation of oil aggregates, the micellization behavior of nonionic surfactants in aqueous solution, and the micellization behavior of ionic and zwitterionic surfactants in aqueous solution. For each of the systems modeled, the CS-MT model predictions were in reasonable agreement with the experimental data, and in almost all cases were in better agreement with the experimental data than the predictions of the traditional MT model.

The second theoretical approach explored in this thesis is the application of computer simulation free-energy (FE) methods to quantify the thermodynamics of mixed micelle formation. In this theoretical approach, referred to as the CS-FE/MT modeling approach, the traditional MT modeling approach, or experimental data, is first used to determine the free energy of formation of a pure (single) surfactant micelle. Subsequently, computer simulations are used to determine the free-energy change associated with alchemically changing the identity of individual surfactants present in the micelle to that of a second surfactant or solubilizate. This free-energy change, when added to the free energy of single surfactant micellization, yields the free energy associated with mixed micelle formation. The free energy of mixed micelle formation can then be used in the context of a thermodynamic description of the micellar solution to predict bulk solution properties such as the CMC and the equilibrium composition of the mixed micelle. The CS-FE/MT model has been used to model both binary surfactant micellization and micellar solubilization. The CS-FE/MT model was shown to be most accurate when the chemical structures of the mixed micelle components were similar and when small alchemical transformations were performed.

The third theoretical approach explored in this thesis is the use of all-atomistic computer simulations to make direct predictions of surfactant solution properties. Although the computational expense associated with atomistic-level MD simulations restricts their use to the evaluation of a limited subset of surfactant solution properties, these simulations can provide significant insight into the structural characteristics of preformed surfactant aggregates and the self-assembly behavior of surfactant molecules over limited timescales. Simulation of monolayers of a homologous series of structurally complex fluorosurfactants has been conducted in order to explore their behavior at a water/air interface and the origin of their ability to reduce surface tension. In addition, atomistic-level MD simulations have been conducted to study the self-assembly behavior of the triterpenoids asiatic acid (AA) and madecassic acid (MA) in aqueous solution. The computer simulation results were used to obtain information about: i) the kinetics of micelle formation, ii) the structural characteristics of the self-assembled micelles, and iii) micellization thermodynamics.

This thesis presents a detailed, atomistic-level computer simulation and molecular-thermodynamic investigation of the micellar solution behavior of nonionic, zwitterionic, and ionic surfactants in aqueous solutions, as well as of the aqueous micellar solubilization of solubilizates by surfactants. It is hoped that the approaches developed in this thesis to

use computer simulations and molecular-thermodynamic theory in a complementary way will not only extend our ability to make accurate predictions of surfactant solution behavior, but will also contribute to our fundamental knowledge of the solution behavior of surfactants and solubilizates. It is further hoped that this thesis will provide a solid foundation for future research in the area of surfactant science, and, more generally, that it will assist future researchers working to connect atomistic-level computer simulation methods with continuum thermodynamic models.

Thesis Supervisor: Kenneth Beers
Title: Visiting Assistant Professor

Thesis Supervisor: Daniel Blankschtein
Title: Professor

Acknowledgements

Many individuals have contributed to the research presented in this thesis. I would like to thank both of my research advisors, Professor Kenneth Beers and Professor Daniel Blankschtein. Kenneth Beers introduced me to the world of computer simulations and was always willing to provide insightful comments on my research and encouragement throughout the research process. Daniel Blankschtein introduced me to the world of colloids and surfactants, and gave me the freedom to pursue the research ideas I found most interesting. He also motivated me to pay careful attention to every detail of my research, and worked very hard to provide feedback on each of the articles, grant proposals, reports, and talks I have prepared over the past four years.

I would also like to extend my sincere thanks to each of the collaborators I have worked with, each of whom have contributed greatly to this thesis. My sincere thanks to Kate Stafford, who was very helpful in implementing the computer simulation/free-energy methods developed as part of this thesis. Her positive attitude and dedication to her work was a great help, and allowed me to manage the many research projects I juggled towards the end of my stay at MIT. I would also like to thank Professor Carlota Rangel-Yagui, who collaborated with me to experimentally and theoretically characterize ibuprofen solubilization behavior in surfactant solutions. I am also grateful to Dr. Arthur Goldsipe for his help with many aspects of my thesis research, including his assistance during the development of the CS-MT modeling approach. My sincere thanks go to Jonathan Mendenhall for providing invaluable assistance in implementing hybrid computer simulation/molecular-thermodynamic modeling approaches to describe complex surfactant micellization and micellar solubilization behavior. Without his help, it would not have been possible to realistically model many of the most complex surfactant/solubilize systems considered in this thesis. I also greatly appreciate the feedback of Dr. Isaac Reif, who critically reviewed several of the papers which came out of my thesis research.

I am grateful to all past and present members of the Beers and Blankschtein groups

for providing a pleasant, collaborative place to work. In particular, I appreciate the helpful feedback I received from the Blankschtein group during my practice talks. I wish the present group members — Srinivas, Saswata, Jonathan, Amanda, Jennifer, Baris, and Shangchao — success in their future research. Jonathan Mendenhall is exploring a coupled-term mean-field modeling approach to enable more accurate estimation of the free-energy contributions associated with micelle self-assembly, and I wish him success with this novel area of research. Shangchao Lin is exploring several interesting applications of the CS-MT model, and I also wish him success in all his research endeavors.

Most of all I would like to thank my family, from grandparents to siblings, who have helped me through graduate school with their love and support. My parents in particular have contributed in many ways to the completion of this thesis, from always being supportive of my education to providing encouragement through the ups and downs of thesis research. This thesis is dedicated to them both.

Finally, I am grateful for the award of a Presidential Fellowship at MIT, and to MIT's chemical engineering department for providing financial support for this research.

Contents

PART I: APPLICATION OF COMPUTER SIMULATIONS TO OBTAIN MOLECULAR-THERMODYNAMIC INPUTS

1	Introduction	42
1.1	Motivation	42
1.2	Introduction to Surfactant Micellization and Micellar Solubilization .	47
1.2.1	Surfactant Micellization	48
1.2.2	Micellar Solubilization	48
1.3	Theoretical Models of Micellization and Micellar Solubilization . . .	54
1.3.1	Molecular-Thermodynamic Models of Micellization	54
1.3.2	Molecular-Thermodynamic Models of Solubilization	55
1.3.3	Limitations of Previous Molecular-Thermodynamic Modeling Approaches	58
1.4	Introduction to Computer Simulation Methods	60
1.5	Computer Simulation Studies of Micellization and Micellar Solubilization	77
1.5.1	Computer Simulation of Preformed Surfactant/Solubilize Sys- tems	64
1.5.2	Computer Simulation of Micelle Self-Assembly	65
1.5.3	Determination of the Free Energy of Micelle Formation	67
1.6	Combined Computer Simulation/Molecular Thermodynamic Models .	68
1.7	Thesis Objectives	70

1.8	Thesis Overview	71
2	Complementary Use of Simulations and Molecular-Thermodynamic Theory to Model Micellization	95
2.1	Introduction	95
2.2	Molecular-Thermodynamic Approach	99
2.2.1	Thermodynamic Framework	99
2.2.2	Molecular Model of Micellization	101
2.3	Molecular Dynamics Simulations	104
2.3.1	Computational Approach	104
2.3.2	Simulation Parameters	105
2.3.3	System Preparation and Equilibration	106
2.3.4	Data Analysis Method	107
2.4	Simulation Results and Discussion	110
2.4.1	Sodium Dodecyl Sulfate (SDS)	110
2.4.2	Cetyltrimethylammonium Bromide (CTAB)	112
2.4.3	Dodecylphosphocholine (DPC)	114
2.4.4	Dodecyl Poly(Ethylene Oxide) (C ₁₂ E ₈)	115
2.4.5	3-Hydroxy Sulfonate (AOS)	117
2.4.6	Decanoyl-n-Methylglucamide (MEGA-10)	120
2.5	Molecular-Thermodynamic Modeling Based on Computer Simulation	
	Inputs	121
2.5.1	Sodium Dodecyl Sulfate (SDS)	122
2.5.2	Cetyltrimethylammonium Bromide (CTAB)	124
2.5.3	Dodecylphosphocholine (DPC)	126
2.5.4	Dodecyl Octa(Ethylene Oxide) (C ₁₂ E ₈)	127
2.5.5	3-Hydroxy Sulfonate (AOS)	128
2.5.6	Decanoyl-n-Methylglucamide (MEGA-10)	129
2.6	Conclusions	133

3	Experimental and Theoretical Investigation of the Micellar-Assisted Solubilization of Ibuprofen in Aqueous Media	145
3.1	Introduction	145
3.2	Materials, Experimental Methods, and Experimental Results	149
3.2.1	Materials	149
3.2.2	Experimental Methods	149
3.2.3	Experimental Results	151
3.3	Theoretical Modeling	153
3.3.1	Molecular Dynamics Simulations	158
3.3.2	Molecular-Thermodynamic Approach	162
3.3.3	Molecular-Thermodynamic Modeling Based on Computer Simulation Inputs	165
3.4	Conclusions	183
4	Complementary Use of Simulations and Molecular-Thermodynamic Theory to Model Solubilization. I. Theory	193
4.1	Introduction	193
4.1.1	Introduction to Surfactant Micellization and Micellar Solubilization	195
4.1.2	Theoretical Modeling Approaches	197
4.1.3	Computer Simulation Approaches	200
4.1.4	Combined Computer Simulation/Molecular-Thermodynamic Modeling Approach	202
4.1.5	Motivation and Research Objectives	204
4.2	Computer Simulations	207
4.2.1	Methodology	207
4.2.2	Simulation Methods and Parameters	209
4.2.3	System Preparation and Equilibration	212
4.2.4	Data Analysis Method	221

4.3	Simulation Results and Discussion	227
4.4	Molecular-Thermodynamic Theory of Solubilization	233
4.4.1	Introduction	233
4.4.2	Thermodynamic Framework to Model the Free Energy of the Micellar Solution	234
4.4.3	Molecular Model of Micellar Solubilization	237
4.5	Conclusions	260
4.6	Appendix 4-A: Equilibration Results for the Cylindrical and Spherical Micelles	263
4.7	Appendix 4-B: Contact Analysis Results	280
5	Complementary Use of Simulations and Molecular-Thermodynamic Theory to Model Solubilization. II. Application	303
5.1	Introduction	303
5.2	Overview of Computer Simulation Results	305
5.3	Overview of Molecular-Thermodynamic Model for Micellar Solubilization	306
5.4	Molecular-Thermodynamic Modeling Based on Computer Simulation Inputs	309
5.4.1	Selection of Heads and Tails for Molecular-Thermodynamic Mod- eling	309
5.4.2	Molecular Parameters Used in Molecular-Thermodynamic Mod- eling	314
5.4.3	Implementation of Molecular Model	316
5.5	Molecular-Thermodynamic Modeling Results	324
5.5.1	Free-Energy Predictions	326
5.5.2	Predictions of Micellar Solubilization Characteristics	336
5.5.3	Sensitivity of the Predictions to Salt Concentration	345
5.6	Conclusions	348
6	Quantifying the Hydrophobic Effect: I. A Computer Simulation/	

Molecular-Thermodynamic Model for the Self-Assembly of Hydrophobic and Amphiphilic Solutes in Aqueous Solution	357
6.1 Introduction	357
6.2 Molecular-Thermodynamic Modeling Approach	364
6.2.1 Introduction	364
6.2.2 Thermodynamic Framework	365
6.2.3 Traditional Molecular-Thermodynamic Model of Surfactant Micellization and Micellar Solubilization	367
6.3 The Computer Simulation/Molecular Thermodynamic (CS-MT) Modeling Approach	373
6.3.1 Introduction	373
6.3.2 Theoretical Framework	373
6.3.3 The Free Energy of Dehydration, g_{dehydr}	375
6.3.4 The Free Energy of Hydration, g_{hydr}	377
6.3.5 Extension of the CS-MT Model to Predict Aggregate Shape and Size	380
6.3.6 Evaluating the Validity and Accuracy of the CS-MT Model	381
6.4 Molecular Dynamics Simulations	384
6.4.1 Introduction	382
6.4.2 Modeling Approach	383
6.4.3 Simulation Methods and Parameters	383
6.4.4 System Preparation and Equilibration	385
6.4.5 Data Analysis Method	390
6.5 Simulation Results and Discussion	396
6.5.1 Fractional Hydration Results	396
6.5.2 Solvent Accessible Surface Area (SASA) Results	401
6.6 Molecular-Thermodynamic Modeling Based on Computer Simulation Inputs	404
6.7 Conclusions	409

6.8	Appendix 6-A: Extension of the CS-MT Model to Predict Aggregate Shape and Size	412
6.9	Appendix 6-B: Mathematical Demonstration of the Equivalence of the CS-MT Model and the Traditional MT Model for Completely Hydrophobic Solutes	417
7	Quantifying the Hydrophobic Effect: II. A Computer Simulation/Molecular-Thermodynamic Model for the Micellization of Nonionic Surfactants in Aqueous Solution	430
7.1	Introduction	430
7.1.1	Review of the CS-MT Model	431
7.1.2	Modeling Nonionic Surfactant Micellization	435
7.2	Molecular Dynamics Simulations	437
7.2.1	Modeling Approach	437
7.2.2	Simulation Methods and Parameters	437
7.2.3	System Preparation and Equilibration	439
7.2.4	Data Analysis Method	443
7.3	Simulation Results and Discussion	446
7.3.1	Octyl Glucoside (OG)	447
7.3.2	Dodecyl Maltoside (DM)	449
7.3.3	Octyl Sulfinyl Ethanol (OSE)	451
7.3.4	Decyl Dimethyl Phosphine Oxide (C ₁₀ PO)	453
7.3.5	Decyl Methyl Sulfoxide (C ₁₀ SO)	453
7.3.6	Dodecyl Octa(Ethylene Oxide) (C ₁₂ E ₈)	455
7.3.7	Decanoyl- <i>n</i> -Methylglucamide (MEGA-10)	458
7.3.8	Evaluation of Approximations Made in Traditional Molecular-Thermodynamic Modeling	458
7.4	Molecular-Thermodynamic Modeling Based on Computer Simulation Inputs	466

7.4.1	Using the CS-MT Modeling Approach to Predict Surfactant Micellization Behavior	466
7.4.2	Modeling Results for Octyl Glucoside (OG)	471
7.4.3	Modeling Results for Dodecyl Maltoside (DM)	475
7.4.4	Modeling Results for Octyl Sulfinyl Ethanol (OSE)	476
7.4.5	Modeling Results for Decyl Dimethyl Phosphine Oxide (C ₁₀ PO)	477
7.4.6	Modeling Results for Decyl Methyl Sulfoxide (C ₁₀ SO)	478
7.4.7	Modeling Results for Binary Mixtures of C ₁₀ PO and C ₁₀ SO .	479
7.4.8	Modeling Results for Dodecyl Octa(Ethylene Oxide) (C ₁₂ E ₈) .	481
7.4.9	Modeling Results for Decanoyl- <i>n</i> -Methylglucamide (MEGA-10)	484
7.4.10	Effect of the Definition of Hydrating Contacts on the Modeling Results	485
7.5	Conclusions	487
7.6	Appendix 7-A: Normalized SASA Profiles	490
8	Quantifying the Hydrophobic Effect: III. A Computer Simulation/ Molecular-Thermodynamic Model for the Micellization of Ionic and Zwitterionic Surfactants in Aqueous Solution	498
8.1	Introduction	498
8.1.1	Overview of the CS-MT Model	499
8.1.2	Modeling Ionic and Zwitterionic Surfactant Micellization . . .	503
8.2	Molecular Dynamics Simulations	505
8.2.1	Modeling Approach	505
8.2.2	Simulation Methods and Parameters	505
8.2.3	System Preparation and Equilibration	506
8.2.4	Data Analysis Method	508
8.3	Simulation Results and Discussion	511
8.3.1	Sodium Dodecyl Sulfate (SDS)	511
8.3.2	Dodecylphosphocholine (DPC)	513

8.3.3	Cetyltrimethylammonium Bromide (CTAB)	515
8.3.4	Sodium 3-Hydroxy Sulfonates (AOS-12 and AOS-16)	515
8.3.5	$C_{12}H_{25}C_NH_{2N+1}N(CH_3)_2Br$ Surfactants (DC ₁ AB-DC ₆ AB)	517
8.4	Molecular-Thermodynamic Modeling Based on Computer Simulation	
	Inputs	521
8.4.1	Using the CS-MT Modeling Approach to Predict the Micellization Behavior of Ionic and Zwitterionic Surfactants	521
8.4.2	Modeling Results for Simple Surfactants	522
8.4.3	Modeling Results for Complex Surfactants	529
8.5	Conclusions	537
8.6	Appendix 8-A: Normalized SASA Profiles	540

PART II: FREE-ENERGY CALCULATIONS USING COMPUTER SIMULATION

9	Free-Energy Calculations Using Computer Simulations: Theory	548
9.1	Background	549
9.2	Overview of CS-FE/MT Modeling Approach	552
9.3	Formulation of the Thermodynamic Framework Used in the CS-FE/MT Model	553
9.4	Introduction to Computer Simulation Free-Energy Methods	559
	9.4.1 Methods for the Evaluation of Free-Energy Differences	560
	9.4.2 Thermodynamic Integration	561
9.5	Free-Energy Calculations Made in the CS-FE/MT Model	564
9.6	Conclusions	568
10	Free-Energy Calculations Using Computer Simulations: Implementation and Results	574
10.1	Implementation of Alchemical Free-Energy Calculations	576
	10.1.1 Selection of λ -Dependent Energy Functions	576

10.1.2	Single vs. Dual-Topology Approaches	579
10.1.3	Description of Alchemical Topologies	579
10.2	Simulation Methods and Parameters	586
10.3	Simulation Preparation and Equilibration	587
10.3.1	Aqueous Simulations	587
10.3.2	Micellar Simulations	588
10.4	Alchemical Simulations and Results	594
10.4.1	Evaluation of $\Delta\Delta G$ from ΔG_1 and ΔG_2	592
10.4.2	$\Delta\Delta G$ Results Based on Simulation at Additional λ Values	619
10.5	Conclusions	539
10.6	Appendix 10-A: Validation of Alchemical Free-Energy Methods Used to Implement the CS-FE/MT Model	627

PART III: DIRECT PREDICTION OF SURFACTANT SOLUTION PROPERTIES USING COMPUTER SIMU- LATIONS

11	Determination of the Interfacial Characteristics of a Series of Bo- laamphiphilic Poly(fluorooxetane) Surfactants through Molecular Dy- namics Simulation	641
11.1	Introduction	641
11.2	Simulation Methodology	646
11.2.1	Simulation Parameters	646
11.2.2	System Preparation and Equilibration	647
11.3	Results and Discussion	654
11.3.1	Saturated Interfacial Areas per Surfactant Molecule	654
11.3.2	Interfacial Areas per Surfactant Molecule as a Function of Ap- plied Surface Tension	656
11.3.3	Visualization of Surfactant Conformation	658

11.3.4	Interfacial Density Profiles	661
11.3.5	Degree of Hydration and Counterion Binding	672
11.3.6	Order Parameters	674
11.4	Conclusions	676
12	Molecular Dynamics Investigation of the Self-Assembly of the Triterpenoids Asiatic Acid and Madecassic Acid in Aqueous Solution	686
12.1	Introduction	686
12.2	Methods	691
12.2.1	Simulation Methodology and Parameters	691
12.2.2	System Preparation and Equilibration	692
12.3	Computer Simulation Results and Analysis	693
12.3.1	Self-Assembly Behavior	693
12.3.2	Number of Micelles and Micelle Aggregation Number	693
12.3.3	Monomer Concentration	699
12.3.4	Micelle Principal Moments of Gyration	701
12.3.5	Orientational Order Parameters	703
12.3.6	Radial Distribution Functions	705
12.3.7	Extent of Hydration	707
12.3.8	Solvent Accessible Surface Area	709
12.4	Computer Simulation/Molecular-Thermodynamic Model to Investigate Micellization Thermodynamics	710
12.4.1	Thermodynamic Framework	713
12.4.2	Molecular Model of Single-Surfactant Micellization	715
12.4.3	Implementation of the CS-MT Model	720
12.5	Conclusions	724
13	Conclusions and Future Research Directions	736
13.1	Thesis Summary	737

13.2	Future Research Directions: Application of Computer Simulation to Obtain Inputs for MT Theory	745
13.2.1	Head and Tail Identification through Water/Oil Interface Simulation	746
13.2.2	Head and Tail Identification through Micellar Simulation . . .	748
13.2.3	CS-MT Modeling of Surfactants and Solubilizates	749
13.3	Future Research Directions: Application of Computer Simulation to Determine Free-Energy Changes	757
13.3.1	Selection of the Optimal Transition Path	757
13.3.2	Alternative Free-Energy Methods	759
13.4	Future Research Directions: Application of Computer Simulation to Make Direct Predictions of Surfactant Solution Properties	760
13.5	Concluding Remarks	762

List of Figures

1-1	Regions of solubilization in a surfactant micelle.	52
1-2	Examples of challenging surfactants to model using molecular-thermo- dynamic theory.	59
1-3	Sequence of steps involved in molecular dynamics (MD) simulation. . .	62
2-1	Scaled contact ratios predicted using simulations for each SDS surfac- tant group, where the scaled contact ratio is defined as the number of contacts of each surfactant group with water divided by the number of contacts of the same group with octane.	111
3-1	Chemical structure of the drug ibuprofen.	147
3-2	Experimentally-determined solubility curve of ibuprofen as a function of SDS concentration in 5 mM phosphate buffer at pH 7.4 and 25 °C. . .	152
3-3	Experimentally-determined solubility curve of ibuprofen as a function of DTAB concentration in 5 mM phosphate buffer at pH 7.4 and 25 °C. . .	154
3-4	Experimentally-determined solubility curve of ibuprofen as a function of C ₁₂ E ₈ concentration in 5 mM phosphate buffer at pH 7.4 and 25 °C. . .	155
3-5	Predicted and experimental values of the micellar composition of ibupro- fen (X_{ibu}), defined as the mole fraction of ibuprofen in the micellar aggregate, as a function of SDS concentration in phosphate buffer at pH 7.4 and 25 °C.	169
3-6	Predicted and experimental values of ibuprofen solubility as a function of SDS concentration in phosphate buffer at pH 7.4 and 25 °C.	172

3-7	Predicted and experimental values of micellar composition of ibuprofen (X_{ibu}), defined as the mole fraction of ibuprofen in the micellar aggregate, as a function of DTAB concentration in phosphate buffer at pH 7.4 and 25 °C.	176
3-8	Predicted and experimental values of ibuprofen solubility as a function of DTAB concentration in phosphate buffer at 25 °C.	178
3-9	Predicted and experimental values of micellar composition of ibuprofen (X_{ibu}), defined as the mole fraction of ibuprofen in the micellar aggregate, as a function of C ₁₂ E ₈ concentration in phosphate buffer at pH 7.4 and 25 °C.	181
3-10	Predicted and experimental values of ibuprofen solubility as a function of C ₁₂ E ₈ concentration in phosphate buffer at pH 7.4 and 25 °C. . .	182
4-1	Chemical structures of the solubilizates modeled in this chapter. . .	182
4-2	Representative snapshot of a water/oil interface (A), a cylindrical micelle (B), and a spherical micelle (C) after equilibration.	213
4-3	Solvent accessible surface area (SASA) profiles for the cylindrical (A) and spherical (B) SDS/ibuprofen micelles and SDS/acetophenone micelles as a function of simulation time.	219
4-4	Distance between several surfactant groups defined in the text and the micelle center of mass ($d_{SO_4-MIC_{COM}}$, $d_{CH_2-MIC_{COM}}$, $d_{CH_3-MIC_{COM}}$) and ibuprofen and the micelle center of mass ($d_{SOL_{COM}-MIC_{COM}}$) in the cylindrical (A) and spherical (B) SDS/ibuprofen micelles.	221
4-5	Distance between several surfactant groups defined in the text and the micelle center of mass ($d_{SO_4-MIC_{COM}}$, $d_{CH_2-MIC_{COM}}$, $d_{CH_3-MIC_{COM}}$) and acetophenone and the micelle center of mass ($d_{SOL_{COM}-MIC_{COM}}$) in the cylindrical (A) and spherical (B) SDS/ibuprofen micelles.	222
4-6	Head and tail identifications made from water/oil interface simulation.	228
4-7	Head and tail identifications made from cylindrical micelle simulation.	229
4-8	Head and tail identifications made from spherical micelle simulation. .	229

4-9	Two-dimensional representation of a spherical or cylindrical micelle core, depicting the L layers concentric to the micelle core and the three Euler angles describing the overall orientation of the surfactant tail with respect to the micelle core/water interface, α , β , and γ	249
4-A1	Solvent accessible surface area (SASA) for the cylindrical and spherical SDS/ibuprofen micelles as a function of simulation time.	266
4-A2	Solvent accessible surface area (SASA) for the cylindrical and spherical SDS/benzamide micelles as a function of simulation time.	267
4-A3	Solvent accessible surface area (SASA) for the cylindrical and spherical SDS/acetophenone micelles as a function of simulation time.	268
4-A4	Solvent accessible surface area (SASA) for the cylindrical and spherical SDS/benzonitrile micelles as a function of simulation time.	269
4-A5	Solvent accessible surface area (SASA) for the cylindrical and spherical SDS/ <i>o</i> -aminobenzoate micelles as a function of simulation time. . . .	270
4-A6	Solvent accessible surface area (SASA) for the cylindrical and spherical SDS/ <i>m</i> -aminobenzoate micelles as a function of simulation time. . . .	271
4-A7	Solvent accessible surface area (SASA) for the cylindrical and spherical SDS/ <i>p</i> -aminobenzoate micelles as a function of simulation time. . . .	272
4-A8	Distance between several surfactant groups defined in the text and the micelle center of mass ($d_{\text{SO}_4-\text{MIC}_{\text{COM}}}$, $d_{\text{CH}_2-\text{MIC}_{\text{COM}}}$, $d_{\text{CH}_3-\text{MIC}_{\text{COM}}}$) and the ibuprofen and the micelle center of mass ($d_{\text{SOL}_{\text{COM}}-\text{MIC}_{\text{COM}}}$) in the cylindrical (A) and spherical (B) SDS/ibuprofen micelles. The average value of each distance over 25 ns of simulation is reported in a table below the figure.	273

4-A9	Distance between several surfactant groups defined in the text and the micelle center of mass ($d_{\text{SO}_4\text{-MIC}_{\text{COM}}}$, $d_{\text{CH}_2\text{-MIC}_{\text{COM}}}$, $d_{\text{CH}_3\text{-MIC}_{\text{COM}}}$) and the benzamide and the micelle center of mass ($d_{\text{SOL}_{\text{COM}}\text{-MIC}_{\text{COM}}}$) in the cylindrical (A) and spherical (B) SDS/benzamide micelles. The average value of each distance over 25 ns of simulation is reported in a table below the figure.	274
4-A10	Distance between several surfactant groups defined in the text and the micelle center of mass ($d_{\text{SO}_4\text{-MIC}_{\text{COM}}}$, $d_{\text{CH}_2\text{-MIC}_{\text{COM}}}$, $d_{\text{CH}_3\text{-MIC}_{\text{COM}}}$) and the acetophenone and the micelle center of mass ($d_{\text{SOL}_{\text{COM}}\text{-MIC}_{\text{COM}}}$) in the cylindrical (A) and spherical (B) SDS/acetophenone micelles. The average value of each distance over 25 ns of simulation is reported in a table below the figure.	275
4-A11	Distance between several surfactant groups defined in the text and the micelle center of mass ($d_{\text{SO}_4\text{-MIC}_{\text{COM}}}$, $d_{\text{CH}_2\text{-MIC}_{\text{COM}}}$, $d_{\text{CH}_3\text{-MIC}_{\text{COM}}}$) and the benzonitrile and the micelle center of mass ($d_{\text{SOL}_{\text{COM}}\text{-MIC}_{\text{COM}}}$) in the cylindrical (A) and spherical (B) SDS/benzonitrile micelles. The average value of each distance over 25 ns of simulation is reported in a table below the figure.	276
4-A12	Distance between several surfactant groups defined in the text and the micelle center of mass ($d_{\text{SO}_4\text{-MIC}_{\text{COM}}}$, $d_{\text{CH}_2\text{-MIC}_{\text{COM}}}$, $d_{\text{CH}_3\text{-MIC}_{\text{COM}}}$) and the <i>o</i> -aminobenzoate and the micelle center of mass ($d_{\text{SOL}_{\text{COM}}\text{-MIC}_{\text{COM}}}$) in the cylindrical (A) and spherical (B) SDS/ <i>o</i> -aminobenzoate micelles. The average value of each distance over 25 ns of simulation is reported in a table below the figure.	277

4-A13	Distance between several surfactant groups defined in the text and the micelle center of mass ($d_{\text{SO}_4-\text{MIC}_{\text{COM}}}$, $d_{\text{CH}_2-\text{MIC}_{\text{COM}}}$, $d_{\text{CH}_3-\text{MIC}_{\text{COM}}}$) and the <i>m</i> -aminobenzoate and the micelle center of mass ($d_{\text{SOL}_{\text{COM}}-\text{MIC}_{\text{COM}}}$) in the cylindrical (A) and spherical (B) SDS/ <i>m</i> -aminobenzoate micelles. The average value of each distance over 25 ns of simulation is reported in a table below the figure.	278
4-A14	Distance between several surfactant groups defined in the text and the micelle center of mass ($d_{\text{SO}_4-\text{MIC}_{\text{COM}}}$, $d_{\text{CH}_2-\text{MIC}_{\text{COM}}}$, $d_{\text{CH}_3-\text{MIC}_{\text{COM}}}$) and the <i>p</i> -aminobenzoate and the micelle center of mass ($d_{\text{SOL}_{\text{COM}}-\text{MIC}_{\text{COM}}}$) in the cylindrical (A) and spherical (B) SDS/ <i>p</i> -aminobenzoate micelles. The average value of each distance over 25 ns of simulation is reported in a table below the figure.	279
5-1	Chemical structures of the solubilizates modeled in this chapter. . . .	304
5-2	Summary of head and tail identification results presented in Chapter 4.	307
5-3	Head and tail identifications made for molecular-thermodynamic modeling of g_{tr} and g_{int}	311
5-4	Head and tail identifications made for molecular-thermodynamic modeling of g_{pack}	313
5-5	Predicted values of g_{pack} (in units of $k_{\text{B}}T$) as a function of l_{c} and α_{mic} for <i>o</i> -aminobenzoate solubilization in cylindrical SDS micelles (A), <i>m</i> -aminobenzoate solubilization in cylindrical SDS micelles (B), and <i>p</i> -aminobenzoate solubilization in cylindrical SDS micelles (C).	330
5-6	Predicted values of g_{pack} (in units of $k_{\text{B}}T$) as a function of l_{c} and α_{mic} for <i>o</i> -aminobenzoate solubilization in spherical CTAB micelles (A), <i>m</i> -aminobenzoate solubilization in cylindrical CTAB micelles (B), and <i>p</i> -aminobenzoate solubilization in spherical CTAB micelles (C). . . .	333

5-7	Predicted values of ΔV_{core} (in units of \AA^3) as a function of l_c and α_{mic} for <i>o</i> -aminobenzoate solubilization in cylindrical SDS micelles (A), <i>m</i> -aminobenzoate solubilization in cylindrical SDS micelles (B), and <i>p</i> -aminobenzoate solubilization in cylindrical SDS micelles (C).	335
5-8	The effect of NaCl concentration on the micelle/water partition coefficient for the solubilization of actophenone (K_s), benzamide (K_s), and <i>o</i> -aminobenzoate ($\ln(K_x)$) in SDS micelles.	346
5-9	The effect of NaCl concentration on the micelle/water partition coefficient for the solubilization of actophenone (K_s), benzamide (K_s), and <i>o</i> -aminobenzoate ($\ln(K_x)$) in CTAB micelles.	347
6-1	Examples of surfactants and solubilizates for which making head and tail assignments is not trivial and which therefore are difficult to model using the traditional molecular-thermodynamic modeling approach.	361
6-2	Sequence of steps followed in the molecular-thermodynamic cycle used in the CS-MT modeling approach presented in the context of the micellization of a cationic surfactant and a nonionic hydrophobic solubilize.	368
6-3	Solvent accessible surface area (SASA) as a function of simulation time for three representative simulated oil aggregates: a small octane sphere, a large octane cylinder, and an octane slab.	391
6-4	Snapshots of the post-equilibration structures of: (i) two dodecane spherical aggregates (of aggregation numbers 17 and 33), (ii) two dodecane cylindrical aggregates (of periodic lengths 2.85 nm and 3.85 nm), and (iii) a dodecane slab.	392
6-5	The average fractional degree of hydration (f) corresponding to each of the groups in octane for each of the five simulated aggregate geometries: (i) a small spherical aggregate, (ii) a large spherical aggregate, (iii) a small cylindrical aggregate, (iv) a large cylindrical aggregate, and (v) a planar slab.	398

6-6	The average fractional degree of hydration (f) corresponding to each of the groups in dodecane for each of the five simulated aggregate geometries: (i) a small spherical aggregate, (ii) a large spherical aggregate, (iii) a small cylindrical aggregate, (iv) a large cylindrical aggregate, and (v) a planar slab.	399
6-7	The average fractional degree of hydration (f) corresponding to each of the groups in hexadecane for each of the five simulated aggregate geometries: (i) a small spherical aggregate, (ii) a large spherical aggregate, (iii) a small cylindrical aggregate, (iv) a large cylindrical aggregate, and (v) a planar slab.	400
6-8	The ratio of the solvent accessible surface area (SASA) to the geometrically-defined surface area (A) for each of the octane, dodecane, and hexadecane oil aggregates simulated, grouped according to geometry.	402
6-9	Theoretical predictions of the hydration free energy difference (Δg_{wc}) associated with hydrating contacts in the aggregate state and in the bulk water state are shown as a function of curvature made using: (i) theoretical predictions based on values of $SASA_{core}/A_{core}$ computed from the simulation results, and (ii) theoretical predictions based on values of $SASA_{core}/A_{core}$	405
7-1	Solvent accessible surface area (SASA) normalized by the average value of SASA as a function of simulation time for micelles of three representative nonionic surfactants: dodecyl maltoside (DM), dodecyl octa(ethylene oxide) ($C_{12}E_8$), and decanoyl- <i>n</i> -methylglucamide (MEGA-10).	444
7-2	Snapshots of the post-equilibration structures of the seven simulated micelles considered in Chapter 7.	443
7-3	The average fractional degree of hydration for each of the groups in octyl glucoside (OG), where results are reported for f , f_{water} , and f_{head}	448

7-4	The average fractional degree of hydration for each of the groups in dodecyl maltoside (DM), where results are reported for f , f_{water} , and f_{head}	450
7-5	The average fractional degree of hydration for each of the groups in octyl sulfinyl ethanol (OSE), where results are reported for f , f_{water} , and f_{head}	452
7-6	The average fractional degree of hydration for each of the groups in decyl dimethyl phosphine oxide (C_{10}PO), where results are reported for f , f_{water} , and f_{head}	454
7-7	The average fractional degree of hydration for each of the groups in decyl ethyl sulfoxide (C_{10}SO), where results are reported for f , f_{water} , and f_{head}	456
7-8	The average fractional degree of hydration for each of the groups in dodecyl octa(ethylene oxide) (C_{12}E_8), where results are reported for f , f_{water} , and f_{head}	457
7-9	The average fractional degree of hydration for each of the groups in decanoyl- <i>n</i> -methylglucamide (MEGA-10), where results are reported for f , f_{water} , and f_{head}	459
7-10	The number of hydrating contacts experienced in bulk water for 8 hydrophobic CH_2 or CH_3 groups in hexadecane, in octyl glucoside (OG), and in octyl sulfinyl ethanol (OSE).	464
7-11	The number of hydrating contacts experienced in bulk water for 12 hydrophobic CH_2 or CH_3 groups in hexadecane, in dodecyl maltoside (DM), and in dodecyl octa(ethylene oxide) (C_{12}E_8).	463
7-12	Predicted and experimental CMCs of mixtures of C_{10}PO and C_{10}SO , where theoretical predictions are made using both the CS-MT model and the traditional MT model.	480

7-13	Predicted and experimental values of the CMC, where theoretical predictions have been made using the CS-MT model with: (i) f values taken as input to evaluate g_{dehydr} and g_{hydr} , and (ii) f_{water} values taken as input to evaluate g_{dehydr} and g_{hydr}	486
7-A1	Solvent accessible surface area (SASA) normalized by the average value of SASA as a function of simulation time for: octyl glucoside (OG), dodecyl maltoside (DM), dodecyl octa(ethylene oxide) (C_{12}E_8), and decanoyl- <i>n</i> -methylglucamide (MEGA-10) during the 5 ns data-gathering simulation run.	489
7-A2	Solvent accessible surface area (SASA) normalized by the average value of SASA as a function of simulation time for: octyl sulfinyl ethanol (OSE), decyl dimethyl phosphine oxide (C_{10}PO), and decyl methyl sulfoxide (C_{10}SO) during the 5 ns data-gathering simulation run.	491
8-1	Solvent accessible surface area (SASA) normalized by the average value of SASA as a function of simulation time for micelles of three representative ionic and zwitterionic surfactants: sodium dodecyl sulfate (SDS), dodecylphosphocholine (DPC), and 3-hydroxy dodecyl sulfonate (AOS-12).	509
8-2	Snapshots of the post-equilibration structures of the simulated micelles corresponding to each of the nine ionic and zwitterionic surfactants considered in this chapter.	510
8-3	The average fractional degree of hydration, f , of each of the groups in sodium dodecyl sulfate (SDS).	512
8-4	The average fractional degree of hydration, f , of each of the groups in dodecylphosphocholine (DPC).	514
8-5	The average fractional degree of hydration, f , of each of the groups in cetyltrimethylammonium bromide (CTAB).	516

8-6	The average fractional degree of hydration, f , of each of the groups in 3-hydroxy dodecyl sulfonate (AOS-12, see A) and 3-hydroxy hexadecyl sulfonate (AOS-16, see B).	518
8-7	The average fractional degree of hydration, f , of each of the groups in decyltrimethylammonium bromide (DC ₁ AB, see A), C ₁₂ H ₂₅ C ₂ H ₅ N(CH ₃) ₂ Br (DC ₂ AB, see B), C ₁₂ H ₂₅ C ₄ H ₉ N(CH ₃) ₂ Br (DC ₄ AB, see C), and C ₁₂ H ₂₅ C ₆ H ₁₃ N(CH ₃) ₂ Br (DC ₆ AB, see D).	519
8-8	Comparison of the CMCs predicted using the CS-MT model and the CMCs predicted using three traditional MT modeling limits with experimental CMC data for decyltrimethylammonium bromide (DC ₁ AB), C ₁₂ H ₂₅ C ₂ H ₅ N(CH ₃) ₂ Br (DC ₂ AB), C ₁₂ H ₂₅ C ₄ H ₉ N(CH ₃) ₂ Br (DC ₄ AB), and C ₁₂ H ₂₅ C ₆ H ₁₃ N(CH ₃) ₂ Br (DC ₆ AB).	533
8-A1	Solvent accessible surface area (SASA) normalized by the average value of SASA as a function of simulation time for: sodium dodecyl sulfate (SDS), 3-hydroxy dodecyl sulfonate (AOS-12), 3-hydroxy hexadecyl sulfonate (AOS-16), and dodecylphosphocholine (DPC) during the 5 ns data-gathering simulation run.	540
8-A2	Solvent accessible surface area (SASA) normalized by the average value of SASA as a function of simulation time for: cetyltrimethylammonium bromide (CTAB), decyltrimethylammonium bromide (DC ₁ AB), C ₁₂ H ₂₅ C ₂ H ₅ N(CH ₃) ₂ Br (DC ₂ AB), C ₁₂ H ₂₅ C ₄ H ₉ N(CH ₃) ₂ Br (DC ₄ AB), and C ₁₂ H ₂₅ C ₆ H ₁₃ N(CH ₃) ₂ Br (DC ₆ AB) during the 5 ns data-gathering simulation run (see text).	541
9-1	Computational strategy used in the CS-FE/MT model.	552
9-2	Comparison of alchemical pathways used to determine $\Delta\Delta G$ for substrate-enzyme binding and for composition change in a micelle.	565
10-1	Alchemical free-energy pathway used in the CS-FE/MT model	575
10-2	Comparison of the single and dual topology approaches	582

10-3	Topologies for surfactant to solubilizate transformation: the sodium dodecyl sulfate (SDS)/ibuprofen (IBU) topology is shown on the left, and the octyl glucoside (OG)/ <i>p</i> -aminobenzoate (PAB) topology is shown on the right.	583
10-4	Topologies for surfactant to cosurfactant transformation: the <i>n</i> -decyl dimethyl phosphine oxide (C ₁₀ PO)/ <i>n</i> - decyl methyl sulfoxide (C ₁₀ SO) topology is shown on the left, the (octylsulfinyl) ethanol (C ₈ SE)/ (decylsulfinyl) ethanol (C ₁₀ SE) topology is shown in the center, and the <i>n</i> -decyl methyl sulfoxide (C ₁₀ SO)/ <i>n</i> -octyl methyl sulfoxide (C ₈ SO) topology is shown on the right.	585
10-5	Solvent accessible surface area (SASA) as a function of simulation time for the SDS (A) and OG (B) micelles during the 10 ns of equilibration conducted prior to beginning alchemical transformation.	591
10-6	Solvent accessible surface area (SASA) as a function of simulation time for the C ₁₀ PO (A), C ₈ SE (B), and C ₁₀ SO (C) micelles during the 10 ns of equilibration conducted prior to beginning alchemical transformations.	592
10-7	Snapshots of the post-equilibration structures of the SDS, OG, C ₁₀ PO, C ₈ SE, and C ₁₀ SO micelles used as the starting point for free-energy calculations.	593
10-8	Computed values of $\partial G/\partial \lambda$ as a function of data gathering time for the transformation of SDS into IBU in aqueous solution (A) and in the micellar environment (B) at three values of λ : 0.0, 0.5, and 1.0. . . .	604
10-9	Computed values of $\partial G/\partial \lambda$ as a function of data gathering time for the transformation of OG into PAB in aqueous solution (A) and in the micellar environment (B) at three values of λ : 0.0, 0.5, and 1.0. . . .	605
10-10	Computed values of $\partial G/\partial \lambda$ as a function of data gathering time for the transformation of C ₁₀ PO into C ₁₀ SO in aqueous solution (A) and in the micellar environment (B) at three values of λ : 0.0, 0.5, and 1.0. . . .	607

10-11	Computed values of $\partial G/\partial\lambda$ as a function of data gathering time for the transformation of C ₈ SE into C ₁₀ SE in aqueous solution (A) and in the micellar environment (B) at three values of λ : 0.0, 0.5, and 1.0.	608
10-12	Computed values of $\partial G/\partial\lambda$ as a function of data gathering time for the transformation of C ₁₀ SO into C ₈ SO in aqueous solution (A) and in the micellar environment (B) at three values of λ : 0.0, 0.5, and 1.0.	609
10-13	Computed values of $\langle\partial G/\partial\lambda\rangle_\lambda$ as a function of λ for the transformation of SDS into IBU in aqueous solution and in the micellar environment.	611
10-14	Computed values of $\langle\partial G/\partial\lambda\rangle_\lambda$ as a function of λ for the transformation of OG into PAB in aqueous solution and in the micellar environment.	612
10-15	Computed values of $\langle\partial G/\partial\lambda\rangle_\lambda$ as a function of λ for the transformation of C ₁₀ PO into C ₁₀ SO in aqueous solution and in the micellar environment.	614
10-16	Computed values of $\langle\partial G/\partial\lambda\rangle_\lambda$ as a function of λ for the transformation of C ₈ SE into C ₁₀ SE in aqueous solution and in the micellar environment.	615
10-17	Computed values of $\langle\partial G/\partial\lambda\rangle_\lambda$ as a function of λ for the transformation of C ₁₀ SO into C ₈ SO in aqueous solution and in the micellar environment.	616
10-A1	Profiles of $\langle\partial G/\partial\lambda\rangle_\lambda$ calculated for hexane in vacuo and in water as a function of the value of the coupling parameter λ	628
10-A2	Schematic representation of the ethane to ethane and the propane to propane self-transformation; below the schematics, profiles of $\langle\partial G/\partial\lambda\rangle_\lambda$ calculated for the ethane to ethane and propane to propane “self-transformations” are shown as a function of the value of the coupling parameter λ	630
10-A3	Schematic representation of the alchemical and non-alchemical free-energy path used to evaluate the difference in the hydration free energies of benzene and hexane.	632

10-A4 Schematic representation of the alchemical and non-alchemical free-energy path used to evaluate the difference in the hydration free energies of benzoate and propionate.	633
11-1 Chemical structures of three poly(fluorooxetane)s and 3M Fluorad FC-129.	643
11-2 Sequence of steps followed to form and equilibrate simulation cells containing monolayers of surfactants 1 -4	649
11-3 Simulation cell x (or equivalently y) dimension [nm] equilibration curves for 1) surfactant 1 , 2) surfactant 2 , 3) surfactant 3 , and 4) surfactant 4	653
11-4 Representative snapshots of surfactant 3 at the water/air interface at (a) low surface concentration and (b) saturation.	658
11-5 Representative snapshot (from below the water surface) of a monolayer of surfactant 2	660
11-6 Number density profile for surfactant 1 at the water/air interface, where S refers to the two sulfur atoms in each surfactant, O-S to each of the four oxygen atoms bonded to each sulfur atom, O-back to each oxygen atom present in the carbon-oxygen surfactant backbone, C-back to the average density of each carbon atom in the carbon-oxygen surfactant backbone, and O-R _f to the average density of each R _f group (as defined in Figure 1) and the oxygen atom connecting the R _f group to the surfactant backbone.	662

11-7	Number density profile for surfactant 2 at the water/air interface, where S refers to the two sulfur atoms in each surfactant, O-S to each of the four oxygen atoms bonded to each sulfur atom, O-back to each oxygen atom present in the carbon-oxygen surfactant backbone, C-back to the average density of each carbon atom in the carbon-oxygen surfactant backbone, and O-R _f to the average density of each R _f group (as defined in Figure 1) and the oxygen atom connecting the R _f group to the surfactant backbone.	661
11-8	Number density profile for surfactant 3 at the water/air interface, where S refers to the two sulfur atoms in each surfactant, O-S to each of the four oxygen atoms bonded to each sulfur atom, O-back to each oxygen atom present in the carbon-oxygen surfactant backbone, C-back to the average density of each carbon atom in the carbon-oxygen surfactant backbone, and O-R _f to the average density of each R _f group (as defined in Figure 1) and the oxygen atom connecting the R _f group to the surfactant backbone.	664
11-9	Number density profile for surfactant 4 at the water/air interface, where CO ₂ refers to the carboxylate group, CH ₂ -CO ₂ to the CH ₂ group attached to the CO ₂ group, N to the nitrogen atom, CH ₃ CH ₂ -N to the ethyl group attached to the nitrogen atom, SO ₂ to the sulfur atom and the two oxygen atoms attached to it, and F(CF ₂) ₈ to the average density of the carbon and fluorine groups comprising the linear fluorocarbon chain.	665
11-10	Scaled density profiles for surfactant 3 at the water/air interface, where simulation data is shown as points, and the curve fits are shown as solid lines.	669
11-11	Scaled density profiles for surfactant 4 at the water/air interface, where simulation data is shown as points, and the curve fits generated by fitting are shown as solid lines.	670

11-12	Average degree of hydration for surfactants 1-4 , as measured by the number of water oxygen atoms within 0.5 nm of selected groups of surfactant atoms, where results are presented for 1) surfactant 1 , 2) surfactant 2 , 3) surfactant 3 , and 4) surfactant 4	673
12-1	The chemical structures of asiatic acid (AA) and madecassic acid (MA).687	
12-2	Starting and ending configuration of the AA (A) and MA (B) simulations.694	
12-3	The number of micellar aggregates identified using the hydrophobic contact criterion).	696
12-4	The average aggregation number of the AA and MA micelles).	698
12-5	The number of monomers identified in the AA and MA simulation cells).700	
12-6	The radial distribution functions $g(r)_{\text{O}^--\text{H}_2\text{O}}$ and $g(r)_{\text{OH}-\text{H}_2\text{O}}$ (see text) for AA and MA.	706
12-7	The radial distribution function $g(r)_{\text{O}^--\text{Na}^+}$ (see text) for AA and MA. 707	
12-8	Degree of hydration for O^- , for OH, and for the carbon ring measured during 75 ns of molecular dynamics simulation.	708
12-9	The total, hydrophobic, and hydrophilic solvent accessible surface area (SASA) measured during 75 ns of molecular dynamics simulation. . .	710
12-10	The thermodynamic cycle used to evaluate the free energy of micelle formation, g_{mic} , associated with AA and MA micelle formation. . . .	716

List of Tables

2.1	Simulated scaled contact ratios (SCR) and standard errors (SE) for SDS based on the assignment of: i) CHelpG atomic charges, and ii) OPLS-AA atomic charges.	113
2.2	Simulated scaled contact ratios (SCR) and standard errors (SE) for CTAB based on the assignment of: i) CHelpG atomic charges, and ii) OPLS-AA atomic charges.	114
2.3	Simulated scaled contact ratios (SCR) and standard errors (SE) for DPC based on the assignment of: i) CHelpG atomic charges, and ii) OPLS-AA atomic charges.	117
2.4	Simulated scaled contact ratios (SCR) and standard errors (SE) for C ₁₂ E ₈ based on the assignment of: i) CHelpG atomic charges, and ii) OPLS-AA atomic charges.	117
2.5	Simulated scaled contact ratios (SCR) and standard errors (SE) for n = 12 and n = 16 (where n is the alkyl chain length of group 8) 3-hydroxy sulfonate (AOS) based on the assignment of: i) CHelpG atomic charges, and ii) OPLS-AA atomic charges. Scaled contact ratios corresponding to the surfactant "head" are shown in bold.	119
2.6	Simulated scaled contact ratios (SCR) and standard errors (SE) for MEGA-10 based on the assignment of: i) CHelpG atomic charges, and ii) OPLS-AA atomic charges.	121

2.7	Molecular-thermodynamic modeling results and experimental data for SDS using the head and tail identifications predicted based on computer simulation, including: (i) the predicted transfer (g_{tr}), interfacial (g_{int}), packing (g_{pack}), steric (g_{st}), and electrostatic (g_{elec}) contributions to the free energy of micellization (g_{mic}), (ii) the theoretical predictions for the CMC and the weight-average micelle the weight-average aggregation number, and (iii) experimental data on the CMC and the weight-average micelle aggregation number.	123
2.8	Molecular-thermodynamic modeling results and experimental data for CTAB using the head and tail identifications predicted based on: i) the CHelpG atomic charges, and ii) the OPLS-AA atomic charges, including: the predicted free energy of micellization (g_{mic}), the predicted transfer free-energy contribution (g_{tr}), the predicted CMC, and the predicted weight-average micelle aggregation number $\langle N \rangle_w$	125
2.9	Molecular-thermodynamic modeling results and experimental data for DPC using the head and tail identifications predicted based on: i) the CHelpG atomic charges, and ii) the OPLS-AA atomic charges, including: the predicted free energy of micellization (g_{mic}), the predicted transfer free-energy contribution (g_{tr}), the predicted CMC, and the predicted weight-average micelle aggregation number $\langle N \rangle_w$	127
2.10	Molecular-thermodynamic modeling results and experimental data for C ₁₂ E ₈ using the head and tail identifications predicted based on: i) the CHelpG atomic charges, and ii) the OPLS-AA atomic charges, including: the predicted free energy of micellization (g_{mic}), the predicted transfer free-energy contribution (g_{tr}), the predicted CMC, and the predicted weight-average micelle aggregation number $\langle N \rangle_w$	128

2.11	Molecular-thermodynamic modeling results and experimental data for $n = 12$ and $n = 16$ 3-hydroxy sulfonates using the head and tail identifications predicted based on: i) the CHelpG atomic charges, and ii) the OPLS-AA atomic charges, including: the predicted free energy of micellization (g_{mic}), the predicted transfer free-energy contribution (g_{tr}), the predicted CMC, and the predicted weight-average micelle aggregation number.	129
2.12	Molecular-thermodynamic modeling results and experimental data for MEGA-10 using the head and tail identifications predicted based on: i) the CHelpG atomic charges, and ii) the OPLS-AA atomic charges, including: the predicted free energy of micellization (g_{mic}), the predicted transfer free-energy contribution (g_{tr}), the predicted CMC, and the predicted weight-average micelle aggregation number.	132
3.1	Experimentally-determined critical micelle concentrations (CMCs) of SDS, DTAB, and $C_{12}E_8$ in water, phosphate buffer at pH 7.4, and ibuprofen-saturated (4 mM) phosphate buffer at pH 7.4.	151
3.2	Simulated scaled contact ratios (SCRs) and standard errors (SEs) for groups of atoms in ibuprofen based on the assignment of: i) CHelpG atomic charges, and ii) OPLS-AA atomic charges.	162
3.3	Input parameters for the molecular-thermodynamic modeling of the surfactants SDS, DTAB, and $C_{12}E_8$	166
4.1	Oil/water interface, cylindrical micelle, and spherical micelle simulation results for ibuprofen.	281
4.2	Oil/water interface, cylindrical micelle, and spherical micelle simulation results for benzamide.	282
4.3	Oil/water interface, cylindrical micelle, and spherical micelle simulation results for acetophenone.	283
4.4	Oil/water interface, cylindrical micelle, and spherical micelle simulation results for benzonitrile.	285

4.5	Oil/water interface, cylindrical micelle, and spherical micelle simulation results for o-aminobenzoate.	285
4.6	Oil/water interface, cylindrical micelle, and spherical micelle simulation results for m-aminobenzoate.	286
4.7	Oil/water interface, cylindrical micelle, and spherical micelle simulation results for p-aminobenzoate.	287
5.1	Geometric parameters for all surfactants and solubilizates.	315
5.2	Molecular properties of the tail fragments of each surfactant and solubilizate.	317
5.3	Molecular-thermodynamic modeling results for solubilization in anionic surfactants.	328
5.4	Molecular-thermodynamic modeling results for solubilization in nonionic surfactants.	328
5.5	Molecular-thermodynamic modeling results for solubilization in cationic surfactants.	328
5.6	Solubilization predictions made using the molecular-thermodynamic model: solubilization in anionic surfactants.	340
5.7	Solubilization predictions made using the molecular-thermodynamic model: solubilization in nonionic surfactants.	340
5.8	Solubilization predictions made using the molecular-thermodynamic model: solubilization in cationic surfactants.	340
6.1	Geometric characteristics of each of the five octane aggregates simulated, including the aggregation number (n), the aggregate volume (V), the aggregate surface area (A), the aggregate core-minor radius (l_c), the periodic length (PL) of each cylinder and slab, and the degree of curvature (C).	385

6.2	Geometric characteristics of each of the five dodecane aggregates simulated, including the aggregation number (n), the aggregate volume (V), the aggregate surface area (A), the aggregate core-minor radius (l_c), the periodic length (PL) of each cylinder and slab, and the degree of curvature (C).	387
6.3	Geometric characteristics of each of the five hexadecane aggregates simulated, including the aggregation number (n), the aggregate volume (V), the aggregate surface area (A), the aggregate core-minor radius (l_c), the periodic length (PL) of each cylinder and slab, and the degree of curvature (C).	388
6.4	Computer simulation/molecular-thermodynamic (CS-MT) and traditional molecular-thermodynamic (MT) modeling results for g_{dehydr} , g_{hydr} , and g_{form} corresponding to each of the five octane, dodecane, and hexadecane aggregate geometries simulated and modeled in this chapter.	407
6.5	Predicted values of $g_{\text{tr,CS-MT}}$ for octane, dodecane, and hexadecane.	414
6.6	Predicted values of g_{form} , $g_{\text{form, max}}$, and $g_{\text{form, min}}$ for the five simulated geometries of dodecane obtained using the CS-MT model.	415
7.1	The number of surfactant and water molecules and the total number of atoms corresponding to each of the seven nonionic surfactant micelles simulated in Chapter 7.	440
7.2	Simulation results for the number of hydrating contacts (N_{cont}), the change in the number of hydrating contacts relative to the corresponding oil aggregate ($\Delta N_{\text{cont}} - \Delta N_{\text{cont,oil agg}}$), and the “Shielded Area” corresponding to the area at the micelle core/water interface that is shielded from hydrating contacts by the surfactant heads for octane, octyl glucoside (OG), octyl sulfinyl ethanol (OSE), dodecane, dodecyl maltoside (DM), and dodecyl octa(ethylene oxide) ($C_{12}E_8$) in the aggregate environment.	466

7.3	Computer simulation/molecular-thermodynamic (CS-MT) and traditional molecular-thermodynamic (MT) modeling results for each of the seven simulated nonionic surfactant micelles considered in this article, where CS-MT model predictions are reported for g_{dehydr} , g_{hydr} , \hat{g}_{int} , and $g_{\text{tr,CS-MT}}$ and traditional MT modeling results for g_{tr} are presented for comparison with $g_{\text{tr,CS-MT}}$	472
7.4	Computer simulation/molecular-thermodynamic (CS-MT) and traditional molecular-thermodynamic (MT) modeling results for each of the seven nonionic surfactants considered in this article.	473
7.5	Comparison of the CS-MT and traditional MT model predictions for g_{form} and the CMC obtained using the values of $g_{\text{tr,CS-MT}}$ and g_{tr} reported in Table 3, respectively.	474
8.1	The geometry, the number of surfactant and water molecules, and the total number of atoms corresponding to each of the ionic and zwitterionic micelle simulations discussed in Chapter 8.	507
8.2	The traditional MT model identifications of heads and tails and molecular parameters used to model each surfactant using the CS-MT model and the traditional MT model (a_{h} , the cross-sectional area of the surfactant head, d_{charge} , the distance between the beginning of the surfactant tail and the location of the charge in the surfactant head, and l_{hg} , the length of the surfactant head).	523
8.3	Computer simulation/molecular-thermodynamic (CS-MT) and traditional molecular-thermodynamic (MT) modeling results for each of the nine simulated ionic and zwitterionic surfactant micelles considered in this article, where CS-MT model predictions are reported for g_{dehydr} , g_{hydr} , \hat{g}_{int} , and $g_{\text{tr,CS-MT}}$ and traditional MT modeling results for g_{tr} are presented for comparison with $g_{\text{tr,CS-MT}}$	525

8.4	Computer simulation/molecular-thermodynamic (CS-MT) and traditional molecular-thermodynamic (MT) modeling results for each of the nine ionic and zwitterionic surfactants considered in this article. . . .	525
8.5	Modeling results for the optimal micelles, where the CS-MT and the traditional MT model predictions of g_{form} were obtained using the values of $g_{\text{tr,CS-MT}}$ and g_{tr} reported in Table 4, respectively.	526
10.1	The number of surfactant and water molecules, and the total number of atoms corresponding to the starting point for each alchemical simulation in the micellar environment.	589
10.2	Transformation free energies computed using the CS-FE/MT model.	595
10.3	Transformation free energies computed using the CS-FE/MT model with additional windows.	618
11.1	Values of the interfacial area per surfactant molecule at saturation reported by Kausch et al. based on fitting experimental surface tension data to the Davies and Gibbs adsorption isotherms.	642
11.2	Computer simulation estimates of the interfacial area per surfactant molecule at saturation for surfactants 1-4	654
11.3	Effect of applied surface tension on the interfacial area per surfactant molecule for surfactants 1-4	657
11.4	Estimates of the amplitude of fluctuations for surfactants 1-4 at the water/air interface expected based on $1 k_B T$ of energy.	659
11.5	The width (w_{air}) and location (z_{air}^o) of the air interface in nanometers, the width (w_{water}) and location (z_{water}^o) of the water interface in nanometers, the width of the Gaussian distribution of surfactant density and the location (z_{surf}^o) of the peak of the Gaussian distribution in nanometers, the separation distance between the location of the air and water interfaces, $ \Delta z $, and values of the penetration parameter for each surfactant.	671

11.6	Order parameters with respect to the x , y , and z -axis for the side chains of surfactants 1-3 and the fluorocarbon chain of surfactant 4 .	675
12.1	Principal moments of the gyration tensor ($\lambda_x, \lambda_y, \lambda_z$) and the radius of gyration (R_g) computed for AA and MA micelles.	702
12.2	Micellar (P_{mic}) and nearest neighbor ($P_{\text{n.n.}}$) order parameters computed for AA and MA micelles.	704

PART I

APPLICATION OF COMPUTER SIMULATIONS TO OBTAIN MOLECULAR-THERMODYNAMIC INPUTS

Chapter 1

Introduction

1.1 Motivation

Surfactants are used in many pharmaceutical, industrial, and environmental applications because of their unique solution properties. When dissolved in water, at concentrations that exceed the critical micelle concentration (CMC), surfactant molecules self-assemble into micellar aggregates, with their hydrophobic portions shielded from water in the aggregate interior, and their hydrophilic portions exposed to water at the aggregate surface. This self-assembly is driven primarily by the hydrophobic effect, although van der Waals, hydrogen-bonding, and screened electrostatic interactions (in the case of charged surfactants) also play an important role in determining how micellization occurs [1].

The solubility of hydrophobic or partly hydrophobic substances in aqueous solution can be increased through the addition of surfactants to the solution at concentrations that exceed the CMC and solubilization of the hydrophobic substances within the micelle interior [2–5]. In general, solubilization can be thought of as occurring in three general ways: (i) formation of a pure droplet of solubilize in the micelle core, (ii) solubilization within the surfactant tails, or (iii) solubilization in the head-shell region. Solubilization may lead to changes in micelle shape and size and can therefore influence the bulk solution properties of micellar solutions. For example, the

solubilization of aromatic hydrocarbons can result in a micelle shape transition from spherical to rodlike. Such a shape transition serves to increase the bulk viscosity of the surfactant solution [3].

A wide variety of industrial, pharmaceutical, and biological processes make use of surfactants [2,3]. The ability of surfactants to aid in the mixing of hydrophobic and hydrophilic molecules is used extensively in the chemical industry in applications such as the removal of oily materials from a substrate, reaction rate enhancement in polymerization reactions, and separation processes [2,3,6]. Surfactants also have potential application in the pharmaceutical industry to solubilize water-insoluble drugs in aqueous solutions for subsequent injection into a patient's body [7]. Examples of biological processes involving surfactants include the role of phospholipid biosurfactants in the gastrointestinal tract during digestion, and the body's use of bile salts to solubilize cholesterol [2].

Because micellar solubilization is such a broadly applicable phenomenon, gaining a fundamental understanding of the factors that affect micellar solubilization is of great academic as well as practical interest. Frequently, a specific set of micellar solution and solubility characteristics are desired for a given application. These characteristics include the CMC and the shape and size of the micellar aggregates that form in solution. Other characteristics include the extent of solubilization, which can be quantified in a number of ways, and the location of the solubilize within the micelle, referred to as the locus of solubilization.

The development of theoretical modeling approaches that both (i) provide fundamental, molecular-level understanding of micellization phenomena, and (ii) enable prediction of bulk solution (CMC, extent of solubilization) and microstructural (locus of solubilization, micelle shape and size) properties would significantly reduce the effort and cost associated with surfactant solution formulation. For example, in detergency applications, it is important to maximize the amount of material solubilized. For this application, theoretical prediction of the extent of solubilization for various classes of surfactants is directly relevant. For drug delivery, a wide range of criteria

must be met, including: (i) low toxicity, (ii) sufficient residence time in the body, (iii) high solubilization capacity, and (iv) the ability to deliver the drug to the desired site in the body. To develop a surfactant solution capable of meeting each of these criteria, it is important to know the extent of solubilization, the micelle shape and size, and the locus of solubilization. In many cases, theoretical predictions of bulk micellar solution properties such as the CMC and the extent of solubilization, and the theoretical prediction of micelle microstructure can be correlated with other bulk solution properties of practical relevance. For example, researchers have reported correlations between the geometry and size of micelles with solution viscosity, and between the monomer and micelle concentrations with the potential of a surfactant to induce skin irritation [8].

With the above motivation in mind, this thesis explores the application of three approaches to model surfactant micellization and micellar solubilization. The first approach involves the use of computer simulations (CS) to obtain input parameters for molecular-thermodynamic (MT) modeling of surfactant micellization and micellar solubilization. Development of a hybrid computer simulation/molecular-thermodynamic modeling approach is motivated by the limitations inherent in computer simulations (namely, the high computational expense of modeling self-assembly) and MT modeling approaches (their restriction to structurally and chemically simple surfactants and solubilizates). A key input required for traditional MT modeling is the identification of the hydrated and the unhydrated portions (head and tail) of surfactants and solubilizates in a self-assembled micellar aggregate. Prior to this thesis, no approach was developed to determine this information for structurally complex surfactants and solubilizates. By conducting simulations of surfactants and solubilizates at a water/oil interface (modeling the water/micelle core interface) or in a micellar environment, we have determined hydration information for both simple and complex surfactants and solubilizates. This information has been successfully used as an input to MT modeling, and has been shown to extend the applicability of the traditional MT modeling approach to more complex surfactant and solubilizate

systems than had been possible to date. In total, 46 surfactant and solubilizate systems have been modeled with this approach, including systems of anionic, cationic, zwitterionic, and nonionic surfactants. For each of the systems modeled, theoretical predictions have been compared with experimental data available in the literature and with experimental data gathered by our research collaborators in São Paulo, Brazil. A novel, alternative approach has also been developed to more accurately quantify the hydrophobic driving force for micelle formation. This new approach is referred to as the computer simulation/molecular-thermodynamic (CS-MT) model. In the CS-MT modeling approach, atomistic molecular dynamics (MD) simulations are used to quantify the hydration changes that take place during self-assembly. This hydration information is then used in a new MT model to quantify the hydrophobic effect, which is decomposed into two components: (1) the free-energy change associated with the dehydration of solute hydrophobic groups that accompanies aggregate self-assembly (as captured in g_{dehydr}), and (2) the change in hydration free energy experienced by these same hydrophobic groups during aggregate self-assembly (as captured in g_{hydr}). The CS-MT model is formulated to allow the prediction of the free-energy change associated with aggregate formation of solute aggregates of any shape and size by performing only two computer simulations — one of the solute in bulk water and the second of the solute in an aggregate of arbitrary shape and size. The CS-MT modeling approach has been validated by using it to model the formation of 15 different oil aggregates of various shapes and sizes in aqueous solution, the micellization behavior of seven different simple and complex nonionic surfactants in aqueous solution, and the micellization behavior of nine different ionic and zwitterionic surfactants in aqueous solution. For each of the systems modeled, the CS-MT model predictions were in reasonable agreement with the experimental data, and in most cases, were in better agreement with the experimental data than the predictions of the traditional MT model.

The second approach explored in this thesis involves the use of computer simulation free-energy methods in the context of micellization and micellar solubilization.

This effort was motivated by the desire to understand how successfully alchemical free-energy methods can be used to compute the free-energy change associated with changing micellar composition — whether by adding a solubilize or a different type of surfactant to the micelle. In this approach, traditional MT modeling, or experimental data, is first used to determine the free energy of formation of a pure (single) surfactant micelle and the pure surfactant micelle aggregation number. Subsequently, computer simulations are used to determine the free-energy change associated with alchemically changing the identity of individual surfactants present in the micelle into a different type of surfactant or into a solubilize. This free-energy difference, when added to the free energy of micellization already determined, yields the free energy of formation (g_{form}) associated with the mixed micellar aggregate. In principle, the free energy of formation can then be used in the context of a thermodynamic description of the micellar solution to estimate bulk solution properties such as the CMC and the equilibrium composition of the mixed micelle. This modeling approach has been used to model both binary surfactant micellization and micellar solubilization, and the results have been compared with the predictions of the traditional MT model and with experimental data.

The third approach explored in this thesis involves using all-atomistic computer simulations to directly predict surfactant solution properties. Although the computational expense of atomistic-level MD simulations limits their use to the evaluation of a limited subset of surfactant solution properties, these simulations can provide a great deal of insight into the structural characteristics of preformed surfactant aggregates and into the self-assembly behavior of a limited number of surfactant molecules over limited timescales. Simulation of monolayers of a homologous series of structurally complex fluorosurfactants has been conducted in order to explore their behavior at a water/air interface and the origin of their ability to reduce surface tension. In addition, atomistic-level MD simulations have been conducted to study the self-assembly behavior of the triterpenoids asiatic acid (AA) and madecassic acid (MA) in aqueous solution. The computer simulation results were used to obtain information about:

i) the dynamics of aggregate formation, ii) the rates of monomer association and dissociation into aggregates, iii) aggregate microstructure, iv) the local environment of different surfactant groups within the aggregate, v) surfactant monomer concentrations, and vi) the average aggregation numbers of the self-assembled aggregates.

The remainder of this chapter is organized as follows. In Section 1.2, general background information on surfactants and their micellar solution behavior is presented. This section also includes a discussion of micellar solubilization, including a description of the main experimental observations. Section 1.3 presents an overview of theoretical models that have been used to model micellization and micellar solubilization. Section 1.4 presents a brief introduction to computer simulation modeling approaches that can be used to study micellization and micellar solubilization. This is followed in Section 1.5 by a review of previous computer simulation studies of micellization and micellar solubilization. In Section 1.7, the specific objectives of this thesis are stated. Finally, in Section 1.8, an overview of the thesis material is presented along with a discussion of the organization of the remainder of the thesis.

1.2 Introduction to Surfactant Micellization and Micellar Solubilization

Surfactants, or surface-active agents, are dual-natured molecules that contain both hydrophilic and hydrophobic moieties. The hydrophilic moiety of the surfactant molecule (conventionally referred to as the “head”) may be anionic, cationic, zwitterionic, or nonionic. The hydrophobic moiety (referred to as the “tail”) is frequently composed of either linear or branched hydrocarbons or fluorocarbons. Benzene rings may also be present in the surfactant tail. The dual “water-loving” and “water-fearing” nature of surfactants can result in highly complex solution behavior when placed in either aqueous or non-polar solvents, including self-assembly into micelles [9]. When poorly-water soluble compounds (solubilizates) are also present in aqueous solution, they partition into surfactant micelles because the hydrophobic nature of the micelle

interior provides a more favorable environment than the aqueous solution.

1.2.1 Surfactant Micellization

Self-assembly of surfactants into a significant number of micellar aggregates begins to occur when the surfactant concentration exceeds a value known as the critical micelle concentration (CMC). Once micelles begin to form, the concentration of free surfactant monomers in aqueous solution becomes independent, or only weakly dependent, on the total concentration of added surfactant [1]. The CMC depends on the chemical structure of the surfactant and the solution conditions, including the temperature, the pressure, and (particularly in the case of ionic surfactants) the ionic strength. Micelles may form in a number of different geometries. Spherical, or globular, micelles typically are observed when total surfactant concentrations are low and/or repulsions among the surfactant heads are strong. At higher surfactant concentrations, one-dimensional growth into cylindrical micelles, or two-dimensional growth into planar disklike micelles, may occur. For ionic surfactants, the addition of counterions, reducing the extent of electrostatic repulsions between the surfactant heads, can result in a sphere-to-cylinder or a sphere-to-disk shape transition [1]. Reduction of electrostatic repulsions between the surfactant heads occurs through counterion binding (i.e. counterions that intercalate among the surfactant heads in the micelle), as well as through association of non-bound counterions within the diffuse region beyond the micelle Stern layer [10, 11].

1.2.2 Micellar Solubilization

In the context of the research undertaken in this thesis, micellar solubilization is defined as the spontaneous dissolution of a material by reversible interaction with micelles to form a thermodynamically stable isotropic solution which exhibits reduced thermodynamic activity of the solubilized material [9]. For the purposes of this thesis, a solubilize may be considered to be a molecule which has a solubility

limit in aqueous solution. A solubilizate may be completely hydrophobic, or may contain some hydrophilic and hydrophobic moieties as part of its chemical structure. Solubilizates which contain both hydrophilic and hydrophobic moieties may be viewed as being similar to surfactants in that they are dual-natured and can be thought of as possessing a head and a tail. However, unlike surfactants, solubilizates do not spontaneously self-assemble into micelles in aqueous solution, and therefore do not have a CMC. However, solubilizates with both hydrophilic and hydrophobic groups may behave much like conventional surfactants within a mixed micelle.

Two key characteristics associated with how micellar solubilization occurs are the extent of solubilization and the locus of solubilization, both of which are discussed below.

Extent of Solubilization

Experimental determinations of the extent of solubilization can be carried out through several methods, including measuring changes in the surfactant CMC, measuring vapor pressures, calorimetry, head-space gas chromatography, semiequilibrium dialysis, fluorescence, and UV/Vis spectrophotometry. Often, the experimental observations allow determination of information about either the infinite dilution limit of the solubilizate (the Henry's law limit) or the saturation limit of the solubilizate in the aqueous micellar solution [3, 4, 12–14].

The extent of solubilization is traditionally quantified by several parameters [2, 3], which include:

1. The Partition Coefficient (K): This parameter is used in the context of the pseudophase separation model of micellization, which considers the micelles to be a separate, infinite phase [15]. K is defined as the ratio of the solubilizate solubility in the aggregate (X_m) to its solubility in the aqueous phase (X_w), that is, $K = X_m/X_w$. Both X_m and X_w are usually expressed as mole fractions, but the use of molarity units is also encountered. The free energy of solubilization (ΔG) can then be defined as $\Delta G = -RT \ln(K)$ [4].

Solubilization isotherms, or the observed extent of solubilization as a function of solubilize concentration at a fixed temperature, have been measured for a variety of surfactant/solubilize systems [3, 14, 16]. Most of these studies report solubilization results in the infinite-dilution limit. The experimental data indicate that K is frequently a function of the solubilize concentration within the micelle. The following empirical expression has been found to apply to many surfactant/solubilize systems [3, 12, 14]:

$$K = K_o(1 - BX_m)^2 \quad (1.1)$$

where K_o is the partition coefficient in the limit of zero solubilize concentration, and the parameter B corresponds to the initial slope of the solubilization isotherm, and is a function of the type of surfactant and solubilize present. Because non-infinite dilution conditions cannot be considered ideal, the observed dependence of K on concentration (X_m) is not surprising.

2. The Saturation Concentration: The concentration at which no more solubilize will solubilize within the micelle while remaining in a single, isotropic solution is defined as the Maximum Additive Concentration (MAC). Saturation can be estimated by detecting an increase in the turbidity of the solution. However, because the measured turbidity also increases when phase separation occurs, and upon the formation of stable microemulsions, the appearance of a pure solute phase constitutes a more rigorous method to identify the MAC [2, 3].

3. The Molar Solubilization Ratio (MSR): The MSR is defined as the ratio of the total number of solubilize molecules associated with the micelle to the total number of surfactant molecules associated with the micelle (which is equal to $X_m/(1-X_m)$) [5]. In practice, the MSR can be calculated as follows:

$$MSR = \frac{C_{sol} - C_{sat}}{C_{sur} - CMC} \quad (1.2)$$

where C_{sol} is the solubilize concentration in the solution, C_{sat} is the solubilize aqueous solubility, C_{sur} is the surfactant concentration in solution, and the CMC is

the critical micelle concentration.

The extent of solubilization depends on the surfactant structure [2, 17–45], on the solubilize structure [2, 4, 5, 13, 17, 18, 35, 46–49], and on the solution conditions [14, 17, 18, 21, 48, 50, 51]. Many experimental studies have been conducted to measure the extent of solubilization of various surfactant/solubilize systems at different solution conditions. In addition, a variety of theoretical models (see Section 1.3.2) have been formulated to predict the extent of solubilization.

Locus of Solubilization

The locus of solubilization plays an important role in determining the extent of solubilization, the rate of micellar reactions where the solubilize acts as a reactant or as a catalyst, and the rate at which solubilize diffusion out of the micelle occurs [52]. The locus of solubilization also affects the way in which the solubilize may influence solution properties such as the CMC and the micelle shape and size.

The location of the solubilize within micelles can be determined by direct experimental measurement (using techniques such as IR spectroscopy or fluorescence), or it can be inferred indirectly using thermodynamic data such as partition coefficients [3–5, 13, 53, 54]. Experimental studies have indicated that there are three distinct regions within a micelle where solubilization may occur: (i) the core region, or deep interior of the micelle, (ii) the palisade layer, which refers to the region consisting of the surfactant tails, and (iii) the corona region, which refers to the region comprising the polymeric surfactant heads in the case of polymer-like surfactants such as the alkyl ethoxylates (C_iE_js). These three solubilization regions are depicted in Figure 1-1 [2, 3, 55], where the smaller circles represent solubilize molecules and the larger circles or the thick grey lines represent surfactant heads. Solubilization may, of course, take place simultaneously in more than one region.

Below, I discuss solubilization in each region separately:

1. Core Region: Here, solubilization takes place within the deep interior of the aggregate, and may even result in the formation of a separate phase within the aggregate

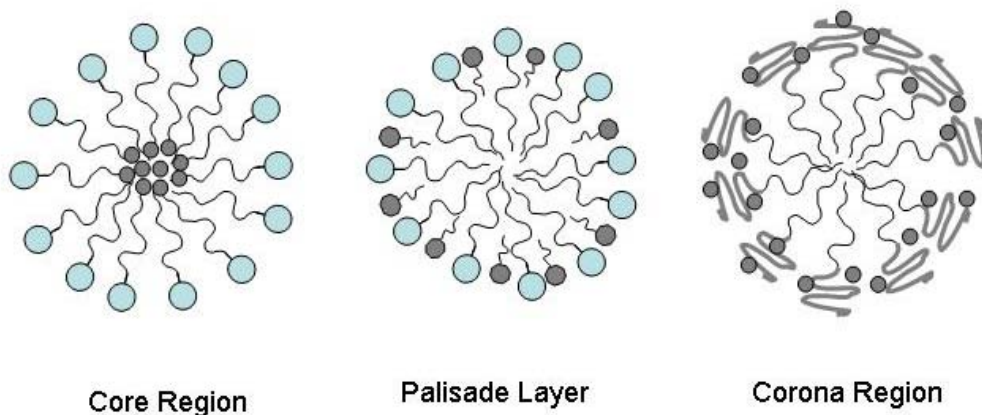


Figure 1-1: Regions of solubilization in a surfactant micelle.

core. This has been shown to occur in the case of aliphatic hydrocarbons. However, theoretical predictions by Srinivasan and Blankschtein [56] for the SDS/hexane system indicate that there is not necessarily a sharp transition between the hydrophobic core phase and the rest of the aggregate. The number of solubilize molecules that are dispersed among the surfactant tails instead of being located in a separate phase in the aggregate core is strongly dependent on l_c , the aggregate core-minor radius [56]. Spherical surfactant/solubilize aggregates possessing such a solubilize-rich core are also referred to as oil-in-water (o/w) droplet microemulsions [1]. In some systems, such as SDS/alcohol, it has been shown that, at low alcohol concentrations, alcohol solubilization in the core region does occur, but that at higher alcohol concentrations, the additional alcohol molecules are located in the Palisade Layer [57].

2. Palisade Layer: This layer refers to the region composed of the surfactant tails within the dry hydrophobic micelle core, and extends further to include the surfactant heads (unless the surfactant heads are polymeric, in which case the surfactant-head region is referred to as the corona region). Solubilizates that are located within this region do not form a separate phase in the micelle core. Depending on the nature and the concentration of the solubilize, the solubilize molecules may be located

closer to, or farther away from, the micelle core/water interface [18,46]. Partly hydrophilic solubilizates may, much like surfactants, localize at the micelle core/water interface with their hydrophilic moieties exposed to water and their hydrophobic moieties shielded from water within the micelle core, as shown in Figure 1-1. Solubilizates that exhibit this behavior include salicylates, alcohols, and amines [57,58]. Semipolar compounds such as benzene can exhibit interesting locus of solubilization behavior, where the locus of solubilization may be influenced by the solubilizate concentration and by the type of surfactants present in the micelle [4,18,47]. Experimental evidence suggests that, in cationic surfactant micelles, benzene is solubilized near the micelle interfacial region because of attractions between the p-electrons in benzene and the positively charged surfactant heads. However, in anionic surfactant micelles, benzene is solubilized deeper within the micelle core [18].

3. Corona Region: Here, solubilization takes place among the heads of surfactants containing polymeric headgroups, such as those having a number of poly(ethylene oxide) groups. Solubilization in this region may be preferred by semipolar solubilizates such as chloroxylenol or benzene [19].

Influence of Solubilization on Micelle Characteristics

Micelle characteristics such as CMCs, shapes, and aggregation numbers may all be affected by solubilization. The addition of solubilizate decreases the CMC relative to that of the surfactant in the absence of solubilizate. Theoretical descriptions of the CMC as a function of the solubilizate partition coefficient have been advanced [56,59].

The effect of the solubilizate on micelle shape and aggregation number depends upon the locus of solubilization. In the case of ionic surfactants, charged solubilizates that solubilize within the micelle head-shell region can act essentially as counterions and facilitate a decrease in the electrostatic repulsions between the charged surfactant heads. This promotes the formation of cylindrical or discoidal aggregates [58,60–65]. This micelle shape transition has been predicted using the molecular-thermodynamic theory of solubilization developed by the Blankschtein group, as well as observed ex-

perimentally for the SDS/alcohol/NaCl system [56]. Solubilization in the micelle core region, on the other hand, increases the micelle core radius, and favors a shape transition from rodlike to spherical or globular micelles [60,62]. Solubilization in the micelle interfacial region of the palisade layer favors the elongation of cylindrical micelles, or a shape transition to a disklike micelle. For some aliphatic compounds possessing short chain lengths, it has been shown that as the chain length decreases, radial growth is favored progressively over axial growth [61,66]. For semipolar compounds such as aromatics, the locus of solubilization, and hence, the effect of solubilization on micelle shape, may be a function of solubilize concentration [60,61,66,67].

1.3 Theoretical Models of Micellization and Micellar Solubilization

In this section, an overview of the theoretical approaches that have been introduced to study micellization and micellar solubilization is presented. Emphasis is given to molecular-thermodynamic models because these represent the most successful and predictive models of micellization and micellar solubilization that have been developed to date.

1.3.1 Molecular-Thermodynamic Models of Micellization

A significant number of researchers have conducted important theoretical work to model micellization in aqueous solution and enable the *a priori* prediction of bulk solution properties such as the CMC and the structure of micellar aggregates from knowledge of the chemical structures of the surfactants present in solution and the solution conditions [8,19,68–71]. Groundbreaking work by Tanford resulted in the development of a phenomenological theory providing significant insight into the physical processes underlying micelle formation [72]. Next, Israelachvili developed a geometric packing theory to model micellization, providing an approach to make predictions of

micelle shape and aggregation number based on the surfactant geometry [1]. These models were followed by the development of molecular-thermodynamic modeling approaches, that have been used by a number of researchers, including Nagarajan and Ruckenstein [4, 5, 19, 47, 53, 73–85].

Currently, the most accurate theoretical models of surfactant micellization make use of a predictive molecular-thermodynamic approach [10]. In the molecular-thermodynamic approach, the free energy of micellization is calculated as the sum of several free-energy contributions, all of which can be computed molecularly given the chemical structures of the surfactants present in the solution and the solution conditions. The free energy of micellization is defined as the free-energy change per surfactant molecule associated with transferring the surfactant monomers and the counterions (in the case of ionic surfactants) from the bulk aqueous solution to the aggregate. The micellization description introduced by Nagarajan and Ruckenstein permits prediction of the CMC and of the shape and size of micellar aggregates composed of nonionic, zwitterionic, and ionic surfactants [19]. In recent years, the Blankschtein group has made important progress in the molecular modeling of surfactant solution behavior, both in the bulk solution [8, 10, 11, 86–90] and at interfaces [91–95].

1.3.2 Molecular-Thermodynamic Models of Solubilization

Molecular-thermodynamic models of solubilization combine thermodynamic descriptions of self-assembly with a molecular approach to estimate the free energy of solubilization, or the free-energy change per surfactant molecule associated with transferring the surfactant monomers, the counterions (in the case of ionic surfactants), and the solubilizates from the bulk aqueous solution to the micelle. Important contributions to the development of molecular-thermodynamic descriptions of solubilization have been made by Landgren and coworkers [96–98], by Nagarajan and coworkers [4, 5, 19, 47, 53, 77, 78, 80, 81, 85], and very recently, by Srinivasan and Blankschtein [56]. Below, I briefly review these contributions.

Landgren and coworkers developed a Poisson-Boltzmann Cell Model (PBCM) to

model solubilization in isotropic solutions and in liquid crystalline phases [96–98]. Their model includes inter-aggregate interactions, which makes it suitable for use at high surfactant concentrations. These authors developed two models to describe isotropic solutions, each applicable to different types of solubilizates. In the first model, all molecules (including the solubilizates) are considered to be anchored at the micelle surface. In the second model, solubilization is considered to take place either in a pure solubilizate domain in the aggregate center, or within the palisade layer. The maximum amount of solubilizate that can be solubilized is not considered in either model. In addition, because both models apply only to spherical aggregates, they do not describe the effect of the solubilized solute on the aggregate shape. Furthermore, the chain conformations inside the aggregate and their contribution to the free energy of aggregate formation are assumed to be a function of the interfacial area per surfactant molecule in the aggregate. An empirical Taylor series expansion of this free-energy dependence is then used to describe the free-energy contribution associated with the chain conformations.

Nagarajan and coworkers developed a solubilization model that allows the prediction of the locus and the extent of solubilization, as well as of the effect of solubilization on micelle shape and size [4, 5, 19, 47, 53, 77, 78, 80, 81, 85]. Their model takes as input the surfactant and the solubilizate molecular structures. The effects of molecular size, aromaticity, interfacial activity, and enthalpic interactions between the solubilizate and the surfactant tails (as described by Flory-Huggins interaction parameters) are accounted for. However, in modeling solubilization in the core region, the authors assume a uniform solution of surfactant tails and solubilizates in the micelle core, and utilize polymeric theories to estimate the packing free energy that are not strictly applicable in the case of surfactants possessing short tails. These authors also developed two limiting models to describe the head-head interactions of surfactants possessing large (>10 monomers) poly(ethylene oxide) heads. Micelles composed of surfactants with large poly(ethylene oxide) heads form spherical or cylindrical micelles, because the steric interactions between the heads are too large for a planar

(discoidal) micelle geometry to be favored. The first model considers the head-shell region to have a uniform polymer segment concentration, and a nonuniform deformation along the radial coordinate characterizing the micelle geometry. The second model treats the polymer chains as being uniformly deformed, while having a radial concentration variation of the polymer segments in the head-shell region. However, these authors did not consider solubilization in the corona region of micelles formed by surfactants with poly(ethylene oxide) polymeric heads [19].

The methods used by Landgren and coworkers and by Nagarajan and coworkers to calculate the packing free energy associated with the micelle core are only applicable in the case of surfactants having linear hydrocarbon tails, and for solubilizates having relatively simple chemical structures. In an effort to overcome some of these limitations, Srinivasan and Blankschtein recently calculated more rigorously the packing free energy associated with the micelle core for a variety of surfactant tail structures and solubilizates [56]. These authors generalized a mean-field approach, introduced originally by Ben-Shaul, Szleifer, and Gelbart, to compute the packing free energy of surfactants having linear alkane tails, branched alkane tails, and alkylbenzene tails, and of solutes, such as salicylate, alcohols, and aromatics [99]. In their packing calculations, only repulsive interactions were considered, although attractive interactions could also have been included through the use of pairwise interaction energies or Flory-Huggins χ parameters. These interactions are likely to be important for polarizable surfactant tails and solubilizates. Srinivasan and Blankschtein also developed a computational framework to model counterion binding onto the aggregate head-shell region of ionic surfactant micelles [10, 11]. The existence of counterion binding has long been believed to play an important role in controlling the aggregate shape, size, and ability to solubilize solutes [1, 100]. The theoretical methodology developed by Srinivasan and Blankschtein is capable of predicting the locus and the extent of solubilization, CMCs, and micelle shapes and sizes for relatively simple solubilizates and ionic surfactants in the presence of counterion binding. Their methodology uses the concept of effective “head” and “tail” regions for the solubilizates as well as for any

lipophilic counterions, which is most applicable in the case of relatively simple structures where it is clear *a priori* how the solubilizate is located and oriented relative to the micelle core/water interface [56].

1.3.3 Limitations of Previous Molecular-Thermodynamic Modeling Approaches

Although significant progress has been made, molecular-thermodynamic approaches to model surfactant micellization and micellar solubilization have been successfully applied only to relatively simple surfactants and solubilizates. The most severe limitation associated with molecular-thermodynamic modeling is that to apply it, the hydrated and the unhydrated portions of surfactants and solubilizates within a micelle must be known *a priori*. This information is used to assign a head and a tail to each of the species present, and is one of the most important inputs required to evaluate the free-energy change associated with micelle formation.

Based on experimental evidence, it is possible to make educated guesses about which portions of a surfactant or a solubilizate will be hydrated for simple chemical structures, such as surfactants with linear or branched hydrocarbon tails attached to a single anionic, cationic, zwitterionic, or nonionic head [10, 11, 15, 19]. For ionic and zwitterionic surfactants of this type, the approximation is made that every carbon except the first carbon attached to the hydrophilic moieties in the surfactant is included as part of the surfactant tail. For nonionic surfactants of this type, every carbon attached to the hydrophilic moieties is included as part of the tail. However, for more complicated chemical structures it is much more difficult to make reasonable head and tail assignments. Examples of such challenging surfactants are shown in Figure 1-2.

In the case of the surfactant alkyl 3-hydroxy sulfonate (AOS), the presence of the two hydrophobic CH₂ groups between the two hydrophilic groups (SO₃⁻ and OH) makes the head and the tail identification challenging. In the case of the surfactant

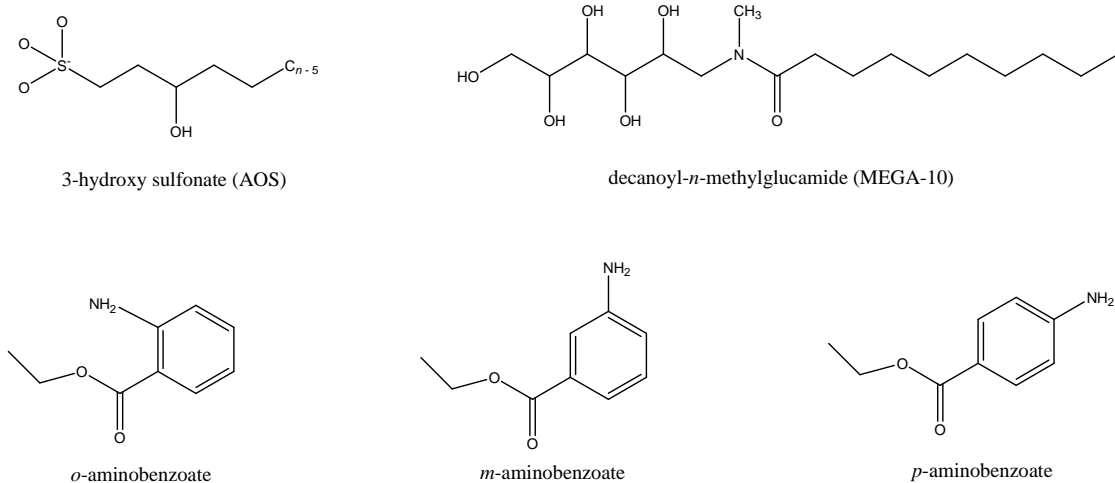


Figure 1-2: Examples of challenging surfactants to model using molecular-thermodynamic theory.

decanoyl-*n*-methylglucamide (MEGA-10), it is difficult to determine the micellar hydration state of each of the three groups bonded to the nitrogen atom (CH_3 , CH_2 , and the carbonyl group). In the case of *o*-, *m*-, and *p*-aminobenzoate, it is unclear what the effect of changing the location of the NH_2 group within the molecule will have on head and tail identification. In addition, it is unclear whether the ethyl ester group attached to the benzene ring should be modeled as being part of the solubilize head or tail.

A key need, therefore, to extend molecular-thermodynamic modeling to more chemically and structurally complex surfactants and solubilizes is the *a priori* knowledge of the hydration states of molecules in the post self-assembly, micellar state. For even slightly complex surfactants and solubilizes such as those shown in Figure 1-2, no simple rule of thumb can be used to make such an identification. The prediction of such information is beyond the ability of simple group-contribution methods, because the hydration state (and therefore the head and tail identification) for various moieties within a complex surfactant or solubilize is intimately related to the way in which the moieties are connected. Although it may be possible in the

future to develop a group-contribution approach that takes molecular connectivity information into account, the approach must be parameterized based on a training set of detailed hydration data for relatively complex surfactants and solubilizates. At the present time, such data is not available. However, computer simulations represent a promising approach to gather such data on a surfactant-by-surfactant or solubilizate-by-solubilizate basis.

1.4 Introduction to Computer Simulation Methods

The objective of computer simulation methods of molecular systems is to estimate time averages or ensemble averages in order to estimate properties of the system. Two of the most popular computer simulation methods used today are molecular dynamics (MD) and Monte Carlo (MC) simulations. Both methods can be used to determine equilibrium properties, but only MD can also be used to determine dynamic properties. Computer simulations allow researchers to explore complex, many-body systems for which analytical, closed-form solutions do not exist.

Frequently, properties of interest depend on the positions and momenta of all the particles present in a system. Given this dependence, the instantaneous value of the property of interest A can be expressed as $A(p^N(t), r^N(t))$, where $p^N(t)$ represents the momenta of the N particles at time t , and $r^N(t)$ represents the positions of the N particles at time t . The instantaneous value of the property A may fluctuate with time, and it is frequently useful to determine the time average value of the property through integration [101]:

$$\langle A \rangle_{t \in [0, \tau]} = \lim_{\tau \rightarrow \infty} \frac{1}{\tau} \int_{t=0}^{\tau} A(p^N(t), r^N(t)) dt \quad (1.3)$$

In molecular dynamics simulation, the time evolution of a system is determined by

solving Newton’s equations of motion. To this end, a potential energy model (referred to as a force field) must be used to describe the intermolecular and intramolecular interactions of each of the system components. The forces acting on each particle in the system are determined through differentiation of the potential energy model. Once the force acting on each atom is known, movement of the atoms in response to these forces is computed numerically by incrementing forward in time with small timesteps and using an integration technique such as the velocity Verlet or the leap-frog algorithm [102]. For unconstrained chemical systems, very small timesteps of approximately 1 femtosecond (fs) must be taken because of the high frequency of bond vibrations. A flowchart illustrating the computational steps involved in an MD simulation in GROMACS (Groningen Machine for Chemical Simulations), a powerful open-source molecular dynamics program, are shown in Figure 1-3 [102].

At the end of an MD simulation with S timesteps, averaged properties are determined as follows:

$$\langle A \rangle = \frac{1}{S} \sum_{i=1}^S A(p^N, r^N) \quad (1.4)$$

An alternative to determining a time average value of the property A of interest is to instead calculate the ensemble average, or expectation value. In this approach, a large number of replicas of the system of interest are considered simultaneously. The ensemble average can be expressed mathematically as follows:

$$\langle A \rangle = \int A(p^N, r^N) \rho(p^N, r^N) dp^N dr^N \quad (1.5)$$

where $\rho(p^N, r^N)$ is the probability of finding a configuration with momenta p^N and positions r^N . Although only a single integral sign is shown, in reality integration must be carried out over all $6N$ momenta and positions of the particles present in the system. Therefore, in this approach, the average value of the property A is determined by averaging over all possible configurations of the system rather than by taking a time average. In MC simulation, changes in the system configuration

THE GLOBAL MD ALGORITHM

1. Input initial conditions

Potential interaction V as a function of atom positions

Positions \mathbf{r} of all atoms in the system

Velocities \mathbf{v} of all atoms in the system

↓

repeat 2,3,4 for the required number of steps:

2. Compute forces

The force on any atom

$$\mathbf{F}_i = -\frac{\partial V}{\partial \mathbf{r}_i}$$

is computed by calculating the force between non-bonded atom pairs:

$$\mathbf{F}_i = \sum_j \mathbf{F}_{ij}$$

plus the forces due to bonded interactions (which may depend on 1, 2, 3, or 4 atoms), plus restraining and/or external forces.

The potential and kinetic energies and the pressure tensor are computed.

↓

3. Update configuration

The movement of the atoms is simulated by numerically solving Newton's equations of motion

$$\frac{d^2 \mathbf{r}_i}{dt^2} = \frac{\mathbf{F}_i}{m_i}$$

$$\frac{d\mathbf{r}_i}{dt} = \mathbf{v}_i; \quad \text{or} \quad \frac{d\mathbf{v}_i}{dt} = \frac{\mathbf{F}_i}{m_i}$$

↓

4. if required: Output step

write positions, velocities, energies, temperature, pressure, etc.

Figure 1-3: Sequence of steps involved in molecular dynamics (MD) simulation. Taken from [102].

are proposed, and the proposed configurations are accepted or rejected using a set of criteria that ensures that the probability that the proposed configuration will be present in the new system is equal to the Boltzmann factor, or $\exp(-V(r^N)/k_B T)$, where $V(r^N)$ is the potential energy of the system given the positions of the N particles comprising the system [101]. A wide variety of potential moves can be proposed, including particle translations, particle exchanges, particle insertions, and changes in the system volume. For every accepted configuration, the value of the property A is determined. The average value of A based on the simulation results is then calculated as:

$$\langle A \rangle = \frac{1}{S} \sum_{i=1}^S A(r^N) \quad (1.6)$$

where S is the total number of property values calculated.

1.5 Computer Simulation Studies of Micellization and Micellar Solubilization

In recent years, a growing number of researchers have been exploring the use of computer simulations to examine the structural characteristics of micelles and to model the self-assembly of surfactants in solution. The majority of the research reported in recent years have used either molecular dynamics or Monte Carlo simulation. In theory, MD and MC simulations based on atomistic force fields have the advantage of being able to model arbitrarily complex chemical structures. However, computer simulation of micelle formation is computationally challenging because: (i) micellar systems may consist of many surfactant and solvent molecules, (ii) of the high liquid-like density of micellar systems, and (iii) of the long time scales involved in surfactant self-assembly. As a result, researchers have been forced to either simulate coarse-grained systems to gain a simplified insight into self-assembly, or have been restricted to simulating small systems over short periods of time with more realistic, fully atomistic, models of the system components and of the intramolecular interac-

tions [103]. An additional area of research still in its infancy is the use of computer simulations to assess the free energy of micelle formation. In Sections 1.5.1, 1.5.2, and 1.5.3, computer simulation of preformed surfactant systems, computer simulation of surfactant self-assembly, and computer simulation estimation of the free energy of micelle formation are discussed, respectively.

1.5.1 Computer Simulation of Preformed Surfactant/Solubilize Systems

Simulation of preformed surfactant systems (whether of monolayers [104–114] or of micelles [115–125]) to obtain information about their equilibrium structure and dynamics in solution is computationally feasible. Recently, a large number of computer simulation studies of surfactant systems, including a number of studies of SDS monolayers and micelles, have appeared in the literature. Although such simulations provide a wealth of structural information, they do not provide insight into the self-assembly process of these systems and cannot be used by themselves to predict many of the properties that are of most interest in micellar solubilization applications, including the CMC, the extent of solubilization, and the aggregation number. Only a limited number of simulation studies of solubilization in surfactant micelles have been reported. In an early study, Karaborni et al. investigated oil solubilization in surfactant solutions by performing MD simulations using a simplified model for water, oil, and surfactant [126]. More recently, Kholov et al. studied n-butanol behavior in SDS micelles using realistic models of the system components, and reported rotational diffusion coefficients and rotational correlation times for SDS and n-butanol within the micelle [127]. Kuhn et al. conducted an all-atomistic study investigating solubilization of pentanol in a sodium octanoate micelle [128]. They report simulation results for the micelle radius, the effect of pentanol on micelle shape, the locus of pentanol solubilization, radial distribution functions for various micelle components, and trans-to-gauche ratios of the SDS alkyl chains.

1.5.2 Computer Simulation of Micelle Self-Assembly

Although simulations of micelle formation with atomistic-level detail are possible, because the simulation time is severely limited by the size and the density of the micellar systems, such simulations have only been performed well above the CMC [103]. To accurately identify the CMC, extended simulations of large surfactant/solvent systems would be necessary at a range of low surfactant concentrations and over prohibitively long time scales [103]. To reduce the computational complexity, researchers have implemented a number of approaches. Several researchers have used lattice models to study surfactant self-assembly [129–133]. These lattice model studies have used simplified models of the intermolecular interactions of the system components. For example, Larson et al. modeled oil, water, and surfactant by treating the surfactant head and tail segments as water and oil “beads” [131, 132]. Floriano et al. modeled the interactions between surfactant heads and between surfactant heads and water molecules as having no energy, while interactions between surfactant tails were treated as having negative energies [133]. Using this model, they identified the CMC of two model surfactants by performing lattice grand-canonical MC simulations and identifying a kink in the osmotic pressure as the surfactant concentration was varied. They report observing a decrease in the CMC with increasing surfactant tail length and an increase in the CMC with decreasing solution temperature. Such behavior corresponds to what has been observed experimentally for nonionic surfactants in aqueous solution. Obviously, however, the simplified models used to describe the system components and their interactions in such lattice studies are not capable of predicting solution behavior with quantitative accuracy. Several researchers have also used off-lattice simulations to study surfactant self-assembly, but the majority of these studies have also used coarse-grained models of surfactants and solvent with approximate models for the interactions of the system components [103, 134–136].

Several researchers have simulated spontaneous micelle, vesicle, and bilayer formation in water at an atomistic level of detail. Maillet et al. conducted large scale molecular dynamics simulation of the self-assembly process of short-chain and long-chain

cationic surfactants [137]. In their work, simulations of *n*-nonyltrimethylammonium chloride (C₉TAC) and erucyl *bis* [2-hydroxyethyl] methylammonium chloride (EMAC) surfactants were conducted for up to 3 ns. Starting from an isotropic distribution of surfactant molecules in solution, spontaneous micelle formation was observed and analyzed in terms of generalized classical nucleation theory. They concluded that for systems far from equilibrium, or for systems at high surfactant concentration, the basic aggregation and fragmentation mechanism was of Smoluchowski type (cluster-cluster coalescence and break up); however, for systems closer to equilibrium, or for systems at lower surfactant concentrations, the aggregation and fragmentation mechanism followed a Becker-Döring process (stepwise addition or removal of surfactant monomers). Marrink et al. have simulated the spontaneous aggregation of phospholipids into bilayers during simulations between 10 and 100 ns in duration. From the self-assembly results, they identified several time scales characterizing the aggregation process, and determined that the rate-limiting process in phospholipid bilayer formation is the gradual disappearance of hydrophilic, water-filled transmembrane pores [138]. Marrink et al. have simulated the self-assembly of 54 dodecylphosphocholine (DPC) surfactant molecules in water at two concentrations above the CMC [139]. Self-assembly was observed to occur after 1 to 12 ns of simulation. Marrink et al. also studied the self-assembly behavior and micelle structure of micelles modeling human bile using MD simulations of up to 50 ns [140]. In their study, Marrink et al. compared MD results on the internal structure of mixed micelles of long-chain phosphatidylcholine lipids and bile salts with two proposed structures for the mixed micelles, the “stacked disk” structure and the “radial shell” structure. Their MD results, which showed that phospholipids are packed radially in the micelle with bile salts wedged between the phospholipid heads, supported the radial shell micelle model. Marrink et al. simulated the formation, structure, and dynamics of small dipalmitoylphosphatidylcholine (DPPC) vesicles [141]. They found that by mixing 25% dipalmitoylphosphatidylethanolamine (DPPE) or lysoPC the aggregation process took less time to come to completion. From their results, they were able

to shed light on the mechanism of vesicle fusion [142]. More recently, de Vries et al. studied the spontaneous formation of an oblong DPPC vesicle in water through 90 ns of molecular dynamics simulation [143]. Braun et al. simulated the formation of a complete SDS micelle around glycophorin A (GpA) transmembrane helices starting from isotropically distributed SDS monomers in an aqueous solution over the course of 32 ns of simulation [144]. The authors found that the characteristics of the self-assembled SDS micelle around the GpA dimer was indistinguishable from that of a preformed SDS micelle surrounding the dimer that was equilibrated for 2.5 ns.

1.5.3 Determination of the Free Energy of Micelle Formation

To date, only a small number of researchers have attempted to use computer simulations to determine the free energy of micelle formation. However, if the system of interest has a low CMC, free-energy methods may provide a more computationally efficient method to determine the CMC than brute force simulation of self-assembly because only a single micelle must be simulated in aqueous solution.

Recently, Pool et al. reported determining the free energy of micelle formation for five different model surfactants in a Lennard-Jones solvent through computer simulation [103]. The authors developed a hybrid MD/MC semi-grand canonical simulation approach to estimate the critical micelle concentration. In this approach, umbrella sampling and configurational bias techniques are used to obtain better estimates of the free energy of micelle formation as a function of micelle aggregation number and total surfactant concentration. The five surfactants investigated by Pool et al. were modeled as containing several hydrophobic tail beads (with each bead being equivalent in size to three CH_2 groups) and a single hydrophilic head bead. The ratio of the size of the head bead to that of the tail bead was different for each of the five surfactants considered. CMCs for each surfactant were determined in a Lennard-Jones solvent, where each “solvent” molecule in the simulation was of roughly the same size as that of seven water molecules. In the future, the approach that they outline could be used with more realistic models of surfactants and solubilizates, although

this would involve a large increase in computational expense.

1.6 Combined Computer Simulation/Molecular Thermodynamic Models

As discussed in Section 1.5.3, determining the free energy of micelle formation through computer simulations is difficult and computationally expensive. To circumvent the limitations associated with implementing a purely computer simulation approach, Mohanty et al. developed an approach that combines free-energy determination through computer simulations with molecular-thermodynamic modeling. The authors used this approach to model a system consisting of cetyltrimethylammonium bromide (CTAB) and sodium salicylate (NaSal) [58]. Mohanty et al. obtained reasonable estimates of the effect of the salicylate ions on the CMC, on the aggregate geometry, and on the aggregate size. From their simulation results, they also obtained detailed structural information about the manner in which salicylate ions locate and orient themselves within the micelle.

In the approach of Mohanty et al., a MC simulation was first performed to determine the equilibrium characteristics of a preformed, mixed CTAB/salicylate micelle. Based on this information, the micelle was compartmentalized into a “head-shell” region and a “core” region. The core region was defined as the spherical or cylindrical kernel that contained no part of the salicylate ions. The shell was defined as the rest of the micelle, including the salicylate ions, the CTAB heads, and a short segment of each CTAB tail. After compartmentalization, a molecular-thermodynamic model of micelle formation was used to determine the free-energy associated with the formation of the CTAB micelle. Next, a MC simulation was used to calculate the free-energy change associated with exchanging salicylate ions with CTAB surfactants within the shell region. The objective of these simulations was to determine the free energy of CTAB within the micelle shell at a given composition with respect to the free energy of CTAB in a single-surfactant (pure) CTAB micelle. These simulations were con-

ducted in the semi-grand canonical ensemble (constant N_{tot} , P , T , and μ_{sal}). In this simulation, the composition and volume (or aggregation number) of the micelle was equilibrated at a specified value of μ_{sal} , or the salicylate chemical potential. In their MC simulation, the core of the micelle was not modeled explicitly. Instead, surfactant heads were constrained to lie on the surface of a sphere of appropriate volume given the aggregation number of the micelle. To prevent this shell of surfactant heads from collapsing, movement of the heads into the micelle core, or outwards into the aqueous solution, were penalized with roughly-estimated free-energy penalties. The size of the constraining sphere was allowed to change as the aggregation number of the micelle varied over the course of the simulation, and an appropriate pressure-volume work free-energy correction was applied to account for the associated change in free energy. Counterion interactions with the charged species present at the surface of the micelle were modeled with the Poisson-Boltzmann equation. It is important to note that Mohanty et al. only accounted for the presence of water using a mean field term calculated separately from simulations using the method of Bocker et al. [123]. Mohanty et al. report CMC estimates for spherical CTAB micelles within 25% of the experimental value, and CMC estimates for CTAB wormlike micelles within 83% of the experimental value. The author's theoretical estimate of the spherical and the sphere-to-wormlike shape transition was within 20% of the experimental data. Although the results, particularly for the sphere-to-wormlike shape transition, appear quite reasonable, given the large number of approximations made during the simulation (including the implementation of approximate constraints to maintain the structure of the shell region, the use of approximate models to account for the interactions of the micelle components with counterions and water, and the approximate molecular-thermodynamic modeling of the core region) the level of agreement that the authors obtained with the experimental data could well have been fortuitous. No additional articles using the Complementary Model of surfactant micellization have been published since the article by Mohanty et al. was published in 2001.

1.7 Thesis Objectives

The central objective of my thesis has been to develop modeling approaches to enable prediction of micellar solution properties based on the chemical structures of the solution components and the solution conditions. As part of this thesis, I have developed approaches to predict the CMC, the locus and the extent of solubilization, micelle shape and size, the degree of counterion binding, and information on micelle dynamics. To accomplish this, I have explored computer simulation (CS), molecular-thermodynamic (MT), and combined computer simulation/molecular-thermodynamic (CS-MT) modeling approaches. My thesis research can be divided into the following three parts:

1. Part I: Application of Computer Simulations to Obtain Molecular-Thermodynamic Inputs. This part of the thesis can be further subdivided into two research areas:
 - Extension of micellization modeling by: (i) using computer simulations to obtain input parameters for MT modeling, and (ii) conducting MT modeling based on the computer simulation inputs. This approach was shown to yield accurate results for simple surfactants, and to enable the extension of the molecular-thermodynamic modeling approach to more complex surfactants than had been possible to date. A number of approaches to combine computer simulation results with MT modeling have been explored, including using computer simulations to make head and tail identifications, and the development of a CS-MT modeling approach that takes water contact data from computer simulations as an input to determine the hydrophobic contributions to the free energy of micelle formation.
 - Extension of solubilization modeling by: (i) using simulations to obtain input parameters for MT modeling, and (ii) conducting MT modeling based on the computer simulation inputs. This modeling approach was used to

model 7 different solubilizates, and was shown to yield reasonable predictions of solution properties. Computer simulations were used both to make head and tail identifications for MT modeling, and also to determine water contact information that was used as an input to the newly-developed CS-MT model.

2. Part II: Free-Energy Calculations Using Molecular Dynamics Simulations.

- Modeling of binary micellization and solubilization by combining an MT model of micellization to determine the free energy associated with the formation of a single surfactant micelle with atomistic-level simulations to determine the free-energy change associated with changing the composition of the micelle by adding either a different type of surfactant or solubilizate. This approach was applied to both ionic and nonionic systems, as well as to micellar systems with varying degrees of structural dissimilarity between the various micellar components.

3. Part III: Direct Prediction of Surfactant Solution Properties Using Molecular Dynamics Simulations.

- Implementation of atomistic-level MD simulations to characterize the behavior of surfactants in monolayers and surfactants in micellar environments. From such simulations, detailed structural and dynamic information about monolayers and micelles, as well as information about the self-assembly behavior of surfactants, was obtained.

1.8 Thesis Overview

The remainder of this thesis is organized as follows. In Chapter 2, a computer simulation/molecular-thermodynamic modeling approach is described in which computer simulations are used to obtain head and tail input parameters for MT modeling.

This is accomplished by simulation of surfactant molecules at infinite dilution at a flat water/oil interface (modeling the water/micelle core interface) to determine the extent of hydration of different portions of each surfactant molecule. A computational approach is developed to identify the head and tail groups of each surfactant from the simulation results. The approach is used to determine the heads and tails for the simple surfactants sodium dodecyl sulfate (SDS), cetyltrimethylammonium bromide (CTAB), dodecylphosphocholine (DPC), and octa(ethylene oxide) ($C_{12}E_8$), as well as for three more complex surfactants, 3- and 4-hydroxy sulfonate (AOS) and decanoyl-*n*-methylglucamide (MEGA-10). The sensitivity of the head and tail assignments obtained to the method used to assign atomic charges is evaluated and discussed. The theoretical predictions are also compared with the experimental data.

In Chapter 3, the micellar solubilization of the drug ibuprofen in aqueous solution is investigated theoretically and experimentally for three surfactants — the anionic surfactant SDS, the cationic surfactant dodecyltrimethylammonium bromide (DTAB), and the nonionic surfactant $C_{12}E_8$ — each having the same hydrocarbon tail length but differing in their hydrophilic heads. Simulations of ibuprofen are conducted at a water/oil interface to identify the head and tail portions of this molecule. Using the input parameters determined from computer simulation, MT theory is then used to predict: (i) the micelle composition as a function of surfactant concentration, (ii) the aqueous solubility of ibuprofen as a function of surfactant concentration, and (iii) the micellar solubilization capacity. The theoretical predictions are compared with experimental solubilization data provided by our research collaborators at the University of São Paulo in Brazil [145].

In Chapter 4, computer simulations are used to determine head and tail input parameters for 7 solubilizates (ibuprofen, benzamide, acetophenone, benzonitrile, *o*-aminobenzoate, *m*-aminobenzoate, and *p*-aminobenzoate). To accomplish this, 21 extended MD simulations of solubilizates at a water/oil interface, in a spherical SDS micelle, and in a cylindrical SDS micelle are performed. Simulations in different environments were conducted to evaluate the effect of curvature, ordering of the

surfactant tails, and the presence of the surfactant heads on the simulation results. In addition, the traditional MT modeling approach used to evaluate g_{tr} , g_{int} , and g_{pack} are generalized for solubilizates, and an approach to couple g_{int} and g_{pack} is discussed.

In Chapter 5, MT modeling results are presented for each of the 7 solubilizates introduced in Chapter 4, and MT modeling is implemented using each of the head and tail identifications made in Chapter 4. MT predictions of: (i) the free energy of micelle formation, (ii) micelle shape and size, (iii) micelle composition, and (iv) the micelle/water partition coefficient have been made and are reported. When possible, the theoretical predictions are compared with experimental data.

In Chapter 6, a computer simulation/molecular-thermodynamic (CS-MT) modeling approach is introduced. In the CS-MT modeling approach, atomistic MD simulations are used to quantify the hydration changes that take place during self-assembly. This hydration information is then used in a new MT model to quantify the hydrophobic effect, which is decomposed into g_{dehydr} , the free-energy change associated with the dehydration of solute hydrophobic groups that accompanies aggregate self-assembly, and g_{hydr} , the change in hydration free energy during aggregate self-assembly. The CS-MT model is formulated to allow the prediction of the free-energy change associated with aggregate formation of solute aggregates of any shape and size by performing only two computer simulations — one of the solute in bulk water and the second of the solute in an aggregate of arbitrary shape and size. To test the validity and the accuracy of the new CS-MT modeling approach, it is used to model the formation of 15 different oil aggregates of various shapes and sizes in aqueous solution, and the results are compared with the predictions of the traditional MT model.

In Chapter 7, the validity and accuracy of the CS-MT model is further evaluated by using it to predict the micellization behavior of seven different nonionic surfactants in aqueous solution — octyl glucoside (OG), dodecyl maltoside (DM), octyl sulfinyl ethanol (OSE), decyl methyl sulfoxide (C_{10}SO), decyl dimethyl phosphine oxide (C_{10}PO), and decanoyl-*n*-methylglucamide (MEGA-10). Detailed information

about the changes in hydration that occur upon the self-assembly of each surfactant into micelles is obtained through MD simulation, and subsequently used to compute the hydrophobic driving force for micelle formation. To enable a straightforward estimation of g_{dehydr} and g_{hydr} in the case of nonionic surfactants, a number of approximations are made. The CMC predictions of the CS-MT model are compared with experimental CMC data because the CMC depends exponentially on g_{form} , and as such, it provides a stringent quantitative test with which to evaluate the predictive accuracy of the CS-MT model. The accuracy of the approximations made to implement the CS-MT model in the case of nonionic surfactants is discussed.

In Chapter 8, the validity and accuracy of the CS-MT model is further evaluated by using it to model the micellization behavior of nine ionic and zwitterionic surfactants in aqueous solution — SDS, dodecylphosphocholine (DPC), CTAB, two 3-hydroxy sulfonate surfactants (AOS-12 and AOS-16), and a homologous series of four cationic DC_NA surfactants with a dimethylammonium bromide head attached to a dodecyl alkyl tail and to an alkyl sidechain of length C_N, having the chemical formula C₁₂H₂₅C_NH_{2N+1}N(CH₃)₂Br, with $N = 1$ (DC₁AB), 2 (DC₂AB), 4 (DC₄AB), and 6 (DC₆AB). Both the CS-MT model and the traditional MT model are used to predict the micellization behavior of simple and complex ionic and zwitterionic surfactants. The accuracy of the approximations made in Chapter 7 to model nonionic surfactants is evaluated in the context of modeling ionic and zwitterionic surfactant micellization, and the CMC predictions of the CS-MT model are compared with experimental CMC data.

Chapter 9 discusses the development of a new computer simulation-free energy/molecular-thermodynamic (CS-FE/MT) modeling approach. In the CS-FE/MT model, traditional MT modeling, or experimental data, are used to determine the free energy of formation of a single (pure) surfactant micelle and the single surfactant micelle aggregation number. A micelle with the theoretically or the experimentally determined aggregation number is then built and equilibrated in aqueous solution in a simulation cell. Computer simulations are then used to compute the free-energy change associ-

ated with: (i) changing the identity of surfactant molecules of type A to surfactant molecules of type B (to model binary surfactant micellization), or (ii) with changing the identity of surfactant molecules of type A to solubilize molecules of type B (to model micellar solubilization). The free-energy change associated with this process is referred to as $\Delta g_{exchange}$, reflecting the fact that a new molecule is exchanged with the original molecule.

In Chapter 10, the CS-FE/MT model is implemented for spherical micellar geometries using a dual-topology thermodynamic integration approach in which molecules of type A are exchanged with molecules of type B as a function of a coupling parameter, λ . To evaluate the accuracy of the CS-FE/MT model, MD simulation results for $\Delta g_{exchange}$ for the exchange of ibuprofen with SDS, p -aminobenzoate with OG, octyl sulfoxide with decyl sulfoxide, (octylsulfinyl)ethanol with (decylsulfinyl)ethanol, and decyl sulfoxide with decyl phosphine oxide are compared with the predictions of the traditional MT model and with experimental data.

In Chapter 11, atomistic-level MD simulations are used to determine and understand the interfacial behavior of a homologous series of structurally complex fluorosurfactants. Constant surface tension ($N\gamma T$) and constant volume (NVT) MD simulations are conducted on a series of bolaamphiphilic α, ω -(diammonium disulfato)poly(fluorooxetane)s with several perfluoroalkyl chain lengths and a typical “long-chain” anionic fluorosurfactant used to improve the flow-and-leveling characteristics of aqueous coatings, in order to compare their behavior at a water/air interface. Recent research has shown that these poly(fluorooxetane) surfactants are an effective substitute for traditional fluorosurfactants used in flow-and-leveling applications [146]. From MD simulation, the saturated interfacial area per surfactant molecule, the interfacial area per surfactant molecule as a function of surface tension, density profiles, order parameters, the degree of hydration of various atoms in each surfactant molecule, and the degree of counterion binding are each determined. A geometrically defined penetration parameter is calculated from the density profiles to evaluate the ability of each surfactant to separate the air and water phases and to re-

duce enthalpically unfavorable contacts. The degree of hydration is also determined for different atoms in poly(fluorooxetane) during simulation.

In Chapter 12, extended MD simulations are used to study the self-assembly of the triterpenoids asiatic acid (AA) and madecassic acid (MA) from randomly distributed monomers to micelles in aqueous solution. A total of 50 ns of MD simulation was conducted, requiring roughly 8,000 CPU hours. The computer simulation results are used to obtain information about: i) the dynamics of micelle formation, ii) the rates of monomer association and dissociation into micelles, iii) the micelle microstructure, iv) the local environments of hydrophobic and hydrophilic groups within each AA and MA molecule, v) the AA and the MA monomer concentrations (which are compared with experimental data), and vi) the average aggregation numbers of the self-assembled AA and MA micelles.

Finally, Chapter 13 summarizes the main results of the thesis, presents concluding remarks, and proposes possible directions for future research. The future research directions proposed include: (i) improvements to the approaches developed in Part I of this thesis to use computer simulations to obtain inputs for MT theory (including head and tail identification through water/oil interface simulation, head and tail identification through micellar simulation, and CS-MT modeling of surfactants and solubilizates), (ii) extensions to the approaches developed in Part II of this thesis to use computer simulations to determine free-energy changes (including selection of the optimal transition path and alternative free-energy models), and further exploration of the research discussed in Part III of this thesis to use computer simulations to make direct predictions of surfactant solution properties.

Bibliography

- [1] Israelachvili, J. N., *Intermolecular and Surface Forces*, Academic Press, 2nd ed., 1991.
- [2] Elworthy, P. H., Florence, A. T., and Macfarlane, C. B., *Solubilization by Surface Active Agents*, Chapman and Hall, London, 1968.
- [3] Dunaway, C. S., Christian, S. D., and Scamehorn, J. F., *Solubilization in Surfactant Aggregates. Surfactant Science Series 55*, Marcel Dekker, New York, 1995.
- [4] Nagarajan, R., “Solubilization in aqueous solutions of amphiphiles,” *Current Opinion in Colloid and Interface Science*, Vol. 1, 1996, pp. 391–401.
- [5] Nagarajan, R., “Solubilization by amphiphilic aggregates,” *Current Opinion in Colloid and Interface Science*, Vol. 2, 1997, pp. 282–293.
- [6] Broze, B., Ward, T., Ward, K. D., Christian, S. D., and Scamehorn, J. F., *Solubilization in Surfactant Aggregates. Surfactant Science Series 55*, Marcel Dekker, New York, 1995.
- [7] Hagan, S. A., Coombes, G. A., Garnett, M. C., Dunn, S. E., and Davies, M. C., “Polylactide-poly(ethylene glycol) copolymers as drug delivery systems: 1. Characterization of water dispersible micelle-forming systems,” *Langmuir*, Vol. 12, 1996, pp. 2153–2161.

- [8] Shiloach, A. and Blankschtein, D., "Predicting micellar solution properties of binary surfactant mixtures," *Langmuir*, Vol. 14, 1998, pp. 1618–1636.
- [9] Rosen, M., *Surfactants and Interfacial Phenomena*, John Wiley and Sons, New York, 10th ed., 1989.
- [10] Srinivasan, V. and Blankschtein, D., "Effect of counterion binding on micellar solution behavior: 1. Molecular-thermodynamic theory of micellization of ionic surfactants," *Langmuir*, Vol. 19, 2003, pp. 9932–9945.
- [11] Srinivasan, V. and Blankschtein, D., "Effect of counterion binding on micellar solution behavior: 2. Prediction of micellar solution properties of ionic surfactant-electrolyte systems," *Langmuir*, Vol. 19, 2003, pp. 9946–9961.
- [12] Rouse, J. D., Sabatini, D. A., Deeds, N. E., and Brown, R. E., "Micellar solubilization of unsaturated hydrocarbon concentrations as evaluated by semi-equilibrium dialysis," *Environmental Science and Technology*, Vol. 29, 1995, pp. 2484–2489.
- [13] In Christian, S. D. and Scamehorn, J. F., *Solubilization in Surfactant Aggregates. Surfactant Science Series 55*, Marcel Dekker, New York, 1995.
- [14] Christian, S. D., Smith, L. S., Bushong, D. S., and Tucker, E. E., "Solubilization of benzene and cyclohexane by sodium deoxycholate micelles," *Journal of Colloid and Interface Science*, Vol. 89, 1982, pp. 514–522.
- [15] Puvvada, S. and Blankschtein, D., "Molecular thermodynamic approach to predict micellization, phase behavior and phase separation of micellar solutions. 1. Application to nonionic surfactants," *The Journal of Chemical Physics*, Vol. 92, 1990, pp. 3710–3724, and references cited therein.
- [16] Takeuchi, M. and Moroi, Y., "Solubilization of n-alkylbenzenes into 1-dodecanesulfonic acid micelles," *Langmuir*, Vol. 11, 1995, pp. 4719–4723.

- [17] Moroi, Y. and Matuura, R. J., "Thermodynamics of solubilization into surfactant micelles: Effect of hydrophobicity of both solubilizate and surfactant molecules," *Journal of Colloid and Interface Science*, Vol. 125, 1988, pp. 456–462.
- [18] Gadelle, F., Koros, W. J., and Schechter, R. S., "Solubilization isotherms of aromatic solutes in surfactant aggregates," *Journal of Colloid and Interface Science*, Vol. 170, 1995, pp. 57–64.
- [19] Nagarajan, R. and Ruckenstein, E., "Theory of surfactant self-assembly: A predictive molecular thermodynamic approach," *Langmuir*, Vol. 7, 1991, pp. 2934–2969.
- [20] Kissa, E., *Fluorinated Surfactants*, Marcel Dekker, New York, 1993.
- [21] Saito, H. and Shinoda, K., "The solubilization of hydrocarbons in aqueous solutions of nonionic surfactants," *Journal of Colloid and Interface Science*, Vol. 24, 1967, pp. 10–15.
- [22] Pusicaro, E., Pelizzetti, E., Bongiovanni, R., and Borgarello, E., "Perfluorinated surfactants - properties and applications. 1. Thermodynamic properties," *Colloids and Surfaces*, Vol. 48, 1990, pp. 259–275.
- [23] Shinoda, K., Hato, M., and Hayashi, T., "Physicochemical properties of aqueous solutions of fluorinated surfactants," *The Journal of Physical Chemistry*, Vol. 76, 1972, pp. 909–914.
- [24] Carlfors, J. and Stilbs, P., "Solubilization in sodium perfluorooctanoate micelles: A multicomponent self-diffusion study," *Journal of Colloid and Interface Science*, Vol. 103, 1985, pp. 332–336.
- [25] Russel, J. C. and Whitten, D. G., "Photochemical reactivity in organized assemblies. 24. Solute partitioning in aqueous surfactant assemblies: Comparison

- of hydrophobic-hydrophilic interactions in micelles, alcohol-swollen micelles, microemulsions, and synthetic vesicles,” *Journal of the American Chemical Society*, Vol. 104, 1982, pp. 5937–5942.
- [26] Kunieda, H. and Shinoda, K., “Krafft points, critical micelle concentrations, surface tension, and solubilizing power of aqueous solutions of fluorinated surfactants,” *The Journal of Physical Chemistry*, Vol. 80, 1976, pp. 2468–2470.
- [27] Bongiovanni, R., Borgarello, E., Carlini, F. M., Fisicaro, E., and Pelizzetti, E., “Perfluorinated surfactants - properties and applications. 2. Monophasic perfluorinated oil surfactant water-system,” *Colloids and Surfaces*, Vol. 48, 1990, pp. 277–283.
- [28] Mathis, G., Ravey, J. C., and Buzier, M., *In Microemulsions*, Robb-Plenum, 1982.
- [29] Ravoo, G. J. and Engberts, J. B. F. N., “Single-tail phosphates containing branched alkyl chains. Synthesis and aggregation in water of a novel class of vesicle-forming surfactants,” *Langmuir*, Vol. 10, 1994, pp. 1735–1740.
- [30] Engberts, J. B. F. N. and Nuslder, J. J. H., “The effect of chain packing on surfactant aggregation in aqueous solution,” *Pure and Applied Chemistry*, Vol. 62, 1990, pp. 47–55.
- [31] Nusselder, J. J. H. and Engberts, J. B. F. N., “Relation between surfactant structure and properties of spherical micelles. 1-alkyl-4-alkylpyridinium halide surfactants,” *Langmuir*, Vol. 7, 1991, pp. 2089–2096.
- [32] Kolthoff, I. M. and Stricks, “Solubilization of dimethylaminoazobenzene in solutions of detergents,” *Journal of Physical Colloid Chemistry*, Vol. 52, 1948, pp. 915–943.

- [33] Eda, Y., Takisawa, N., and Shirahama, K., "Solubilization of 1-alkanols in ionic micelles measured by piezoelectric gas sensors," *Langmuir*, Vol. 12, 1996, pp. 325–329.
- [34] Sagitani, H., Suzuki, T., and Shinoda, K., "Solubilization of cyclohexane in aqueous solutions of sodium A-alkyl alkanoates," *Journal of Colloid and Interface Science*, Vol. 87, 1982, pp. 11–17.
- [35] Klevens, H. B., "Solubilization," *Chemical Reviews*, Vol. 47, 1950, pp. 1–78.
- [36] Rosen, M., "Geminis: A new generation of surfactants. These materials have better properties than conventional ionic surfactants as well as positive synergistic effects with non-ionics," *CHEMTECH*, Vol. 23, 1993, pp. 30–33.
- [37] Zana, R., Benrraou, M., and Rueff, R., "Gemini (dimeric) surfactants," *Current Opinion in Colloid and Interface Science*, Vol. 1, 1996, pp. 566–571.
- [38] De, S., Aswal, V. K., Gyal, P. S., and Bhattacharya, S., "Role of spacer chain length in dimeric micellar organization. Small angle neutron scattering and fluorescence studies," *The Journal of Physical Chemistry*, Vol. 100, 1996, pp. 11664–11663.
- [39] Zana, R., Benrraou, M., and Rueff, R., "Alkanediyl-alpha,omega-bis(dimethylalkylammonium bromide) surfactants. 1. Effect of the spacer chain length on the critical micelle concentration and micelle ionization degree," *Langmuir*, Vol. 7, 1991, pp. 1072–1075.
- [40] Rosen, M., *Journal In Advanced Technology Conference*, Vol. 9, 1998.
- [41] Hirata, H., Hattori, N., Ishida, M., Okabayashi, H., Fruzaka, M., and Zana, R., "Small-angle neutron-scattering study of bis(quaternary ammonium bromide) surfactant micelles in water. Effect of the spacer chain length on micellar structure," *The Journal of Physical Chemistry*, Vol. 99, 1995, pp. 17778–17784.

- [42] Devinsky, F., Lacko, I., and Imam, T., "Relationship between structure and solubilization properties of some bisquaternary ammonium amphiphiles," *Journal of Colloid and Interface Science*, Vol. 143, 1991, pp. 336–342.
- [43] Dam, T., Engberts, J. B. F. N., Karthausr, J., Karaboni, S., and van Os, N. M., "Synthesis, surface properties and oil solubilisation capacity of cationic gemini surfactants," *Colloids and Surfaces A: Physicochemical and Engineering Aspects*, Vol. 118, 1996, pp. 41–49.
- [44] Diamant, H. and Andelman, D., "Dimeric surfactants: Spacer chain conformation and specific area at the air/water interface," *Langmuir*, Vol. 10, 1994, pp. 2910–2916.
- [45] Diamant, H. and Andelman, D., "Dimeric surfactants: A simplified model for the spacer chain," *Langmuir*, Vol. 11, 1995, pp. 3605–3606.
- [46] Moroi, Y., Mitsunobu, K., Morisue, T., Kadobayashi, Y., and Sakai, M., "Solubilization of benzene, naphthalene, anthracene, and pyrene in 1-dodecanesulfonic acid micelle," *The Journal of Physical Chemistry*, Vol. 99, 1995, pp. 2372–2376.
- [47] Chaiko, M. A., Nagarajan, R., and Ruckenstein, E., "Solubilization of single-component and binary mixtures of hydrocarbons in aqueous micellar solutions," *Journal of Colloid and Interface Science*, Vol. 99, 1984, pp. 168–182.
- [48] Moroi, Y., Morisue, T., Take'uchi, M., and Shibata, O., "Solubilization of arenes and n-alkylbenzenes into ionic surfactant micelles," *Colloids and Surfaces A: Physicochemical and Engineering Aspects*, Vol. 109, 1996, pp. 201–208.
- [49] Talsani, S. K., Rodriguez-Guadarrama, L. A., Mohanty, K. K., and Rajagopalan, R., "Phase behavior and solubilization in surfactant-solute-solvent systems by Monte Carlo simulations," *Langmuir*, Vol. 14, 1998, pp. 2684–2692.

- [50] Smith, G. A., Christian, S. D., Tucker, E. E., and Scamehorn, J. F., “Solubilization of hydrocarbons by surfactant micelles and mixed micelles,” *Journal of Colloid and Interface Science*, Vol. 130, 1989, pp. 254–265.
- [51] Ozeki, S. and Ikeda, S., “The difference in solubilization power between spherical and rodlike micelles of dodecyldimethylammonium chloride in aqueous solutions,” *The Journal of Physical Chemistry*, Vol. 89, 1985, pp. 5088–5093.
- [52] Heijnen, J., *Olefin Epoxidations Catalyzed by Micelle-Incorporated Homogeneous Catalysts*, Ph.D. thesis, Eindhoven University, 2003.
- [53] Nagarajan, R., “Locus of solubilization of benzene in surfactant micelles,” *The Journal of Physical Chemistry*, Vol. 87, 1983, pp. 2916–2922.
- [54] Goldenberg, M. S., Bruno, L. A., and Rennwanz, E. L., “Determination of solubilization sites and efficiency of water-insoluble agents in ethylene oxide-containing nonionic micelles,” *Journal of Colloid and Interface Science*, Vol. 158, 1993, pp. 351–363.
- [55] Nagakawa, T. and In Schick, M. J., *Nonionic Surfactants. Surfactant Science Series 55*, Marcel Dekker, New York, 1995.
- [56] Srinivasan, V., *Theoretical Modeling of Micellization and Solubilization in Ionic Surfactant Systems*, Ph.D. thesis, Massachusetts Institute of Technology, 2003, and references cited therein.
- [57] Blokhuis, A. M., Hoiland, H., Gilje, E., and Backlund, S., “The effect of inorganic salt on the solubilization of alcohols in aqueous surfactant solutions,” *Journal of Colloid and Interface Science*, Vol. 124, 1988, pp. 125–129.
- [58] Mohanty, S., Davis, H. T., and McCormick, A. V., “Complementary use of simulations and free energy models for CTAB/NaSal systems,” *Langmuir*, Vol. 17, 2001, pp. 7160–7171.

- [59] Treiner, C., Christian, S. D., and Scamehorn, J. F., *Solubilization in Surfactant Aggregates. Surfactant Science Series 55*, Marcel Dekker, New York, 1995.
- [60] Tornblom, M. and Henriksson, U., “Effect of solubilization of aliphatic hydrocarbons on size and shape of rodlike C(16)TABr micelles studied by H-2 NMR relaxation,” *The Journal of Physical Chemistry*, Vol. 101, 1997, pp. 6028–6035.
- [61] Hoffmann, H. and Ulbricht, W., “Transition of rodlike to globular micelles by the solubilization of additives,” *Journal of Colloid and Interface Science*, Vol. 129, 1989, pp. 388–405.
- [62] Reekmans, S., Luo, H., van der Auweraer, M., and de Schryver F., “Influence of alcohols and alkanes on the aggregation behavior of ionic surfactants in water,” *Langmuir*, Vol. 6, 1990, pp. 628–637.
- [63] Thimons, K. L., Brazdil, L. C., Harrison, D., and Fisch, M. R., “Effects of pentanol isomers on the growth of SDS micelles in 0.5 M NaCl,” *The Journal of Physical Chemistry B*, Vol. 101, 1997, pp. 11087–11091.
- [64] Forland, G. M., Samseth, J., Gjerde, M. I., Holland, H., Jensen, A. O., and Mortensen, K., “Influence of alcohol on the behavior of sodium dodecylsulfate micelles,” *Journal of Colloid and Interface Science*, Vol. 203, 1997, pp. 328–334.
- [65] ud Din, K., Kumar, S., Kirti, and Goyal, P. S., “Micellar growth in presence of alcohols and amines: A viscometric study,” *Langmuir*, Vol. 12, 1996, pp. 1490–1494.
- [66] Bayer, O., Hoffmann, H., Ulbricht, W., and Thurn, H., “The influence of solubilized additives on surfactant solutions with rodlike micelles,” *Advances in Colloid and Interface Science*, Vol. 26, 1996, pp. 177–203.
- [67] Heindl, A., Strnad, J., and Kohler, H. H., “Effect of aromatic solubilizates on the shape of CTABr micelles,” *The Journal of Physical Chemistry*, Vol. 97, 1993, pp. 742–746.

- [68] Gunnarsson, G., Jonsson, B., and Wennerstrom, H., "Surfactant association into micelles - An electrostatic approach," *The Journal of Physical Chemistry*, Vol. 84, 1980, pp. 3114–3121.
- [69] Jonsson, B. and Wennerstrom, H., "Thermodynamics of ionic amphiphile-water systems," *Journal of Colloid and Interface Science*, Vol. 80, 1981, pp. 482–496.
- [70] Evans, D. F., Mitchell, D. J., and Ninham, B. W., "Ion binding and dressed micelles," *The Journal of Physical Chemistry*, Vol. 88, 1984, pp. 6344–6348.
- [71] Hayter, J. B., "A self-consistent theory of dressed micelles," *Langmuir*, Vol. 8, 1992, pp. 2873–2876.
- [72] Tanford, C., *The Hydrophobic Effect: Formation of Micelles and Biological Membranes*, John Wiley and Sons, New York, 1991.
- [73] Ruckenstein, E. and Beunen, J. A., "Effect of counterion binding on micellization," *Langmuir*, Vol. 4, No. 1, 1988, pp. 77–90.
- [74] Ruckenstein, E. and Nagarajan, R., *Micellization, Solubilization, and Microemulsions*, Plenum Press, 1977.
- [75] Nagarajan, R. and Ruckenstein, E., "A transition point for micellar size distribution: A statistical thermodynamical approach," *Journal of Colloid and Interface Science*, Vol. 60, 1977, pp. 221–231.
- [76] Nagarajan, R. and Ruckenstein, E., "Aggregation of amphiphiles as micelles or vesicles in aqueous media," *Journal of Colloid and Interface Science*, Vol. 71, 1979, pp. 580–604.
- [77] Nagarajan, R. and Ruckenstein, E., "Solubilization as a separation process," *Separation Science and Technology*, Vol. 16, 1981, pp. 1429–1465.
- [78] Nagarajan, R. and Ruckenstein, E., *Surfactants in Solution*, Plenum Press, 1984.

- [79] Nagarajan, R., “Molecular theory for mixed micelles,” *Langmuir*, Vol. 1, 1985, pp. 331–341.
- [80] Nagarajan, R., “Micellization, mixed micellization and solubilization: The role of interfacial interactions,” *Advances in Colloid and Interface Science*, Vol. 26, 1986, pp. 205–264.
- [81] Nagarajan, R., “Thermodynamics of micelles, mixed micelles and solubilization: The role of interfacial interactions,” *Advances in Colloid and Interface Science*, Vol. 26, 1986, pp. 205–264.
- [82] Nagarajan, R., *Mixed Surfactant Systems*, Vol. Surfactant Science Series 70, chap. 4, ACS Symposium Series 501, Washington, D. C., 1992, pp. 54–95.
- [83] Nagarajan, R., *Theory of Micelle Formation: Quantitative Approach to Predicting Micellar Properties from Surfactant Molecular Structure*, chap. 1, Marcel Dekker, New York, 1997, pp. 1–81.
- [84] Camesano, T. A. and Nagarajan, R., “Micelle formation and CMC of gemini surfactants: A thermodynamic model,” *Colloids and Surfaces A: Physico Chem. Eng. Aspects*, Vol. 167, 2000, pp. 165–178.
- [85] Rao, I. V. and Ruckenstein, E., “Micellization behavior in the presence of alcohols,” *Journal of Colloid and Interface Science*, Vol. 113, 1986, pp. 375–387.
- [86] Reif, I., Mulqueen, M., and Blankshtein, D., “Molecular-thermodynamic prediction of critical micelle concentrations of commercial surfactants,” *Langmuir*, Vol. 17, 2001, pp. 5801–5812.
- [87] Shiloach, A. and Blankshtein, D., “Measurement and prediction of ionic/nonionic mixed micelle formation and growth,” *Langmuir*, Vol. 14, 1998, pp. 7166–7182.

- [88] Shiloach, A. and Blankschtein, D., “Prediction of critical micelle concentrations of nonideal ternary surfactant mixtures,” *Langmuir*, Vol. 14, 1998, pp. 4105–4114.
- [89] Shiloach, A. and Blankschtein, D., “Prediction of critical micelle concentrations and synergism of binary surfactant mixtures containing zwitterionic surfactants,” *Langmuir*, Vol. 13, 1997, pp. 3968–3981.
- [90] Zoeller, N., Lue, L., and Blankschtein, D., “A statistical-thermodynamic framework to model nonionic micellar solutions,” *Langmuir*, Vol. 13, 1997, pp. 5258–5275.
- [91] Mulqueen, M. and Blankschtein, D., “Theoretical and experimental investigation of the equilibrium oil-water interfacial tensions of solutions containing surfactant mixtures,” *Langmuir*, Vol. 18, 2002, pp. 365–376.
- [92] Nikas, Y., Puvvada, S., and Blankschtein, D., “Surface tensions of aqueous nonionic surfactant mixtures,” *Langmuir*, Vol. 8, 1992, pp. 2680–2689.
- [93] Mulqueen, M. and Blankschtein, D., “Prediction of equilibrium surface tension and surface adsorption of aqueous surfactant mixtures containing ionic surfactants,” *Langmuir*, Vol. 15, 1999, pp. 8832–8848.
- [94] Mulqueen, M., Stebe, K., and Blankschtein, D., “Dynamic interfacial adsorption in aqueous surfactant mixtures: Theoretical study,” *Langmuir*, Vol. 17, 2001, pp. 5196–5207.
- [95] Mulqueen, M., Datwani, S., Stebe, K., and Blankschtein, D., “Dynamic surface tension of aqueous surfactant mixtures: Experimental investigation,” *Langmuir*, Vol. 17, 2001, pp. 5801–5812.
- [96] Aamodt, M., Landgren, M., and Jonsson, B., “Solubilization of uncharged molecules in ionic surfactant aggregates. 1. The micellar phase,” *The Journal of Physical Chemistry*, Vol. 96, 1992, pp. 945–950.

- [97] Landgren, M., Aamodt, M., and Jonsson, B., “Solubilization of uncharged molecules in ionic surfactant aggregates. 2. Phase equilibria,” *The Journal of Physical Chemistry*, Vol. 96, 1992, pp. 950–961.
- [98] Jonsson, B., Landgren, M., Olofsson, G., and In Christian, S. D., *Solubilization in Surfactant Aggregates. Surfactant Science Series 55*, Marcel Dekker, New York, 1995.
- [99] Gelbart, W. M., Ben-Shaul, A., and Roux, D., *Micelles, Membranes, Microemulsions, and Monolayers*, Springer, Berlin, 1994, and references cited therein.
- [100] Telo de Gama, M. M. and Gubbins, K. E., “Adsorption and orientation of amphiphilic molecules at a liquid-liquid interface,” *Molecular Physics*, Vol. 59, 1986, pp. 227–239.
- [101] Leach, A., *Molecular Modeling: Principles and Applications*, Prentice Hall, 2nd ed., 2001.
- [102] van der Spoel, D., Lindahl, E., Hess, B., van Buuren, A., Apol, E., Meulenhoff, P., Tieleman, D., Sijbers, A., Feenstra, K., van Drunen, R., and Berendsen, H., *Gromacs User Manual version 3.2*, www.gromacs.org, 2004.
- [103] Pool, R. and Bolhuis, P. G., “Accurate free energies of micelle formation,” *The Journal of Physical Chemistry B*, Vol. 109, 2005, pp. 6650–6657.
- [104] Tarek, M., Tobias, D. J., and Klein, M. L., “Molecular dynamics simulation of tetradecyltrimethylammonium bromide monolayers at the air-water interface,” *The Journal of Physical Chemistry*, Vol. 99, 1995, pp. 1393–1402.
- [105] Wijmans, C. M. and Linse, P., “Surfactant self-assembly at a hydrophilic surface. A Monte Carlo simulation study,” *The Journal of Physical Chemistry*, Vol. 100, 1996, pp. 12583–12591.

- [106] Schweighofer, K. J., Essmann, U., and Berkowitz, M., “Structure and dynamics of water in the presence of charged surfactant monolayers at the water-CCl₄ interface. A molecular dynamics study,” *The Journal of Physical Chemistry*, Vol. 101, 1997, pp. 10775–10780.
- [107] Kuhn, H. and Rehage, H., “Molecular dynamics computer simulations of surfactant monolayers: Monododecyl pentaethylene glycol at the surface between air and water,” *The Journal of Physical Chemistry B*, Vol. 103, 1999, pp. 8493–8501.
- [108] Kuhn, H. and Rehage, H., “Molecular orientation of monododecyl pentaethylene glycol (C12E5) surfactants at infinite dilution at the air/water interface. A molecular dynamics computer simulation study,” *Physical Chemistry Chemical Physics*, Vol. 2, 2000, pp. 1023–1028.
- [109] Kuhn, H. and Rehage, H., “Molecular orientation of monododecyl pentaethylene glycol at water/air and water/oil interfaces. A molecular dynamics computer simulation study,” *Colloid and Polymer Science*, Vol. 114-118, 2000, pp. 278.
- [110] da Rocha, S. R. P., Johnston, K. P., and Rossky, P. J., “Surfactant-modified CO₂-water interface: A molecular view,” *The Journal of Physical Chemistry*, Vol. 106, 2002, pp. 13250–13261.
- [111] Stone, M. T., da Rocha, S. R. P., Rossky, P. J., and Johnston, K. P., “Molecular differences between hydrocarbon and fluorocarbon surfactants at the CO₂/water interface,” *The Journal of Physical Chemistry B*, Vol. 107, 2003, pp. 10185–10192.
- [112] Rekvig, L., Hafskjold, B., and Smit, B., “Simulating the effect of surfactant structure on bending moduli of monolayers,” *The Journal of Chemical Physics*, Vol. 120, 2004, pp. 4897–4905.

- [113] Rekvig, L., Hafskjold, B., and Smit, B., “Chain length dependencies of the bending modulus of surfactant monolayers,” *Physical Review Letters*, Vol. 92, 2004, pp. 116101.
- [114] Dominguez, H., “Computer simulations of surfactant mixtures at the liquid/liquid interface,” *The Journal of Physical Chemistry B*, Vol. 106, 2002, pp. 5915–5924.
- [115] Schweighofer, K. J., Essmann, U., and Berkowitz, M., “Simulation of sodium dodecyl sulfate at the water-vapor and water-carbon tetrachloride interfaces at low surface coverage,” *The Journal of Physical Chemistry B*, Vol. 101, 1997, pp. 3793–3799.
- [116] Bruce, C., Berkowitz, M., Perera, L., and Forbes, M., “Molecular dynamics simulation of sodium dodecyl sulfate micelle in water: Micellar structural characteristics and counterion distribution,” *The Journal of Physical Chemistry B*, Vol. 106, 2002, pp. 3788–3793.
- [117] MacKerell, A. D., “Molecular dynamics simulation analysis of a sodium dodecyl sulfate micelle in aqueous solution: Decreased fluidity of the micelle hydrocarbon interior,” *The Journal of Physical Chemistry*, Vol. 99, 1995, pp. 1846–1855.
- [118] Bruce, C., Senapati, S., Berkowitz, M., Perera, L., and Forbes, M., “Molecular dynamics simulations of sodium dodecyl sulfate micelle in water: The behavior of water,” *The Journal of Physical Chemistry B*, Vol. 106, 2002, pp. 10902–10907.
- [119] Dominguez, H., “Computer simulation studies of surfactant monolayer mixtures at the water/oil interface: Charge distribution effects,” *Journal of Colloid and Interface Science*, Vol. 274, 2004, pp. 665–672.

- [120] Dominguez, H. and Berkowitz, M. L., “Computer simulations of sodium dodecyl sulfate at liquid/liquid and liquid/vapor interfaces,” *The Journal of Physical Chemistry B*, Vol. 104, 2000, pp. 5302–5308.
- [121] Gao, J., Ge, W., Hu, G., and Li, J., “From homogeneous dispersion to micelles - A molecular dynamics simulation on the compromise of the hydrophilic and hydrophobic effects of sodium dodecyl sulfate in aqueous solution,” *Langmuir*, Vol. 21, 1989, pp. 5223–5229.
- [122] Bogusz, S., Venable, R. M., and Pastor, R. W., “Molecular dynamics simulations of octyl glucoside micelles: Structural properties,” *The Journal of Physical Chemistry B*, Vol. 104, 2000, pp. 5462–5470.
- [123] Bocker, J., Brickmann, J., and Bopp, P., “Molecular dynamics simulation study of an n-dodecyltrimethylammonium chloride micelle in water,” *The Journal of Physical Chemistry*, Vol. 98, 1994, pp. 712–717.
- [124] Rakitin, A. R. and Pack, G. R., “Molecular dynamics simulations of ionic interactions with dodecyl sulfate micelles,” *The Journal of Physical Chemistry B*, Vol. 108, 2004, pp. 2712–2716.
- [125] Pal, S., Balasubramanian, S., and Bagchi, B., “Identity, energy, and environment of interfacial water molecules in a micellar solution,” *The Journal of Physical Chemistry B*, Vol. 107, 2003, pp. 5194–5202.
- [126] Karaborni, S., van Os, N. M., Esselink, K., and Hilbers, P. A. J., “Molecular dynamics simulations of oil solubilization in surfactant solutions,” *Langmuir*, Vol. 9, 1993, pp. 1175–1178.
- [127] Kholov, K. N., Mamatkulov, S. I., Saidov, A. A., Khabibullaev, P. K., and Berkowitz, M. L., “Molecular dynamics study of alcohol solubilization process in micellar solutions,” *Uzbek Journal of Physics*, Vol. 5, 2003, pp. 145–149.

- [128] Kuhn, H., Breitzke, B., and Rehage, H., “A molecular modeling study of pentanol solubilized in a sodium octanoate micelle,” *Journal of Colloid and Interface Science*, Vol. 249, 2002, pp. 152–161.
- [129] Rodriguez-Guadarrama, L. A., Talsania, S. K., Mohanty, K. K., and Rajagopalan, R., “Thermodynamics of aggregation of amphiphiles in solution from lattice Monte Carlo simulations,” *Langmuir*, Vol. 15, 1999, pp. 437–446.
- [130] Care, C. M. and Dalby, T., “Packing entropy in micelle self-assembly,” *Europhysics Letters*, Vol. 45, 1999, pp. 38–44.
- [131] Larson, R. G., “Monte Carlo simulation of microstructural transitions in surfactant systems,” *The Journal of Chemical Physics*, Vol. 96, 1992, pp. 7904–7918.
- [132] Larson, R. G., Scriven, L. E., and Davis, H. T., “Monte Carlo simulation of model amphiphilic oil-water systems,” *The Journal of Chemical Physics*, Vol. 83, 1985, pp. 2411–2420.
- [133] Floriano, M. A., Caponetti, E., and Panagiotopoulos, A. Z., “Micellization in model surfactant systems,” *Langmuir*, Vol. 15, 1999, pp. 3143–3151.
- [134] Smit, B., Hilbers, P. A. J., Esselink, K., Rupert, L. A. M., van Os, N. M., and Schlijper, A. G., “Computer simulations of a water oil interface in the presence of micelles,” *Nature*, Vol. 348, 1990, pp. 624–625.
- [135] Smit, B., Esselink, K., Hilbers, P. A. J., van Os, N. M., Rupert, L. A. M., and Szlifer, I., “Computer simulations of surfactant self-assembly,” *Langmuir*, Vol. 9, 1993, pp. 9–11.
- [136] Smit, B., Hilbers, P. A. J., Esselink, K., Rupert, L. A. M., van Os, N. M., and Schlijper, A. G., “Structure of a water/oil interface in the presence of micelles: A computer simulation study,” *The Journal of Physical Chemistry*, Vol. 95, 1991, pp. 6361–6368.

- [137] Maillet, J. B., Lachet, V., and Coveney, P. V., “Large scale molecular dynamics simulation of self-assembly processes in short and long chain cationic surfactants,” *Physical Chemistry Chemical Physics*, Vol. 1, 1999, pp. 5277.
- [138] Marrink, S., Lindahl, E., Edholm, O., and Mark, A., “Simulation of the spontaneous aggregation of phospholipids into bilayers,” *Journal of the American Chemical Society*, Vol. 123, 2001, pp. 8638–8639.
- [139] Marrink, S. J., Tieleman, D. P., and Mark, A. E., “Molecular dynamics simulation of the kinetics of spontaneous micelle formation,” *The Journal of Physical Chemistry B*, Vol. 104, 2000, pp. 12165–12173.
- [140] Marrink, S. J. and Mark, A. E., “Molecular dynamics simulations of mixed micelles modeling human bile,” *Biochemistry*, Vol. 41, 2002, pp. 5375–5382.
- [141] Marrink, S. and Mark, A., “Molecular dynamics simulation of the formation, structure, and dynamics of small phospholipid vesicles,” *Journal of the American Chemical Society*, Vol. 125, 2003, pp. 15233–15242.
- [142] Marrink, S. J. and Mark, A. E., “The mechanism of vesicle fusion as revealed by molecular dynamics simulations,” *Journal of the American Chemical Society*, Vol. 125, 2003, pp. 11144–11145.
- [143] de Vries, A., Mark, A., and Marrink, S., “Molecular dynamics simulation of the spontaneous formation of a small DPPC vesicle in water in atomistic detail,” *Journal of the American Chemical Society*, Vol. 126, 2004, pp. 4488–4489.
- [144] Braun, R., Engelman, D. M., and Schulten, K., “Molecular dynamics simulations of micelle formation around dimeric glycophorin A transmembrane helices,” *Biophysical Journal*, Vol. 87, 2004, pp. 754–763.
- [145] Yagui et al., C. R., 2004., Ongoing Collaboration.

- [146] Kausch, C. M., Kim, Y., Russell, V. M., Medsker, R. E., and Thomas, R. R., “Surface tension and adsorption properties of a series of bolaamphiphilic poly(fluorooxetane)s,” *Langmuir*, Vol. 19, 2003, pp. 7182–7187.

Chapter 2

Complementary Use of Simulations and Molecular-Thermodynamic Theory to Model Micellization

2.1 Introduction

Surfactants are used in many pharmaceutical, industrial, and environmental applications because of their unique solution properties. When dissolved in water, surfactant molecules self-assemble into micellar aggregates, with their hydrophobic tails shielded from water in the aggregate interior, and their hydrophilic heads exposed to water at the aggregate surface. This self-assembly is driven primarily by the hydrophobic effect, although van der Waals, hydrogen-bonding, and screened electrostatic interactions (in the case of charged surfactants) also play an important role in determining how micellization occurs [1].

Because micellization is such a broadly applicable phenomenon, gaining a fundamental understanding of the factors that affect it is of great academic as well as practical relevance. Frequently, a highly specific set of micellar solution characteristics is required for a given application. These characteristics typically include the critical micelle concentration (CMC) and the shape and size of the micellar aggregates

that form in solution.

Theoretical work has been carried out in the past to enable the *a priori* prediction of the CMC and the structure of the micellar aggregates from knowledge of the chemical structures of the surfactant(s) present in solution [2–7]. However, to date, theoretical methodologies have been developed only for relatively simple surfactant systems. The most advanced theoretical descriptions that have been developed can be used to model surfactants with linear and branched hydrocarbon (or fluorocarbon) tails and a single, rigid head, such as, sodium dodecyl sulfate (SDS) and cetyl trimethyl ammonium bromide (CTAB), or a polymeric head group such as poly(ethylene oxide) [3, 8–10].

Currently, the most accurate theoretical models of surfactant micellization make use of a predictive molecular-thermodynamic approach [9]. A number of researchers have worked on this approach in the past [2, 3, 8, 9]. The micellization description introduced by Nagarajan and Ruckenstein allows prediction of the CMC and the shape and size of micellar aggregates composed of nonionic, zwitterionic, and ionic surfactants [3]. In the molecular-thermodynamic approach, the free-energy change associated with the formation of the surfactant aggregate is expressed as the sum of several free-energy contributions, all of which can be computed molecularly given the chemical structures of the surfactant. In recent years, our group has made important progress in the molecular modeling of surfactant solution behavior, both in the bulk solution [2, 9–15] and at interfaces [16–20].

Molecular-thermodynamic modeling works well for surfactants that possess a relatively simple chemical structure. However, a major current challenge to use the molecular-thermodynamic approach to model surfactant micellization is that for the approach to yield accurate predictions, a reasonable *a priori* estimate must be made about how a given surfactant will position and orient itself within the micelle. Such an identification is necessary because the interaction energies involved depend on the specific position and orientation of the surfactant molecule within the micelle. In the case of surfactants possessing more complex chemical structures, devoid of clearly

identifiable hydrophilic and hydrophobic moieties, it may be difficult to determine what portions of a surfactant molecule should be modeled as the head and what portions should be modeled as the tail in the context of molecular-thermodynamic micellization theories.

An alternative to using molecular-thermodynamic descriptions of micellization is to use molecular dynamics (MD) or Monte Carlo (MC) computer simulations to simulate the formation of micelles. In theory, MD and MC simulations based on an atomistic forcefield have the advantage of being capable of modeling arbitrarily complex chemical structures. Recently, various researchers have explored this approach [21–42]. However, an atomistic-level description of micelle formation is computationally challenging because: (i) micelles may consist of many surfactant molecules, and (ii) of the liquid-like density of micelles. Although simulations of micelle formation with atomistic-level detail are possible, because simulation time is severely limited by the size and density of micellar systems, such simulations have only been performed well *above* the CMC [31]. Indeed, at or around the CMC, computer simulation of micelle formation requires simulation of a large-sized system over prohibitively long time scales [31]. To reduce the computational complexity, researchers have implemented coarse-grained models when attempting to estimate the CMC. Lattice and off-lattice models have been used with simple intermolecular interaction potentials [23–31]. Significant simplifications have been made in these studies to reduce the computational demands on the simulation. For example, Larson et al. modeled oil, water, and surfactant by treating the surfactant head and tail segments as being identical to water and oil beads. Such simplified descriptions are not capable of accurately predicting solution behavior, and have prevented these researchers from obtaining more accurate predictions using simulations than using free-energy models [43].

Given the shortcomings of the current modeling approaches, there is a need to develop a predictive, molecular-level theoretical description that can predict the solution behavior of complex surfactant systems. Molecular-thermodynamic methods are

most applicable for systems with relatively simple surfactant chemical structures, and computer simulations, although capable of modeling complex chemical structures, are computationally very expensive.

With this in mind, McCormick et al. developed an approach which combines computer simulations and a molecular-thermodynamic model of micellization, and applied it to model a system consisting of cetyltrimethylammonium bromide (CTAB) and sodium salicylate (NaSal) [43]. These authors used computer simulations to: (i) determine how a complex counterion (salicylate) would locate and orient itself in a CTAB micelle, and (ii) calculate the free-energy change associated with exchanging the Sal^- ions with the surfactant molecules. McCormick et al. obtained reasonable estimates of the effect of the Sal^- ions on the CMC, the aggregate geometry, and the aggregate size. To accomplish (i), the salicylate ion was simulated in a micellar environment using Monte Carlo simulations. This information was then used in (ii) to divide the micelle into a “core” region, modeled solely using molecular-thermodynamic modeling, and a “head-shell” region, modeled using both molecular-thermodynamic models of micellization and computer simulation.

In this chapter, we show that molecular dynamics simulations of complex surfactant molecules at an oil/water interface (modeling the micelle core/water interface) can be used to identify what portions of the surfactant should be modeled as the head and what portions should be modeled as the tail in the context of molecular-thermodynamic theories of micelle formation. Instead of simulating the surfactant molecule in a micellar environment, as was done by McCormick et al., we will show that simulation of a single surfactant molecule at a flat oil/water interface is sufficient in many cases to determine input parameters for the molecular-thermodynamic modeling approach. When appropriate, simulation at a flat interface has the advantage of computational simplicity—*simulation times are kept to a minimum by simulating a single surfactant molecule instead of the entire micelle.* By combining computer simulations and molecular-thermodynamic theory, we will show that it is possible to model more complex surfactants with less computational expense than has been

possible to date.

The remainder of this chapter is organized as follows. The molecular-thermodynamic approach to model surfactant self-assembly is reviewed in Section 2.2. Section 2.3 describes the computer simulation approach used in this chapter. Computer simulation results are presented in Section 2.4. Molecular-thermodynamic modeling results based on computer simulation inputs are described and compared with available experimental data in Section 2.5. Concluding remarks are presented in Section 2.6.

2.2 Molecular-Thermodynamic Approach

The molecular-thermodynamic approach relies on a thermodynamic framework to describe the micellar solution [9]. This framework permits the calculation of solution properties, such as the critical micelle concentration (CMC), the distribution of aggregate shapes and sizes, and microstructural characteristics of the aggregate (such as its core minor radius) from the free energy of micellization. In Section 2.2.1, we briefly describe the thermodynamic framework that relates the free energy of micellization to various micellar solution characteristics, and in Section 2.2.2, we review molecular-thermodynamic techniques that have been developed and used in the past to calculate the free energy of micellization [8–10].

2.2.1 Thermodynamic Framework

The theoretical framework considered here is applicable for nonionic, zwitterionic, and ionic surfactants with bound counterions at the micellar surface. Consider a solution of N_w water molecules and a distribution $\{N_{n_s n_c}\}$ of micellar aggregates at thermodynamic equilibrium at temperature T and pressure P , where n_s is the number of surfactant molecules (component s) and n_c is the number of bound counterions (component c) in each aggregate. Micellar aggregates will form in solution if the surfactant concentration exceeds the CMC.

According to the multiple-chemical equilibrium model [1], each aggregate can be considered as a distinct chemical species in equilibrium with the other aggregates and with the individually-dispersed molecules present in the solution. At thermodynamic equilibrium, the solution free energy attains its minimum value, which implies that [9]:

$$\mu_{n_s n_c} = n_s \mu_s + n_c \mu_c \quad (2.1)$$

The chemical potential, $\mu_{n_s n_c}$, in Eq. 2.1 can be calculated by taking the partial derivative of the total solution free energy with respect to $N_{n_s n_c}$ [9,10]. The chemical potentials of the surfactant monomers, μ_s , and of the unbound counterions, μ_c , are obtained by setting $\{n_s = 1, n_c = 0\}$ and $\{n_c = 1, n_s = 0\}$, respectively, in the resulting expression for $\mu_{n_s n_c}$ [9,10].

Using the resulting expressions for μ_s and μ_c in Eq. 1, the following expression is obtained for the population distribution of $n_s n_c$ -mers:

$$X_{n_s n_c} = \left(\frac{1}{e}\right) (X_s e)^{n_s} (X_c e)^{n_c} \exp \left[-\frac{1}{k_B T} (\mu_{n_s n_c}^o - n_s \mu_s^o - n_c \mu_c^o) \right] \quad (2.2)$$

In Eq. 2.2, X_s is the mole fraction of the monomeric surfactant and X_c is the mole fraction of the unbound counterions (where $X_i = N_i/N$, $i = s$ or c). Note that the factors of e appearing in Eq. 2.2 reflect the manner in which we have defined mole fractions, which is different from the more conventional definition, $X_i = N_i / (N_w + \sum_{n_s} \sum_{n_c} \sum_{n_a} N_{n_s n_c n_a})$ [8,44].

Alternatively, Eq. 2.2 can be expressed in terms of the degree of counterion binding (β_j , defined as $\beta_j = n_{c_j}/n_s$). Using this definition in the case where multiple counterion species are present, the resulting aggregates can be treated as $n_s \{\beta_j\}$ -mers, where β_j is the degree of counterion binding of counterion species j . Defining g_{mic}

as the free-energy gain of micellization per surfactant molecule, Eq. 2.2 becomes:

$$X_{n_s\{\beta_j\}} = \left(\frac{1}{e}\right) X_s^{n_s} \exp\left(-\frac{n_s g_{mic}}{k_B T}\right) \quad (2.3)$$

where

$$g_{mic} = \left[\frac{\mu_{n_s n_c}^o}{n_s} - \bar{\mu}_s^o - \sum_j \beta_j \bar{\mu}_{c_j}^o \right] - \sum_j \beta_j k_B T \ln X_{c_j} \quad (2.4)$$

with $\bar{\mu}_i^o = \mu_i^o + k_B T$.

The free energy of micellization, g_{mic} , reflects the free-energy changes associated with transferring the surfactant monomers and the counterions in their corresponding standard states from the aqueous solution to form an aggregate in its standard state (the term in the square brackets in Eq. 4), as well as with the translational entropic penalty associated with localizing the counterions (the second term in Eq. 4) when that aggregate is formed [9].

For the values of n_s , β_j , and the micellar shape (S) that minimize g_{mic} (denoted as n_s^* , β_j^* , and S^*), g_{mic} has a minimum value denoted as g_{mic}^* . Due to the exponential dependence of $X_{n_s n_c}$ on $n_s \cdot g_{mic}$ in Eq. 2.3, small deviations from g_{mic}^* yield $X_{n_s n_c}$ values that are negligibly small. Accordingly, by solving for g_{mic}^* as a function of n_s^* , β_j^* , and S^* , the optimal aggregation number, n_s^* , can be predicted. In addition, the CMC of the surfactant is given by [9]:

$$CMC = \exp\left(\frac{g_{mic}^*}{k_B T}\right) \quad (2.5)$$

Note that Eq. 2.5 is obtained as an upper bound of the surfactant monomer concentration (X_s).

2.2.2 Molecular Model of Micellization

The evaluation of g_{mic} , using as little experimental information as possible, has been the subject of much investigation. The most recent theoretical description of g_{mic}

requires knowledge of the chemical structures of the surfactants and the counterions, as well as an estimate of how the surfactants will locate and orient themselves within the micellar aggregate [9].

A surfactant aggregate can be characterized as follows: (i) the aggregate geometry (S), (ii) the aggregate composition (β_j), and (iii) the aggregate core minor radius (l_c). Minimization of g_{mic} with respect to each of these variables enables the prediction of aggregate characteristics and of the CMC [8,9].

The free energy of micellization (g_{mic}) is modeled as the sum of various free-energy contributions (each a function of S , β_j , and l_c), and of the translational entropy loss of the bound counterions. The quantity g_{mic} is calculated using the following expression [9]:

$$g_{mic} = g_{tr} + g_{int} + g_{pack} + g_{st} + g_{elec} + g_{ent} - k_B T \left(1 + \sum_j \beta_j \right) - \sum_j \beta_j k_B T \ln(X_{c_j}) \quad (2.6)$$

where each term is discussed below.

Approaches have been developed to calculate each contribution listed in Eq. 2.6. Specifically, g_{tr} , or the transfer free energy, is typically computed from experimental solubility data [45]. The interfacial free energy, g_{int} , is computed from the surfactant tail/water interfacial tension data, mixing rules, and the use of the Gibbs-Tolman-Koenig-Buff equation to approximate the dependence of the tail/water interfacial tension on curvature [8]. A relatively complex numerical procedure is used to compute the packing free-energy contribution (g_{pack}), in which a large number of the possible conformations of the surfactant tails within the aggregate core are generated to determine the free energy required to fix the tail moieties at the aggregate/water interface [9]. Analytical techniques have been developed to compute the steric free-energy contribution (g_{st}) that arises from packing the surfactant heads at the aggregate/water interface [46]. The electrostatic free-energy contribution (g_{elec}) results from the electrostatic repulsions between ionic groups, if present, in the micellar aggregate [9]. Analytical approximations have been developed to calculate this contribution that

are based on the Poisson-Boltzmann equation or its modifications [47].

Each of the free-energy contributions appearing in Eq. 2.6 depends on how the surfactant molecule is identified as being located and oriented within the micelle. Surfactant segments that are shielded from water in the micelle core contribute directly to the transfer (g_{tr}) and to the packing (g_{pack}) free-energy contributions. The steric (g_{st}) and the electrostatic (g_{elec}) free-energy contributions reflect interactions that operate within the head-shell region of the micelle, where water molecules are also present. Finally, the interfacial free-energy contribution, g_{int} , depends on what portions of the surfactant molecule are identified as lying at the aggregate/water interface. As a result, to accurately calculate the free energy of micellization in Eq. 6, it is imperative to know how the surfactant molecules will locate and orient themselves within the micelle.

Previously, the approximate hydrophilicity or hydrophobicity of the various atoms comprising the surfactant molecules was determined using Molecular Modelling Pro [48], a computer program that makes use of a proprietary group-contribution method to estimate the hydrophilic and the hydrophobic portions of molecules [49]. For relatively simple surfactants such as sodium dodecyl sulfate (SDS), Molecular Modeling Pro identifies the sulfate (SO_4^-) group as being quite hydrophilic, and the first methylene (CH_2) group attached to SO_4^- as also being somewhat hydrophilic [9]. Therefore, in previous studies, the first CH_2 group in the alkyl chain attached to the SO_4^- group was not included as contributing to g_{tr} or to g_{pack} . On this basis, the SO_4^- and the first CH_2 group were identified as the surfactant head. For alkyl poly(ethylene oxide) surfactants, Molecular Modeling Pro indicates that only the ethylene oxide groups are hydrophilic, implying that all the CH_2 groups in the alkyl chain are shielded from water. Making these assumptions in identifying the heads and tails of relatively simple surfactants has yielded reasonable predictions in previous studies [8, 10].

The group-contribution approach underlying Molecular Modeling Pro, although successfully applied to relatively simple surfactants with clearly identifiable hydrophilic

and hydrophobic portions, is not adequate in the case of surfactants possessing a more complex chemical structure. Indeed, more complex surfactants can have multiple hydrophilic and hydrophobic portions within their structure, and therefore, in such cases, it is not clear *a priori* how such molecules will orient within a micellar aggregate. Because of these shortcomings, in this chapter, computer simulations at an oil/water interface (modeling the micelle core/water interface) are used to identify the hydrophilic and hydrophobic portions of surfactant molecules.

2.3 Molecular Dynamics Simulations

2.3.1 Computational Approach

In this section, we describe our efforts to use computer simulations to determine the effective head and tail of the surfactant involved in the micellization process. By performing a simple molecular dynamics (MD) simulation, the average position of a surfactant molecule at an oil/water interface has been determined. The interactions between each atom comprising the surfactant molecule and its environment are described using the all-atom Optimized Performance for Liquid Systems (OPLS-AA) force field [50]. This method permits the determination of the effective head and the effective tail portions of the surfactant, even in cases where the chemical structure is sufficiently complex that such a division is not apparent *a priori*.

The computer simulation approach presented here is most applicable to a surfactant that adopts a consistent position and orientation relative to an oil/water interface which is similar to the position and orientation that it will adopt within a micellar environment. When the surfactant position and orientation depends strongly on factors such as the interface radius of curvature and the presence of neighboring surfactant molecules, this relatively simple method may not be applicable, because the input parameters for the molecular-thermodynamic theory may not be constant (specifically, they may become functions of aggregate shape, aggregation number, and aggregate composition). In such cases, the method presented here may not be accu-

rate. However, it is noteworthy that full-micellar simulations that we have conducted recently—the results of which are currently in preparation for publication—indicate that water/oil interface simulations serve as an effective proxy for full-micellar simulations in determining molecular-thermodynamic input parameters for a wide range of chemical structures.

2.3.2 Simulation Parameters

We have carried out computer simulations of sodium dodecyl sulfate (SDS), cetyltrimethylammonium bromide (CTAB), dodecylphosphocholine (DPC), dodecyl poly(ethylene oxide) (C₁₂E₈), 3-hydroxy sulfonate (AOS), and decanoyl-*n*-methylglucamide (MEGA-10) using the OPLS-AA forcefield. Some additional parameters (needed to describe angles and angle vibrations) were taken from the literature in order to more accurately model the sulfate (SO₄⁻) head in SDS [51]. Dodecylphosphocholine (DPC) was modeled using the united-atom GROMACS forcefield with parameters implemented by Tieleman et al. [52]. It is noteworthy that the GROMACS forcefield [53] is not an all-atom forcefield, and treats all methylene (CH₂) and methyl (CH₃) groups as unified atoms. Water was treated explicitly using the simple extended point-charge model (SPC-E) for water [54]. Van der Waals interactions were treated using a cutoff distance of 1.2 nm, and Coulombic interactions were described using Particle Mesh Ewald (PME) summation. All simulations were run using fixed bond lengths, which allowed the simulation timestep to be set at 2 fs.

Two different approaches were used to assign atomic charges to the surfactant and the oil molecules. In the first set of simulations, atomic charges were assigned based on the atomic charges specified within the OPLS-AA forcefield. Because charge parameterization was not available for SO₄⁻ in the OPLS-AA forcefield, atomic charges implemented by other researchers in their computer simulations of SDS micelles were used instead [51]. In the second set of simulations, the atomic charges were determined using the CHelpG method implemented in *Gaussian 98* [55]. The CHelpG algorithm assigns atomic charges to fit calculated electrostatic potentials at a number

of points on the van der Waals surface. This method is frequently used to estimate atomic charges for molecular mechanics simulations [56]. Octane was selected as our model “oil” for all the computer simulations. We believe, based on full-micellar simulation results that are currently in preparation for publication, that similar results should be obtained using both longer and shorter alkane molecules. Atomic charges on each surfactant, with the exception of SDS, and on octane were predicted using the *RBLYP* density functional and the *6-31G(d)* basis set [56]. Because of the presence of the sulfur atom in SDS, a larger *6-31+G(3df)* basis set was used to predict atomic charges for this surfactant. To ensure self-consistency of the simulation parameters, the same charge assignment method was used in each simulation for both the surfactant and the octane molecules. In other words, when OPLS-AA atomic charges were used to model the surfactant molecule in a simulation, OPLS-AA atomic charges were also used to model the octane molecules. Because SPC-E charge groups have been carefully optimized to match experimental data of the physical and structural characteristics of water, these charge parameters were not changed [54].

2.3.3 System Preparation and Equilibration

All the reported simulations were performed using the GROMACS software package, version 3.2 [57,58]. For each interfacial simulation, a single surfactant molecule was placed between a layer of water and a layer of octane, with the interface oriented parallel to the x - y plane. The water and the octane layers, in turn, were surrounded by vacuum. Each simulation cell was specified to be 4.0 nm long in the x and y dimensions, a distance large enough to approximate “infinite dilution” for the simulated surfactant molecule. The thicknesses of the simulated oil and water layers varied from 10 to 30 nm, and were specified such that approximately 10 nm separated the surfactant molecule from the surrounding vacuum to prevent the presence of vacuum (as opposed to bulk water or octane) from affecting the simulation results. The presence of the vacuum made it unnecessary to adjust the simulation cell dimensions to attain pressure equilibration. As a result, all the reported simulations were

carried out at a constant volume. In both the equilibration and the data-gathering simulation runs, the simulation cell temperature was maintained at 300 K using a Berendsen temperature coupling algorithm implemented in GROMACS [59].

After constructing the water-surfactant-octane system, each simulation cell was allowed to equilibrate for at least 100 ps before gathering data. In the case of $C_{12}E_8$, 1-2 ns was required for the initially fully-extended E_8 head to reach its equilibrium position relative to the octane/water interface. However, the other surfactants simulated appeared to reach an equilibrium configuration at the interface much more rapidly (within 100 ps). This was verified by showing that the local environment of each surfactant molecule had stabilized using the data analysis method described in the following section.

2.3.4 Data Analysis Method

To identify the local environment of each surfactant atom, two analysis methods were investigated. In the first analysis method, the number of contacts per timestep experienced by different surfactant atoms with water and with octane was counted over the course of a simulation run. In this method, a contact was defined as two atoms approaching each other within a set distance at any time during the simulation. Because the van der Waals radii of the simulated atoms ranged between 0.12–0.19 nm, a reasonable minimum distance to identify such contacts is twice the maximum van der Waals radii, or around 0.38 nm. The distance was set at 0.4, 0.5, and 0.6 nm, and the results were found not to be sensitive to the value of the distance chosen. Both the size of the atom and its local environment affect the number of contacts that it experiences with water and with octane. The larger the surfactant atom under consideration, the greater the number of water or octane molecules that will surround it, and the greater the number of contacts that will be recorded during a simulation. By computing the ratio of the number of contacts with water and the number of contacts with octane for each surfactant atom, these size effects cancel out and it is possible to determine whether the surfactant atom is surrounded primarily by water

or by octane. Computer simulations conducted on a surfactant molecule surrounded entirely by water, as well as on the same surfactant molecule surrounded entirely by octane, revealed that a surfactant molecule in bulk water is contacted 1.13 times as often as a surfactant molecule in bulk octane. Based on this result, any surfactant atom contacting water over 1.13 times as often as it contacts octane is surrounded, on average, more by water than by octane. For the purpose of carrying out molecular-thermodynamic modeling, any surfactant atom that is surrounded primarily by water will be approximated as being entirely in the water phase, and will therefore be included as part of the surfactant head. To make the presentation of the results more intuitive, each contact ratio has been scaled by a factor of $1/1.13$, or 0.88. On this basis, a scaled contact ratio greater than one indicates that a surfactant atom makes more contacts with water than with octane, and is therefore part of the surfactant head. Conversely, a scaled contact ratio smaller than one indicates that a surfactant atom is part of the surfactant tail. Note that the scaling factor of 0.88 corrects for the atom density difference between octane and water, and therefore, should not be a strong function of the chemical structure of the surfactant simulated in order to determine this correction factor.

An estimate of the error in the evaluation of each scaled contact ratio was carried out using block averaging, a useful technique to analyze correlated data [60–62]. In general, error estimates for correlated data (such as data obtained from MD simulations) are underestimated. Block averaging removes the effect of this correlation to yield an accurate estimate of error by dividing the simulation data into blocks and then computing averages for each block. If each block is sufficiently large, successive blocks become uncorrelated and an accurate estimate of the error can be obtained. This approach was implemented by computing the the standard error of the mean from the variance between averages of each block of data, and increasing the block size until the standard error estimate stopped increasing. To aid in the identification of this asymptotic value, an analytical block average curve (based on the assumption that the autocorrelation in the data can be described as the sum of two exponentials)

was fit to the standard error versus block size data [60–62].

In the second analysis method, we computed density profiles along the z -axis of each simulation cell for water, for octane, and for each surfactant atom. Each surfactant atom fluctuates around an average position relative to the water-octane interface. The distribution of the positions of each atom is broadened by capillary waves at the water/octane interface. Experimental and computer simulation results indicate that this distribution is well described by a Gaussian function [63–65]. Accordingly, the density distribution for each surfactant atom generated from the computer simulation results was fit to a Gaussian curve. Each atom was then identified as part of the surfactant head or tail by comparing the peak of the atom’s Gaussian density distribution to the location of the water/octane interface. The location of the water/octane interface was determined by first normalizing the water and the octane density profiles by the bulk densities of pure water and pure octane, respectively, and then by identifying the point at which the water and the surfactant densities were equal. Very similar results were obtained using both number-weighted and mass-weighted density profiles. With sufficient simulation time, the density profile for each surfactant atom should generate a smooth Gaussian curve [63–65]. The second analysis method was used to analyze each of the surfactants considered in this chapter. However, the density profiles generated during the course of the 1-6 ns simulations that we conducted did not result in a smooth, Gaussian profile for the surfactant atom density distribution. The noise in the density data made the identification of the surfactant head or tail groups using this method approximate. More generally, the identification of the surfactant head and tail based on the contact analysis method is more reliable than that based on the second method because: (i) the density histogram data is too noisy to accurately fit a Gaussian function to the data in all cases, and (ii) the contact data conveys direct information about the local environment of each surfactant atom at any given time step during the simulation. In addition, the contact analysis method provides a convenient method to quantitatively determine the standard error. Therefore, in the remainder of the chapter, we will

only present results based on the contact analysis method.

2.4 Simulation Results and Discussion

To determine the accuracy of the proposed computer simulation approach, we first modeled a relatively simple anionic (SDS), cationic (CTAB), zwitterionic (DPC), and nonionic ($C_{12}E_8$) surfactant. Extensive experimental data is available in the literature for these surfactants, thus enabling comparison with our theoretical predictions of CMCs and weight-average micelle aggregation numbers. Following that, we studied two additional surfactants, possessing more complex chemical structures, to further test the range of applicability of the proposed approach. The first surfactant, AOS, is anionic, and the second one, MEGA-10, is nonionic. In Sections 2.4.1-2.4.6, we discuss each of these six surfactants separately.

2.4.1 Sodium Dodecyl Sulfate (SDS)

SDS is a widely-used, anionic surfactant for which extensive experimental micellization data is available. A sample simulated scaled contact ratio profile for SDS located at the water-octane interface is shown in Figure 2-1, where the data presented is based on a 1 ns simulation of SDS using OPLS-AA atomic charge assignments. In Figure 2-1, the simulated scaled contact ratio (as described in Section 2.3.4) is shown for groups of surfactant atoms. The horizontal dashed line denotes a scaled contact ratio of one. Surfactant groups whose scaled contact ratios are greater than one (above the horizontal dashed line) are identified as being part of the surfactant head. Conversely, surfactant groups whose scaled contact ratios are smaller than one (below the horizontal dashed line) are identified as being part of the surfactant tail. Figure 2-1 shows that both the SO_4^- group and the first CH_2 group experience more scaled contacts with water than with octane, and both are therefore part of the surfactant head. All the other groups have a scaled contact ratio smaller than one, and are therefore part of the surfactant tail.

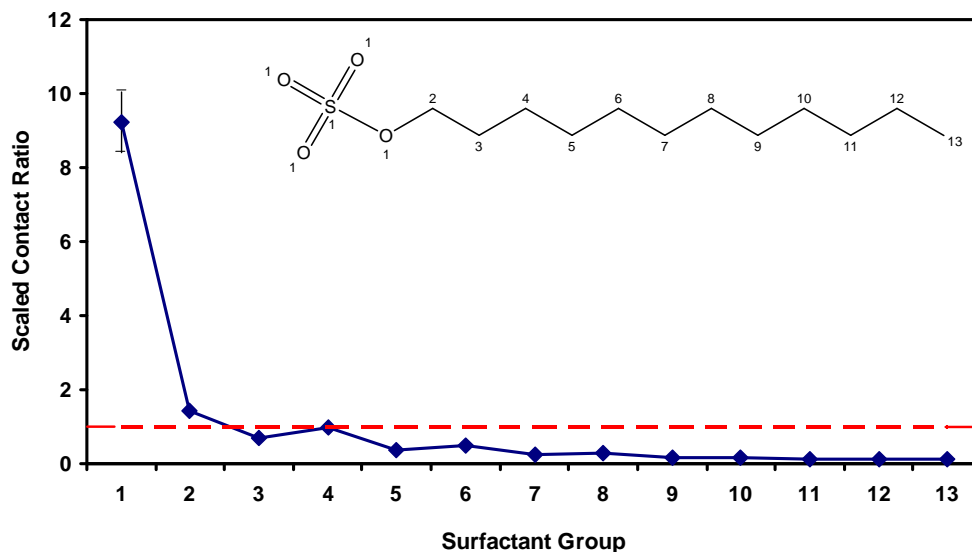


Figure 2-1: Scaled contact ratios predicted using simulations are plotted for each SDS surfactant group, where the scaled contact ratio is defined as the number of contacts of each surfactant group with water divided by the number of contacts of the same group with octane (for details, see Section 2.3.4). Each ratio is based on contact data averaged over the course of a 1 ns simulation run. Error bars are shown for each scaled contact ratio, although only the error associated with the sulfate group is large enough to be visible. The dashed horizontal line is drawn at a contact ratio of one, which represents the dividing line between what we identify to be part of the surfactant “head” (scaled contact ratio > 1) or part of the surfactant “tail” (scaled contact ratio < 1).

In Table 2.1, we list scaled contact ratios and standard errors for SDS determined from simulations based on the assignments of CHelpG and OPLS-AA atomic charges. The scaled contact ratios are reported in the same form as that shown in Figure 2-1. In some cases, averaged results for groups of several atoms (as in the case of SO_4^-) are presented to reduce the amount of reported data. Note that scaled contact ratios corresponding to the surfactant head are shown in bold. In Tables 2.1-2.6, which report our computer simulation results, only those atoms that are part of either the surfactant head or the surfactant tail have been grouped together. The standard error of the mean for each scaled contact ratio (calculated through the block averaging approach discussed in Section 2.3.4) is reported to provide a measure of the statistical significance of the results. If the scaled contact ratio for each group is changed by plus or minus the standard error computed for that group, none of the head and tail assignments reported in Table 2.1 would change. Therefore, we consider the head and tail assignment for each group to be statistically significant. As shown in Table 2.1, both methods of assigning atomic charges indicate that SO_4^- and the first CH_2 group attached to the sulfate moiety are part of the surfactant head. If n denotes the total number of carbon atoms in the surfactant alkyl chain, then the computer simulation results indicate that the number of carbon atoms that should actually be included in the surfactant tail is $(n - 1)$.

2.4.2 Cetyltrimethylammonium Bromide (CTAB)

CTAB is a commonly-used cationic surfactant for which extensive experimental micellization data is available. In Table 2.2, we list scaled contact ratios determined for CTAB using simulations based on the assignment of CHelpG and OPLS-AA atomic charges. In some cases, averaged results for groups of several atoms (as in the case of each methyl group attached to nitrogen) are presented to reduce the amount of reported data. The standard error of the mean for each scaled contact ratio is reported to provide a measure of the statistical significance of the results. Based on the criteria discussed in Section 2.4.1, all the head and tail assignments made are statisti-

CHelpG Atomic Charge Assignments, 1 ns Simulation													
Group	1	2	3	4	5	6	7	8	9	10	11	12	13
SCR	7.37	1.11	0.72	0.66	0.37	0.36	0.24	0.24	0.19	0.20	0.18	0.25	0.17
SE	0.45	0.09	0.05	0.04	0.03	0.04	0.04	0.05	0.04	0.05	0.04	0.07	0.04

OPLS-AA Atomic Charge Assignments, 1 ns Simulation													
Group	1	2	3	4	5	6	7	8	9	10	11	12	13
SCR	9.23	1.43	0.69	0.92	0.38	0.48	0.22	0.27	0.17	0.17	0.14	0.13	0.13
SE	0.80	0.08	0.05	0.07	0.03	0.06	0.03	0.05	0.04	0.06	0.06	0.07	0.07

Table 2.1: Simulated scaled contact ratios (SCR) and standard errors (SE) for SDS based on the assignment of: i) CHelpG atomic charges, and ii) OPLS-AA atomic charges. Scaled contact ratios corresponding to the surfactant "head" are shown in bold.

cally significant. Our results indicate that either ($n-2$) carbon atoms are part of the surfactant tail, as predicted using the CHelpG assignment of atomic charges, or that ($n-3$) carbon atoms are part of the surfactant tail, as predicted using the OPLS-AA assignment of atomic charges. Note that both estimates differ from the ($n-1$) value predicted for SDS (see Table 2.1). The predicted ($n-3$) value appears too small for reasons that will be discussed in more detail in Section 2.5.2. The scaled contact ratios deduced from all our simulations were quite noisy in the case of CTAB, and relatively long (2 to 3 ns) simulations were necessary to reduce the magnitude of the error in the simulated scaled contact ratios in order to obtain statistically meaningful results.

The OPLS-AA assignment of atomic charges yields a slightly more polarized charge distribution than that obtained using the CHelpG algorithm. Our simulation results show that this increased polarity has a significant effect on the simulation results, and therefore, on the identification of the surfactant head and tail in the case of CTAB. Clearly, the correct assignment of atomic charges is of paramount importance

CHelpG Atomic Charge Assignments, 2 ns Simulation											
Group	1	2	3	4	5	6	7	8	9	10	11
SCR	5.56	9.30	3.87	7.02	2.64	1.21	0.91	0.47	0.20	0.06	0.04
SE	1.10	1.44	0.53	0.56	0.22	0.11	0.06	0.05	0.04	0.04	0.03

OPLS-AA Atomic Charge Assignments, 3 ns Simulation											
Group	1	2	3	4	5	6	7	8	9	10	11
SCR	7.37	8.99	7.72	7.83	3.83	1.81	1.11	0.62	0.29	0.12	0.11
SE	1.03	1.58	1.81	0.79	0.37	0.13	0.08	0.05	0.05	0.07	0.07

Table 2.2: Simulated scaled contact ratios (SCR) and standard errors (SE) for CTAB based on the assignment of: i) CHelpG atomic charges, and ii) OPLS-AA atomic charges. Scaled contact ratios corresponding to the surfactant "head" are shown in bold.

to correctly identify the surfactant head and tail.

2.4.3 Dodecylphosphocholine (DPC)

DPC is a popular zwitterionic surfactant used as a model membrane system for the NMR study of lipid-bound peptides and proteins because it resembles common phosphatidylcholine lipids [66]. DPC was selected for this study because it is zwitterionic, and because experimental and computer simulation results are available for this surfactant [52, 66, 67].

The forcefield parameters used in our simulations are the same as those used by Tieleman et al. in their computer simulation work [?, 52, 66, 67]. We have determined the head and the tail of DPC using both the CHelpG atomic charge assignments and the atomic charge parameters used by Tieleman et al.

As Table 2.3 shows, predictions based on the CHelpG atomic charge assignments indicate that all the carbon atoms in the dodecyl chain attached to PO_4^- are part of the surfactant tail, while those based on the atomic charge assignments of Tieleman et

CHelpG Atomic Charge Assignments, 3 ns Simulation															
Group	1	2	3	4	5	6	7	8	9	10	11	12	13	14	15
SCR	4.40	2.39	2.41	4.21	1.84	2.08	0.66	0.35	0.28	0.18	0.15	0.11	0.10	0.08	0.08
SE	0.69	0.31	0.41	0.29	0.17	0.12	0.05	0.03	0.04	0.04	0.03	0.03	0.02	0.02	0.02

Tieleman Atomic Charge Assignments, 3 ns Simulation															
Group	1	2	3	4	5	6	7	8	9	10	11	12	13	14	15
SCR	50.85	27.71	32.99	81.79	46.25	4.26	1.05	0.80	0.36	0.23	0.15	0.10	0.09	0.08	0.07
SE	16.32	9.85	19.16	39.80	18.11	0.18	0.05	0.05	0.02	0.02	0.03	0.02	0.03	0.03	0.03

Table 2.3: Simulated scaled contact ratios (SCR) and standard errors (SE) for DPC based on the assignment of: i) CHelpG atomic charges, and ii) OPLS-AA atomic charges. Scaled contact ratios corresponding to the surfactant "head" are shown in bold.

al. indicate that the first CH_2 group attached to PO_4^- should not be included as part of the surfactant tail. Averaged results for groups of several carbon and hydrogen atoms have been reported near the tail end of the surfactant to reduce the amount of reported data. The standard error of the mean for each scaled contact ratio is reported, and show that all the head and tail assignments made are statistically significant. A discussion of the modeling results obtained based on both identifications of the surfactant head and tail, including commentary on which identification is most accurate, is presented in Section 2.5.5.

2.4.4 Dodecyl Poly(Ethylene Oxide) (C_{12}E_8)

C_{12}E_8 was selected as our model nonionic surfactant. This surfactant has been the subject of considerable study because of its industrial relevance [68]. The interaction of this nonionic surfactant with the water/octane environment lacks the strong electrostatic forces present in the case of the ionic surfactants SDS and CTAB considered above. Before conducting the simulations, it was not clear whether the ionic, zwitterionic, or nonionic surfactants considered would have their head and tail groups predicted most accurately using the OPLS-AA forcefield.

Each of the ethylene oxide (EO) groups present in $C_{12}E_8$ was found, after extended simulation time, to come to equilibrium sandwiched between the water and the octane layers, rather than to extend into the water layer. Most likely, this conformation was adopted to shield the maximum possible number of water molecules from the octane molecules, and hence, to maximize the entropy of water. Unfortunately, because the EO groups were wedged between the water and the octane molecules, it was more difficult to accurately identify the head and the tail of $C_{12}E_8$. In a micellar environment, of course, such a conformation would not be possible because crowding by neighboring surfactant heads would force the E_8 moiety away from the aggregate core/water interface and into the water phase. Scaled contact ratios and standard errors of the mean for $C_{12}E_8$ are presented in Table 2.4. In Table 2.4, to reduce the amount of reported data, we have reported averaged results for groups of several atoms. Results vary significantly based on the atomic charge assignments made. One should note that the standard errors on the mean of the scaled contact ratios are large enough to prevent statistically significant head or tail identification for several groups, in particular, for groups 8, 9, and 11 when CHelpG atomic charges were used, and for groups 2, 7, and 8 when OPLS-AA atomic charges were used.

Based on extensive modeling work done by other researchers and by our own research group, as well as on experimental NMR evidence, we conclude that the head and tail identifications made using the CHelpG atomic charge assignments shown in Table 2.4 are not appropriate for modeling the micellization of $C_{12}E_8$ because the existing evidence suggests that each EO group in a $C_{12}E_8$ micelle is hydrated [3, 8, 63, 69]. Although the scaled contact ratio results based on the assignment of OPLS-AA atomic charges are more reasonable, the fact that EO groups 1 and 2 and CH_2 group 12 are identified as being part of the surfactant tail suggests that infinite-dilution simulation of polymeric, nonionic surfactants at an interface does not give reliable results for molecular-thermodynamic modeling. However, group 13 listed in Table 2.4 is identified as being part of the surfactant head, while group 14 is identified as being part of the surfactant tail, which is consistent with previous work

CHelpG Atomic Charge Assignments, 3 ns Simulation																
Group	1	2	3	4	5	6	7	8	9	10	11	12	13	14	15	16
SCR	1.68	1.07	0.65	0.71	0.81	0.69	0.90	0.99	1.06	1.08	1.06	0.70	0.75	0.51	0.34	0.16
SE	0.10	0.05	0.04	0.04	0.07	0.06	0.08	0.10	0.09	0.07	0.11	0.06	0.05	0.04	0.04	0.09

OPLS-AA Atomic Charge Assignments, 3 ns Simulation																
Group	1	2	3	4	5	6	7	8	9	10	11	12	13	14	15	16
SCR	0.10	0.90	1.21	2.56	3.88	1.75	1.03	1.16	1.44	1.67	1.74	0.88	1.11	0.61	0.43	0.18
SE	0.20	0.13	0.17	0.65	1.23	0.44	0.13	0.28	0.30	0.13	0.19	0.07	0.05	0.05	0.05	0.06

Table 2.4: Simulated scaled contact ratios (SCR) and standard errors (SE) for $C_{12}E_8$ based on the assignment of: i) CHelpG atomic charges, and ii) OPLS-AA atomic charges. Scaled contact ratios corresponding to the surfactant “head” are shown in bold.

which suggests that n carbon atoms should be included as part of the $C_{12}E_8$ tail. Molecular-thermodynamic modeling results based on this identification of the head and the tail of $C_{12}E_8$ are presented in Section 2.5.4.

Because of the flat conformation adopted by the E_8 moiety at the water/octane interface, it is not surprising that subtle differences in the assignment of atomic charges have a significant impact on the identification of the $C_{12}E_8$ head and tail using the computer simulation approach presented here.

2.4.5 3-Hydroxy Sulfonate (AOS)

Sodium α -olefinsulfonates (AOS) are ionic surfactants used frequently in household and industrial formulations [70]. These surfactants are useful because of their salient wetting and detergency attributes, as well as for their tolerance for hard water ions. AOS, as it is used industrially, is a mixture of several chemical species, composed of: 60-70% sodium alkenesulfonate, 30% hydroxyalkanesulfonate, and 0-10% sodium disulfonate. The hydroxyalkanesulfonate fraction is present in both the 3-hydroxy sulfonate and the 4-hydroxy sulfonate forms [70]. In addition, the hydroxyalkanesulfonate backbone can contain between 12 and 18 carbon atoms.

We have selected two hydroxyalkanesulfonates for modeling to determine if computer simulations can be used to correctly identify the head and tail portions of surfactants with: (i) two hydrophilic groups (SO_3^- and OH) connected by hydrophobic CH_2 groups, and (ii) two different carbon backbone lengths ($n = 12$ and 16 carbons).

Scaled contact ratios and standard errors for the ($n = 12$ and 16) 3-hydroxy sulfonate surfactants at a water/octane interface are presented in Table 2.5. In some cases, averaged results for groups of several atoms are reported to reduce the amount of reported data. Both simulations based on CHelpG atomic charges were conducted for 3 ns, which gave statistically significant results for all the groups with the exception of groups 3 and 4 in the 12 carbon 3-hydroxy sulfonate. The scaled contact ratio values deduced from all our simulations were quite noisy, and for the simulations using OPLS-AA atomic charges, 6 ns simulations were required to reduce the magnitude of the error in the calculated contact ratios and to obtain statistically meaningful results.

The simulation results presented in Table 2.5, based on the CHelpG and the OPLS-AA assignments of atomic charges, indicate that both surfactants should be modeled as having ($n-3$) carbon atoms in the surfactant tail. Based on the CHelpG results, groups 3 and 4 in the 12 carbon 3-hydroxy sulfonate cannot be assigned conclusively to be part of the surfactant head or of the surfactant tail given the statistical uncertainty in their scaled contact ratios. However, the OPLS-AA data for this surfactant is statistically significant, and indicates that both groups are part of the surfactant head. In spite of the hydrophobicity of groups 2 and 3, our results indicate that the close proximity of the SO_3^- and the OH moieties forces these groups into the water phase. For a surfactant such as 3-hydroxy sulfonate, which possesses two hydrophilic groups separated by a carbon backbone, computer simulations provide important insight into which groups are hydrated and which are not.

CHelpG Atomic Charge Assignments, $n = 12$, 3 ns Simulation								
Group	1	2	3	4	5	6	7	8
SCR	7.82	1.32	0.94	1.02	1.89	0.48	0.52	0.20
SE	0.71	0.13	0.10	0.13	0.19	0.04	0.11	0.06
CHelpG Atomic Charge Assignments, $n = 16$, 3 ns Simulation								
Group	1	2	3	4	5	6	7	8
SCR	10.87	3.57	1.54	2.83	2.34	0.59	0.81	0.17
SE	1.67	0.73	0.30	0.21	0.18	0.07	0.15	0.03
OPLS-AA Atomic Charge Assignments, $n = 12$, 6 ns Simulation								
Group	1	2	3	4	5	6	7	8
SCR	9.27	1.78	2.02	1.11	2.48	0.62	0.43	0.16
SE	0.35	0.10	0.08	0.08	0.13	0.03	0.04	0.02
OPLS-AA Atomic Charge Assignments, $n = 16$, 6 ns Simulation								
Group	1	2	3	4	5	6	7	8
SCR	9.37	1.81	2.43	1.11	2.25	0.71	0.47	0.15
SE	0.53	0.10	0.25	0.07	0.17	0.04	0.04	0.02

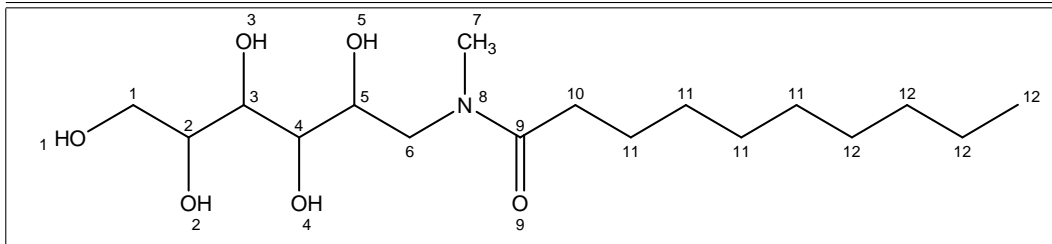
Table 2.5: Simulated scaled contact ratios (SCR) and standard errors (SE) for $n = 12$ and $n = 16$ (where n is the alkyl chain length of group 8) 3-hydroxy sulfonate (AOS) based on the assignment of: i) CHelpG atomic charges, and ii) OPLS-AA atomic charges. Scaled contact ratios corresponding to the surfactant "head" are shown in bold. The results for $n = 12$ and $n = 16$ were identical, and are therefore reported together.

2.4.6 Decanoyl-*n*-Methylglucamide (MEGA-10)

Recently, alkylpolyglucoside (APG) nonionic surfactants such as MEGA-10 have generated great interest because of their unique solution properties [71]. APG surfactants are both more strongly lipophobic and hydrophilic when compared with ethoxylated C_iE_j nonionic surfactants [71]. In addition, they have great practical value because they are biodegradable and dermatologically safe [71]. As a nonionic surfactant with a relatively complex hydrophilic moiety, MEGA-10 allows us to further test the range of applicability of the proposed computer simulation approach to identify the head and tail portions of surfactants possessing a more complex chemical structure. Note that MEGA-10 is considered a relatively complex surfactant because it contains an amide group (groups 8 and 9 in Table 2.6), which is a structure that has not been modeled in the past using molecular-thermodynamic models of micellization due to the difficulty in identifying the appropriate head and tail portions of this surfactant.

As shown in Table 2.6, the simulation results depend on the method used to assign atomic charges. Averaged results for groups of similar atoms are presented in some cases to reduce the amount of reported data. The standard error of the mean for each scaled contact ratio is reported to provide a measure of the statistical significance of the results. The standard errors of the mean for the scaled contact ratios are large enough to prevent statistically significant head or tail identification for several groups. This is the case for group 4 when CHelpG atomic charges are used, and for group 3 when OPLS-AA atomic charges are used. Some of the unexpected head or tail assignments (particularly for group 4) are due to the nonionic glucoside moieties spreading out between the water and the oil layers, as opposed to extending into the water phase. This is similar to what was observed for the E_8 moiety in $C_{12}E_8$. In a micellar environment, of course, such a spread conformation would not be allowed because of crowding by neighboring surfactant heads. As a result, each of the C-OH groups in MEGA-10 will be considered as part of the surfactant head in molecular-thermodynamic modeling.

The main difference between the CHelpG and the OPLS-AA atomic charge assign-



CHelpG Atomic Charge Assignments, 3 ns Simulation												
Group	1	2	3	4	5	6	7	8	9	10	11	12
SCR	1.86	2.63	1.59	0.91	1.75	0.64	0.34	1.17	0.89	0.68	0.56	0.45
SE	0.37	0.83	0.42	0.26	0.23	0.22	0.06	0.09	0.05	0.07	0.10	0.34
OPLS-AA Atomic Charge Assignments, 3 ns Simulation												
Group	1	2	3	4	5	6	7	8	9	10	11	12
SCR	2.25	3.69	1.01	0.42	1.24	0.30	0.39	0.68	0.55	0.70	0.56	0.25
SE	0.27	1.01	0.13	0.04	0.23	0.04	0.08	0.09	0.03	0.16	0.09	0.04

Table 2.6: Simulated scaled contact ratios (SCR) and standard errors (SE) for MEGA-10 based on the assignment of: i) CHelpG atomic charges, and ii) OPLS-AA atomic charges. Scaled contact ratios corresponding to the surfactant "head" are shown in bold.

ments is that the nitrogen atom (group 8) is identified as being part of the surfactant head when the CHelpG atomic charges are used, while it is identified as being part of the surfactant tail when the OPLS-AA atomic charges are used. In both cases, all n carbon atoms in the linear alkyl chain are included as part of the surfactant tail. Molecular-thermodynamic modeling results using both estimates for the MEGA-10 head and tail portions are presented and discussed in Section 2.5.6.

2.5 Molecular-Thermodynamic Modeling Based on Computer Simulation Inputs

In Section 2.4, a computer simulation approach was introduced to determine surfactant head and tail input parameters for use in molecular-thermodynamic modeling. Specifically, we used this approach to identify the head and tail portions of SDS, CTAB, DPC, C₁₂E₈, AOS, and MEGA-10. In this section, the head and

tail portions of each surfactant determined in Section 2.4 are used as inputs in a molecular-thermodynamic theory of micellization developed by our group to predict various useful micellization properties of the surfactants considered [8–10]. Using the thermodynamic framework presented in Section 2.2.1 and the molecular model of micellization presented in Section 2.2.2, CMCs and weight-average micelle aggregation numbers for each surfactant are predicted, and the results are compared with available experimental data in Sections 2.5.1-2.5.6.

2.5.1 Sodium Dodecyl Sulfate (SDS)

As discussed in Section 2.4.1, computer simulation results, based both on the CHelpG and the OPLS-AA charge assignments, indicate that the SO_4^- group and the CH_2 group attached to it should be modeled as being part of the surfactant head. If the number of surfactant carbons is denoted by n , the number of carbons shielded from water within the micelle core is therefore equal to $(n-1)$. Using this information, a number of parameters needed as inputs for molecular-thermodynamic modeling can be defined based on the proposed surfactant chemical structure. First, a_h —the cross-sectional area of the surfactant head—must be specified, and can be estimated from knowledge of the chemical structure of the surfactant head. Specifically, the cross-sectional area of $\text{SO}_4\text{-CH}_2$ is equal to that of the larger SO_4^- group. Based on the sulfur-oxygen bond length and the cross-sectional area of oxygen, a_h was estimated to be 25 \AA^2 . To accurately treat electrostatic effects (that is, the repulsions between the negatively-charged SO_4^- groups), the distance between the beginning of the surfactant tail and the location of the charge in the surfactant head must be specified. This distance (d_{charge}) includes the length of the CH_2 group attached to the SO_4^- group, and is equal to 3.7 \AA . Finally, the length of the surfactant head (l_{hg}), or the distance from the tip of the surfactant head to the start of the surfactant tail, must be specified, and is equal to 5.57 \AA . Using these inputs, it is possible to estimate each of the contributions to the free energy of micellization shown in Eq. 2.6. Theoretical predictions for each of these free-energy contributions are reported in Table 2.7 to

g_{mic}	g_{tr}	g_{int}	g_{pack}	g_{st}	g_{elec}	CMC _{pred}	$\langle N \rangle_w$, pred	CMC _{expt}	$\langle N \rangle_w$, expt
-8.67 kT	-18.45 kT	4.34 kT	2.51 kT	1.09 kT	4.36 kT	9.6 mM	44	8.1 mM	74

Table 2.7: Molecular-thermodynamic modeling results for SDS using the “head” and “tail” identifications predicted based on computer simulation. The predicted transfer (g_{tr}), interfacial (g_{int}), packing (g_{pack}), steric (g_{st}), and electrostatic (g_{elec}) contributions to the free energy of micellization (g_{mic}) are presented, and theoretical predictions for the CMC and the weight-average micelle aggregation number $\langle N \rangle_w$ are presented and compared with the corresponding experimental values. The following input parameters were used: $a_h = 25 \text{ \AA}^2$, $d_{\text{charge}} = 3.7 \text{ \AA}$, and $l_{hg} = 5.57 \text{ \AA}$ (see text).

allow comparison of the relative contribution that each makes to g_{mic} . Molecular-thermodynamic modeling has been performed for an SDS/water solution at 25 °C, the temperature at which experimental CMC and weight-average micelle aggregation numbers were measured [1, 72].

Our predictions of the CMC and the weight-average micelle aggregation number, $\langle N \rangle_w$, using the head and tail surfactant portions determined from computer simulation are also reported in Table 2.7. Our predicted CMC is 9.6 mM, in close agreement with the experimental value of 8.1 mM [1]. The $\langle N \rangle_w$ value is predicted to be 44, which is significantly lower than the experimental value of 74 [72]. The smaller $\langle N \rangle_w$ value predicted reflects the fact that in the current molecular-thermodynamic description, micellar aggregates are approximated as being either perfectly spherical, cylindrical, or flat in geometry. In the case of SDS, a spherical shape was predicted by the model to be the optimal shape, and as a result, a perfect spherical geometry was used to model the SDS micelle. In fact, SDS micelles are somewhat non-spherical under the solution conditions considered here, allowing them to have an aggregation number which is larger than what has been predicted [1].

The identification of the surfactant head and tail made for SDS through computer simulation is fully consistent with what was assumed previously in performing molecular-thermodynamic modeling [9]. Modeling an SDS micelle as having water penetration up to the first CH_2 group attached to the polar surfactant head is also consistent with experimental evidence obtained from NMR measurements of SDS micelles [73]. For purposes of comparison, if the first CH_2 group attached to SO_4^-

in SDS is taken to be part of the tail instead of part of the head, our molecular-thermodynamic theory predicts a much lower CMC of 4.27 mM, which is almost two times smaller than the experimentally reported CMC of 8.1 mM. This reflects the more negative transfer free-energy contribution associated with transferring the additional CH₂ group from the water phase to the micelle core. The sensitivity of the predictions to the proper identification of what atoms should be included in the surfactant head and tail, and the close agreement between our theoretical predictions and experiments, suggests that the computer simulation results that we have obtained for SDS are valid.

2.5.2 Cetyltrimethylammonium Bromide (CTAB)

As discussed in Section 2.4.2, our computer simulation results indicate that the first two (based on the CHelpG assignment of atomic charges) or three (based on the OPLS-AA assignment of atomic charges) CH₂ groups attached to the trimethyl ammonium (CH₃)₃-N moiety in CTAB should be modeled as being part of the surfactant head. Input parameters (a_h , d_{charge} , and l_{hg}) required to model CTAB using molecular-thermodynamic theory have been estimated based on both head and tail identifications using the same approach described for the modeling of SDS in Section 2.5.1. Molecular thermodynamic modeling results obtained using both sets of input parameters are reported in Table 2.8. The surfactant head predicted based on the CHelpG atomic charges results in a CMC prediction of 1.32 mM and in a weight-average micelle aggregation number prediction of 50. The head predicted using the OPLS-AA atomic charges results in a CMC prediction of 2.56 mM and in a weight-average micelle aggregation number prediction of 42. The most important free-energy term contributing to the difference in CMC predictions based on the CHelpG and OPLS-AA atomic charges is the transfer free energy (g_{tr}). As can be seen in Table 2.8, including an additional CH₂ group as part of the surfactant head makes g_{tr} less negative by approximately $1.5 k_B T$. The experimental CMC and weight-average micelle aggregation number for CTAB are 0.9 mM and 90, respec-

CHelpG Atomic Charges: head = (CH ₃) ₃ N-CH ₂ -CH ₂ -				
g_{tr}	CMC _{pred}	$\langle N \rangle_{w, pred}$	CMC _{expt}	$\langle N \rangle_{w, expt}$
-22.93 kT	1.32 mM	50	0.9 mM	90
OPLS-AA Atomic Charges: head = (CH ₃) ₃ N-CH ₂ -CH ₂ -CH ₂ -				
g_{tr}	CMC _{pred}	$\langle N \rangle_{w, pred}$	CMC _{expt}	$\langle N \rangle_{w, expt}$
-21.44 kT	2.56 mM	42	0.9 mM	90

Table 2.8: Molecular-thermodynamic modeling results for CTAB using the “head” and “tail” identifications predicted based on: i) the CHelpG atomic charges, and ii) the OPLS-AA atomic charges. The predicted free energy of micellization (g_{mic}) and transfer free-energy contribution (g_{tr}) are presented for the “head” and “tail” identifications made. Theoretical predictions of the CMC and the weight-average micelle aggregation number $\langle N \rangle_w$ are reported and compared with the corresponding experimental values. Based on the CHelpG “head” and “tail” assignment, the following input parameters were used: $a_h = 32 \text{ \AA}^2$, $d_{charge} = 3.8 \text{ \AA}$, and $l_{hg} = 6.36 \text{ \AA}$ (see text). Based on the OPLS-AA “head” and “tail” assignment, the following input parameters were used: $a_h = 32 \text{ \AA}^2$, $d_{charge} = 5.1 \text{ \AA}$, and $l_{hg} = 7.66 \text{ \AA}$ (see text).

tively [74].

Clearly, the CHelpG predictions for the surfactant head are in closer agreement with the experimental values than the predictions based on the OPLS-AA atomic charges [74]. The OPLS-AA forcefield is not well-parameterized for the (CH₃)₃N⁺-CH₂- group present in CTAB, and the atomic charge assignment used in this case was based on similar, but not exactly analogous, compounds. The nitrogen in (CH₃)₃-N⁺-CH₂- contains three CH₃ groups adjacent to the positively-charged nitrogen, and unfortunately, only atomic charge parameters for a simple CH₃ group adjacent to NH₃⁺ were available. Therefore, it is not particularly surprising that the OPLS-AA results are not as accurate. Our results suggest that using the CHelpG atomic charges is more accurate than using the OPLS-AA atomic charges determined based on ionic surfactants which are not completely analogous to the actual surfactant under consideration.

It is also interesting to compare the CHelpG results that we have obtained with the results that would be obtained using the $(n - 1)$ convention that has been used previously in molecular-thermodynamic modeling of ionic micelles [9]. If the $(n - 1)$

convention is used, molecular-thermodynamic theory predicts a CMC of 0.68 and a weight-average micelle aggregation number of 50. Therefore, in moving from modeling the system with the $(n - 1)$ convention to the $(n - 2)$ prediction based on the CHelpG computer simulation results, the CMC goes from being slightly underpredicted to being slightly overpredicted. Both the $(n - 1)$ and the $(n - 2)$ carbon atom assignments for the CTAB tail yield reasonable results for the CMC, and therefore, both tail assignments appear acceptable from a molecular-thermodynamic modeling perspective.

2.5.3 Dodecylphosphocholine (DPC)

As discussed in Section 2.4.3, application of the atomic charge assignments used by Tieleman et al. indicates that the first carbon atom in DPC's linear alkyl chain should be included as part of the surfactant head. On the other hand, the CHelpG atomic charge assignments indicate that all the carbon atoms should be included as part of the surfactant tail. The head cross-sectional area (a_h) and the distance separating the two charges present in the zwitterionic surfactant head (d_{sep}) were each identified based on the chemical structure of the surfactant and the two surfactant head and tail identifications made (they are the same in both cases), and were used as inputs for molecular-thermodynamic modeling.

Molecular-thermodynamic modeling results for DPC are shown in Table 2.9. The surfactant head identified based on the CHelpG atomic charges yields a CMC prediction of 0.24 mM and a weight-average micelle aggregation number prediction of 56. The surfactant head identified using the OPLS-AA atomic charge yields a CMC prediction of 0.95 mM and a weight-average micelle aggregation number prediction of 48. The experimental values are 1.0 mM for the CMC and 44 for the weight-average micelle aggregation number [66].

Our theoretical results based on the OPLS-AA atomic charge assignments are in excellent agreement with the experimental results for DPC, while those based on the CHelpG atomic charge assignments underpredict the CMC by a factor of 4 [66].

CHelpG Atomic Charges			
CMC _{pred}	$\langle N \rangle_w$, pred	CMC _{expt}	$\langle N \rangle_w$, expt
0.24 mM	56	1.0 mM	44 ± 5
OPLS-AA Atomic Charges			
CMC _{pred}	$\langle N \rangle_w$, pred	CMC _{expt}	$\langle N \rangle_w$, expt
0.95 mM	48	1.0 mM	44 ± 5

Table 2.9: Molecular-thermodynamic modeling results for DPC using the “head” and “tail” identifications predicted based on: i) the CHelpG atomic charges, and ii) the OPLS-AA atomic charges. The predicted free energy of micellization (g_{mic}) and the theoretically predicted CMC and weight-average micelle aggregation number $\langle N \rangle_w$ are reported and compared with the corresponding experimental values. The following input parameters were used: $a_h = 32 \text{ \AA}^2$ and $d_{sep} = 4.33 \text{ \AA}$ (see text).

The micelle aggregation number predicted using the OPLS-AA atomic charges is also in closer agreement with the experimental value than that predicted based on the CHelpG atomic charges [66].

2.5.4 Dodecyl Octa(Ethylene Oxide) ($C_{12}E_8$)

As discussed in Section 2.4.4, we had difficulty in determining the head and tail portions of $C_{12}E_8$ using near infinite-dilution simulations of $C_{12}E_8$ at the octane/water interface. Nevertheless, the head and tail results based on the OPLS-AA atomic charge assignments indicated that all n carbons in the linear alkyl chain of $C_{12}E_8$ should be included as part of the surfactant tail—a result that appears reasonable based on specular neutron reflectivity measurements and hydrogen/deuterium isotopic labelling, as well as on previous molecular-thermodynamic modeling experience [8, 65].

To use molecular-thermodynamic theory to model micellization of non-ionic surfactants, only the head cross-sectional area, a_h , must be specified [8]. An estimate of a_h for the E_8 head was made based on previous theoretical and experimental studies of C_iE_j surfactants conducted within our group. In these studies, correlations were developed to predict the average E_j head size in a micellar environment as a function of temperature and the concentration of salt present in the solution [8].

Theoretical results are presented in Table 2.10 based on the head and tail identifi-

CMC _{pred}	$\langle N \rangle_w$, pred	CMC _{expt}	$\langle N \rangle_w$, expt
0.53 mM	41	0.1 mM	69

Table 2.10: Molecular-thermodynamic modeling results for C₁₂E₈ using the “head” and “tail” identifications predicted based on computer simulation. The predicted free energy of micellization (g_{mic}) and the theoretically predicted CMC and weight-average micelle aggregation number $\langle N \rangle_w$ are reported and compared with the corresponding experimental values. Correlations developed to predict the average E₈ “head” size in a micellar environment ($a_h = 61.1 \text{ \AA}^2$) were used (see text).

cations made using the OPLS-AA computer simulation results and our estimate of a_h based on the head identification. The predicted values for the CMC (0.53 mM) and for the weight-average micelle aggregation number (41) are in reasonable agreement with the experimental values (0.1 mM and 69, respectively) [68].

2.5.5 3-Hydroxy Sulfonate (AOS)

The computer simulation results presented in Section 2.4.5 indicate that each 3-hydroxy sulfonate surfactant has ($n-3$) carbon atoms that should be included as part of the surfactant tail. The head cross-sectional area (a_h), the charge distance (d_{charge}), and the length of the head (l_{hg}) have been identified for each of the two surfactants based on their chemical structures. For each surfactant, a_h was derived from the cross-sectional area of SO₃⁻, the bulkiest group in the surfactant head.

Molecular-thermodynamic modeling predictions for the CMC of 3-hydroxy sulfonates with carbon chains of length $n = 12$ and $n = 16$ are presented in Table 2.11, along with the experimental CMC values [75]. Theoretical modeling was done at 30 °C in a pure water/3-hydroxy sulfonate solution—the same solution conditions corresponding to the experimental data. Micelle aggregation number predictions are not shown because only CMC experimental data was available for this system. The theoretically predicted CMCs, based on the computer simulation inputs, are in excellent agreement with the experimental values. The agreement obtained confirms that the head and tail identifications made based on computer simulations are appropriate for molecular-thermodynamic modeling. In fact, the head and tail identifications made

$n = 12$	
CHelpG and OPLS-AA Atomic Charges	
CMC _{pred}	CMC _{expt}
25.4 mM	24.8 mM
$n = 16$	
CHelpG and OPLS-AA Atomic Charges	
CMC _{pred}	CMC _{expt}
1.48 mM	1.45 mM

Table 2.11: Molecular-thermodynamic modeling results for $n = 12$ and $n = 16$ 3-hydroxy sulfonates using the “head” and “tail” identifications made using simulations. Since the “head” and “tail” predicted based on the CHelpG atomic charges and the OPLS-AA atomic charges were the same, the results are reported together. Theoretically predicted CMCs are reported and compared with the experimental CMC values. The following input parameters were used: $a_h = 23 \text{ \AA}^2$, $d_{\text{charge}} = 5.27 \text{ \AA}$, and $l_{hg} = 7.14 \text{ \AA}$ (see text).

result in the best possible agreement with the available experimental CMC data. Changing the tail identification to include ($n-2$) or ($n-4$) carbon atoms for either of the AOS surfactants considered here would lead to a significant underprediction and overprediction of the CMC, respectively.

2.5.6 Decanoyl-*n*-Methylglucamide (MEGA-10)

As discussed in Section 2.4.6, the computer simulation identification of the head and tail portions for MEGA-10 was found to depend on the atomic charge assignment method used. Simulations based on the OPLS-AA atomic charge assignment indicated that nitrogen should be included as part of the surfactant tail, while the CHelpG atomic charge assignment indicated that it should be included as part of the surfactant head.

The tail structure identified for MEGA-10 is significantly more complex than the linear or the branched hydrocarbons that have been modeled in the past using molecular-thermodynamic theory. In modeling relatively simple surfactants having linear alkyl chains, a simple empirical correlation describing aqueous solubility as a

function of chain length and of the solution temperature has been used in previous studies [3,8–10]. Aqueous solubility is related to the transfer free energy by the relationship $g_{tr} = k_B T \ln(s)$, where s is the aqueous solubility of the compound expressed on a mole fraction basis. In order to determine g_{tr} for the more complex tail moiety of MEGA-10, which includes both hydrophobic and hydrophilic groups as well as a branched structure, a generalized approach was needed in order to estimate aqueous solubilities for more complex chemical structures.

Estimation of aqueous solubility from molecular structure has been the subject of much research, since solubility is an important physical property in many practical applications, including drug delivery [76]. Aqueous solubility depends strongly on the presence of functional groups with the ability to hydrogen-bond, such as carboxyl and amino groups [76]. Accurate determination of aqueous solubility is complicated by the fact that it is a function of both temperature and salt concentration. Property-solubility relationships, structure-solubility relationships, and group-contribution approaches can all be used to estimate solubilities [76]. Property-solubility relationships relate solubility to another physical property that is experimentally known or which can be estimated. Structure-solubility relationships and group-contribution approaches rely on relating molecular size, shape, and connectivity indices to solubility. Some of the better-known approaches are Quantitative Structure-Water Solubility Relationships (QSWSRs), and group-contribution methods such as those developed by Kopman, Wang, and Blthasar, by Wkita, Yoshimoto, Miyamoto, and Watanabe, or those based on the AQUAFAC approach [76].

In the case of MEGA-10, we have used a computer program developed by Tetko et al., based on the use of associative neural networks for the prediction of lipophilicity, to estimate the aqueous solubility of the tail group identified using the CHelpG atomic charges and the OPLS-AA atomic charges. This program was developed using 1,291 test molecules, and the predictions using the program were found to fit experimental data with an RMS of 0.49 and a standard deviation of 0.38 [77, 78].

Similar to the case of $C_{12}E_8$ discussed in Section 2.5.4, it was only necessary to

estimate the head cross-sectional area, a_h , to use molecular-thermodynamic theory to model the micellization of the MEGA-10 surfactant. The cross-sectional area of the short, polymeric hydroxyl sugar moiety present in MEGA-10 depends on the conformations that it adopts in a micellar environment. An estimate of a_h was made by extracting the average radius of gyration of the head from our computer simulation results. In a micellar environment, the area per surfactant head would be expected to be smaller because of crowding effects. Therefore, estimates obtained in this manner should be regarded as an upper-bound estimate for the head cross-sectional area. The values of a_h obtained through this analysis are 62 \AA^2 and 68 \AA^2 based on the CHelpG and OPLS-AA atomic charge assignments, respectively. Using these a_h estimates, molecular-thermodynamic modeling indicates that MEGA-10 forms spherical micelles.

Table 2.12 presents theoretical predictions for the free energy of micellization (g_{mic}), the transfer free energy (g_{tr}), the CMC, and the weight-average micelle aggregation number, $\langle N \rangle_w$, for MEGA-10 based on the CHelpG and the OPLS-AA atomic charge predictions of the surfactant head and tail. Using the CHelpG atomic charge results, a CMC of 8.16 mM and a weight-average micelle aggregation number of 42 are predicted. This is in reasonable agreement with the experimental values of 5 mM and 71 for the CMC and the weight-average micelle aggregation number, respectively [71]. If the surfactant head area, a_h , is lowered by just 10%, the predicted CMC decreases from 8.16 mM to 4.66 mM, in very close agreement with the experimental value. Since the a_h value used represents an upper-bound on the surfactant head area, the results suggest that a more realistic method of determining the head area of MEGA-10 in a micellar environment would yield better predictions.

Using the OPLS-AA atomic charge results, the predicted CMC and weight-average micelle aggregation number are 663.8 mM and 33, respectively. These predictions, based on only a slightly different head and tail identification, are in poor agreement with the experimental results. In this case, the effect of including the nitrogen atom in the surfactant tail has a large effect on the modeling results. Because this

CHelpG Atomic Charges				
g_{tr}	CMC _{pred}	$\langle N \rangle_w$, pred	CMC _{expt}	$\langle N \rangle_w$, expt
-16.89 kT	8.16 mM	42	5 ± 0.05 mM	71
OPLS-AA Atomic Charges				
g_{tr}	CMC _{pred}	$\langle N \rangle_w$, pred	CMC _{expt}	$\langle N \rangle_w$, expt
-13.09 kT	663.8 mM	33	5 ± 0.05 mM	71

Table 2.12: Molecular-thermodynamic modeling results for MEGA-10 using the “head” and “tail” identifications predicted based on: i) the CHelpG atomic charges, and ii) the OPLS-AA atomic charges. The predicted free energy of micellization (g_{mic}) and the predicted transfer free-energy contribution (g_{tr}) are provided for the two “head” and “tail” identifications made. Theoretically predicted CMCs and weight-average micelle aggregation numbers $\langle N \rangle_w$ are reported and compared with the corresponding experimental values. The following input parameters were used: $a_h = 62 \text{ \AA}^2$ (based on the CHelpG results) and 68 \AA^2 (based on the OPLS-AA results) (see text).

group is hydrophilic, its inclusion in the surfactant tail makes the transfer free-energy contribution (g_{tr}) less favorable (less negative) than that of the tail identified using the CHelpG atomic charge results. This, in turn, makes micellization less favorable and greatly increases the CMC.

Clearly, the CHelpG predictions of the surfactant head yield more reasonable predictions than those obtained using the OPLS-AA atomic charges. This is similar to what was observed in modeling CTAB [74]. Unfortunately, the OPLS-AA forcefield is not well-parameterized for the tertiary ammino geometry present in MEGA-10, just as it was not well-parameterized for the trimethyl amino geometry present in CTAB. As a result, the atomic charge assignments used in this case were based on secondary amines that are similar, but not exactly analogous, in structure. Our results suggest that using CHelpG assignments for atomic charges is more accurate for both ionic and nonionic surfactants than applying OPLS charge assignments which were determined for compounds that are not perfectly analogous to the actual surfactant under consideration.

2.6 Conclusions

We have presented a novel modeling approach that incorporates inputs from atomistic-level computer simulations in a molecular-thermodynamic description of micellar self-assembly. The central goal of implementing computer simulations in the relatively simple manner presented in this chapter was to extend the range of applicability of molecular-thermodynamic descriptions to model surfactants possessing more complex chemical structures by providing information about how such surfactants will localize and orient themselves within a micellar aggregate.

Two methods were used to determine atomic charges for each surfactant considered in this chapter. The first method involves using the CHelpG approach, in which atomic charges are assigned to fit electrostatic potentials at a number of points on the van der Waals surface [55]. The second method involves using the atomic charges recommended in the OPLS-AA forcefield or, if these are not available, using atomic charge assignments reported in the literature. The computer simulation results were found, in general, to be quite sensitive to the atomic charge assignment method used. Our results indicate that the charge assignments recommended within the OPLS-AA forcefield give more reasonable results than those obtained using the CHelpG algorithm if the molecular structures present in the surfactant of interest have been specifically parameterized in the forcefield. This is to be expected, since in proper forcefield parametrization, atomic charges are one degree of freedom that is tuned so that the computer simulation predictions agree as closely as possible with the experimental structural and physical properties. However, our results for CTAB and MEGA-10 indicate that if a forcefield has not been adequately parameterized for the surfactant of interest, the CHelpG method can provide a useful approach to estimate appropriate atomic charges.

A contact ratio analysis method was implemented to determine the head and tail portions of the surfactants considered in this chapter. In this method, the number of contacts made by a surfactant atom with water and with octane are recorded during

the course of a simulation. By taking the ratio of the number of contacts recorded for each atom with water and with octane, it is possible to infer whether the atom is surrounded primarily by water or by octane during the simulation run. We also attempted to use a density profile analysis to determine the average location of each surfactant atom relative to the location of the octane/water interface. However, noise in the density data and the fact that this method does not convey direct information about the local environment of each surfactant atom makes the results based on this analysis method less reliable than those obtained using the contact analysis method. For this reason, results based on the density profile analysis method were not reported.

Good agreement between our theoretical predictions and the experimental data was observed as long as adequate atomic charges were used in the computer simulations. Because predicted micellar properties are highly sensitive to the surfactant head and tail identifications made, our results suggest that when a properly parameterized forcefield is used, computer simulation results are reasonably accurate. With the exception of $C_{12}E_8$, simulation of an individual surfactant molecule at a flat octane/water interface was found to be a reasonable substitute for simulating the surfactant molecule at a curved, micelle/water interface. In the case of $C_{12}E_8$, the flexible, polymeric nature of the E_8 moiety allowed it to localize between the water and the octane layers, and prevented appropriate head and tail identifications from an infinite-dilution octane/water interface simulation. Although octane/water interface simulations gave reasonable results for every surfactant considered in this chapter except $C_{12}E_8$, such simulations may not be appropriate for more complex surfactants with multiple hydrophobic and hydrophilic “pockets” present in their molecular structure. For such surfactants, where location and orientation within a micellar aggregate may depend on a delicate balance of electrostatic, hydrogen-bonding, and van der Waals interactions, a simulation that incorporates the effect of neighboring surfactant molecules and of the curvature of the micellar aggregate may be necessary to accurately identify the appropriate surfactant head and tail portions for input into

the molecular-thermodynamic modeling. We are currently developing other modeling approaches to predict the micellization behavior of such complex surfactants.

The results presented in this chapter indicate that using computer simulations to determine input parameters for molecular-thermodynamic theories of micellization can extend the range of applicability of such theories to allow modeling of surfactants possessing more complex chemical structures. In the case of surfactants such as 3-hydroxy sulfonate or MEGA-10, the relatively complex chemical structures of these molecules makes the *a priori* identification of how they will locate and orient themselves in a micellar aggregate difficult and highly speculative. However, as shown in this chapter, by performing relatively simple computer simulations of such surfactants at a flat octane/water interface, appropriate head and tail identifications can be made for use as inputs for successful molecular-thermodynamic modeling of micellization.

In the next chapter, Chapter 3, the computer simulation/molecular-thermodynamic modeling approach developed here will be used to model the micellar solubilization of ibuprofen by nonionic, anionic, and cationic surfactants. In the modeling presented in Chapter 3, simplifying approximations will be made to allow evaluation of the packing free-energy contribution, g_{pack} , using the same mean-field chain packing model used in this chapter. In addition, predictions of the micellar solubilization behavior of ibuprofen will be made using what is effectively a binary surfactant micellization model. In Chapter 4, a general computer simulation/molecular-thermodynamic model of micellar solubilization will be presented. Computer simulation results for solubilize head and tail and the molecular-thermodynamic model of micellar solubilization introduced in Chapter 4 will be used in Chapter 5 to make predictions of the micellar solubilization of seven different solubilizes by nonionic, anionic, and cationic surfactants.

Bibliography

- [1] Israelachvili, J. N., *Intermolecular and Surface Forces*, Academic Press, 2nd ed., 1991.
- [2] Shiloach, A. and Blankschtein, D., “Predicting micellar solution properties of binary surfactant mixtures,” *Langmuir*, Vol. 14, 1998, pp. 1618–1636.
- [3] Nagarajan, R. and Ruckenstein, E., “Theory of surfactant self-assembly: A predictive molecular thermodynamic approach,” *Langmuir*, Vol. 7, 1991, pp. 2934–2969.
- [4] Gunnarsson, G., Jonsson, B., and Wennerstrom, H., “Surfactant association into micelles - An electrostatic approach,” *The Journal of Physical Chemistry*, Vol. 84, 1980, pp. 3114–3121.
- [5] Jonsson, B. and Wennerstrom, H., “Thermodynamics of ionic amphiphile-water systems,” *Journal of Colloid and Interface Science*, Vol. 80, 1981, pp. 482–496.
- [6] Evans, D. F., Mitchell, D. J., and Ninham, B. W., “Ion binding and dressed micelles,” *The Journal of Physical Chemistry*, Vol. 88, 1984, pp. 6344–6348.
- [7] Hayter, J. B., “A self-consistent theory of dressed micelles,” *Langmuir*, Vol. 8, 1992, pp. 2873–2876.
- [8] Puvvada, S. and Blankschtein, D., “Molecular thermodynamic approach to predict micellization, phase behavior and phase separation of micellar solutions. 1.

Application to nonionic surfactants,” *The Journal of Chemical Physics*, Vol. 92, 1990, pp. 3710–3724, and references cited therein.

- [9] Srinivasan, V. and Blankschtein, D., “Effect of counterion binding on micellar solution behavior: 1. Molecular-thermodynamic theory of micellization of ionic surfactants,” *Langmuir*, Vol. 19, 2003, pp. 9932–9945.
- [10] Srinivasan, V. and Blankschtein, D., “Effect of counterion binding on micellar solution behavior: 2. Prediction of micellar solution properties of ionic surfactant-electrolyte systems,” *Langmuir*, Vol. 19, 2003, pp. 9946–9961.
- [11] Reif, I., Mulqueen, M., and Blankschtein, D., “Molecular-thermodynamic prediction of critical micelle concentrations of commercial surfactants,” *Langmuir*, Vol. 17, 2001, pp. 5801–5812.
- [12] Shiloach, A. and Blankschtein, D., “Measurement and prediction of ionic/nonionic mixed micelle formation and growth,” *Langmuir*, Vol. 14, 1998, pp. 7166–7182.
- [13] Shiloach, A. and Blankschtein, D., “Prediction of critical micelle concentrations of nonideal ternary surfactant mixtures,” *Langmuir*, Vol. 14, 1998, pp. 4105–4114.
- [14] Shiloach, A. and Blankschtein, D., “Prediction of critical micelle concentrations and synergism of binary surfactant mixtures containing zwitterionic surfactants,” *Langmuir*, Vol. 13, 1997, pp. 3968–3981.
- [15] Zoeller, N., Lue, L., and Blankschtein, D., “A statistical-thermodynamic framework to model nonionic micellar solutions,” *Langmuir*, Vol. 13, 1997, pp. 5258–5275.
- [16] Mulqueen, M. and Blankschtein, D., “Theoretical and experimental investigation of the equilibrium oil-water interfacial tensions of solutions containing surfactant mixtures,” *Langmuir*, Vol. 18, 2002, pp. 365–376.

- [17] Nikas, Y., Puvvada, S., and Blankschtein, D., "Surface tensions of aqueous non-ionic surfactant mixtures," *Langmuir*, Vol. 8, 1992, pp. 2680–2689.
- [18] Mulqueen, M. and Blankschtein, D., "Prediction of equilibrium surface tension and surface adsorption of aqueous surfactant mixtures containing ionic surfactants," *Langmuir*, Vol. 15, 1999, pp. 8832–8848.
- [19] Mulqueen, M., Stebe, K., and Blankschtein, D., "Dynamic interfacial adsorption in aqueous surfactant mixtures: Theoretical study," *Langmuir*, Vol. 17, 2001, pp. 5196–5207.
- [20] Mulqueen, M., Datwani, S., Stebe, K., and Blankschtein, D., "Dynamic surface tension of aqueous surfactant mixtures: Experimental investigation," *Langmuir*, Vol. 17, 2001, pp. 5801–5812.
- [21] Groot, R. D. and Warren, P. W., "Dissipative particle dynamics: Bridging the gap between atomistic and mesoscopic simulation," *The Journal of Chemical Physics*, Vol. 107, 1997, pp. 4423–4435.
- [22] Groot, R. D., "Mesoscopic simulation of polymer-surfactant aggregation," *Langmuir*, Vol. 16, 2000, pp. 7493–7502.
- [23] Rodriguez-Guadarrama, L. A., Talsania, S. K., Mohanty, K. K., and Rajagopalan, R., "Thermodynamics of aggregation of amphiphiles in solution from lattice Monte Carlo simulations," *Langmuir*, Vol. 15, 1999, pp. 437–446.
- [24] Care, C. M. and Dalby, T., "Packing entropy in micelle self-assembly," *European Physics Letters*, Vol. 45, 1999, pp. 38–44.
- [25] Larson, R. G., "Monte Carlo simulation of microstructural transitions in surfactant systems," *The Journal of Chemical Physics*, Vol. 96, 1992, pp. 7904–7918.
- [26] Larson, R. G., Scriven, L. E., and Davis, H. T., "Monte Carlo simulation of model amphiphilic oil-water systems," *The Journal of Chemical Physics*, Vol. 83, 1985, pp. 2411–2420.

- [27] Floriano, M. A., Caponetti, E., and Panagiotopoulos, A. Z., “Micellization in model surfactant systems,” *Langmuir*, Vol. 15, 1999, pp. 3143–3151.
- [28] Smit, B., Hilbers, P. A. J., Esselink, K., Rupert, L. A. M., van Os, N. M., and Schlijper, A. G., “Computer simulations of a water oil interface in the presence of micelles,” *Nature*, Vol. 348, 1990, pp. 624–625.
- [29] Smit, B., Esselink, K., Hilbers, P. A. J., van Os, N. M., Rupert, L. A. M., and Szlifer, I., “Computer simulations of surfactant self-assembly,” *Langmuir*, Vol. 9, 1993, pp. 9–11.
- [30] Smit, B., Hilbers, P. A. J., Esselink, K., Rupert, L. A. M., van Os, N. M., and Schlijper, A. G., “Structure of a water/oil interface in the presence of micelles: A computer simulation study,” *The Journal of Physical Chemistry*, Vol. 95, 1991, pp. 6361–6368.
- [31] Pool, R. and Bolhuis, P. G., “Accurate free energies of micelle formation,” *The Journal of Physical Chemistry B*, Vol. 109, 2005, pp. 6650–6657.
- [32] Talsani, S. K., Rodriguez-Guadarrama, L. A., Mohanty, K. K., and Rajagopalan, R., “Phase behavior and solubilization in surfactant-solute-solvent systems by Monte Carlo simulations,” *Langmuir*, Vol. 14, 1998, pp. 2684–2692.
- [33] Mackie, A. D., Onur, K., and Panagiotopoulos, A. Z., “Phase equilibria of a lattice model for an oil-water-amphiphile mixture,” *The Journal of Chemical Physics*, Vol. 104, 1996, pp. 3718–3725.
- [34] Telo de Gama, M. M. and Gubbins, K. E., “Adsorption and orientation of amphiphilic molecules at a liquid-liquid interface,” *Molecular Physics*, Vol. 59, 1986, pp. 227–239.
- [35] Widom, B., “Correlation and scattering functions in a lattice model of oil-water-amphiphile solutions,” *The Journal of Chemical Physics*, Vol. 90, 1989, pp. 2437–2433.

- [36] Larson, R. G., “Molecular simulation of ordered amphiphilic phases,” *Chemical Engineering Science*, Vol. 49, 1994, pp. 2833–2850.
- [37] Larson, R. G., “Simulation of lamellar phase transitions in block copolymers,” *Macromolecules*, Vol. 27, 1994, pp. 4198–4203.
- [38] Nelson, P. H., Rutledge, G. C., and Hatton, T. A., “On the size and shape of self-assembled micelles,” *The Journal of Chemical Physics*, Vol. 107, 1997, pp. 10777–10781.
- [39] Nelson, P. H., Rutledge, G. C., and Hatton, T. A., “Asymmetric growth in micelles containing oil,” *The Journal of Chemical Physics*, Vol. 110, 1999, pp. 9673–9680.
- [40] Marrink, S., Lindahl, E., Edholm, O., and Mark, A., “Simulation of the spontaneous aggregation of phospholipids into bilayers,” *Journal of the American Chemical Society*, Vol. 123, 2001, pp. 8638–8639.
- [41] Marrink, S. and Mark, A., “Molecular dynamics simulation of the formation, structure, and dynamics of small phospholipid vesicles,” *Journal of the American Chemical Society*, Vol. 125, 2003, pp. 15233–15242.
- [42] de Vries, A., Mark, A., and Marrink, S., “Molecular dynamics simulation of the spontaneous formation of a small DPPC vesicle in water in atomistic detail,” *Journal of the American Chemical Society*, Vol. 126, 2004, pp. 4488–4489.
- [43] Mohanty, S., Davis, H. T., and McCormick, A. V., “Complementary use of simulations and free energy models for CTAB/NaSal systems,” *Langmuir*, Vol. 17, 2001, pp. 7160–7171.
- [44] Blankschtein, D., Thurston, G. M., and Benedek, G. B., “Phenomenological theory of equilibrium thermodynamic properties and phase separation of micellar solutions,” *The Journal of Physical Chemistry*, Vol. 85, 1986, pp. 7268–7288.
- [45] Tanford, C., *The Hydrophobic Effect: Formation of Micelles and Biological Membranes*, John Wiley and Sons, New York, 1991.

- [46] Puvvada, S. and Blankschtein, D., “Theoretical and experimental investigations of micellar properties of aqueous solutions containing binary mixtures of nonionic surfactants,” *The Journal of Physical Chemistry*, Vol. 96, 1992, pp. 5579–5592.
- [47] Ohshima, H., Healy, T. W., and White, L. R., “Accurate analytic expressions for the surface charge density/surface potential relationship and double-layer potential distribution for a spherical colloidal particle,” *Journal of Colloid and Interface Science*, Vol. 90, 1982, pp. 17–26.
- [48] ChemSW, Inc., Fairfield, CA., *Molecular Modeling Pro version 3.2*, 2003.
- [49] Quinn, J. A., “A new method for the calculation of hydrophilic surface area (HSA) from structure,” 2003, Norgwyn Montgomery Software Inc., North Wales, PA.
- [50] Jorgensen, W. L., Maxwell, D. S., and Tirado-Rives, J., “Development and testing of the OPLS all-atom force field on conformational energetics and properties of organic liquids,” *Journal of the American Chemical Society*, Vol. 118, 1996, pp. 11225–11236.
- [51] Schweighofer, K. J., Essmann, U., and Berkowitz, M., “Simulation of sodium dodecyl sulfate at the water-vapor and water-carbon tetrachloride interfaces at low surface coverage,” *The Journal of Physical Chemistry B*, Vol. 101, 1997, pp. 3793–3799.
- [52] Tieleman, D. P. and Berendsen, H. J. C., “Molecular dynamics simulations of a fully hydrated dipalmitoyl phosphatidylcholine bilayer with different macroscopic boundary conditions and parameters,” *The Journal of Chemical Physics*, Vol. 105, 1996, pp. 4871–4880.
- [53] van der Spoel, D., Lindahl, E., Hess, B., van Buuren, A. R., Apol, E., Meulenhoff, P. J., Tieleman, D. P., Sijbers, A. L. T. M., Feenstra, K. A., van Drunen, R., and Berendsen, H. J. C., *Gromacs User Manual*, www.gromacs.org, 2004.

- [54] Berendsen, H. J. C., Grigera, J. R., and Straatsma, T. P., “The missing term in effective pair potentials,” *The Journal of Physical Chemistry*, Vol. 91, 1987, pp. 6269–6271.
- [55] Breneman, C. and Wiberg, K., “Determining atom-centered monopoles from molecular electrostatic potentials: The need for high sampling density in formamide,” *Journal of Computational Chemistry*, Vol. 11, 1990, pp. 361–373.
- [56] Foresman, J. and Frisch, A., *Exploring Chemistry with Electronic Structure Methods*, Gaussian, Inc., Pittsburgh, Pennsylvania, 1996.
- [57] Berendsen, H. J. C., van der Spoel, D., and van Drunen, R., “GROMACS: A message-passing parallel molecular dynamics implementation,” *Computational Physics Community*, Vol. 91, 1995, pp. 43–56.
- [58] Lindahl, E., Hess, B., and van der Spoel, D., “Gromacs 3.0: A package for molecular simulation and trajectory analysis,” *Journal of Molecular Modeling*, Vol. 7, 2001, pp. 306–317.
- [59] van der Spoel, D., Lindahl, E., Hess, B., van Buuren, A., Apol, E., Meulenhoff, P., Tieleman, D., Sijbers, A., Feenstra, K., van Drunen, R., and Berendsen, H., *Gromacs User Manual version 3.2*, www.gromacs.org, 2004.
- [60] Flyvbjerg, H. and Petersen, H. G., “Error estimates on averages of correlated data,” *The Journal of Chemical Physics*, Vol. 91, 1989, pp. 461–466.
- [61] Hess, B., *Stochastic Concepts in Molecular Simulation*, Ph.D. thesis, Rijksuniversiteit Groningen, Groningen, 1999.
- [62] Hess, B., “Determining the shear viscosity of model liquids from molecular dynamics simulations,” *The Journal of Chemical Physics*, Vol. 116, 2001, pp. 209–217.
- [63] Penfold, J. and Thomas, R. K., “Solvent distribution in non-ionic surfactant monolayers,” *Physical Chemistry Chemical Physics*, Vol. 4, 2002, pp. 2648–2652.

- [64] Bocker, J., Schlenkrich, M., Bopp, P., and Brinkmann, J., “Molecular dynamics simulation of a n-hexadecyltrimethylammonium chloride monolayer,” *The Journal of Chemical Physics*, Vol. 96, 1992, pp. 9915–9922.
- [65] Tarek, M., Tobias, D. J., and Klein, M. L., “Molecular dynamics simulation of tetradecyltrimethylammonium bromide monolayers at the air-water interface,” *The Journal of Physical Chemistry*, Vol. 99, 1995, pp. 1393–1402.
- [66] Kallick, D. A., Tessmer, M. R., Watts, C. R., and Li, C.-Y., “The use of dodecylphosphocholine micelles in solution NMR,” *Journal of Magnetic Resonance*, Vol. 109, 1995, pp. 60–65.
- [67] Tieleman, D. P., van der Spoel, D., and Berendsen, H. J. C., “Molecular dynamics simulations of dodecylphosphocholine micelles at three different aggregate sizes: Micellar structure and lipid chain relaxation,” *The Journal of Physical Chemistry B*, Vol. 104, 2000, pp. 6380–6388.
- [68] Alargova, R. G., Kochijashky, I. I., Sierra, M. L., and Zana, R., “Micelle aggregation numbers of surfactants in aqueous solutions: A comparison between the results from steady-state and time-resolved fluorescence quenching,” *Langmuir*, Vol. 14, 1998, pp. 5412–5418.
- [69] Sarmoria, C. and Blankschtein, D., “Conformational characteristics of short poly(ethylene oxide) chains terminally attached to a wall and free in aqueous solution,” *The Journal of Physical Chemistry*, Vol. 96, 1992, pp. 1978–1983.
- [70] Van Os, N. M., Van Ginkel, R., Van Zon, A., Heywood, F. W., Berryman, E. L., and Borchardt, J. K., *Solubilization in Surfactant Aggregates. Surfactant Science Series 56*, Marcel Dekker, New York, 1996.
- [71] Hierrezuelo, J. M., Aguiar, J., and Ruiz, C. C., “Stability, interaction, size, and microenvironmental properties of mixed micelles of decanoyl-N-methylglucamide and sodium dodecyl sulfate,” *Langmuir*, Vol. 20, 2004, pp. 10419–10426.

- [72] Cabane, B., Duplessix, R., and Zemb, T., "High-resolution neutron-scattering on ionic surfactant micelles - SDS in water," *Journal de Physique*, Vol. 46, 1985, pp. 2161–2178.
- [73] Cabane, B., "Structure of the water-surfactant interface in micelles: An NMR-study of SDS micelles labeled with paramagnetic-ions," *Journal de Physique*, Vol. 42, 1981, pp. 847–859.
- [74] Hansson, P., Jonsson, B., Strom, C., and Soderman, O., "Determination of micellar aggregation numbers in dilute surfactant systems with the fluorescence quenching method," *The Journal of Physical Chemistry B*, Vol. 104, 2000, pp. 3496–3506.
- [75] Van Os, N. M., Rupert, L. A. M., and Haak, J. R., *Physico-Chemical Properties of Selected Anionic, Cationic and Nonionic Surfactants*, Elsevier, Amsterdam, 1993.
- [76] Reinhard, M. and Drefahl, A., *Estimating physiochemical properties of organic compounds*, John Wiley and Sons, Inc., New York, 1999.
- [77] Tetko, I. and Tanchuk, V. Y., "Virtual Computational Chemistry Laboratory webpage," 2005.
- [78] Tetko, I. and Tanchuk, V. Y., "Application of associative neural networks for prediction of lipophilicity in ALOGPS 2.1 program," *Journal of Chemical Information and Computer Science*, Vol. 42, 2002, pp. 1136–1145.

Chapter 3

Experimental and Theoretical Investigation of the Micellar-Assisted Solubilization of Ibuprofen in Aqueous Media

3.1 Introduction

An important property of surfactants is their ability to form colloidal-sized aggregates in aqueous solutions, known as micelles. Micelles are particularly useful in pharmaceutical applications due to their ability to increase the solubility of sparingly water-soluble substances [1]. In this context, solubilization is defined as the spontaneous dissolution of a material by reversible interaction with micelles to form a thermodynamically stable isotropic solution which exhibits reduced thermodynamic activity of the solubilized material [2]. It is noteworthy that the spatial position of a drug solubilized within a micelle depends on the drug polarity.

Numerous drug delivery and drug targeting systems have been studied in an attempt to minimize drug degradation and loss, to prevent harmful side effects, and to increase drug bioavailability [3–7]. The utilization of micelles as drug carriers in aque-

ous media presents some advantages when compared to other alternatives such as the use of water-soluble polymers and liposomes. Micellar systems can solubilize drugs that are poorly soluble in water, increasing bioavailability by lengthening retention in the body to provide gradual accumulation in the required area. In addition, the small size of micelles permits them to accumulate in areas with leaky vasculature [7,8].

Frequently, the solubilization of a drug molecule by a micellar surfactant is characterized by the molar solubilization capacity, χ [9]. The χ value is defined as the number of moles of the solute (drug) that can be solubilized by one mole of micellar surfactant, and can be calculated based on the following general equation for micellar solubilization:

$$\chi = \frac{S_{tot} - S_W}{C_{surf} - CMC} \quad (3.1)$$

where S_{tot} is the total drug solubility, S_W is the drug solubility in water, C_{surf} is the total molar concentration of surfactant in the solution, and CMC denotes the critical micelle concentration [10]. Since above the CMC the surfactant monomer concentration remains approximately constant at the CMC value, the term $(C_{surf} - CMC)$ in Eq. 1 is approximately equal to the concentration of surfactant in micellar form. Accordingly, χ in Eq. 3.1 can be viewed as the ratio of the drug concentration in the micelles $(S_{tot} - S_W)$ to the surfactant concentration in micellar form $(C_{surf} - CMC)$.

Ibuprofen (2-(4-isobutylphenyl)propanoic acid), $pK_a = 4.8$, is a non-steroidal, anti-inflammatory drug that is widely used to treat inflammation (see Figure 3-1) [11]. The main disadvantages of this family of drugs include a relatively short plasma half-life, significant gut-toxicity, and significant nephro-toxicity [12]. Therefore, the development of a drug delivery system that enables the controlled release of ibuprofen would be highly beneficial, particularly in high dose-dependent treatments, such as in the treatment of chronic diseases like rheumatoid arthritis. Studies have been conducted on the transdermal delivery of ibuprofen aimed at reducing the side effects associated with long-term treatment. Transdermal ibuprofen delivery systems based on polymers, alkyl poly(ethylene oxide) nonionic surfactant solutions, and liposomes

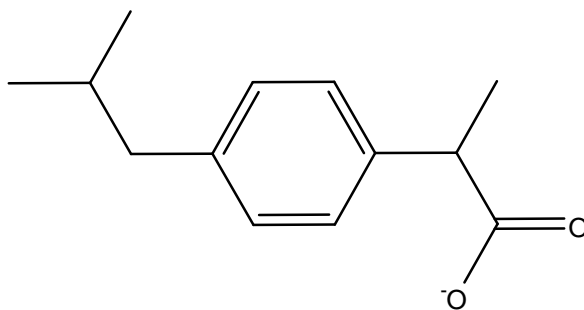


Figure 3-1: Chemical structure of the drug ibuprofen.

have been investigated [13–16].

Ibuprofen is a poorly water-soluble drug [11]. Yazdanian et al. have reported a solubility value of 11 mM (2.3 mg/mL) in 20 mM phosphate buffer at pH 7.4 [17], while the therapeutic dose is approximately 600 mg [18]. This low solubility presents an important challenge in ibuprofen formulation. Therefore, studies directed towards obtaining a better understanding of the aqueous micellar solubilization of ibuprofen may contribute to the development of more effective ibuprofen delivery vehicles. In this respect, very recent work has been published investigating the formulation of intravenous preparations of ibuprofen [19]. In addition, some recent work on ibuprofen solubilization aiming at oral liquid formulations has also been published [20,21]. In this chapter, the micellar solubilization of ibuprofen is investigated experimentally and theoretically in aqueous solutions of three surfactants: the anionic surfactant sodium dodecyl sulfate, SDS, the cationic surfactant dodecyltrimethylammonium bromide, DTAB, and the nonionic surfactant dodecyl octa(ethylene oxide), $C_{12}E_8$, all having the same hydrocarbon tail length but differing in their hydrophilic head groups. In spite of the fact that the micellar systems selected are not adequate for injectable formulations, by studying the solubilization behavior of ibuprofen in model anionic, cationic, and nonionic surfactants we hope to contribute to the development of a fundamental understanding of the micellar solubilization behavior of ibuprofen in aqueous media. In future studies, we plan to investigate solubilization in polymeric

micelles, which are more stable and show more promise from a pharmaceutical point of view.

In addition to the practical benefits discussed above, from a theoretical perspective, ibuprofen serves as an interesting test case to determine the range of applicability of a recently-developed combined computer simulation/molecular thermodynamic modeling approach to model self-assembly. This theoretical approach has been used recently to model the micellization behavior of simple and complex *single* surfactants [22], but has not yet been used to model micellar-assisted solubilization. The combined computer simulation/molecular-thermodynamic modeling approach used in this chapter uses molecular-dynamics simulations of ibuprofen at an oil/water interface (modeling the micelle core/water interface) to identify the hydrated and the unhydrated portions of ibuprofen in a micellar environment. Using this information, along with knowledge of the chemical structures of ibuprofen, SDS, DTAB, and C₁₂E₈, it is possible to use molecular-thermodynamic theory to predict the solubilization behavior of ibuprofen in the three micellar solutions considered. Molecular-thermodynamic theory enables the prediction of the change in free energy associated with transferring the surfactant monomers, the ibuprofen molecules, and the counterions (in the case of SDS and DTAB) from their reference states in the aqueous solution to a micellar aggregate [23–25]. This free-energy change can then be used, along with a thermodynamic description of the micellar solution, to predict various solubilization-related properties, including the aggregate composition as a function of surfactant concentration, the solubility of ibuprofen as a function of surfactant concentration, and the molar solubilization capacity (χ) [23].

The remainder of the chapter is organized as follows. In Section 2, we describe materials (Section 2.1), experimental methods (Section 2.2), and experimental results on ibuprofen solubilization (Section 2.3). The theoretical modeling of ibuprofen is discussed in Section 3.3. Specifically, Section 3.3.1 describes the computer simulation approach employed, including a discussion of simulation methodology (Section 3.3.1), simulation parameters (Section 3.3.1), system preparation and equilibration

(Section 3.3.1), our data analysis method (Section 3.3.1), and simulation results (Section 3.3.1). The molecular-thermodynamic approach is introduced in Section 3.3.2, including a discussion of the thermodynamic framework underlying the approach (Section 3.3.2) and the molecular model of binary surfactant micellization (Section 3.3.2). Molecular-thermodynamic modeling results based on computer simulation inputs, including a comparison with experimental results, are presented in Section 3.3.3. Finally, concluding remarks are presented in Section 3.4.

3.2 Materials, Experimental Methods, and Experimental Results

3.2.1 Materials

Ibuprofen and DTAB were obtained from Sigma (St. Louis, MO). SDS was obtained from Pharmacia Biotech (Uppsala, Sweden). $C_{12}E_8$ was obtained from Nikko Chemicals (Tokyo, Japan). All chemicals were used as received. Solutions were prepared in a 5 mM phosphate buffer of pH 7.4 (ionic strength = 0.011 M), using water purified through a Millipore Milli-Q ion-exchange system (Bedford, MA). Note that a pH of 7.4 was specified to approximate the pH of human blood. At this pH, the carboxylic group in ibuprofen is 99.7% dissociated, making the drug negatively-charged. All the other reagents were of analytical grade. The glassware used was washed in a 50:50 ethanol:1 M sodium hydroxide bath, followed by a 1 M nitric acid bath, rinsed copiously with Milli-Q water, and finally dried in an oven.

3.2.2 Experimental Methods

Determination of Ibuprofen Concentrations

Ibuprofen concentrations were determined spectrophotometrically at $\lambda = 273$ nm in a BECKMAN DU 640 (Fullerton, CA) spectrophotometer. In order to eliminate

any possible influence of the surfactant in the absorption measurements, a solution of pure surfactant at the same concentration as the sample containing ibuprofen was used as the control. The extinction coefficient of ibuprofen at this wavelength is $256.5 \text{ M}^{-1}\text{cm}^{-1}$ [26].

Determination of Critical Micelle Concentrations

The CMCs of the three surfactants studied were measured at 25 °C in pure water, in phosphate buffer at pH 7.4, and in phosphate buffer with 4 mM of ibuprofen (corresponding to the saturation limit of ibuprofen in the buffer solution). CMC determinations for SDS and DTAB were based on the change in conductance with surfactant concentration. Measurements were performed in a MPC 227 Mettler-Toledo (Columbus, OH) conductivity meter [27]. The accuracy of the conductance measurements was $\pm 5 \text{ mS/cm}$. CMC determinations for C_{12}E_8 were based on the change in surface tension with surfactant concentration. A Du Noüy ring tensiometer (TE 1C/3 Lauda-Königshefen, Germany) was used to measure surface tensions with an accuracy of $\pm 1 \text{ mN/m}$. The effect of curvature was accounted for using the Harkins and Jordan correction factor [28,29]. Each conductivity/surface tension measurement was carried out in triplicate, and the typical error in the CMC determination was less than 5%.

Determination of Ibuprofen Solubilities

The solubilities of ibuprofen in the SDS, DTAB, and C_{12}E_8 solutions were measured at surfactant concentrations between 0 and 80 mM. Excess amounts of ibuprofen were added to vials containing 2.0 mL of the buffered surfactant solutions. The sample vials were then agitated at 8 rpm in an end-to-end rotator (Barnstead/Thermolyne, Dubuque, IW) at 25 °C for 24 hours. After agitation, the samples were filtered through a $0.20 \mu\text{m}$ Minisart RC 25 system (Sartorius, Goettingen, Germany), and the concentration of ibuprofen in solution was determined spectrophotometrically as described in Section 2.2.1. All the solubility measurements were carried out in

Surfactant	Critical Micelle Concentration – CMC (mM)		
	H ₂ O	Buffer	Buffer + Ibuprofen
SDS	8.7	4.7	4.7
DTAB	15.9	13.5	11.0
C ₁₂ E ₈	0.08	0.09	0.05

Table 3.1: Experimentally-determined critical micelle concentrations (CMCs) of SDS, DTAB, and C₁₂E₈ in water, phosphate buffer at pH 7.4, and ibuprofen-saturated (4 mM) phosphate buffer at pH 7.4.

triplicate, and the typical accuracy of the measurements was $\pm 10\%$.

3.2.3 Experimental Results

The experimentally-determined CMCs of SDS, DTAB, and C₁₂E₈ are summarized in Table 3.1. The CMCs of DTAB and C₁₂E₈ are lower in the ibuprofen-saturated buffer than in the buffer, whereas no change is observed in the CMC of SDS. The CMCs measured in water are consistent with what has been reported in the literature [30]: 8.2 mM for SDS, 16.0 mM for DTAB, and 0.088 mM for C₁₂E₈. The low CMCs of nonionic surfactants such as C₁₂E₈, reflecting micelle formation at low surfactant concentrations, combined with the low relative toxicity of nonionic surfactants, makes this class of surfactants particularly appropriate for drug delivery applications.

Figures 3-2, 3-3, and 3-4 show the experimentally-determined solubility curves of ibuprofen as a function of surfactant concentration for aqueous solutions of SDS, DTAB, and C₁₂E₈, respectively. As can be seen in the three figures, the solubility of ibuprofen increases linearly with increasing surfactant concentration. This behavior results from the association of the ibuprofen molecules with the micellar aggregates, and will be discussed further in Section 3.3.3. The solubility curves of ibuprofen in the SDS and the DTAB micellar solutions clearly show that micellar-assisted solubilization is taking place, since increased ibuprofen solubility is observed only at surfactant concentrations that exceed the respective CMCs (4.7 mM for SDS and 11 mM for DTAB). On the other hand, a clear correlation between the onset of micelle formation and an increased ibuprofen solubility is not observed in the solubility curve of

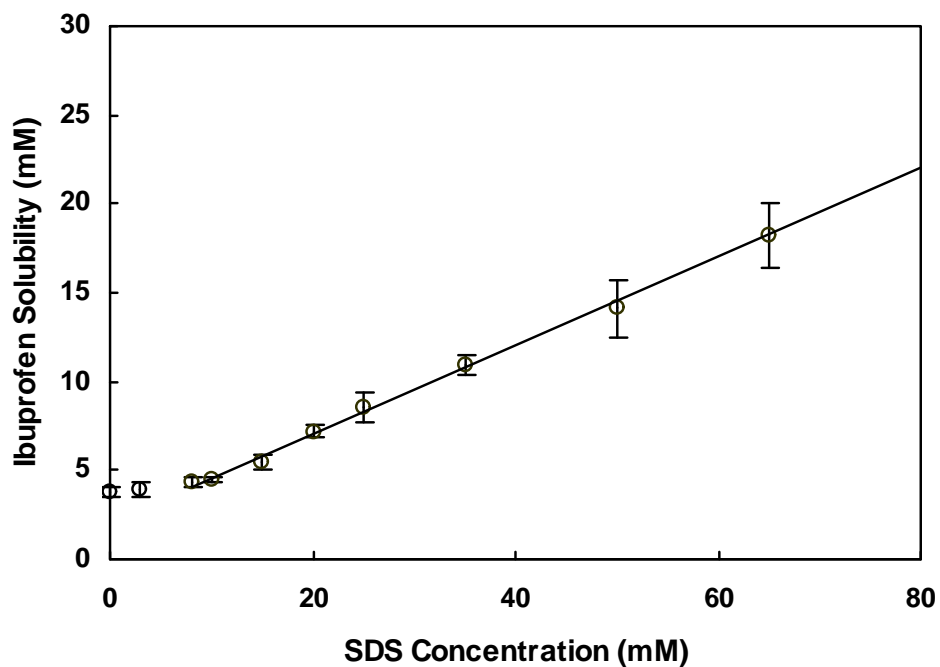


Figure 3-2: Experimentally-determined solubility curve of ibuprofen as a function of SDS concentration in 5 mM phosphate buffer at pH 7.4 and 25 °C. The error bars represent 95% confidence limits for the measurements. The line shown in the figure was fit to the solubility data above the CMC, and has the functional form: $y = 0.250x + 2.057$, with an R^2 value of 0.999.

ibuprofen in the $C_{12}E_8$ micellar solution (see Figure 3-4), due to the very low CMC of this nonionic surfactant (0.05 mM). Nevertheless, ibuprofen solubility measurements at $C_{12}E_8$ concentrations below the CMC (data not shown) revealed no increase in ibuprofen solubility, confirming the correlation between increased ibuprofen solubility and micelle formation for $C_{12}E_8$ as well.

As shown in Figure 3-2, there is a 5.5-fold increase in the solubility of ibuprofen relative to that in the aqueous buffer solution upon the addition of 80 mM SDS. As shown in Figure 3-3, there is a 16-fold increase in the solubility of ibuprofen relative to that in the aqueous buffer solution upon the addition of 80 mM DTAB. Figure 3-4 shows the solubility results for ibuprofen in the $C_{12}E_8$ micellar solution, which are quite similar to those observed in the DTAB micellar solution.

The molar solubilization capacity (χ) was determined for the three surfactants using Eq. 3.1. DTAB was found to have the highest molar solubilization capacity ($\chi = 0.97$), followed by $C_{12}E_8$ ($\chi = 0.72$), and finally by SDS ($\chi = 0.23$). A discussion of the physical mechanisms underlying the observed solubility behavior of ibuprofen in the three surfactant systems studied, including a comparison with our theoretical results, will be presented in Section 3.3.3.

3.3 Theoretical Modeling

Molecular-thermodynamic theory can be used to model the micellar-assisted aqueous solubilization behavior of solubilizates consisting entirely of hydrophobic groups, which localize within the micelle hydrophobic core upon solubilization, or of solubilizates which contain both hydrophilic and hydrophobic groups, and which may also localize at the micelle/water interface. The objective of molecular-thermodynamic modeling is to determine the free-energy change associated with transferring the surfactant monomers, the solubilizates, and the counterions (in the case of ionic surfactants) from their standard states in the aqueous solution to form a micellar aggregate in its standard state [23]. For solubilizates which localize within the micelle core,

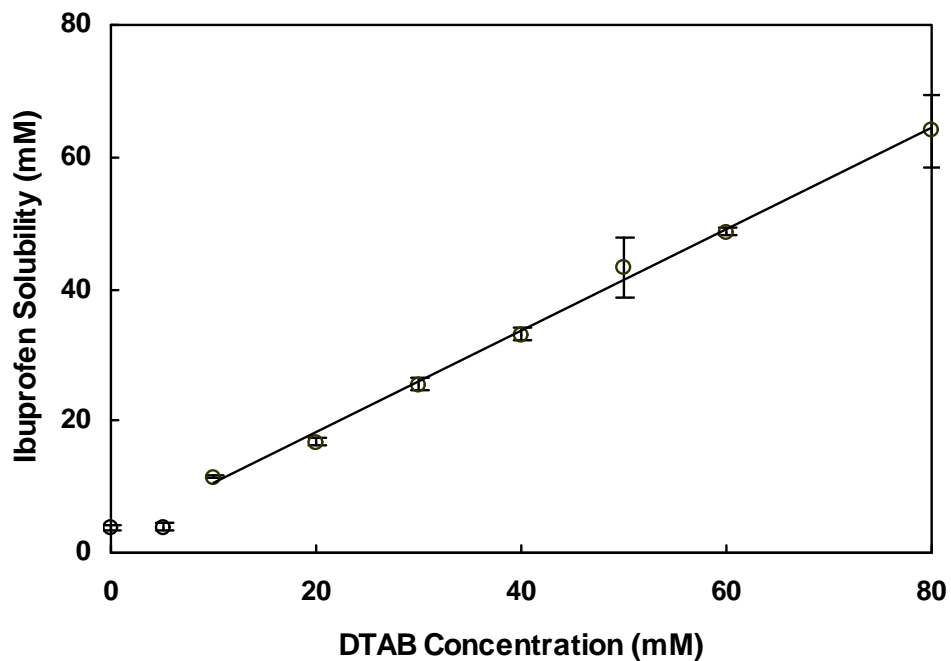


Figure 3-3: Experimentally-determined solubility curve of ibuprofen as a function of DTAB concentration in 5 mM phosphate buffer at pH 7.4 and 25 °C. The error bars represent 95% confidence limits for the measurements. The line shown in the figure was fit to the solubility data above the CMC, and has the functional form: $y = 0.768x + 2.825$, with an R^2 value of 0.997.

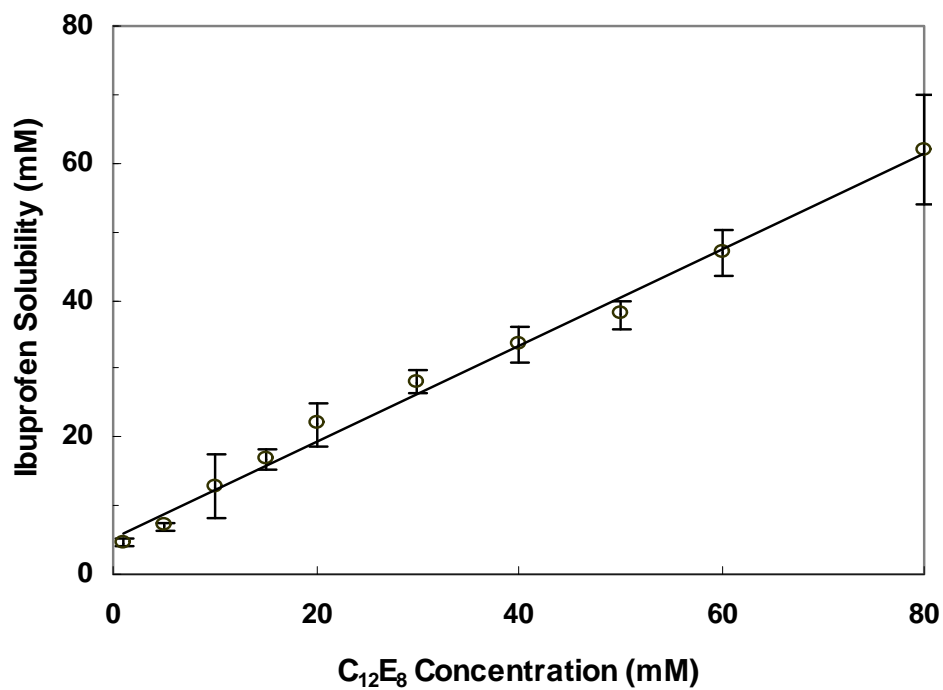


Figure 3-4: Experimentally-determined solubility curve of ibuprofen as a function of C₁₂E₈ concentration in 5 mM phosphate buffer at pH 7.4 and 25 °C. The error bars represent 95% confidence limits for the measurements. The line shown in the figure was fit to the solubility data above the CMC, and has the functional form: $y = 0.720x + 4.317$, with an R^2 value of 0.993.

the free-energy change associated with transferring a solubilizate from the aqueous solution to an environment consisting of: i) unhydrated surfactant tails, and ii) other solubilizates, must be determined [23]. For solubilizates which localize at the micelle/water interface, only a portion of the molecule is transferred from the aqueous solution to the micelle core. The remainder of the molecule is hydrated and interacts with: i) hydrated surfactant heads, ii) other hydrated solubilizate heads, and iii) water molecules. Solubilizates of this type behave like surfactants within a micellar environment, in the sense that they contain both hydrated and unhydrated moieties. As a result, their micellization behavior can be modeled in a manner similar to that of conventional surfactants. However, it is important to note that solubilizates of this type differ from conventional surfactants in that they do not have a CMC and, without added surfactant, cannot form micellar aggregates in aqueous solution. Instead, they have an aqueous solubility limit, which corresponds to the maximum concentration of solubilizate that can exist in the aqueous solution. When modeling the behavior of these solubilizates in a micellar solution, their aqueous solubility limit corresponds to the maximum concentration of solubilizate that can exist outside the micelles in the aqueous solution.

The drug ibuprofen has a relatively complex structure which contains both hydrophilic and hydrophobic moieties (see Figure 3-1). To successfully apply molecular-thermodynamic theory to model the aqueous solubilization behavior of ibuprofen, it was necessary to determine: i) whether ibuprofen localizes within the micelle core or at the micelle/water interface, and ii) if localization at the micelle/water interface does occur, what portions of ibuprofen are exposed to the aqueous solution (referred to as the head) and what portions reside in the micelle core (referred to as the tail). For the three surfactants considered in this chapter (SDS, DTAB, and $C_{12}E_8$), the head and tail portions were already known from previously conducted computer simulation/molecular-thermodynamic modeling [22].

A rough identification of the head and the tail portions of simple surfactant or solubilizate molecules that localize at the micelle/water interface can be made us-

ing group-contribution methods to determine the hydrophilic and the hydrophobic portions of such molecules [31]. However, this type of approach is not suitable to determine the head and tail portions of surfactant or solubilize molecules that possess complex chemical structures. Indeed, complex surfactants and solubilizates can have multiple hydrophilic and hydrophobic portions within their structure, and therefore, in such cases, it is not clear *a priori* how molecules of this type will locate and orient themselves within a micellar aggregate. Because of this challenge, we recently conducted computer simulations of anionic, cationic, zwitterionic, and nonionic surfactants at an oil/water interface (modeling the micelle core/water interface) in order to identify the head and tail portions of these surfactants [22]. Because of the relatively complex structure of ibuprofen, molecular dynamics simulations were first used to estimate how ibuprofen localizes in a micellar aggregate using molecular dynamics simulations described in Section 3.3.1.

The modeling approach presented in this chapter relies on a thermodynamic framework to describe the micellar solution [24,25,32]. This theoretical framework permits the calculation of micellar solution properties, including the critical micelle concentration (CMC), the distribution of aggregate shapes and sizes, and microstructural characteristics of the aggregate (such as the core minor radius), from the free energy of aggregate formation. A brief overview of this theoretical framework is presented in Section 3.3.2. Because our computer simulations indicate that ibuprofen does localize at the micelle/water interface, and therefore behaves like a typical surfactant within a micellar environment, a molecular-thermodynamic theory developed to model binary surfactant micellization was used to model the solubilization of ibuprofen in aqueous solutions of SDS, DTAB, and $C_{12}E_8$. This binary surfactant micellization theory is reviewed in Section 3.3.2. Subsequently, the head and tail identifications made for ibuprofen are used as inputs to the molecular-thermodynamic theory, and the predictions made are discussed and compared with the experimental results in Section 3.3.3.

3.3.1 Molecular Dynamics Simulations

Methodology

To identify the head and tail of ibuprofen, molecular dynamics computer simulations of ibuprofen at a flat octane/water interface were carried out to estimate how ibuprofen locates and orients itself within a micellar aggregate. Note that octane was arbitrarily selected as the model “oil” in all the computer simulations. Similar results should be obtained using both longer and shorter alkane molecules. Computer simulations were used because the chemical structure of ibuprofen is too complex (with a hydrophilic carboxylate group, a slightly hydrophobic benzyl group, and a hydrophobic alkyl chain, see Figure 3-1) to allow use of group-contribution theory to accurately identify the head and the tail of the molecule.

The infinite-dilution computer simulation approach used here is most applicable to solubilizates that adopt a consistent position and orientation relative to an octane/water interface which is similar to the position and orientation that they would adopt within a micellar environment. When the solubilizate orientation depends strongly on factors such as the interface radius of curvature and the presence of additional surfactant molecules, this relatively simple computational strategy may not be applicable, because the input parameters for the molecular-thermodynamic theory may not be constant (specifically, they may become functions of aggregate shape, aggregation number, and aggregate composition). With this in mind, ibuprofen, being a relatively complex solubilizate with both hydrophilic and hydrophobic moieties, serves as an interesting test case to determine the applicability of inputting the results of solubilizate simulation at a flat octane/water interface to model the solubilization of ibuprofen in curved micellar aggregates.

Simulation Parameters

Computer simulations were carried out using the OPLS-AA forcefield [33]. Because ibuprofen was 99.7% deprotonated in the experiments conducted, the carboxylate

group in ibuprofen was treated as being fully dissociated and negatively-charged. Water was treated explicitly using the simple extended point-charge (SPC-E) model for water [34]. Octane was used as the model “oil” in all the computer simulations. Van der Waals interactions were treated using a cutoff distance of 1.2 nm, and Coulombic interactions were described using Particle Mesh Ewald (PME) summation. All simulations were run using fixed bond lengths, which allowed a simulation timestep of 2 fs.

Two different approaches were used to assign atomic charges for ibuprofen and octane. In one set of simulations, atomic charges were assigned based on the atomic charges specified within the OPLS-AA forcefield. In another set of simulations, *Gaussian 98* was used to determine atomic charges using the CHelpG method [35]. The CHelpG algorithm assigns atomic charges to fit calculated electrostatic potentials at a number of points on the van der Waals surface. This method is frequently used to estimate atomic charges for molecular mechanics calculations [36]. Atomic charges for ibuprofen and octane were determined using the *rblyp* density functional and the *6-31G(d)* basis set [36]. To ensure self-consistency of the simulation parameters, the same charge assignment method was used in each simulation for both the ibuprofen and the octane molecules. Because the SPC-E charge groups for water have been carefully optimized, these charge parameters were not changed [34].

System Preparation and Equilibration

Simulations using both OPLS-AA and CHelpG atomic charges were performed using the GROMACS software package, version 3.2 [37, 38]. A single ionized ibuprofen molecule was placed between 20 nm-thick layers of octane and water. The octane and water layers, in turn, were surrounded by vacuum. Each simulation cell was specified to be 4.0 nm long parallel to the octane/water interface. The simulation cell temperature was maintained at 300 K using a Berendsen temperature coupling algorithm implemented in GROMACS, and simulations were carried out at a constant volume [39].

After constructing the octane-ibuprofen-water system, the simulation cell was allowed to equilibrate for 250 ps before gathering data. During this equilibration run, the ibuprofen molecule appeared to reach an equilibrium configuration relative to the octane/water interface. This was verified by confirming that the local environment of each atom in ibuprofen had stabilized using the analysis approach described in the next section.

Data Analysis Method

After equilibration, a 3 ns run was initiated during which data was gathered. To identify the local environment of each atom in ibuprofen from the simulation results, the number of contacts per timestep experienced by different atoms in ibuprofen with octane and with water was counted over the course of a simulation run. In this method, a contact was defined as two atoms approaching each other to within a set cutoff distance at any time during the simulation. Because the van der Waals radii of the simulated atoms ranged between 0.12–0.14 nm, a reasonable minimum cutoff to identify such contacts is twice the maximum van der Waals radii, or around 0.28 nm. However, few contacts were observed at 0.28 nm. Accordingly, to improve statistics, the cutoff distance was set at 0.4, 0.5, and 0.6 nm. It is noteworthy that the identification of what atoms in ibuprofen are part of the head and the tail was found not to be sensitive to the size of the cutoff distance chosen. The ratio of the number of contacts with water to the number of contacts with octane was computed for each atom in ibuprofen to determine whether a given atom is surrounded primarily by water or by octane. As we reported recently, each contact ratio must be scaled by a factor of 0.88 to account for the fact that an atom in bulk water is contacted slightly more frequently than an atom in bulk octane [22]. Using this approach, any atom having a scaled contact ratio greater than one has been identified as being part of ibuprofen’s head. Conversely, any atom having a scaled contact ratio smaller than one has been identified as being part of ibuprofen’s tail.

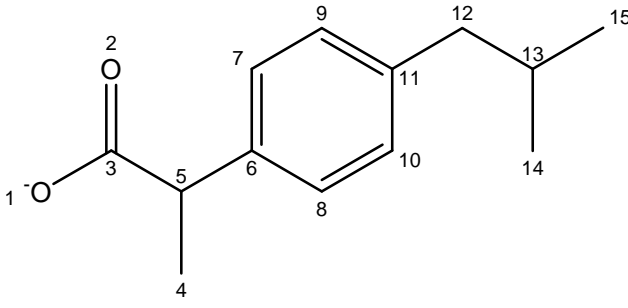
An estimate of the error of each scaled contact ratio was determined through the

use of block averaging [40–42]. The standard error for the scaled contact ratios was computed from the variance between averages of blocks of data, and the block size was increased until the standard error estimate became constant. An analytical block average curve (based on the assumption that the autocorrelation in the data can be described as the sum of two exponentials) was fit to the standard error versus block size data to assist in identifying the correct standard error values [40–42].

Simulation Results and Discussion

In Table 3.2, we list scaled contact ratios (SCRs) and standard errors (SEs) for atoms in ibuprofen determined from molecular dynamics simulations based on the assignment of CHelpG and OPLS-AA atomic charges. In some cases, averaged results for groups of several atoms (for example, CH₃) are presented to reduce the amount of reported data. Scaled contact ratios corresponding to the ibuprofen head are shown in bold. The standard error of the mean for each scaled contact ratio (calculated through the block averaging approach discussed in Section 3.3.1) is reported to provide a measure of the statistical significance of the results.

The computer simulation results show that both head and tail groups are present in ibuprofen, indicating that ibuprofen should localize at the micelle/water interface. Although group 4 in ibuprofen is identified as being part of the tail using CHelpG atomic charges and as being part of the head using OPLS-AA atomic charges, this difference is not statistically significant given the level of uncertainty in both scaled contact ratios. If the scaled contact ratio for group 4 is changed by plus or minus the standard error computed for group 4, the head and tail identification changes for this group because the scaled contact ratio is extremely close to one. Therefore, based on our simulation results, we cannot unambiguously determine whether group 4 should be included as part of ibuprofen’s head or as part of ibuprofen’s tail. Because the scaled contact ratio for group 4 is very close to one, in a micellar environment this methyl group is likely to be partly, rather than fully, shielded from water. Consequently, in Section 3.3.3, we report molecular-thermodynamic modeling results for ibuprofen



CHelpG Atomic Charge Results, 3 ns Simulation															
Group	1	2	3	4	5	6	7	8	9	10	11	12	13	14	15
SCR	14.2	11.0	9.39	0.99	1.78	1.33	0.84	0.88	0.46	0.47	0.45	0.26	0.26	0.16	0.22
SE	1.50	0.71	0.62	0.03	0.06	0.06	0.05	0.05	0.05	0.05	0.03	0.06	0.03	0.02	0.03
OPLS-AA Atomic Charge Results, 3 ns Simulation															
Group	1	2	3	4	5	6	7	8	9	10	11	12	13	14	15
SCR	15.3	16.4	11.0	1.00	1.74	1.31	0.98	0.84	0.55	0.48	0.47	0.23	0.28	0.17	0.24
SE	1.15	1.40	0.66	0.04	0.09	0.06	0.06	0.07	0.03	0.05	0.02	0.03	0.03	0.02	0.03

Table 3.2: Simulated scaled contact ratios (SCRs) and standard errors (SEs) for groups of atoms in ibuprofen based on the assignment of: i) CHelpG atomic charges, and ii) OPLS-AA atomic charges. Scaled contact ratios corresponding to the ibuprofen head are shown in bold.

both with group 4 included as part of ibuprofen’s head and as part of ibuprofen’s tail.

3.3.2 Molecular-Thermodynamic Approach

Since the computer simulation results presented in Section 3.3.1 indicate that ibuprofen behaves like a conventional surfactant in a micellar environment, its solubilization in a micellar solution can be modeled as a binary mixed micellization process involving the “real” surfactant (SDS, DTAB, or $C_{12}E_8$), denoted hereafter as surfactant *A*, and ibuprofen, denoted hereafter as surfactant *B* (see also Section 3.3.2). Note, however, that in this modeling approach, the aqueous solubility limit of ibuprofen in the aqueous solution outside the micelles must be enforced.

Thermodynamic Framework

In the multiple-chemical equilibrium model [32, 43], each micellar aggregate is considered as a distinct chemical species in equilibrium with the other aggregates and with the individually-dispersed molecules present in the solution. By equating the chemical potentials of the micellar aggregates, the surfactant A and B monomers, and the counterions (denoted hereafter as c) in the case of SDS and DTAB, an expression is obtained that describes the population distribution of micellar aggregates, $X_{n\alpha\hat{\beta}}$, containing $n\alpha$ surfactant A molecules (where n is the total number of surfactant molecules in the micellar aggregate and $\alpha =$ the ratio of the number of surfactant A molecules to the total number of surfactant molecules in the micellar aggregate), $n(1 - \alpha)$ surfactant B molecules, and $\hat{\beta}$ bound counterions per surfactant molecule in the micellar aggregate [25]. Specifically,

$$X_{n\alpha\hat{\beta}} = \frac{1}{e} X_{1A}^{n\alpha} X_{1B}^{n(1-\alpha)} X_{1c}^{n\hat{\beta}} \exp \left[-\frac{n}{k_B T} g_{mic} (S, l_c, \alpha, \hat{\beta}) \right] \quad (3.2)$$

where the free energy of micellization, g_{mic} , is defined as follows:

$$g_{mic} = \frac{1}{n} \mu_{n\alpha\hat{\beta}}^o - \left[\alpha \mu_A^o + (1 - \alpha) \mu_B^o + \hat{\beta} \mu_c^o \right] - k_B T (1 + \hat{\beta}) \quad (3.3)$$

In Eq. 3.3, μ_i^o is the standard-state chemical potential of species i (where $i =$ a micellar aggregate $n\alpha\hat{\beta}$, a surfactant A monomer, a surfactant B monomer, or a counterion), k_B is the Boltzmann constant, and T is the absolute temperature [25]. The variables X_{1A} , X_{1B} , and X_{1c} in Eq. 3.2 are the mole fractions of the surfactant A monomers, the surfactant B monomers, and the counterions, respectively. As shown in Eq. 3.2, g_{mic} is a function of the aggregate shape (S), the aggregate core minor radius (l_c), the aggregate composition (α), and the degree of counterion binding ($\hat{\beta}$). The free energy of micellization, g_{mic} , reflects the free-energy change associated with transferring the surfactant A monomers, the surfactant B monomers, and the

counterions in their corresponding standard states from the aqueous solution to form a micellar aggregate in its standard state.

For the values of S , l_c , α , and $\hat{\beta}$ that minimize g_{mic} (denoted as S^* , l_c^* , α^* , and $\hat{\beta}^*$), g_{mic} has a minimum value denoted hereafter as g_{mic}^* . Due to the exponential dependence of $X_{n\alpha\hat{\beta}}$ on $n \cdot g_{mic}$ in Eq. 3.2, small deviations from g_{mic}^* yield $X_{n\alpha\hat{\beta}}$ values that are essentially zero. Accordingly, by solving for g_{mic}^* as a function of S , l_c , α , and $\hat{\beta}$, the optimal aggregate shape, S^* , core minor radius, l_c^* , composition, α^* , and degree of counterion binding, $\hat{\beta}^*$, can be predicted. In addition, the CMC of the surfactant A /surfactant B (ibuprofen)/counterion system is given by [25]:

$$CMC = \exp \left(\frac{g_{mic}^* (S^*, l_c^*, \alpha^*, \hat{\beta}^*)}{k_B T} \right) \quad (3.4)$$

Molecular Model of Binary Surfactant Micellization

A molecular-thermodynamic model of binary surfactant micellization can then be used to predict g_{mic} for the surfactant A molecules, the surfactant B (ibuprofen) molecules, and the counterions. This model estimates g_{mic} based on the chemical structures of surfactant A , surfactant B , and the counterion, as well as on an estimate of how surfactants A and B localize within a micellar aggregate [25].

The free energy of binary surfactant micellization, g_{mic} , can be expressed as the sum of the following six free-energy contributions [24]:

$$g_{mic} = g_{tr} + g_{int} + g_{pack} + g_{st} + g_{elec} + g_{ent} \quad (3.5)$$

In Eq. 3.5, the transfer free-energy contribution, g_{tr} , represents the free-energy change associated with transferring the surfactant tails from the aqueous solution to a bulk solution of surfactant tails [44]. The interfacial free-energy contribution, g_{int} , represents the free-energy change associated with forming an interface between the

surfactant tails and the aqueous solution [32]. The packing free-energy contribution represents the free-energy change required to fix one end of the surfactant tail moieties at the aggregate/water interface [24]. The steric free-energy contribution, g_{st} , arises from organizing the surfactant heads at the aggregate/water interface [45]. The electrostatic free-energy contribution, g_{elec} , results from the electrostatic repulsions between ionic groups, if present, in the micellar aggregate [24,25]. The entropic free-energy contribution, g_{ent} , arises from the entropy gain associated with mixing the surfactants and the counterions within the micelle. Modeling approaches have been developed to calculate each of these free-energy contributions [23]. Detailed information about how this is done for binary surfactant mixtures (allowing for counterion binding) has been reported in the literature [24,25,43].

3.3.3 Molecular-Thermodynamic Modeling Based on Computer Simulation Inputs

The head and tail identifications for ibuprofen discussed in Section 3.3.1 have been used as inputs to the molecular-thermodynamic framework presented in Sections 3.3.2 and 3.3.2 to predict: (i) the micellar composition as a function of surfactant concentration, (ii) the ibuprofen solubility as a function of surfactant concentration, and (iii) the molar solubilization capacity, χ , for the three surfactants considered (SDS, DTAB, and C₁₂E₈). As discussed earlier, ibuprofen differs from the three surfactants studied in this chapter in that it does not spontaneously form micellar aggregates in aqueous solution. However, because the computer simulations discussed in Section 3.3.1 indicate that it should behave like a conventional surfactant within a micellar environment, we have been able to model its micellar-assisted solubilization behavior using the binary surfactant molecular-thermodynamic micellization theory discussed in Section 3.3.2. To predict the free energy of micellization (g_{mic}), the free-energy contributions listed in Eq. 3.5 have been computed for each surfactant/ibuprofen mixture.

	SDS	DTAB	C₁₂E₈
a_h	25 Å ²	32 Å ²	61 Å ²
d_{charge}	3.7 Å	5.1 Å	N/A
l_{hg}	5.6 Å	7.7 Å	N/A

Table 3.3: Input parameters for the molecular-thermodynamic modeling of the surfactants SDS, DTAB, and C₁₂E₈, where a_h , d_{charge} , and l_{hg} have been defined in the text.

Using the head and tail identifications made from computer simulations, a number of parameters necessary for molecular-thermodynamic modeling were estimated. These include a_h , the cross-sectional area of the surfactant or ibuprofen head, d_{charge} , the distance between the beginning of the surfactant tail and the location of the charge in the surfactant head, and l_{hg} , the distance from the beginning of the surfactant tail to the tip of the surfactant head. The parameters used for SDS, DTAB, and C₁₂E₈ have been reported recently [22], and are listed in Table 3.3 for completeness.

For ibuprofen, a_h is equal to the cross-sectional area of the carboxylate group (20 Å²), and the distance d_{charge} was estimated to be 3.43 Å based on the energy-minimized geometry of ibuprofen in vacuum. The four free-energy contributions, g_{int} , g_{st} , g_{elec} , and g_{ent} , in Eq. 3.5 were estimated in a straightforward manner using these values of a_h and d_{charge} . However, additional work was needed (see below) to estimate ibuprofen’s transfer free-energy contribution, g_{tr} , and its effect on the packing free-energy contribution, g_{pack} .

The quantity g_{tr} is one of the most important free-energy contributions listed in Eq. 3.5 in terms of the magnitude of its contribution to g_{mic} . It can be estimated for relatively simple surfactants having linear alkyl chains using an empirical correlation describing aqueous solubility as a function of chain length and the solution temperature [24, 32, 46]. Aqueous solubility is related to the transfer free energy by the relationship $g_{\text{tr}} = k_B T \ln(s)$, where s is the aqueous solubility of the compound expressed on a mole fraction basis. However, the tail group identified for ibuprofen is more complex than a linear hydrocarbon – it includes branched hydrocarbon chains and the majority of a benzene ring.

A computer program developed by Tetko et al., based on the use of associative neural networks for the prediction of lipophilicity, was used to estimate the aqueous solubility of the tail group identified for ibuprofen (with and without the inclusion of group 4), see Section 3.3.1 [47, 48]. A similar approach was used in a recently-published study on the computer simulation and molecular-thermodynamic modeling of the micellization of the surfactant decanoyl-n-methylglucamide (MEGA-10) [22]. Without the inclusion of group 4, the ibuprofen tail was estimated to have a solubility of $6.61 \cdot 10^{-5}$ M, giving a g_{tr} value of $-13.63 k_B T$. In this case, experimental solubility data was also available for the same tail group, giving an experimental solubility value of $7.59 \cdot 10^{-5}$ M [47], which corresponds to a g_{tr} value of $-13.50 k_B T$. By comparison, the transfer free energy of a linear chain of eight CH_2 groups and a CH_3 group is $-13.97 k_B T$. With this observation in mind, in order to simplify the implementation of the molecular-thermodynamic theory, the ibuprofen tail without the inclusion of group 4 was approximated as being equivalent to a *nine carbon linear alkyl chain*. With the inclusion of group 4, the ibuprofen tail was approximated as being equivalent to a *ten carbon linear alkyl chain* (for which $g_{tr} = -15.46 k_B T$). These approximations allowed straightforward determination of the effect of ibuprofen on g_{pack} using a previously-developed mean-field theoretical approach to model chain packing in micelles [24]. Previous work comparing g_{pack} for linear alkyl tails and alkylbenzene tails indicates that modeling the ibuprofen tail as a linear alkyl chain should not introduce significant error to the estimation of the packing free-energy contribution [23].

Ibuprofen Solubilization in SDS Micelles

Molecular-thermodynamic modeling of SDS in water and of SDS in the same buffered solution that was used to gather the experimental data reported in Section 2.3 yielded CMC predictions (based on the use of Eq. 3.4 for a single surfactant, that is, with $\alpha^* = 0$) of 7.54 mM and 3.99 mM, respectively. The predicted CMCs are in good agreement with the experimentally-determined CMCs of 8.7 mM and 4.7 mM reported in Table 3.1, indicating that SDS is modeled reasonably well using the molecular-

thermodynamic modeling approach.

The molecular-thermodynamic approach presented in Section 3.3.2 can be used to predict the shape, core minor radius, and composition of micellar aggregates at a specified temperature and solution composition. In addition, the molecular-thermodynamic approach can be used to predict the solubility limit of a solubilizate such as ibuprofen in a surfactant solution at a specified temperature, salt concentration, and surfactant concentration. To perform these theoretical predictions, however, the aqueous solubility limit of ibuprofen (*in the absence of surfactant*) at the solution temperature and salt concentration of interest must be enforced in the molecular-thermodynamic modeling. This solubility limit can be determined through experimental measurement, as was done here, or it can be predicted theoretically, and its value can then be used without further change as an input in modeling ibuprofen solubility in the presence of any surfactant. Several approaches are available to theoretically predict the solubility limit of organic compounds in aqueous media, including group-contribution approaches [22, 49].

To test the combined computer simulation/molecular-thermodynamic modeling approach presented in this chapter, both the micellar composition and the solubility limit of ibuprofen in the micellar solution were predicted and compared with the experimental data. Theoretical predictions were made based on the computer simulation inputs for the head and the tail of ibuprofen presented in Section 3.3.1. In making micellar composition predictions, our objective was to compare the predicted and the experimentally-determined micellar compositions at the same solution composition. Accordingly, micellar composition predictions were made at the experimentally-measured SDS and ibuprofen solution concentrations. However, we would like to stress that molecular-thermodynamic theory can also be used to predict the micellar composition at the *theoretically-predicted* solubility limit of ibuprofen in the micellar solution.

Micellar composition estimates were made using both tail identifications for ibuprofen (with and without the inclusion of group 4). These results are presented in Fig-

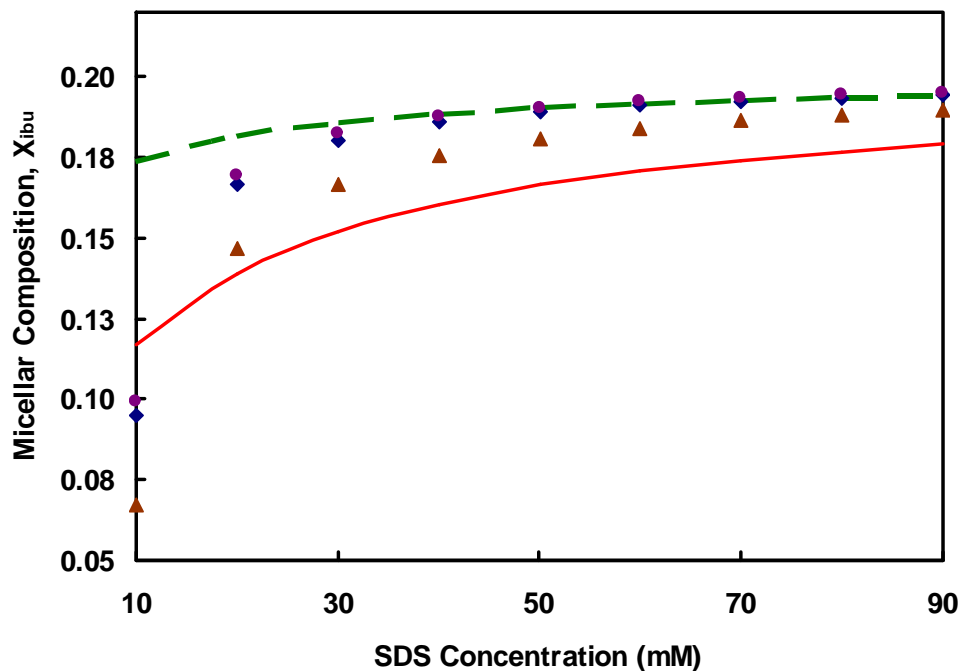


Figure 3-5: Micellar composition of ibuprofen (X_{ibu}), defined as the mole fraction of ibuprofen in the micellar aggregate, as a function of SDS concentration in phosphate buffer at pH 7.4 and 25 °C. The theoretical predictions are based on modeling ibuprofen with the inclusion of group 4 (dashed line) and without the inclusion of group 4 (solid line) as part of the ibuprofen tail. The experimental values are based on the approximation that: (i) the SDS monomeric concentration remains constant at its CMC value of 4.7 mM (diamonds), (ii) the SDS monomeric concentration is equal to that predicted using the molecular-thermodynamic theory with the inclusion of group 4 in the ibuprofen tail (circles), and (iii) the SDS monomeric concentration is equal to that predicted using the molecular-thermodynamic theory without the inclusion of group 4 in the ibuprofen tail (triangles).

ure 3-5, where the theoretically-predicted micellar composition (X_{ibu} , or equivalently $(1 - \alpha^*)$, see Section 3.3.2) is plotted as a function of SDS concentration. Note that X_{ibu} corresponds to the mole fraction of ibuprofen in the micelle. The dashed line is the theoretical prediction based on the inclusion of group 4 in the ibuprofen tail, and the solid line is the theoretical prediction based on the exclusion of group 4 from the ibuprofen tail. Experimental data on the solubility limit of ibuprofen in the presence of SDS have been converted to obtain the “experimental” micellar composition as a function of SDS concentration. This was done by applying a mole balance to the entire solution (consisting of the monomer and the micellar pseudophases). Upon applying such a mole balance, the following equation relating the experimental ibuprofen solubility data to the micellar composition is obtained:

$$X_{ibu} = \frac{(C_{ibu} - 4.0 \text{ mM})}{(C_{SDS} - C_{1SDS}) + (C_{ibu} - 4.0 \text{ mM})} \quad (3.6)$$

where C_{ibu} is the experimentally-measured concentration of ibuprofen solubilized in the solution, 4.0 mM is the experimentally-measured solubility limit of ibuprofen in the buffer solution with no surfactant present (see Section 2.2), C_{SDS} is the concentration of SDS added to the solution, and C_{1SDS} is the concentration of monomeric SDS in the aqueous solution.

Three different approximations were made to determine C_{1SDS} . The first, and simplest, approximation (see the diamonds in Figure 3-5) was to specify the monomeric concentration of SDS as remaining constant at 4.7 mM, which is the experimentally-measured CMC of SDS in the buffer solution saturated with 4.0 mM ibuprofen (see Table 3.1). The second and third approximations were to specify the monomeric concentration of SDS based on the theoretical predictions of the molecular-thermodynamic theory, in one case with inclusion of group 4 in the ibuprofen tail (the triangles in Figure 3-5), and in the other without inclusion of group 4 in the ibuprofen tail (the circles in Figure 3-5). In the molecular-thermodynamic approach, the SDS monomeric concentration is determined by solving for the equilibrium monomeric SDS concentration

corresponding to the free-energy minimum for the entire solution [32]. Each approximation for the SDS monomeric concentration yielded somewhat different estimates of the micellar composition (X_{ibu}) as a function of SDS concentration.

Without group 4 included in the ibuprofen tail (solid line in Figure 3-5), the theoretical predictions of X_{ibu} underestimate the concentration of ibuprofen in the micellar aggregates over most of the SDS concentration range. With the inclusion of group 4 in the ibuprofen tail (dashed line in Figure 3-5), more accurate estimates of X_{ibu} are obtained at all but the lowest SDS concentrations. However, overall, both tail assignments yield reasonable predictions. The worst theoretical predictions, with and without the inclusion of group 4, are obtained at the lowest SDS concentration considered (10 mM). At very low concentrations of SDS in the solution, the experimental results indicate that the micelles are composed almost entirely of SDS. Our theoretical predictions overestimate the tendency of ibuprofen to solubilize at low concentrations of SDS, where the solubility predictions are most sensitive to the accuracy of our modeling approach for SDS and ibuprofen.

Figure 3-6 compares theoretical predictions of ibuprofen solubility as a function of SDS concentration with the experimental solubility data taken from Figure 3-2 above the CMC (note that error bars are not shown for clarity). As expected based on the results shown in Figure 3-5, the inclusion of group 4 in the ibuprofen tail (dashed line) yields the best ibuprofen solubility predictions. With the inclusion of group 4, the solubility enhancement of ibuprofen due to the presence of SDS is predicted very accurately. Using this modeling approach, the theoretically-predicted value of the molar solubilization capacity, χ , is 0.23. Without the inclusion of group 4, the ibuprofen solubility is somewhat underpredicted (solid line), and this underprediction increases as the SDS concentration increases. Without group 4, the theoretically-predicted value of χ is 0.17. The average value of χ based on both tail approximations is 0.20, which is in reasonable agreement with the experimentally-measured value of 0.23 reported in Section 2.3.

Because theoretical predictions of micellar composition and of ibuprofen solubility

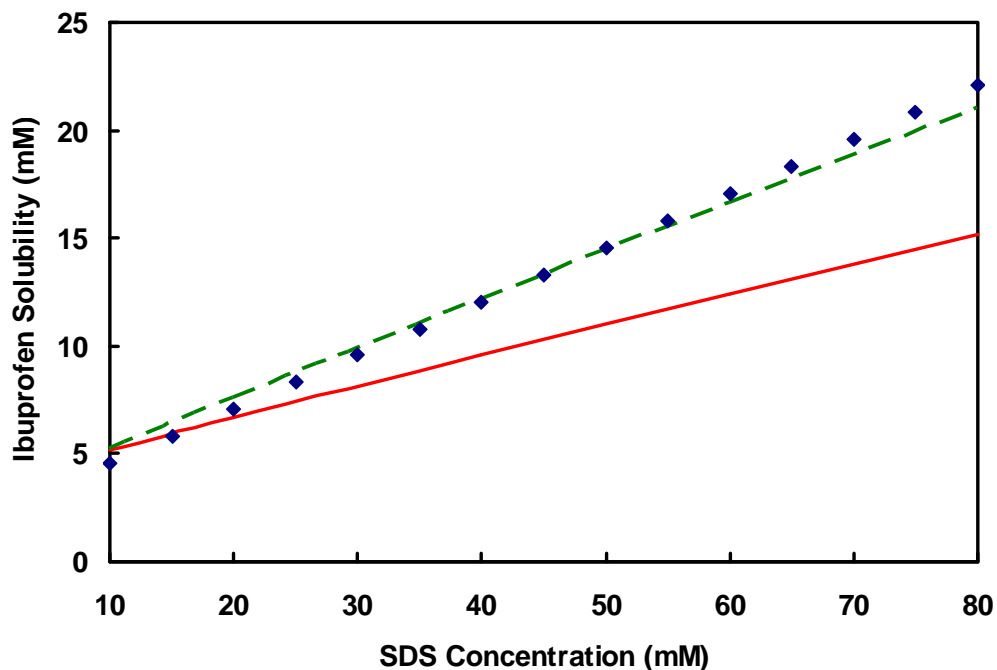


Figure 3-6: Ibuprofen solubility as a function of SDS concentration in phosphate buffer at pH 7.4 and 25 °C. The theoretical predictions are based on modeling ibuprofen with the inclusion of group 4 (dashed line) and without the inclusion of group 4 (solid line) as part of the ibuprofen tail. The experimental solubility data (diamonds), taken from Figure 2 above the CMC, is provided for comparison. Note that error bars are not shown for clarity.

as a function of SDS concentration appear to be very sensitive to the head and tail assignments made for ibuprofen, the results in Figures 3-5 and 3-6 indicate that the computer simulation method that was used to identify the head and tail portions of ibuprofen provided accurate inputs for the molecular-thermodynamic theory. Given the complexity of ibuprofen's chemical structure, without using computer simulations to identify the head and the tail of ibuprofen, it would not have been possible to obtain the type of agreement between theory and experiment shown in Figures 3-5 and 3-6.

As Figure 3-5 shows, only a limited amount of ibuprofen is solubilized in the SDS micelles, and the experimental X_{ibu} values are between 7% and 19% over the entire range of SDS concentrations examined. The lack of synergistic interactions between the negatively-charged SDS heads and the ibuprofen heads would be expected to limit solubility. Mall et al. observed a similarly low level of solubility for sulfanilamide, an acidic drug with a pKa of 10.4, in the presence of SDS [1]. In addition to the lack of synergistic electrostatic interactions between the SDS and the ibuprofen heads, the ibuprofen also has a less negative transfer free-energy contribution ($g_{tr} = -13.95 k_B T$ or $-15.46 k_B T$, depending on tail assignment) than SDS ($g_{tr} = -16.95 k_B T$). This makes the inclusion of ibuprofen in an SDS micelle less favorable than the inclusion of SDS, and further limits the solubilization of ibuprofen.

As stated in Section 2.1, ibuprofen is an acidic drug that is 99.7% dissociated at pH 7.4. As a result, ibuprofen has been modeled here as being fully dissociated (both in the molecular dynamics simulations and in the molecular-thermodynamic modelling). It is noteworthy, however, that the pKa of ibuprofen is expected to shift to a higher value in the presence of SDS micelles, decreasing the ionized fraction of ibuprofen [50]. To check the validity of the fully-dissociated approximation, a recently-developed molecular-thermodynamic model of pH-sensitive micellization was used to estimate the ionized fraction of ibuprofen in an SDS micelle at the experimental conditions examined [25]. This recently-developed theory is capable of predicting the extent of dissociation of pH-sensitive micellar components based on minimization of the solution free energy and the pKa values of each component in pure water. Our

calculations showed that over 93% of ibuprofen molecules are ionized in an SDS micelle, indicating that the fully-ionized approximation made to model this system is reasonable. Similar calculations showed that the fully-dissociated approximation is also appropriate to model the ibuprofen/DTAB and the ibuprofen/C₁₂E₈ micellar systems.

Ibuprofen Solubilization in DTAB Micelles

Recent computer simulation and molecular-thermodynamic modeling of DTAB indicate that this surfactant should be modeled as possessing either 10 or 11 carbon atoms in the surfactant tail [22]. This conclusion was reached by computer simulations of DTAB at an octane/water interface, and by the subsequent comparison of theoretical predictions of CMCs and micelle aggregation numbers with the experimental values. With this in mind, both tail approximations have been used for the theoretical predictions made in this chapter. Molecular-thermodynamic modeling of DTAB in water and of DTAB in the same buffered solution that was used to gather the experimental data reported in Section 2.3 yielded CMC predictions of 41.16 mM and 35.98 mM, respectively, when the DTAB tail was treated as containing 10 carbons, and CMC predictions of 10.34 mM and 6.25 mM, respectively, when the DTAB tail was treated as containing 11 carbons. These predictions bound the experimentally-measured CMCs reported in Table 3.1, which are 15.9 mM in water and 13.5 mM in the buffer solution, indicating that DTAB is modeled reasonably well using the molecular-thermodynamic modeling approach.

Theoretical predictions of the ibuprofen micellar composition (X_{ibu}) as a function of DTAB concentration are shown in Figure 3-7. The theoretical predictions were made based on both tail identifications for ibuprofen (with and without the inclusion of group 4), and both tail identifications for DTAB (including either 10 or 11 carbon atoms in the DTAB tail). In Figure 3-7, the modeling results presented for ibuprofen are an average of the results obtained based on both DTAB tail identifications. Note that X_{ibu} reported in Figure 3-7 corresponds to the mole fraction of ibuprofen in the

micelle, and that the DTAB concentration reported in Figure 3-7 corresponds to the amount of DTAB added to the solution. Because cationic and anionic surfactant mixtures are known to precipitate [51], we specifically checked for precipitation of a mixture of DTAB and ibuprofen and confirmed that this did not take place at the conditions examined (data not shown). In Figure 3-7, experimental values of X_{ibu} are presented along with the theoretical X_{ibu} predictions for comparison, where X_{ibu} was calculated from the experimental ibuprofen solubility data assuming that: (i) the DTAB monomeric concentration remains constant at the experimentally-determined CMC value of DTAB in a buffer solution saturated with 4.0 mM ibuprofen, or (ii) the DTAB monomeric concentration is estimated using molecular-thermodynamic modeling. Because the DTAB monomeric concentration was found to be approximately the same regardless of whether DTAB was modeled as containing 10 or 11 carbons in its tail or whether the ibuprofen tail was modeled with or without the inclusion of group 4, the experimental results presented in Figure 3-7 are based on an average of these approximations.

The experimental ibuprofen solubility data that was converted into “experimental” micellar compositions based on molecular-thermodynamic estimates of the monomeric DTAB concentration (the circles in Figure 3-7) are expected to be much more accurate than the experimental data converted based on the assumption that the monomeric DTAB concentration remains constant at its CMC value (the diamonds in Figure 3-7). Experimental measurements have shown that cationic/anionic surfactant mixtures have a lower CMC (and hence, a lower monomeric surfactant concentration) than the CMCs of either surfactant component taken individually [51]. By analogy, the DTAB monomeric concentration is expected to decrease below its pure CMC value upon ibuprofen solubilization because of the electrostatic synergy between the positively-charged DTAB and the negatively-charged ibuprofen. Strictly, therefore, our theoretical predictions should be compared with the circles shown in Figure 3-7.

A comparison of Figures 3-5 and 3-7 shows that the theoretical modeling results for X_{ibu} in the DTAB case are less accurate than those obtained in the SDS case. For

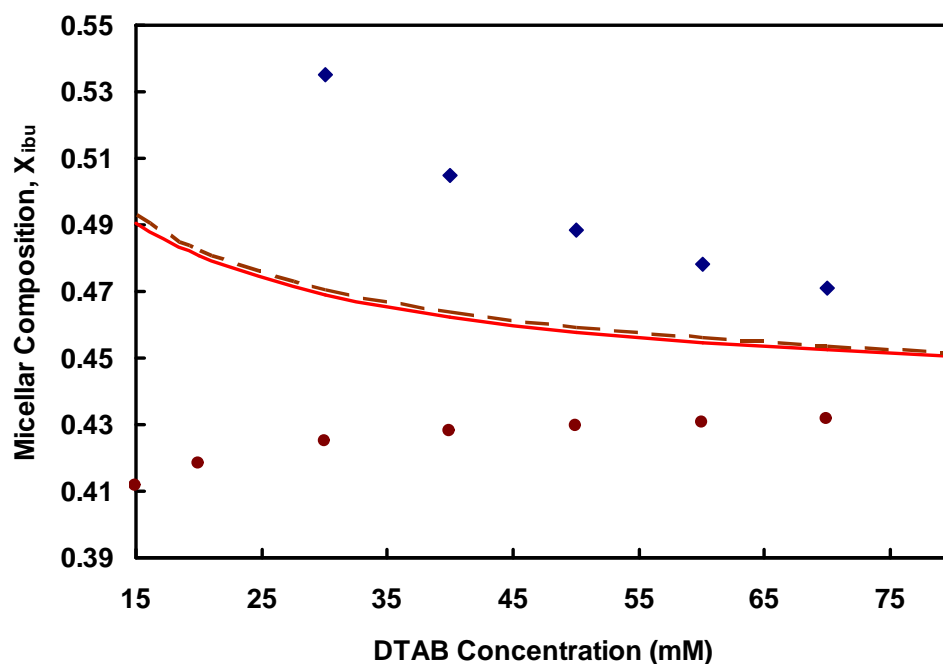


Figure 3-7: Micellar composition of ibuprofen (X_{ibu}), defined as the mole fraction of ibuprofen in the micellar aggregate, as a function of DTAB concentration in phosphate buffer at pH 7.4 and 25 °C. Theoretical predictions are presented for: (i) average results based on modeling DTAB as having an 11 or 12 carbon atom tail, and modeling ibuprofen with the inclusion of group 4 in its tail (dashed line), and (ii) average results based on modeling DTAB as having an 11 or 12 carbon atom tail, and modeling ibuprofen without the inclusion of group 4 in its tail (solid line). The experimental values are based on the approximation that: (a) the DTAB monomeric concentration remains constant at its CMC value of 11.0 mM (diamonds), (b) the DTAB monomeric concentration is equal to an average of the theoretical predictions for the DTAB monomeric concentration based on modeling using approximations (i)-(ii) listed above (circles).

this system, the degree of electrostatic synergy between the oppositely-charged DTAB and ibuprofen molecules appears to be overestimated by the theory, leading to an overprediction of the micellar ibuprofen concentration (X_{ibu}). For systems exhibiting significant electrostatic synergy, it is more difficult to accurately quantify the free-energy contribution associated with the electrostatic interactions (g_{elec}). The term g_{elec} is positive, implying that there is always a penalty for “charging” the surfactants and the solubilizates at the surface of the micelle. In the DTAB/ibuprofen case, we appear to underestimate the magnitude of g_{elec} , leading to an overprediction of the synergy between the oppositely-charged DTAB and ibuprofen molecules.

The solubility limit of ibuprofen in the presence of DTAB has also been predicted theoretically using both head and tail identifications for ibuprofen, as well as both estimates for the DTAB tail length. In Figure 3-8, the experimental data on ibuprofen solubility, taken from Figure 3-3 above the CMC (note that error bars are not shown for clarity), and the theoretical predictions of ibuprofen solubility are presented as a function of the DTAB concentration. Note that the theoretical predictions for ibuprofen are an average of the results obtained based on both DTAB tail approximations. As expected based on the results shown in Figure 3-7, the solubility of ibuprofen is overestimated for both of the ibuprofen tail identifications used in the theoretical modeling (solid and dashed lines). On average, over the range of DTAB concentrations examined, when group 4 is included in the ibuprofen tail, ibuprofen solubility is overestimated by a factor of 1.9 (dashed line). For comparison, when group 4 is not included in the ibuprofen tail, ibuprofen solubility is overestimated by a factor of 1.7. This overprediction is also reflected in our theoretical estimate of χ (based on an average of all the tail approximations), which at 2.11 is about a factor of two larger than the experimental value of 0.97 that we reported in Section 2.3.

Molecular-thermodynamic modeling reveals that the large extent of ibuprofen solubility in the DTAB micellar solution results from the favorable electrostatic attractions between the positively-charged DTAB molecules and the negatively-charged ibuprofen molecules. Because ibuprofen has a less negative transfer free-energy con-

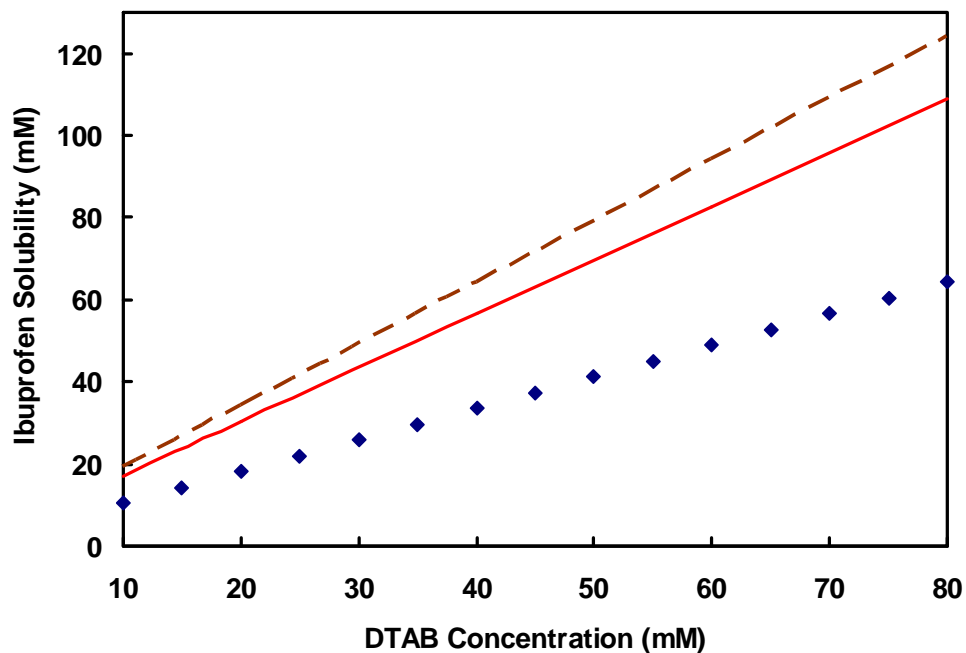


Figure 3-8: Ibuprofen solubility as a function of DTAB concentration in phosphate buffer at 25 °C. Theoretical predictions are presented for: (i) average results based on modeling DTAB as having an 11 or 12 carbon atom tail, and modeling ibuprofen with the inclusion of group 4 in its tail (dashed line), and (ii) average results based on modeling DTAB as having an 11 or 12 carbon atom tail, and modeling ibuprofen without the inclusion of group 4 in its tail (solid line). The experimental solubility data (diamonds), taken from Figure 3 above the CMC, is provided for comparison. Note that error bars are not shown for clarity.

tribution ($g_{tr} = -13.95 k_B T$ or $-15.46 k_B T$, depending on tail assignment) than DTAB ($g_{tr} = -15.46 k_B T$ or $-16.96 k_B T$, depending on tail assignment), g_{tr} favors micellar aggregates that contain more DTAB than ibuprofen. This is similar to what was observed in the case of ibuprofen solubilization in SDS micelles reported in Section 3.3.3. However, in solutions of DTAB and ibuprofen, the solubilization of additional ibuprofen is favored because of the synergistic electrostatic interactions between the oppositely-charged DTAB and ibuprofen heads. Caetano et al. observed a similar behavior in mixtures of the negatively-charged surfactant SDS and the positively-charged trifluoperazine, an amphiphilic drug used as an antipsychotic and a tranquilizer [52].

Ibuprofen Solubilization in $C_{12}E_8$ Micelles

Recent molecular-thermodynamic modeling studies of $C_{12}E_8$ conducted by our group indicate that every ethylene oxide (EO) group in this nonionic surfactant should be included as part of the surfactant head, and that every carbon atom in the linear alkyl chain should be included as part of the surfactant tail [22]. Molecular-thermodynamic modeling of $C_{12}E_8$ in water and of $C_{12}E_8$ in the same buffer solution that we used to gather the experimental data in Section 2.3 yielded CMC predictions of 0.53 and 0.52 mM, respectively, which are larger than the experimental CMCs of 0.08 mM and 0.09 mM reported in Table 3.1, but which nevertheless indicate that $C_{12}E_8$ is modeled reasonably well using the molecular-thermodynamic modeling approach.

Theoretical predictions of the ibuprofen micellar composition (X_{ibu}) as a function of $C_{12}E_8$ concentration are presented in Figure 3-9, using the same approach described in Section 3.3.3. The variable X_{ibu} in Figure 3-9 corresponds to the mole fraction of ibuprofen in the micelle. Theoretical predictions have been made using both head and tail identifications for ibuprofen (with and without the inclusion of group 4 in the tail). Experimental values of ibuprofen micellar compositions, estimated based on the same three approximations for the $C_{12}E_8$ monomeric concentration described in Section 3.3.3, are shown for comparison. Because the $C_{12}E_8$ monomeric concentration is very

low, similar estimates of X_{ibu} were obtained using all three approximations. As shown in Figure 3-9, the closest agreement with the experimental results is obtained without including group 4 in the ibuprofen tail (solid line). However, X_{ibu} is also predicted reasonably well with the inclusion of group 4 (dashed line), and the experimentally-determined X_{ibu} values are bounded by the two theoretical X_{ibu} predictions. Without inclusion of group 4, the theoretically-predicted value of χ is 0.62. With inclusion of group 4, χ is predicted to be 1.19. The average of the two predicted χ values is equal to 0.87, which is in reasonable agreement with the experimental value of 0.72 reported in Section 2.3.

The solubility limit of ibuprofen in the presence of $C_{12}E_8$ was also predicted theoretically using both tail identifications for ibuprofen. These theoretical predictions are presented in Figure 3-10 along with the experimental ibuprofen solubility data taken from Figure 3-4 above the CMC (note that error bars are not shown for clarity). As expected based on the results shown in Figure 3-9, the experimental solubility values lie in between the theoretical predictions based on the inclusion or the exclusion of group 4 in the ibuprofen tail. Both methods of modeling ibuprofen yield reasonable predictions of ibuprofen solubility. Because the theoretical predictions of compositions and ibuprofen solubilities are very sensitive to the head and tail assignments made for ibuprofen, our results indicate that the computer simulation method used to identify the head and the tail portions of ibuprofen provided accurate inputs for the molecular-thermodynamic theory.

It is noteworthy that the solubility of ibuprofen in the $C_{12}E_8$ micellar solution is similar to what is observed in the DTAB micellar solution, in spite of the fact that the molar solubilization capacity of DTAB ($\chi = 0.97$) is higher than that of $C_{12}E_8$ ($\chi = 0.72$). In other words, although the number of moles of ibuprofen solubilized per mole of surfactant is greater for DTAB than for $C_{12}E_8$, the nonionic surfactant is almost equally effective at increasing ibuprofen solubility. The reason for this behavior is the low CMC of $C_{12}E_8$ relative to DTAB, which indicates that $C_{12}E_8$ has a stronger tendency than DTAB to form micelles in aqueous solution. As a result,

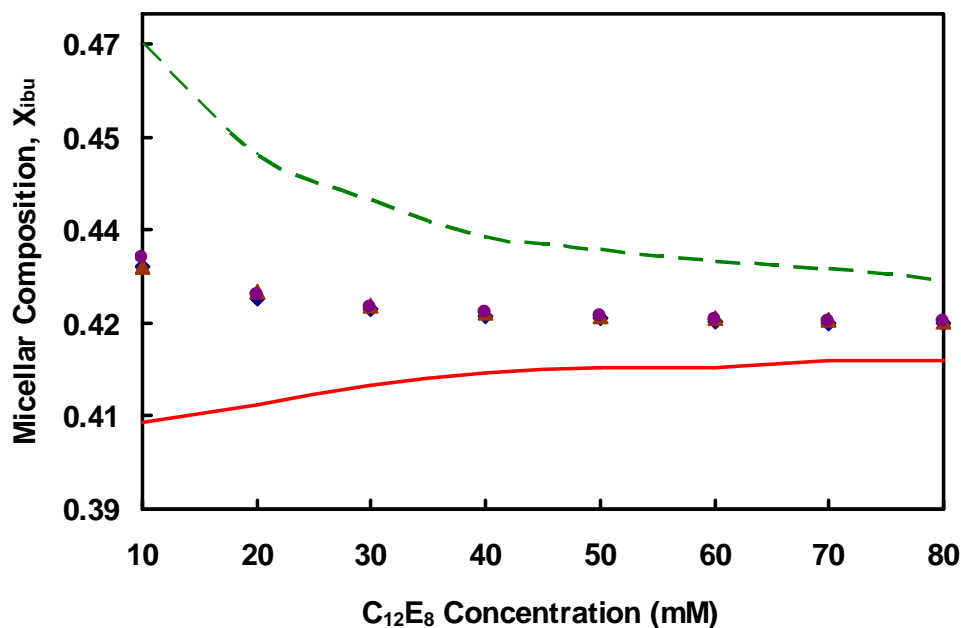


Figure 3-9: Micellar composition of ibuprofen (X_{ibu}), defined as the mole fraction of ibuprofen in the micellar aggregate, as a function of $C_{12}E_8$ concentration in phosphate buffer at pH 7.4 and 25 °C. The theoretical predictions are based on modeling ibuprofen with the inclusion of group 4 in its tail (dashed line) and without the inclusion of group 4 in its tail (solid line). The experimental values are based on the approximation that: (i) the $C_{12}E_8$ monomeric concentration remains constant at its CMC value of 0.05 mM (diamonds), (ii) the $C_{12}E_8$ monomeric concentration is equal to that predicted using the molecular-thermodynamic theory with the inclusion of group 4 in the ibuprofen tail (circles), and (iii) the $C_{12}E_8$ monomeric concentration is equal to that predicted using the molecular-thermodynamic theory without the inclusion of group 4 in the ibuprofen tail (triangles).

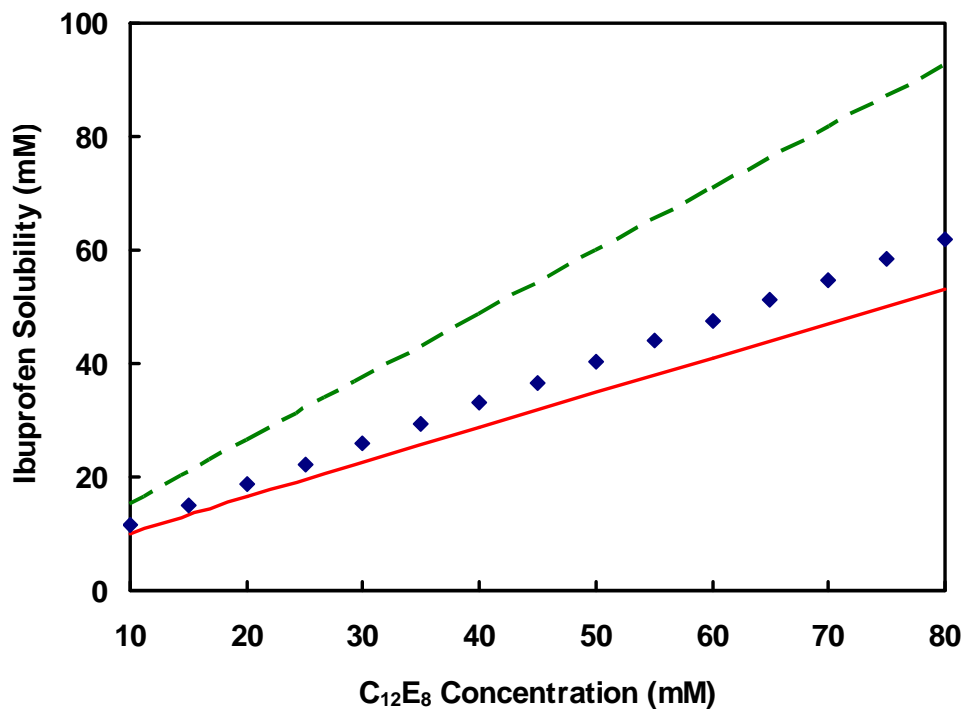


Figure 3-10: Ibuprofen solubility as a function of C₁₂E₈ concentration in phosphate buffer at pH 7.4 and 25 °C. The theoretical predictions are based on modeling ibuprofen with the inclusion of group 4 in its tail (dashed line) and without the inclusion of group 4 in its tail (solid line). The experimental solubility data (diamonds), taken from Figure 4 above the CMC, is provided for comparison. Note that error bars are not shown for clarity.

a large fraction of $C_{12}E_8$ in the micellar solution is present in micellar form, thus creating more locations within the solution at which ibuprofen may be solubilized.

3.4 Conclusions

In this chapter, the extent of micellar-assisted aqueous solubilization of ibuprofen in anionic (SDS), cationic (DTAB), and nonionic ($C_{12}E_8$) micelles was investigated both experimentally and theoretically. The anionic surfactant SDS exhibited the worst ibuprofen solubility profile. Solubility profiles for ibuprofen in the presence of DTAB and $C_{12}E_8$ were quite similar to each other. Although the molar solubilization ratio of $C_{12}E_8$ ($\chi = 0.72$) was found to be lower than that of DTAB ($\chi = 0.97$), $C_{12}E_8$ has a much lower CMC than DTAB, which facilitates its ability to form micelles and to solubilize ibuprofen. Therefore, from a pharmaceutical standpoint, nonionic surfactants like $C_{12}E_8$ may be the best choice for the micellar-assisted solubilization of ibuprofen in aqueous media, since they provide a reasonable molar solubilization capacity combined with a low CMC. In addition, the low relative toxicity of nonionic surfactants makes them particularly useful for solubilization and drug delivery purposes.

A combined computer simulation/molecular-thermodynamic modeling approach was used to model the aqueous solubility of ibuprofen in the presence of the three surfactants considered in this chapter. Molecular dynamics simulations of ibuprofen at an octane/water interface were used to estimate what portions of ibuprofen are hydrated in a micellar environment (the ibuprofen head), and what portions of ibuprofen are shielded from water within the micellar core (the ibuprofen tail). The simulation data was analyzed by counting the number of contacts made by the water molecules and by the octane molecules with each atom in ibuprofen. Through measuring the relative frequency of contacts between each atom and either water or octane, it was possible to infer whether each ibuprofen atom was surrounded primarily by water or by octane during the simulation run. The OPLS-AA forcefield

was implemented to describe the interactions between ibuprofen, SPC-E water, and octane. In addition, two methods were used to determine atomic charge parameters. The first method made use of the CHelpG approach, in which atomic charges are assigned to fit the electrostatic potential at a number of points on the van der Waals surface. The second method simply used the atomic charge parameters recommended in the OPLS-AA forcefield. Equivalent head and tail identifications were made for ibuprofen based on both sets of atomic charges.

Our theoretical predictions of the ibuprofen micellar composition (X_{ibu}) and of the solubility of ibuprofen in aqueous solutions of SDS and C₁₂E₈ compare well with the experimental data, indicating that: (i) the head and the tail identifications made for ibuprofen based on the computer simulation results are reasonable, and (ii) the molecular-thermodynamic approach accurately predicts solution properties based on the computer simulation inputs. Our theoretical estimates of X_{ibu} and of the solubility of ibuprofen in aqueous solutions of DTAB were also reasonable, although the predicted degree of electrostatic synergy due to the opposite charges of ibuprofen and DTAB was overestimated, leading to an overprediction of the ibuprofen solubility in the DTAB case.

In the case of molecules with relatively complex chemical structures, such as ibuprofen, the *a priori* identification of how such molecules will locate and orient themselves in a micellar aggregate is challenging and often speculative. The results presented in this chapter indicate that computer simulations of ibuprofen at an oil/water interface (modeling the micelle core/water interface) are sufficient to determine inputs for molecular-thermodynamic modeling of the micellar-assisted solubilization of ibuprofen in aqueous solution.

In the next chapter, Chapter 4, a general computer simulation/molecular-thermodynamic model of micellar solubilization will be presented. In this general model, the mean-field model used in this chapter to evaluate g_{pack} will be generalized to allow evaluation of g_{pack} for more complex surfactant and solubilizate tails (including tails with ringed structures). In addition, through the inclusion of what will be referred to as a “neu-

tral groups,” the mean-field model will be extended to allow more physically realistic modeling of surfactant/solubilizate tail groups that spend a significant amount of time both inside and outside the micelle core (as indicated by molecular dynamics simulation results). Computer simulation results for solubilizate head, tail, and neutral groups and the molecular-thermodynamic model of micellar solubilization introduced in Chapter 4 will be used in Chapter 5 to make predictions of the micellar solubilization of seven different solubilizates by nonionic, anionic, and cationic surfactants.

Bibliography

- [1] Mall, S., Buckton, G., and Rawlins, D. A., “Dissolution behaviour of sulphonamides into sodium dodecyl sulfate micelles: A thermodynamic approach,” *Journal of Pharmaceutical Sciences*, Vol. 85, 1996, pp. 75–78.
- [2] Rosen, M., *Surfactants and Interfacial Phenomena*, John Wiley and Sons, New York, 10th ed., 1989.
- [3] Allen, T. M., Hansen, C. B., and Menenez, D. E. L., “Pharmacokinetics of long-circulating liposomes,” *Advanced Drug Delivery Reviews*, Vol. 16, 1995, pp. 267–284.
- [4] Canto, G. S., Dalmora, S. L., and Oliveira, A. G., “Piroxicam encapsulated in liposomes: Characterization and in vivo evaluation of topical anti-inflammatory effect,” *Drug Development and Industrial Pharmacy*, Vol. 25, 1999, pp. 1235–1239.
- [5] Gref, R., Minamitake, Y., Peracchia, M. T., Trubetskoy, V. S., Torchilin, V. P., and Langer, R., “Biodegradable long-circulating polymeric nanospheres,” *Science*, Vol. 263, 1994, pp. 1600–1603.
- [6] Jones, M. C. and Leroux, J. C., “Polymeric micelles - A new generation of colloidal drug carriers,” *European Journal of Pharmaceutics and Biopharmaceutics*, Vol. 48, 1999, pp. 101–111.
- [7] Torchilin, V. P., Trubetskoy, V. S., Whiteman, K. R., Caliceti, P., Ferruti, P., and Veronese, F. M., “New synthetic amphiphilic polymers for steric protection of

- liposomes in-vivo,” *Journal of Pharmaceutical Sciences*, Vol. 84, 1995, pp. 1049–1053.
- [8] Torchilin, V. P., “Structure and design of polymeric surfactant-based drug delivery systems,” *Journal of Controlled Release*, Vol. 73, 2001, pp. 137–172.
- [9] Attwood, D. and Florence, A. T., *Surfactant Systems: Their Chemistry, Pharmacology and Biology*, Chapman and Hall, New York, 1983.
- [10] Alvarez-Nunez, F. A. and Yalkowsky, S. H., “Relationship between polysorbate 80 solubilization descriptors and octanol-water partition coefficients of drugs,” *International Journal of Pharmaceutics*, Vol. 200, 2000, pp. 217–222.
- [11] Janjikhel, R. K. and Adeyeye, C. M., “Dissolution of ibuprofen enantiomers from coprecipitates and suspensions containing chiral excipients,” *Pharmaceutical Development Technology*, Vol. 4, 1999, pp. 9–17.
- [12] Simo, C., Gallardo, A., San Roman, J., Barbas, C., and Cifuentes, A., “Fast and sensitive capillary electrophoresis method to quantitatively monitor ibuprofen enantiomers released from polymeric drug delivery systems,” *Journal of Chromatography B*, Vol. 767, 2002, pp. 35–43.
- [13] Suedee, R., Srichana, T., and Rattananont, T., “Enantioselective release of controlled delivery granules based on molecularly imprinted polymers,” *Drug Delivery*, Vol. 9, 2002, pp. 19–30.
- [14] Liso, P. A., Rebueta, M., Sandroman, J., Gallardo, A., and Villar, A. M., “Antinociceptive and antipyretic properties of a new conjugated ibuprofen-methacrylic polymeric controlled delivery system,” *Journal of Controlled Release*, Vol. 33, 1995, pp. 429–436.
- [15] Park, E. S., Chang, S. Y., Hahn, M., and Chi, S. C., “Enhancing effect of polyoxyethylene alkyl ethers on the skin permeation of ibuprofen,” *International Journal of Pharmaceutics*, Vol. 209, 2000, pp. 109–119.

- [16] Bula, D. and Ghaly, E. S., “Liposome delivery systems containing ibuprofen,” *Drug Development and Industrial Pharmacy*, Vol. 21, 1995, pp. 1621–1629.
- [17] Yazdanian, M., Briggs, K., Jankovsky, C., and Hawi, A., “The ‘high solubility’ definition of the current FDA Guidance on Biopharmaceutical Classification System may be too strict for acidic drugs,” *Pharmaceutical Research*, Vol. 21, 2004, pp. 293–299.
- [18] Portoles, A., Vargas, E., Burgos, A., Moreno, E., Garcia, M., Terleira, A., Caturla, M. C., and Moreno, A., “Pharmacokinetic study of a new ibuprofen 600mg plus codeine 30mg combination versus ibuprofen or codeine alone in single oral doses in healthy volunteers,” *Clinical Drug Investigation*, Vol. 22, 2002, pp. 41–49.
- [19] Zhao, X., Chen, D., Gao, P., Ding, P., and Li, K., “Synthesis of ibuprofen eugenol ester and its microemulsion formulation for parenteral delivery,” *Chemical and Pharmaceutical Bulletin*, Vol. 53, 2005, pp. 1246–1250.
- [20] Yong, C. S., Lee, M. K., Park, Y. J., Kong, K. H., Xuan, J. J., Kim, J. H., Kim, J. A., Lyoo, W. S., Han, S. S., Rhee, J. D., Kim, J. O., Yang, C. H., Kim, C. K., and Choi, H. G., “Enhanced oral bioavailability of ibuprofen in rats by poloxamer gel using poloxamer 188 and menthol,” *Drug Development and Industrial Pharmacy*, Vol. 31, 2005, pp. 615–622.
- [21] Nerurkar, J., Beach, J. W., Park, M. O., and Jun, H. W., “Solubility of guaifenesin in the presence of common pharmaceutical additives,” *Pharmaceutical Development and Technology*, Vol. 10, 2003, pp. 385–396.
- [22] Stephenson, B. C., Beers, K., and Blankschtein, D., “Complementary use of simulations and molecular-thermodynamic theory to model micellization,” *Langmuir*, Vol. 22, 2006, pp. 1500–1513.

- [23] Srinivasan, V., *Theoretical Modeling of Micellization and Solubilization in Ionic Surfactant Systems*, Ph.D. thesis, Massachusetts Institute of Technology, 2003, and references cited therein.
- [24] Srinivasan, V. and Blankschtein, D., “Effect of counterion binding on micellar solution behavior: 1. Molecular-thermodynamic theory of micellization of ionic surfactants,” *Langmuir*, Vol. 19, 2003, pp. 9932–9945.
- [25] Goldsipe, A. and Blankschtein, D., “Modeling counterion binding in ionic-nonionic and ionic-zwitterionic binary surfactant mixtures,” *Langmuir*, Vol. 22, 2005, pp. 9850–9865.
- [26] Ridell, A., Evertsson, H., Nilsson, S., and Sundelof, L. O., “Amphiphilic association of ibuprofen and two nonionic cellulose derivatives in aqueous solution,” *Journal of Pharmaceutical Sciences*, Vol. 88, 1999, pp. 1175–1181.
- [27] Shah, S. S., Jamroz, N. U., and Sharif, Q. M., “Micellization parameters and electrostatic interactions in micellar solution of sodium dodecyl sulfate (SDS) at different temperatures,” *Colloids and Surfaces A: Physicochemical and Engineering Aspects*, Vol. 178, 2001, pp. 199–206.
- [28] Hu, R. Y. Z., Wang, A. T. A., and Hartnett, J. P., “Surface-tension measurement of aqueous polymer solutions,” *Experimental Thermal and Fluid Science*, Vol. 4, 1991, pp. 723–729.
- [29] Theander, K. and Pugh, R. J., “The influence of pH and temperature on the equilibrium and dynamic surface tension of aqueous solutions of sodium oleate,” *Journal of Colloid and Interface Science*, Vol. 239, 2001, pp. 209–216.
- [30] Prete, P. S. C., Gomes, K., Malheiros, S. V. P., Meireles, N. C., and De Paula, E., “Solubilization of human erythrocyte membranes by non-ionic surfactants of the polyoxyethylene alkyl ethers series,” *Biophysical Chemistry*, Vol. 97, 2002, pp. 45–54.

- [31] ChemSW, Inc., Fairfield, CA., *Molecular Modeling Pro version 3.2*, 2003.
- [32] Puvvada, S. and Blankschtein, D., “Molecular thermodynamic approach to predict micellization, phase behavior and phase separation of micellar solutions. 1. Application to nonionic surfactants,” *The Journal of Chemical Physics*, Vol. 92, 1990, pp. 3710–3724, and references cited therein.
- [33] Jorgensen, W. L., Maxwell, D. S., and Tirado-Rives, J., “Development and testing of the OPLS all-atom force field on conformational energetics and properties of organic liquids,” *Journal of the American Chemical Society*, Vol. 118, 1996, pp. 11225–11236.
- [34] Berendsen, H. J. C., Grigera, J. R., and Straatsma, T. P., “The missing term in effective pair potentials,” *The Journal of Physical Chemistry*, Vol. 91, 1987, pp. 6269–6271.
- [35] Breneman, C. and Wiberg, K., “Determining atom-centered monopoles from molecular electrostatic potentials: The need for high sampling density in formamide,” *Journal of Computational Chemistry*, Vol. 11, 1990, pp. 361–373.
- [36] Foresman, J. and Frisch, A., *Exploring Chemistry with Electronic Structure Methods*, Gaussian, Inc., Pittsburgh, Pennsylvania, 1996.
- [37] Berendsen, H. J. C., van der Spoel, D., and van Drunen, R., “GROMACS: A message-passing parallel molecular dynamics implementation,” *Computational Physics Community*, Vol. 91, 1995, pp. 43–56.
- [38] Lindahl, E., Hess, B., and van der Spoel, D., “Gromacs 3.0: A package for molecular simulation and trajectory analysis,” *Journal of Molecular Modeling*, Vol. 7, 2001, pp. 306–317.
- [39] van der Spoel, D., Lindahl, E., Hess, B., van Buuren, A., Apol, E., Meulenhoff, P., Tieleman, D., Sijbers, A., Feenstra, K., van Drunen, R., and Berendsen, H., *Gromacs User Manual version 3.2*, www.gromacs.org, 2004.

- [40] Flyvbjerg, H. and Petersen, H. G., “Error estimates on averages of correlated data,” *The Journal of Chemical Physics*, Vol. 91, 1989, pp. 461–466.
- [41] Hess, B., *Stochastic Concepts in Molecular Simulation*, Ph.D. thesis, Rijksuniversiteit Groningen, Groningen, 1999.
- [42] Hess, B., “Determining the shear viscosity of model liquids from molecular dynamics simulations,” *The Journal of Chemical Physics*, Vol. 116, 2001, pp. 209–217.
- [43] Shiloach, A. and Blankschtein, D., “Predicting micellar solution properties of binary surfactant mixtures,” *Langmuir*, Vol. 14, 1998, pp. 1618–1636.
- [44] Tanford, C., *The Hydrophobic Effect: Formation of Micelles and Biological Membranes*, John Wiley and Sons, New York, 1991.
- [45] Puvvada, S. and Blankschtein, D., “Theoretical and experimental investigations of micellar properties of aqueous solutions containing binary mixtures of nonionic surfactants,” *The Journal of Physical Chemistry*, Vol. 96, 1992, pp. 5579–5592.
- [46] Srinivasan, V. and Blankschtein, D., “Effect of counterion binding on micellar solution behavior: 2. Prediction of micellar solution properties of ionic surfactant-electrolyte systems,” *Langmuir*, Vol. 19, 2003, pp. 9946–9961.
- [47] Tetko, I. and Tanchuk, V. Y., “Virtual Computational Chemistry Laboratory webpage,” 2005.
- [48] Tetko, I. and Tanchuk, V. Y., “Application of associative neural networks for prediction of lipophilicity in ALOGPS 2.1 program,” *Journal of Chemical Information and Computer Science*, Vol. 42, 2002, pp. 1136–1145.
- [49] Reinhard, M. and Drefahl, A., *Estimating physiochemical properties of organic compounds*, John Wiley and Sons, Inc., New York, 1999.

- [50] Caetano, W. and Tabak, M., “Interaction of chlorpromazine and trifluoperazine with ionic micelles: Electronic absorption spectroscopy studies,” *Spectrochimica Acta A*, Vol. 55, 1999, pp. 2513–2528.
- [51] Scamehorn, J. F. and Harwell, J. H., *Mixed Surfactant Systems. Surfactant Science Series 46*, Marcel Dekker, New York, 1993.
- [52] Caetano, W., Gelamo, E. L., Tabak, M., and Itri, R., “Chlorpromazine and sodium dodecyl sulfate mixed micelles investigated by small angle X-ray scattering,” *Journal of Colloid and Interface Science*, Vol. 248, 2002, pp. 149–157.

Chapter 4

Complementary Use of Computer Simulations and Molecular-Thermodynamic Theory to Model Micellar Solubilization.

I. Theory

4.1 Introduction

The solubility of hydrophobic, or partly hydrophobic, substances in aqueous solutions can be increased through the addition of surfactants. Surfactants consist of a hydrophilic moiety, known as the head, attached to a hydrophobic moiety, known as the tail. When dissolved in water, surfactant molecules self-assemble into aggregates (micelles), with their hydrophobic tails and any solubilized hydrophobic substances (referred to as solubilizates) shielded from water in the aggregate interior, and their hydrophilic heads exposed to water at the aggregate surface. This self-assembly is driven by hydrophobic, van der Waals, hydrogen-bonding, and (in the case of charged

surfactants and solubilizates) screened electrostatic interactions [1].

A wide variety of industrial, pharmaceutical, and biological processes make use of micellar solubilization processes. The ability of surfactants to aid in the mixing of hydrophobic and hydrophilic molecules is used extensively in the chemical industry for: (i) the removal of oily materials from a substrate, (ii) reaction rate enhancement in polymerization reactions, and (iii) separation processes [1–3]. Surfactants can also be used to solubilize water-insoluble drugs in aqueous solutions for subsequent injection into a patient's body [4]. Examples of biological processes involving biological surfactants include the role of phospholipid biosurfactants in the gastrointestinal tract during digestion, and the body's use of bile salts to solubilize cholesterol [2]. Because micellar solubilization is such a broadly applicable phenomenon, gaining a fundamental understanding of the factors that affect micellar solubilization is of great academic as well as practical interest.

4.1.1 Introduction to Surfactant Micellization and Micellar Solubilization

In the context of the research undertaken in this thesis, micellar solubilization is defined as the spontaneous dissolution of a material by reversible interaction with micelles to form a thermodynamically stable isotropic solution which exhibits reduced thermodynamic activity of the solubilized material [5]. For the purposes of this chapter, a solubilizate may be considered to be a molecule which has a solubility limit in aqueous solution. A solubilizate may be completely hydrophobic, or may contain some hydrophilic and hydrophobic moieties as part of its chemical structure. Solubilizates which are amphiphilic may be viewed as being similar to surfactants in that they are dual-natured and can be thought of as possessing a head and a tail. Amphiphilic solubilizates may behave much like conventional surfactants within a mixed micelle. However, unlike surfactants, solubilizates do not spontaneously self-assemble into micelles in aqueous solution, and therefore, do not have a CMC.

Two key characteristics associated with how micellar solubilization occurs are the extent of solubilization and the locus of solubilization, both of which are discussed below.

The Extent of Solubilization

Experimental determination of the extent of solubilization can be accomplished through several methods, including measuring changes in the surfactant CMC, measuring vapor pressures, calorimetry, head-space gas chromatography, semiequilibrium dialysis, fluorescence, and UV/Vis spectrophotometry. Often, the experimental observations allow determination of information about either the infinite dilution limit of the solubilize (the Henry's law limit) or the saturation limit of the solubilize in the aqueous micellar solution [3, 6–9].

The extent of solubilization is traditionally quantified by several parameters [2, 3], which include:

1. K_x : The dimensionless partition ratio K_x is defined as the solubilize solubility in the micelles, $X_{\text{sol}}^{\text{mic}}$, divided by its solubility in the aqueous solution, $X_{\text{sol}}^{\text{aq}}$ [10]:

$$K_x = \frac{X_{\text{sol}}^{\text{mic}}}{X_{\text{sol}}^{\text{aq}}} \quad (4.1)$$

Both $X_{\text{sol}}^{\text{mic}}$ and $X_{\text{sol}}^{\text{aq}}$ are usually expressed as mole fractions, but the use of molarity units is also encountered.

2. K_s : The equilibrium constant K_s is defined as the concentration of solubilize in the micelles, $C_{\text{sol}}^{\text{mic}}$, divided by the product of the concentration of solubilize in the aqueous solution, $C_{\text{sol}}^{\text{aq}}$, and the concentration of surfactant in the micelles, $C_{\text{surf}}^{\text{mic}}$ [10]. K_s can also be expressed in terms of the mole fraction of solubilize in the micelles, $X_{\text{sol}}^{\text{mic}}$, and the concentration of solubilize in the aqueous solution, $C_{\text{sol}}^{\text{aq}}$:

$$K_s = \frac{C_{\text{sol}}^{\text{mic}}}{C_{\text{sol}}^{\text{aq}} C_{\text{surf}}^{\text{mic}}} = \frac{(n_{\text{sol}}^{\text{mic}}/V_{\text{tot}})/n_{\text{mic}}^{\text{tot}}}{C_{\text{sol}}^{\text{aq}} (n_{\text{surf}}^{\text{mic}}/V_{\text{tot}})/n_{\text{mic}}^{\text{tot}}} = \frac{X_{\text{sol}}^{\text{mic}}}{C_{\text{sol}}^{\text{aq}} (1 - X_{\text{sol}}^{\text{mic}})} \quad (4.2)$$

where $n_{\text{sol}}^{\text{mic}}$ and $n_{\text{surf}}^{\text{mic}}$ are the total number of solubilize and surfactant molecules

associated with the micelles, respectively, V_{tot} is the total volume of the micelles, and $n_{\text{mic}}^{\text{tot}}$ is the total number of surfactant and solubilizate molecules in the micelles.

3. The Molar Solubilization Ratio (MSR): The MSR is defined as the ratio of the total number of solubilizate molecules associated with the micelles to the total number of surfactant molecules associated with the micelles [11]:

$$MSR = \frac{n_{\text{sol}}^{\text{mic}}}{n_{\text{surf}}^{\text{mic}}} = \frac{n_{\text{sol}}^{\text{mic}}/n_{\text{mic}}^{\text{tot}}}{n_{\text{surf}}^{\text{mic}}/n_{\text{mic}}^{\text{tot}}} = \frac{X_{\text{sol}}^{\text{mic}}}{X_{\text{surf}}^{\text{mic}}} = \frac{X_{\text{sol}}^{\text{mic}}}{(1 - X_{\text{sol}}^{\text{mic}})} \quad (4.3)$$

Solubilization isotherms, or the observed extent of solubilization as a function of solubilizate concentration at a fixed temperature, have been measured for a variety of surfactant/solubilizate systems [3, 9, 12]. Many of these studies report solubilization results in the infinite-dilution limit. The experimental data indicate that the micelle/water partition coefficient, K , is frequently a function of the solubilizate concentration within the micelle. The following empirical expression has been found to apply to many surfactant/solubilizate systems [3, 7, 9]:

$$K = K_o(1 - BX_{\text{sol}}^{\text{mic}})^2 \quad (4.4)$$

where K_o is the micelle/water partition coefficient in the limit of zero solubilizate concentration, and the parameter B corresponds to the initial slope of the solubilization isotherm, and is a function of the type of surfactant and solubilizate present. Because non-infinite dilution conditions cannot be considered ideal, the observed dependence of K on concentration ($X_{\text{sol}}^{\text{mic}}$) in Eq. 4.4 is not surprising.

The Locus of Solubilization

The locus (location) of solubilization plays an important role in determining the extent of solubilization, the rate of micellar reactions where the solubilizate acts as a reactant or as a catalyst, and the rate at which solubilizate diffusion out of the micelle occurs [13]. The locus of solubilization also affects the way in which the solubilizate may influence solution properties such as the CMC and the micelle shape and size.

The location of the solubilize within micelles can be determined by direct experimental measurement (using techniques such as IR spectroscopy or fluorescence), or it can be inferred indirectly using thermodynamic data such as partition coefficients [3, 6, 8, 11, 14, 15]. Experimental studies have indicated that there are three distinct regions within a micelle where solubilization may occur: (i) the core region, or deep interior of the micelle, (ii) the palisade layer, which refers to the region consisting of the surfactant tails, and (iii) the corona region, which refers to the region consisting of the surfactant heads in the case of surfactants with polymeric heads such as the alkyl poly(ethylene oxide), C_iE_j , nonionic surfactants (see Chapter 1 for a schematic depiction of these three solubilization regions).

4.1.2 Theoretical Modeling Approaches

A number of theoretical studies have focused on modeling surfactant micellization and micellar solubilization in aqueous media [16–21]. The objective of these studies has been to enable the *a priori* prediction of the CMC, of the structure of the micellar aggregates, and (in the case of micellar solubilization) of the locus and the extent of solubilization from knowledge of the chemical structures of the surfactant(s)/solubilize(s) present in the aqueous solution and of the solution conditions (including total surfactant/solubilize concentration, temperature, pH, and ionic strength).

The most accurate theoretical models of micellar solubilization make use of a predictive molecular-thermodynamic approach. Molecular-thermodynamic models of solubilization combine molecular information about the system components with a thermodynamic description of self-assembly to estimate various contributions to the free energy of solubilization, which is defined as the free-energy change per surfactant molecule associated with transferring the surfactant monomers, the counterions (in the case of ionic surfactants/solubilizes), and the solubilizes from bulk aqueous solution to the aggregate. Important contributions to the development of molecular-thermodynamic descriptions of solubilization have been made by Landgren

and coworkers, by Nagarajan and coworkers [6, 11, 14, 17, 22–27], and very recently, by Srinivasan and Blankshtein [28]. Landgren and coworkers developed a Poisson-Boltzmann Cell Model (PBCM) to model solubilization in isotropic solutions and in liquid crystalline phases [29–31]. Their model includes inter-aggregate interactions, which makes it suitable for use at high surfactant concentrations. These authors developed two models to describe isotropic solutions, each applicable to different types of solubilizates. In the first model, all molecules (including the solubilizates) are considered to be anchored at the micelle surface. In the second model, solubilization is considered to take place either in a pure solubilizate domain in the aggregate center, or within the palisade layer. The maximum amount of solubilizate that can be solubilized is not considered in either model. In addition, because both models apply only to spherical aggregates, they do not describe the effect of the solubilized solute on the aggregate shape. Furthermore, the chain conformations inside the aggregate and their contribution to the free energy of aggregate formation are assumed to be a function of the interfacial area per surfactant molecule in the aggregate. An empirical Taylor series expansion of this free-energy dependence is then used to describe the free-energy contribution associated with the chain conformations.

Nagarajan and coworkers developed a solubilization model that allows the prediction of the locus and the extent of solubilization, as well as of the effect of solubilization on micelle shape and size [6, 11, 14, 17, 22–27]. This model requires as input the surfactant and the solubilizate molecular structures. The effects of molecular size, aromaticity, interfacial activity, and enthalpic interactions between the solubilizate and the surfactant tails (as described by Flory-Huggins interaction parameters) are accounted for. However, in modeling solubilization in the core region, the authors assume a uniform solution of surfactant tails and solubilizates in the micelle core, and utilize polymeric theories to estimate the packing free energy that are not strictly applicable in the case of surfactants possessing short tails. These authors also developed two limiting models to describe the head-head interactions of surfactants possessing large (>10 monomers) poly(ethylene oxide) heads. Micelles composed of surfactants

with large poly(ethylene oxide) heads form spherical or cylindrical micelles, because the steric interactions between the heads are too large for a planar (discoidal) micelle geometry to be favored. The first model considers the head-shell region to have a uniform polymer segment concentration, and a nonuniform deformation along the radial coordinate characterizing the micelle geometry. The second model treats the polymer chains as being uniformly deformed, while having a radial concentration variation of the polymer segments in the head-shell region. However, these authors did not consider solubilization in the corona region of micelles formed by surfactants with poly(ethylene oxide) polymeric heads [17].

The methods used by Landgren and coworkers and by Nagarajan and coworkers to calculate the packing free energy associated with the micelle core are only applicable in the case of surfactants having linear hydrocarbon tails, and for solubilizates having relatively simple chemical structures. In an effort to overcome some of these limitations, Srinivasan and Blankschtein recently calculated more rigorously the packing free energy associated with the micelle core for a variety of surfactant tail structures and solubilizates [28]. These authors generalized a mean-field approach, introduced originally by Ben-Shaul, Szeleifer, and Gelbart [32], to compute the packing free energy of surfactants having linear alkane tails, branched alkane tails, and alkylbenzene tails, and of solutes, such as salicylate, alcohols, and aromatics [28]. In their packing calculations, only repulsive interactions were considered, although attractive interactions could also have been included through the use of pairwise interaction energies or Flory-Huggins χ parameters. These interactions are likely to be important for polarizable surfactant tails and solubilizates. Srinivasan and Blankschtein also developed a computational framework to model counterion binding onto the aggregate head-shell region of ionic surfactant micelles [33, 34]. The existence of counterion binding has long been believed to play an important role in controlling the aggregate shape, size, and ability to solubilize solutes [35, 36]. The theoretical methodology developed by Srinivasan and Blankschtein is capable of predicting the locus and the extent of solubilization, CMCs, and micelle shape and size for relatively simple solubilizates and

ionic surfactants in the presence of counterion binding. Their methodology uses the concept of effective “head” and “tail” regions for the solubilizates as well as for any lipophilic counterions, which is most applicable in the case of relatively simple structures where it is clear *a priori* how the solubilizate is located and oriented relative to the micelle core/water interface [28].

4.1.3 Computer Simulation Approaches

An alternative to using molecular-thermodynamic descriptions of micellization and micellar solubilization is to use computer simulations to simulate the self-assembly of surfactants and solubilizates into micelles. To reduce the computational complexity associated with simulating the self-assembly process, researchers have used a number of approaches. Early on, a number of researchers used lattice models to study surfactant self-assembly [37–41]. These lattice model studies used simplified models of the intermolecular interactions of the system components. For example, Larson et al. modeled oil, water, and surfactant by treating the surfactant head and tail segments as water and oil “beads” [39,40]. Floriano et al. modeled the interactions among surfactant heads and between surfactant heads and water molecules as having no energy, while interactions between surfactant tails were treated as having negative energy [41]. Using this model, they identified the CMC of two model surfactants by performing lattice grand-canonical MC simulations and identifying a kink in the osmotic pressure as the surfactant concentration was varied. These authors reported observing a decrease in the CMC with increasing surfactant tail length and an increase in the CMC with decreasing solution temperature. Such behavior corresponds to what has been observed experimentally for nonionic surfactants in aqueous solution. Several researchers have also used off-lattice simulations to study surfactant self-assembly, but the majority of these studies have also used coarse-grained models of surfactants and solvent with approximate models for the interactions of the system components [42–45]. The simplified models used to describe the system components and their interactions in these early off-lattice and lattice studies are not capable of

predicting the solution behavior with quantitative accuracy.

In theory, molecular dynamics (MD) and Monte Carlo (MC) computer simulations based on an atomistic forcefield have the advantage of being capable of modeling arbitrarily complex chemical structures and enabling quantitatively or semiquantitatively accurate predictions of micellization and micellar solubilization phenomena. However, although simulations of micelle formation with atomistic-level detail are possible, such simulations have only been performed well above the CMC, because simulation times are severely limited by the size and the density of the micellar systems [45]. To accurately identify the CMC, extended simulations of large surfactant/solvent systems would be necessary over a range of low surfactant concentrations and over prohibitively long time scales [45]. Nevertheless, a number of researchers have simulated spontaneous micelle, vesicle, and bilayer formation in water at an atomistic level of detail. Maillet et al. conducted large scale molecular dynamics simulation of the self-assembly process of short and long chain cationic surfactants (*n*-nonyltrimethylammonium chloride (C_9TAC) and erucyl *bis* [2-hydroxyethyl] methylammonium chloride) [46]. Marrink et al. simulated the spontaneous aggregation of phospholipids into bilayers using simulations between 10 and 100 ns in duration [47], the self-assembly of 54 dodecylphosphocholine (DPC) surfactant molecules in water at two concentrations above the CMC [48], the self-assembly behavior and micelle structure of micelles modeling human bile using MD simulations of up to 50 ns [49], and the formation of small dipalmitoylphosphatidylcholine (DPPC) vesicles [50, 51]. More recently, de Vries et al. studied the spontaneous formation of an oblong DPPC vesicle in water through 90 ns of molecular dynamics simulation [52]. Braun et al. simulated the formation of a complete SDS micelle around glycoporphin A (GpA) transmembrane helices starting from isotropically distributed SDS monomers in an aqueous solution over the course of 32 ns of simulation [53].

Simulation of preformed surfactant systems (whether of monolayers [54–64] or of micelles [65–75]) to obtain information about their equilibrium structure and dynamics in solution is much less computationally expensive than simulation of surfactant

self-assembly. Recently a large number of computer simulation studies of preformed surfactant systems have appeared in the literature. Although such simulations provide a wealth of structural information about surfactant aggregates, they do not provide insight into the self-assembly process of these systems and cannot be used by themselves to predict many of the properties that are of most interest in micellar solubilization applications, including the CMC, the extent of solubilization, and the aggregation number. Only a limited number of studies of solubilization in surfactant micelles have been reported. In an early study, Karaborni et al. investigated oil solubilization in surfactant solutions by performing MD simulations using a simplified model of water, oil, and surfactant [76]. More recently, Kholov et al. studied n-butanol behavior in SDS micelles using realistic models of the system components, and reported rotational diffusion coefficients and rotational correlation times for SDS and n-butanol within the micelle [77]. Kuhn et al. conducted an all-atomistic study investigating the solubilization of pentanol in a sodium octanoate micelle [78]. These authors report simulation results for the micelle radius, the effect of pentanol on micelle shape, the locus of pentanol solubilization, radial distribution functions for the various micelle components, and trans-to-gauche ratios of the sodium octanoate alkyl chains.

4.1.4 Combined Computer Simulation/Molecular-Thermodynamic Modeling Approach

To overcome the limitations of molecular-thermodynamic modeling (namely, its applicability to relatively simple surfactant and solubilizate systems) and computer simulations (the high computational cost of modeling self-assembly with atomistic detail), we have developed a hybrid computer simulation/molecular-thermodynamic modeling approach. This approach involves conducting MD simulations of surfactants or solubilizates at an oil/water interface (modeling the micelle core/water interface), or of solubilizates in a micellar environment, to estimate the hydrated and the unhydrated

portions of each molecule in a micelle, a key input for molecular-thermodynamic modeling. Using this information, along with knowledge of the chemical structures of the surfactants and the solubilizates, it is possible to use molecular-thermodynamic theory to predict the change in free energy associated with transferring the surfactant monomers, the solubilizate molecules, and the counterions (for ionic systems) from their reference state in the aqueous solution to form a micellar aggregate [33,34,79,80]. This free-energy change is then used, along with a thermodynamic description of the micellar solution, to predict various solubilization-related properties, including CMCs, micelle shape and size, aggregate composition as a function of surfactant concentration, the solubility of each solubilizate as a function of surfactant concentration, and the molar solubilization capacity [16,28,81,82].

Recently, a hybrid computer simulation/molecular-thermodynamic modeling approach was used to model the micellization behavior of three relatively complex surfactants—the anionic surfactant 3-hydroxy sulfonate (AOS) with two different linear alkyl chain lengths and the nonionic surfactant decanoyl-n-methylglucamide (MEGA-10) [80]. This modeling approach was also used to model the solubilization behavior of the relatively complex solubilizate ibuprofen in sodium dodecyl sulfate (SDS), dodecyltrimethylammonium bromide (DTAB), and dodecyl octa(ethylene oxide) ($C_{12}E_8$) micelles [82]. The results of this study were reported in Chapter 3. AOS is considered relatively complex because it contains two hydrophilic groups (SO_3^- and OH) connected by hydrophobic CH_2 groups. MEGA-10 is considered relatively complex because it contains an amide group. Ibuprofen is relatively complex because it contains a hydrophilic carboxylate group, a slightly hydrophobic benzyl group, and a hydrophobic alkyl chain. For each of these molecules, it was not clear *a priori* how they would be hydrated in a micellar environment. To determine the hydrated and the unhydrated portions of each of these molecules, MD simulations were conducted for a single surfactant or solubilizate molecule at near-infinite dilution at an oil/water interface. For each of these molecules, we showed that simulation of a single surfactant or solubilizate molecule at a flat oil/water interface was sufficient

to determine input parameters for the molecular-thermodynamic modeling approach. When appropriate, simulation at a flat interface has the advantage of computational simplicity — simulation times are kept to a minimum by simulating a single surfactant/solubilize molecule instead of the entire micelle. However, such a computer simulation approach is most applicable to a surfactant that adopts a consistent position and orientation relative to an oil/water interface which is similar to the position and orientation that it will adopt within a micellar environment. When the surfactant/solubilize position and orientation depend strongly on factors such as the interface radius of curvature and the presence of neighboring surfactant/solubilize molecules, this relatively simple method may not be applicable, because the input parameters for the molecular-thermodynamic theory may not be constant (specifically, they may become functions of aggregate shape, aggregation number, and aggregate composition). The effects of interface radius of curvature and the presence of neighboring surfactant molecules on the input parameters for molecular-thermodynamic theory will be investigated in detail in this chapter.

4.1.5 Motivation and Research Objectives

Given the shortcomings of the current computer simulation and molecular-thermodynamic modeling approaches, there is a need to develop a predictive, molecular-level theoretical description that can predict the solution behavior of complex surfactant and solubilize systems. Molecular-thermodynamic methods are most applicable to systems with relatively simple surfactant/solubilize chemical structures, and computer simulations, although capable of modeling complex chemical structures, are very computationally expensive. With this in mind, in this chapter, I explore ways in which computer simulations may be used to improve the predictive ability of molecular thermodynamic models of solubilization. This is done by: (i) using computer simulations to determine input parameters for a number of solubilizates in the context of molecular-thermodynamic modeling, and (ii) presenting a molecular-thermodynamic modeling approach that uses the computer simulation inputs to make predictions of micel-

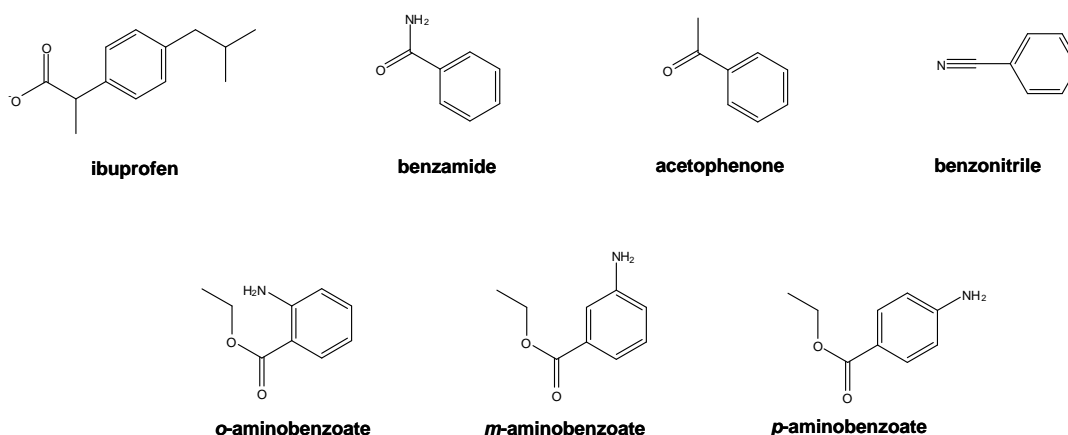


Figure 4-1: Chemical structures of the seven solubilizers modeled in this chapter.

lar solubilization behavior. To accomplish these two objectives, I have conducted atomistic-level computer simulations of seven different solubilizers at an oil/water interface and within spherical and cylindrical SDS micelles. SDS was selected for each micellar simulation because it is a commonly used, well-characterized anionic surfactant which has been extensively studied both experimentally [35, 83–88] and through computer simulation [65–68, 70, 71]. The seven solubilizers modeled are ibuprofen, benzamide, acetophenone, benzonitrile, *o*-aminobenzoate, *m*-aminobenzoate, and *p*-aminobenzoate. The chemical structures of each of the seven solubilizers are shown in Figure 4-1.

The seven solubilizers studied here were selected based on the availability of several sources of experimental data describing their solubilization behavior in nonionic, anionic, and cationic surfactant micelles and their suitability to assess the validity of the hybrid computer simulation/molecular-thermodynamic modeling approach introduced in this chapter. Each solubilizer contains both hydrophobic and hydrophilic moieties, making accurate head and tail identification for these molecules difficult without computer simulation inputs. As such, these molecules represent important systems for which computer simulations are expected to enable theoretical predictions of micellar solubilization behavior. Note that although results from an experimental

and a theoretical study of the solubilization behavior of ibuprofen in $C_{12}E_8$, SDS, and DTAB micelles were presented in Chapter 3, in this chapter, the solubilization behavior of ibuprofen will be modeled more rigorously by: (i) comparing the head and tail identifications made based on water/oil interface simulation with the head and tail identifications made based on simulations in cylindrical and spherical SDS micelles, and (ii) rigorously computing the packing (g_{pack}) and interfacial (g_{int}) free-energy contributions to the free energy of aggregate formation. In Chapter 3, g_{pack} and g_{int} for the surfactant/ibuprofen aggregate were evaluated by approximating the ibuprofen tail as either a nine-carbon linear alkyl chain or as a ten-carbon linear alkyl chain. Although these approximations simplify the implementation of the molecular-thermodynamic theory, they are not expected to be as physically realistic as computing g_{pack} and g_{int} based on the actual structure of the ibuprofen tail. Benzamide, acetophenone, benzonitrile, and *o*-, *m*-, and *p*-aminobenzoate were selected for study because these solubilizates possess: (i) varying degrees of amphiphilicity, and (ii) relatively complex tail structures. In addition, the micellar solubilization behavior of *o*-, *m*-, and *p*-aminobenzoate is quite interesting from a theoretical standpoint. Although only small structural differences exist between these three solubilizates, they exhibit significant differences in their micelle/water partition coefficients.

By simulating these seven solubilizates at an oil/water interface and comparing the results with those obtained by conducting simulations in a micellar environment, we have been able to examine in detail the effects of curvature and crowding on the hydration states of the solubilizate molecules considered. Furthermore, although not reported in this chapter, by comparing the detailed structural information obtained from computer simulations with similar structural information predicted using molecular-thermodynamic modeling, it has been possible to assess the accuracy of the molecular-thermodynamic modeling predictions of micelle structure.

The remainder of the chapter is organized as follows. Section 4.2 describes the computer simulation approach used in this chapter, including the computer simulation methodology (Section 4.2.1), the simulation methods and parameters (Section 4.2.2),

system preparation and equilibration (Section 4.2.3), and a discussion of the approach used to analyze the simulation data (Section 4.2.4). Computer simulation results are presented in Section 4.3. The molecular-thermodynamic approach to model surfactant and solubilize self-assembly, as informed by computer simulation inputs, is discussed in Section 4.4, including an introduction to the model (Section 4.4.1), a discussion of the thermodynamic framework used in the molecular-thermodynamic model (Section 4.4.2), and a discussion of the molecular model used to describe the micellar solubilization process (Section 4.4.3). Concluding remarks are presented in Section 4.5. Molecular-thermodynamic modeling results based on the computer simulation inputs for each of the seven solubilizates considered in this chapter will be presented in Chapter 5.

4.2 Computer Simulations

4.2.1 Methodology

To identify the “head” and “tail” of each of the seven solubilizates considered in this chapter, molecular dynamics computer simulations of each solubilizate were carried out at a flat octane/water interface (modeling the micelle core/water interface). Octane was arbitrarily selected as the model “oil” in all the computer simulations. We anticipate that similar results should be obtained using alkane molecules of different lengths [80, 82]. Each oil/water interface simulation was conducted in a constant number of molecules, constant normal pressure, and constant temperature ensemble ($NP_N T$). As will be discussed in greater detail in Section 4.2.2, simulation cell dimensions parallel to the oil/water interface (x and y) were fixed, but the simulation cell dimension perpendicular to the interface (z) was allowed to change in response to a constant normal pressure of 1.0 bar.

As discussed in Section 4.1, oil/water interface simulations are expected to yield accurate molecular-thermodynamic inputs for solubilizates that adopt a position and orientation relative to the octane/water interface that is similar to the position and

orientation that they would adopt within a micellar environment. When the solubilize orientation depends strongly on factors such as the interface radius of curvature and the presence of other surfactant and solubilize molecules, this relatively simple computational strategy may not be applicable. To evaluate the effects of interfacial curvature and of crowding from other surfactants in a micellar environment, each of the seven solubilizes was also simulated in spherical and cylindrical SDS micelles. Simulations within an SDS bilayer (being most analogous in geometry to the oil/water interface simulations) were also attempted, but the resulting bilayers were found to be unstable and quickly collapsed (within 200 ps) to form discoidal micellar aggregates during computer simulation. The breakup of the simulated SDS bilayers was not surprising, because all simulations were carried out in pure water without any added salt, making the electrostatic repulsions between the SO_4^- heads of SDS in a planar configuration quite strong. As will be discussed in Sections 4.2.3 and 4.2.3, five solubilize molecules were included in each spherical and cylindrical SDS micelle, yielding a sufficiently low solubilize concentration that solubilize/solubilize interactions are much less frequent than surfactant/solubilize interactions. Because simulations were conducted at only one solubilize concentration in the spherical and in the cylindrical SDS micelles, the simulations conducted in this chapter do not provide information about the effects of solubilize concentration on the input parameters obtained for molecular-thermodynamic theory. Although such effects are beyond the scope of the present study, they represent an important area for future research.

Each cylindrical and spherical micelle simulation was conducted in a constant total number of particles, constant pressure, and constant temperature (NPT) ensemble. This ensemble is rigorously correct for spherical micelle simulations, but is only an approximation of reality for cylindrical micelle simulations. In the cylindrical micelle simulations, only a short “slice” of each cylindrical micelle was simulated to minimize computational time. The axis of this “slice” was oriented parallel to the z axis. During simulation, the cylindrical micelle was in direct contact with

the periodic reflecting walls on two of the six sides of the cubic simulation cell (the sides perpendicular to the z axis). With simulations conducted in this manner, the “end caps” of the cylindrical micelle that would be present in an actual micellar solution [89] are not modeled. Therefore, the appropriate boundary condition for the surfaces perpendicular to the z axis is a physically realistic surface tension, rather than the constant pressure that was chosen. However, without experimental information on the value of this surface tension, it was not possible to perform simulations in a thermodynamically valid $N\gamma T$ ensemble for the cylindrical micelles. As a result, an NPT ensemble was used in which the pressure applied parallel to the z axis was 1.0 bar and the pressure applied perpendicular to the z axis was 0.0 bar. An alternative approach would involve conducting a constant number of particles, constant volume, and constant temperature (NVT) simulation on a cylinder performed with an experimentally measured area per surfactant head, but this would have required accurate experimental data on the aggregation number for each surfactant/solubilizate system that was not available. Based on research into the effect of surface tension on interfacial area conducted by other researchers [90–92] (see also Chapter 11), we do not believe that the NPT ensemble approximation adopted here will introduce significant error. The simulations in cylindrical micelles conducted here, although approximate, serve their primary purpose of quantitatively evaluating the effect of interface curvature and of surfactant crowding on the hydration states of solubilizates in a micellar environment.

4.2.2 Simulation Methods and Parameters

All system components, with the exception of water, were modeled with the bonded and nonbonded interaction potentials included in a fully atomistic OPLS-AA force field [93]. Some additional parameters for angles and angle vibrations were taken from the literature to more accurately model the sulfate (SO_4^-) head in SDS [94]. Water was modeled using the simple extended point-charge (SPC/E) model for water. The SPC/E model represents an improvement over the SPC model in which a

correction is made to account for the self-polarization of water [95]. Atomic charges were assigned to each molecule based on the default atomic charge values specified in the OPLS-AA force field. In two previous studies, we investigated the sensitivity of the head and tail assignments obtained from computer simulation to the method used to assign atomic charges. In general, we found that the results were quite sensitive to the atomic charges used, and that the charge assignments recommended within the OPLS-AA forcefield yield more reasonable results than those obtained using the CHelpG algorithm (as implemented in Gaussian 98), in which atomic charges are assigned to fit the electrostatic potential at a number of points on the van der Waals surface [96], as long as the molecular structure of the surfactant or the solubilize of interest was specifically parameterized for in the forcefield. The CHelpG algorithm is a method frequently used to estimate atomic charges for molecular mechanics simulations [97]. Fortunately, this was the case for the seven solubilizes modeled in this chapter. However, atomic charges for the SO_4^- - CH_2 group of SDS were taken from the literature because the charges for this group were not available in the OPLS-AA force field [94]. These charges were found to correspond closely with atomic charges that we obtained for each atom in this group by modeling SDS using the *RBLYP* density functional and the *6-31G(d)* basis set in Gaussian 98 and using the CHelpG algorithm to determine atomic charges [97,98]. Van der Waals interactions were treated using a cutoff distance of 0.9 nm, and Coulombic interactions were described using 3D particle mesh Ewald (PME) summation. Although the van der Waals cutoff used here is shorter than the cutoff used in many studies reported in the literature (where the reported cutoffs are frequently as large as 0.14 nm), a trade-off exists between using longer cutoffs to try to capture more accurately the nonbonded interactions present in the system and using the same cutoffs implemented during the original force field parameterization. Other researchers have shown that truncation schemes for electrostatic interactions give qualitatively incorrect results when compared with newer and more accurate methods such as the use of reaction field treatment of electrostatics or Ewald summation [99]. Accordingly, 3D PME summa-

tion was used in each of our simulations. However, using the OPLS-AA force field, Shirts et al. recently demonstrated that applying relatively short-range cutoffs for van der Waals interactions along with long-range dispersion corrections yields reasonable results [100–102]. In modeling short-ranged nonbonded interactions, a neighbor list of 9.0 Å was maintained and updated every 10 steps. A long-range dispersion correction was used to more accurately estimate the energy and the pressure of the system. Both corrections are negative; however, while the energy correction is small, the pressure correction is significant and must be included to obtain accurate results [103]. Each simulation was carried out using fixed bond lengths, which allowed an increase in simulation timestep from 1 fs to 2 fs. Bond lengths were constrained using the SHAKE algorithm as implemented in GROMACS [104].

In each simulation, the cell temperature was maintained at 300 K using a Berendsen temperature coupling algorithm, which mimics weak coupling to an external heat bath with first order kinetics [103]. A Berendsen pressure coupling algorithm was used to maintain each box at the specified pressure of 1.0 bar [103]. To allow only the simulation cell dimension perpendicular to the interface to change in size during the $NP_N T$ oil/water interface simulations, a semi-isotropic implementation of Berendsen pressure coupling was used which allows the use of a different liquid compressibility in the x and y dimensions than in the z dimension. By specifying a compressibility of zero in the x and y dimensions, only the cell dimension perpendicular to the interface was allowed to change. Each dimension of the simulation cell was allowed to change in the NPT micellar simulations. Each oil/water interface simulation was carried out using the GROMACS software package, version 3.2 [105, 106]. The micellar simulations were carried out using a 2006 developer’s version of GROMACS. By using the parallelized molecular dynamics code GROMACS, it was possible to conduct these simulations on relatively long time scales (up to 50 ns), which has allowed a thorough equilibration of each surfactant/solubilizate system as well as the collection of simulation data over an extended period of time.

4.2.3 System Preparation and Equilibration

Water/Oil Interface Simulations

Each water/oil interface (with the exception of the interface containing ibuprofen) was constructed by placing a single solubilize molecule between a ≈ 15 Å thick layer of water and a ≈ 20 Å thick layer of octane. Each simulation cell was 1.9 nm long parallel to the octane/water interface (in the x and y dimensions). A representative oil/water simulation cell is shown in Figure 4-2A. In this figure, one solubilize molecule is located at the water/oil interface. Each solubilize atom is depicted using its van der Waals radii to improve the solubilize visibility, and water molecules are not shown for clarity. The location of the rectangular periodic boundary conditions used during the oil/water interface simulation are indicated. Note that because of the 3D periodic boundary conditions, two water/octane interfaces are present in the simulation cell. A relatively small simulation cell size was used for each water/oil interface simulation to permit long simulation times and thereby improve the statistical significance of the simulation results. In previous studies to determine the head and tail of surfactants [80] (see Chapter 2) and ibuprofen (see Chapter 3) [82], we used a simulation cell size that was 4.0 nm in both dimensions parallel to the octane/water interface to approximate near-infinite dilution and determine if, even at very low interfacial concentrations, reasonable information about hydration could be obtained for molecular-thermodynamic modeling. Even at near-infinite dilution, the head and tail identifications made for molecular-thermodynamic modeling yielded reasonable modeling results [80, 82]. The higher interfacial concentrations present in the oil/water interface simulations conducted in this chapter to determine the head and tail of benzamide, acetophenone, benzonitrile, *o*-aminobenzoate, *m*-aminobenzoate, and *p*-aminobenzoate approximate an environment where a significant amount of solubilize is present in the surfactant micelle, and are expected to be more physically realistic than simulations conducted at infinite solubilize dilution.

Water/oil interface simulations were conducted for extended periods of time to

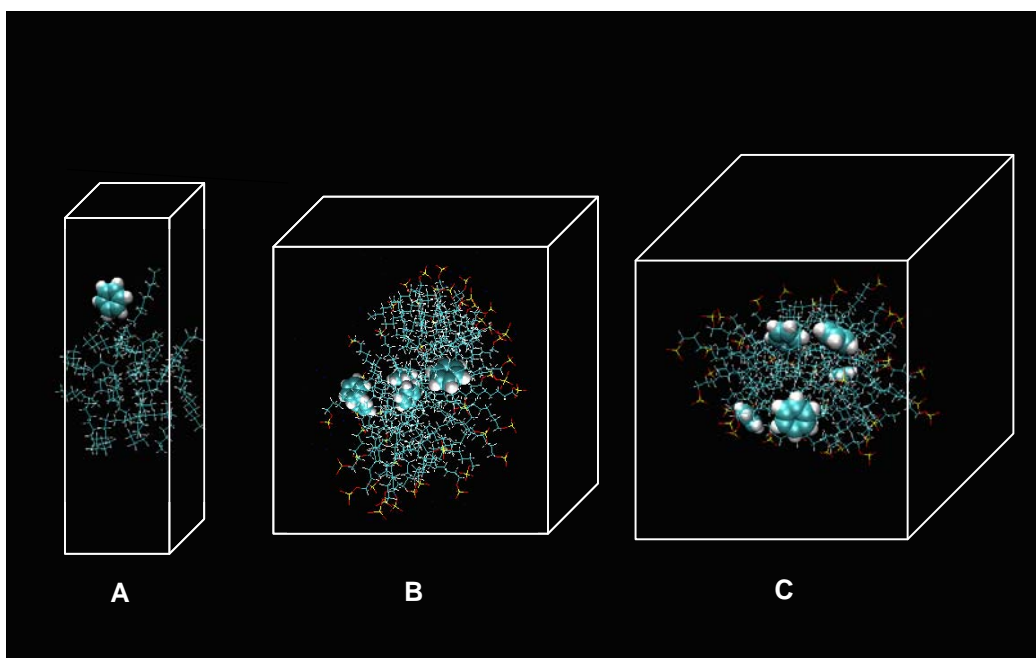


Figure 4-2: Representative snapshot of a water/oil interface (A), a cylindrical micelle (B), and a spherical micelle (C) after equilibration. The white lines denote the location of the periodic boundary conditions. Solubilize molecules are shown using their van der Waals radii, octane (see A) or sodium dodecyl sulfate (SDS) molecules are shown as lines (see B and C), and water molecules are omitted for clarity.

improve the statistical significance of the simulation results. Each simulation cell was allowed to equilibrate for at least 100 ps before gathering data. Each of the solubilizates considered appeared to reach an equilibrium configuration at the interface within that period of time, as verified by confirming that the local environment of each solubilizate atom had stabilized using the data analysis method described in the following section (results not shown). After equilibration, long data gathering runs were initiated. Depending on the solubilizate, oil/water interface simulations were conducted for between 3 ns and 50 ns. Head and tail identifications obtained from water/oil interface simulation using default OPLS-AA atomic charges have already been reported for ibuprofen (see Chapter 3), but are included here to allow comparison with the micellar simulation results [82]. With the exception of ibuprofen, which was simulated for 3 ns, the other six solubilizates were simulated for at least 10 ns. The longest simulations were conducted for *o*-, *m*-, and *p*-aminobenzoate at an oil/water interface in order to improve the statistical significance of the head and tail assignments.

Cylindrical Micelle Simulations

A cylindrical SDS micelle was performed using an initial guess of 45 \AA^2 for the surface area per surfactant head. This initial area was selected arbitrarily, although it was found to be sufficiently close to the final equilibrated surface area per surfactant head to make the initial micelle configuration stable. The total number of surfactant molecules included in the simulation cell after performing the micelle was 54, which was found to be a sufficiently large number for the simulation cell to maintain a z dimension (parallel to the cylinder axis) of greater than two times the van der Waals and electrostatics cutoff distances applied during simulation. The cylindrical micelle was performed by placing the SDS molecules in close proximity with the hydrophilic SO_4 group in each SDS molecule oriented radially outward from the axis of the micelle. A total of 1,520 water molecules were included in the simulation cell around the cylindrical micelles, along with 54 counterions (giving a total of approximately 7,000

atoms). Bruce et al. have observed that counterions are the slowest component of an SDS surfactant/water system to come to an equilibrium distance from the center of mass of the micelle, taking approximately 1 ns to come to equilibrium [66]. To speed the equilibration of our system, counterions were added by replacing water molecules experiencing the greatest electrostatic potential, with the potential being recalculated after every ion insertion. The preformed micelle was equilibrated for 25 ns, after which the ending configuration was used as the starting point to make the 7 surfactant/solubilize micelles.

Each surfactant/solubilize micelle was created by exchanging 5 SDS molecules with five solubilize molecules and placing them at the micelle core/water interface. The final number of surfactant molecules in each micelle was therefore 49. Five solubilizes were inserted into each micelle to allow: (i) averaging of computer simulation results over multiple solubilizes, and (ii) evaluation of the uncertainty associated with the simulation results. Each of the solubilizes was initially placed at the micelle core/water interface at the same location previously occupied by the SO_4 head of the SDS molecule that it replaced. This initial location was selected because all of the simulated solubilizes possess semipolar benzene rings and some polar atoms; therefore, it was considered most appropriate to initially introduce the solubilizes into an environment containing both polar groups (water molecules, surfactant heads, and counterions) and nonpolar groups (the surfactant tails), and allow them to diffuse from this initial location to their equilibrium location within the micelle. After introducing the solubilizes, the number of counterions present in each simulation cell was adjusted if necessary to preserve electroneutrality. The fully-constructed surfactant/solubilize micelle was then equilibrated for an additional 15 ns in the *NPT* ensemble. A semi-isotropic implementation of Berendsen pressure coupling was used to apply 1 atm of pressure parallel to the axis of the micelle and 0 atm of pressure perpendicular to the axis of the micelle [103]. As discussed in Section 4.2.1, the appropriate boundary condition to use perpendicular to the z axis is a finite surface tension value. However, in the absence of experimental data on the value of this

surface tension, the pressure perpendicular to this axis was set to 0 bar. After initial equilibration, an additional 10 ns of simulation in the *NPT* ensemble was performed during which data was gathered. A number of metrics were used to verify that adequate equilibration of the surfactant/solubilizate system had taken place. These metrics include: the system potential energy, the micelle solvent accessible surface area (SASA), and the distance from the micelle center of mass to various surfactant segments and to the solubilizate center of mass. A discussion of the equilibration results will be presented in Section 4.2.3.

A representative snapshot of an SDS/solubilizate cylindrical micelle after simulation for 25 ns is shown in Figure 4-2B. Each atom in the solubilizate molecule is depicted using its van der Waals radius to improve visibility. Water molecules are not shown for clarity. The location of the rectangular periodic boundary conditions used during the cylindrical micelle simulation are shown in the figure. In order to minimize computational cost, the z dimension of each post-equilibration simulation cell was only approximately 2.5 nm in length. The x and y dimensions of the simulation cells were approximately 5.5 nm in length.

Spherical Micelle Simulations

A spherical SDS micelle was performed at an aggregation number of 43 that was determined based on molecular-thermodynamic modeling of SDS micelles in water. In performing molecular-thermodynamic modeling, we made the assumption that the micelle is perfectly spherical [16,81]. As a result, we tend to underpredict aggregation numbers [80]. The observation has been made that given the relatively large aggregation number of SDS micelles that are observed experimentally to form in aqueous solution, the shape of the SDS micelles must be somewhat nonspherical (the aggregation number of SDS in aqueous solution has been reported to be 69.6 by Almgren et al. [88] and 74 by Cabane et al. [107], whereas the largest aggregation number that is geometrically possible for a perfectly spherical SDS micelle is 56 [35]). Therefore, the aggregation number that we have used for our computer simulation study is a


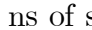
lower-bound limit to the aggregation number, which would correspond to micelles which form when the concentration of SDS in the solution corresponds to the CMC of SDS. This low aggregation number was selected because it both: (i) minimizes computational time, and (ii) corresponds to the maximum curvature state of spherical SDS micelles and allows us to better evaluate the effect of curvature on solubilize hydration. After determining the aggregation number, a single SDS micelle was performed as a spherical aggregate by placing SDS molecules in close proximity with the hydrophilic SO_4 group of each SDS molecule oriented radially outwards from the micelle center. A total of 3,347 water molecules and 43 counterions were also included in the simulation cell (corresponding to a total of approximately 12,000 atoms). Similar to what was done in the cylindrical micelle simulations, to speed equilibration the 43 counterions were placed at locations experiencing the greatest electrostatic potential. After preparing the surfactant/counterion/water system, equilibration was performed for 25 ns in the NPT ensemble. This ending configuration was used as the starting point for each of the 7 surfactant/solubilize micelles considered. Each surfactant/solubilize micelle was created by exchanging five surfactant molecules with five solubilize molecules in each spherical micelle, yielding a final number of 38 surfactant molecules in each system. Each of the solubilizes was initially placed at the micelle core/water interface at the same location previously occupied by the SO_4 head of the SDS molecule that it replaced for the same reasons discussed in Section 4.2.3. If necessary, the number of counterions was adjusted after solubilize addition and surfactant deletion to maintain electroneutrality. Each surfactant/solubilize system was then simulated for 15 ns of equilibration, and data was gathered for the last 10 ns of simulation. A discussion of the equilibration results will be presented in Section 4.2.3.

A representative snapshot of a spherical SDS/solubilize micelle after simulation for 25 ns is shown in Figure 4-2C. Each solubilize atom is depicted using its van der Waals radius to improve its visibility. Water molecules are not shown for clarity. The location of the cubic periodic boundary conditions used during spherical

micelle simulation are shown in the figure. The x , y , and z dimensions of each post-equilibration simulation cell were approximately 5 nm in length.

Equilibration Results for Cylindrical and Spherical Micelles

For the seven cylindrical and seven spherical micelles simulated, potential energy was found to equilibrate and begin fluctuating about an equilibrium value within a small fraction of the total 25 ns simulation time (results not shown).

SASA equilibration and fluctuation was found to occur on a much longer timescale than that corresponding to potential energy equilibration and fluctuation. In Figure 4-3, we plot SASA results for SDS/ibuprofen micelles () and for SDS/acetophenone micelles () obtained during the entire 25 ns of simulation. Results are reported for cylindrical micelles in Figure 4-3A and for spherical micelles in Figure 4-3B. To calculate SASA, we used the double cubic lattice method as implemented in GROMACS. The solvent accessible surface was determined by rolling a probe sphere of radius 0.14 nm (the approximate size of a water molecule) around each molecule within the micelle [103]. As will be shown in Section 4.3, ibuprofen has a charged carboxylate group that is very hydrated in the micellar environment, whereas acetophenone has a carbonyl group that is only moderately hydrated in the micellar environment. The results presented in Figure 4-3 are representative of the SASA profiles obtained for micelles containing each of the other 5 solubilizates.

It is interesting to point out that the SDS/ibuprofen cylindrical and spherical micelles have a higher value of SASA on average than the SDS/acetophenone cylindrical and spherical micelles, an effect which may be due to the fact that: (i) ibuprofen has a larger molecular volume than acetophenone, so the SDS/ibuprofen micelle is slightly larger than the SDS/acetophenone micelle, and (ii) the charged, highly hydrated carboxylate group present in ibuprofen may cause the surface of the SDS/ibuprofen micelle to be somewhat rougher than the surface of the SDS/acetophenone micelle.

As can be seen in Figure 4-3, the SASA values exhibit no noticeable upward or downward drift during the data-gathering simulation. SASA profiles for each of the

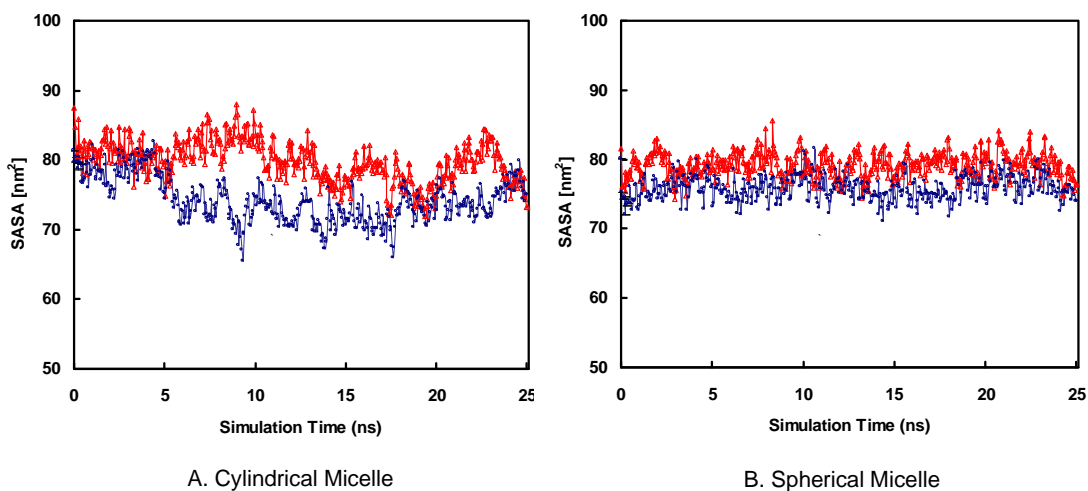


Figure 4-3: Solvent accessible surface area (SASA) profiles for the cylindrical (A) and spherical (B) SDS/ibuprofen micelles ($\text{---}\triangle\text{---}$) and SDS/acetophenone micelles ($\text{---}\circ\text{---}$) as a function of simulation time.

seven SDS/solubilizate cylindrical and spherical micelles are included in Appendix A of this chapter. However, it is interesting to note that the SASA results for the spherical micelles are more stable in terms of the magnitude of fluctuations observed than those for the cylindrical micelles (see discussion in Appendix A). For both cylindrical and spherical micelles, it appears that the total simulation time is sufficient to ensure sampling of a large number of different micellar conformations with different corresponding values of SASA.

The distances from the micelle center of mass (COM) to the center of mass of: (i) the sulfate (SO_4) group in SDS ($d_{\text{SO}_4\text{-MIC}_{\text{COM}}}$, see the \circ results), (ii) the sixth CH_2 group away from the sulfate group in SDS ($d_{\text{CH}_2\text{-MIC}_{\text{COM}}}$, see the \circ results), and (iii) the terminal CH_3 group in SDS ($d_{\text{CH}_3\text{-MIC}_{\text{COM}}}$, see the \circ results) are plotted in Figures 4-4 and 4-5 for ibuprofen and acetophenone, respectively. Each reported point reflects an average value for all the surfactant molecules (49 in the cylindrical micelles and 38 in the spherical micelles). The distances from the micelle center of mass to the solubilizate center of mass is also reported ($d_{\text{SOL}_{\text{COM}}\text{-MIC}_{\text{COM}}}$, see the \circ results)

for ibuprofen in Figure 4-4 and for acetophenone in Figure 4-5. Each reported point reflects an average value for the 5 solubilizates present in the micelles. Figure 4-4 presents results for spherical (4-4A) and for cylindrical (4-4B) SDS/ibuprofen micelles. Figure 4-5 presents results for cylindrical (4-5A) and for spherical (4-5B) SDS/acetophenone micelles. The results presented in Figures 4-4 and 4-5 are representative of distance results obtained for micelles containing each of the other 5 solubilizates. The most striking characteristic of each distance profile shown is its variability — each distance fluctuates substantially (up to 2 nm) during the course of the 25 ns simulation. The large magnitude of distance fluctuations observed is consistent with the relatively high level of fluctuations observed in micelle shape upon visualization of the MD trajectories. Although significant fluctuations in the distance values are observed, no consistent drift in the distance results is apparent for the SDS/ibuprofen and for the SDS/acetophenone micelles. Distance profiles for all seven solubilizates considered in the cylindrical and the spherical SDS micelles are included in Appendix A of this chapter. In addition, the average values of $d_{\text{SO}_4-\text{MIC}_{\text{COM}}}$, $d_{\text{CH}_2-\text{MIC}_{\text{COM}}}$, $d_{\text{CH}_3-\text{MIC}_{\text{COM}}}$, and $d_{\text{SOL}_{\text{COM}}-\text{MIC}_{\text{COM}}}$ over all 25 ns of simulation performed are reported in various tables presented in Appendix A. In general, the solubilizates do not have a significant influence on the distance results for the three surfactant groups examined because only five solubilizates are present in each cylindrical and spherical micelle.

The potential energy, the SASA, and the distance to the micelle center of mass results discussed above suggest that: (i) the 15 ns of equilibration conducted for each micelle is sufficient, and (ii) the data recorded during the 10 ns data-gathering simulation should be sufficient to sample the equilibrium state of the micelle reasonably well. In total, the simulations reported in this chapter required approximately 25,000 CPU hours to complete. The water/oil interface simulations required ≈ 3 CPU hours per nanosecond of simulation, the cylindrical micelle simulations required ≈ 25 CPU hours per nanosecond of simulation, and the spherical micelle simulations required ≈ 35 CPU hours per nanosecond of simulation. Clearly, water/oil interface simulations

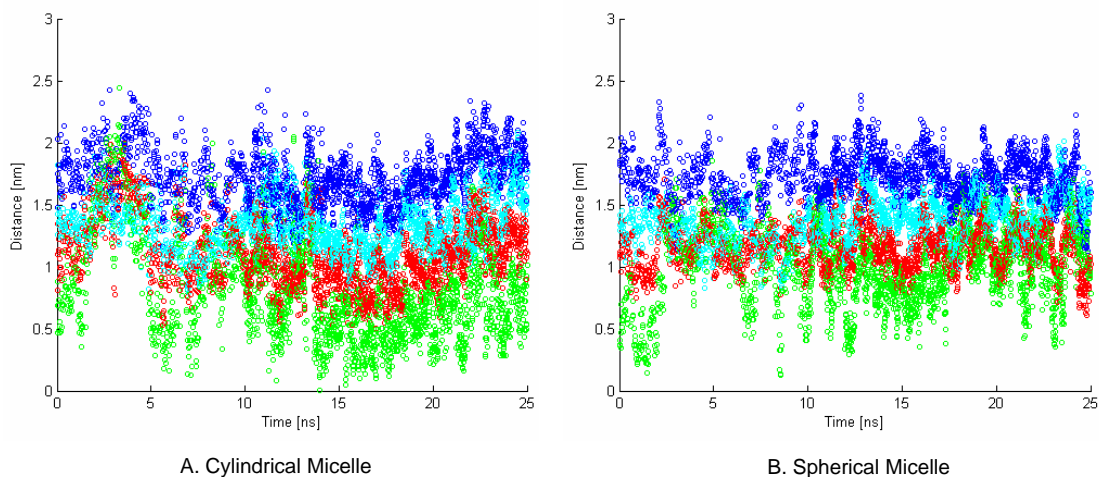


Figure 4-4: Distances between several surfactant groups defined in the text and the micelle center of mass ($d_{\text{SO}_4-\text{MIC}_{\text{COM}}}$, see the \bullet results; $d_{\text{CH}_2-\text{MIC}_{\text{COM}}}$, \circ ; and $d_{\text{CH}_3-\text{MIC}_{\text{COM}}}$, \circ), and between the center of mass of ibuprofen and the micelle center of mass ($d_{\text{SOL}_{\text{COM}}-\text{MIC}_{\text{COM}}}$, \circ) in the cylindrical (A) and the spherical (B) SDS/ibuprofen micelles.

are much less computationally expensive than simulating in a micellar environment. Therefore, if reasonable inputs can be obtained for molecular-thermodynamic modeling from water/oil interface simulations, this simulation approach is the preferred one.

4.2.4 Data Analysis Method

Oil/Water Interface Simulations

To characterize the local environment of each atom in the solubilize from the oil/water simulation results, the number of contacts per timestep experienced by different atoms in the solubilize with octane and with water was counted over the course of a simulation run. A contact was defined as two atoms approaching each other to within a set cutoff distance at any time during the simulation. Because the van der Waals radii of the simulated atoms ranged between 0.12–0.19 nm, a reason-

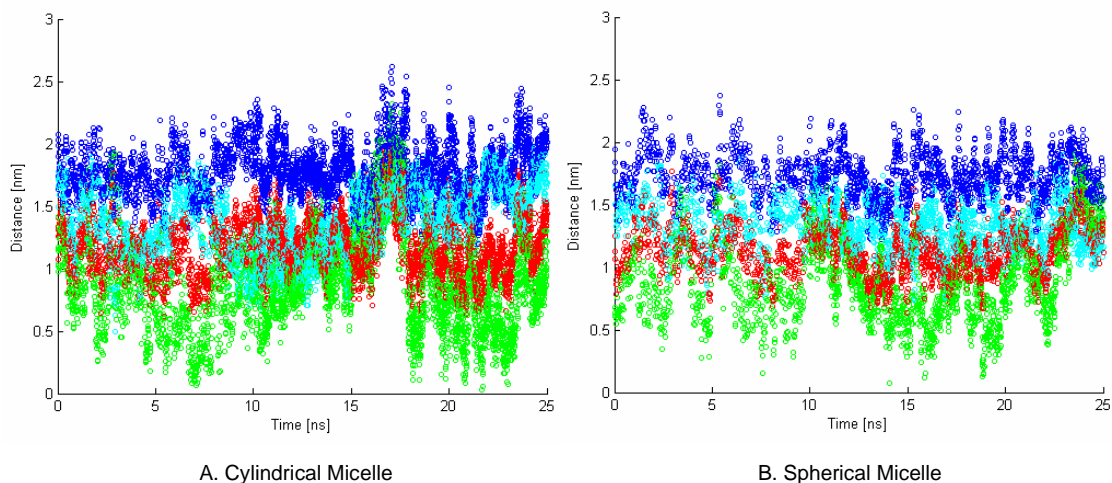


Figure 4-5: Distances between several surfactant groups defined in the text and the micelle center of mass ($d_{\text{SO}_4\text{-MICCOM}}$, see the \circ results; $d_{\text{CH}_2\text{-MICCOM}}$, \circ ; and $d_{\text{CH}_3\text{-MICCOM}}$, \circ), and between the center of mass of acetophenone and the micelle center of mass ($d_{\text{SOLCOM-MICCOM}}$, \circ) in the cylindrical (A) and the spherical (B) SDS/acetophenone micelles.

able minimum cutoff distance to identify such contacts is twice the maximum van der Waals radius, or around 0.38 nm. As shown in a previous study [80], in which the size of the cutoff distance was set at 0.4, 0.5, and 0.6 nm, the size of the cutoff distance does not have a significant effect on the head and tail assignment results. In this study, as well as in our previous two studies, a 0.5 nm cutoff distance was used [80,82]. The ratio of the number of contacts with water to the number of contacts with octane was computed for each atom in the solubilize considered to determine whether a given atom is surrounded primarily by water or by octane. As we reported recently, each contact ratio must be scaled by a factor of 0.88 to account for the fact that an atom in bulk water experiences slightly more contacts than an atom in bulk octane [80]. Any atom having a scaled contact ratio greater than 1.0 is identified as being part of the solubilize head. Conversely, any atom having a scaled contact ratio smaller than 1.0 is identified as being part of the solubilize tail.

An estimate of the error of each scaled contact ratio was determined through the use of block averaging [108–110]. The standard error for the scaled contact ratios was computed from the variance between averages of blocks of data, and the block size was increased until the standard error estimate became constant. This analysis approach allows estimation of the true standard error in correlated data sets. An analytical block average curve (based on the assumption that the autocorrelation in the data can be described as the sum of two exponentials) was fit to the standard error versus block size data to assist in identifying the correct standard error values [108–110].

Unfortunately, a single simulation is usually not adequate to demonstrate the statistical significance of the simulation results. Other researchers have commented on this problem in the context of free energy calculations made through computer simulation (see additional discussion in Chapter 9) [101, 111]. It is typically necessary to run multiple independent simulations to check and verify that the uncertainty estimates obtained through block averaging are reasonable [99, 102, 104]. Due to the rapidly diverging nature of molecular dynamics simulation results, simulations can be made independent simply by changing the seed number used to randomly assign initial velocities [112]. To simultaneously determine the effect of simulation duration on variance in the scaled contact ratios and on the level of run-to-run variance, three independent runs were conducted for the *o*-, *m*-, and *p*-aminobenzoate solubilizates of duration 10, 25, and 50 ns. Run-to-run variance was found to be comparable in magnitude (typically within a factor of 2) to the block average estimates of standard error for each of these solubilizates. Accordingly, and because of the high computational cost associated with conducting multiple simulations, independent simulations were not considered necessary for the other four solubilizates simulated.

By computing standard errors in the scaled contact ratios, it is possible to evaluate the statistical significance of the head and tail assignment made for each solubilizate group. If the scaled contact ratio for any specific group is within a standard error of 1.0, the head or tail assignment for that group is not considered to be statistically significant. For ibuprofen, benzamide, *m*-aminobenzoate, and *p*-aminobenzoate, the

level of noise observed in the simulation results led to non-statistically significant head and tail assignments for a total of 5 different groups (see Section 4.3).

Cylindrical and Spherical Micelle Simulations

To identify the solubilizate head and tail in a micellar environment, a different approach is necessary. In a micellar environment, a solubilizate molecule located at the micelle core/water interface makes contacts not only with water and with surfactant tail atoms, but also with surfactant head atoms and with atoms in other solubilizate molecules. Consequently, taking the ratio of the number of contacts with water to the number of contacts with surfactant tails would yield an inaccurate head and tail assignment for each solubilizate atom (particularly because, as will be shown in Chapter 6, contacts with surfactant heads are most appropriately treated as hydrating contacts, similar to contacts with water molecules). Instead, the approach adopted here to identify the head and tail of solubilizates based on cylindrical and spherical micelle simulation results involves calculating the ratio of the number of contacts per timestep experienced by different atoms in the solubilizate molecule with water to the number of total contacts experienced by the same atoms per timestep. Note that the total number of contacts per timestep includes contacts with water, with counterions (if present), with surfactant heads, with surfactant tails, and with other solubilizates. This ratio, which we define as the micellar contact ratio (MCR), was also calculated for each atom in the surfactants present in the micellar system. To minimize error in the results, the MCR for each surfactant and solubilizate atom was averaged for all the 5 solubilizates and for all the 38 (in the case of spherical micelles) or 49 (in the case of cylindrical micelles) surfactants considered. The MCR calculated for each atom quantifies the degree of hydration of that atom in the micellar environment. As shown in Chapter 2, the appropriate head and tail assignment for SDS in the context of molecular-thermodynamic modeling is that the SO_4 group and the first CH_2 group attached to it comprise the SDS head. Each of the remaining CH_2 groups and the terminal CH_3 group in the dodecyl chain of SDS comprise the SDS tail [81].

After determining MCR for each solubilize atom, a metric must be used to determine whether or not the MCR value computed for each atom indicates that the atom is part of the solubilize head or part of the solubilize tail. To assign each solubilize atom as either head or tail, the MCR for each solubilize atom is compared to the MCRs of the surfactant atoms, where the groups that are part of the surfactant head and tail are assumed to be known. Using the simulation results obtained in this chapter, solubilize atoms were identified as head or tail as follows: if the MCR of the solubilize atom (or group of atoms) was greater than the average of the MCRs of the first and the second CH₂ groups in SDS (i.e., greater than the average of the last head group and the first tail group in SDS), the solubilize atom was assigned to be part of the solubilize head in molecular-thermodynamic modeling. Otherwise, if the MCR of the solubilize atom was less than that of the average of the MCRs of the first and the second CH₂ groups in SDS, then the solubilize atom was considered to be part of the solubilize tail in molecular-thermodynamic modeling. The difference between the MCR of a solubilize group and the average MCR of the last head group and the first tail group in the surfactant tail will be referred to as ΔMCR . If ΔMCR is positive, the group is part of the head, and if ΔMCR is negative, the group is part of the tail.

To apply the computational approach just described, the head and tail of the surfactant must be known *a priori*. It is not difficult to determine the head and tail of simple anionic, cationic, zwitterionic, and nonionic surfactants [80, 82]. For surfactants with charged (anionic, cationic, or zwitterionic), hydrophilic atoms attached to a linear alkyl chain, the first CH₂ group attached to the surfactant head is quite hydrated and should be modeled as part of the surfactant head. However, for surfactants with nonionic hydrophilic atoms attached to a linear alkyl chain, the first CH₂ group attached to the surfactant head is relatively unhydrated and should be modeled as being part of the surfactant tail [80, 82]. These rules-of-thumb have been determined based on experimental evidence and the computer simulation results presented in Chapter 2.

For more structurally complex surfactants where it is not immediately obvious what portions of the molecule should be assigned to be part of the head and the tail, the surfactant molecule may be first simulated at a water/oil interface to determine head and tail assignments using the analysis approach described in Section 4.2.4 and in Chapter 2. Following such assignment, a micelle containing both the surfactant and solubilizate may be performed and simulated in aqueous solution in order to determine the head and tail for each solubilizate using the method described in this section. Determination of the surfactant head and tail may also be accomplished by simulation in a micellar environment, but in this case analysis is complicated by the fact that no reference condition can be defined with which to evaluate ΔMCR values from the MCR values computed for each surfactant group. Determination of the surfactant head and tail may be accomplished in the micellar environment using an alternative computer simulation/molecular-thermodynamic modeling approach (referred to as the CS-MT modeling approach) that is introduced in Chapters 6, 7, and 8. In the CS-MT modeling approach, surfactant groups that are part of the head and part of the tail are determined by counting “hydrating contacts” (contacts with hydrogen bonding or coordinate bonding atoms) in the micellar state and in bulk aqueous solution to determine what is referred to as the “fractional hydration” of each surfactant group. In Chapter 7, a value of fractional hydration that serves as the division between groups that are part of the head and part of the tail is proposed.

The same approach used to compute the standard errors of the SCRs described in Section 4.2.4 was used to compute the standard errors of the MCRs. Because head and tail assignments made from cylindrical and spherical micelle simulations requires comparison of the MCR for a specific solubilizate group with the average MCR for the last head and first tail group in a surfactant, errors in all three MCR values contribute to the uncertainty in the head and tail assignment. Fortunately, the standard error in the MCRs computed for the surfactants were found to be very small because the results were averaged over a large number of SDS molecules. Consequently, the standard error in each ΔMCR value for each solubilizate group was found to be close

to the standard error in the MCR value for that solubilizate group. If the ΔMCR value for any specific solubilizate group is within a standard error of 0.0, the head or tail assignment for that group is not considered to be statistically significant. Using the cylindrical micelle simulation data, the head or tail assignments made for one group in ibuprofen, one group in benzamide, one group in acetophenone, and two groups in *p*-aminobenzoate were not statistically significant. Using the spherical micelle simulation data, the head or tail assignment made for one group in ibuprofen, one group in benzamide, two groups in acetophenone, one group in benzonitrile, one group in *o*-aminobenzoate and *m*-aminobenzoate, and two groups in *p*-aminobenzoate were not statistically significant (see Section 4.3).

4.3 Simulation Results and Discussion

Head and tail assignments made for groups of atoms in each solubilizate using water/oil interface simulations, cylindrical micelle simulations, and spherical micelle simulations are presented in Figures 4-6, 4-7, and 4-8, respectively. In these figures, averaged results for groups of several atoms (for example, CH_3) are presented to reduce the complexity of the reported data. For clarity, no hydrogen atoms are shown in the figures. The solubilizates are shown in the same order that they appear in Figure 4-1, which more clearly identifies the chemical identity of each group. In each figure, groups that are identified as being part of the head are colored in blue, groups that are identified as being part of the tail are colored in red, and groups that could not be assigned as being part of the head or the tail with statistical significance are colored in grey. Recall that the criteria used to determine the statistical significance of head and tail assignment was described in Section 4.2.4. In Tables 1-7 in Appendix B, we list scaled contact ratios (SCRs), differences in the solubilizate and surfactant micellar contact ratios (ΔMCRs), and standard errors (SEs) computed from the water/oil interface simulation, cylindrical micelle simulation, and spherical micelle simulation data for groups of atoms in each solubilizate. In these tables,

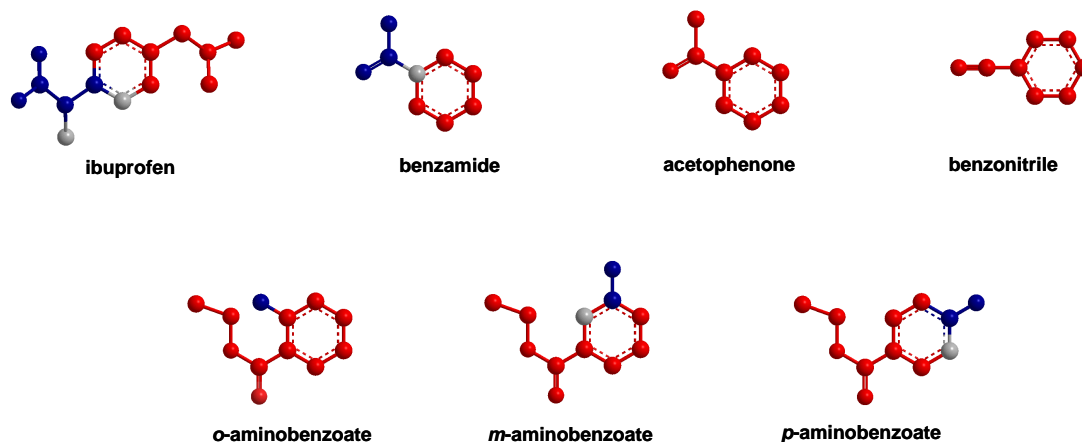


Figure 4-6: Head and tail identifications made based on water/oil interface simulations.

groups that are identified as being part of the head are shown in bold.

In general, the head and tail assignments made using water/oil interface simulation data, cylindrical micelle simulation data, and spherical micelle simulation data are similar. A total of 13 groups are assigned to be part of the head based on the water/oil interface simulation data, 10 are assigned to be part of the head based on the cylindrical micelle simulation data, and 12 are assigned to be part of the head based on the spherical micelle simulation data. Five groups could not be assigned to be part of the head or the tail with statistical significance based on the water/oil interface simulation data, five groups could not be assigned to be part of the head or the tail with statistical significance based on the cylindrical micelle simulation data, and nine groups could not be assigned to be part of the head or the tail with statistical significance based on the spherical micelle simulation data. Finally, a total of 59 groups were assigned to be part of the tail based on the water/oil interface simulation data, 62 groups were assigned to be part of the tail based on the cylindrical micelle simulation data, and 57 groups were assigned to be part of the tail based on the spherical micelle simulation data.

Important differences do exist, however, between the head and tail assignments

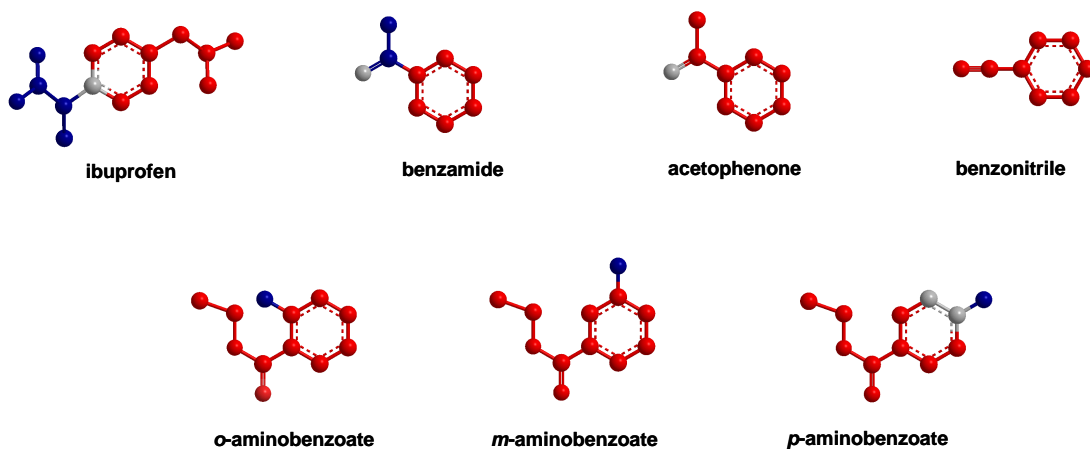


Figure 4-7: Head and tail identifications made based on cylindrical micelle simulations.

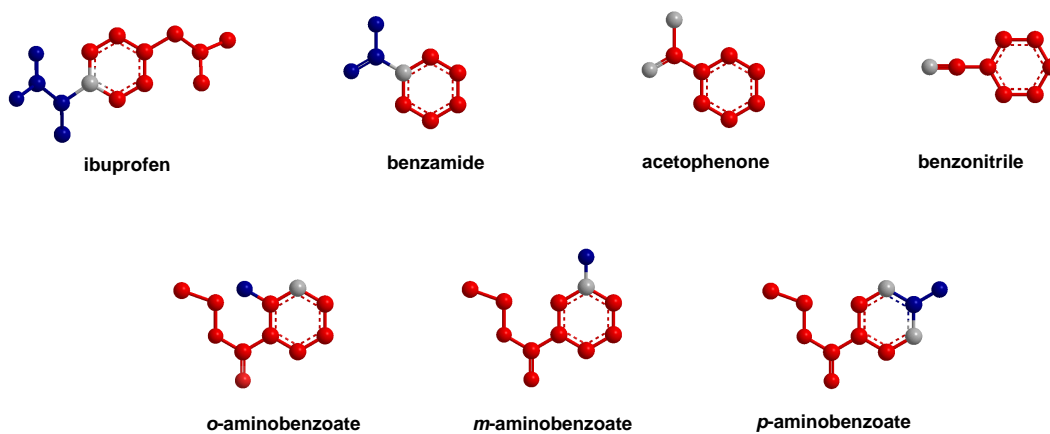


Figure 4-8: Head and tail identifications made based on spherical micelle simulations.

obtained from simulation in the three different geometries. For example, the entire acetophenone molecule is assigned to be tail based on the water/oil interface simulation results. Based on the cylindrical micelle simulation results, however, the oxygen atom in the carbonyl group in acetophenone cannot be assigned to be part of the head or part of the tail with statistical significance. Based on the spherical micelle simulation results, both the oxygen atom in the carbonyl group and the CH₃ group adjacent to the carbonyl group in acetophenone cannot be assigned to be part of the head or part of the tail with statistical significance.

The cylindrical and the spherical micelle simulations are expected to yield more physically accurate head and tail assignments than the water/oil interface simulations (albeit at the cost of greater computational expense). However, several important differences do exist between the cylindrical and the spherical micelle simulation head and tail assignment results. For example, in addition to the difference in the head and tail assignments made for acetophenone discussed above, the entire benzonitrile molecule is assigned to be tail based on the cylindrical micelle simulation results, while the nitrogen in benzonitrile has no statistically significant head or tail assignment based on the spherical micelle simulation results.

The observed differences between the head and tail assignments based on the three methods reflect two factors. The first factor is that the degree of curvature, the ordering present in the oil/micelle core phase, and the presence/spacing of the surfactant heads differs in the three cases, which would naturally be expected to influence the position and the orientation of the solubilizates relative to the micelle core/water interface to some extent. Therefore, we would expect that real, physical differences between the head and the tail identifications may be obtained for some solubilizates using the three different methods. The second factor is that the water contact data obtained using the three methods is quite noisy, and the results presented here indicate that it is not always possible, even with extended simulation times (up to 50 ns for the water/oil interface simulations and 25 ns for the cylindrical and the spherical micelle simulations) to make statistically significant head and tail

assignments for solubilizates with structures such as those modeled in this chapter.

Close inspection of the actual SCR and Δ MCR data included in Appendix B clarifies this picture somewhat, providing additional information about the extent to which the two factors discussed above contribute to the observed differences in head and tail assignments. In fact, statistically significant differences in the Δ MCR results obtained from cylindrical and spherical micelle simulation data do exist for a significant number of groups. Analysis of the results presented in Appendix B shows that 29 of the 77 Δ MCR results for groups in the seven solubilizates considered here are different to a statistically significant extent. Statistical significance in this case has been assessed by comparing the absolute value of the difference between the Δ MCR value for a given group obtained based on the cylindrical and the spherical micelle simulation data with the sum of the SE values associated with the two Δ MCR values. If the absolute value of the difference in Δ MCR is greater than the sum of the two SE values, the difference is considered statistically significant. A more stringent test of statistical significance (corresponding to a 95% level of confidence) is whether the absolute value of the difference in the Δ MCR values is greater than twice the sum of the two SE values. Using this more stringent criteria, 16 out of 77 Δ MCR assignments made using the cylindrical and the spherical micelle simulation data are different to a statistically significant extent.

Although statistically significant differences in the Δ MCR values do exist, it is not clear to what extent these differences will impact the predictions made by the molecular-thermodynamic model. One of the main free-energy contributions affected by the head and tail assignment is the transfer free-energy contribution, g_{tr} . This free-energy contribution is the primary driving force for micelle formation, and has the largest (in magnitude) free-energy contribution to the free energy of micelle formation in aqueous solution (see Section 4.4.3). An assumption is made in traditional MT modeling that g_{tr} (which is linearly related to the number of tail groups) can be considered to be independent of micelle shape and size. The computer simulation results presented here, which indicate that to some extent the head and tail assignments

are a function of micelle curvature, of the extent of ordering in the surfactant tails, and/or of the spacing of the surfactant heads, indicate that this assumption is an approximation. However, it is important to note that the molecular-thermodynamic model has been shown to yield quantitatively, or semi-quantitatively, accurate predictions of the micellization behavior of a wide range of structurally simple nonionic, zwitterionic, anionic, and cationic surfactants [16, 80, 81]. Consequently, we anticipate that selecting heads and tails based on an average of the results presented in Figures 4-6, 4-7, and 4-8, or based on one of the three methods discussed in this chapter (simulation at a water/oil interface, in a cylindrical micelle, or in a spherical micelle) should yield reasonable molecular-thermodynamic modeling results.

If reasonable results can be obtained with all three methods, for the types of solubilizates considered in this chapter (which are relatively small and rigid), determination of head and tail parameters through simulation at a water/oil interface would be recommended because it is much less computationally expensive than simulation in a micellar environment. However, in Chapter 5, head and tail assignments made based on the spherical micelle simulation results will be used in molecular-thermodynamic modeling because these assignments are expected to be the most physically realistic, and in Chapter 5 we wish to use the best possible head and tail input parameters determined through computer simulation in order to evaluate whether the hybrid computer simulation/molecular-thermodynamic model is capable of making accurate predictions of micellar solubilization behavior that are in agreement with the available experimental data. Head and tail assignments obtained through simulation in spherical micelles are expected to yield the most physically realistic of the head and tail assignments discussed in this chapter because: (i) unlike simulation at a water/oil interface, simulation in a spherical micelle includes the effects of curvature at the micelle/core water interface, ordering of the surfactant tails, and the presence of the surfactant heads, and (ii) unlike simulation in a cylindrical micelle, the boundary conditions applied during simulation in a spherical micelle are physically realistic (see Sections 4.2.3 and 4.2.3). Groups that could not be assigned to be part of the head

or the tail with statistical significance based on the spherical micelle simulation data will be modeled in a new way when implementing a mean-field model to evaluate the packing free-energy contribution (g_{pack}) associated with micelle formation. In general, those groups for which statistically significant head and tail assignments could not be made will be modeled as “neutral” groups in the packing model presented in Section 4.4.3.

4.4 Molecular-Thermodynamic Theory of Solubilization

4.4.1 Introduction

In this section, a general molecular-thermodynamic theory of solubilization is reviewed and extended. The development of a molecular-thermodynamic theory of solubilization involves combining: (i) a thermodynamic description of the surfactant and solubilizate solution with (ii) a molecular model to evaluate the free-energy change associated with transferring surfactants and solubilizates from their reference state in aqueous solution to form a surfactant/solubilizate micellar aggregate.

To simplify notation, both the thermodynamic framework and the molecular model for the free energy of micelle formation presented in this section will be formulated for the solubilization of a single ionic or nonionic solubilizate species in a micelle containing a single ionic or nonionic surfactant species, where multiple counterion species may be present in aqueous solution. However, the theory presented here may be generalized in a straightforward manner to model the self-assembly of multiple surfactant species and multiple solubilizate species into micelles.

The molecular-thermodynamic theory of solubilization presented here builds on the theory developed by Srinivasan and Blankschtein [28]. A number of refinements, such as the introduction of a new “neutral group” approach to the mean-field packing model and the use of regular solution theory to more accurately model sur-

factant/solubilize interactions in the micelle core, are presented for the first time here. Both refinements have been necessary to make the theory more physically realistic for complex surfactants and solubilizates.

4.4.2 Thermodynamic Framework to Model the Free Energy of the Micellar Solution

In the thermodynamic framework developed here, we denote the number of water molecules by N_w and the number of micellar aggregates consisting of n_s surfactant molecules, $\{n_{c_j}\}_{j=1}^J$ counterions (each species indexed by j with a total of J species present in solution), and n_a solubilizates in solution by $N_{n_s\{n_{c_j}\}n_a}$. The distribution of these micellar aggregates — referred to as $n_s\{n_{c_j}\}n_a$ -mers — includes all monomeric species in bulk aqueous solution: (i) surfactant monomers, corresponding to $n_s = 1$, $\{n_{c_j}\} = \{0\}$, and $n_a = 0$; (ii) unbound counterions, corresponding to $n_s = 0$, $\{n_{c_j \neq k}\} = \{0\}$, $n_{c_j=k} = 1$, and $n_a = 0$, for each species k present; and (iii) solubilize monomers, corresponding to $n_s = 0$, $\{n_{c_j}\} = 0$, and $n_a = 1$. The mole fraction $X_{n_s\{n_{c_j}\}n_a}$ for a given $n_s\{n_{c_j}\}n_a$ -mer is defined here to be $N_{n_s\{n_{c_j}\}n_a}/N$, where N is the total number of molecules in solution; that is, $N = N_w + \sum_{n_s} \sum_{\{n_{c_j}\}} \sum_{n_a} (n_s + \sum_j n_{c_j} + n_a) N_{n_s\{n_{c_j}\}n_a}$, where $\sum_{\{n_{c_j}\}} \equiv \sum_{n_{c_1}} \sum_{n_{c_2}} \dots \sum_{n_{c_J}}$ and the summations are understood to range from 0 to ∞ in each case. Note that this definition differs from the conventional mole fraction definition, where $X_{n_s\{n_{c_j}\}n_a} = N_{n_s\{n_{c_j}\}n_a}/(N_w + \sum_{n_s} \sum_{\{n_{c_j}\}} \sum_{n_a} N_{n_s\{n_{c_j}\}n_a})$ [28].

In the multiple-chemical equilibrium model [16, 81], each micellar aggregate is considered to be a distinct chemical species in equilibrium with the other aggregates (including monomers). By equating the overall chemical potential of a micellar aggregate, or $n_s\{n_{c_j}\}n_a$ -mer, with the sum of the chemical potentials of all the aggregate constituents (n_s surfactants, $\{n_{c_j}\}$ bound counterions, and n_a solubilizates), an expression is obtained for the mole fraction of that aggregate, $X_{n_s\{n_{c_j}\}n_a}$ [28].

Specifically,

$$X_{n_s\{n_{c_j}\}n_a} = \left(\frac{1}{e}\right) (X_s e)^{n_s} (X_a e)^{n_a} \left(\prod_j (X_{c_j} e)^{n_{c_j}}\right) \quad (4.5)$$

$$\cdot \exp\left[-\frac{1}{kT} \left(\mu_{n_s\{n_{c_j}\}n_a}^\circ - n_s \mu_s^\circ - n_a \mu_a^\circ - \sum_j n_{c_j} \mu_{c_j}^\circ\right)\right]$$

$$= \left(\frac{1}{e}\right) (X_s + X_a)^{n_{agg}} \quad (4.6)$$

$$\cdot \exp\left[\begin{array}{l} -\frac{1}{kT} \left[\mu_{n_s\{n_{c_j}\}n_a}^\circ - n_s \mu_s^\circ - n_a \mu_a^\circ - \sum_j n_{c_j} \mu_{c_j}^\circ\right] + \\ n_s \left(1 + \ln\left(\frac{X_s}{X_s + X_a}\right)\right) + n_a \left(1 + \ln\left(\frac{X_a}{X_s + X_a}\right)\right) + \\ \sum_j n_{c_j} (1 + \ln(X_{c_j})) \end{array}\right]$$

$$= \left(\frac{1}{e}\right) (X_s + X_a)^{n_{agg}} \exp[-n_{agg} \cdot g_f] \quad (4.7)$$

where X_s , X_{c_j} , and X_a are the mole fractions of the surfactant monomers, the unbound counterions of type j , and the solubilize monomers in the bulk aqueous solution, respectively; μ_i° is the standard-state (infinite dilution) chemical potential of species i , where i represents a micellar aggregate, a surfactant monomer, an unbound counterion of species j , or a solubilize monomer; k_B is the Boltzmann constant; T is the absolute temperature; n_{agg} is the aggregation number of the micellar aggregate (i.e. the number of core constituents: $n_{agg} = n_s + n_a$); and g_f is the modified free energy of micelle formation. Note that all free energies, enthalpies, and entropies represented by the symbols g , h , and s , respectively and regardless of subscript, are intensive quantities, defined on a per n_{agg} basis with units of $k_B T$. This convention will be used throughout the remainder of this chapter.

The modified free energy of micelle formation, g_f , is defined as follows [79]:

$$g_f = \left[\mu_{n_s\{n_{c_j}\}n_a}^\circ - n_s \mu_s^\circ - n_a \mu_a^\circ - \sum_j n_{c_j} \mu_{c_j}^\circ\right] - k_B T n_s \left(1 + \ln\left(\frac{X_s}{X_s + X_a}\right)\right) \quad (4.8)$$

$$- k_B T n_a \left(1 + \ln\left(\frac{X_a}{X_s + X_a}\right)\right) - k_B T \sum_j n_{c_j} (1 + \ln(X_{c_j}))$$

$$= g_{form} + g_{ent} - \left(1 + \sum_j \beta_j\right) \quad (4.9)$$

where

$$g_{\text{form}} = \frac{1}{k_{\text{B}}T} \left(\frac{\mu_{n_{\text{s}}\{n_{c_j}\}n_{\text{a}}}^{\circ}}{n_{\text{agg}}} - \alpha_{\text{s}}\mu_{n_{\text{s}}}^{\circ} - \alpha_{\text{a}}\mu_{n_{\text{a}}}^{\circ} - \sum_j \beta_{c_j}\mu_{c_j}^{\circ} \right) \quad (4.10)$$

and

$$g_{\text{ent}} = - \left[\alpha_{\text{s}} \ln \left(\frac{X_{\text{s}}}{X_{\text{s}} + X_{\text{a}}} \right) + \alpha_{\text{a}} \ln \left(\frac{X_{\text{a}}}{X_{\text{s}} + X_{\text{a}}} \right) + \sum_j \beta_{c_j} \ln (X_{c_j}) \right] \quad (4.11)$$

$$= - \left[\alpha_{\text{s}} \ln (\alpha_{\text{s}}^{\text{bulk}}) + \alpha_{\text{a}} \ln (\alpha_{\text{a}}^{\text{bulk}}) + \sum_j \beta_{c_j} \ln (X_{c_j}) \right] \quad (4.12)$$

where $\alpha_{\text{s}} = n_{\text{s}}/n_{\text{agg}}$ and $\alpha_{\text{a}} = n_{\text{a}}/n_{\text{agg}}$ are the surfactant and solubilize mole fractions in the micellar aggregate, respectively; $\alpha_{\text{s}}^{\text{bulk}} = X_{\text{s}}/(X_{\text{s}}+X_{\text{a}})$ and $\alpha_{\text{a}}^{\text{bulk}} = X_{\text{a}}/(X_{\text{s}}+X_{\text{a}})$ are the relative fractions of surfactant and solubilize in the bulk state ($\alpha_{\text{s}}^{\text{bulk}} + \alpha_{\text{a}}^{\text{bulk}} = 1$), respectively; and $\beta_{c_j} = n_{c_j}/n_{\text{agg}}$ is the degree of counterion binding for counterion species j .

The factor of e that appears in each of the pre-exponential factors in Eq. 4.5 results from the ‘individual entity’ definition of X_i used in the equation, rather than the conventional mole fraction definition. In Eq. 4.7, the pre-exponential factor $(X_{\text{s}} + X_{\text{a}})^{n_{\text{agg}}}$ captures the translational entropy loss associated with localizing the n_{s} monomeric surfactants and n_{a} monomeric solubilizes in the micellar aggregate, while g_{f} reflects both: (i) the free-energy advantage associated with the transfer of the surfactant monomers, the counterions, and the solute monomers from their corresponding standard-states in the bulk aqueous solution to the micellar aggregate (given by g_{form}), and (ii) the entropic disadvantage associated with the loss in translational entropy of the bound counterions and the solubilized solutes resulting from their association with the micellar aggregate (given by g_{ent}).

A theoretical challenge in solving Eq. 4.9 is determining the reference state chemical potentials of the micellar aggregates and monomers (including the surfactant, the solubilize, and the counterions of interest). Historically, the functional form of g_{form} , which contains these terms, has been determined by constructing a thermodynamic path from a solution containing all the constituents in monomeric form at infinite

dilution in bulk aqueous solution to a solution containing a single micelle at infinite dilution in bulk aqueous solution. As a state function, g_{form} may be calculated from any reversible path; in previous research published by our group, we have postulated the following functional form for g_{form} , where the six terms appearing below on the right-hand side of the equation are distinct free-energy contributions. Specifically,

$$g_{\text{form}} = g_{\text{tr}} + g_{\text{int}} + g_{\text{pack}} + g_{\text{mix}} + g_{\text{st}} + g_{\text{elec}} \quad (4.13)$$

Each of these distinct free-energy contributions is computed molecularly based on the chemical structures of the surfactants, the counterions, and the solubilizates. The six free-energy contributions in Eq. 4.13 are discussed in detail in the following section, which introduces a molecular model to determine the magnitude of each contribution.

Note that, in the discussion that follows, we make frequent use of the index i to represent either the surfactant or solubilizate species (i.e. the core constituents). In the remainder of this chapter, we will only explicitly indicate the definition of i where it is additionally used to index the counterion species.

4.4.3 Molecular Model of Micellar Solubilization

In the molecular model of micellar solubilization presented here, the formation of a micellar aggregate from the surfactant monomers, the counterions, and the solubilizate monomers in their standard states in aqueous solution can be modeled by computing the free-energy contributions associated with the formation of the micelle interfacial shell and the free-energy contributions associated with the formation of the micelle core.

Formation of the Micelle Interfacial Shell

In this section, we discuss the evaluation of the free-energy changes associated with assembling the micelle interfacial shell, which includes the surfactant heads, the sol-

ubilizate heads (if present), and the bound counterions (in the case of ionic systems). A key assumption underlying the molecular-thermodynamic modeling approach is that the micelle is modeled as having a sharp micelle core/water interface, so that the free-energy contributions associated with the formation of the micelle interfacial shell are independent of the internal microstructure of the micelle (which is determined through the packing model described in Section 4.4.3), and depend solely on the micelle geometry and composition.

The Steric Free-Energy Contribution In previous work on the micellization of ionic surfactants with counterion binding, the effect of excluded area at the interface due to surfactant heads and bound counterions on the lateral mobility of these entities across the interfacial surface has been modeled through a steric free-energy contribution, g_{st} , given by:

$$g_{st} = - \left(\alpha_h + \sum_j \beta_{c_j} \right) \ln \left(1 - \frac{A_h}{A} \right) \quad (4.14)$$

$$= - \left(\alpha_h + \sum_j \beta_{c_j} \right) \ln \left(1 - \frac{\alpha_a a_{h,a} + \alpha_s a_{h,s} + \sum_j \beta_{c_j} a_{h,c_j}}{(S/l_{core})v_{avg}} \right) \quad (4.15)$$

In Eq. 4.15, $a_{h,a}$, $a_{h,s}$, a_{h,c_j} are the lateral head areas of the solubilizate, the surfactant, and the j th species of counterion, respectively, projected onto the micelle surface of area A . A_h is the total surface area occupied by the projection of these heads (i.e., $A_h = n_a a_{h,a} + n_s a_{h,s} + \sum_j n_{c_j} a_{h,c_j}$), such that the ratio A_h/A represents the occupied fraction of the micelle surface area; the argument of the logarithm is therefore the fractional free surface area at the micelle surface. It is convenient to divide both A_h and A in equation 4.14 by n_{agg} to eliminate explicit reference to the number of molecules, and the formula $A/n_{agg} = (A/V)v_{avg} = (S/l_{core})v_{avg}$ is further used to develop equation 4.15, where V is the micelle volume, S is the micelle shape factor ($S = 1$ for bilayers, 2 for cylinders, and 3 for spheres), l_{core} is the micelle core-minor radius, and v_{avg} is the average core constituent tail volume ($v_{avg} = \alpha_s v_s + \alpha_a v_a$, with v_s and v_a the molecular tail volumes of the surfactant and

solubilize, respectively). The term multiplying the logarithm in Eqs. 4.14 and 4.15, $\alpha_h + \sum_j \beta_{c_j}$, represents the fraction of constituents with heads relative to the number of core constituents (n_{agg}), where α_h is defined below and is dependent on whether the solubilize is localized entirely within the surfactant core (zero head area) or has amphiphilic character (nonzero head area).

$$\alpha_h = \begin{cases} \alpha_s + \alpha_a = 1, & \text{if } a_{h,a} > 0 \\ \alpha_s, & \text{if } a_{h,a} = 0 \end{cases} \quad (4.16)$$

The Electrostatic Free-Energy Contribution The electrostatic free-energy contribution includes two separate terms: (i) the free-energy change associated with discharging the charged surfactant/solubilize heads in bulk aqueous solution, g_{disch} , and (ii) the free-energy change associated with charging the micellar aggregate to the appropriate surface charge density in aqueous solution, g_{charge} . The electrostatics free-energy model used in modeling micellar solubilization is identical to a model developed for ionic, zwitterionic, and pH-sensitive surfactant mixtures [33, 34, 79]. Solubilizes that localize in the micelle core are typically nonionic, and therefore do not contribute to g_{elec} . The electrostatic free-energy contribution is computed using the following expression:

$$g_{\text{elec}} = g_{\text{disch}} + g_{\text{charge}} \quad (4.17)$$

$$= g_{\text{disch}} + \int_0^{q_f} \psi_0(q) dq \quad (4.18)$$

where $\psi_0(q)$ is the instantaneous micelle surface potential, expressed as a function of the instantaneous micelle charge, q , and $\int_0^{q_f} \psi_0(q) dq$ is the work required to charge the micelle surface against this instantaneous potential from an uncharged state ($q = 0$) to the final state of charge ($q = q_f$).

The first term in Eq. 4.17 is evaluated using the Debye-Huckel expression, and is

given by:

$$g_{\text{disch}} = \alpha_a g_{\text{disch},a} + \alpha_s g_{\text{disch},s} + \sum_j \beta_{c_j} g_{\text{disch},c_j} \quad (4.19)$$

$$= -\frac{e_0^2}{4\pi\eta_b\epsilon_0 (k_B T)^2} \left(\alpha_a \frac{z_a^2}{r_{h,a}(1+\kappa r_{h,a})} + \alpha_s \frac{z_s^2}{r_{h,s}(1+\kappa r_{h,s})} + \frac{\sum_j \beta_{c_j} \frac{z_{c_j}^2}{r_{h,c_j}(1+\kappa r_{h,c_j})}}{\sum_j \beta_{c_j} \frac{z_{c_j}^2}{r_{h,c_j}(1+\kappa r_{h,c_j})}} \right) \quad (4.20)$$

where e_0 is the electronic charge, η_b is the dielectric constant for the bulk aqueous solvent, ϵ_0 is the dielectric permittivity of vacuum, and z_i and $r_{h,i}$ are the charge and the hydrated radius of species i , respectively (including the J counterion species). Note that Eq. 4.20 contains contributions for all ionic species in the solution that are present in the final aggregate, including charged surfactants, bound counterions, and solubilizates. For nonionic components $z_i = 0$, and therefore $g_{\text{disch},i} = 0$.

The magnitude of the integral in the second term of Eq. 4.18 is dictated by the number and charge of the ionic constituents in the micellar aggregate and in bulk aqueous solution. The solution of this integral involves solving a Laplace equation for the Stern region of the micelles, and approximating the Poisson-Boltzmann equation using the Ohshima, Healy, and White approximation [33].

Formation of the Micelle Core

In this section, the free-energy contributions associated with the formation of the micelle core are discussed. These free-energy contributions include: (i) two free-energy contributions associated with changes in hydration (the transfer free-energy contribution, g_{tr} , and the interfacial free-energy contribution, g_{int}), (ii) a free-energy contribution associated with mixing of the surfactants, the counterions, and the solubilizates in the micelle, g_{mix} , and (iii) a free-energy contribution associated with the constrained arrangement of the surfactant and the solubilizate tails in the micelle core, g_{pack} .

Free-Energy Contributions Due to Hydration The transfer (g_{tr}) and the interfacial (g_{int}) free-energy contributions both reflect the free-energy changes associated

with changes in surfactant and solubilize hydration that occur during micelle formation. The transfer free-energy contribution for tail i reflects the free-energy change associated with complete dehydration of each surfactant/solubilize tail as it is transferred to a bulk solution of tails of type i , while the interfacial free-energy contribution reflects the free-energy change associated with forming the micelle core/water interface, causing atoms in the tails that lie at or near the interface to be partially rehydrated.

The Transfer Free-Energy Contribution The transfer free energy, $g_{\text{tr},i}$, of the hydrophobic tail of component i is modeled by equating the chemical potential of that tail in monomer state, $\mu_{\text{aq},i}$, in aqueous solution with its chemical potential in a pure bulk phase of tails, $\mu_{\text{pure},i}$, as shown below:

$$\mu_{\text{aq},i} = \mu_{\text{aq},i}^0 + k_{\text{B}}T \ln X_{\text{aq},i} = \mu_{\text{pure},i}^0 = \mu_{\text{pure},i} \quad (4.21)$$

where $\mu_{\text{aq},i}^0$ is the standard-state chemical potential of component i in the aqueous bulk phase, $\mu_{\text{pure},i}^0$ is the standard-state chemical potential of component i in the pure component i bulk tail phase, and $X_{\text{aq},i}$ is the mole fraction of component i in aqueous solution in equilibrium with the pure tail phase resulting from the equality of the chemical potentials in Eq. 4.21. This mole fraction is then equal to that at the solubility limit of component i by the definition of this equilibrium. Note, however, that this tail is often not a physically realizable independent entity in the case of amphiphilic compounds; for example, for surfactants with linear alkane tails, the tail does not have a methyl group connected to the surfactant head and is therefore not a true linear alkane. In practice, in this example, we make the assumption that the linear alkane analogous to the surfactant tail is an appropriate substitute molecule for calculations utilizing Eq. 4.21 involving the standard-state chemical potentials and tail solubility.

Rearranging Eq. 4.21, we arrive at an expression for the difference in standard-state chemical potentials, $\mu_{\text{pure},i}^0 - \mu_{\text{aq},i}^0$, which we define as $k_{\text{B}}Tg_{\text{tr},i}$, where $g_{\text{tr},i}$ is given

by:

$$g_{\text{tr},i} = \frac{\mu_{\text{pure},i}^0 - \mu_{\text{aq},i}^0}{k_{\text{B}}T} = \ln \frac{S_{\text{aq},i}}{S_{\text{aq},i} + 55.6} \quad (4.22)$$

where $X_{\text{aq},i}$ has been written explicitly in terms of the molar solubility limit of the hydrophobic tail of component i , $S_{\text{aq},i}$, and 55.6 corresponds to the molarity of pure water.

To calculate g_{tr} for a multicomponent micelle, we weight each $g_{\text{tr},i}$ by the micellar mole fraction of that component, α_i . Specifically, in the case of a single surfactant and a single solubilize considered here, one obtains:

$$g_{\text{tr}} = \alpha_{\text{s}}g_{\text{tr},\text{s}} + \alpha_{\text{a}}g_{\text{tr},\text{a}} \quad (4.23)$$

In practice, it is usually straightforward to estimate $S_{\text{aq},i}$ for surfactant and solubilize tails with relatively simple structures that have physically realistic close analogues because aqueous solubility data is readily available for a large set of organic compounds. However, in cases where experimental solubility data is not available, especially in cases where the tail has no immediate realistic analogue (e.g., a fragment of an aromatic ring), the solubility must be predicted theoretically, for example by using a group-contribution approach. Such approaches will be discussed in greater detail in Chapter 5.

The Interfacial Free-Energy Contribution The interfacial free-energy contribution, g_{int} , is computed as the reversible work associated with creating an interface between water and a phase consisting of a mixture of surfactant/solubilize tails, with this interface having a characteristic interfacial tension, σ . We evaluate g_{int} using the macroscopic interfacial tension of the micelle core/water interface, σ , and an estimate of the area of the interface, A , that is exposed to water. The value of A is equal to the difference between the total micelle area, A_{tot} , which is obtained geometrically based on the volume of the surfactant/solubilize tails, and the total area of the micelle that is shielded from water contacts by the heads that reside at

the interface, A_0 . Note that, in general, A_0 has a value different from A_h (which appears in Eq. 4.14), since the two areas are conceptually different, although both are related to the presence of head groups. Alternatively, g_{int} can be expressed in terms of the area per molecule in the micelle, a , which can be formulated in terms of the micelle shape factor, S ($S = 1$ for bilayers, 2 for cylinders, and 3 for spheres); the micelle core-minor radius, l_{core} ; and the average tail volume, v_{avg} . Specifically,

$$g_{\text{int}} = \sigma \frac{(A - A_0)}{n_{\text{agg}}} = \sigma (a - a_0) = \sigma \left(\frac{S}{l_{\text{core}}} v_{\text{avg}} - a_{0,\text{avg}} \right) \quad (4.24)$$

where n_{agg} is the total number of molecules in the micellar aggregate, $a = A/n_{\text{agg}}$, $a_0 = A_0/n_{\text{agg}}$, $v_{\text{avg}} = \sum_i \alpha_i v_i$, and $a_{0,\text{avg}} = \sum_j \alpha_j a_{0,j}$, where the index j includes only surfactants and solubilizates that possess heads.

To compute σ , the interfacial tension between water and the micelle core, the surfactant tail/water interfacial tension, σ_s , and the solubilizate tail/water interfacial tension, σ_a , are weighted by the volume fractions of each component near the micelle core/water interface, $\eta_{\text{int},i}$, as follows:

$$\sigma = \eta_{\text{int},s} \sigma_s + \eta_{\text{int},a} \sigma_a \quad (4.25)$$

As will be discussed in Section 4.4.3, the term $\eta_{\text{int},i}$ refers to the volume fraction of tail i in a layer within the micelle core extending from the micelle core/water interface 1.54 \AA toward the micelle center. Volume fractions in the outer layer are used instead of area fractions at the micelle surface in order to capture the impact on the interfacial tension of solubilizates which are located fully within the micelle core (with no heads) but near the interface. Solubilizates present deeper in the micelle core are assumed not to contribute to the characteristics of the interface. Due to this construction, Eq. 4.25 is a general formula that may be used regardless of the locus of solubilization. For solubilizates without a head, $\eta_{\text{int},i}$ must be calculated within the context of the mean-field model used to compute the packing free-energy contribution, g_{pack} . However, for solubilizates with a head, $\eta_{\text{int},i}$ can be approximated

as being equal to α_i . In this case, Eq. 4.25 may be rewritten as follows:

$$\sigma = \alpha_s \sigma_s + \alpha_a \sigma_a \quad (4.26)$$

The curvature-corrected interfacial tensions, σ_i , are determined using the Gibbs-Tolman-Koenig-Buff equation [113–116]:

$$\sigma_i = \frac{\sigma_{0,i}}{\left(1 + \frac{(S-1)\delta}{l_{\text{core}}}\right)} \quad (4.27)$$

where $\sigma_{0,i}$ is the interfacial tension of component i with water at a flat interface (having a typical value of about 50 mN/m for linear hydrocarbons), δ is the Tolman distance [116], and S is the shape factor defined above. Typically, an empirical correlation is used to determine $\sigma_{0,i}$ for alkyl chains of varying length and as a function of temperature, although, if available, the experimental $\sigma_{0,i}$ values may be used [117]. The Tolman distance, δ , is computed using the following expression [81].

$$\delta(n_t) = \delta(n_t = 11) l_{\text{max}}(n_t) / l_{\text{max}}(n_t = 11) \quad (4.28)$$

where n_t is the number of carbons in the alkyl tail, and $l_{\text{max}}(n_t) = 1.54 + 1.265n_t$ is the fully-extended length of the alkyl tail (in Å) [118].

For some solubilizates, experimental values of $\sigma_{0,a}$ are available. When these are not available, $\sigma_{0,a}$ may be estimated using an equation developed by Girifalco and Good, which enables estimation of the interfacial tension between two bulk phases based on their respective surface tensions and a parameter, Φ , which depends on the molecular structure of the phase constituents as follows:

$$\sigma_{0,a} = \gamma_i + \gamma_w - 2\Phi_{iw}(\gamma_i\gamma_w)^{1/2} \quad (4.29)$$

where γ_i is the surface tension of the surfactant or solubilizate tail i ; γ_w is the surface tension of pure water, or 72.8 mN/m; and Φ_{iw} is the value of Φ specific to the

component i /water interface. Note that Φ_{iw} is typically determined for classes of compounds with similar chemical functionality by back-calculating using experimental measurements to determine the interfacial and surface tensions in Eq. 4.29. This equation enables use of the larger body of literature values for surface tension to predict interfacial tensions when experimental interfacial tension data is not available, although the determination of Φ_{iw} for complex molecules has not been well characterized in the literature.

The Mixing Free-Energy Contribution The mixing free-energy contribution, g_{mix} , models two distinct types of mixing associated with micellar solubilization, which we will refer to as $g_{\text{mix,I}}$ and $g_{\text{mix,II}}$ in the ensuing discussion. The first type of mixing, $g_{\text{mix,I}}$, involves the effects of mixing solubilize tails with surfactant tails within the micelle core. In an extension of the previous molecular-thermodynamic model of solubilization, we have chosen to model the mixing of the surfactant/solubilize tails using regular solution theory, which accounts for both entropic and enthalpic contributions to the free energy of mixing. Note that, for solubilizates that have no head, and that therefore are free to move within the micelle core, an additional translational entropy term is required. This additional translational entropy term is included in g_{pack} and will be discussed in Section 4.4.3. The second type of mixing entropy, $g_{\text{mix,II}}$, involves the mixing of counterions, surfactant heads, and solubilize heads (when applicable), in the micelle interfacial shell.

Both $g_{\text{mix,I}}$ and $g_{\text{mix,II}}$ are specific applications of a more general model of mixing, given by:

$$g_{\text{mixing}} = \sum_i \alpha_i \ln a_i = h_{\text{mixing}} - Ts_{\text{mixing}} \quad (4.30)$$

where, in a micellar system, i can index any of: the surfactant head or tail, the solubilize head or tail, and any one of the J counterion species, as applicable; α_i is the mole fraction of species i (relative to n_{agg}); and a_i is the activity of species i .

In developing an expression for $g_{\text{mix,I}}$ from Eq. 4.30, we make use of the regular solution model proposed by Hildebrand for a binary system [119], which in our case

is the system comprised of the surfactant tail and solubilize tail within the micelle core. Specifically,

$$k_{\text{B}}T \ln a_s = v_s \eta_a^2 (\delta_s - \delta_a)^2 + k_{\text{B}}T \ln \alpha_s \quad (4.31a)$$

$$k_{\text{B}}T \ln a_a = v_a \eta_s^2 (\delta_s - \delta_a)^2 + k_{\text{B}}T \ln \alpha_a \quad (4.31b)$$

where v_i is the tail volume of species i , $\eta_i = \alpha_i v_i / v_{\text{avg}}$ is the volume fraction of species i , and δ_i is the solubility parameter for species i , which can be determined either experimentally or using group-contribution methods.

By combining Eq. 4.30 with Eqs. 4.31a and 4.31b, we arrive at the following expression for $g_{\text{mix,I}}$, which has been written in a manner that emphasizes the enthalpic and the ideal entropic contributions to the free energy:

$$\begin{aligned} g_{\text{mix,I}} &= (h_{\text{mix,I}}) - T (s_{\text{mix,I}}) \\ &= \left(\frac{\eta_s \eta_a (\delta_s - \delta_a)^2 v_{\text{avg}}}{k_{\text{B}}T} \right) - T \left(-\frac{\alpha_s \ln \alpha_s + \alpha_a \ln \alpha_a}{T} \right) \end{aligned} \quad (4.32)$$

In equation 4.32, it is a difference in solubility parameters between the two mixed species that captures the non-idealities of the surfactant tail/solubilize tail mixing. When these parameters are equal, $h_{\text{mix,I}}$ becomes zero, and the free energy of mixing is a function of the ideal entropy alone, which corresponds to ideal mixing. Note that it is by definition of a regular solution that decomposition into a nonideal enthalpic component and an ideal entropic component is possible [119].

To evaluate $g_{\text{mix,II}}$, the mixing of bound counterions, surfactant heads, and solubilize heads, as applicable, is modeled as ideal. That is, we assume that the solubility parameters of these species are very similar, such that the enthalpic term tends to zero. This assumption greatly simplifies evaluation of the mixing free energy; for micellar solutions where multiple counterions are present, implementation of a regular solution model to compute the mixing free energy would require consideration of all pairwise interactions. With this in mind, the following simple expression is used to

determine $g_{\text{mix,II}}$ [28]:

$$g_{\text{mix,II}} = -T (s_{\text{mix,II}}) = \begin{cases} \alpha_s \ln \frac{\alpha_s}{\alpha_s + \sum_j \beta_{c_j}} + \sum_j \beta_{c_j} \ln \frac{\beta_{c_j}}{\alpha_s + \sum_j \beta_{c_j}}, & \text{if } a_{h,a} = 0 \\ \alpha_a \ln \frac{\alpha_a}{1 + \sum_j \beta_{c_j}} + \alpha_s \ln \frac{\alpha_s}{1 + \sum_j \beta_{c_j}} + \sum_j \beta_{c_j} \ln \frac{\beta_{c_j}}{1 + \sum_j \beta_{c_j}}, & \text{if } a_{h,a} > 0 \end{cases} \quad (4.33)$$

where the first case represents ideal mixing of surfactant heads and J bound counterion species, and the second case represents ideal mixing of surfactant heads, solubilize heads, and J bound counterion species.

The mixing free-energy contribution, g_{mix} , is equal to the sum of $g_{\text{mix,I}}$ and $g_{\text{mix,II}}$:

$$g_{\text{mix}} = g_{\text{mix,I}} + g_{\text{mix,II}} \quad (4.34)$$

$$= \begin{cases} \frac{\eta_s \eta_a (\delta_s - \delta_a)^2 v_{\text{avg}}}{k_B T} + \alpha_s \left(\ln \alpha_s + \ln \frac{\alpha_s}{\alpha_s + \sum_j \beta_{c_j}} \right) + \\ \alpha_a (\ln \alpha_a) + \sum_j \beta_{c_j} \left(\ln \frac{\beta_{c_j}}{\alpha_s + \sum_j \beta_{c_j}} \right), & \text{if } a_{h,a} = 0 \\ \frac{\eta_s \eta_a (\delta_s - \delta_a)^2 v_{\text{avg}}}{k_B T} + \alpha_s \left(\ln \alpha_s + \ln \frac{\alpha_s}{1 + \sum_j \beta_{c_j}} \right) + \\ \alpha_a \left(\ln \alpha_a + \ln \frac{\alpha_a}{1 + \sum_j \beta_{c_j}} \right) + \sum_j \beta_{c_j} \left(\ln \frac{\beta_{c_j}}{1 + \sum_j \beta_{c_j}} \right), & \text{if } a_{h,a} > 0 \end{cases}$$

The Packing Free-Energy Contribution The free-energy penalty associated with attachment of the surfactant and amphiphilic solubilize tails to the micelle core/water interface is captured in g_{pack} , the packing free-energy contribution. This free-energy contribution includes: (i) the conformational penalty associated with packing the surfactant and the solubilize tails in the micelle core, and (ii) the entropic gain associated with mixing the surfactant tails and unattached solubilize tails within the micelle core.

In this section, a chain packing theory to model protein adsorption onto solid surfaces grafted with polymer chains originally developed by Ben-Shaul, Szleifer, and Gelbart is generalized to model packing within micellar systems [120, 121]. Here, an extension of Szleifer's model developed by Srinivasan and Blankshtein, which incor-

porates the presence of solubilizates in the micelle core, is reviewed. Surfactant tails, because of their chemical bonds with the surfactant heads, are effectively attached to the micelle core/water interface [28]. If an amphiphilic solubilizate is present in the micelle, the solubilizate tail is also attached to the micelle core/water interface. To make the mean-field model more physically realistic when modeling complex surfactants and amphiphilic solubilizates possessing head groups, a novel modeling approach has been developed that models certain surfactant/solubilizate groups as “neutral” groups. This approach is reported for the first time in this section.

System Definition In the mean-field theory used to compute g_{pack} , the micelle hydrophobic core is divided into L concentric layers (see Figure 4-9). The label l , where $l = 1, 2, 3 \dots L$ starting from the micelle center towards the micelle surface, will be used to number each of the layers in the micelle core. The value of L is typically chosen so that the width of each layer is between 1.5-2.0 Å, which is close to the length of a carbon-carbon bond [28]. The volume of the micelle core will be denoted by V , and therefore, the overall volume fraction of the solubilized solute in the micelle core is defined as $\eta_a = n_a v_a / V$, where n_a and v_a are the number and molecular tail volume of the solubilizate present in the micelle, respectively.

In the mean-field packing model, the conformations of a single surfactant tail and a single solubilizate tail are considered. The intramolecular bonded interactions of the surfactant and the solubilizate are modeled rigorously, while the intermolecular interactions with the other surfactant and solubilizate tails are treated using a mean-field approximation. Both the surfactant and the solubilizate tails are modeled at a united-atom level of detail, in which hydrogen atoms are modeled as being part of their parent atoms (for example, each CH₂ group is modeled as a single entity).

To introduce an increased level of physical realism into the model for the packing free-energy contribution (g_{pack}), we have introduced a new modeling approach in which each group in a surfactant or solubilizate tail can be modeled as a head group, a tail group, or a “neutral” group when performing packing calculations. In earlier

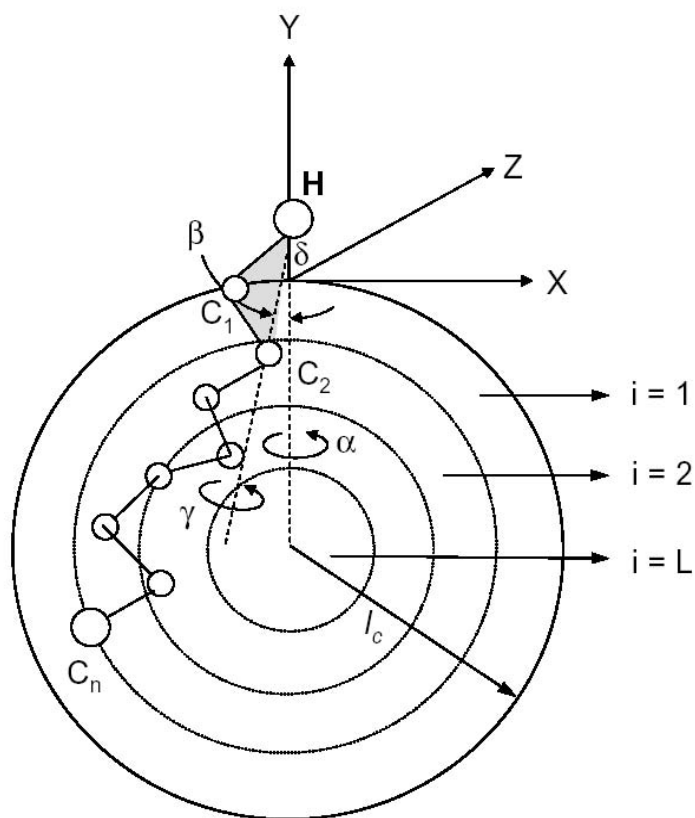


Figure 4-9: Two-dimensional representation of a spherical or cylindrical micelle core. The micelle core is divided into L layers parallel to the micelle core-water interface. The Cartesian reference frame $\{X, Y, Z\}$ is chosen with the Y -axis passing through the surfactant head (\mathbf{H}) and oriented normal to the micelle core/water interface. The three Euler angles describing the overall orientation of the surfactant tail with respect to the micelle core/water interface (α , β , and γ) are discussed in the text. The variable δ denotes the position of the surfactant head outside the micelle core/water interface. Figure and explanation are taken from [28].

implementations of the packing model, all head groups were modeled as a single combined entity (see the group denoted **H** in Figure 4-9). In the new implementation, the packing model is made more physically realistic by modeling each group that is part of the surfactant/solubilize head explicitly. A single group in the head (typically a very hydrophilic group, such as the charged group in an ionic surfactant head) is selected as the group that is “rooted” at a position δ beyond the micelle core/water interface. Although the other head groups are not rooted at a specific coordinate and all conformations of the head group are sampled during modeling, they are not permitted to cross the micelle core/water interface to enter the micelle core. Similarly, tail groups are forced to remain within the micelle core. In contrast to both head and tail groups, neutral groups are groups that are modeled as being allowed to adopt positions in both the aqueous phase and within the micelle core. We believe that modeling certain groups in this manner makes the packing model more physically realistic by relaxing the traditional approximation that the micelle core/water interface is completely sharp. In reality (and as observed in our MD simulations), micelles are dynamic entities characterized by a rough micelle core/water interface. Many solubilize groups in the 14 micelles simulated in this chapter spent a significant amount of time in both the aqueous phase and the micelle core. As such, modeling the micelle core/water interface as a sharp boundary and assigning such groups to be either head groups (which are not allowed to enter the micelle core), or tail groups (which are not allowed to enter the aqueous solution), is not physically realistic and can result in large, unphysical g_{pack} values (results not shown).

The identification of an individual group in a surfactant or solubilize as a head group, a tail group, or a neutral group is made based on the computer simulation results. In the new proposed implementation of g_{pack} , neutral groups are defined as groups that are observed to spend a significant amount of time both outside and inside of the micelle core during MD simulation. It is important to note that surfactant/solubilize groups that cannot be identified as head groups or as tail groups with statistical significance (for the solubilizes simulated in this chapter, such groups are

shown in grey in Figures 4-6, 4-7, and 4-8) either: (i) have an average SCR value that is very close to 1.0 or a ΔMCR value that is very close to 0.0, or (ii) have a high degree of variation in their SCR or ΔMCR values. We believe that such groups will be modeled in a more physically realistic manner if they are modeled as neutral groups.

A single conformation of the surfactant tail is denoted by Ω . This conformational state can be separated into two components: (i) Ω_{int} , or the internal dihedral conformation of the tail, and (ii) Ω_{ext} , or the external conformation of the tail, which specifies the rotational orientation of the tail with respect to the micelle core/water interface [28].

If a solubilize does not possess a head, then it may be distributed throughout the micelle core, and therefore it is necessary to consider conformations for the molecule throughout the micelle core. The position of a solubilize that has no head within the micelle core is denoted by p , where the value of p ranges from 1 to L . The value of p can refer to the position of any arbitrarily selected segment of the solubilize within the micelle core. The conformation of a solubilize positioned in layer p is denoted by ω_p . Just like the surfactant tail, the conformational state of the solubilize tail can be separated into two components: (i) $\omega_{p,\text{int}}$, or the solubilize internal dihedral conformation, and (ii) $\omega_{p,\text{ext}}$, or the solubilize external conformation, which specifies the rotational orientation of the solubilize tail with respect to the micelle core/water interface [28].

Internal Conformations of the Surfactant/Solubilize Tail Internal conformations reflect only the dihedral, or torsional, conformations of the surfactant or solubilize tail; both bond angles and bond lengths are modeled as being fixed at their average values. Dihedral conformations for molecules with rotatable bonds are modeled using the Rotational Isomeric State (RIS) model, which has been shown to be effective at describing the conformational statistics of chain-like molecules in the liquid state [122, 123]. RIS replaces a continuous dihedral potential for a given

rotatable bond with a set of discrete dihedral angles and energies that correspond to the minima observed in the continuous potential. Energies are reported as differences between each discrete state energy and the minimum state energy (typically referred to as the *trans* state), ϵ . For linear alkanes, for example, each $\text{CH}_2\text{-CH}_2$ bond is assigned three states, the *trans* state (180°) and two higher energy *gauche* states (a " g^- " state at 60° and a " g^+ " state at 300°). Boltzmann factors based on these energy differences, of the form $\exp(-\epsilon/k_{\text{B}}T)$, can then be used to determine the probability of the dihedral state being occupied in a canonical ensemble of surfactant or solubilizate tail configurations.

Although, in principle, the dihedral potential may be a function of the state of every other dihedral in a molecule, only the effect of nearest neighbor states are considered in the RIS approximation. For example, in the case of linear alkanes, one type of *gauche* state followed by the other type (e.g. g^+g^- or g^-g^+) leads to the unfavorable "pentane" effect, which involves the steric overlap of some hydrogen atoms. This conformation is assigned an infinite energy, which leads to a Boltzmann factor of 0.

For the seven solubilizates modeled in this chapter, several, including ibuprofen and the aminobenzoates, have adjacent pairs of rotatable bonds that are amenable to modeling with the RIS approach. However, the RIS model has the most impact on the computed values of g_{pack} when modeling longer, more flexible alkyl chains, since changes in dihedrals in one part of the tail (chain) have a large influence on the position of atoms further down the chain.

To implement the mean-field model, an internal Cartesian coordinate system is specified for each atom within the surfactant/solubilizate tail. In Figure 4-9, the coordinate system for each carbon atom, C_k (where k ranges between 1 and n), would be represented by a coordinate system $\{\mathbf{x}_k, y_k, z_k\}$. This coordinate system has been described in detail elsewhere [28], and therefore is not discussed any further here.

External Conformations of the Surfactant/Solubilize Tail External conformations reflect the orientation of the surfactant/solubilize tail and the position of the surfactant/solubilize head (denoted by \mathbf{H} in Figure 4-9), with respect to the micelle core/water interface. Positions of the surfactant/solubilize head are generated randomly such that $\delta \leq 1.5 \text{ \AA}$, thereby allowing the surfactant head to fluctuate in the region immediately outside the micelle core/water interface (in what is referred to as “piston-like” motion). For each head position, a number of different orientations of the surfactant/solubilize tail are sampled, each of which is characterized by the three Euler angles, $\{\alpha, \beta, \gamma\}$, which describe the orientation of the $\mathbf{H-C}_1\text{-C}_2$ triangle shown in Figure 4-9. As shown in Figure 4-9, α is the angle between the projection of the $\mathbf{H-C}_2$ line on the X-Z plane and the X-axis, β is the angle between the Y axis and the imaginary $\mathbf{H-C}_2$ line, and γ is the angle describing the rotation of the tail about the $\mathbf{H-C}_2$ line. Additional details of this coordinate system and of the coordinate system used to describe the entire micelle, $\{X, Y, Z\}$, have been presented elsewhere [28], and therefore are not discussed any further here.

For solubilizates with no head, external conformations are generated in the same manner as for solubilizates attached to the micelle core/water interface, with the difference that piston-like motion is not considered. Because both internal and external conformations of such solubilizates must be sampled in each layer within the micelle core, the total number of conformations that must be included during the analysis is increased.

Evaluation of the Conformational Free Energy In this section, the equations that must be solved to evaluate g_{pack} are introduced and discussed briefly. An in-depth discussion of the origin of these expressions and their physical meaning has been reported elsewhere [28]. The value of g_{pack} in Eq. 4.13 is computed as the composition-weighted average of g_{pack} for the surfactant ($g_{\text{pack},s}$) and for the solubi-

lize ($g_{\text{pack},a}$) as follows:

$$g_{\text{pack}} = \alpha_s g_{\text{pack},s} + \alpha_a g_{\text{pack},a} \quad (4.35)$$

However, it is important to note that the two packing free-energies in Eq. 4.35, $g_{\text{pack},s}$ and $g_{\text{pack},a}$, cannot be calculated independently, since the partition functions governing the distribution of surfactant and solubilize tail configurations are coupled through the mean field via space-filling constraints in the micelle core [28]. This will be discussed in detail shortly.

The packing free-energy contribution of micelle component i , $g_{\text{pack},i}$, is equal to the difference between the conformational free energy of a surfactant/solubilize tail of type i in the micellar environment ($A_{c,s}$ and $A_{c,a}$ for the surfactant and the solubilize, respectively) and the conformational free energy of the same surfactant/solubilize tail in a bulk phase of surfactant/solubilize tails of type i ($A_{c,s}^{\text{free}}$ and $A_{c,a}^{\text{free}}$ for the surfactant and the solubilize, respectively). Specifically [28],

$$g_{\text{pack},s} = A_{c,s} - A_{c,s}^{\text{free}} \quad (4.36)$$

$$g_{\text{pack},a} = A_{c,a} - A_{c,a}^{\text{free}} \quad (4.37)$$

The conformational free energy of the surfactant tail is given by the following expression [28]:

$$A_{c,s} = E_{c,s} - TS_{c,s} \quad (4.38)$$

$$= \sum_{\Omega} \epsilon_s(\Omega) P_s(\Omega) + k_B T \sum_{\Omega} P_s(\Omega) \ln P_s(\Omega) \quad (4.39)$$

$$= - \sum_l \pi_l \langle \phi_s(l, \Omega) \rangle - k_B T \ln y_s \quad (4.40)$$

where $E_{c,s}$ is the internal energy of the central surfactant tail, $S_{c,s}$ is the conformational entropy of the central surfactant tail, $\epsilon_s(\Omega)$ is the internal energy of the central surfactant tail in conformation Ω , $P_s(\Omega)$ is the probability that the central surfactant tail will adopt conformation Ω , π_l is the Lagrange multiplier for layer l required to

satisfy volume-filling constraints, $\langle \phi_s(l, \Omega) \rangle$ is the average volume of the surfactant tail in layer l , and y_s is the normalization factor for $P_s(\Omega)$ that is obtained by enforcing $\sum_{\Omega} P_s(\Omega) = 1$.

The conformational free energy of a solubilize tail, in the case of an amphiphilic solubilize that is attached to the micelle interface, has a functional form which is identical to that of the surfactant tail, since there are no translational entropy effects and all solubilize tails originate in the same (outer) layer:

$$A_{c,a} = - \sum_l \pi_l \langle \phi_a(l, \Omega) \rangle - k_B T \ln y_a \quad (4.41)$$

where $\langle \phi_a(l, \Omega) \rangle$ and y_a are the average volume of the solubilize tail in layer i and normalization factor, respectively, with both calculated analogously to the surfactant case.

The conformational free energy of the solubilize tail, in the case of a hydrophobic solubilize that is mobile within the micelle core, is given by the following expression, which involves a sum over each layer p within the micelle core:

$$A_{c,a} = \sum_{p=1}^L \left(\frac{n_a^p}{n_a} \right) A_{c,a}^p \quad (4.42)$$

where n_a^p/n_a is the fraction of mobile solubilizes originating in layer p . The value of n_a^p/n_a is evaluated using normalization constants (see below). The conformational free energy of the solubilize tail in layer p is expressed as follows [28]:

$$A_{c,a}^p = E_{c,a}^p - T(S_{c,a}^p + S_{t,a}^p) \quad (4.43)$$

$$= \sum_{\omega_p} \epsilon_a(\omega_p) P_a(\omega_p) + k_B T \left(\sum_{\omega_p} P_a(\omega_p) \ln P_a(\omega_p) + \ln(\rho_a^p v_a) \right) \quad (4.44)$$

$$= - \sum_l \pi_l \langle \phi_a(l, \omega_p) \rangle - k_B T \ln y_a^p + k_B T \ln \left(\frac{n_a^p v_a}{V_p} \right) \quad (4.45)$$

$$= - \sum_l \pi_l \langle \phi_a(l, \omega_p) \rangle - k_B T \ln y_a^p + k_B T \ln \left(\frac{n_a^p/n_a}{F_p} \eta_a \right) \quad (4.46)$$

$$= - \sum_l \pi_l \langle \phi_a(l, \omega_p) \rangle - k_B T \ln \sum_{p=1}^L F_p y_a^p + k_B T \ln \eta_a \quad (4.47)$$

where $E_{c,a}^p$ is the internal energy of the central solubilize tail originating in layer p ; $S_{c,a}^p$ is the conformational entropy of the central solubilize tail originating in layer p ; $S_{t,a}^p$ is the translational entropy of the central solubilize molecule originating in layer p ; $\epsilon_a(\omega_p)$ is the internal energy of the central solubilize tail in conformation ω_p ; $P_a(\omega_p)$ is the probability that the central solubilize tail will adopt conformation ω_p ; ρ_a^p is the number density of solubilizates originating in layer p , given by $\rho_a^p = n_a^p/V_p$ (where V_p is the volume of layer p); π_l , the lateral pressure in layer l , is the Lagrange multiplier for layer l required to satisfy volume-filling constraints; $\langle \phi_a(l, \omega_p) \rangle$ is the average volume that the solubilize tail originating in layer p occupies in layer l when in conformation ω_p ; y_a^p is the normalization factor for $P_a(\omega_p)$ that is obtained by enforcing $\sum_{\omega_p} P_a(\omega_p) = 1$; and F_p is the ratio of the volume of layer p to the total volume of the micelle core (i.e. $F_p = V_p/V$).

The conformational free energy of a surfactant tail in a bulk phase of surfactant tails is defined as follows [28]:

$$A_{c,s}^{\text{free}} = -k_B T \ln \left(\sum_{\Omega} \exp \left(-\frac{\epsilon(\Omega)}{k_B T} \right) \right) \quad (4.48)$$

The conformational free energy of a solubilize tail is defined as follows for: (i) an amphiphilic solubilize attached to the interface:

$$A_{c,a}^{\text{free}} = -k_B T \ln \left(\sum_{\omega} \exp \left(-\frac{\epsilon(\omega)}{k_B T} \right) \right) \quad (4.49)$$

and (ii) a hydrophobic solubilize that is mobile within the micelle core:

$$A_{c,a}^{\text{free}} = -k_B T \ln \left(\frac{\sum_{\omega} \exp \left(-\frac{\epsilon(\omega)}{k_B T} \right)}{L} \right) \quad (4.50)$$

where ω denotes a conformation of the solubilize tail in the bulk tail phase. The factor of L , the number of layers chosen in the micelle, in Eq. 4.50 reflects the isotropy of the bulk solubilize tail phase. In other words, in the micelle, the

external conformation of a mobile solubilize tail includes the originating layer p ; this distinction between originating layers has no meaning in the bulk phase state, and therefore, for an unbiased sampling of p , division by L prevents overcounting in determining the Helmholtz free energy of the bulk solubilize tail phase. The expressions for $A_{c,s}^{\text{free}}$ and $A_{c,a}^{\text{free}}$ are derived by setting each of the Lagrange multipliers π_i equal to zero in Eqs. 4.40 and 4.47, respectively, and, for mobile solubilizes, also by setting η_a equal to 1.0 in Eq. 4.47. It is important to note that all neutral groups are included in the calculation of $A_{c,s}^{\text{free}}$ and $A_{c,a}^{\text{free}}$.

As shown in Eqs. 4.39 and 4.44, $A_{c,s}$ and $A_{c,a}^p$ depend on the quantities $P_s(\Omega)$, $P_a(\omega_p)$, and n_a^p (or equivalently, $\rho_a^p = n_a^p/V_p$). Determination of the functional forms of these quantities is accomplished through a minimization of a functional containing $A_{c,s}$ and $A_{c,a}^p$, a PV work term containing the lateral pressures $\{\pi_l\}$, and any additional, coupled free energy terms. In the case of micellar solubilization, there are three scenarios considered in this chapter: (i) the solubilize is attached to the interface, in which case no coupled free energy terms are included and Eq. 4.41 is used for $A_{c,a}$ ($A_{c,s} + A_{c,a} + \sum_l \pi_l V_l$ is minimized); (ii) the solubilize is mobile in the micelle core but has the same interfacial tension against water as the surfactant (i.e. a nonpolar solubilize), and Eq. 4.42 is used for $A_{c,a}$ ($A_{c,s} + A_{c,a} + \sum_l \pi_l V_l$ is minimized); and (iii) the solubilize is mobile in the core but has a different interfacial tension against water than the surfactant (i.e. a polar solubilize), and Eq. 4.42 is used for $A_{c,a}$ ($A_{c,s} + A_{c,a} + G_{\text{int}} + \sum_l \pi_l V_l$ is minimized). This procedure has been presented elsewhere [28], and therefore, only the results for the three cases are presented below [28]:

In all three cases, the minimization results in the following expression for $P_s(\Omega)$ and y_s :

$$P_s(\Omega) = \frac{\exp\left(-\frac{\epsilon(\Omega)}{k_B T}\right) \exp\left(-\frac{\sum_l \pi_l \phi_s(l, \Omega)}{k_B T}\right)}{y_s} \quad (4.51)$$

$$y_s = \sum_{\Omega} \exp\left(-\frac{\epsilon(\Omega)}{k_B T}\right) \exp\left(-\frac{\sum_l \pi_l \phi_s(l, \Omega)}{k_B T}\right) \quad (4.52)$$

For case (i), a similar expression is developed for $P_a(\omega)$ and y_a :

$$P_a(\omega) = \frac{\exp\left(-\frac{\epsilon(\omega)}{k_B T}\right) \exp\left(-\frac{\sum_l \pi_l \phi_a(l, \omega)}{k_B T}\right)}{y_a} \quad (4.53)$$

$$y_a = \sum_{\omega} \exp\left(-\frac{\epsilon(\omega)}{k_B T}\right) \exp\left(-\frac{\sum_l \pi_l \phi_a(l, \omega)}{k_B T}\right) \quad (4.54)$$

For case (ii), for each layer p , $P_a(\omega_p)$ and y_a^p are of the forms:

$$P_a(\omega_p) = \frac{\exp\left(-\frac{\epsilon(\omega_p)}{k_B T}\right) \exp\left(-\frac{\sum_l \pi_l \phi_a(l, \omega_p)}{k_B T}\right)}{y_a^p} \quad (4.55)$$

$$y_a^p = \sum_{\omega_p} \exp\left(-\frac{\epsilon(\omega_p)}{k_B T}\right) \exp\left(-\frac{\sum_l \pi_l \phi_a(l, \omega_p)}{k_B T}\right) \quad (4.56)$$

For case (iii), for each layer p , $P_a(\omega_p)$ and y_a^p are of the forms:

$$P_a(\omega_p) = \frac{\exp\left(-\frac{\epsilon(\omega_p)}{k_B T}\right) \exp\left(-\frac{\sum_l \pi_l \phi_a(l, \omega_p)}{k_B T}\right) \exp\left(-\frac{(\sigma_a - \sigma_s)}{k_B T (V_L/A)} \phi_a(L, \omega_p)\right)}{y_a^p} \quad (4.57)$$

$$y_a^p = \sum_{\omega_p} \exp\left(-\frac{\epsilon(\omega_p)}{k_B T}\right) \exp\left(-\frac{\sum_l \pi_l \phi_a(l, \omega_p)}{k_B T}\right) \cdot \exp\left(-\frac{(\sigma_a - \sigma_s)}{k_B T (V_L/A)} \phi_a(L, \omega_p)\right) \quad (4.58)$$

where σ_a and σ_s are the interfacial tensions of the mobile solubilize and of the interface-attached surfactant tail against water, respectively, and V_L is the volume of the outer shell (i.e. the shell in which the volume fractions of its constituents govern the calculation of g_{int} , as described in Section 4.4.3).

In cases (ii) and (iii), the number of solubilizates originating in layer p is found, through the minimization procedure, to be:

$$n_a^p = n_a \frac{y_a^p V_p}{\sum_{p=1}^L y_a^p V_p} = n_a \frac{y_a^p F_p}{\sum_{p=1}^L y_a^p F_p} \quad (4.59)$$

Given the functional forms for $P_s(\Omega)$, $P_a(\omega_p)$, and n_a^p just described, it is possible to solve the volume-filling constraints for the micellar system. The volume-filling constraints, expressed in a general form, are given by the following expression for each layer l :

$$n_s \langle \phi_s(l, \Omega) \rangle + \sum_{p=1}^L n_a^p \langle \phi_a(l, \omega_p) \rangle = V_l = F_l V \quad (4.60)$$

The average tail volume for tails containing neutral groups depends on $\langle v_s(\Omega) \rangle$ and $\langle v_a(\omega_p) \rangle$ and is given by the following expression:

$$v_{\text{avg}} = \left(\alpha_s \langle v_s(\Omega) \rangle + \sum_{p=1}^L \alpha_a^p \langle v_a(\omega_p) \rangle \right) \quad (4.61)$$

where $\alpha_s = n_s/n_{\text{agg}}$, $\alpha_a^p = n_a^p/n_{\text{agg}}$, and $n_{\text{agg}} = n_s + n_a$. This dependence of v_{avg} on conformations in turn implies a similar dependence for $n_{\text{agg}} = V/v_{\text{avg}}$, which indicates that the aggregation number, in addition to being a function of the core-minor radius, shape, and composition, also depend upon molecular properties, such as the component interfacial tension against water in the case of mobile solubilizes, and the temperature, which governs the distribution of dihedral states.

A rearrangement of Eq. 4.60 into the form that is solved to determine each of the Lagrange multipliers, π_l , is given below for case (i) (see Eq. 4.62) and for cases (ii) and (iii) (see and Eq. 4.63):

$$\alpha_s \sum_{\Omega} P(\Omega) [\phi_s(l, \Omega) - F_l v_s(\Omega)] + \alpha_a \sum_{\omega} P(\omega) [\phi_a(l, \omega) - F_l v_a(\omega)] = 0 \quad (4.62)$$

and

$$\alpha_s \sum_{\Omega} P(\Omega) [\phi_s(l, \Omega) - F_l v_s(\Omega)] + \sum_{p=1}^L \alpha_a^p \sum_{\omega_p} P(\omega_p) [\phi_a(l, \omega_p) - F_l v_a(\omega_p)] = 0 \quad (4.63)$$

The Lagrange multipliers determined by solving each of the L volume-filling constraints given in Eq. 4.62 or Eq. 4.63 are then inserted in the expressions given in Eq. 4.40 to determine $A_{c,s}$ and either Eq. 4.41, to determine $A_{c,a}$, for case (i), or Eq.

4.47 to determine $A_{c,a}^p$, for cases (ii) and (iii). Subsequently, $A_{c,s}^{\text{free}}$ is calculated using Eq. 4.48 and $A_{c,a}^{\text{free}}$ is calculated using Eq. 4.49 for case (i) or Eq. 4.50 for cases (ii) and (iii), which allows the evaluation of $g_{\text{pack},s}$ and $g_{\text{pack},a}$ using Eqs. 4.36 and 4.37, respectively.

4.5 Conclusions

In this chapter, a hybrid computer simulation/molecular-thermodynamic modeling approach was presented to model micellar solubilization. The objective of this new approach is to overcome the limitations associated with molecular-thermodynamic modeling (its applicability only to relatively simple surfactant and solubilize systems) and computer simulations (the high computational cost of simulating self-assembly). The hybrid modeling approach presented here utilizes MD simulations of solubilizates at an oil/water interface (modeling the micelle core/water interface), or solubilizates in a cylindrical or spherical micelle, to estimate the hydrated and the unhydrated portions of each solubilize in a micellar environment. From such information, head and tail identifications are made for each solubilize.

We have conducted atomistic-level computer simulations of seven different solubilizates at an oil/water interface and within spherical and cylindrical SDS micelles in order to make head and tail identifications. The seven solubilizates simulated included ibuprofen, benzamide, acetophenone, benzonitrile, *o*-aminobenzoate, *m*-aminobenzoate, and *p*-aminobenzoate. Each solubilize was selected based on the availability of experimental solubilization data and on their appropriateness to evaluate the validity of the hybrid modeling approach presented in this chapter.

The approaches used to initialize, equilibrate, and gather data for each water/oil interface simulation and for each micellar simulation were discussed, including a discussion of the appropriate simulation ensemble for each type of simulation. A data analysis approach was presented in which the solubilize head and tail are determined from water/oil interface simulation data by computing the scaled contact ratio (SCR)

of each group in the solubilizate molecule. A different computational approach was presented to analyze the micellar simulation data in which head and tail assignments are made by computing the difference in micellar contact ratios (ΔMCR) between each group in the solubilizate molecule and the micellar contact ratio characterizing the division between the head and the tail for the surfactant molecules. Head and tail identifications made based on the water/oil interface, the cylindrical micelle, and the spherical micelle simulation data were each presented.



In general, the head and tail assignments made using water/oil interface, cylindrical micelle, and spherical micelle simulation data are quite similar, although several important differences were found to exist. An analysis of the cylindrical and the spherical micelle simulation results showed that 16 out of 77 ΔMCR assignments made using the cylindrical and the spherical micelle simulation data were different to a 95% confidence level. For the small, relatively rigid solubilizates considered in this chapter, reasonable assignments of head and tail appear to have been obtained using water/oil interface simulations. Although the cylindrical and the spherical micelle simulations are expected to yield more physically realistic head and tail assignments than the water/oil interface simulation, micellar simulations come at the cost of greater computational expense.

A general molecular-thermodynamic theory of solubilization was reviewed and extended. The molecular-thermodynamic theory of solubilization introduced in this chapter has two components: (i) a thermodynamic description of the surfactant and solubilizate solution, and (ii) a molecular model that is used to evaluate the free-energy change associated with transferring surfactants and solubilizates from their standard states in aqueous solution to form a surfactant/solubilizate micellar aggregate. Several extensions to the molecular model of solubilization were introduced. A new free-energy term, g_{mix} , was included in the molecular model to incorporate both the entropic and the enthalpic contributions to the free energy associated with mixing the surfactant and the solubilizate tails in the micelle core ($g_{\text{mix},\text{I}}$, modeled using the regular solution model proposed by Hildebrand), and the mixing of counterions with

surfactant heads, and of solubilize heads with surfactant heads in the head-shell region of the micelle ($g_{\text{mix,II}}$, modeled with an ideal solution model). The molecular model was also extended by generalizing the mean-field model for g_{pack} to model each group in a surfactant or solubilize molecule in one of three ways: (i) as a head group, (ii) as a tail group, or (iii) as a “neutral” group. By introducing the concept of neutral groups for the first time into the packing model, we allow groups which are identified through computer simulation to spend a significant amount of time in both the micelle core and in the aqueous solution to not be constrained to lie on only one side of the micelle core/water interface or the other. This, in turn, relaxes to some extent the assumption made in previous implementations of the mean-field packing model that there is a sharp micelle core/water interface. We therefore expect this generalization of the mean-field model used to compute g_{pack} to provide a significantly more physically realistic description of g_{pack} for complex surfactants and for complex amphiphilic solubilizes. Identification of whether a surfactant, or a solubilize, group should be modeled as being part of the head, as being part of the tail, or as being neutral when implementing the mean-field packing model can be made based on the computer simulation SCR, ΔMCR , and standard error (SE) computed for each of the SCR and ΔMCR results. Those groups whose SE values are too large to permit statistically significant head and tail assignment will be modeled as “neutral” groups in the packing model.

In Chapter 5, the computer-simulation based identifications of head, tail, and neutral groups and the molecular-thermodynamic theory of solubilization presented in this chapter will be used to model the micellar solubilization behavior of the seven solubilizes considered here in anionic, nonionic, and cationic surfactant micelles.

4.6 Appendix 4-A: Equilibration Results for the Cylindrical and Spherical Micelles

As discussed in Section 4.2.3, three different metrics were used to: (i) verify that adequate equilibration of each surfactant/solubilizate system had occurred after the 15 ns equilibration simulation runs, and (ii) assess the extent to which the data gathered during the 10 ns data-gathering simulation should be sufficient to sample the equilibrium state of the micelle with reasonable accuracy. The three metrics that were selected include the system potential energy, the micelle solvent accessible surface area (SASA), and the distance from the micelle center of mass (COM) to various surfactant groups and to the solubilizate center of mass. For the seven cylindrical and seven spherical micelles simulated, potential energy was found to equilibrate and begin fluctuating about an equilibrium value within a small fraction of the total 25 ns simulation time. Therefore, potential energy results are not presented. However, both SASA profiles and distance profiles are reported in this appendix for all the seven surfactant/solubilizate systems considered. As discussed in Section 4.2.3, SASA was calculated using the double cubic lattice method as implemented in GROMACS with a probe sphere of radius 0.14 nm [103]. In Figures A1 to A12, SASA profiles are reported for solubilizates in both cylindrical () and in spherical () micelles.

The variability observed in the SASA results for the cylindrical micelles is higher, on average, than the variability observed in the SASA results for the spherical micelles. The average difference between the maximum and the minimum SASA values calculated for all seven cylindrical micelles was 26.6% of the average SASA value for the cylindrical micelles. In contrast, the average difference between the maximum and the minimum SASA value calculated for all seven spherical micelles was only 14.1% of the average SASA value for the spherical micelles. Examination of the SASA profiles suggests that this difference is primarily due to the fact that the initial configuration of the cylindrical micelles appears to have been further away from

the equilibrium configuration than the initial configuration of the spherical micelles. In general, after the first 15 ns of simulation, no consistent upwards or downwards drift in the SASA profiles is apparent, which indicates that the 15 ns of equilibration conducted for the micellar systems was more than adequate to allow each simulated micelle to equilibrate. In addition, because the 10 ns data-gathering simulation time appears larger than the characteristic timescale associated with SASA fluctuation, the SASA results suggest that the data-gathering simulation run should provide reasonably thorough sampling of the equilibrium state of the cylindrical and the spherical micelles. SASA does not convey any information about internal micelle structure, however. To evaluate internal equilibration, distances have been measured between several micelle components and the micelle center of mass.

Distance profiles for all 14 cylindrical and spherical SDS/solubilizate micelles have been computed and are reported in Figures A13 to A24 in this appendix. As discussed in Section 4.6, the distance from the micelle center of mass to the center of mass of the sulfate (SO_4) group in SDS ($d_{\text{SO}_4-\text{MIC}_{\text{COM}}}$, see the ○ results), the distance from the sixth CH_2 group away from the sulfate group in SDS to the micelle center of mass ($d_{\text{CH}_2-\text{MIC}_{\text{COM}}}$, see the ○ results), and the distance from the terminal CH_3 group in SDS to the micelle center of mass ($d_{\text{CH}_3-\text{MIC}_{\text{COM}}}$, see the ○ results) are each reported. It is important to note that each reported point reflects an average value for all surfactant molecules (49 in the cylindrical micelles and 38 in the spherical micelles). The distance from the micelle center of mass to the solubilizate center of mass is also reported ($d_{\text{SOL}_{\text{COM}}-\text{MIC}_{\text{COM}}}$, see the ○ results), and each reported point reflects an average value for the 5 solubilizates present in the micelle. Results are reported for the entire 25 ns of simulation.

The average values of $d_{\text{SO}_4-\text{MIC}_{\text{COM}}}$, $d_{\text{CH}_2-\text{MIC}_{\text{COM}}}$, $d_{\text{CH}_3-\text{MIC}_{\text{COM}}}$, and $d_{\text{SOL}_{\text{COM}}-\text{MIC}_{\text{COM}}}$ are reported in the tables accompanying each figure showing the distance results. As discussed in Section 4.6, the solubilizates do not have a significant impact on the distance results for the three surfactant groups because only five solubilizates are present in each cylindrical and spherical micelle. For example, values of $d_{\text{SO}_4-\text{MIC}_{\text{COM}}}$ for the

cylindrical micelles are all between 1.70 nm and 1.73 nm, and for the spherical micelles they are all between 1.84 nm and 1.94 nm. The most striking characteristic of each of the distance profiles is their variability — each distance fluctuates substantially (up to 2 nm) during the course of the 25 ns simulation. The high degree of distance fluctuations observed is consistent with the relatively high level of fluctuations observed in micelle shape upon visualizing the MD trajectories. Although significant fluctuations in the distance values are observed, no consistent drifts in the distance results are apparent for any of the solubilizate-containing SDS micelles considered.

Based on an average of the cylindrical and spherical micelle results, the following ranking of solubilizate distances to the micelle center of mass was obtained: *p*-aminobenzoate (1.42 nm) > benzamide (1.41 nm) > ibuprofen (1.39 nm) > *m*-aminobenzoate (1.39 nm) > acetophenone (1.37 nm) > *o*-aminobenzoate (1.33 nm) > benzonitrile (1.29 nm).

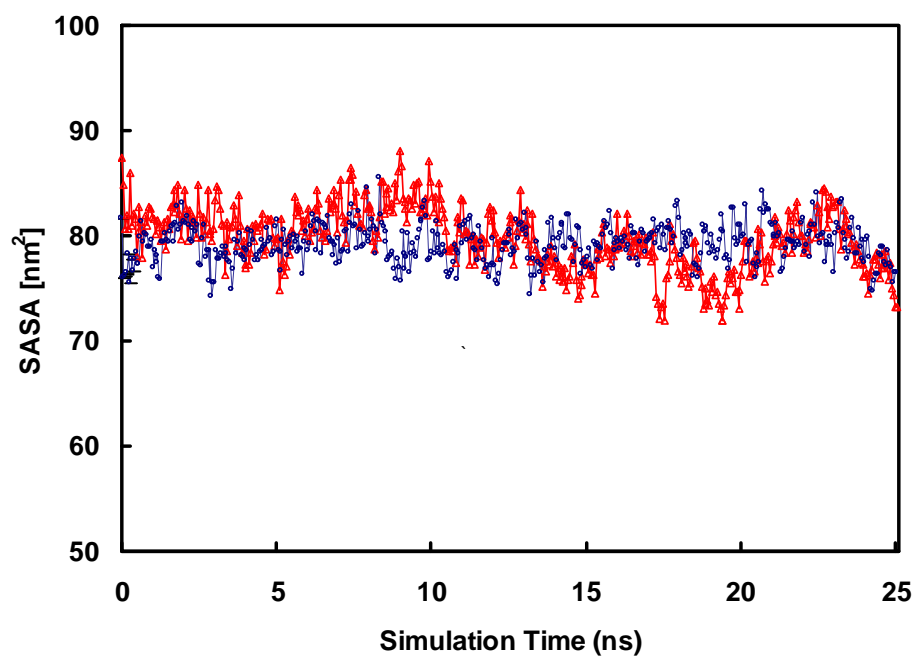


Figure 4-A1: Solvent accessible surface area (SASA) for the cylindrical ($\text{---}\triangle\text{---}$) and the spherical ($\text{---}\circ\text{---}$) SDS/ibuprofen micelles as a function of simulation time.

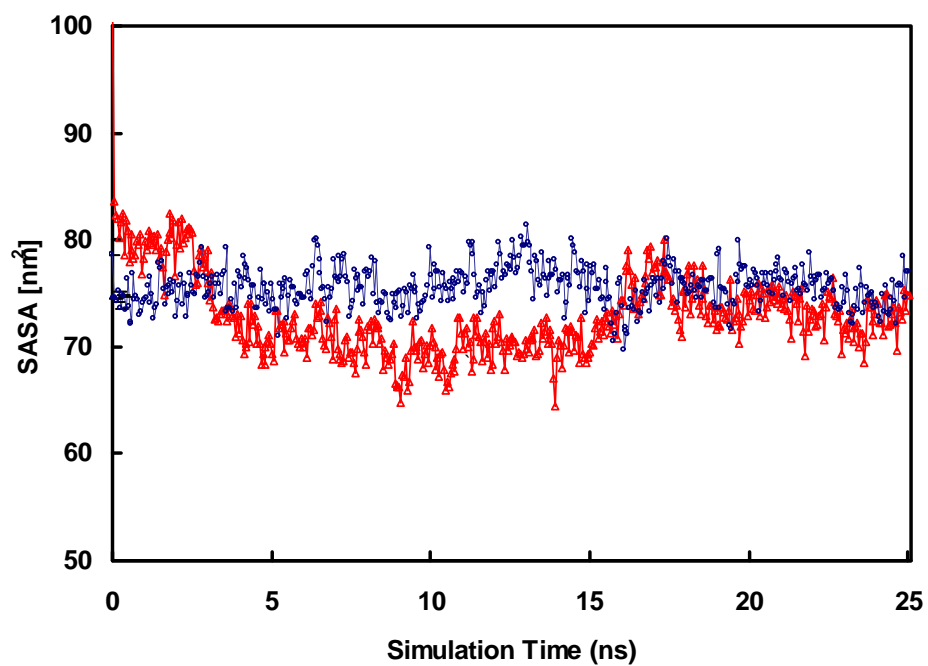


Figure 4-A2: Solvent accessible surface area (SASA) for the cylindrical (— Δ —) and the spherical (— \circ —) SDS/benzamide micelles as a function of simulation time.

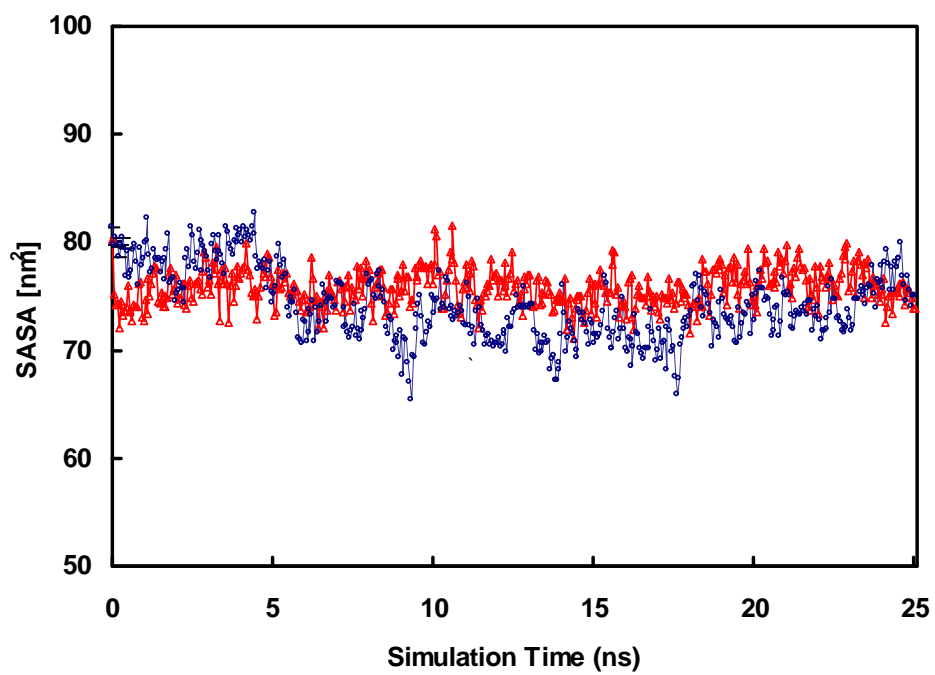


Figure 4-A3: Solvent accessible surface area (SASA) for the cylindrical (—△—) and the spherical (—○—) SDS/acetophenone micelles as a function of simulation time.

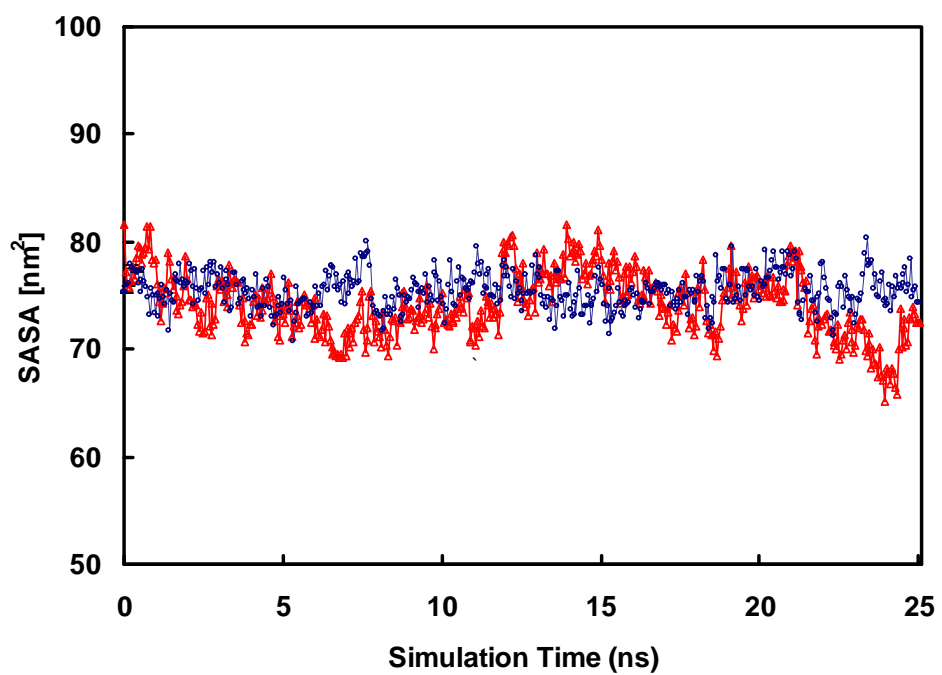


Figure 4-A4: Solvent accessible surface area (SASA) for the cylindrical (—△—) and the spherical (—○—) SDS/benzonitrile micelles as a function of simulation time.

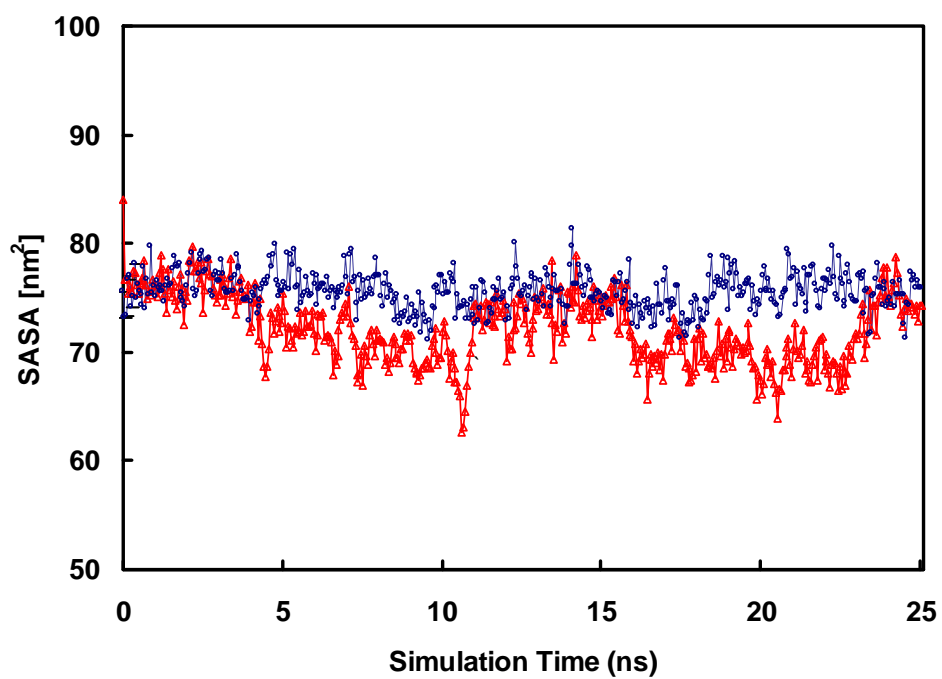


Figure 4-A5: Solvent accessible surface area (SASA) for the cylindrical ($\text{---}\triangle\text{---}$) and the spherical ($\text{---}\circ\text{---}$) SDS/*o*-aminobenzoate micelles as a function of simulation time.

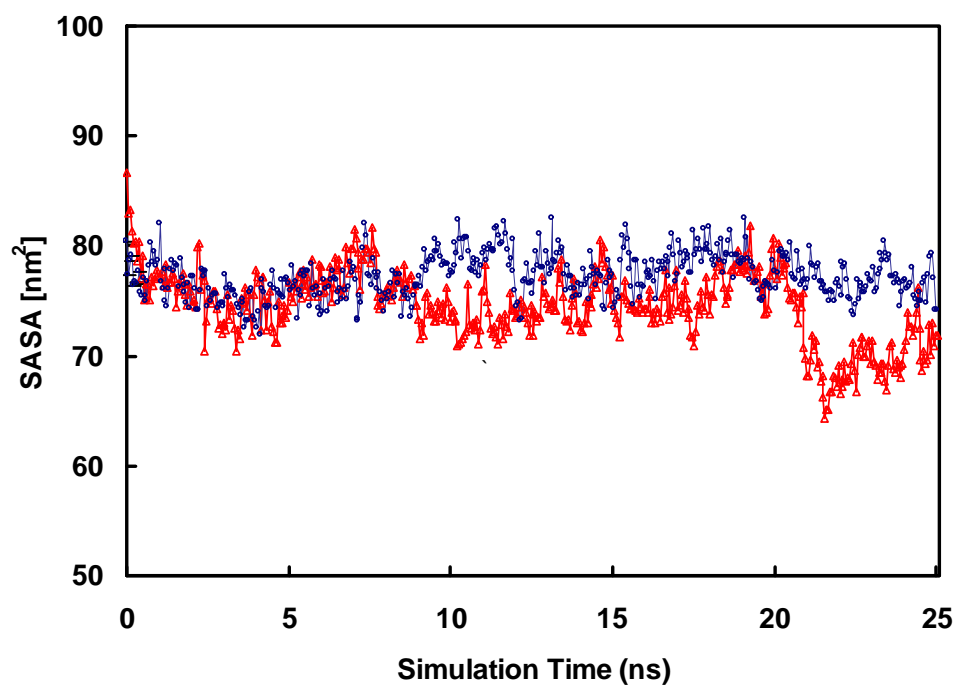


Figure 4-A6: Solvent accessible surface area (SASA) for the cylindrical ($\text{---}\triangle\text{---}$) and the spherical ($\text{---}\circ\text{---}$) SDS/*m*-aminobenzoate micelles as a function of simulation time.

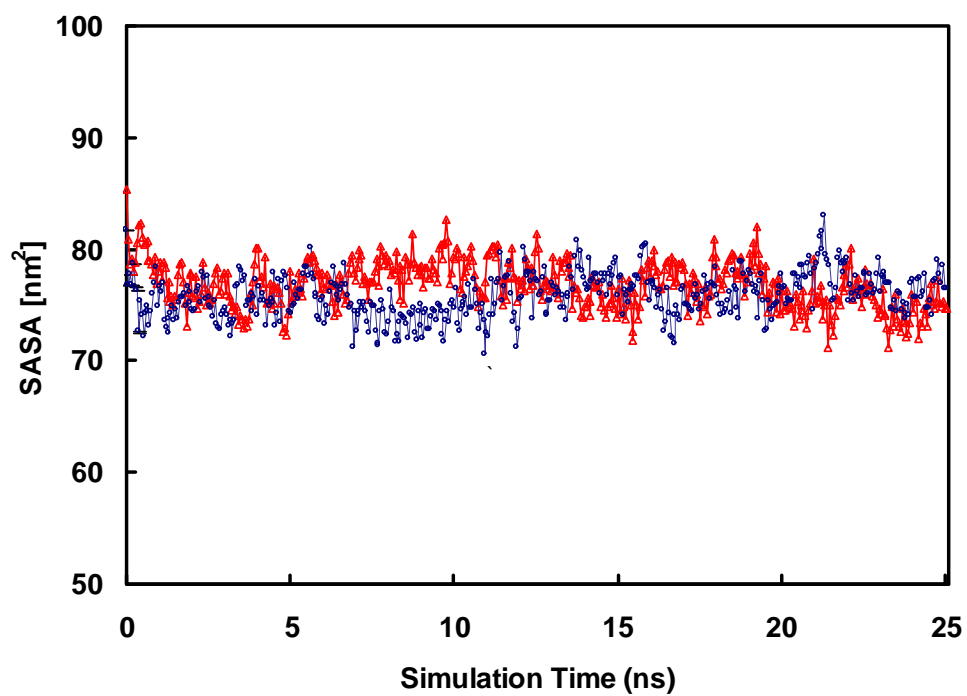
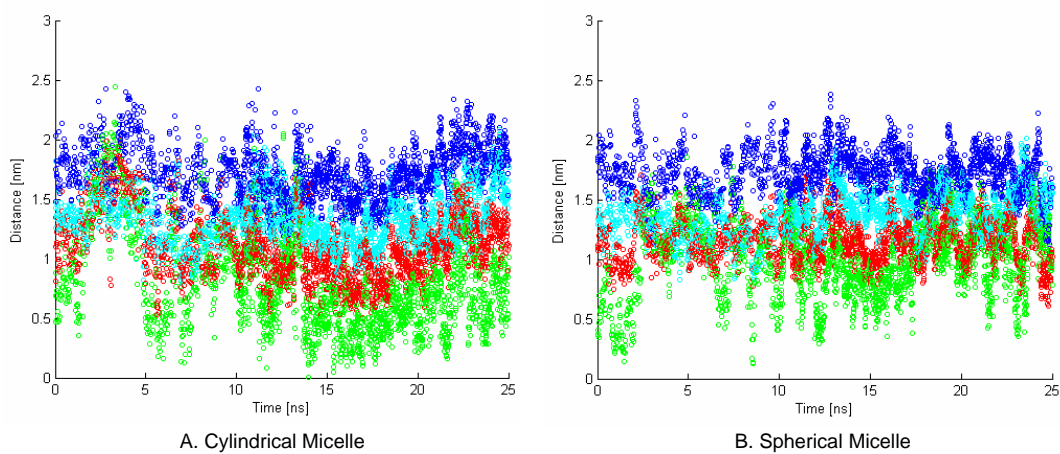
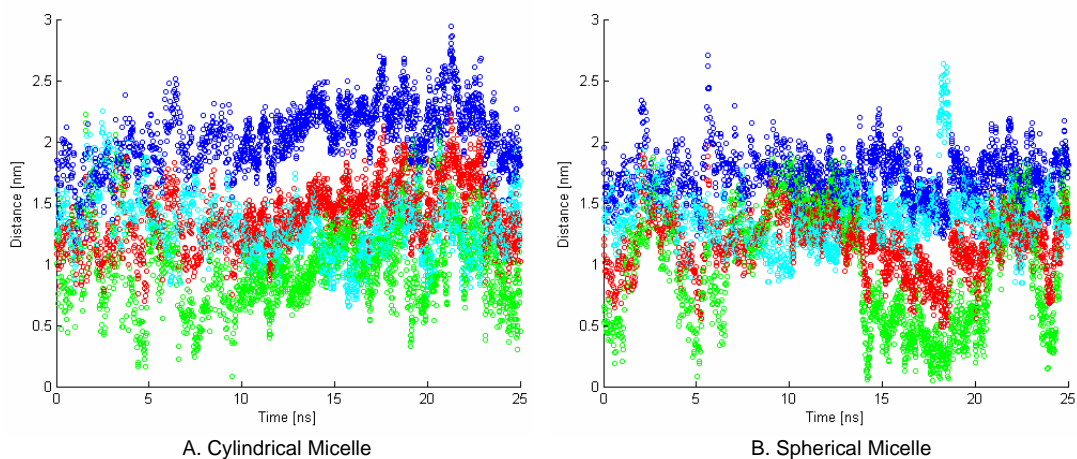


Figure 4-A7: Solvent accessible surface area (SASA) for the cylindrical (—△—) and the spherical (—○—) SDS/*p*-aminobenzoate micelles as a function of simulation time.



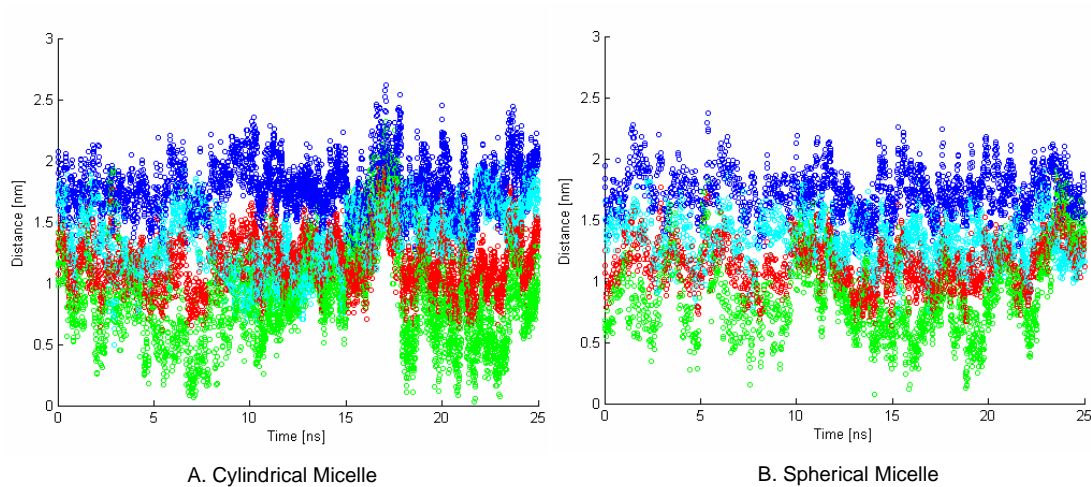
Distance	Avg. Cylindrical Micelle Results [nm]	Avg. Spherical Micelle Results [nm]
$d_{\text{SO}_4-\text{MIC}_{\text{COM}}}$	1.73	1.86
$d_{\text{CH}_2-\text{MIC}_{\text{COM}}}$	1.14	1.28
$d_{\text{CH}_3-\text{MIC}_{\text{COM}}}$	0.93	1.02
$d_{\text{SOL}-\text{MIC}_{\text{COM}}}$	1.40	1.38

Figure 4-A8: Distances between several surfactant groups defined in the text and the micelle center of mass ($d_{\text{SO}_4-\text{MIC}_{\text{COM}}}$, see the \circ results; $d_{\text{CH}_2-\text{MIC}_{\text{COM}}}$, \bullet ; $d_{\text{CH}_3-\text{MIC}_{\text{COM}}}$, \bullet) and between the center of mass of ibuprofen and the micelle center of mass ($d_{\text{SOL}_{\text{COM}}-\text{MIC}_{\text{COM}}}$, \bullet) in the cylindrical (A) and the spherical (B) SDS/ibuprofen micelles. The average values of each distance over the 25 ns of simulation are presented in the table.



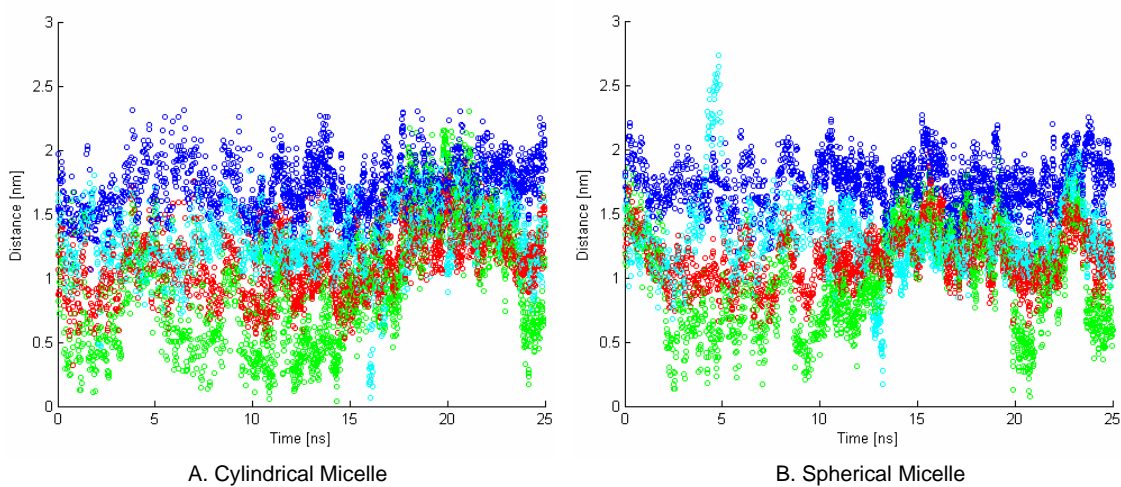
Distance	Avg. Cylindrical Micelle Results [nm]	Avg. Spherical Micelle Results [nm]
$d_{\text{SO}_4\text{-MIC}_{\text{COM}}}$	1.70	1.90
$d_{\text{CH}_2\text{-MIC}_{\text{COM}}}$	1.12	1.28
$d_{\text{CH}_3\text{-MIC}_{\text{COM}}}$	0.94	0.97
$d_{\text{SOL}_{\text{COM}}\text{-MIC}_{\text{COM}}}$	1.38	1.44

Figure 4-A9: Distances between several surfactant groups defined in the text and the micelle center of mass ($d_{\text{SO}_4\text{-MIC}_{\text{COM}}}$, see the \circ results; $d_{\text{CH}_2\text{-MIC}_{\text{COM}}}$, \circ ; $d_{\text{CH}_3\text{-MIC}_{\text{COM}}}$, \circ) and between the center of mass of benzamide and the micelle center of mass ($d_{\text{SOL}_{\text{COM}}\text{-MIC}_{\text{COM}}}$, \circ) in the cylindrical (A) and the spherical (B) SDS/benzamide micelles. The average values of each distance over the 25 ns of simulation are presented in the table.



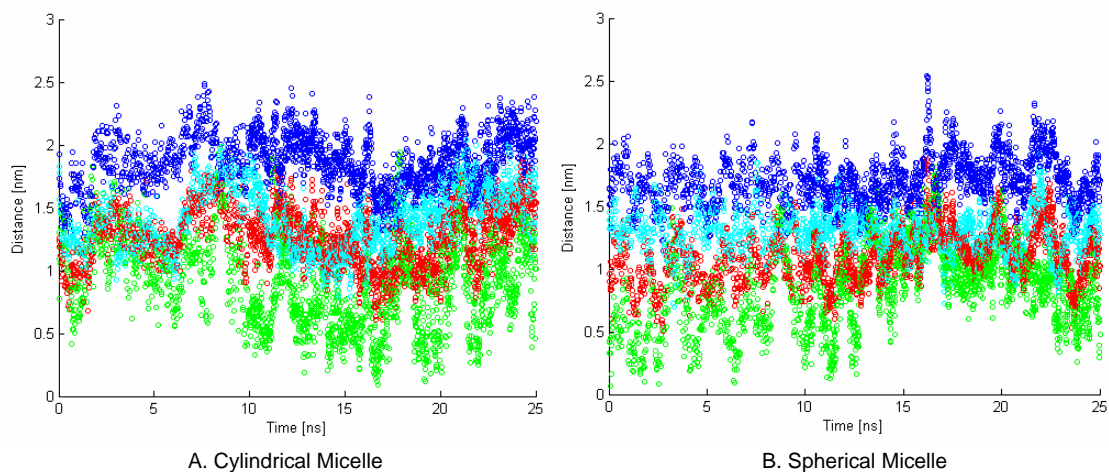
Distance	Avg. Cylindrical Micelle Results [nm]	Avg. Spherical Micelle Results [nm]
$d_{\text{SO}_4-\text{MIC}_{\text{COM}}}$	1.71	1.90
$d_{\text{CH}_2-\text{MIC}_{\text{COM}}}$	1.13	1.28
$d_{\text{CH}_3-\text{MIC}_{\text{COM}}}$	0.93	0.97
$d_{\text{SOL}_{\text{COM}}-\text{MIC}_{\text{COM}}}$	1.32	1.42

Figure 4-A10: Distances between several surfactant groups defined in the text and the micelle center of mass ($d_{\text{SO}_4-\text{MIC}_{\text{COM}}}$, see the \circ results; $d_{\text{CH}_2-\text{MIC}_{\text{COM}}}$, \bullet ; $d_{\text{CH}_3-\text{MIC}_{\text{COM}}}$, \bullet) and between the center of mass of acetophenone and the micelle center of mass ($d_{\text{SOL}_{\text{COM}}-\text{MIC}_{\text{COM}}}$, \bullet) in the cylindrical (A) and the spherical (B) SDS/acetophenone micelles. The average values of each distance over the 25 ns of simulation are presented in the table.



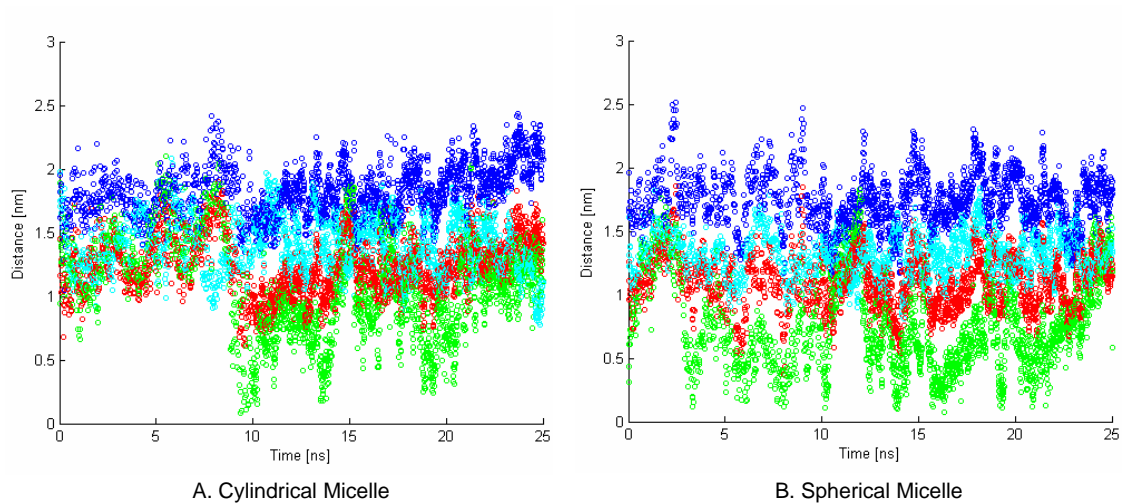
Distance	Avg. Cylindrical Micelle Results [nm]	Avg. Spherical Micelle Results [nm]
$d_{\text{SO}_4-\text{MIC}_{\text{COM}}}$	1.71	1.84
$d_{\text{CH}_2-\text{MIC}_{\text{COM}}}$	1.12	1.26
$d_{\text{CH}_3-\text{MIC}_{\text{COM}}}$	0.94	1.00
$d_{\text{SOL}_{\text{COM}}-\text{MIC}_{\text{COM}}}$	1.25	1.32

Figure 4-A11: Distances between several surfactant groups defined in the text and the micelle center of mass ($d_{\text{SO}_4-\text{MIC}_{\text{COM}}}$, see the \circ results; $d_{\text{CH}_2-\text{MIC}_{\text{COM}}}$, \bullet ; $d_{\text{CH}_3-\text{MIC}_{\text{COM}}}$, \bullet) and between the center of mass of benzonitrile and the micelle center of mass ($d_{\text{SOL}_{\text{COM}}-\text{MIC}_{\text{COM}}}$, \circ) in the cylindrical (A) and the spherical (B) SDS/benzonitrile micelles. The average values of each distance over the 25 ns of simulation are presented in the table.



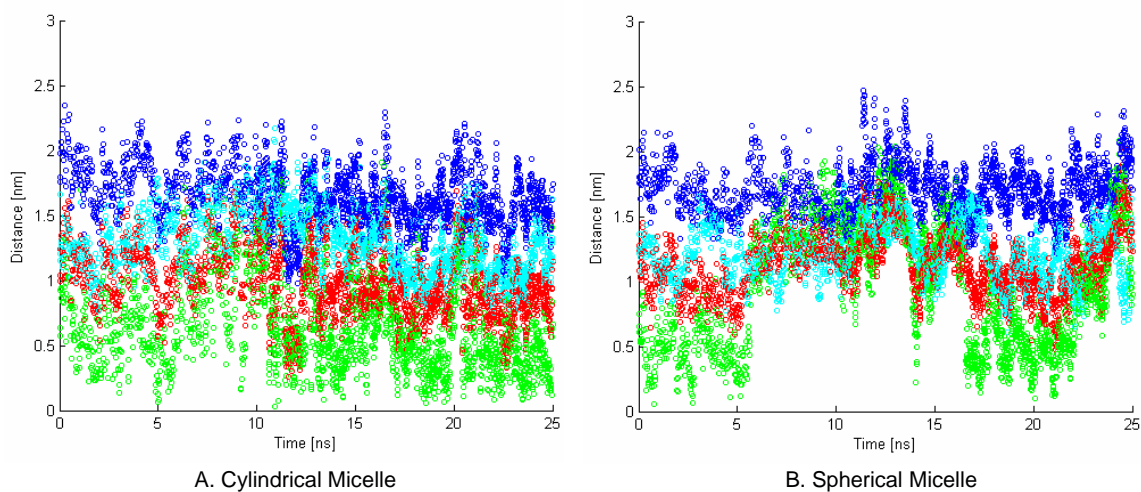
Distance	Avg. Cylindrical Micelle Results [nm]	Avg. Spherical Micelle Results [nm]
$d_{\text{SO}_4-\text{MIC}_{\text{COM}}}$	1.72	1.91
$d_{\text{CH}_2-\text{MIC}_{\text{COM}}}$	1.13	1.29
$d_{\text{CH}_3-\text{MIC}_{\text{COM}}}$	0.94	0.97
$d_{\text{SOL}-\text{MIC}_{\text{COM}}}$	1.27	1.40

Figure 4-A12: Distances between several surfactant groups defined in the text and the micelle center of mass ($d_{\text{SO}_4-\text{MIC}_{\text{COM}}}$, see the \circ results; $d_{\text{CH}_2-\text{MIC}_{\text{COM}}}$, \circ ; $d_{\text{CH}_3-\text{MIC}_{\text{COM}}}$, \circ) and between the center of mass of *o*-aminobenzoate and the micelle center of mass ($d_{\text{SOL}_{\text{COM}}-\text{MIC}_{\text{COM}}}$, \circ) in the cylindrical (A) and the spherical (B) SDS/*o*-aminobenzoate micelles. The average values of each distance over the 25 ns of simulation are presented in the table.



Distance	Avg. Cylindrical Micelle Results [nm]	Avg. Spherical Micelle Results [nm]
$d_{\text{SO}_4-\text{MIC}_{\text{COM}}}$	1.72	1.86
$d_{\text{CH}_2-\text{MIC}_{\text{COM}}}$	1.13	1.27
$d_{\text{CH}_3-\text{MIC}_{\text{COM}}}$	0.94	1.00
$d_{\text{SOL}-\text{MIC}_{\text{COM}}}$	1.46	1.30

Figure 4-A13: Distances between several surfactant groups defined in the text and the micelle center of mass ($d_{\text{SO}_4-\text{MIC}_{\text{COM}}}$, see the \circ results; $d_{\text{CH}_2-\text{MIC}_{\text{COM}}}$, \bullet ; $d_{\text{CH}_3-\text{MIC}_{\text{COM}}}$, \bullet) and between the center of mass of *m*-aminobenzoate and the micelle center of mass ($d_{\text{SOL}_{\text{COM}}-\text{MIC}_{\text{COM}}}$, \circ) in the cylindrical (A) and the spherical (B) SDS/*m*-aminobenzoate micelles. The average values of each distance over the 25 ns of simulation are presented in the table.



Distance	Avg. Cylindrical Micelle Results [nm]	Avg. Spherical Micelle Results [nm]
$d_{\text{SO}_4-\text{MIC}_{\text{COM}}}$	1.72	1.84
$d_{\text{CH}_2-\text{MIC}_{\text{COM}}}$	1.13	1.25
$d_{\text{CH}_3-\text{MIC}_{\text{COM}}}$	0.94	1.01
$d_{\text{SOL}-\text{MIC}_{\text{COM}}}$	1.29	1.55

Figure 4-A14: Distances between several surfactant groups defined in the text and the micelle center of mass ($d_{\text{SO}_4-\text{MIC}_{\text{COM}}}$, see the \circ results; $d_{\text{CH}_2-\text{MIC}_{\text{COM}}}$, \circ ; $d_{\text{CH}_3-\text{MIC}_{\text{COM}}}$, \circ) and between the center of mass of *p*-aminobenzoate and the micelle center of mass ($d_{\text{SOL}_{\text{COM}}-\text{MIC}_{\text{COM}}}$, \circ) in the cylindrical (A) and the spherical (B) SDS/*p*-aminobenzoate micelles. The average values of each distance over the 25 ns of simulation are presented in the table.

4.7 Appendix B: Contact Analysis Results

In Tables B1 to B7 in this appendix, we list scaled contact ratios (SCRs), Δ MCRs, and standard errors (SEs) computed from the water/oil interface, cylindrical micelle, and spherical micelle simulations for groups of atoms in each of the seven solubilizates considered in this chapter. Groups that are identified as being part of the head are shown in bold. A description of the way in which each SCR, Δ MCR, and SE value has been computed is presented in Section 4.2.4.

Oil/Water Interface Simulation Results															
Group	1	2	3	4	5	6	7	8	9	10	11	12	13	14	15
SCR	15.27	16.44	10.95	1.00	1.74	1.31	0.98	0.84	0.55	0.48	0.47	0.23	0.28	0.17	0.24
SE	1.15	1.40	0.66	0.04	0.09	0.06	0.06	0.07	0.03	0.05	0.02	0.03	0.03	0.02	0.03
Cylindrical Micelle Simulation Results															
Group	1	2	3	4	5	6	7	8	9	10	11	12	13	14	15
Δ MCR	0.34	0.33	0.29	0.04	0.09	0.00	-0.06	-0.05	-0.14	-0.13	-0.15	-0.19	-0.18	-0.19	-0.17
SE	0.01	0.02	0.02	0.01	0.01	0.01	0.01	0.01	0.01	0.01	0.01	0.01	0.02	0.01	0.01
Spherical Micelle Simulation Results															
Group	1	2	3	4	5	6	7	8	9	10	11	12	13	14	15
Δ MCR	0.34	0.34	0.30	0.05	0.11	-0.01	-0.05	-0.06	-0.14	-0.14	-0.17	-0.20	-0.20	-0.20	-0.19
SE	0.01	0.01	0.01	0.01	0.01	0.01	0.01	0.01	0.01	0.01	0.01	0.01	0.02	0.01	0.01

Table 4.1: Oil/water interface, cylindrical micelle, and spherical micelle simulation results for ibuprofen.

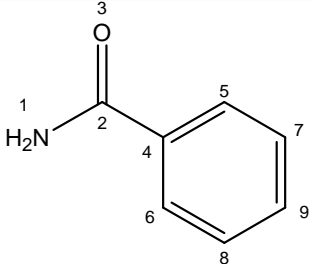
									
Oil/Water Interface Simulation Results									
Group	1	2	3	4	5	6	7	8	9
SCR	2.52	1.59	1.71	0.99	0.74	0.73	0.39	0.39	0.27
SE	0.06	0.03	0.03	0.02	0.03	0.04	0.01	0.02	0.01
Cylindrical Micelle Simulation Results									
Group	1	2	3	4	5	6	7	8	9
Δ MCR	0.05	0.03	0.01	-0.07	-0.11	-0.11	-0.17	-0.17	-0.20
SE	0.01	0.02	0.01	0.01	0.01	0.01	0.01	0.01	0.01
Spherical Micelle Simulation Results									
Group	1	2	3	4	5	6	7	8	9
Δ MCR	0.11	0.09	0.06	-0.02	-0.05	-0.06	-0.10	-0.10	-0.12
SE	0.01	0.01	0.01	0.02	0.02	0.01	0.02	0.01	0.01

Table 4.2: Oil/water interface, cylindrical micelle, and spherical micelle simulation results for benzamide.

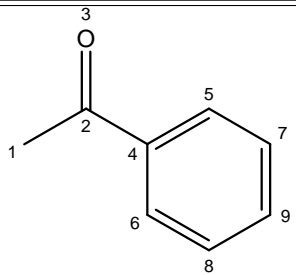
									
Oil/Water Interface Simulation Results									
Group	1	2	3	4	5	6	7	8	9
SCR	0.62	0.77	0.86	0.81	0.58	0.49	0.48	0.35	0.35
SE	0.02	0.02	0.03	0.03	0.02	0.02	0.02	0.01	0.01
Cylindrical Micelle Simulation Results									
Group	1	2	3	4	5	6	7	8	9
Δ MCR	-0.02	-0.03	0.00	-0.12	-0.14	-0.13	-0.17	-0.17	-0.18
SE	0.01	0.01	0.01	0.01	0.01	0.01	0.02	0.01	0.02
Spherical Micelle Simulation Results									
Group	1	2	3	4	5	6	7	8	9
Δ MCR	0.00	-0.02	0.01	-0.10	-0.11	-0.11	-0.13	-0.12	-0.13
SE	0.01	0.01	0.01	0.01	0.01	0.01	0.02	0.01	0.02

Table 4.3: Oil/water interface, cylindrical micelle, and spherical micelle simulation results for acetophenone.

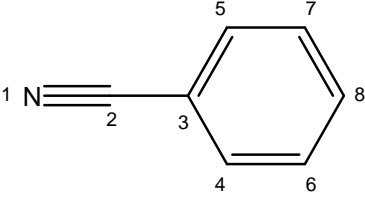
								
Oil/Water Interface Simulation Results								
Group	1	2	3	4	5	6	7	8
SCR	0.64	0.57	0.46	0.41	0.41	0.32	0.31	0.27
SE	0.02	0.02	0.02	0.02	0.02	0.01	0.02	0.02
Cylindrical Micelle Simulation Results								
Group	1	2	3	4	5	6	7	8
Δ MCR	-0.04	-0.07	-0.10	-0.12	-0.11	-0.13	-0.12	-0.13
SE	0.02	0.02	0.02	0.02	0.01	0.02	0.01	0.03
Spherical Micelle Simulation Results								
Group	1	2	3	4	5	6	7	8
Δ MCR	0.01	-0.04	-0.09	-0.11	-0.10	-0.12	-0.11	-0.12
SE	0.03	0.02	0.02	0.02	0.02	0.01	0.02	0.01

Table 4.4: Oil/water interface, cylindrical micelle, and spherical micelle simulation results for benzonitrile.

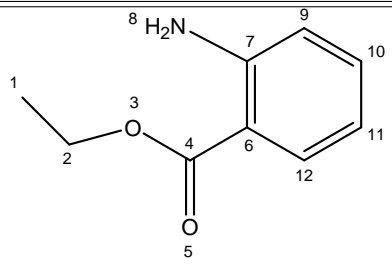
												
Oil/Water Interface Simulation Results												
Group	1	2	3	4	5	6	7	8	9	10	11	12
SCR	0.36	0.57	0.47	0.67	0.80	0.58	0.91	1.18	0.82	0.43	0.25	0.26
SE	0.03	0.02	0.02	0.01	0.02	0.01	0.01	0.04	0.02	0.01	0.01	0.02
Cylindrical Micelle Simulation Results												
Group	1	2	3	4	5	6	7	8	9	10	11	12
Δ MCR	-0.13	-0.08	-0.14	-0.10	-0.05	-0.13	-0.03	0.03	-0.04	-0.12	-0.19	-0.21
SE	0.05	0.04	0.03	0.02	0.02	0.03	0.01	0.01	0.02	0.03	0.02	0.03
Spherical Micelle Simulation Results												
Group	1	2	3	4	5	6	7	8	9	10	11	12
Δ MCR	-0.09	-0.06	-0.13	-0.11	-0.05	-0.14	-0.03	0.06	0.01	-0.09	-0.19	-0.22
SE	0.02	0.01	0.03	0.01	0.01	0.01	0.01	0.02	0.01	0.01	0.02	0.03

Table 4.5: Oil/water interface, cylindrical micelle, and spherical micelle simulation results for o-aminobenzoate.

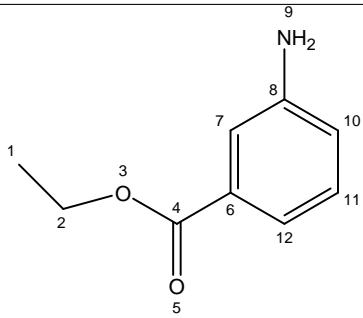
												
Oil/Water Interface Simulation Results												
Group	1	2	3	4	5	6	7	8	9	10	11	12
SCR	0.27	0.38	0.37	0.49	0.58	0.55	1.02	1.04	1.31	0.68	0.34	0.27
SE	0.09	0.01	0.06	0.01	0.02	0.01	0.05	0.02	0.03	0.01	0.09	0.08
Cylindrical Micelle Simulation Results												
Group	1	2	3	4	5	6	7	8	9	10	11	12
Δ MCR	-0.16	-0.16	-0.18	-0.17	-0.16	-0.16	-0.09	-0.03	0.04	-0.05	-0.16	-0.21
SE	0.02	0.01	0.02	0.01	0.01	0.01	0.01	0.01	0.01	0.04	0.04	0.01
Spherical Micelle Simulation Results												
Group	1	2	3	4	5	6	7	8	9	10	11	12
Δ MCR	-0.06	-0.05	-0.12	-0.11	-0.06	-0.12	-0.04	0.00	0.06	-0.04	-0.13	-0.18
SE	0.02	0.02	0.02	0.01	0.01	0.01	0.01	0.01	0.02	0.01	0.02	0.02

Table 4.6: Oil/water interface, cylindrical micelle, and spherical micelle simulation results for m-aminobenzoate.

Oil/Water Interface Simulation Results												
Group	1	2	3	4	5	6	7	8	9	10	11	12
SCR	0.21	0.27	0.31	0.39	0.40	0.50	0.45	0.69	1.02	1.22	0.98	0.64
SE	0.01	0.01	0.01	0.02	0.01	0.02	0.02	0.02	0.01	0.02	0.07	0.04
Cylindrical Micelle Simulation Results												
Group	1	2	3	4	5	6	7	8	9	10	11	12
Δ MCR	-0.16	-0.15	-0.16	-0.15	-0.13	-0.13	-0.07	-0.01	0.01	0.06	-0.07	-0.15
SE	0.02	0.02	0.02	0.02	0.02	0.01	0.02	0.01	0.01	0.01	0.01	0.01
Spherical Micelle Simulation Results												
Group	1	2	3	4	5	6	7	8	9	10	11	12
Δ MCR	-0.13	-0.12	-0.15	-0.13	-0.10	-0.12	-0.09	-0.01	0.03	0.09	-0.01	-0.09
SE	0.03	0.03	0.02	0.03	0.03	0.02	0.02	0.01	0.01	0.01	0.01	0.01

Table 4.7: Oil/water interface, cylindrical micelle, and spherical micelle simulation results for p-aminobenzoate.

Bibliography

- [1] Broze, B., Ward, T., Ward, K. D., Christian, S. D., and Scamehorn, J. F., *Solubilization in Surfactant Aggregates. Surfactant Science Series 55*, Marcel Dekker, New York, 1995.
- [2] Elworthy, P. H., Florence, A. T., and Macfarlane, C. B., *Solubilization by Surface Active Agents*, Chapman and Hall, London, 1968.
- [3] Dunaway, C. S., Christian, S. D., and Scamehorn, J. F., *Solubilization in Surfactant Aggregates. Surfactant Science Series 55*, Marcel Dekker, New York, 1995.
- [4] Hagan, S. A., Coombes, G. A., Garnett, M. C., Dunn, S. E., and Davies, M. C., "Polylactide-poly(ethylene glycol) copolymers as drug delivery systems: 1. Characterization of water dispersible micelle-forming systems," *Langmuir*, Vol. 12, 1996, pp. 2153–2161.
- [5] Rosen, M., *Surfactants and Interfacial Phenomena*, John Wiley and Sons, New York, 10th ed., 1989.
- [6] Nagarajan, R., "Solubilization in aqueous solutions of amphiphiles," *Current Opinion in Colloid and Interface Science*, Vol. 1, 1996, pp. 391–401.
- [7] Rouse, J. D., Sabatini, D. A., Deeds, N. E., and Brown, R. E., "Micellar solubilization of unsaturated hydrocarbon concentrations as evaluated by semi-equilibrium dialysis," *Environmental Science and Technology*, Vol. 29, 1995, pp. 2484–2489.

- [8] In Christian, S. D. and Scamehorn, J. F., *Solubilization in Surfactant Aggregates. Surfactant Science Series 55*, Marcel Dekker, New York, 1995.
- [9] Christian, S. D., Smith, L. S., Bushong, D. S., and Tucker, E. E., "Solubilization of benzene and cyclohexane by sodium deoxycholate micelles," *Journal of Colloid and Interface Science*, Vol. 89, 1982, pp. 514–522.
- [10] Dunaway, C. S., Christian, S. D., Scamehorn, J. F., and In Christian, S. D., *Solubilization in Surfactant Aggregates. Surfactant Science Series 55*, Marcel Dekker, New York, 1995.
- [11] Nagarajan, R., "Solubilization by amphiphilic aggregates," *Current Opinion in Colloid and Interface Science*, Vol. 2, 1997, pp. 282–293.
- [12] Takeuchi, M. and Moroi, Y., "Solubilization of n-alkylbenzenes into 1-dodecanesulfonic acid micelles," *Langmuir*, Vol. 11, 1995, pp. 4719–4723.
- [13] Heijnen, J., *Olefin Epoxidations Catalyzed by Micelle-Incorporated Homogeneous Catalysts*, Ph.D. thesis, Eindhoven University, 2003.
- [14] Nagarajan, R., "Locus of solubilization of benzene in surfactant micelles," *The Journal of Physical Chemistry*, Vol. 87, 1983, pp. 2916–2922.
- [15] Goldenberg, M. S., Bruno, L. A., and Rennwanz, E. L., "Determination of solubilization sites and efficiency of water-insoluble agents in ethylene oxide-containing nonionic micelles," *Journal of Colloid and Interface Science*, Vol. 158, 1993, pp. 351–363.
- [16] Shiloach, A. and Blankshtein, D., "Predicting micellar solution properties of binary surfactant mixtures," *Langmuir*, Vol. 14, 1998, pp. 1618–1636.
- [17] Nagarajan, R. and Ruckenstein, E., "Theory of surfactant self-assembly: A predictive molecular thermodynamic approach," *Langmuir*, Vol. 7, 1991, pp. 2934–2969.

- [18] Gunnarsson, G., Jonsson, B., and Wennerstrom, H., "Surfactant association into micelles - An electrostatic approach," *The Journal of Physical Chemistry*, Vol. 84, 1980, pp. 3114–3121.
- [19] Jonsson, B. and Wennerstrom, H., "Thermodynamics of ionic amphiphile-water systems," *Journal of Colloid and Interface Science*, Vol. 80, 1981, pp. 482–496.
- [20] Evans, D. F., Mitchell, D. J., and Ninham, B. W., "Ion binding and dressed micelles," *The Journal of Physical Chemistry*, Vol. 88, 1984, pp. 6344–6348.
- [21] Hayter, J. B., "A self-consistent theory of dressed micelles," *Langmuir*, Vol. 8, 1992, pp. 2873–2876.
- [22] Rao, I. V. and Ruckenstein, E., "Micellization behavior in the presence of alcohols," *Journal of Colloid and Interface Science*, Vol. 113, 1986, pp. 375–387.
- [23] Chaiko, M. A., Nagarajan, R., and Ruckenstein, E., "Solubilization of single-component and binary mixtures of hydrocarbons in aqueous micellar solutions," *Journal of Colloid and Interface Science*, Vol. 99, 1984, pp. 168–182.
- [24] Nagarajan, R., "Micellization, mixed micellization and solubilization: The role of interfacial interactions," *Advances in Colloid and Interface Science*, Vol. 26, 1986, pp. 205–264.
- [25] Nagarajan, R., "Thermodynamics of micelles, mixed micelles and solubilization: The role of interfacial interactions," *Advances in Colloid and Interface Science*, Vol. 26, 1986, pp. 205–264.
- [26] Nagarajan, R. and Ruckenstein, E., *Surfactants in Solution*, Plenum Press, 1984.
- [27] Nagarajan, R. and Ruckenstein, E., "Solubilization as a separation process," *Separation Science and Technology*, Vol. 16, 1981, pp. 1429–1465.

- [28] Srinivasan, V., *Theoretical Modeling of Micellization and Solubilization in Ionic Surfactant Systems*, Ph.D. thesis, Massachusetts Institute of Technology, 2003, and references cited therein.
- [29] Aamodt, M., Landgren, M., and Jonsson, B., “Solubilization of uncharged molecules in ionic surfactant aggregates. 1. The micellar phase,” *The Journal of Physical Chemistry*, Vol. 96, 1992, pp. 945–950.
- [30] Landgren, M., Aamodt, M., and Jonsson, B., “Solubilization of uncharged molecules in ionic surfactant aggregates. 2. Phase equilibria,” *The Journal of Physical Chemistry*, Vol. 96, 1992, pp. 950–961.
- [31] Jonsson, B., Landgren, M., Olofsson, G., and In Christian, S. D., *Solubilization in Surfactant Aggregates. Surfactant Science Series 55*, Marcel Dekker, New York, 1995.
- [32] Gelbart, W. M., Ben-Shaul, A., and Roux, D., *Micelles, Membranes, Microemulsions, and Monolayers*, Springer, Berlin, 1994, and references cited therein.
- [33] Srinivasan, V. and Blankschtein, D., “Effect of counterion binding on micellar solution behavior: 1. Molecular-thermodynamic theory of micellization of ionic surfactants,” *Langmuir*, Vol. 19, 2003, pp. 9932–9945.
- [34] Srinivasan, V. and Blankschtein, D., “Effect of counterion binding on micellar solution behavior: 2. Prediction of micellar solution properties of ionic surfactant-electrolyte systems,” *Langmuir*, Vol. 19, 2003, pp. 9946–9961.
- [35] Israelachvili, J. N., *Intermolecular and Surface Forces*, Academic Press, 2nd ed., 1991.
- [36] Telo de Gama, M. M. and Gubbins, K. E., “Adsorption and orientation of amphiphilic molecules at a liquid-liquid interface,” *Molecular Physics*, Vol. 59, 1986, pp. 227–239.

- [37] Rodriguez-Guadarrama, L. A., Talsania, S. K., Mohanty, K. K., and Rajagopalan, R., “Thermodynamics of aggregation of amphiphiles in solution from lattice Monte Carlo simulations,” *Langmuir*, Vol. 15, 1999, pp. 437–446.
- [38] Care, C. M. and Dalby, T., “Packing entropy in micelle self-assembly,” *European Physics Letters*, Vol. 45, 1999, pp. 38–44.
- [39] Larson, R. G., “Monte Carlo simulation of microstructural transitions in surfactant systems,” *The Journal of Chemical Physics*, Vol. 96, 1992, pp. 7904–7918.
- [40] Larson, R. G., Scriven, L. E., and Davis, H. T., “Monte Carlo simulation of model amphiphilic oil-water systems,” *The Journal of Chemical Physics*, Vol. 83, 1985, pp. 2411–2420.
- [41] Floriano, M. A., Caponetti, E., and Panagiotopoulos, A. Z., “Micellization in model surfactant systems,” *Langmuir*, Vol. 15, 1999, pp. 3143–3151.
- [42] Smit, B., Hilbers, P. A. J., Esselink, K., Rupert, L. A. M., van Os, N. M., and Schlijper, A. G., “Computer simulations of a water oil interface in the presence of micelles,” *Nature*, Vol. 348, 1990, pp. 624–625.
- [43] Smit, B., Esselink, K., Hilbers, P. A. J., van Os, N. M., Rupert, L. A. M., and Szlifer, I., “Computer simulations of surfactant self-assembly,” *Langmuir*, Vol. 9, 1993, pp. 9–11.
- [44] Smit, B., Hilbers, P. A. J., Esselink, K., Rupert, L. A. M., van Os, N. M., and Schlijper, A. G., “Structure of a water/oil interface in the presence of micelles: A computer simulation study,” *The Journal of Physical Chemistry*, Vol. 95, 1991, pp. 6361–6368.
- [45] Pool, R. and Bolhuis, P. G., “Accurate free energies of micelle formation,” *The Journal of Physical Chemistry B*, Vol. 109, 2005, pp. 6650–6657.

- [46] Maillet, J. B., Lachet, V., and Coveney, P. V., “Large scale molecular dynamics simulation of self-assembly processes in short and long chain cationic surfactants,” *Physical Chemistry Chemical Physics*, Vol. 1, 1999, pp. 5277.
- [47] Marrink, S., Lindahl, E., Edholm, O., and Mark, A., “Simulation of the spontaneous aggregation of phospholipids into bilayers,” *Journal of the American Chemical Society*, Vol. 123, 2001, pp. 8638–8639.
- [48] Marrink, S. J., Tieleman, D. P., and Mark, A. E., “Molecular dynamics simulation of the kinetics of spontaneous micelle formation,” *The Journal of Physical Chemistry B*, Vol. 104, 2000, pp. 12165–12173.
- [49] Marrink, S. J. and Mark, A. E., “Molecular dynamics simulations of mixed micelles modeling human bile,” *Biochemistry*, Vol. 41, 2002, pp. 5375–5382.
- [50] Marrink, S. J. and Mark, A. E., “The mechanism of vesicle fusion as revealed by molecular dynamics simulations,” *Journal of the American Chemical Society*, Vol. 125, 2003, pp. 11144–11145.
- [51] Marrink, S. and Mark, A., “Molecular dynamics simulation of the formation, structure, and dynamics of small phospholipid vesicles,” *Journal of the American Chemical Society*, Vol. 125, 2003, pp. 15233–15242.
- [52] de Vries, A., Mark, A., and Marrink, S., “Molecular dynamics simulation of the spontaneous formation of a small DPPC vesicle in water in atomistic detail,” *Journal of the American Chemical Society*, Vol. 126, 2004, pp. 4488–4489.
- [53] Braun, R., Engelman, D. M., and Schulten, K., “Molecular dynamics simulations of micelle formation around dimeric glycophorin A transmembrane helices,” *Biophysical Journal*, Vol. 87, 2004, pp. 754–763.
- [54] Tarek, M., Tobias, D. J., and Klein, M. L., “Molecular dynamics simulation of tetradecyltrimethylammonium bromide monolayers at the air-water interface,” *The Journal of Physical Chemistry*, Vol. 99, 1995, pp. 1393–1402.

- [55] Wijmans, C. M. and Linse, P., “Surfactant self-assembly at a hydrophilic surface. A Monte Carlo simulation study,” *The Journal of Physical Chemistry*, Vol. 100, 1996, pp. 12583–12591.
- [56] Schweighofer, K. J., Essmann, U., and Berkowitz, M., “Structure and dynamics of water in the presence of charged surfactant monolayers at the water-CCl₄ interface. A molecular dynamics study,” *The Journal of Physical Chemistry*, Vol. 101, 1997, pp. 10775–10780.
- [57] Kuhn, H. and Rehage, H., “Molecular dynamics computer simulations of surfactant monolayers: Monododecyl pentaethylene glycol at the surface between air and water,” *The Journal of Physical Chemistry B*, Vol. 103, 1999, pp. 8493–8501.
- [58] Kuhn, H. and Rehage, H., “Molecular orientation of monododecyl pentaethylene glycol (C12E5) surfactants at infinite dilution at the air/water interface. A molecular dynamics computer simulation study,” *Physical Chemistry Chemical Physics*, Vol. 2, 2000, pp. 1023–1028.
- [59] Kuhn, H. and Rehage, H., “Molecular orientation of monododecyl pentaethylene glycol at water/air and water/oil interfaces. A molecular dynamics computer simulation study,” *Colloid and Polymer Science*, Vol. 114-118, 2000, pp. 278.
- [60] da Rocha, S. R. P., Johnston, K. P., and Rossky, P. J., “Surfactant-modified CO₂-water interface: A molecular view,” *The Journal of Physical Chemistry*, Vol. 106, 2002, pp. 13250–13261.
- [61] Stone, M. T., da Rocha, S. R. P., Rossky, P. J., and Johnston, K. P., “Molecular differences between hydrocarbon and fluorocarbon surfactants at the CO₂/water interface,” *The Journal of Physical Chemistry B*, Vol. 107, 2003, pp. 10185–10192.

- [62] Rekvig, L., Hafskjold, B., and Smit, B., “Simulating the effect of surfactant structure on bending moduli of monolayers,” *The Journal of Chemical Physics*, Vol. 120, 2004, pp. 4897–4905.
- [63] Rekvig, L., Hafskjold, B., and Smit, B., “Chain length dependencies of the bending modulus of surfactant monolayers,” *Physical Review Letters*, Vol. 92, 2004, pp. 116101.
- [64] Dominguez, H., “Computer simulations of surfactant mixtures at the liquid/liquid interface,” *The Journal of Physical Chemistry B*, Vol. 106, 2002, pp. 5915–5924.
- [65] Schweighofer, K. J., Essmann, U., and Berkowitz, M., “Simulation of sodium dodecyl sulfate at the water-vapor and water-carbon tetrachloride interfaces at low surface coverage,” *The Journal of Physical Chemistry B*, Vol. 101, 1997, pp. 3793–3799.
- [66] Bruce, C., Berkowitz, M., Perera, L., and Forbes, M., “Molecular dynamics simulation of sodium dodecyl sulfate micelle in water: Micellar structural characteristics and counterion distribution,” *The Journal of Physical Chemistry B*, Vol. 106, 2002, pp. 3788–3793.
- [67] MacKerell, A. D., “Molecular dynamics simulation analysis of a sodium dodecyl sulfate micelle in aqueous solution: Decreased fluidity of the micelle hydrocarbon interior,” *The Journal of Physical Chemistry*, Vol. 99, 1995, pp. 1846–1855.
- [68] Bruce, C., Senapati, S., Berkowitz, M., Perera, L., and Forbes, M., “Molecular dynamics simulations of sodium dodecyl sulfate micelle in water: The behavior of water,” *The Journal of Physical Chemistry B*, Vol. 106, 2002, pp. 10902–10907.

- [69] Dominguez, H., “Computer simulation studies of surfactant monolayer mixtures at the water/oil interface: Charge distribution effects,” *Journal of Colloid and Interface Science*, Vol. 274, 2004, pp. 665–672.
- [70] Dominguez, H. and Berkowitz, M. L., “Computer simulations of sodium dodecyl sulfate at liquid/liquid and liquid/vapor interfaces,” *The Journal of Physical Chemistry B*, Vol. 104, 2000, pp. 5302–5308.
- [71] Gao, J., Ge, W., Hu, G., and Li, J., “From homogeneous dispersion to micelles - A molecular dynamics simulation on the compromise of the hydrophilic and hydrophobic effects of sodium dodecyl sulfate in aqueous solution,” *Langmuir*, Vol. 21, 1989, pp. 5223–5229.
- [72] Bogusz, S., Venable, R. M., and Pastor, R. W., “Molecular dynamics simulations of octyl glucoside micelles: Structural properties,” *The Journal of Physical Chemistry B*, Vol. 104, 2000, pp. 5462–5470.
- [73] Bocker, J., Brickmann, J., and Bopp, P., “Molecular dynamics simulation study of an n-dodecyltrimethylammonium chloride micelle in water,” *The Journal of Physical Chemistry*, Vol. 98, 1994, pp. 712–717.
- [74] Rakitin, A. R. and Pack, G. R., “Molecular dynamics simulations of ionic interactions with dodecyl sulfate micelles,” *The Journal of Physical Chemistry B*, Vol. 108, 2004, pp. 2712–2716.
- [75] Pal, S., Balasubramanian, S., and Bagchi, B., “Identity, energy, and environment of interfacial water molecules in a micellar solution,” *The Journal of Physical Chemistry B*, Vol. 107, 2003, pp. 5194–5202.
- [76] Karaborni, S., van Os, N. M., Esselink, K., and Hilbers, P. A. J., “Molecular dynamics simulations of oil solubilization in surfactant solutions,” *Langmuir*, Vol. 9, 1993, pp. 1175–1178.

- [77] Kholov, K. N., Mamatkulov, S. I., Saidov, A. A., Khabibullaev, P. K., and Berkowitz, M. L., “Molecular dynamics study of alcohol solubilization process in micellar solutions,” *Uzbek Journal of Physics*, Vol. 5, 2003, pp. 145–149.
- [78] Kuhn, H., Breitzke, B., and Rehage, H., “A molecular modeling study of pentanol solubilized in a sodium octanoate micelle,” *Journal of Colloid and Interface Science*, Vol. 249, 2002, pp. 152–161.
- [79] Goldsipe, A. and Blankschtein, D., “Modeling counterion binding in ionic-nonionic and ionic-zwitterionic binary surfactant mixtures,” *Langmuir*, Vol. 22, 2005, pp. 9850–9865.
- [80] Stephenson, B. C., Beers, K., and Blankschtein, D., “Complementary use of simulations and molecular-thermodynamic theory to model micellization,” *Langmuir*, Vol. 22, 2006, pp. 1500–1513.
- [81] Puvvada, S. and Blankschtein, D., “Molecular thermodynamic approach to predict micellization, phase behavior and phase separation of micellar solutions. 1. Application to nonionic surfactants,” *The Journal of Chemical Physics*, Vol. 92, 1990, pp. 3710–3724, and references cited therein.
- [82] Stephenson, B. C., Rangel-Yagui, C. O., Pessoa, A., Tavares, L. C., Beers, K. J., and Blankschtein, D., “Experimental and theoretical investigation of the micellar-assisted solubilization of ibuprofen in aqueous media,” *Langmuir*, Vol. 22, 2006, pp. 1514–1525.
- [83] Stigter, D., “On density, hydration, shape, and charge of micelles of sodium dodecyl sulfate and dodecyl ammonium chloride,” *Journal of Colloid and Interface Science*, Vol. 23, 1966, pp. 379–388.
- [84] Shah, S. S., Jamroz, N. U., and Sharif, Q. M., “Micellization parameters and electrostatic interactions in micellar solution of sodium dodecyl sulfate (SDS)

- at different temperatures,” *Colloids and Surfaces A: Physicochemical and Engineering Aspects*, Vol. 178, 2001, pp. 199–206.
- [85] Mall, S., Buckton, G., and Rawlins, D. A., “Dissolution behaviour of sulphonamides into sodium dodecyl sulfate micelles: A thermodynamic approach,” *Journal of Pharmaceutical Sciences*, Vol. 85, 1996, pp. 75–78.
- [86] Hierrezuelo, J. M., Aguiar, J., and Ruiz, C. C., “Stability, interaction, size, and microenvironmental properties of mixed micelles of decanoyl-N-methylglucamide and sodium dodecyl sulfate,” *Langmuir*, Vol. 20, 2004, pp. 10419–10426.
- [87] Caetano, W., Gelamo, E. L., Tabak, M., and Itri, R., “Chlorpromazine and sodium dodecyl sulfate mixed micelles investigated by small angle X-ray scattering,” *Journal of Colloid and Interface Science*, Vol. 248, 2002, pp. 149–157.
- [88] Almgren, M. and Swarup, S., “Size of sodium dodecyl sulfate micelles in the presence of additives. 2. Aromatic and saturated hydrocarbons,” *The Journal of Physical Chemistry*, Vol. 86, 1982, pp. 4212–4216.
- [89] Srinivasan, V. and Blankschtein, D., “Prediction of conformational characteristics and micellar solution properties of fluorocarbon surfactants,” *Langmuir*, Vol. 21, 2004, pp. 1647–1660.
- [90] Tieleman, D. and Berendsen, H., “Molecular dynamics simulations of a fully hydrated dipalmitoyl phosphatidylcholine bilayer with different macroscopic boundary conditions and parameters,” *Journal of Chemical Physics*, Vol. 105, 1996, pp. 4871–4880.
- [91] Shin, S., Collazo, N., and Rice, S., “A molecular dynamics study of the packing structures in monolayers of partially fluorinated amphiphiles,” *The Journal of Chemical Physics*, Vol. 96, 1992, pp. 1352–1366.

- [92] Shin, S., Collazo, N., and Rice, S., “Comment on molecular dynamics simulations of monolayers of fluorinated amphiphiles,” *The Journal of Chemical Physics*, Vol. 98, 1993, pp. 3469–3474.
- [93] Jorgensen, W. L., Maxwell, D. S., and Tirado-Rives, J., “Development and testing of the OPLS all-atom force field on conformational energetics and properties of organic liquids,” *Journal of the American Chemical Society*, Vol. 118, 1996, pp. 11225–11236.
- [94] Schweighofer, K. J., Essmann, U., and Berkowitz, M., “Simulation of sodium dodecyl sulfate at the water-vapor and water-carbon tetrachloride interfaces at low surface coverage,” *The Journal of Physical Chemistry B*, Vol. 101, 1997, pp. 3793–3799.
- [95] Berendsen, H. J. C., Grigera, J. R., and Straatsma, T. P., “The missing term in effective pair potentials,” *The Journal of Physical Chemistry*, Vol. 91, 1987, pp. 6269–6271.
- [96] Breneman, C. and Wiberg, K., “Determining atom-centered monopoles from molecular electrostatic potentials: The need for high sampling density in formamide,” *Journal of Computational Chemistry*, Vol. 11, 1990, pp. 361–373.
- [97] Foresman, J. and Frisch, A., *Exploring Chemistry with Electronic Structure Methods*, Gaussian, Inc., Pittsburgh, Pennsylvania, 1996.
- [98] Chirlian, L. E. and Francl, M. M., “Atomic charges derived from electrostatic potentials: A detailed study,” *Journal of Computational Chemistry*, Vol. 8, 2004, pp. 894–905.
- [99] Bader, J. S. and Chandler, D., “Computer-simulation study of the mean forces between ferrous and ferric ions in water,” *The Journal of Physical Chemistry*, Vol. 96, 1992, pp. 6423–6427.

- [100] Shirts, M. R., Pitera, J. W., Swope, W. C., and Pande, V. S., “Extremely precise free energy calculations of amino acid side chain analogs: Comparison of common molecular mechanics force fields for proteins,” *The Journal of Chemical Physics*, Vol. 119, 2003, pp. 5740–5760.
- [101] Shirts, M. R. and Pande, V. S., “Solvation free energies of amino acid side chain analogs for common molecular mechanics water models,” *The Journal of Chemical Physics*, Vol. 122, 2005, pp. 134508.
- [102] Shirts, M., *Calculating Precise and Accurate Free Energies in Biomolecular Systems*, Ph.D. thesis, Stanford, 2005, and references cited therein.
- [103] van der Spoel, D., Lindahl, E., Hess, B., van Buuren, A., Apol, E., Meulenhoff, P., Tieleman, D., Sijbers, A., Feenstra, K., van Drunen, R., and Berendsen, H., *Gromacs User Manual version 3.2*, www.gromacs.org, 2004.
- [104] van Gunsteren, W. F. and Berendsen, J. J. C., “A leap-frog algorithm for stochastic dynamics,” *Journal of Computational Chemistry*, Vol. 18, 1997, pp. 1463–1472.
- [105] Berendsen, H. J. C., van der Spoel, D., and van Drunen, R., “GROMACS: A message-passing parallel molecular dynamics implementation,” *Computational Physics Community*, Vol. 91, 1995, pp. 43–56.
- [106] Lindahl, E., Hess, B., and van der Spoel, D., “Gromacs 3.0: A package for molecular simulation and trajectory analysis,” *Journal of Molecular Modeling*, Vol. 7, 2001, pp. 306–317.
- [107] Cabane, B., Duplessix, R., and Zemb, T., “High-resolution neutron-scattering on ionic surfactant micelles - SDS in water,” *Journal de Physique*, Vol. 46, 1985, pp. 2161–2178.
- [108] Flyvbjerg, H. and Petersen, H. G., “Error estimates on averages of correlated data,” *The Journal of Chemical Physics*, Vol. 91, 1989, pp. 461–466.

- [109] Hess, B., *Stochastic Concepts in Molecular Simulation*, Ph.D. thesis, Rijksuniversiteit Groningen, Groningen, 1999.
- [110] Hess, B., “Determining the shear viscosity of model liquids from molecular dynamics simulations,” *The Journal of Chemical Physics*, Vol. 116, 2001, pp. 209–217.
- [111] Pearlman, D. A. and Kollman, P. A., “The lag between the hamiltonian and the system configuration in free-energy perturbation calculations,” *The Journal of Chemical Physics*, Vol. 91, 1989, pp. 7831–7839.
- [112] Pearlman, D. A. and Rao, B. G., *Free Energy Calculations: Methods and Applications*, John Wiley & Sons, Ltd., New York, 1998.
- [113] Gibbs, J. W., *The Scientific Papers of J.W. Gibbs*, Vol. 1, Dover, New York, 1961.
- [114] Koenig, F. O., “On the thermodynamic relation between surface tension and curvature,” *The Journal of Chemical Physics*, Vol. 18, 1950, pp. 449.
- [115] Buff, F. P., “The spherical interface. I. Thermodynamics,” *The Journal of Chemical Physics*, Vol. 19, 1951, pp. 1591.
- [116] Tolman, R. C., “Consideration of the Gibbs theory of surface tension,” *The Journal of Chemical Physics*, Vol. 16, 1948, pp. 758.
- [117] Aveyard, R., Briscoe, B. J., and Chapman, J., “Adhesion at the alkane/water and ester/water interfaces,” *Journal of the Chemical Society, Faraday Transactions*, Vol. 68, 1972, pp. 10.
- [118] Tanford, C., *The Hydrophobic Effect: Formation of Micelles and Biological Membranes*, John Wiley and Sons, New York, 1991.
- [119] Hildebrand, J. H., Prausnitz, J. M., and Scott, R. L., *Regular and Related Solutions*, Van Nostrand Reinhold Company, 1971.

- [120] Szleifer, I., “Protein adsorption on surfaces with grafted polymers: A theoretical approach,” *Biophysical Journal*, Vol. 72, 1997, pp. 595–612.
- [121] Szleifer, I., “Protein adsorption on tethered polymer layers: Effect of polymer chain architecture and composition,” *Physica A: Statistical Mechanics and Its Applications*, Vol. 244, 1997, pp. 370–388.
- [122] Mattice, W. L. and Suter, U. W., *Conformational Theory of Large Molecules: The Rotational Isomeric State Model in Macromolecular Systems*, Wiley, New York, 1994.
- [123] Flory, P., *Statistical Mechanics of Chain Molecules*, Wiley, New York, 1969.

Chapter 5

Complementary Use of Computer Simulations and Molecular-Thermodynamic Theory to Model Micellar Solubilization.

II. Application

5.1 Introduction

In Chapter 4, a hybrid computer simulation/molecular thermodynamic modeling approach was developed to model micellar solubilization in aqueous solution. In this approach, molecular dynamics (MD) simulations are used to quantify the extent of hydration of atoms within each solubilizate in a micellar environment. From this hydration information, head, tail, and neutral groups are identified and used as inputs in a molecular-thermodynamic (MT) model for micellar solubilization in aqueous solution.

In Chapter 4, simulations of seven solubilizates were conducted at a water/oil

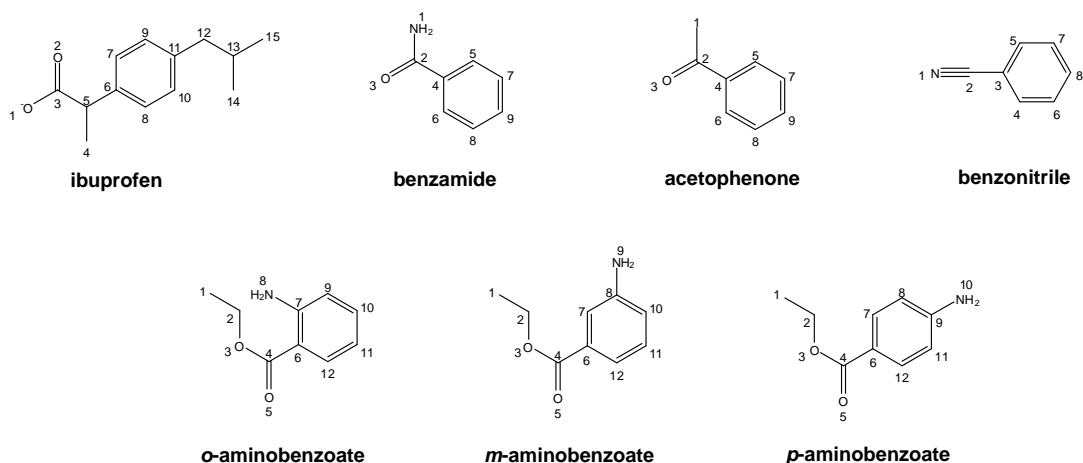


Figure 5-1: Chemical structures of the seven solubilizates modeled in this chapter.

interface, used as a model for the water/micelle core interface, and within cylindrical and spherical sodium dodecyl sulfate (SDS) micelles. The seven solubilizates modeled included: ibuprofen, benzamide, acetophenone, benzonitrile, *o*-aminobenzoate, *m*-aminobenzoate, and *p*-aminobenzoate. The chemical structures of these seven solubilizates are shown again in Figure 5-1 for completeness.

In this chapter, hydration information obtained from the computer simulations discussed in Chapter 4 will be used, along with the molecular-thermodynamic theory of solubilization presented in Chapter 4, to model the micellar solubilization behavior of these seven solubilizates in anionic, nonionic, and cationic surfactant micelles. Theoretical predictions will be made of: (i) the modified free energy of micelle formation (g_f), and (ii) each of the seven free-energy contributions to g_f (g_{tr} , g_{int} , g_{pack} , g_{mix} , g_{st} , g_{elec} , and g_{ent}). Theoretical predictions will also be made of: (i) the micelle shape, S (where $S = 1$ for bilayers, 2 for cylinders, and 3 for spheres), (ii) the micelle core-minor radius, l_c , (iii) the degree of counterion binding for each counterion type present, β_{c_j} – defined as the number of bound counterions of type j per total number of molecules in the core of the micelle (that is, per total number of surfactant and solubilizate molecules present), (iv) the critical micelle concentration (CMC), (v) the micelle composition, α_{mic} – defined as the mole fraction of surfactant in the micelle,

and (vi) the micelle/water partition coefficients defined in Eqs. 4.1 and 4.2 in Chapter 4.

5.2 Overview of Computer Simulation Approach and Results

In Chapter 4, head and tail identifications were made for each solubilize using hydration data obtained from simulation of the solubilize: (i) at a water/oil interface, (ii) within a cylindrical SDS surfactant micelle, and (iii) within a spherical SDS surfactant micelle.

Based on simulation data from the water/oil interface simulations, head and tail assignments were made by computing contacts experienced by each of the numbered solubilize groups shown in Figure 5-1 with water and with oil. The degree of hydration of each group was quantified using a scaled contact ratio (SCR), where any solubilize group with an SCR value greater than 1.0 was assigned as being part of the solubilize head while any solubilize group with an SCR value less than 1.0 was assigned as being part of the solubilize tail.

Based on simulation data for the cylindrical and spherical micelles, head and tail assignments were made by computing contacts with water and with all the atoms present in the micellar system. The degree of hydration of each group was quantified using the micellar contact ratio (MCR), where any solubilize group with a ΔMCR value greater than 0.0 (that is, the difference between the solubilize MCR value and a reference MCR value identified as the dividing value between head and tail as determined based on surfactant MCR data) was assigned as being part of the solubilize head. Conversely, any solubilize group with a calculated ΔMCR value less than 0.0 was assigned as being part of the solubilize tail (see Chapter 4 for details).

The head and tail identifications made based on computer simulation data obtained in the three different environments were similar but not identical, reflecting

the fact that: (i) the water/oil interface simulation does not account for the effect of curvature, ordering of surfactant tails, or the presence of surfactant heads, (ii) the cylindrical and spherical micelle environments have different degrees of curvature, a different level of ordering of the surfactant tails, and a different degree of spacing between surfactant heads, and (iii) the SCR and Δ MCR data obtained are quite noisy and it was difficult in some cases to make a statistically significant assignment of a specific solubilize group as being part of the solubilize head or tail (see Chapter 4 for details).

For completeness, the head and tail identifications for the seven solubilizes shown in Figure 5-1 made based on the water/oil interface simulations, the cylindrical micelle simulations, and the spherical micelle simulations reported in Chapter 4 are summarized in Figure 5-2. The head and tail assignments shown in Figure 5-2 provide the necessary information to implement the MT model to quantify the micellar solubilization behavior of the seven solubilizes considered.

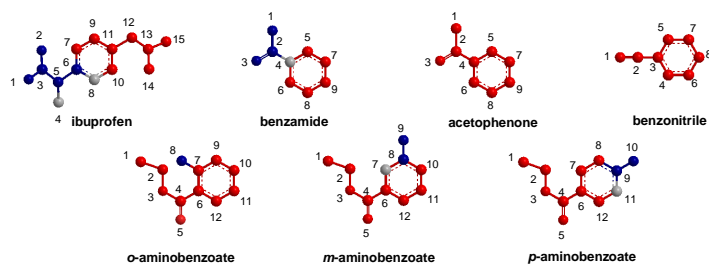
5.3 Overview of the Molecular-Thermodynamic Model of Micellar Solubilization

The molecular-thermodynamic model of micellar solubilization presented in Chapter 4 determines the modified free-energy of surfactant/solubilize micelle formation (g_f) as the sum of the following seven free-energy contributions and a conversion factor:

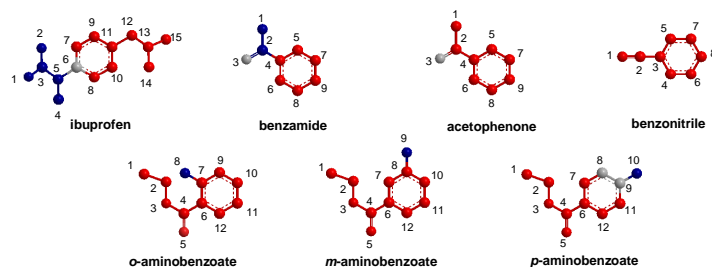
$$g_f = g_{tr} + g_{int} + g_{pack} + g_{mix} + g_{st} + g_{elec} + g_{ent} - \left(1 + \sum_j \beta_j\right) \quad (5.1)$$

where g_{tr} is the transfer free-energy contribution, g_{int} is the interfacial free-energy contribution, g_{pack} is the packing free-energy contribution, g_{mix} is the mixing free-energy contribution, g_{st} is the steric free-energy contribution, g_{elec} is the electrostatic free-energy contribution, g_{ent} is the entropic free-energy contribution, and the term $-\left(1 + \sum_j \beta_j\right)$ is a conversion factor that arises from the way in which chemical

Water/Oil Interface Simulation Results



Cylindrical Micelle Simulation Results



Spherical Micelle Simulation Results

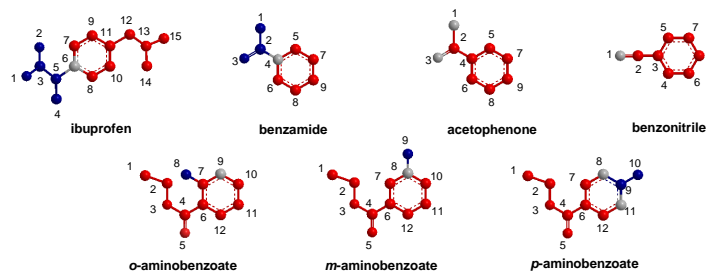


Figure 5-2: Summary of the head and tail identification results presented in Chapter 4 for the seven solubilizates shown in Figure 5-1. Head groups are shown in blue, tail groups are shown in red, and groups which could not be identified as head or tail with statistical significance are shown in grey.

potentials have been defined (see Chapter 4). Theoretical models used to determine each free-energy contribution were discussed in detail in Chapter 4.

After determining g_f , the population distribution (mole fractions) of micellar aggregates, $X_{n_s\{n_{c_j}\}n_a}$, containing n_s surfactant molecules, n_{c_j} bound counterions of type j , and n_a solubilize molecules can be determined using the following equation [1]:

$$X_{n_s\{n_{c_j}\}n_a} = \left(\frac{1}{e}\right) (X_s + X_a)^{n_{\text{agg}}} \exp[-n_{\text{agg}} \cdot g_f] \quad (5.2)$$

where X_s is the mole fraction of surfactant monomers, X_a is the mole fraction of solubilize monomers, and n_{agg} is the total number of core constituents in the micelle ($n_{\text{agg}} = n_s + n_a$). The modified free-energy of micelle formation, g_f , depends on: the micelle shape (S), the micelle core-minor radius (l_c), the micelle composition (α_{mic}), and the micelle degree of counterion binding of each counterion of type j (β_{c_j}).

At the values of S , l_c , α_{mic} , and β_{c_j} that minimize g_f (denoted as S^* , l_c^* , α_{mic}^* , and β^*), g_f has an optimal value denoted as g_f^* . Due to the exponential dependence of $X_{n_s\{n_{c_j}\}n_a}$ on $(n_{\text{agg}} \cdot g_f)$ in Eq. 5.2, small deviations of g_f from g_f^* yield $X_{n_s\{n_{c_j}\}n_a}$ values that are essentially zero. Accordingly, by solving for g_f^* , the optimal micelle shape, S^* , the optimal micelle core-minor radius, l_c^* , the optimal micelle composition, α_{mic}^* , and the optimal micelle degree of counterion binding, $\beta_{c_j}^*$, can be predicted. In addition, the CMC in mole fraction units is computed from g_f^* as follows [2]:

$$\text{CMC} \approx X_{\text{surf}}^{\text{aq}} \exp\left(\frac{g_f^*(S^*, l_c^*, \alpha_{\text{mic}}^*, \beta_{c_j}^*)}{k_B T}\right) \quad (5.3)$$

where $X_{\text{surf}}^{\text{aq}}$ is the mole fraction of surfactant in the aqueous solution, k_B is the Boltzmann constant, and T is the temperature in degrees Kelvin.

5.4 Molecular-Thermodynamic Modeling Based on Computer Simulation Inputs

5.4.1 Selection of Heads and Tails for Molecular-Thermodynamic Modeling

Surfactants

In this chapter, solubilization will be modeled in a number of different surfactant micelles in order to make predictions that can be compared with available experimental solubilization data. The surfactants modeled in this chapter include: the anionic surfactant sodium dodecyl sulfate, SDS, two different nonionic surfactants (dodecyl octa(ethylene oxide), $C_{12}E_8$, and a commercial-grade dodecyl poly(ethylene oxide) surfactant with an average degree of ethoxylation of 23, $C_{12}E_{23}$ or Brij-35), and a cationic surfactant (cetyltrimethylammonium bromide, CTAB). Because of their simple chemical structures (each surfactant has a single linear alkyl chain attached to a single charged or uncharged hydrophilic moiety), the head and tail of each of these surfactants can be identified without computer simulation using simple rules of thumb described in previous publications [2–5]. These rules of thumb are suggested by group-contribution approaches which indicate that the first CH_2 group attached to a charged or dipolar head possesses hydrophilic character, while the remainder of the CH_2 groups and the terminal CH_3 group in the linear alkyl chain remain hydrophobic [6]. As a result, the approximation is made in this chapter that the head of each ionic surfactant (SDS and CTAB) is composed of each of the hydrophilic atoms as well as the first CH_2 group in the linear alkyl chain attached to the hydrophilic atoms. On the other hand, all the CH_2 groups and the terminal CH_3 group in a linear alkyl chain attached to an uncharged polar head are hydrophobic in character. Consequently, for the nonionic surfactants $C_{12}E_8$ and $C_{12}E_{23}$, the approximation is made that each ethylene oxide (E) group is included in the head, and that the entire linear alkyl chain attached to the head (C_{12}) is the tail.

Solubilizates

Based on the computer simulation head and tail identifications summarized in Figure 5-2, we have selected appropriate head and tail groups to use as inputs when evaluating g_{tr} and g_{int} , and we have also identified reasonable head, tail, and neutral groups to use as inputs when evaluating g_{pack} in the context of molecular-thermodynamic modeling. The head and tail group assignments made to evaluate g_{tr} and g_{int} are shown in Figure 5-3, where the blue groups correspond to head groups and the red groups correspond to tail groups. The head, tail, and neutral group assignments made to evaluate g_{pack} are shown in Figure 5-4, where the black group corresponds to the reference head group that is positioned at a range of distances within 1.54 Å of the micelle core/water interface (1.54 Å is the length of a carbon-carbon bond, and corresponds to the distance used by Szleifer in his mean-field packing model [7]) when implementing the mean-field packing model (see Chapter 4), the blue groups correspond to head groups, the red groups correspond to tail groups, and the light grey groups correspond to neutral groups. The assignments shown in Figures 5-3 and 5-4 are discussed in the following two sections.

Assignment of Heads and Tails to Evaluate g_{tr} and g_{int} All surfactant/solubilizate groups must be assigned as being part of the head or tail in order to evaluate g_{tr} and g_{int} ; neutral groups have no meaning in this context. In the MT modeling approach, any group that is identified as tail will contribute to g_{tr} to the extent that it affects the overall solubility of the surfactant/solubilizate tail. In addition, any group that is identified as tail will contribute to g_{int} because g_{int} is directly proportional to the interfacial tension of the micelle core/water interface, which in turn depends on the chemical nature of each of the groups present at the interface. In an ensemble average of surfactant/solubilizate tail configurations, most (if not all) of the surfactant/solubilizate tail groups will spend at least some time at the micelle core/water interface.

As shown in Figure 5-2 (as well as in the SCR and ΔMCR data reported in Ap-

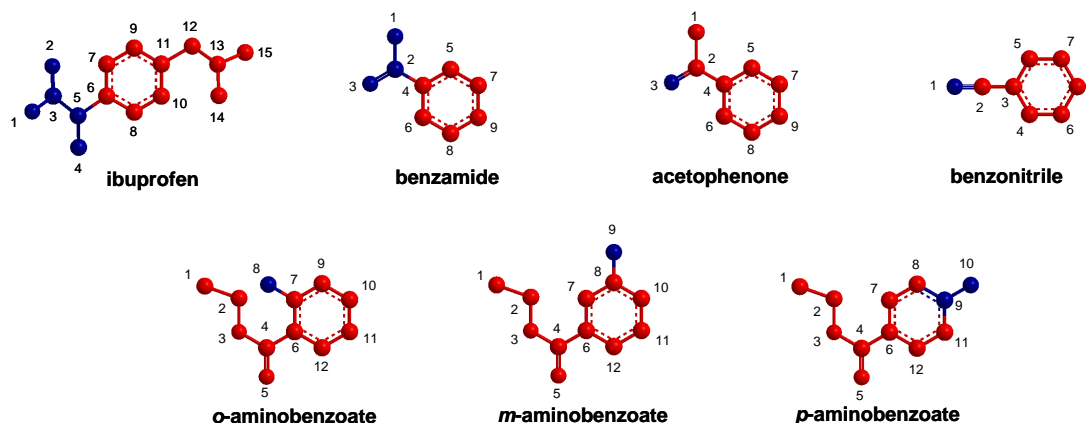


Figure 5-3: Head and tail identifications made for molecular-thermodynamic modeling of g_{tr} and g_{int} .

pendix B of Chapter 4), there are differences between the water/oil interface, the cylindrical micelle, and the spherical micelle assignments of head and tail groups. As discussed in Chapter 4, the head and tail assignments made using spherical micelle simulations are expected to be the most physically realistic because: (i) unlike simulation at a water/oil interface, simulation in a spherical micelle includes the effects of curvature at the micelle/core water interface, ordering of the surfactant tails, and the presence of the surfactant heads, and (ii) unlike simulation in a cylindrical micelle, the boundary conditions applied during simulation in a spherical micelle are physically realistic. Consequently, in this chapter, heads and tails identified based on the spherical micelle simulation results were selected to evaluate g_{tr} and g_{int} . If a particular group had a ΔMCR value greater than 0.0 based on the spherical micelle simulation results, it was assigned as head. Conversely, if that group had a ΔMCR value less than 0.0 based on the spherical micelle simulation results, it was assigned as tail. Because all groups must be assigned as part of the head or the tail in order to evaluate g_{tr} and g_{int} , the statistical significance of the head and tail assignments was ignored when assigning head and tail groups for MT modeling — the only information used was the ΔMCR data.

As shown in Figure 5-3, groups 1-5 in ibuprofen are identified as head and groups 6-15 are identified as tail for the purpose of evaluating g_{tr} and g_{int} . However, to enable direct comparison with the molecular-thermodynamic modeling results for ibuprofen presented in Chapter 3, MT modeling was also carried out for ibuprofen where g_{tr} was evaluated with groups 1, 2, 3, and 5 being identified as head and groups 4 and 6-15 being identified as tail. In Chapter 3, we showed that these two modeling limits, which we will refer to as Limit I and Limit II, respectively, yield molecular-thermodynamic modeling predictions that slightly underpredict (Limit I) and slightly overpredict (Limit II) the molar solubilization ratio of ibuprofen.

As shown in Figure 5-2, all acetophenone groups are assigned as part of the tail based on the water/oil interface simulation results, while groups 1-2 and 4-9 of acetophenone are assigned as part of the tail based on the cylindrical micelle simulation results. In addition, all groups in benzonitrile are assigned as being part of the tail based on the water/oil interface and the cylindrical micelle simulation results. Therefore, even though molecular-thermodynamic modeling is carried out here based on the spherical micelle simulation results (in which, as shown in the data presented in Appendix B of Chapter 4, group 3 of acetophenone and group 1 of benzonitrile are identified as head), in an upcoming publication we will examine an alternative molecular-thermodynamic modeling approach in which, in accordance with the water/oil interface and cylindrical simulation results, the entire acetophenone and benzonitrile molecules are modeled as tail.

Assignment of Heads and Tails to Evaluate g_{pack} In the mean-field packing model described in Chapter 4, it is necessary to define four different types of groups: (i) a single head group which is positioned at a range of locations outside of the micelle core/water interface (referred to hereafter as the “reference head group”), (ii) other head groups (if present) that are constrained to remain on the aqueous side of the micelle core/water interface, (iii) tail groups, which are constrained to remain within the micelle core, and (iv) neutral groups, which are allowed to reside in both

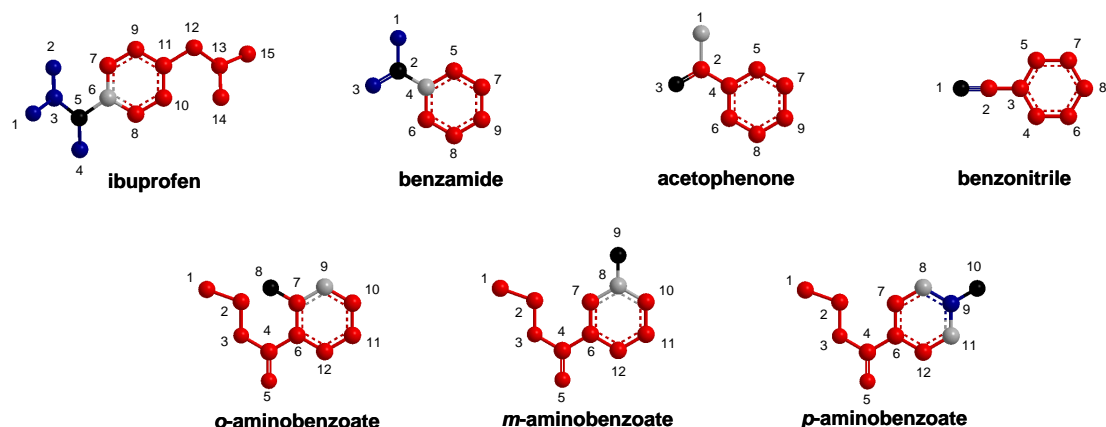


Figure 5-4: Head and tail identifications made for molecular-thermodynamic modeling of g_{pack} .

the aqueous phase and within the micelle core.

In the mean-field model for g_{pack} introduced in Chapter 4, neutral groups are defined as groups that are observed to spend a significant amount of time both outside and inside of the micelle core during the course of an MD simulation. Therefore, modeling certain solubilizate groups as neutral is expected to yield more physically realistic estimates of g_{pack} because it relaxes, to some extent, the approximation made in the mean-field packing model that the micelle core/water interface is completely sharp. In previous implementations of the packing model, all groups were defined as either head groups or tail groups [1, 8]. No tail groups were ever allowed to exit the micelle, and no head groups were ever allowed to enter the micelle. A number of groups in the seven solubilizates modeled here were observed to spend a significant amount of time in both the aqueous phase and the micelle core. Consequently, modeling the micelle core/water interface as a sharp boundary is not physically realistic. Solubilizate groups shown in Figure 5-2 that could not be identified as head groups or as tail groups with statistical significance based on the spherical micelle simulation data either: (i) have a ΔMCR value that is very close to 0.0, or (ii) exhibit a high degree of variation in their ΔMCR values. Because groups which could not be as-

signed with statistical significance as being part of the head or part of the tail spend a substantial amount of time both outside and inside the micelle core, we have chosen to model those groups without a statistically significant head or tail assignment as neutral groups in the evaluation of g_{pack} .

Note that it was not necessary to model any surfactant groups as neutral groups because: (i) the simple linear alkyl chain structure of the surfactant tails considered here is such that at most one CH_2 group (the CH_2 group adjacent to the surfactant head) may qualify as neutral based on the computer simulation results, and (ii) previous implementation of the g_{pack} model for surfactants with linear alkyl chains has demonstrated that reasonable estimates of g_{pack} may be obtained without modeling any groups as being neutral [4]. The head, tail, and neutral group assignments to evaluate g_{pack} were made based on the spherical micelle head and tail assignments reported in Figure 5-2. As shown in Figure 5-4, the single head group selected to be fixed at a designated position outside the micelle core/water interface in implementing the packing model is the head group closest to the micelle core/water interface (e.g., the head group adjacent to a neutral group).

5.4.2 Molecular Parameters Used in Molecular-Thermodynamic Modeling

Based on the head and tail assignments made for each surfactant considered, and the head and tail assignments made to calculate g_{tr} and g_{int} for each solubilize discussed in Section 5.4.1 (see Figure 5-3), three geometric parameters were estimated for each surfactant/solubilize based on the chemical structures of the surfactant/solubilize heads, and were subsequently used as inputs in MT modeling [2–5, 8]. These geometric parameters are reported in Table 5.1 for the four surfactants and the seven solubilizes considered. The first geometric parameter is a_{h} — the cross-sectional area of the surfactant/solubilize head. The second geometric parameter is d_{charge} — the distance from the location of the charge in the surfactant/solubilize head to

Surfactant	Geometric Parameters		
	a_h [\AA^2]	d_{charge} [\AA]	l_{hg} [\AA]
SDS	25.0	3.70	6.30
C_{12}E_8	62.1	N/A	22.8
Brij-35 ($\text{C}_{12}\text{E}_{23}$)	53.3	N/A	N/A
CTAB	32.0	3.80	6.40
Solubilizate	Geometric Parameters		
Ibuprofen	20.0	3.43	6.00
Benzamide	18.0	N/A	N/A
Acetophenone	6.34	N/A	N/A
Benzonitrile	8.45	N/A	N/A
<i>o</i> -Aminobenzoate	15.0	N/A	N/A
<i>m</i> -Aminobenzoate	15.0	N/A	N/A
<i>p</i> -Aminobenzoate	15.0	N/A	N/A

Table 5.1: Geometric parameters of the four surfactants and the seven solubilizates considered in this chapter.

the beginning of the surfactant/solubilizate tail. The third geometric parameter is l_{hg} — the length of the surfactant/solubilizate head, or the distance from the tip of the surfactant/solubilizate head to the beginning of the surfactant/solubilizate tail. The parameter a_h is needed to calculate g_{st} (see Eq. 4.15 in Chapter 4) and the parameters d_{charge} and l_{hg} are needed to calculate g_{elec} (see Eq. 4.18 in Chapter 4) [4, 8]. Note that for nonionic surfactants and solubilizates, d_{charge} and l_{hg} are not needed to implement the molecular-thermodynamic model [5]. As traditionally done in MT modeling, the geometric parameters a_h , d_{charge} , and l_{hg} were estimated based on the energy minimized geometry of the surfactant or solubilizate in vacuum [4].

5.4.3 Implementation of the Molecular Model of Micellar Solubilization

As discussed in Chapter 4, estimates of several physical properties are also needed to implement the MT model. These properties include: (i) the solubility of each surfactant/solubilizate tail i , which is needed to determine g_{tr} , (ii) the surface tension of

the micelle core/water interface, which is needed to determine g_{int} , and (iii) solubility parameters for each surfactant/solubilize tail, which are needed to determine g_{mix} . The approach used to estimate each of these physical properties and to evaluate the free-energy contributions to g_f listed in Eq. 5.1 (g_{tr} , g_{int} , g_{pack} , g_{mix} , g_{st} , g_{elec} , and g_{ent}) are each discussed separately below.

Evaluation of g_{tr}

As discussed in Chapter 4, the transfer free-energy contribution of tail i is computed using the following expression:

$$g_{\text{tr},i} = \ln \frac{S_{\text{aq},i}}{S_{\text{aq},i} + 55,600} \quad (5.4)$$

where $S_{\text{aq},i}$ is the aqueous solubility of tail i in mM. The value of g_{tr} corresponding to a multicomponent micelle is evaluated by weighting $g_{\text{tr},i}$ values of each tail i by the micelle mole fraction of that component, α_i . Specifically, for the micellization of a single surfactant and a single solubilize type, one has:

$$g_{\text{tr}} = \alpha_s g_{\text{tr},s} + \alpha_a g_{\text{tr},a} \quad (5.5)$$

where α_s is the surfactant mole fraction in the micelle, $g_{\text{tr},s}$ is the transfer free energy of the surfactant tail, α_a is the solubilize mole fraction in the micelle, and $g_{\text{tr},a}$ is the transfer free energy of the solubilize tail.

For linear alkyl tails, correlations have been developed to express solubility as a function of alkyl chain length, temperature, and the concentration of added salt in aqueous solution [4, 9]. These correlations were used here to estimate the solubility of the SDS, C₁₂E₈, Brij-35, and CTAB surfactant tails. The estimated surfactant tail solubilities are reported in Table 5.2. The solubility of each solubilize tail i was determined using either experimental data, or, when experimental data was not available, using the Virtual Computational Chemistry Laboratory ALOGPS software developed by Tetko et al. [10, 11], which is based on the use of associative neural

Surfactants						
Tail Identity	$S_{\text{aq},i}$ [mM]	$\rho_{\text{liq},i}$ [g/cm ³]	Φ_{iw}	γ_i [dyn/cm]	$\sigma_{0,i}$ [dyn/cm]	δ_i [MPa ^{1/2}]
C ₁₁ (SDS)	5.36×10^{-4}	-	-	-	52.4	15.3
C ₁₂ (Brij35, C ₁₂ E ₈)	1.20×10^{-4}	-	-	-	52.6	15.3
C ₁₅ (CTAB)	3.05×10^{-7}	-	-	-	53.1	15.6
Solubilizates						
Tail Identity	$S_{\text{aq},i}$ [mM]	$\rho_{\text{liq},i}$ [g/cm ³]	Φ_{iw}	γ_i [dyn/cm]	$\sigma_{0,i}$ [dyn/cm]	δ_i [MPa ^{1/2}]
Ibuprofen (Limit I)	0.08	0.89	0.64	33.2	42.7	17.0
Ibuprofen (Limit II)	2.26×10^{-3}	0.89	0.64	33.2	42.7	17.0
Benzamide	23.0	1.17	0.70	54.1	39.0	17.3
Acetophenone	6.17	-	-	-	17.4 (expt.)	17.6
Benzonitrile	6.17	-	-	-	28.0 (expt.)	17.6
<i>o</i> -Aminobenzoate	4.80	1.06	0.82	35.2	25.0	20.2
<i>m</i> -Aminobenzoate	4.80	1.06	0.82	35.2	25.0	20.2
<i>p</i> -Aminobenzoate	21.8	1.04	0.82	41.0	24.2	20.2

Table 5.2: Molecular properties of the tail fragments of each surfactant and solubilizate considered in this chapter. $S_{\text{aq},i}$ is the aqueous solubility of tail i , $\rho_{\text{liq},i}$ is the liquid density of tail i , Φ_{iw} is the value of the parameter Φ (see text) specific to the tail i /water interface, γ_i is the surface tension of surfactant or solubilizate tail i , $\sigma_{0,i}$ is the interfacial tension of surfactant or solubilizate tail i at a flat interface, and δ_i is the Tolman distance for tail i . Values of $\rho_{\text{liq},i}$, Φ_{iw} , and γ_i are not reported for surfactant/solubilizate tails for which the group-contribution approach described in the text was not needed to evaluate $\sigma_{0,i}$.

networks. Each measured or predicted solubilizate tail solubility is also listed in Table 5.2.

Evaluation of g_{int}

As discussed in Chapter 4, for the surfactant/solubilizate systems modeled here (where each solubilizate is modeled as possessing a head), g_{int} may be computed using the following expression (see Eq. 4.24 in Chapter 4):

$$g_{\text{int}} = (\alpha_s \sigma_s + \alpha_a \sigma_a) \left(\frac{S}{l_c} v_{\text{avg}} - a_{0,\text{avg}} \right) \quad (5.6)$$

where σ_s is the curvature-corrected surfactant tail/water interfacial tension, σ_a is

the curvature-corrected solubilizate tail/water interfacial tension, v_{avg} is the average molecular volume of the surfactant and solubilizate tails (computed using the chemistry software Molecular Modeling Pro [6]), and $a_{0,\text{avg}}$ is the average area shielded by the surfactant and solubilizate heads at the micelle core/water interface. In previous publications, it has been assumed that each bond that crosses the interface shields 21 Å² of area [4, 12]. Accordingly, for all the molecules with heads considered here, we have used a value of 21 Å² for the shielded molecular area, $a_{0,i}$, of molecule i .

The curvature-corrected interfacial tensions, σ_i , were determined using the Gibbs-Tolman-Koenig-Buff equation [13–16]:

$$\sigma_i = \frac{\sigma_{0,i}}{\left(1 + \frac{(S-1)\delta}{l_c}\right)} \quad (5.7)$$

where $\sigma_{0,i}$ is the interfacial tension of tail i at a flat interface (having a typical value of about 50 dyn/cm² for linear hydrocarbons), and δ is the Tolman distance [16]. An empirical correlation was used to estimate the Tolman distance, δ , for both the surfactant and solubilizate tails [4]. Specifically,

$$\delta(n_t) = \delta(n_t = 11)l_{\text{max}}(n_t)/l_{\text{max}}(n_t = 11) \quad (5.8)$$

where n_t is the number of carbons in the surfactant/solubilizate tail, and $l_{\text{max}}(n_t) = 1.54 + 1.265n_t$ (in Å) is the fully-extended length of the surfactant/solubilizate tail [17]. The value of $\delta(n_t = 11)$ used in this chapter is 2 Å, as justified in a previous publication by Goldsipe and Blankschtein [2].

An empirical correlation was used to estimate $\sigma_{0,s}$ for each surfactant tail [18]. For acetophenone and benzonitrile, experimentally measured values of $\sigma_{0,a}$ were found in the literature [19, 20]. For each of the five other solubilizates, $\sigma_{0,a}$ was estimated using an expression developed by Girifalco and Good, which enables estimation of the interfacial tension between two bulk phases based on their respective surface tensions and a parameter, Φ , which depends on the molecular structure of the phase

constituents [21]. Specifically,

$$\sigma_{0,i} = \gamma_i + \gamma_w - 2\Phi_{iw}(\gamma_i\gamma_w)^{1/2} \quad (5.9)$$

where Φ_{iw} is the value of Φ specific to the tail i /water interface, γ_i is the surface tension of surfactant or solubilizate tail i , and γ_w is the surface tension of water, or 72.8 dyn/cm.

Girifalco and Good determined values of Φ_{iw} for a variety of compounds containing a single functional group, and demonstrated that molecules containing the same functional groups (e.g. ketones) tend to have similar values of Φ_{iw} . For several of the solubilizates studied here, multiple functional groups are present, and it is not clear how to correctly estimate Φ_{iw} . As a first approximation, we decided to determine an average value of Φ_{iw} for a class of compounds with a common functional group (f), which is designated as $\Phi_{iw,f}$. For each solubilizate tail i , we identify the functional groups present, and then average each appropriate $\Phi_{iw,f}$ value using the number of functional groups of each type (n_f) present. Specifically,

$$\Phi_{iw} = \frac{\sum_f n_f \Phi_{iw,f}}{\sum_f n_f} \quad (5.10)$$

Although there is no theoretical basis for this type of weighting, we have found it useful to allow modeling of simple compounds in the absence of an established group-contribution method. Other weighting schemes may be used, and future work will involve developing a more accurate group-contribution approach to determine Φ_{iw} . Estimated values of Φ_{iw} obtained using this approach are listed in Table 5.2.

Equation 5.9 enables use of the larger body of literature values for surface tension to predict interfacial tensions when experimental interfacial tension data is not available. However, for some solubilizates, liquid surface tensions are not available or cannot be measured experimentally, since many single solubilizates are in a solid state. Moreover, for amphiphilic solubilizates, the tail may be a fragment of a molecule (e.g. a fraction of an aromatic ring), for which no surface tension measurements are avail-

able. As a result of some of these limitations, we have used a group-contribution approach to estimate an effective surface tension using parachor [22]. The parachor associated with tail i (s or a) is defined as follows:

$$parachor_i = \frac{\gamma_i^{1/4} M_i}{\rho_{liq,i} - \rho_{vap,i}} \approx \frac{\gamma_i^{1/4} M_i}{\rho_{liq,i}} \quad (5.11)$$

where γ_i is the surface tension of tail i , M_i is the molecular weight of tail i , and $\rho_{liq,i}$ and $\rho_{vap,i}$ are the liquid and vapor densities of tail i . Since $\rho_{liq,i} \gg \rho_{vap,i}$ for many organic molecules, we have neglected $\rho_{vap,i}$ in Eq. 5.11.

An interesting group-contribution approach to estimate $parachor_i$ was developed by McGowan, and is given by [22]:

$$parachor_i = \sum_k n_{k,i} A_k - 19N_{bonds,i} \quad (5.12)$$

where N_{bonds} is the total number of bonds in the molecule or molecular fragment i , $n_{k,i}$ is the number of atoms of type k , and A_k is a group parameter assigned to atoms of type k . We have used $A_k = 24.7$ for hydrogen, 47.6 for carbon, 41.9 for nitrogen, and 36.2 for oxygen atoms [22].

After calculating parachor for a surfactant/solubilizate tail according to Eq. 5.12, γ_i may be calculated if $\rho_{liq,i}$ and M_i are known. In the case of molecular fragments and solubilizates for which liquid densities are not available (e.g. solubilizates which are solids at room temperature), an effective liquid density can be estimated using another group-contribution method due to Girolami [22]. Using this group-contribution approach, a scaled volume for species i , $V_{scale,i}$, is calculated from atomic contributions. This property, in addition to the molecular weight of the species, can be used to estimate $\rho_{liq,i}$ as follows [22]:

$$\rho_{liq,i} = \frac{M_i}{5V_{scale,i}} \quad (5.13)$$

In implementing this approach, following the periodic table in terms of groups of

atoms, each hydrogen contributes 1, each atom in the Li to F series contributes 2, and each atom in the Na to Cl series contributes 4 to $V_{\text{scale},i}$. In using Eq. 5.13, the calculated liquid density, $\rho_{\text{liq},i}$, must be increased by 10% for each hydroxyl group, carboxylic acid group, primary or secondary amino group, amide group, sulfoxide group, and unfused ring [22]. An increase of 7.5% should be used on each ring of a system of fused rings. Estimated values of $\rho_{\text{liq},i}$ obtained using this approach are listed in Table 5.2.

In summary, after determining $\rho_{\text{liq},i}$ using Eq. 5.13 and parachor_i using Eq. 5.12, γ_i can be calculated using Eq. 5.11 and then used with an estimate for Φ_{iw} , calculated using Eq. 5.10, to calculate $\sigma_{0,a}$ using Eq. 5.9. Equation 5.7 can then be used to determine the curvature-corrected value of the micelle core/water interfacial tension, σ_i . Finally, g_{int} can be estimated using Eq. 5.6. For any of the estimated quantities reported in Table 5.2, we consider experimental inputs to be superior. Nevertheless, the group-contribution approach outlined above has allowed the estimation of σ_i for ibuprofen, benzamide, and *o*-, *m*-, and *p*-aminobenzoate for which experimental data was not available. Each estimated or experimentally measured value of $\sigma_{0,i}$ is listed in Table 5.2.

As an illustration, we discuss the estimation of the interfacial tension of the tail of benzamide against water using the group-contribution approaches discussed above. The tail of benzamide is very similar to benzene, having a six-carbon aromatic ring but with only five hydrogen atoms (the sixth position occupied by the bond fragment connecting the benzamide tail to the NH_2 head) and eleven total bonds. Using Eq. 5.12, parachor is calculated to be 200.1. The benzamide tail molecular weight is 77.1 g/mol. Using the approach just described, V_{scale} is computed to be 17, and Eq. 5.13 is used to estimate ρ_{liq} as being equal to 0.998 (scaled by 1.1 due to the presence of the aromatic group). Using Eq. 5.11, the surface tension of the benzamide tail is then calculated to be 45.0 dyn/cm. Using Eq. 5.10, and recognizing that the aromatic group is the only functional group in the benzamide tail, Φ_{iw} is calculated to be 0.70. Finally, using Eq. 5.9, the predicted interfacial tension is calculated to

be 37.6 dyn/cm, which is in good agreement with the experimental value for liquid benzene, 35 dyn/cm. Performing a similar calculation with six hydrogens instead of five reduces the predicted interfacial tension by only 0.4 dyn/cm.

Evaluation of g_{pack}

The packing free-energy contribution, g_{pack} , has been evaluated using the mean-field packing model described in Chapter 4 using information reported in Figure 5-4 as an input. One of the head groups shown in each solubilizate in Figure 5-4 (the black group) was positioned at a range of locations near the micelle core/water interface (a distance denoted by δ in Chapter 4). Other head groups, if present, were constrained to remain on the aqueous side of the micelle core/water interface (the blue groups in Figure 5-4). Conversely, all the tail groups shown in Figure 5-4 (the red groups) were constrained to remain within the micelle core. The neutral groups shown in Figure 5-4 (the grey groups) were allowed to be located in both the aqueous phase and within the micelle core.

The Rotational Isomeric State (RIS) model was used to generate internal conformations for each surfactant tail. In modeling the surfactant tails, the bond angle and carbon-carbon bond length were fixed at their average values of 112° and 1.53 Å, respectively. Three possible torsional states, ϕ_k , were allowed for each surfactant chain: a low energy *trans* state (*t*: $\phi_t = 180^\circ$) and two high energy *gauche* states (g^- : $\phi_{g^-} = 60^\circ$; g^+ : $\phi_{g^+} = 300^\circ$). For a surfactant tail containing n carbon atoms, the total number of internal conformations for the chain is equal to 3^{n-2} . Of these bond sequences, bond sequences containing any g^+g^- or g^-g^+ pairs were discarded because these pairs have very high energies due to steric interactions of hydrogen atoms (i.e. the "pentane" effect). The *gauche* – *trans* energy difference, ϵ_g , was taken to be 500 cal/mol [23, 24]. The allowed torsional states and the energy differences between those states in the RIS model used to describe the internal conformations of the solubilizate molecules were determined using Molecular Modeling Pro [6].

For each set of torsional states, the molecule with corresponding internal con-

formation was oriented at the interface such that the reference head group in the molecule (the black groups in Figure 5-4) was situated at l_{core} . Then, a set of four external descriptors, including 3 Euler angles (α, β, γ) capturing molecular rotation and one offset parameter (δ , capturing piston-like motion), was used to specify the external conformation of the molecule. One thousand external conformations were selected based on random sampling of these four descriptors for each internal conformation. We found that increasing the number of conformations further did not significantly change the calculated values of g_{pack} .

For each of the surfactant/solubilizate systems modeled in this chapter, there is a maximum value of the core-minor radius (typically referred to as l_{max}) beyond which the micelle cannot extend, which can be computed from the maximum extended length of the surfactant and solubilizate tails and the composition of the micelle [4]. For a single-surfactant micelle of SDS, l_{max} is equal to 14.1 nm, for a single-surfactant micelle of C₁₂E₈ or Brij-35, l_{max} is equal to 15.5 nm, and for a single-surfactant micelle of CTAB, l_{max} is equal to 19.1 nm. During minimization of g_f , inequality constraints were used to ensure that the value of l_c for the surfactant/solubilizate micelle considered never exceeded l_{max} .

Evaluation of g_{mix}

As discussed in Chapter 4, the mixing free-energy contribution, g_{mix} , is computed as the sum of $g_{\text{mix,I}}$ and $g_{\text{mix,II}}$. The term $g_{\text{mix,I}}$ captures the free-energy associated with mixing solubilizate tails with surfactant tails in the micelle core, while the term $g_{\text{mix,II}}$ captures the free-energy associated with mixing counterions with surfactants, and solubilizate heads with surfactant heads, in the head shell region of the micelle. We chose to model $g_{\text{mix,I}}$ using regular solution theory, which allows one to account for both entropic and enthalpic contributions to the free-energy of mixing.

The regular solution model expression for $g_{\text{mix,I}}$ has the following form (see Eq.

4.32 in Chapter 4):

$$g_{\text{mix,I}} = \frac{1}{k_{\text{B}}T} (h_{\text{mix,I}}) - \frac{1}{k_{\text{B}}} (s_{\text{mix,I}}) \quad (5.14)$$

$$= \frac{1}{k_{\text{B}}T} (\eta_{\text{s}}\eta_{\text{a}} (\delta_{\text{s}} - \delta_{\text{a}})^2 v_{\text{avg}}) - \frac{1}{k_{\text{B}}} (-k_{\text{B}}\alpha_{\text{s}} \ln \alpha_{\text{s}} - k_{\text{B}}\alpha_{\text{a}} \ln \alpha_{\text{a}}) \quad (5.15)$$

where $\eta_i = \alpha_i v_i / v_{\text{avg}}$ is the volume fraction of component i , and δ_i is the solubility parameter of component i .

Evaluation of $g_{\text{mix,I}}$ requires estimation of the solubility parameters δ_{s} and δ_{a} . To determine $g_{\text{mix,I}}$ for the seven solubilizates modeled in this chapter, solubility parameters were estimated for the solubilizate tails using the three-dimensional group-contribution method of van Krevelen and Hoftyzer, as implemented in Molecular Modeling Pro [6].

Evaluation of $g_{\text{mix,II}}$ is straightforward. Because $g_{\text{mix,II}}$ includes only the ideal mixing of counterions, surfactants, and solubilizate heads in the head shell region of the micelle, it is evaluated using an expression that depends only on α_{s} , α_{a} , and β_{c_j} (see Eq. 4.33 in Chapter 4).

Evaluation of g_{st} , g_{elec} , and g_{ent}

Each of the three remaining free-energy contributions in Eq. 5.1 (g_{st} , g_{elec} , and g_{ent}) were evaluated in a straightforward manner using the theoretical models for each contribution introduced in Chapter 4 and the geometric parameters for each surfactant and solubilizate reported in Table 5.1.

5.5 Molecular-Thermodynamic Modeling Results

We next apply the hybrid computer simulation/molecular-thermodynamic model introduced in Chapter 4 to model micellar solubilization by anionic, nonionic, and cationic surfactants. In Section 5.5.1, we use the hybrid model to predict g_{f} and

each of the free-energy contributions to g_f for each surfactant/solubilize system. In Section 5.5.2, we report the predictions of the hybrid model for micelle shape, core-minor radius, degree of counterion binding, CMC, micelle composition, and either K_s or $\ln(K_x)$. The micelle/water partition coefficients K_s and K_x were defined in Eqs. 4.2 and 4.1 in Chapter 4, respectively. Predicted values of K_s are compared with available experimental K_s data, and predicted values of $\ln(K_x)$ are compared with available experimental $\ln(K_x)$ data.

As discussed in Chapter 4, two separate solubilization limits are frequently investigated experimentally when characterizing micellar solubilization behavior. The first limit is infinite dilution of the solubilize (the Henry's Law limit) in aqueous surfactant solution, and the second limit is the maximum concentration of solubilize that can be added to the aqueous surfactant solution before a separate solubilize phase forms (the saturation limit, or the solubility limit) [25–29]. The theoretical predictions and the experimental data reported in this chapter correspond to the second of these two limits.

All theoretical predictions were made for aqueous surfactant/solubilize solutions at 25 °C containing 20 mM of surfactant and 10 mM of sodium chloride salt. The total surfactant concentration was selected arbitrarily. The surfactant concentration selected for modeling will not affect the predictions of the solubilization model for the reported micelle properties because the theoretical model is based on the assumption that the solution is ideal. At low surfactant concentrations where ideal solution behavior holds, intermicellar interactions can be safely neglected, and the optimal characteristics of the self-assembled micelles are independent of the total surfactant concentration. Consequently, although the total amount of solubilized solubilize in solution is a function of the total surfactant concentration, the characteristics of each self-assembled micelle are independent of the total surfactant concentration above the CMC. The salt concentration was also selected arbitrarily because: (i) our sources of experimental data do not specify the salt concentration added to the solution, and (ii) solubilization measurements are typically made in buffered solutions which can be

modeled reasonably well as having a low salt concentration [25,30,31]. The sensitivity of the theoretical predictions to the salt concentration have been investigated and is discussed in Section 5.5.3.

In this section, theoretical predictions were made only for those systems for which experimental partition coefficient data were available. For surfactant/solubilizate systems for which experimental partition coefficient data was not available (for example, for the ibuprofen/CTAB micellar system) theoretical predictions were not made. Theoretical predictions of K_s were made for those surfactant/solubilizate micellar systems for which experimentally measured K_s values were available, and theoretical predictions of $\ln(K_x)$ were made for those surfactant/solubilizate micellar systems for which experimentally measured $\ln(K_x)$ values were available. Moreover, due to the lack of experimental data, we have been limited to making comparisons between theoretically predicted and experimentally measured micelle/water partition coefficients at the solubilizate saturation limit in aqueous solution. However, to more thoroughly evaluate the accuracy of the hybrid computer simulation/molecular thermodynamic modeling approach, experimental data on other solubilization-related properties (such as micelle/water partition coefficients at the Henry's Law limit, micelle shape, core-minor radius, composition, degree of counterion binding, and CMC) will be gathered and compared with the predictions of the hybrid model in ongoing work being conducted in the Blankschtein group.

5.5.1 Free-Energy Predictions

The hybrid computer simulation/molecular-thermodynamic modeling approach described in Chapter 4 was used to make free-energy predictions for the optimal surfactant/solubilizate micelles which are predicted to form in aqueous solution. Note that free-energy predictions were made only for those surfactant/solubilizate systems for which experimental solubilization data was available in the literature. Free-energy predictions made for solubilization in anionic SDS micelles are reported in Table 5.3. Free-energy predictions made for solubilization in nonionic surfactant micelles ($C_{12}E_8$

in the case of ibuprofen and Brij-35 in the case of benzamide, acetophenone, and benzonitrile) are reported in Table 5.4. Finally, free-energy predictions for solubilization in cationic CTAB micelles are reported in Table 5.5.

For ibuprofen, free-energy predictions were made based on two different modeling limits (Limit I and Limit II) used to estimate g_{tr} . As discussed in Section 5.4.1, these two limits reflect modeling group 4 in ibuprofen as being: (i) part of the head when evaluating g_{tr} , or (ii) part of the tail when evaluating g_{tr} . Results obtained based on both limits (L1 and L2) are reported in Tables 5.3 to 5.5 in order to allow comparison with the theoretical predictions reported in Chapter 3.

The average free-energy values predicted for the solubilization of all seven solubilizates in anionic SDS micelles are as follows: $g_{\text{tr}} = -13.8 k_{\text{B}}T$, $g_{\text{int}} = 2.68 k_{\text{B}}T$, $g_{\text{pack}} = 2.26 k_{\text{B}}T$, $g_{\text{st}} = 1.13 k_{\text{B}}T$, $g_{\text{elec}} = -0.49 k_{\text{B}}T$, $g_{\text{mix}} = -1.15 k_{\text{B}}T$, and $g_{\text{ent}} = 4.41 k_{\text{B}}T$. The average value of g_{f} is $-7.63 k_{\text{B}}T$. Note that in calculating these average values, the Limit I and Limit II modeling results for ibuprofen were preaveraged before including them in the overall average. The average free-energy values predicted for the solubilization of all seven solubilizates in nonionic C₁₂E₈ or Brij-35 micelles are as follows: $g_{\text{tr}} = -15.9 k_{\text{B}}T$, $g_{\text{int}} = 2.84 k_{\text{B}}T$, $g_{\text{pack}} = 2.19 k_{\text{B}}T$, $g_{\text{st}} = 1.42 k_{\text{B}}T$, $g_{\text{elec}} = 0.00 k_{\text{B}}T$, $g_{\text{mix}} = -0.57 k_{\text{B}}T$, and $g_{\text{ent}} = 3.32 k_{\text{B}}T$. The average value of g_{f} is $-7.65 k_{\text{B}}T$. Finally, the average free-energy values predicted for the solubilization of all seven solubilizates in cationic CTAB micelles are as follows: $g_{\text{tr}} = -17.7 k_{\text{B}}T$, $g_{\text{int}} = 2.53 k_{\text{B}}T$, $g_{\text{pack}} = 2.21 k_{\text{B}}T$, $g_{\text{st}} = 1.03 k_{\text{B}}T$, $g_{\text{elec}} = -0.22 k_{\text{B}}T$, $g_{\text{mix}} = -1.15 k_{\text{B}}T$, and $g_{\text{ent}} = 7.04 k_{\text{B}}T$. The average value of g_{f} is $-7.52 k_{\text{B}}T$.

For each of the surfactant/solubilizate systems modeled, g_{tr} , g_{mix} , and, in some cases, g_{elec} are negative, and therefore, drive micelle formation in aqueous solution. The transfer free-energy contribution, g_{tr} , is the largest of the seven free-energy contributions in magnitude, and represents the primary driving force for micelle formation in aqueous solution. The other free-energy contributions are positive, and therefore, all oppose micelle formation.

Several chemical differences exist between the anionic, nonionic, and cationic sur-

Solubilization in Anionic SDS Micelles: Free-Energy Results									
Surf.	Sol.	g_f	g_{tr}	g_{int}	g_{pack}	g_{st}	g_{elec}	g_{mix}	g_{ent}
SDS	Ibuprofen (L1)	-9.11	-18.5	3.49	2.14	1.78	-0.89	-1.13	5.02
SDS	Ibuprofen (L2)	-10.3	-18.3	3.40	2.25	1.79	-1.07	-1.45	3.04
SDS	Benzamide	-6.02	-13.0	2.44	2.17	0.80	0.04	-1.14	3.89
SDS	Acetophenone	-6.88	-14.4	2.33	2.31	0.85	-0.45	-1.36	5.15
SDS	Benzonitrile	-6.17	-11.4	2.24	2.26	0.36	-0.04	-0.77	2.24
SDS	<i>o</i> -Aminobenzoate	-8.45	-16.7	2.71	2.45	1.40	-0.70	-1.22	5.14
SDS	<i>m</i> -Aminobenzoate	-7.69	-14.7	2.20	2.29	1.03	-0.44	-1.04	4.34
SDS	<i>p</i> -Aminobenzoate	-8.50	-8.14	3.42	2.16	1.70	-0.86	-1.20	6.07

Table 5.3: Hybrid computer simulation/molecular thermodynamic free-energy predictions for solubilization in anionic SDS micelles. All free energies are reported in units of $k_B T$, and L1 and L2 denote Limits I and II for ibuprofen discussed in the text.

Solubilization in Nonionic ($C_{12}E_8$ and Brij-35) Micelles: Free-Energy Results									
Surf.	Sol.	g_f	g_{tr}	g_{int}	g_{pack}	g_{st}	g_{elec}	g_{mix}	g_{ent}
$C_{12}E_8$	Ibuprofen (L1)	-11.1	-19.4	4.71	2.43	1.83	-0.06	-0.29	0.65
$C_{12}E_8$	Ibuprofen (L2)	-11.3	-19.2	4.35	2.43	1.52	0.13	-0.57	1.04
Brij-35	Benzamide	-6.13	-14.6	2.38	1.95	1.65	0.00	-0.64	4.11
Brij-35	Acetophenone	-6.95	-15.4	2.38	2.23	1.25	0.00	-0.60	4.17
Brij-35	Benzonitrile	-6.31	-14.2	2.07	2.15	1.12	0.00	-0.61	4.16

Table 5.4: Hybrid computer simulation/molecular thermodynamic free-energy predictions for solubilization in nonionic ($C_{12}E_8$ and Brij-35) surfactant micelles. All free-energies are reported in units of $k_B T$, and L1 and L2 denote Limits I and II for ibuprofen discussed in the text.

Solubilization in Cationic CTAB Micelles: Free-Energy Results									
Surf.	Sol.	g_f	g_{tr}	g_{int}	g_{pack}	g_{st}	g_{elec}	g_{mix}	g_{ent}
CTAB	Benzamide	-6.10	-16.0	2.34	2.19	1.03	0.05	-1.20	6.68
CTAB	Acetophenone	-6.86	-17.5	2.29	2.32	1.06	-0.38	-1.37	8.06
CTAB	Benzonitrile	-6.21	-15.1	2.06	2.18	0.77	-0.28	-1.17	6.56
CTAB	<i>o</i> -Aminobenzoate	-8.99	-17.4	2.46	1.89	0.83	-0.11	-0.98	5.51
CTAB	<i>m</i> -Aminobenzoate	-7.74	-17.7	2.13	2.22	1.19	-0.30	-1.00	7.00
CTAB	<i>p</i> -Aminobenzoate	-9.22	-22.4	3.90	2.47	1.32	-0.30	-1.18	8.45

Table 5.5: Hybrid computer simulation/molecular thermodynamic free-energy predictions for solubilization in cationic CTAB micelles. All free-energies are reported in units of $k_B T$.

factants considered: (i) the charge state of the surfactant head (anionic, nonionic, or cationic) and (if present) of its associated counterion, (ii) the head size ($a_h = 25 \text{ \AA}^2$ for SDS, 62.1 \AA^2 for C_{12}E_8 , 53.3 \AA^2 for Brij-35, and 32 \AA^2 for CTAB), (iii) differences in l_{hg} and d_{charge} , and (iv) the number of carbons in the surfactant tail (11 in SDS, 12 in C_{12}E_8 and Brij-35, and 15 in CTAB). Because each of the free-energy contributions to g_f computed for each solubilizate are coupled through the minimization procedure used to determine the optimal value of g_f , the effect of each of these chemical differences is manifested in all the computed free-energy contributions. Therefore, the size of each surfactant/solubilizate head, for example, not only affects the value of the steric free-energy contribution, g_{st} (see Chapter 4), but also affects the values of g_{tr} , g_{int} , g_{pack} , g_{elec} , g_{mix} , and g_{ent} .

Evaluating the Effect of Neutral Groups

As discussed in Section 5.4.1, neutral groups were identified for six of the seven solubilizates and are modeled differently than head or tail groups in the mean-field packing model. In contrast to head and tail groups, which are constrained to remain outside and inside the micelle core, respectively, these neutral groups are allowed to adopt positions in both the aqueous phase and within the micelle core when determining g_{pack} . In this section, the effect of including neutral groups on the packing free-energy contribution, g_{pack} , and on the volume of the solubilizate tail within the micelle core, v_a , are discussed for several representative cases. In Section 5.5.2, the effect of including neutral groups on the predicted micelle/water partition coefficients of several surfactant/solubilizate systems will be discussed.

In Figure 5-5, predicted g_{pack} values (defined on a per total number of molecules basis, and in $k_B T$ units) for SDS/aminobenzoate micelles are plotted *for the optimal predicted micelle shape* as a function of the core-minor radius, l_c , for fixed values of α_{mic} , given by: (i) $\alpha_{mic} = 0.25$ (—●—), (ii) $\alpha_{mic} = 0.50$ (—■—), (iii) $\alpha_{mic} = 0.75$ (—▲—), and (iv) $\alpha_{mic} = 1.00$ (—✕—). Recall that, as discussed in Section 5.1, $\alpha_{mic} = 1.0$ corresponds to a pure SDS micelle. In Figure 5-5A,

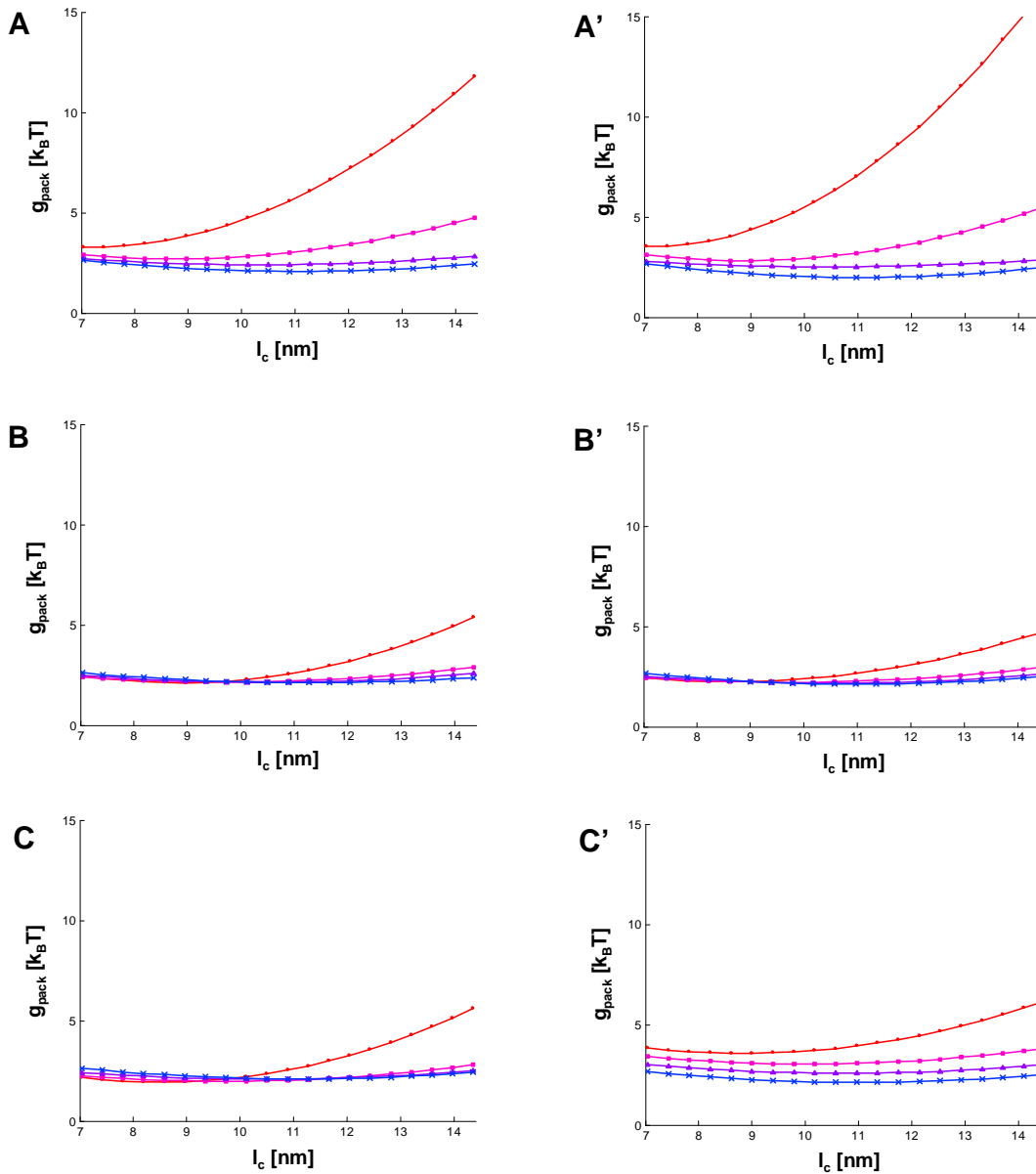


Figure 5-5: Predicted values of g_{pack} (in units of $k_B T$) corresponding to the solubilization of: *o*-aminobenzoate in cylindrical SDS micelles (with neutral groups, A, and without neutral groups, A'), *m*-aminobenzoate in cylindrical SDS micelles (with neutral groups, B, and without neutral groups, B'), and *p*-aminobenzoate in cylindrical SDS micelles (with neutral groups, C, and without neutral groups, C'). Results are presented as a function of l_c , and at four fixed values of α_{mic} : (i) $\alpha_{\text{mic}} = 0.25$ (—●—), (ii) $\alpha_{\text{mic}} = 0.50$ (—■—), (iii) $\alpha_{\text{mic}} = 0.75$ (—▲—), and (iv) $\alpha_{\text{mic}} = 1.00$ (—×—), where $\alpha_{\text{mic}} = 1.00$ corresponds to a pure SDS micelle.

predictions of g_{pack} are presented for cylindrical SDS/*o*-aminobenzoate micelles with neutral groups assigned, in Figure 5-5B, predictions of g_{pack} are presented for cylindrical SDS/*m*-aminobenzoate micelles with neutral groups assigned, and in Figure 5-5C, predictions of g_{pack} are presented for cylindrical SDS/*p*-aminobenzoate micelles with neutral groups assigned. In Figure 5-5A', predictions of g_{pack} are presented for cylindrical SDS/*o*-aminobenzoate micelles with no neutral groups assigned, in Figure 5-5B', predictions of g_{pack} are presented for cylindrical SDS/*m*-aminobenzoate micelles with no neutral groups assigned, and in Figure 5-5C', predictions of g_{pack} are presented for cylindrical SDS/*p*-aminobenzoate micelles with no neutral groups assigned.

Differences between plots A and A', B and B', and C and C' are most evident at large solubilizate concentrations in the micelle (corresponding to the lower α_{mic} values). The inclusion of neutral groups to evaluate g_{pack} has a small effect on the g_{pack} profiles for *o*-aminobenzoate (see A and A') and *m*-aminobenzoate (see B and B'), but it does have a significant effect in the case of *p*-aminobenzoate (see C and C'). Indeed, comparison of Figures 5-5C and 5-5C' shows that, in general, the g_{pack} profiles for *p*-aminobenzoate in SDS micelles are higher without the inclusion of neutral groups.

The g_{pack} values shown in Figures 5-5A, 5-5A', 5-5B, 5-5B', 5-5C, and 5-5C' are smooth functions of both l_c and α_{mic} . The addition of *o*-aminobenzoate increases g_{pack} at all plotted values of l_c and α_{mic} (regardless of whether or not neutral groups are used, see A and A'). In contrast, the addition of *m*-aminobenzoate decreases g_{pack} at small values of the core-minor radius ($l_c \lesssim 9.75$ nm) and increases g_{pack} at large values of the core-minor radius ($l_c \gtrsim 9.75$ nm) (again, regardless of whether or not neutral groups are used, see B and B'). With inclusion of neutral groups, the addition of *p*-aminobenzoate decreases g_{pack} at small values of the core-minor radius ($l_c \lesssim 10$ nm) and increases g_{pack} at large values of the core-minor radius ($l_c \gtrsim 10$ nm, see C). Without inclusion of neutral groups, the addition of *p*-aminobenzoate always leads to an increase in g_{pack} (see C'). Based on the neutral group g_{pack} results,

at the optimal micelle shape, core-minor radius, and composition predicted for each SDS/aminobenzoate micelle (see Section 5.5.2), the g_{pack} values are ranked as follows: p -aminobenzoate > m -aminobenzoate > o -aminobenzoate.

In Figure 5-6, the predicted g_{pack} values (defined on a per total number of molecules basis, and in $k_{\text{B}}T$ units) for CTAB/aminobenzoate micelles are plotted *for the optimal predicted micelle shape* as a function of the core-minor radius, l_c , for fixed values of α_{mic} , given by: (i) $\alpha_{\text{mic}} = 0.25$ (—●—), (ii) $\alpha_{\text{mic}} = 0.50$ (—■—), (iii) $\alpha_{\text{mic}} = 0.75$ (—▲—), and (iv) $\alpha_{\text{mic}} = 1.00$ (—✕—). Recall that $\alpha_{\text{mic}} = 1.0$ corresponds to a pure CTAB micelle. In Figure 5-6A, predictions of g_{pack} are presented for spherical CTAB/ o -aminobenzoate micelles with neutral groups assigned, in Figure 5-6B, predictions of g_{pack} are presented for cylindrical CTAB/ m -aminobenzoate micelles with neutral groups assigned, and in Figure 5-6C, predictions of g_{pack} are presented for spherical CTAB/ p -aminobenzoate micelles with neutral groups assigned. In Figure 5-6A', predictions of g_{pack} are presented for spherical CTAB/ o -aminobenzoate micelles with no neutral groups assigned, in Figure 5-6B', predictions of g_{pack} are presented for cylindrical CTAB/ m -aminobenzoate micelles with no neutral groups assigned, and in Figure 5-6C', predictions of g_{pack} are presented for spherical CTAB/ p -aminobenzoate micelles with no neutral groups assigned.

In contrast to the results presented in Figure 5-5, the use of neutral groups in evaluating g_{pack} has only a minor effect on the g_{pack} profiles of o -aminobenzoate and m -aminobenzoate, but it does have a visible effect on the g_{pack} profiles of p -aminobenzoate. Comparison of Figures 5-5C and 5-5C' shows that the g_{pack} profiles of p -aminobenzoate in the CTAB micelles are higher without the inclusion of neutral groups.

Similar to the g_{pack} profiles computed for SDS/aminobenzoate micelles, the g_{pack} profiles for CTAB/aminobenzoate micelles shown in Figures 5-6A, 5-6A', 5-6B, 5-6B', 5-6C, and 5-6C' are smooth functions of both l_c and α_{mic} . In general, the addition of o -aminobenzoate increases g_{pack} (both with and without neutral groups). The addition of m -aminobenzoate decreases g_{pack} at small values of the core-minor

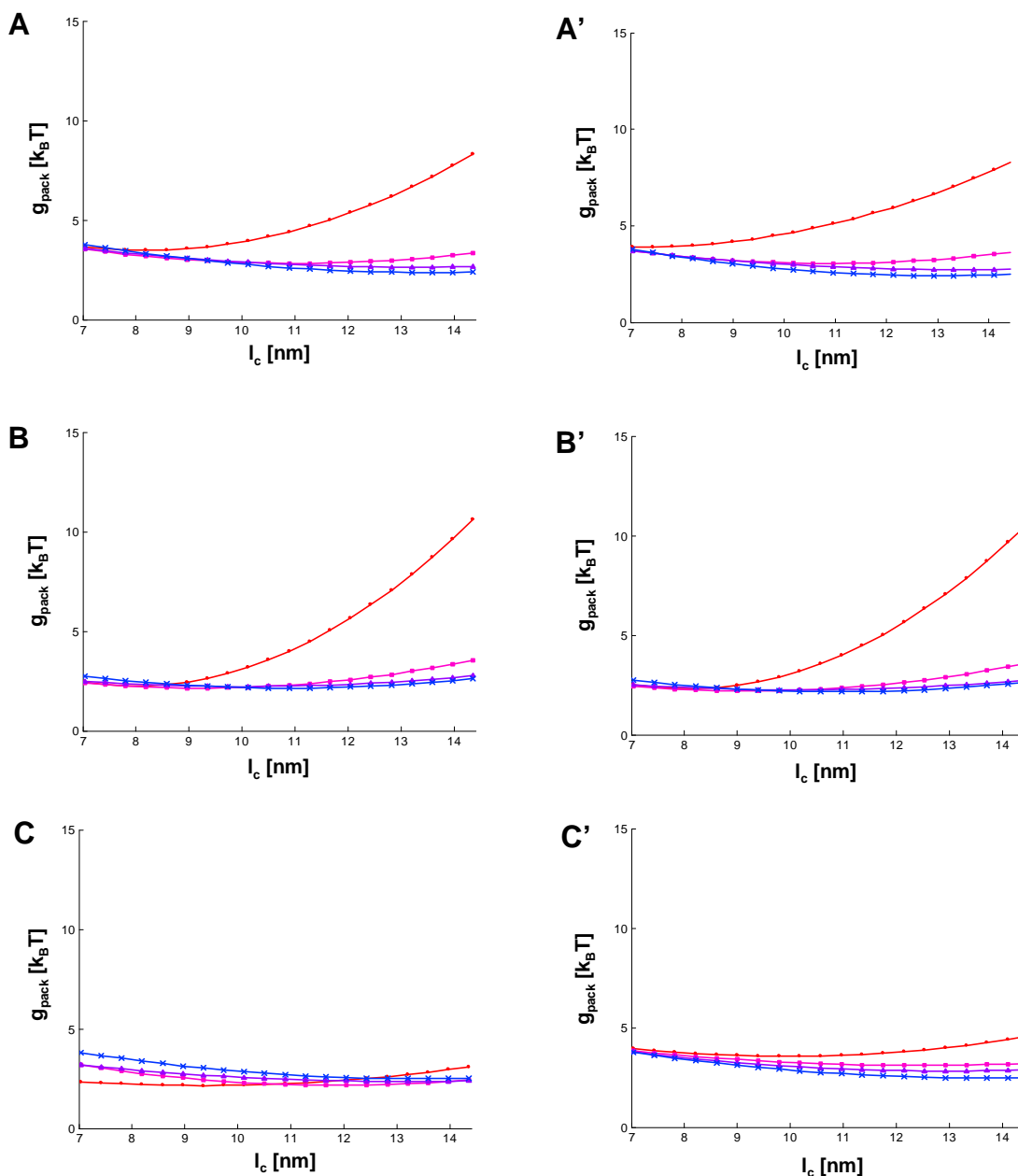


Figure 5-6: Predicted values of g_{pack} (in units of $k_B T$) corresponding to the solubilization of: *o*-aminobenzoate in spherical CTAB micelles (with neutral groups, A, and without neutral groups, A'), *m*-aminobenzoate in cylindrical CTAB micelles (with neutral groups, B, and without neutral groups, B'), and *p*-aminobenzoate in spherical CTAB micelles (with neutral groups, C, and without neutral groups, C'). Results are presented as a function of l_c and at four fixed values of α_{mic} : (i) $\alpha_{\text{mic}} = 0.25$ (—●—), (ii) $\alpha_{\text{mic}} = 0.50$ (—■—), (iii) $\alpha_{\text{mic}} = 0.75$ (—▲—), and (iv) $\alpha_{\text{mic}} = 1.00$ (—×—), where $\alpha_{\text{mic}} = 1.00$ corresponds to a pure CTAB micelle.

radius ($l_c \lesssim 8.5$ nm) and increases g_{pack} at large values of the core-minor radius ($l_c \gtrsim 8.5$ nm) (with and without neutral groups). With the inclusion of neutral groups, the addition of *p*-aminobenzoate decreases g_{pack} for all plotted values of l_c and α_{mic} , with the exception of $l_c \gtrsim 12.8$ nm and $\alpha_{\text{mic}} = 0.25$. However, without the inclusion of neutral groups, the addition of *p*-aminobenzoate increases g_{pack} for all plotted values of l_c and α_{mic} . Based on the neutral group g_{pack} results, at the optimal micelle geometry predicted for each CTAB/aminobenzoate micelle, the g_{pack} values are ranked as follows: *p*-aminobenzoate > *m*-aminobenzoate > *o*-aminobenzoate.

The results presented in Figures 5-5 and 5-6 demonstrate that the inclusion of the selected neutral groups does not always have a significant effect on g_{pack} . Nevertheless, as will be discussed in Section 5.5.2, the inclusion of neutral groups can greatly affect the predicted value of the micelle/water partition coefficient. For example, the micelle/water partition coefficient of *o*-aminobenzoate in SDS micelles was found to change significantly with the inclusion of neutral groups (even though g_{pack} is very similar for *o*-aminobenzoate with and without the inclusion of neutral groups, as shown in Figures 5-5A and 5-5A'). This results from the fact that inclusion of neutral groups causes a shift in the sphere-to-cylinder micelle shape transition point, which in turn results in cylinders being predicted as the optimal micelle shape at the solubility limit. In addition, the micelle/water partition coefficient of *p*-aminobenzoate in SDS micelles was found to change because, as shown in Figures 5-5C and 5-5C', the inclusion of neutral groups has a significant effect on the predicted values of g_{pack} for this solubilize. In all cases tested, the micelle/water partition coefficients predicted using neutral groups are more accurate relative to the experimental values than those predicted without the inclusion of neutral groups. Moreover, we would like to stress that the approach used in this chapter to: (i) identify neutral groups based on the computer simulation results, and (ii) model the neutral groups in the mean-field packing model, is consistent with the approach that was used successfully in a separate study to model the micellization behavior of a homologous series of DC_NAB cationic surfactants (see [32] and Chapter 8).

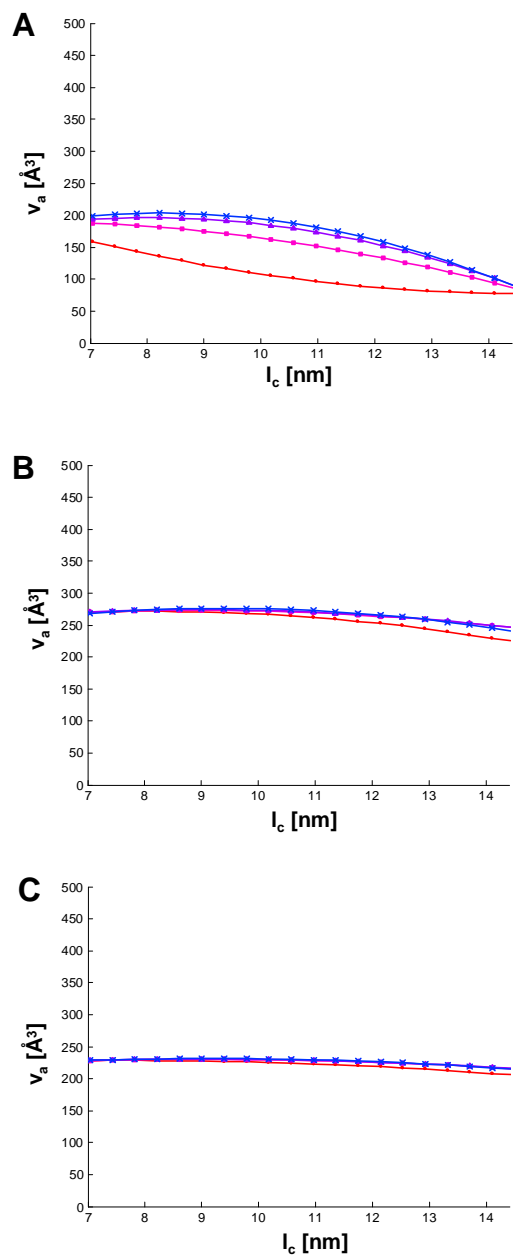


Figure 5-7: Predicted values of v_a (in units of \AA^3) corresponding to the solubilization of: *o*-aminobenzoate in cylindrical SDS micelles (A), *m*-aminobenzoate in cylindrical SDS micelles (B), and *p*-aminobenzoate in cylindrical SDS micelles (C). Results are presented as a function of l_c and at four fixed values of α_{mic} : (i) $\alpha_{\text{mic}} = 0.25$ (—●—), (ii) $\alpha_{\text{mic}} = 0.50$ (—■—), (iii) $\alpha_{\text{mic}} = 0.75$ (—▲—), and (iv) $\alpha_{\text{mic}} = 1.00$ (—×—), where $\alpha_{\text{mic}} = 1.00$ corresponds to a pure SDS micelle.

When one or more solubilizate groups are modeled as neutral groups, the volume of the solubilizate tail (v_a) within the micelle core is no longer a fixed quantity. Instead, v_a depends on both l_c and α_{mic} , and must be predicted using the mean-field packing model. As an illustration, in Figure 5-7, predicted values of v_a (in units of \AA^3) for *o*-, *m*-, and *p*-aminobenzoate solubilizates in SDS micelles are plotted *for the optimal predicted micelle shape* as a function of the core-minor radius, l_c , for fixed values of α_{mic} , given by: (i) $\alpha_{\text{mic}} = 0.25$ (—●—), (ii) $\alpha_{\text{mic}} = 0.50$ (—■—), (iii) $\alpha_{\text{mic}} = 0.75$ (—▲—), and (iv) $\alpha_{\text{mic}} = 1.00$ (—×—). In Figure 5-7A, predictions of v_a are presented for cylindrical SDS/*o*-aminobenzoate micelles, in Figure 5-7B, predictions of v_a are presented for cylindrical SDS/*m*-aminobenzoate micelles, and in Figure 5-7C, predictions of v_a are presented for cylindrical SDS/*p*-aminobenzoate micelles.

The v_a profiles computed for SDS/*o*-aminobenzoate decrease slightly as l_c increases (ranging from approximately 200 \AA^3 for $l_c = 7 \text{ nm}$ and $\alpha_{\text{mic}} = 1.00$ to approximately 75 \AA^3 for $l_c = 13.5 \text{ nm}$ and $\alpha_{\text{mic}} = 0.25$ (see A). In contrast, the v_a profiles for SDS/*m*-aminobenzoate micelles decrease only slightly as l_c increases (ranging from approximately 275 \AA^3 for $l_c = 7 \text{ nm}$ to approximately 225 \AA^3 for $l_c = 14.4 \text{ nm}$), in spite of the fact that *m*-aminobenzoate, like *o*-aminobenzoate, has one neutral group. The v_a profiles computed for SDS/*p*-aminobenzoate decrease slightly as l_c increases (ranging from approximately 230 \AA^3 for $l_c = 7 \text{ nm}$ and $\alpha_{\text{mic}} = 1.00$ to approximately 210 \AA^3 for $l_c = 14.4 \text{ nm}$ and $\alpha_{\text{mic}} = 0.50$). The v_a profiles computed for SDS/*p*-aminobenzoate exhibit less variation as a function of l_c and α_{mic} than those predicted for SDS/*o*-aminobenzoate, in spite of the fact that *p*-aminobenzoate has two neutral groups and *o*-aminobenzoate has only one. The results in Figure 5-7 demonstrate that the predicted v_a values are a complex function of the chemical structures of the surfactant/solubilizate tails, as well as of both the number and connectivity of the identified head, tail, and neutral groups.

5.5.2 Predictions of Micellar Solubilization Characteristics

Predictions of the hybrid computer simulation/molecular-thermodynamic model for the optimal micelle shape, core-minor radius (as characterized by l_c), degree of counterion binding (β_j), CMC, micelle composition (characterized by the surfactant mole fraction in the micelle, α_{mic}), and micelle/water partition coefficient (K_s or $\ln(K_x)$) are reported in Table 5.6 for solubilization in anionic SDS micelles, in Table 5.7 for solubilization in nonionic C₁₂E₈ or Brij-35 micelles, and in Table 5.8 for solubilization in cationic CTAB micelles.

Predictions of Micelle Shape

Both spherical and cylindrical optimal micelle shapes are predicted for the surfactant/solubilize systems modeled, although the majority of the surfactant/solubilize micelles (12 out of 17) are predicted to be cylindrical in shape (see Tables 5.6-5.8).

Predictions of Micelle Core-Minor Radius

There is significant variability in the predicted l_c values for different surfactant/solubilize systems. The smallest predicted l_c value corresponds to the benzonitrile/SDS micellar system ($l_c = 8.97 \text{ \AA}$), and the largest predicted l_c value corresponds to the *p*-aminobenzoate/CTAB system ($l_c = 19.6 \text{ \AA}$). The value of the micelle core-minor radius, l_c , is predicted to be 11.9 \AA on average for the SDS/solubilize micelles, 12.6 \AA on average for the C₁₂E₈ and Brij-35/solubilize micelles, and 15.0 \AA on average for the CTAB/solubilize micelles. In calculating these average values, the Limit I and Limit II modeling results for ibuprofen were preaveraged before being included in the overall average. These l_c results can be rationalized by noting that the anionic surfactant SDS has 11 of its carbon groups in its linear alkyl tail, the nonionic surfactants C₁₂E₈ and Brij-35 have 12 of their carbon groups in their tails, and the cationic surfactant CTAB has 15 of its carbon groups in its tail. In general, surfactants or solubilizates with long tails tend to form micelles with larger values of l_c upon self-assembly.

Predictions of the Degree of Counterion Binding

The average predicted value of $\beta_{\{c_j\}}$ (where $\beta_{\{c_j\}}$ is the average value of β_{c_j} for all the counterions present in the micellar solution) is 0.40 for SDS/solubilizate micelles, 0.01 for C₁₂E₈/ibuprofen micelles (the only nonionic surfactant system with a non-zero degree of counterion binding), and 0.33 for CTAB/solubilizate micelles (where averages have been computed as described in Section 5.5.2). In addition, the average value of $\beta_{\{c_j\}}$ is 0.41 for the cylindrical SDS or CTAB micelles, and 0.27 for the spherical SDS or CTAB micelles. Cylindrical micelles have a lower area per surfactant/solubilizate head than spherical micelles, and therefore, have a larger electrostatic potential at the micelle surface. This, in turn, promotes more counterion binding in the case of cylindrical micelles; consequently, the observed trend in counterion binding with micelle shape is consistent with what would be expected intuitively [8].

Predictions of the Critical Micelle Concentration

The average predicted value of the CMC is 11.0 mM for the anionic SDS/solubilizate system, 10.9 mM for nonionic C₁₂E₈ and Brij-35/solubilizate system, and 9.81 mM for cationic CTAB/solubilizate system (where averages were computed as described in Section 5.5.2). However, there is great variability in the predicted CMC values for different surfactant/solubilizate systems. The largest predicted CMC is for the SDS/benzamide system (18.0 mM), while the smallest predicted CMC is for the Limit 2 modeling of the C₁₂E₈/ibuprofen system (0.50 mM). Unfortunately, we were not able to find experimental CMC data for these systems for comparison with the predicted CMCs.

Predictions of Micelle Composition

The average predicted value of the micelle surfactant mole fraction, α_{mic} , is 0.66 for anionic SDS/solubilizate micelles, 0.61 for nonionic C₁₂E₈ and Brij-35/solubilizate micelles, and 0.57 for cationic CTAB/solubilizate micelles (where averages were computed as described in Section 5.5.2), with predicted values of α_{mic} ranging from 1.00

(predicted for Limit 1 modeling of the SDS/ibuprofen micellar system) to 0.24 (predicted for the SDS/benzonitrile micellar system). The primary driving force for the very large value of α_{mic} for the SDS/ibuprofen micellar system is the large disparity between the g_{tr} values of SDS and ibuprofen ($-11.55 k_{\text{B}}T$ and $-6.55 k_{\text{B}}T$, respectively). In contrast, the primary driving force for the small value of α_{mic} for the CTAB/benzamide micellar system is a combination of the g_{pack} , g_{st} , and g_{elec} free-energy contributions which each favor incorporation of benzamide into micelles in place of SDS.

Predictions of Micelle Partition Coefficients

The K_{s} and $\ln(K_{\text{x}})$ values reported in Tables 5.6, 5.7, and 5.8 include both predicted and experimentally measured micelle/water partition coefficients at the solubilize saturation (solubility) limit in solution. Theoretical predictions of K_{s} are reported for the micellar solubilization of ibuprofen, benzamide, acetophenone, and benzonitrile because K_{s} values were available experimentally. Similarly, theoretical predictions of $\ln(K_{\text{x}})$ are reported for *o*-, *m*-, and *p*-aminobenzoate in order to match the experimental data available in the literature. Partition coefficient results are discussed below separately for each surfactant/solubilize system considered.

K_{s} of Ibuprofen Theoretically predicted and experimental K_{s} values for micellar solutions of SDS/ibuprofen and C_{12}E_8 /ibuprofen are reported in Tables 5.6 and 5.7, respectively. As discussed in Section 5.4.1, two different modeling limits were explored for ibuprofen. In Limit I, group 4 shown in Figure 5-1 is modeled as being head, and in Limit II, it is modeled as being tail. These two limits are reported here because they correspond to the two modeling limits reported for ibuprofen in Chapter 3.

The Limit I theoretical predictions of K_{s} for the SDS/ibuprofen and C_{12}E_8 /ibuprofen micellar systems are 1.45 mol^{-1} and 318 mol^{-1} , respectively, while the experimental values are 605 and 1894, respectively [3]. Both theoretical predictions are in

Solubilization in Anionic SDS Micelles: Micellar Solubilization Results								
Surf.	Sol.	Shape	l_c [Å]	$\beta_{\{c_j\}}$	CMC [mM]	α_{mic}	K_s [mol ⁻¹]	Expt. K_s [mol ⁻¹]
SDS	Ibuprofen (L1)	Cyl.	12.1	0.67	5.99	1.00	1.45	605 [3]
SDS	Ibuprofen (L2)	Cyl.	12.1	0.69	1.53	0.89	429	605 [3]
SDS	Benzamide	Sph.	14.3	0.18	18.0	0.49	9.36	7.6 [33]
SDS	Acetophenone	Cyl.	11.6	0.34	12.7	0.56	17.5	17, 35, 48 [33]
SDS	Benzonitrile	Cyl.	8.97	0.08	15.29	0.24	16.23	33 [33]
							$\ln(K_x)$	Expt. $\ln(K_x)$
SDS	<i>o</i> -Aminobenzoate	Cyl.	12.2	0.52	8.99	0.81	7.52	9.25 [34]
SDS	<i>m</i> -Aminobenzoate	Cyl.	12.4	0.35	9.44	0.59	6.94	8.58 [34]
SDS	<i>p</i> -Aminobenzoate	Cyl.	12.0	0.65	8.89	0.97	5.88	8.81 [34]

Table 5.6: Micellar solubilization predictions made using the hybrid computer simulation/molecular thermodynamic model of solubilization in anionic SDS micelles. L1 and L2 denote Limit I and Limit II for ibuprofen discussed in the text.

Solubilization in Nonionic C ₁₂ E ₈ and Brij-35 Micelles: Micellar Solubilization Results								
Surf.	Sol.	Shape	l_c [Å]	$\beta_{\{c_j\}}$	CMC [mM]	α_{mic}	K_s [mol ⁻¹]	Expt. K_s [mol ⁻¹]
C ₁₂ E ₈	Ibuprofen (L1)	Sph.	15.0	$4.05 \cdot 10^{-4}$	0.77	0.91	318	1894 [3]
C ₁₂ E ₈	Ibuprofen (L2)	Sph.	15.4	0.01	0.50	0.75	908	1894 [3]
Brij-35	Benzamide	Cyl.	11.2	0.00	16.7	0.56	7.27	33 [33]
Brij-35	Acetophenone	Cyl.	12.3	0.00	12.1	0.58	13.7	26 [33]
Brij-35	Benzonitrile	Cyl.	11.8	0.00	14.0	0.47	11.6	23, 16 [33]

Table 5.7: Micellar solubilization predictions made using the hybrid computer simulation/molecular-thermodynamic model of solubilization in nonionic C₁₂E₈ and Brij-35 micelles. L1 and L2 denote Limit I and Limit II for ibuprofen discussed in the text.

Solubilization in Cationic CTAB Micelles: Micellar Solubilization Results								
Surf.	Sol.	Shape	l_c [Å]	$\beta_{\{c_j\}}$	CMC [mM]	α_{mic}	K_s [mol ⁻¹]	Expt. K_s [mol ⁻¹]
CTAB	Benzamide	Sph.	17.9	0.20	16.6	0.49	9.42	12, 10 [33]
CTAB	Acetophenone	Cyl.	14.4	0.55	12.4	0.55	20.2	26, 21, 18 [33]
CTAB	Benzonitrile	Cyl.	12.6	0.22	14.6	0.39	16.5	18, 20, 24 [33]
							$\ln(K_x)$	Expt. $\ln(K_x)$
CTAB	<i>o</i> -Aminobenzoate	Sph.	10.8	0.22	3.18	0.53	8.40	10.07 [34]
CTAB	<i>m</i> -Aminobenzoate	Cyl.	14.9	0.33	8.07	0.55	7.00	8.87 [34]
CTAB	<i>p</i> -Aminobenzoate	Sph.	19.6	0.48	4.00	0.88	7.27	9.33 [34]

Table 5.8: Micellar solubilization predictions made using the hybrid computer simulation/molecular-thermodynamic model of solubilization in cationic CTAB micelles.

poor agreement with the experimental data. The low values of K_s predicted by Limit I modeling are not surprising given the high values of α_{mic} predicted for the SDS/ibuprofen and C₁₂E₈/ibuprofen micelles. In contrast, the Limit II theoretical predictions of K_s for the SDS/ibuprofen and C₁₂E₈/ibuprofen micellar systems are 429 mol⁻¹ and 908 mol⁻¹, respectively, which are in much closer agreement with the experimental values (605 mol⁻¹ and 1894 mol⁻¹). The results indicate that if group 4 (see Figure 5-1) in ibuprofen is modeled as remaining fully hydrated in the micellar state rather than as being dehydrated, the incorporation of ibuprofen into the micellar environment is severely underpredicted. These results highlight the sensitivity of the modeling results to the head and tail assignments made. It is interesting to point out that in Chapter 3, where the solubilization of ibuprofen was modeled in a more approximate way, the Limit I and Limit II predictions for the solubilization of ibuprofen in SDS and C₁₂E₈ micelles bordered the experimental data. Here, the Limit II theoretical K_s predictions are in much better agreement with the experimental data than the Limit I K_s predictions, indicating that the net effect of implementing a more physically realistic description of the interfacial and packing free-energy contributions in the case of ibuprofen has been to decrease the driving force for ibuprofen incorporation into the micelles.

K_s of Benzamide Theoretically predicted K_s values for micellar systems of SDS/benzamide, Brij-35/benzamide, and CTAB/benzamide are 9.36 mol⁻¹, 7.27 mol⁻¹, and 9.42 mol⁻¹, respectively. The experimental K_s values are 7.6 mol⁻¹, 33 mol⁻¹, and either 12 or 10 mol⁻¹, respectively [33]. The predicted K_s values for the SDS/benzamide and CTAB/benzamide micellar systems are in good agreement with the experimental data, but the predicted K_s value for the Brij-35/benzamide micellar system is off by a factor of approximately four. Our theoretical model for g_{elec} favors incorporation of benzamide in anionic and cationic micelles more than it favors its incorporation in nonionic micelles because of the electrostatic benefit associated with the incorporation of a nonionic entity into a charged micelle. This is clearly reflected

in the predicted K_s values obtained using the hybrid model. The experimental result for the solubilization of benzamide in Brij-35 is surprising because it indicates that, in contrast to what is predicted theoretically and what would be expected intuitively, more benzamide is incorporated into Brij-35 micelles than into either SDS or CTAB micelles. The experimental data seems to suggest the existence of some type of specific interaction between benzamide and Brij-35 that is not included in the molecular-thermodynamic model, and that favors the incorporation of benzamide into Brij-35 micelles. Alternatively, the solubilization of benzamide occurs to some extent in the head-shell region (corona region) of the Brij-35 micelles. Solubilization in the corona region has not been accounted for in the molecular-thermodynamic model introduced in Chapter 4. Although neglecting corona-region solubilization is reasonable when modeling solubilization in small-head surfactants such as SDS and CTAB, it may not be a good approximation when modeling solubilization in the case of surfactants with polymeric heads such as Brij-35 (which contains 23 ethylene oxide groups).

K_s of Acetophenone Theoretically predicted K_s values for the SDS/acetophenone, Brij-35/acetophenone, and CTAB/acetophenone micellar systems are 17.5 mol^{-1} , 13.7 mol^{-1} , and 20.2 mol^{-1} , respectively. The experimental K_s values for the SDS/acetophenone micellar system are 17, 35, and 48 mol^{-1} (average = 33 mol^{-1}), 26 mol^{-1} for the Brij-35/acetophenone micellar system, and 26, 21, and 18 mol^{-1} (average = 21.7 mol^{-1}) for the CTAB/acetophenone micellar system [33]. The large variability in the experimental K_s values measured for the SDS/acetophenone and CTAB/acetophenone systems makes it difficult to evaluate the accuracy of the theoretical results. Nevertheless, the theoretical predictions of solubilization in all three surfactant systems considered appear reasonable. The molecular-thermodynamic model predicts that more acetophenone is incorporated into SDS and CTAB surfactant micelles than into Brij-35 surfactant micelles. The theoretical predictions make sense molecularly because, as discussed in the context of benzamide solubilization,

g_{elec} favors incorporation of acetophenone into anionic and cationic micelles more than it favors incorporation into nonionic micelles. Unfortunately, given the large variability observed in the experimental data, it is difficult to determine whether or not the experimental K_s data support the theoretically predicted trend in K_s values.

K_s of Benzonitrile Theoretically predicted K_s values for micellar solutions of SDS/benzonitrile, Brij-35/benzonitrile, and CTAB/benzonitrile are 16.2 mol^{-1} , 11.6 mol^{-1} , and 16.5 mol^{-1} , respectively. Similar to the acetophenone experimental data, the experimental K_s values for the solubilization of benzonitrile in SDS, Brij-35, and CTAB micelles show large variability. The experimental K_s values for the SDS/benzonitrile system is 33 mol^{-1} , the experimental K_s values for the Brij-35/benzonitrile system are 23 and 16 mol^{-1} (average = 19.5 mol^{-1}), and the experimental K_s values for the CTAB/benzonitrile system are 18, 20, and 24 mol^{-1} (average = 20.7 mol^{-1}) [33]. The large variability in the experimental K_s values makes it difficult to evaluate the accuracy of the theoretical K_s results, although in general, the theoretical predictions of solubilization in the three surfactant systems considered appear quite reasonable.

$\ln(K_x)$ of the Aminobenzoates In Tables 5.6 and 5.8, theoretically predicted $\ln(K_x)$ values for *o*-, *m*-, and *p*-aminobenzoate are compared with experimental $\ln(K_x)$ values.

Theoretically predicted $\ln(K_x)$ values for micellar solutions of SDS/*o*-aminobenzoate and CTAB/*o*-aminobenzoate are 7.52 mol^{-1} and 8.40 mol^{-1} , respectively. In comparison, the experimental $\ln(K_x)$ values for micellar solutions of SDS/*o*-aminobenzoate and CTAB/*o*-aminobenzoate are 9.25 mol^{-1} and 10.07 mol^{-1} , respectively [34]. The theoretical $\ln(K_x)$ values are 17.6% smaller on average than the experimental $\ln(K_x)$ values. To evaluate to what extent inclusion of neutral groups in the mean-field packing model affects the predicted $\ln(K_x)$ values, we also modeled the SDS/*o*-aminobenzoate system without the inclusion of any neutral groups and using the head and tail assignments reported in Figure 5-3. Without the inclusion of neutral

groups, the predicted $\ln(K_x)$ value is 3.34 mol^{-1} , and the optimal micelle is predicted to be spherical in shape. Clearly, the inclusion of neutral groups has a significant effect on the predicted value of $\ln(K_x)$ for the SDS/*o*-aminobenzoate system and yields a $\ln(K_x)$ value which is in poor agreement with the experimental $\ln(K_x)$ value (9.25 mol^{-1}). This results from the fact that the optimal micelle shape is predicted to be different with the inclusion (cylindrical) and without the inclusion (spherical) of neutral groups in the evaluation of g_{pack} .

The theoretically predicted $\ln(K_x)$ values for micellar solutions of SDS/*m*-aminobenzoate and CTAB/*o*-aminobenzoate are 6.94 mol^{-1} and 7.00 mol^{-1} , respectively. In comparison, the experimental $\ln(K_x)$ values for micellar systems of SDS/*m*-aminobenzoate and CTAB/*m*-aminobenzoate are 8.58 mol^{-1} and 8.87 mol^{-1} , respectively [34]. The theoretical $\ln(K_x)$ values are 20.1% smaller on average than the experimental $\ln(K_x)$ values. Without the inclusion of neutral groups, the predicted $\ln(K_x)$ value for the SDS/*m*-aminobenzoate system is 6.88 mol^{-1} , and the optimal micelle is predicted to be cylindrical in shape. For this surfactant/solubilizate system, the inclusion of neutral groups shifts the predicted $\ln(K_x)$ value slightly away from the experimental $\ln(K_x)$ value. The predicted $\ln(K_x)$ value for the SDS/*m*-aminobenzoate system does not change appreciably because, as shown in Figures 5-5B and 5-5B', g_{pack} is not greatly affected by the inclusion of neutral groups for this system.

Finally, the theoretically predicted $\ln(K_x)$ values for micellar systems of SDS/*p*-aminobenzoate and CTAB/*o*-aminobenzoate are 5.88 mol^{-1} and 7.27 mol^{-1} , respectively. In comparison, the experimental $\ln(K_x)$ values for micellar systems of SDS/*p*-aminobenzoate and CTAB/*p*-aminobenzoate are 8.81 mol^{-1} and 9.33 mol^{-1} , respectively [34]. The theoretical $\ln(K_x)$ values are 27.7% smaller on average than the experimental $\ln(K_x)$ values. Without the inclusion of neutral groups, the predicted $\ln(K_x)$ value for the SDS/*p*-aminobenzoate system is 4.24 mol^{-1} , and the optimal micelle is predicted to be cylindrical in shape. For this surfactant/solubilizate system, the significant difference in the predicted value of $\ln(K_x)$ arises from the change in g_{pack} associated with the inclusion of neutral groups (see Figures 5-5C and 5-5C').

As discussed in Chapter 4, the micellar solubilization behavior of *o*-, *m*-, and *p*-aminobenzoate is quite interesting from a theoretical perspective. Although only small structural differences exist between these three solubilizates, there are significant differences in their micelle/water partition coefficients. The experimental ranking of micelle/water partition coefficients in both SDS and CTAB surfactant micelles is *o*-aminobenzoate > *p*-aminobenzoate > *m*-aminobenzoate. The ranking predicted theoretically is *o*-aminobenzoate > *m*-aminobenzoate > *p*-aminobenzoate for solubilization in SDS micelles, and *o*-aminobenzoate > *p*-aminobenzoate > *m*-aminobenzoate for solubilization in CTAB micelles.

5.5.3 Sensitivity of the Theoretical Predictions to Salt Concentration

All theoretical predictions were made for aqueous solutions containing 10 mM of sodium chloride. As discussed at the beginning of Section 5.5, this salt concentration was selected because: (i) the ionic species and their concentrations in solution were not specified in our literature sources of experimental data, and (ii) solubilization measurements are typically made in a buffered solution which can be approximated reasonably well as a salt solution of low-concentration [2]. The sensitivity of the predictions of the hybrid computer simulation/molecular-thermodynamic model to salt concentration is discussed briefly in this section.

Molecular-thermodynamic predictions of the micelle/water partition coefficient, K_s , for acetophenone and benzamide, as well as of the natural logarithm of the micelle/water partition coefficient, $\ln(K_x)$, for *m*-aminobenzoate, were made in SDS, Brij-35, and CTAB micellar solutions with 0 mM, 10 mM, 25 mM, and 50 mM of added sodium chloride. The predicted values of K_s and $\ln(K_x)$ were found to be extremely insensitive to the NaCl concentration for the solubilization of the three solubilizates considered in the nonionic Brij-35 micellar systems (results not shown). This result is intuitively expected because the primary effect of NaCl is to affect the

electrostatic free-energy contribution, g_{elec} . Because g_{elec} is equal to zero for each solubilize/Brij-35 system, the addition of NaCl to the aqueous solution has little effect on the predicted K_s or $\ln(K_x)$ values.

In contrast, the concentration of added NaCl in the aqueous solution was found to have a significant effect on the predicted values of K_s and $\ln(K_x)$ for the solubilization of the three solubilizes considered in the anionic SDS and in the cationic CTAB micellar solutions. The dependence of K_s and $\ln(K_x)$ on NaCl concentration for the solubilization of the three solubilizes in SDS micelles is reported in Figure 5-8, and the dependence of K_s and $\ln(K_x)$ on NaCl concentration for the solubilization of the three solubilizes in CTAB micelles is reported in Figure 5-9. In general, the effect of the inclusion of NaCl was to lower K_s or $\ln(K_x)$. As NaCl is added to the aqueous solution, it reduces g_{elec} by decreasing electrostatic repulsions at the micelle surface, which serves to make the incorporation of each nonionic solubilize into anionic SDS or cationic CTAB micelles less thermodynamically favorable than the incorporation of each nonionic solubilize at lower NaCl concentrations.

5.6 Conclusions

In this chapter, a hybrid computer simulation/molecular-thermodynamic modeling approach was used to model the solubilization of ibuprofen, benzamide, acetophenone, benzonitrile, *o*-aminobenzoate, *m*-aminobenzoate, and *p*-aminobenzoate in SDS, C₁₂E₈, Brij-35, and CTAB micelles. The hybrid modeling approach used MD simulations to estimate the hydrated and the unhydrated portions of each solubilize in a micellar environment. From the computer simulation results presented in Chapter 4, inputs were determined for each solubilize in order to implement molecular-thermodynamic modeling. Head and tail identifications were made in order to evaluate g_{tr} and g_{int} , and head, tail, neutral, and reference head group identifications were made in order to evaluate g_{pack} . The molecular-thermodynamic model of solubilization used in this chapter consists of two elements: (i) a macroscopic thermodynamic description of the

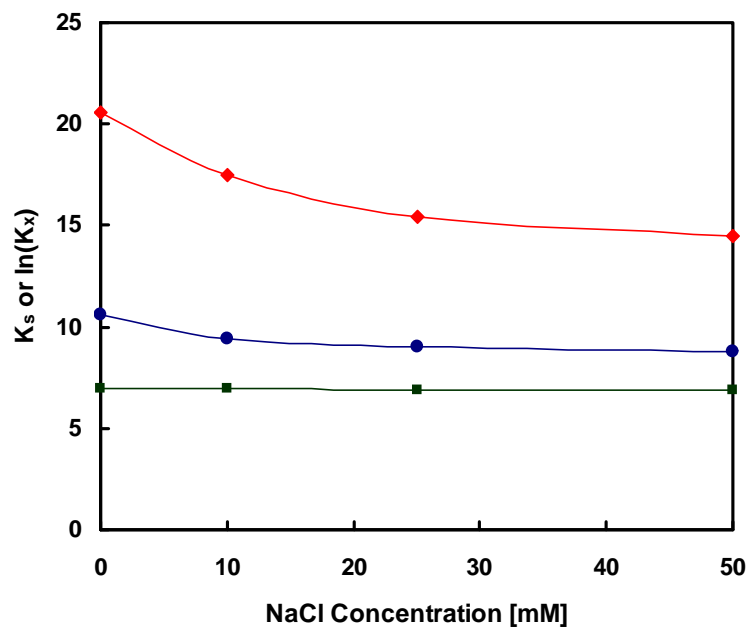


Figure 5-8: Predicted effect of the solution NaCl concentration on the micelle/water partition coefficient for the solubilization of acetophenone in SDS micelles (K_s , —◆—), benzamide in SDS micelles (K_s , —●—), and *m*-aminobenzoate in SDS micelles ($\ln(K_x)$, —■—). The lines are shown as a guide to the eye.

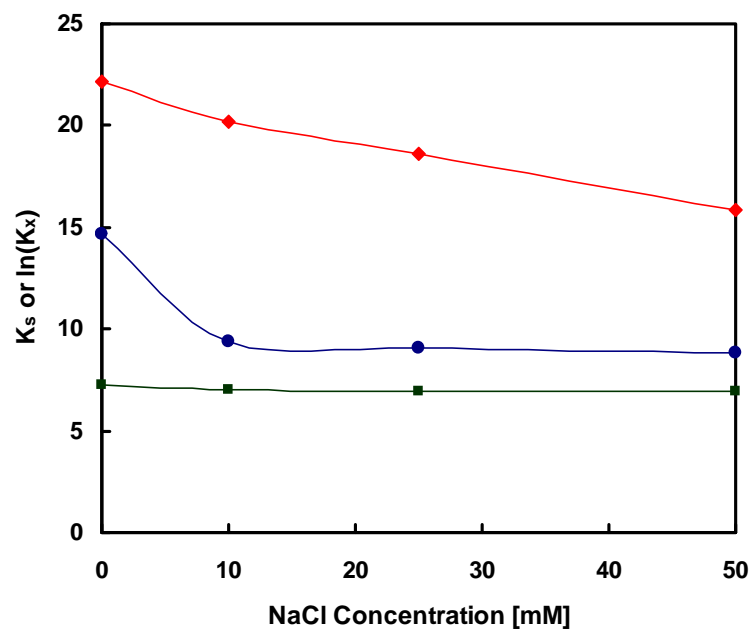


Figure 5-9: Predicted effect of the solution NaCl concentration on the micelle/water partition coefficient for the solubilization of acetophenone in CTAB micelles (K_s , \blacklozenge), benzamide in CTAB micelles (K_s , \bullet), and *m*-aminobenzoate in CTAB micelles ($\ln(K_x)$, \blacksquare). The lines are shown as a guide to the eye.

surfactant and solubilize aqueous solution, and (ii) a molecular model that is used to evaluate the free-energy change associated with transferring surfactants and solubilizes from their reference states in aqueous solution to form a surfactant/solubilize micellar aggregate in aqueous solution.

Using the hybrid computer simulation/molecular-thermodynamic modeling approach, theoretical predictions were made for the free energy associated with micelle formation and for the optimal micelle shape, core-minor radius, degree of counterion binding, CMC, micelle composition, and micelle/water partition coefficient of a total of 17 different surfactant/solubilize systems. Both spherical and cylindrical micelle shapes were predicted for the surfactant/solubilize systems modeled. The average micelle core-minor radius was predicted to be 11.9 Å for SDS/solubilize micelles, 12.6 Å for C₁₂E₈ and Brij-35/solubilize micelles, and 15.0 Å for CTAB/solubilize micelles. The average degree of counterion binding, $\beta_{\{c_j\}}$, was predicted to be 0.41 for the cylindrical ionic surfactant micelles, and 0.27 for the spherical ionic surfactant micelles, indicating that counterion binding is higher in micelles with a higher electrostatic potential at the micelle core/water interface. Predicted values of the surfactant/solubilize CMC and the micelle composition varied significantly from system to system, with the highest predicted CMC of 18.0 mM corresponding to the SDS/benzamide system and the lowest predicted CMC of 0.5 mM corresponding to Limit 2 modeling of the C₁₂E₈/ibuprofen system. Theoretical predictions of the micelle/water partition coefficients, K_s or $\ln(K_x)$, were also made and compared with the experimental K_s or $\ln(K_x)$ values, for each of the 17 surfactant/solubilize systems modeled in this chapter.

The average absolute discrepancy between the theoretically predicted and experimentally measured K_s values reported in this chapter (where the predicted K_s value for ibuprofen was taken as the average of the Limit I and Limit II predictions) is 46.5% for solubilization in SDS micelles, 58.4% for solubilization in C₁₂E₈ or Brij-35 micelles, and 13.7% for solubilization in CTAB micelles. The average absolute discrepancy between the theoretically predicted and experimentally measured $\ln(K_x)$

values reported in this chapter is 23.7% for solubilization in SDS micelles and 19.9% for solubilization in CTAB micelles.

The sensitivity of the theoretically predicted K_s values to the solution concentration of NaCl was investigated for the solubilization of acetophenone, benzamide, and *o*-aminobenzoate in SDS, Brij-35, and CTAB micelles. It was found that for the solubilization of these solubilizates in Brij-35 micelles, the predicted K_s values were very insensitive to the solution NaCl concentration — a finding that is expected because the electrostatic contribution to the free energy of micelle formation is negligible for nonionic systems. However, for some of the ionic surfactant/nonionic solubilizate micellar systems considered, the solution NaCl concentration was found to have a significant effect on the predicted K_s values. For example, the predicted value of K_s for the solubilization of acetophenone in SDS and CTAB micelles decreased by 29.6% and 28.3%, respectively, as the NaCl concentration was increased from 0 mM to 50 mM. In many cases, the composition of salt species and the ionic strength of the aqueous solution corresponding to a specific experimentally measured micelle/water partition coefficient are not reported in the literature. Consequently, care must be taken when comparing theoretically predicted K_s or $\ln(K_x)$ values with experimentally reported values, including the experimental K_s or $\ln(K_x)$ values that were used in this chapter for comparison with the theoretically predicted K_s or $\ln(K_x)$ values.

A useful approach to evaluate the accuracy of the hybrid computer simulation/molecular-thermodynamic modeling approach used in this chapter is to determine the average absolute discrepancy between the experimental K_s or $\ln(K_x)$ values and a K_s or $\ln(K_x)$ value estimated by making the assumption that each micelle is composed of 50% surfactant and 50% solubilizate. As discussed in Chapter 4, $K_s = X_{\text{sol}}^{\text{mic}} / [C_{\text{sol}}^{\text{aq}}(1 - X_{\text{sol}}^{\text{mic}})]$ and $\ln(K_x) = \ln(X_{\text{sol}}^{\text{mic}} / X_{\text{sol}}^{\text{aq}})$, where $X_{\text{sol}}^{\text{mic}}$ is the mole fraction of solubilizate in micelles, $X_{\text{sol}}^{\text{aq}}$ is the mole fraction of solubilizate in aqueous solution, and $C_{\text{sol}}^{\text{aq}}$ is the concentration of solubilizate in aqueous solution in units of moles per liter. Setting $X_{\text{sol}}^{\text{mic}} = 0.5$ in the expressions for K_s and $\ln(K_x)$ yields the following expressions: $K_s = 1/C_{\text{sol}}^{\text{aq}}$ and $\ln(K_x) = \ln(0.5/X_{\text{sol}}^{\text{aq}})$. These two expressions represent the best possible esti-

mate of K_s or $\ln(K_x)$ (i.e. the estimates that on average would yield the least error in comparison with experimental data) that can be made in the absence of a theoretical model that allows prediction of the composition of the micelles that form in solution, or in the absence of experimental data that suggests a more reasonable value of $X_{\text{sol}}^{\text{mic}}$. To be of value, a theoretical model of micellar solubilization (such as the hybrid model used in this chapter) must yield better predictions of K_s or $\ln(K_x)$ on average than the simple formulas $K_s = 1/C_{\text{sol}}^{\text{aq}}$ and $\ln(K_x) = \ln(0.5/X_{\text{sol}}^{\text{aq}})$, respectively. The average absolute discrepancy between the experimentally measured K_s and $\ln(K_x)$ values and the predicted K_s or $\ln(K_x)$ values for all the solubilizates considered is 34.8%, while the average absolute discrepancy between the experimentally measured K_s or $\ln(K_x)$ values and the predictions based on $K_s = 1/C_{\text{sol}}^{\text{aq}}$ and $\ln(K_x) = \ln(0.5/X_{\text{sol}}^{\text{aq}})$ is 47.2%. However, as just discussed, all the K_s and $\ln(K_x)$ values predicted in this chapter were made with an assumed value of 10 mM NaCl concentration in aqueous solution. To more rigorously evaluate the validity and accuracy of the hybrid model, it would be necessary to know the identity and concentration of salt in aqueous solution corresponding to the experimental data, and to make theoretical predictions of solubilization behavior at the same solution conditions. Furthermore, additional testing of the hybrid model of micellar solubilization by comparing other solubilization-related predicted properties (including micelle shape, core-minor radius, composition, degree of counterion binding, and CMC) with experimental data should be carried out.

Although the chemical structures of the solubilizates modeled in this chapter are similar in the sense that they all contain a single semipolar phenyl group and one or more hydrophilic polar groups, a broad range of micellar solubilization behavior is experimentally observed and was predicted using the hybrid computer simulation/molecular-thermodynamic modeling approach used in this chapter. Subtle differences in solubilizate chemical structure can have a large impact on solubilization behavior, as demonstrated by the very different micelle/water partition coefficients observed experimentally in the case of *o*-, *m*-, and *p*-aminobenzoate in SDS and CTAB micellar solutions. This interesting solution behavior arises from a

complex interplay of transfer, interfacial, packing, steric, electrostatic, mixing, and entropic free-energy contributions to the free energy associated with micelle formation. Each of these free-energy contributions can be predicted and understood using the hybrid computer simulation/molecular thermodynamic model used in this chapter, thus providing a fundamental, molecular-level understanding of the predicted properties in addition to quantifying their values.

In the next chapter, Chapter 6, a novel computer simulation/molecular-thermodynamic (CS-MT) modeling approach will be introduced that enables more accurate quantification of the hydrophobic driving force for micelle formation. By more accurately quantifying this hydrophobic driving force, the CS-MT model enables theoretical modeling of the self-assembly of significantly more complex surfactant/solubilizate systems than has been possible to date. The CS-MT modeling approach is validated in Chapter 6 by using it to model the formation of 15 oil aggregates in aqueous solution. In Chapter 7, the CS-MT model is used to model the micellization of seven nonionic surfactants in aqueous solution, and in Chapter 8 the CS-MT model is used to model the micellization of nine anionic, zwitterionic, and cationic surfactants in aqueous solution.

Bibliography

- [1] Srinivasan, V., *Theoretical Modeling of Micellization and Solubilization in Ionic Surfactant Systems*, Ph.D. thesis, Massachusetts Institute of Technology, 2003, and references cited therein.
- [2] Goldsipe, A. and Blankschtein, D., “Modeling counterion binding in ionic-nonionic and ionic-zwitterionic binary surfactant mixtures,” *Langmuir*, Vol. 22, 2005, pp. 9850–9865.
- [3] Stephenson, B. C., Rangel-Yagui, C. O., Pessoa, A., Tavares, L. C., Beers, K. J., and Blankschtein, D., “Experimental and theoretical investigation of the micellar-assisted solubilization of ibuprofen in aqueous media,” *Langmuir*, Vol. 22, 2006, pp. 1514–1525.
- [4] Puvvada, S. and Blankschtein, D., “Molecular thermodynamic approach to predict micellization, phase behavior and phase separation of micellar solutions. 1. Application to nonionic surfactants,” *The Journal of Chemical Physics*, Vol. 92, 1990, pp. 3710–3724, and references cited therein.
- [5] Stephenson, B. C., Beers, K., and Blankschtein, D., “Complementary use of simulations and molecular-thermodynamic theory to model micellization,” *Langmuir*, Vol. 22, 2006, pp. 1500–1513.
- [6] ChemSW, Inc., Fairfield, CA., *Molecular Modeling Pro version 3.2*, 2003.

- [7] Szleifer, I., "Protein adsorption on tethered polymer layers: Effect of polymer chain architecture and composition," *Physica A: Statistical Mechanics and Its Applications*, Vol. 244, 1997, pp. 370–388.
- [8] Srinivasan, V. and Blankschtein, D., "Effect of counterion binding on micellar solution behavior: 1. Molecular-thermodynamic theory of micellization of ionic surfactants," *Langmuir*, Vol. 19, 2003, pp. 9932–9945.
- [9] Smith, R. and Tanford, C., "Hydrophobicity of long chain n-alkyl carboxylic acids, as measured by their distribution between heptane and aqueous solutions," *Proceedings of the National Academy of Sciences*, Vol. 70, 1973, pp. 289–293.
- [10] Tetko, I. and Tanchuk, V. Y., "Virtual Computational Chemistry Laboratory webpage," 2005.
- [11] Tetko, I. and Tanchuk, V. Y., "Application of associative neural networks for prediction of lipophilicity in ALOGPS 2.1 program," *Journal of Chemical Information and Computer Science*, Vol. 42, 2002, pp. 1136–1145.
- [12] Stephenson, B. C., Goldsipe, A., Beers, K. J., and Blankschtein, D., "Quantifying the hydrophobic effect: I. A computer simulation/molecular-thermodynamic model for the aqueous self-assembly of hydrophobic and amphiphilic solutes," *The Journal of Physical Chemistry B*, 2006, pp. (submitted).
- [13] Gibbs, J. W., *The Scientific Papers of J.W. Gibbs*, Vol. 1, Dover, New York, 1961.
- [14] Koenig, F. O., "On the thermodynamic relation between surface tension and curvature," *The Journal of Chemical Physics*, Vol. 18, 1950, pp. 449.
- [15] Buff, F. P., "The spherical interface. I. Thermodynamics," *The Journal of Chemical Physics*, Vol. 19, 1951, pp. 1591.
- [16] Tolman, R. C., "Consideration of the Gibbs theory of surface tension," *The Journal of Chemical Physics*, Vol. 16, 1948, pp. 758.

- [17] Tanford, C., *The Hydrophobic Effect: Formation of Micelles and Biological Membranes*, John Wiley and Sons, New York, 1991.
- [18] Aveyard, R., Briscoe, B. J., and Chapman, J., "Adhesion at the alkane/water and ester/water interfaces," *Journal of the Chemical Society, Faraday Transactions*, Vol. 68, 1972, pp. 10.
- [19] Reddy Karri, S. B. and Mathur, V. K., "Measurement of interfacial tension of immiscible liquids of equal density," *American Institute of Chemical Engineering Journal*, Vol. 34, 1988, pp. 155.
- [20] Lam, A., Sathyagal, A. N., Kumar, S., and Ramkrishna, D., "Maximum stable drop diameter in stirred dispersions," *American Institute of Chemical Engineering Journal*, Vol. 42, 1996, pp. 1547.
- [21] Girifalco, L. A. and Good, R. J., "A theory for the estimation of surface and interfacial energies. I. Derivation and application to interfacial tension," *The Journal of Physical Chemistry*, Vol. 61, 1956, pp. 904.
- [22] Reinhard, M. and Drefahl, A., *Estimating physiochemical properties of organic compounds*, John Wiley and Sons, Inc., New York, 1999.
- [23] Flory, P., *Statistical Mechanics of Chain Molecules*, Wiley, New York, 1969.
- [24] Abe, A., Jernigan, R. L., and Flory, P. J., "Conformational energies of n-alkanes and the random configuration of higher homologs including polymethylene," *Journal of the American Chemical Society*, Vol. 88, 1966, pp. 631.
- [25] Dunaway, C. S., Christian, S. D., and Scamehorn, J. F., *Solubilization in Surfactant Aggregates. Surfactant Science Series 55*, Marcel Dekker, New York, 1995.
- [26] Nagarajan, R., "Solubilization in aqueous solutions of amphiphiles," *Current Opinion in Colloid and Interface Science*, Vol. 1, 1996, pp. 391–401.

- [27] Rouse, J. D., Sabatini, D. A., Deeds, N. E., and Brown, R. E., "Micellar solubilization of unsaturated hydrocarbon concentrations as evaluated by semiequilibrium dialysis," *Environmental Science and Technology*, Vol. 29, 1995, pp. 2484–2489.
- [28] In Christian, S. D. and Scamehorn, J. F., *Solubilization in Surfactant Aggregates. Surfactant Science Series 55*, Marcel Dekker, New York, 1995.
- [29] Christian, S. D., Smith, L. S., Bushong, D. S., and Tucker, E. E., "Solubilization of benzene and cyclohexane by sodium deoxycholate micelles," *Journal of Colloid and Interface Science*, Vol. 89, 1982, pp. 514–522.
- [30] Elworthy, P. H., Florence, A. T., and Macfarlane, C. B., *Solubilization by Surface Active Agents*, Chapman and Hall, London, 1968.
- [31] Dunaway, C. S., Christian, S. D., Scamehorn, J. F., and In Christian, S. D., *Solubilization in Surfactant Aggregates. Surfactant Science Series 55*, Marcel Dekker, New York, 1995.
- [32] Stephenson, B. C., Beers, K. J., and Blankschtein, D., "Quantifying the hydrophobic effect: III. A computer simulation/molecular-thermodynamic model for the micellization of ionic and zwitterionic surfactants," *The Journal of Physical Chemistry B*, 2006, pp. (submitted).
- [33] Quina, F. H., Alonso, E. O., and Farah, J. P. S., "Incorporation of nonionic solutes into aqueous micelles: A linear solvation free energy relationship analysis," *The Journal of Physical Chemistry*, Vol. 99, 1995, pp. 11708–11714.
- [34] Mukerjee, P. and Ko, J.-S., "Solubilization of ethyl o-, m-, and p-aminobenzoates in micelles of different charge types: Interfacial adsorption and orientation effects," *The Journal of Physical Chemistry*, Vol. 96, 1992, pp. 6090–6094.

Chapter 6

Quantifying the Hydrophobic Effect: I. A Computer Simulation/Molecular-Thermodynamic Model for the Self-Assembly of Hydrophobic and Amphiphilic Solutes in Aqueous Solution

6.1 Introduction

Surfactants are molecules consisting of a hydrophilic moiety, referred to as the “head,” attached to a hydrophobic moiety, referred to as the “tail.” This dual nature of surfactants leads to very interesting behavior in aqueous solution. Above a threshold surfactant concentration, known as the critical micelle concentration, or CMC, the

surfactant molecules self-assemble into aggregates known as micelles with their hydrophobic tails partly shielded from water in the aggregate interior (the aggregate core), and their hydrophilic heads exposed to water at the aggregate surface.

The solubility of chemicals that have limited solubility in aqueous solution can be increased through the addition of surfactants [1–4]. These chemicals are frequently referred to as solubilizates, and they may be either completely hydrophobic or amphiphilic (containing both hydrophilic and hydrophobic moieties). Amphiphilic solubilizates may behave much like conventional surfactants within a micellar environment, and their incorporation into micelles can be accurately modeled using theories developed originally to model mixed surfactant micellization [5]. However, unlike surfactants, solubilizates have a solubility limit, rather than a CMC, in aqueous solution, and without added surfactant they do not spontaneously self-assemble to form micelles.

The hydrophobic effect, or the increase in solution free energy observed upon addition of nonpolar solutes to water, is the primary driving force responsible for surfactant self-assembly in aqueous solution [6]. It is also the primary driving force responsible for solubilizate incorporation into surfactant micelles in aqueous solution. In addition to the hydrophobic effect, the process of micelle self-assembly is also mediated by van der Waals, hydrogen-bonding, and screened electrostatic interactions (in the case of charged surfactants) [7].

Gaining a fundamental understanding of the process of micellization and micellar solubilization in aqueous solution is both of academic and practical interest. A number of theoretical approaches have been developed to enable the prediction of equilibrium properties of self-assembled surfactant/solubilizate systems in aqueous solution based on the chemical structures of the solution components and the solution conditions (such as the temperature, the pressure, and the ionic strength) [8–13]. Among the equilibrium micellar solution properties which can be predicted are the CMC, the micelle size distribution, the micelle shape and average size, the extent of micellar solubilization, and the locus (or location) of solubilization within a micelle.

Theoretical efforts have been most successful at modeling the self-assembly of relatively simple surfactant systems, including surfactants that have linear hydrocarbon (or fluorocarbon) tails and a single, rigid head, for example, sodium dodecyl sulfate (SDS) and cetyltrimethylammonium bromide (CTAB). Some progress has also been made in modeling surfactants with long polymeric heads, including those of the alkyl poly(ethylene oxide) variety [8].

The most predictive and accurate theoretical models of surfactant micellization and micellar solubilization implement what is known as the molecular-thermodynamic (MT) modeling approach [8, 14]. In the MT modeling approach, the free-energy change associated with the formation of the surfactant aggregate is expressed as the sum of several free-energy contributions, all of which can be computed molecularly given the chemical structures of the various micellar components. The MT model introduced by Nagarajan and Ruckenstein allows prediction of the CMC and of the shape and size of micellar aggregates composed of nonionic, zwitterionic, and ionic surfactants [8]. In recent years, our group has also contributed to the development of MT models to predict surfactant behavior in aqueous solution [9, 14–22].

Because the hydrophobic effect is the primary driving force for micelle self-assembly in aqueous solution, it is essential to accurately model this contribution to the overall free energy of micelle formation. In order to model the hydrophobic effect in the context of the MT approach, a reasonable *a priori* determination must be made about the way in which the surfactant and the solubilizate molecules are hydrated in the micellar state. By comparing the degree of hydration of various groups within each solute in the micellar state with the degree of hydration of those same groups in the bulk aqueous solution, the changes in hydration that occur upon micelle self-assembly can be determined. From knowledge of such hydration changes, MT theory can then be used to quantify the hydrophobic driving force for micelle formation.

To date, MT models of micellization and micellar solubilization have relied on relatively simple approximations for the micellar hydration states of the surfactants and the solubilizates. In the traditional MT approach, each surfactant molecule is

modeled as being composed of two distinct portions — the head and the tail. The surfactant head is considered to be fully hydrated in both the monomeric and the micellar states. The surfactant tail is considered to be at least partially dehydrated in the micellar state, with the degree of dehydration being a function of the micelle geometry [8,14]. To identify the head and the tail, one approach involves determining the relative degree of hydrophobicity of different groups within a solute molecule using a group-contribution approach such as the one included in the software package Molecular Modeling Pro [23]. Using this type of information, it is possible to make educated guesses about which portions of a simple solute are hydrated in the micellar state. For example, for surfactants with an alkyl group attached to a charged or zwitterionic head, group-contribution approaches suggest that the first CH₂ group attached to the charged or dipolar head also possesses hydrophilic character, while the remainder of the CH₂ groups and the terminal CH₃ group remain hydrophobic. Based on this information, as well as on some experimental evidence for charged and zwitterionic surfactants [5,14], the approximation is made that $n_t = n_c - 1$, where n_c is the total number of CH₂ and CH₃ groups in the hydrocarbon chain and n_t is the number of CH₂ and CH₃ groups that should be modeled as being part of the surfactant tail. For surfactants with an alkyl group attached to a nonionic head, every CH₂ and CH₃ group attached to the hydrophilic head is assumed to be part of the tail, such that $n_t = n_c$ [22].

Unfortunately, in the case of more complex solute chemical structures, making head and tail assignments using simple group-contribution methods is inadequate. Examples of surfactants and solubilizates for which making head and tail assignments is not trivial are shown in Figure 6-1. In the case of the surfactant alkyl 3-hydroxy sulfonate (AOS), the presence of the two hydrophobic CH₂ groups between the two hydrophilic groups (SO₃⁻ and OH) makes the head and the tail identification challenging. In the case of the surfactant decanoyl-*n*-methylglucamide (MEGA-10), it is difficult to determine the micellar hydration state of each of the three groups bonded to the nitrogen atom (CH₃, CH₂, and the carbonyl group). In the case of the solu-

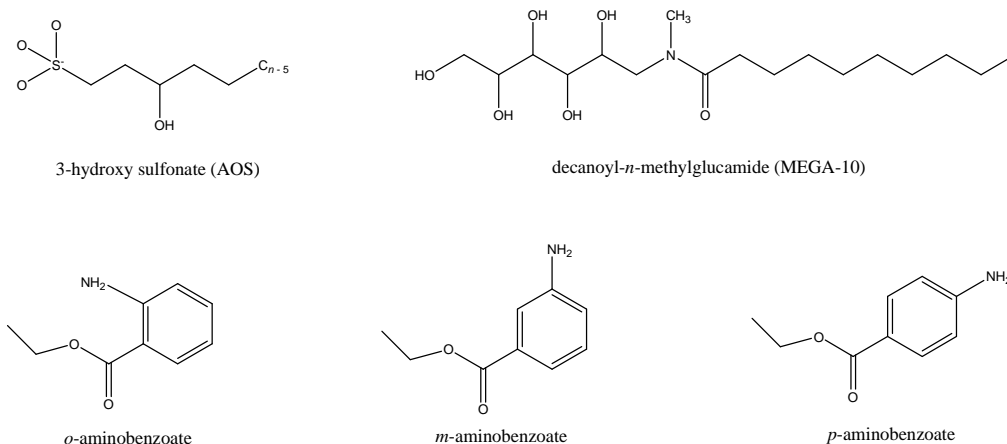


Figure 6-1: Examples of surfactants and solubilizers for which making head and tail assignments is not trivial. As a result, the surfactants shown here are difficult to model using the traditional molecular-thermodynamic (MT) modeling approach.

For solubilizers *o*-, *m*-, and *p*-aminobenzoate, it is unclear what effect changing the relative locations of the NH₂ group and the ethyl ester group within the molecule has on the head and the tail identification. In addition, it is unclear whether the ethyl ester group attached to the benzene ring should be modeled as being part of the solubilizer head or tail.

To extend the applicability of the MT modeling approach to more chemically and structurally complex surfactants and solubilizers, there is a need to accurately estimate the hydration states of these solutes in the micellar state. Even for the relatively simple surfactants and solubilizers shown in Figure 6-1, the prediction of such hydration information is beyond the scope of simple group-contribution methods, because the hydration states of the various chemical groups in the micelle are intimately related to the connectivity of these groups within a given solute. Although it may be possible to develop a suitable group-contribution approach that accounts for this connectivity in order to predict the required hydration information, such an approach must be parameterized based on a training set of detailed micellar hydration data for relatively complex surfactants and solubilizers. Unfortunately, at the present time, such data are not available. Fortunately, however, atomistic-level

computer simulations provide a promising approach to gather such information.

With the above need in mind, we recently reported the development of a traditional MT modeling approach in which molecular dynamics (MD) computer simulations of surfactant molecules at an oil/water interface (serving as a proxy for the hydrophobic micelle core-water interface) were used to determine the head and the tail groups of both structurally simple and relatively complex surfactants [24]. Subsequently, this approach was also used to determine the head and the tail groups of the pharmaceutically-relevant solubilizate ibuprofen [25]. In each case, traditional MT modeling was conducted based on computer simulation assignments of heads and tails, and the theoretical modeling results were compared with the experimental data [24,25]. Reasonable agreement was obtained between the theoretical predictions and the experimental data, with our results indicating that accurate head and tail assignments for traditional MT modeling can indeed be made through the use of MD simulations [24,25].

In this chapter, we present a new theoretical approach that combines hydration information determined through the use of computer simulation (CS) with a new molecular-thermodynamic (MT) model used to quantify the hydrophobic effect. The new theoretical approach can be used to predict the self-assembly behavior of solutes in aqueous solution. This new theoretical approach, which will be referred to hereafter as the CS-MT model, is presented generally for both hydrophobic and amphiphilic solutes, including oil molecules, surfactants, and solubilizates.

The CS-MT model extends previous MT modeling work in the following important ways:

(i) By using hydration data obtained from computer simulation, the CS-MT modeling approach avoids making some of the hydration approximations that have been made in traditional MT models of micellization and micellar solubilization. In addition, the computer simulation results allow one to evaluate the accuracy of the hydration approximations made in traditional MT modeling [14].

(ii) A new theoretical model is developed to make quantitatively accurate esti-

mates of the hydrophobic driving force involved in the self-assembly of hydrophobic and amphiphilic solutes in aqueous solution using hydration data obtained from computer simulation. The CS-MT model decomposes the contribution to free energy from the hydrophobic effect into two parts: (a) a “dehydration” free-energy change associated with the decrease in the number of solute-water contacts with respect to the dilute aqueous solution limit and (b) a “hydration” free energy change describing the change in the free energy of the remaining solute-water contacts as compared to those in a dilute aqueous solution. Using this modeling approach, solute groups that are partially hydrated and reside the majority of the time at the micelle core/water interface can be modeled in a more physically realistic manner than is currently possible using the traditional MT model.

(iii) Through computer simulation of the micellar state, a wealth of information about micelle microstructure can be obtained and used as an input to refine traditional MT or CS-MT modeling. Examples of such structural information are the projected area of each solute head at the micelle core/water interface, the distribution of conformations of the solute tails within the micelle core, the degree of counterion binding (in the case of ionic solutes), and the locus of solubilization. Although the effect of using such structural information to improve MT modeling is not explored in this chapter, we are pursuing such improvements as part of our ongoing research.

To validate and test the implementation of the CS-MT model, we will present CS-MT and traditional MT modeling results for 15 different oil aggregates of various shapes (spheres, cylinders, and slabs) and sizes. These oil aggregates were selected as a starting point to validate the CS-MT modeling approach because they are significantly simpler to model than micelles, in which the presence of the surfactant heads introduces additional complications. In Chapter 7 [26], we describe the implementation of the CS-MT model to predict the micellization behavior of simple and relatively complex nonionic surfactants (where electrostatic effects are absent) in aqueous solution. In Chapter 8, we describe the implementation of the CS-MT model to predict the micellization behavior of ionic and zwitterionic surfactants (where electrostatic

effects are present) [27].

The remainder of the chapter is organized as follows. The traditional MT modeling approach for solute self-assembly is reviewed in Section 6.2, including a description of the thermodynamic framework underlying the traditional MT and the CS-MT models (Section 6.2.2) and an overview of the traditional MT model (Section 6.2.3). The CS-MT model is introduced in Section 6.3. The model is formulated generally for a wide class of solutes, including oil molecules, nonionic and ionic surfactants, and nonionic and ionic solubilizates. Section 6.4 describes the computer simulation approach used to obtain the hydration information required in the CS-MT model, including an overview of the modeling approach (Section 6.4.2), the simulation methods and parameters (Section 6.4.3), and a description of how each system was prepared and equilibrated (Section 6.4.4). The data analysis method used to analyze the MD trajectories is described in Section 6.4.5. Computer simulation results are presented in Section 6.5. In Section 6.6, the CS-MT model is used to model oil aggregates, results are compared with those obtained using the traditional MT model, and the validity and accuracy of the CS-MT model is discussed. Concluding remarks are presented in Section 6.7. Finally, the CS-MT model is extended to allow the prediction of aggregate shape and size in Appendix A, and the equivalence of the CS-MT and the traditional MT modeling approaches is demonstrated mathematically in the case of completely hydrophobic solutes in Appendix B.

6.2 Molecular-Thermodynamic Modeling Approach

6.2.1 Introduction

In this section, we review the traditional MT model, with particular emphasis on how the hydrophobic effect is quantified. The MT model presented here is applicable to a broad class of hydrophobic and amphiphilic solutes, including oil molecules, surfactants, and solubilizates, although as discussed in Section 6.1, it can only be applied to relatively simple solutes without additional information about the hydration states

of each solute in the micellar environment.

The central objective of the MT modeling of micellization and solubilization in aqueous solution is to compute g_{form} , the free-energy change associated with transferring the surfactant monomers, the solubilizates, and any bound counterions (in the case of ionic surfactants) from their standard states in the aqueous solution to a micellar aggregate in its standard state [5, 14, 22]. Quantification of the hydrophobic contribution to g_{form} is essential to accurately model this transfer process. The MT modeling approach relies on a thermodynamic framework to describe the micellar solution [14, 15, 22]. This thermodynamic framework allows the calculation of useful micellar solution properties, including the critical micelle concentration (CMC), the distribution of aggregate shapes and sizes, and microstructural characteristics of the micellar aggregate (such as the locus of solubilization) from g_{form} . A brief overview of the thermodynamic framework is presented in Section 6.2.2. Note that this framework is formulated in the context of modeling a binary mixture of a single surfactant species and a single solubilizate species, but can be reformulated in a straightforward manner to model single surfactant micellization, the micellization of n -component surfactant mixtures, and the micellar solubilization of n -component mixtures of surfactants and solubilizates [5, 14, 22]. After introducing the thermodynamic framework, we briefly review the traditional MT modeling approach in Section 6.2.3.

6.2.2 Thermodynamic Framework

In the multiple-chemical equilibrium model of micellization [9, 14], each micellar aggregate is considered to be a distinct chemical species in equilibrium with the other aggregates and with the individually dispersed solutes present in the aqueous solution. By equating the chemical potentials of the micellar aggregates, the surfactant monomers (s), the solubilizate monomers (sol), and the counterions (c), an expression is obtained that describes the mole fraction of micellar aggregates, $X_{n_s\alpha\beta}$, containing n_s surfactant molecules, n_{sol} solubilizate molecules, and $\beta \cdot n_s$ bound counterions

(where $\alpha = n_s/(n_{\text{sol}} + n_s)$ is the aggregate composition, and β is the degree of counterion binding). Specifically [5],

$$X_{n_s\alpha\beta} = \left(\frac{1}{e}\right) X_{1s}^{n_s} \exp\left[-\frac{n_s g_{\text{form}}(S, l_c, \alpha, \beta)}{k_B T}\right] \quad (6.1)$$

where k_B is the Boltzmann constant, T is the absolute temperature, and g_{form} is defined as follows:

$$g_{\text{form}} = \left[\frac{\mu_{n_s\alpha\beta}^o}{n_s} - \mu_s^o - \beta\mu_c^o - \frac{\alpha}{1-\alpha}\mu_{\text{sol}}^o\right] - k_B T - \beta k_B T \ln(X_{1c}e) - \frac{\alpha}{1-\alpha}k_B T(X_{1\text{sol}}e) \quad (6.2)$$

In Eq. 6.2, μ_i^o is the standard-state chemical potential of species i (where i refers to a $n_s\alpha\beta$ micellar aggregate, to a surfactant monomer, to a solubilize monomer, or to an unbound counterion). The variables X_{1s} , $X_{1\text{sol}}$, and X_{1c} in Eqs. 6.1 and 6.2 are the mole fractions of the surfactant monomers, the solubilize monomers, and the counterions, respectively. As shown in Eq. 6.1, g_{form} is a function of the aggregate shape (S), the aggregate core-minor radius (l_c), the aggregate composition (α), and the degree of counterion binding (β).

At the values of S , l_c , α , and β that minimize g_{form} (denoted as S^* , l_c^* , α^* , and β^*), g_{form} has an optimal value denoted hereafter as g_{form}^* . Due to the exponential dependence of $X_{n_s\alpha\beta}$ on $(n_s \cdot g_{\text{form}})$ in Eq. 6.1, small deviations from g_{form}^* yield $X_{n_s\alpha\beta}$ values that are essentially zero. Accordingly, by solving for g_{form}^* , the optimal aggregate shape, S^* , the optimal core-minor radius, l_c^* , the optimal composition, α^* , and the optimal degree of counterion binding, β^* , can be predicted. In addition, the CMC in mole fraction units is computed as follows [22]:

$$\text{CMC} \approx \exp\left(\frac{g_{\text{form}}^*(S^*, l_c^*, \alpha^*, \beta^*)}{k_B T}\right) \quad (6.3)$$

6.2.3 Traditional Molecular-Thermodynamic Model of Surfactant Micellization and Micellar Solubilization

MT theory can be used to predict g_{form} based on the chemical structures of each of the solutes in the aqueous solution — whether they are oil molecules, surfactants, or solubilizates. As discussed in Section 6.1, important inputs to the MT model are the hydrated and the unhydrated portions of each solute in the micellar state [24]. In the traditional MT modeling approach, g_{form} is expressed as the sum of the following six free-energy contributions [22]:

$$g_{\text{form}} = g_{\text{tr}} + g_{\text{int}} + g_{\text{pack}} + g_{\text{st}} + g_{\text{elec}} + g_{\text{ent}} \quad (6.4)$$

Each of the six contributions in Eq. 6.4 arises from a distinct step in a thermodynamic cycle used to model the process of micelle formation. The various steps involved are shown schematically in Figure 6-2, which depicts the micelle formation process for a binary mixture of a cationic surfactant and a nonionic hydrophobic solubilize in aqueous solution. An analogous thought process may be used to model the formation of a multi-component surfactant micelle or of a multi-component surfactant/solubilize micelle.

In the first step shown in Figure 6-2, the cationic surfactant heads are separated from the surfactant tails and subsequently discharged along with the negative counterions in the aqueous solution. The corresponding discharge free energy is denoted as $g_{\text{discharge}}$ [15, 16].

In the second step shown in Figure 6-2, a hydrophobic micelle core composed of the surfactant tails and the solubilize tails (referred to collectively as the solute tails) is formed. This step is modeled as the sum of three free-energy contributions: g_{tr} , g_{int} , and g_{pack} . The transfer free-energy contribution, g_{tr} , represents the free-energy change associated with transferring the solute tails from the aqueous solution to a bulk solution of solute tails [6]. The interfacial free-energy contribution, g_{int} , represents the free-energy change associated with forming an interface between the

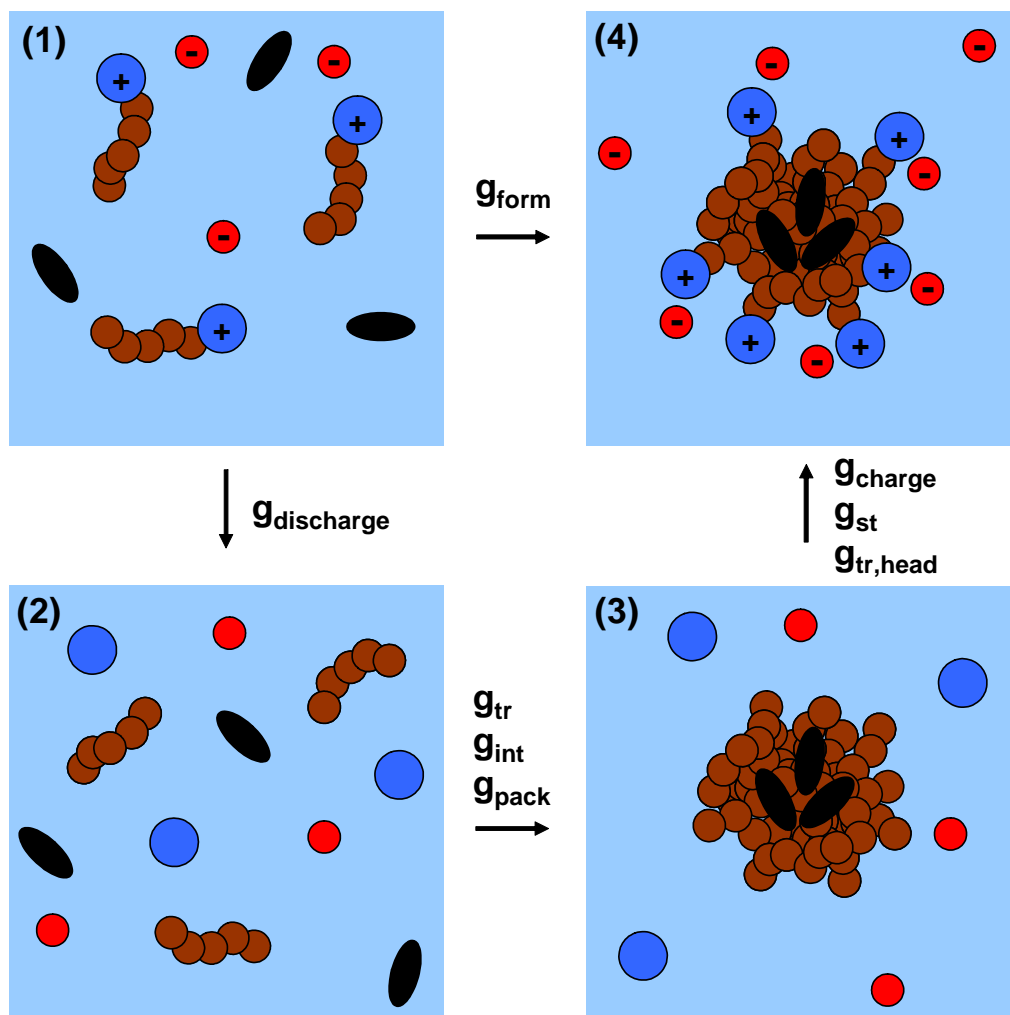


Figure 6-2: Sequence of steps followed in the molecular-thermodynamic cycle used in the CS-MT modeling approach developed in this article. This sequence is presented in the context of the micellization of a cationic surfactant and a nonionic hydrophobic solubilizate. Between frames (1) and (2), the solute heads (the large blue circles carrying positive charges) are separated from the solute tails (the chains consisting of five brown circles), and the solute heads and the counterions (the small red circles carrying negative charges) are discharged (as reflected in $g_{\text{discharge}}$). Between frames (2) and (3), the solute hydrophobic tails and the hydrophobic solubilizates (the black ovals) are grouped to form the micelle core (as reflected in g_{tr} , g_{int} , and g_{pack}). Between frames (3) and (4), the solute heads are reattached to one end of the solute tails (as reflected in g_{st} and $g_{\text{tr,head}}$), and the solute heads and their associated counterions are recharged (as reflected in g_{charge}).

solute tails and the aqueous solution [14]. The packing free-energy contribution, g_{pack} , represents the free-energy change required to fix one end of the amphiphilic solute tails (in the example considered here, only the surfactant tails) at the micelle core/water interface. This free-energy contribution is estimated using a mean-field model first introduced by Ben-Shaul, Szleifer, and Gelbart [28–30], and requires sampling each important conformation and orientation of the solute tail subject to the constraint that the hydrophobic micelle core has uniform density.

In the third step shown in Figure 6-2, the surfactant heads are transferred to the surface of the micelle (with a corresponding free-energy contribution, g_{st}) and recharged along with the counterions (with a corresponding free-energy contribution, g_{charge}) [15, 16, 31]. The steric free-energy contribution, g_{st} , accounts for the steric penalty associated with placing the surfactant heads in close proximity at the aggregate core/water interface [32]. In localizing the surfactant heads at the aggregate core/water interface, the heads are transferred to a different environment than that corresponding to the bulk water reference state. The change in free energy associated with this transfer corresponds to $g_{\text{tr,head}}$. However, in the traditional MT modeling approach, the surfactant heads are assumed to remain fully hydrated in the aggregate state, and therefore, $g_{\text{tr,head}}$ is approximated as being equal to zero. As a result, the free-energy contribution, $g_{\text{tr,head}}$, is not listed in Eq. 6.4. We define the electrostatic free-energy contribution, g_{elec} , in Eq. 6.4 as being equal to the sum of $g_{\text{discharge}}$ and g_{charge} [15, 16]. Note that the entropic free-energy contribution, g_{ent} , although included in Eq. 6.4, is not shown in Figure 6-2 because it can contribute to the thermodynamic cycle at several stages. The entropic free-energy contribution includes the translational entropy loss incurred by the solubilizates upon association with the micelles, the translational entropy loss of the bound counterions, and the mixing entropy associated with a multicomponent micelle [15, 16]. A more detailed description of the conceptual thought process implemented in the traditional MT modeling approach can be found in Refs. 14 and 15.

It is important to note that the salient characteristic of a solubilizate in the con-

text of the MT model is that it has a solubility limit in aqueous solution rather than a CMC. Chemically, solubilize molecules can be amphiphilic like conventional surfactant molecules. If an amphiphilic solubilize is present in the micelle, it may localize at the micelle core/water interface in a manner analogous to a surfactant molecule. If this is the case, only a portion of the amphiphilic solubilize molecule will be transferred to the hydrophobic micelle core and contribute to g_{tr} and g_{int} . In addition, because one end of the solubilize tail is constrained to reside at the micelle core/water interface, the solubilize tails also contribute to g_{pack} . Finally, the solubilize head contributes to g_{st} and $g_{\text{tr,head}}$, and its charge state contributes to g_{elec} .

The sequence of steps outlined above have been used by our group for many years to describe the process of micelle formation [9,14–22]. Recently, Maibaum et al. used a similar sequence of steps to model micelle formation, although the thermodynamic cycle that they proposed was used solely to model nonionic surfactants [33]. Specifically, Maibaum et al. broke up the formation of the hydrophobic micelle core into two steps: the formation of a vapor cavity in aqueous solution, and the transfer of the solute tails to this vapor cavity. The free energy of formation of the vapor cavity was modeled as being equal to the water/vapor surface tension times the surface area of the vapor cavity, plus a pressure-volume work term associated with cavity formation (which is negligible for water at standard conditions). After filling the hydrophobic core with the solute tails, the water/vapor surface tension was corrected to become equal to the interfacial tension of a water/oil interface.

An important aspect of the thermodynamic cycle shown in Figure 6-2 that we would like to highlight is that, in conceptually separating the solute heads from the tails in aqueous solution, and in subsequently reattaching them in the micellar environment, *we do not allow the hydration states of the solute tails to change*. Therefore, the hydration states of the solute tails are assumed to be the same in frames (1) and (2) as well as in frames (3) and (4) in Figure 6-2. The transition involved in moving from frame (2) to frame (3) in Figure 6-2 reflects the formation of the micelle hy-

drophobic core. The changes in hydration incurred in the formation of this micelle core represent the primary driving force for micelle formation. In traditional MT modeling, this driving force is modeled by the two terms, g_{tr} and g_{int} . Because a more general and accurate calculation of the hydrophobic contribution to the free energy of micelle formation is the central aim of this chapter, we will discuss the traditional MT modeling approach used to calculate g_{tr} and g_{int} in more detail in Sections 6.2.3 and 6.2.3, respectively. For a detailed discussion of the other free-energy contributions appearing in Eq. 6.4, the interested reader is referred to Refs. 14, 15, and 22.

The Transfer Free-Energy Contribution, g_{tr}

In the traditional MT modeling approach, only the solute tails contribute to g_{tr} . Therefore, to determine this free-energy contribution, it is first necessary to identify the head and the tail of each component present in the micelle. Various approaches for such identification were described in Section 6.1. After identifying the solute tails, g_{tr} is estimated as a composition-weighted average of g_{tr} for each micellar component expressed on a per surfactant molecule basis. For example, in a micelle containing a single surfactant type and a single solubilize type, the transfer free-energy contribution is estimated as follows [5]:

$$g_{\text{tr}} = g_{\text{tr,s}} + \frac{(1 - \alpha)}{\alpha} g_{\text{tr,sol}} \quad (6.5)$$

where $g_{\text{tr,s}}$ and $g_{\text{tr,sol}}$ are the free-energy contributions associated with transferring a surfactant (s) tail and a solubilize (sol) tail, respectively, to the aggregate core. Note that we divided by α in Eq. 6.5 to obtain an expression on a per surfactant molecule basis. For linear alkyl tails, correlations have been developed to express solubility as a function of alkyl chain length, temperature, and the concentration of added salt in aqueous solution [14, 34, 35]. For more complex solutes, more sophisticated group-contribution methods or experimental data may be used to estimate the tail solubility [24, 25]. Note that aqueous solubility is related to g_{tr} by the relationship

$g_{\text{tr}} = k_{\text{B}}T\ln(s)$, where s is the aqueous solubility of the solute expressed on a mole fraction basis.

The Interfacial Free-Energy Contribution, g_{int}

Some, or all, of the solute tails which are transferred to the aggregate core will reside for some time at the micelle core/water interface. The free-energy penalty associated with partially rehydrating these tail moieties is referred to as the interfacial free-energy contribution (g_{int}), and is modeled in the traditional MT approach using a micelle core/water interfacial tension. In a two-component micelle containing a single surfactant type and a single solubilize type, g_{int} is computed on a per surfactant molecule basis using the following expression [5]:

$$g_{\text{int}} = (a - a_0) \left[\frac{\alpha^{\text{int}}\sigma_{\text{s}} + (1 - \alpha^{\text{int}})\sigma_{\text{sol}}}{\alpha} \right] \quad (6.6)$$

where a is the area available to each solute at the micelle core/water interface, a_0 is the interfacial area that is screened by the solute heads on a per surfactant molecule basis, α^{int} is the mole fraction of surfactant at the micelle core/water interface, and σ_j is the curvature-dependent interfacial tension between water and a bulk phase of solute tails of type j (where $j = \text{s}$ or sol) [14]. Note that we have divided by α in Eq. 6.6 to obtain an expression on a per surfactant molecule basis. The curvature-dependent interfacial tension, σ_j , is determined using the Gibbs-Tolman-Koenig-Buff equation [36–39]:

$$\sigma_j = \frac{\sigma_{0,j}}{\left(1 + \frac{(S-1)\delta}{l_c}\right)} \quad (6.7)$$

where $\sigma_{0,j}$ is the interfacial tension of component j at a flat interface (having a typical value of about 50 mN/m for hydrocarbons), δ is the Tolman distance [39], and S is a shape factor (3 for spheres, 2 for cylinders, and 1 for disks or bilayers). We typically use an empirical correlation to determine $\sigma_{0,j}$ for alkyl chains of varying length and as a function of temperature, although, if available, the experimental $\sigma_{0,j}$ values may be used [40]. The Tolman distance, δ , is computed using the following

expression [14].

$$\delta(n_t) = \delta(n_t = 11)l_{\max}(n_t)/l_{\max}(n_t = 11) \quad (6.8)$$

where n_t is the number of carbons in the solute tail, and $l_{\max}(n_t) = 1.54 + 1.265n_t$ is the fully-extended length of the solute tail (in Å) [6].

6.3 The Computer Simulation/Molecular Thermodynamic (CS-MT) Modeling Approach

6.3.1 Introduction

In this section, we describe a new model for the hydrophobic effect that incorporates hydration information obtained from computer simulation as an input. This new model provides a more general approach to quantify the hydrophobic driving force for aggregate self-assembly than what is traditionally used in MT modeling, which was reviewed in Section 6.2. We develop this new model using a general expression for the extent of hydration. After introducing the new modeling approach in this Section, the simulation approach used to obtain the extent of hydration data required to implement the CS-MT model is discussed in Section 6.4.

6.3.2 Theoretical Framework

As discussed in Section 6.2.3, and shown in Eq. 6.4, in the traditional MT modeling approach, the hydrophobic effect is quantified by the free-energy contributions, g_{tr} and g_{int} . In order to more accurately quantify the hydrophobic effect, we propose to replace the terms g_{tr} , $g_{\text{tr,head}}$, and g_{int} (see Figure 6-2) with: (i) the free-energy contribution associated with dehydration (g_{dehydr}), and (ii) the free-energy contribution associated with hydration (g_{hydr}), that is, to rewrite Eq. 6.4 as follows:

$$g_{\text{form}} = g_{\text{dehydr}} + g_{\text{hydr}} + g_{\text{pack}} + g_{\text{st}} + g_{\text{elec}} + g_{\text{ent}} \quad (6.9)$$

Since we propose to use computer simulation to determine g_{dehydr} and g_{hydr} , we refer to this modeling approach as the CS-MT model. The models used to calculate g_{dehydr} and g_{hydr} are presented in Sections 6.3.3 and 6.3.4, respectively. Each of the remaining four free-energy contributions in Eq. 6.9 are identical to those included in the traditional MT model for g_{form} . Nevertheless, it is important to stress that, in principle, computer simulations could also be used to improve the estimation of g_{pack} and g_{st} (see below).

As discussed in Section 6.2.3, g_{pack} is the free-energy penalty associated with fixing one end of the solute tails at the aggregate core/water interface [15]. In the traditional MT modeling approach, each conformation and orientation of the solute tails (subject to the constraint of constant aggregate core density) is sampled after fixing one end of each tail at the aggregate core/water interface, and the free-energy difference between the constrained and the unconstrained states is estimated using a mean-field description [28–30]. An alternative to generating solute tail conformations in a separate computational step, and using the generated conformations to determine g_{pack} , would be to use the tail conformations recorded during an MD simulation to compute g_{pack} . Such an approach could potentially allow computation of g_{pack} with less computational expense than is currently possible, and would also allow a more seamless integration of the computer simulation and the MT modeling approaches. Although this approach has not yet been implemented, we are investigating the utility of incorporating this type of approach as part of our ongoing modeling work.

The steric free-energy contribution, g_{st} , accounts for the free-energy penalty associated with placing the solute heads in close proximity at the aggregate core/water interface. To determine this contribution, the cross-sectional area of the solute head at the aggregate core/water interface must be estimated. In the case of small, rigid heads, it is straightforward to do so from knowledge of the head chemical structure. However, in the case of larger, polymeric heads, such estimation is quite challenging. In such cases, the head area can be estimated from the computer simulation results by calculating the average projected area of each solute head at the aggregate

core/water interface over the course of the molecular dynamics simulation run. We are investigating this use of computer simulations as part of our ongoing modeling work.

Computer simulation results on the structure of the aggregate state can also be used to check key structural predictions made by traditional MT theory, including: (i) the degree of counterion binding (when ionic solutes are present in the micelle), and (ii) the locus of solubilization (when solubilizates are present in the micelle). By comparing the MD and the MT predictions, it is possible to ascertain to what extent both approaches yield consistent and physically reasonable results. Accurate MT estimates of the degree of counterion binding and of the locus of solubilization are essential to accurately estimate the free-energy contributions in Eq. 6.9. In future publications involving ionic surfactants and solubilizates, we will compare the structural predictions of the MD and the MT modeling approaches, and discuss the implications of our results on both the CS-MT and the traditional MT modeling approaches.

6.3.3 The Free Energy of Dehydration, g_{dehydr}

In the CS-MT model, we quantify hydration using the following general expression, which we refer to as the fractional hydration, f , where:

$$f = \frac{\text{extent of hydration in the aggregate environment}}{\text{extent of hydration in the bulk water environment}} \quad (6.10)$$

Note that $f = 0$ corresponds to complete dehydration and $f = 1$ corresponds to the extent of hydration in the bulk water environment. The fractional dehydration in the aggregate environment is equal to $(1-f)$. The specific manner in which f will be estimated using computer simulation data will be discussed in detail in Section 6.4. However, using the definition of the fractional hydration given in Eq. 6.10, we present here a theoretical model to allow estimation of the hydrophobic driving force for aggregate formation.

Every hydrophobic group in a solute tail, and most groups in a solute head, will experience some degree of dehydration upon aggregate formation. As we discussed in Section 6.2.3, in traditional MT theory, the heads are assumed to remain fully hydrated in the micellar state and do not contribute to the hydrophobic driving force for aggregate formation (in other words, $g_{\text{tr,head}} = 0$ in Figure 6-2). Using the hydration information obtained through computer simulation data, it is no longer necessary to make this approximation in the context of the CS-MT modeling approach. Indeed, here, we propose a more general approach to quantify the free-energy contribution associated with the dehydration of *any* hydrophobic group in the solute, regardless of whether the group is in the solute head or in the solute tail. Specifically, we propose the following model for g_{dehydr} :

$$g_{\text{dehydr}} = \sum_{i=1}^{n_{\text{hyd}}} (1 - f_i) g_{\text{tr}_i} \quad (6.11)$$

where n_{hyd} is the total number of hydrophobic groups in the solute, $(1-f_i)$ is the fractional dehydration associated with group i upon aggregate formation, and g_{tr_i} is the free-energy change associated with transferring group i from the aqueous solution to a bulk phase of hydrophobic tails. Note that in Eq. 6.11, hydrophilic groups are assumed to have a negligible effect on the dehydration free energy, and therefore, are not included in the summation. The validity of this approximation is discussed in greater detail in Chapter 7.

To compute g_{dehydr} using Eq. 6.11, it is necessary to accurately estimate g_{tr_i} for each hydrophobic group in the solute molecule. For the oil molecules considered in this chapter, g_{tr_i} is only needed for the CH_2 and the CH_3 groups that comprise the oil molecule, and is obtained using the same solubility correlations for linear alkyl tails that are used in the traditional MT modeling approach [34].

6.3.4 The Free Energy of Hydration, g_{hydr}

The hydration free-energy contribution in Eq. 6.9 is necessary to account for the difference in free energy associated with hydrating contacts in bulk water and in the core of an aggregate. Hydrating contacts have a different free energy in the two states because the size of a single hydrophobic chain in water is much smaller than the size of an aggregate core. This difference in size, in turn, induces a different extent of disruption of the surrounding water molecules in the two states, leading to a different hydration free energy. The size dependence of hydration thermodynamics is a well-known phenomenon, and has been modeled theoretically in an approach developed by Lum, Chandler, and Weeks (the LCW Theory) [41]. For small solutes (typically smaller than 1 nm in radius), the solute volume is sufficiently small that it does not disrupt the hydrogen bonding network in the surrounding water molecules. For larger solutes (or clusters of solutes), the hydrophobic surface is of sufficiently low curvature that it disrupts the hydrogen bonding network, reducing the density of water near the surface, and creating a solute/water interface [42].

We propose the following model to compute g_{hydr} :

$$g_{\text{hydr}} = \sum_{i=1}^{n_{\text{core}}} \text{SASA}_i f_i \Delta g_{\text{wc}_i} \quad (6.12)$$

where n_{core} is the total number of hydrophobic groups in the solute that adsorb onto, or are incorporated into, the aggregate core, SASA_i is the solvent accessible surface area of group i , f_i is the fractional hydration associated with group i upon aggregate formation, and Δg_{wc_i} is defined as the difference in the free energy per unit of solvent accessible surface area associated with hydration in the aggregate state and in the aqueous solution for group i .

To the extent that a hydrophobic group adsorbed onto, or incorporated into, the aggregate core remains hydrated in the aggregate state, the free-energy change associated with hydrating contacts for that group is accounted for with the term Δg_{wc_i} . For amphiphilic solutes (which contain both a head and a tail), only those

hydrophobic groups that are actually incorporated into the aggregate core contribute to g_{hydr} . Any hydrophobic groups that extend away from the aggregate core into the aqueous solution are best modeled as having the same free energy associated with water contacts in the aggregate state as in the bulk aqueous state, since the extent of disruption of the hydrogen bonding/coordinate bonding network of the solution in both states is very similar.

If desired, the term Δg_{wc_i} in Eq. 6.12 may be used as a fitting parameter to obtain the closest possible agreement between: (i) the traditional MT model and the CS-MT model, or (ii) the experimental data and the theoretical predictions of the CS-MT model. However, in order to develop a predictive model that requires no experimental input, we propose a theoretical approach to estimate Δg_{wc_i} for the oil molecules considered in this chapter.

In general, Δg_{wc_i} depends on the chemical nature of group i . However, the only molecules of interest in this chapter are oils. Because of the chemical similarity of the CH_2 and the CH_3 groups in oil, Δg_{wc_i} can be approximated as being equal for both groups. Note that the size difference between the CH_2 and the CH_3 groups is accounted for through the $SASA_i$ term in Eq. 6.12. With this approximation in mind, in the remainder of this chapter, we will refer to Δg_{wc_i} as Δg_{wc} when modeling each oil aggregate considered.

By predicting Δg_{wc} theoretically for oil aggregates and evaluating the accuracy of the CS-MT modeling results, we will be able to assess the validity and range of applicability of Eqs. 6.9, 6.11, and 6.12. In addition, we will be able to assess the validity of the computer simulation approach that will be described in Sections 6.4 and 6.5. We propose the following theoretical model for Δg_{wc} :

$$\Delta g_{\text{wc}} = \sigma_{\text{core}} - \sigma_{\text{bulk}} = \frac{\sigma A_{\text{core}}}{SASA_{\text{core}}} + \frac{g_{\text{tr}_i}}{SASA_i} \quad (6.13)$$

where σ_{core} is the “microscopic interfacial tension” (interfacial free energy per unit SASA) associated with the aggregate hydrophobic core/water interface, σ_{bulk} is the

“microscopic interfacial tension” (interfacial free energy per unit SASA) associated with the group i (CH_2 or CH_3)/water interface in the aqueous solution, σ is the macroscopic interfacial tension of the aggregate hydrophobic core/water interface (computed using Eq. 6.7), A_{core} is the area of the aggregate hydrophobic core computed geometrically based on the volume of the aggregate subject to the assumption of a perfectly smooth aggregate surface, $SASA_{\text{core}}$ is the solvent accessible surface area of the aggregate hydrophobic core, and $SASA_i$ is the solvent accessible surface area of group i .

In Eq. 6.13, $\sigma_{\text{core}} = \sigma A_{\text{core}}/SASA_{\text{core}}$ and $\sigma_{\text{bulk}} = -g_{\text{tr}_i}/SASA_i$ (recall that g_{tr_i} is < 0). By defining $\sigma_{\text{core}} = \sigma A_{\text{core}}/SASA_{\text{core}}$, we demand that the microscopic interfacial tension experienced at the aggregate interface be equal to the free energy of the aggregate hydrophobic core/water interface per unit of interfacial SASA. By defining $\sigma_{\text{bulk}} = -g_{\text{tr}_i}/SASA_i$, we demand that the microscopic interfacial tension experienced in bulk water at the group i /water interface be equal to the negative of the transfer free energy of group i per unit of solute SASA. The difference between σ_{core} and σ_{bulk} is equal to the free-energy difference per unit SASA associated with the hydrating contacts in the aggregate state and in the bulk water state.

The validity of Eq. 6.13 hinges on whether it is physically reasonable to evaluate Δg_{wc} on a per unit SASA basis, thereby invoking the concept of a microscopic interfacial tension, or microscopic interfacial free energy per unit area. Modeling the aggregate hydrophobic core as having a microscopic interfacial tension (σ_{core}) is reasonable given the size of the oil aggregates considered here (1.15 to 1.48 nm in radius), the typical size of hydrophobic micellar cores (~ 1 nm in radius), and the success obtained in modeling the micellar hydrophobic core using a curvature-corrected interfacial tension in the traditional MT modeling approach (see Eq. 6.7) [14]. However, because a linear alkane is only ~ 0.25 nm in radius in its smallest dimension [14], it is more questionable to model the solvation free energy of an oil molecule in the bulk aqueous solution as being proportional to SASA. For very small solutes, past research suggests that the solvation free energy can be modeled more accurately as being lin-

early related to the solvated volume rather than to the solvated surface area [42]. Nevertheless, a number of researchers, including Tanford, have modeled solubility as a function of SASA for linear and branched alkyl chains with reasonable accuracy, suggesting that the relatively simple model proposed in Eq. 6.13 is adequate [43,44]. The validity of Eq. 6.13 will be discussed in greater detail in Section 6.5 based on the values of σ_{core} and σ_{bulk} determined from our computer simulation results. Although σ_{bulk} is approximately constant, given the dependence of σ on the alkyl tail length and on the aggregate hydrophobic core curvature, σ_{core} is also expected to be a function of alkyl tail length and curvature. In addition, we note that the ratio of $A_{\text{core}}/SASA_{\text{core}}$ may also be a function of these variables. In Section 6.5, we will present results for $A_{\text{core}}/SASA_{\text{core}}$ for 15 oil aggregates of different shapes (spheres, cylinders, and slabs) and sizes. Using the computer simulation results, we will then be able to estimate Δg_{wc} using Eq. 6.13.

6.3.5 Extension of the CS-MT Model to Predict Aggregate Shape and Size

It is important to note that the theoretical framework that we have presented above allows one to determine g_{form} only for an aggregate for which hydration data is available from computer simulation. Because of the computational expense associated with performing atomistic computer simulations of aggregate systems, it is not practical to perform simulations of many aggregates having different shapes and sizes to identify the aggregate geometry that corresponds to the minimum value of g_{form} , which in turn, corresponds to the aggregate geometry that will be realized experimentally.

A salient capability of traditional MT theory is that it enables prediction of g_{form} as a function of aggregate shape and size [14, 15]. From this known functional dependence, it is then possible to predict the optimal aggregate shape and size. In Appendix A, we outline a computational strategy to extend the CS-MT modeling approach to enable prediction of g_{form} as a function of aggregate shape and size.

This is accomplished by combining elements of the CS-MT and the traditional MT models.

6.3.6 Evaluating the Validity and Accuracy of the CS-MT Model

To validate and test the implementation of the CS-MT model, we have selected a total of 15 different oil aggregates for simulation and modeling. Oil aggregates were selected as a starting point to validate the CS-MT modeling approach because of their simplicity. Indeed, unlike nonionic or ionic surfactant micelles, oil aggregates are devoid of solute heads at the aggregate core/water interface. As a result, for each of the 15 oil aggregates considered, there are only two contributions to g_{form} : g_{tr} and g_{int} in the traditional MT modeling approach (see Eq. 6.4), and g_{dehydr} and g_{hydr} in the CS-MT modeling approach (see Eq. 6.9). In other words, g_{pack} , g_{st} , g_{elec} , and g_{ent} in Eqs. 6.4 and 6.9 are all equal to zero, because the oil aggregates: (i) are devoid of solute heads at the aggregate core/water interface (g_{pack} and $g_{\text{st}} = 0$), (ii) are nonionic ($g_{\text{elec}} = 0$), and (iii) are single-component systems ($g_{\text{ent}} = 0$).

Unfortunately, experimental data for g_{form} is not available for these oil aggregates because these structures are not thermodynamically stable except at infinite dilution. As a result, in this chapter, we will compare the predictions of the CS-MT model with those of the traditional MT model. However, in Chapter 7, we discuss the implementation of the CS-MT model to predict the micellization behavior of nonionic surfactants. In that case, the CS-MT model predictions will be compared with both the traditional MT model predictions as well as with experimental CMC data. CMC predictions were selected as the micellar property of interest in Chapter 7 because the CMC depends exponentially on g_{form} (see Eq. 6.3), and as such, it provides an excellent quantitative metric with which to assess the predictive accuracy of the CS-MT model.

The 15 different oil aggregates that were selected for modeling include a total of five

geometries: (i) a spherical oil aggregate of radius ≈ 1.16 nm (the “small” spherical oil aggregate), (ii) a spherical oil aggregate of radius ≈ 1.45 nm (the “large” spherical oil aggregate), (iii) a cylindrical oil aggregate of radius ≈ 1.10 nm (the “small” cylindrical oil aggregate), (iv) a cylindrical oil aggregate of radius ≈ 1.30 nm (the “large” cylindrical oil aggregate), and (v) a planar slab of oil with a half-width ≈ 0.85 nm (the “planar” oil aggregate). In addition, we selected three different types of oil molecules for simulation and modeling in the five chosen aggregate geometries: octane, dodecane, and hexadecane. The three oil molecules selected cover a range of alkyl chain lengths that are frequently encountered in surfactant and solubilize tails.

By conducting simulations for three different types of oil molecules in five different geometries possessing different curvatures, we will be able to thoroughly evaluate the accuracy of the CS-MT modeling approach for the types of hydrocarbon tails and aggregate geometries that are most commonly encountered in modeling micellization and micellar solubilization. In addition, by modeling spherical oil aggregates, cylindrical oil aggregates, and planar oil slabs, we will be able to evaluate the ability of the CS-MT approach to model the three idealized micellar geometries (a perfect sphere, a perfect cylinder, or a perfect bilayer) that are used in the context of the traditional MT modeling approach [9, 14, 15, 22].

6.4 Molecular Dynamics Simulations

6.4.1 Introduction

In this section, we describe a general molecular dynamics simulation approach which can be used for any hydrophobic or amphiphilic solute to determine the detailed hydration information required to more accurately quantify the hydrophobic driving force responsible for self-assembly. This approach is introduced here in the context of the 15 different oil aggregates that were selected to validate the CS-MT model (see Section 6.3.6). The approach presented here has also be used to obtain hydration

information for nonionic surfactants in Chapter 7.

6.4.2 Modeling Approach

To more accurately quantify the hydrophobic driving force associated with the formation of each of the 15 aggregates considered here, we have used atomistic computer simulations to determine the change in hydration of each atom (or group of atoms, such as, a CH₂ group) which is transferred from the aqueous solution environment to the aggregate environment. To accomplish this, two simulations were performed. The first one — the “bulk water” simulation — was of a single solute in a simulation cell containing water. The second one — the “aggregate” simulation — was of the same solute in the aggregate environment. Since it is very computationally expensive to simulate the self-assembly of solutes in aqueous solution into aggregates, for each of the aggregates simulated here, the aggregate was pre-formed in vacuum and subsequently equilibrated in a box of water [45]. Although these equilibration times were sufficient to allow rearrangement and equilibration of the solutes within the aggregate, they were not sufficient to allow a solute to leave the aggregate environment and enter the aqueous environment. Accordingly, the simulated aggregate will not necessarily have the same geometry (shape and size) that would be observed experimentally.

6.4.3 Simulation Methods and Parameters

All the solutes considered were modeled using bonded and non-bonded interaction potentials included in the fully-atomistic OPLS-AA force field [46]. Water was modeled using the simple extended point-charge (SPC/E) model for water. SPC/E represents an improvement over SPC in which a correction is implemented to account for the self-polarization of water [47]. Atomic charges were assigned to each oil molecule based on the default atomic charge values recommended in OPLS-AA. Van der Waals interactions were incorporated using a cutoff distance of 0.9 nm, and

Coulombic interactions were described using 3D particle mesh Ewald (PME) summation [48, 49]. Although the van der Waals cutoff used in this study is shorter than the cutoffs that are frequently reported in the literature (1.2 to 1.4 nm), there is a trade-off between using longer cutoff distances to try to more accurately capture the non-bonded interactions present in the system and using the same cutoff distances used for the original force field parameterization. It has been demonstrated that truncation schemes for electrostatic interactions give qualitatively incorrect results when compared with newer and more accurate methods, such as, reaction field treatment of electrostatics or Ewald summation [50]. However, using relatively short-range cutoffs for van der Waals interactions yields accurate results with the inclusion of long-range dispersion corrections, as shown in recent simulation studies using the OPLS-AA force field carried out by Shirts et al. [51–53]. In our simulations, long-range dispersion corrections were implemented to more accurately model the energy and the pressure of the system. Both dispersion corrections are negative, and while the energy correction is small, the pressure correction is significant and must be included to yield accurate results [54]. In modeling short-range, non-bonded interactions, a neighbor list with a cutoff of 0.9 nm was maintained and updated every 10 simulation steps. Each simulation was carried out with fixed bond lengths using the SHAKE algorithm as implemented in GROMACS [55], which allowed an increase in simulation timestep from 1 fs to 2 fs.

In each simulation, the cell temperature was maintained at 298.15 K using a Berendsen temperature coupling algorithm, which mimics weak coupling to an external heat bath with first-order kinetics [54]. A Berendsen pressure coupling algorithm was used to maintain each simulation cell at the desired pressure of 1.0 bar [54]. All simulations were conducted using a 2006 developers' version of the GROMACS software package [56, 57].

Aggregate Type	n	V	A	l_c	PL	C
		[nm ³]	[nm ²]	[nm]	[nm]	[nm ⁻¹]
small sphere	25	6.75	17.27	1.17	N/A	1.71
large sphere	50	13.5	27.41	1.48	N/A	1.35
small cylinder	54	14.58	26.57	1.10	3.85	0.91
large cylinder	54	14.58	22.83	1.28	2.85	0.78
slab	192	51.84	28.88	0.90	3.80	0.0

Table 6.1: Geometric characteristics of each of the five octane aggregates simulated, including the aggregation number (n), the aggregate volume (V), the aggregate surface area (A), the aggregate core-minor radius (l_c), the periodic length (PL) of each cylinder and slab, and the degree of curvature (C , as defined in Eq. ??).

6.4.4 System Preparation and Equilibration

Bulk Water Simulations

The “bulk water” simulation for each of the oil molecules considered was initialized by placing a single oil molecule in a simulation cell and surrounding it with water molecules. The simulation cell was selected to be sufficiently large that there would always be at least 2.0 nm separating the oil molecule from its periodic image. Computer simulation studies of the propagation of water ordering away from an interface suggest that such a separation distance should be sufficient to prevent the oil molecule from interacting with its periodic image [58]. After a brief equilibration under NPT conditions until the system volume had stabilized, a 2 to 5 ns data-gathering simulation was conducted.

Aggregate Simulations

The geometric characteristics of the five simulated aggregates of octane, dodecane, and hexadecane are listed in Tables 6.1, 6.2, and 6.3, respectively. In total, 15 different aggregate systems were prepared and simulated. It is important to note that, to the extent possible (given the requirement of an integer number of molecules), aggregation numbers for octane, dodecane, and hexadecane were selected such that corresponding aggregate geometries would have the same dimensions. In other words,

the small spherical octane aggregate has the same dimensions as the small spherical hexadecane aggregate. This was done to permit direct comparison of the simulation results for the different oil molecules considered, and to evaluate the effect of the hydrocarbon chain length on these results. The volume, V , of each aggregate reported in Tables 6.1, 6.2, and 6.3 was computed using the formula $V = 54.3 \cdot n_{\text{CH}_3} + 26.9 \cdot n_{\text{CH}_2}$ (\AA^3), where n_{CH_2} is the number of CH_2 groups and n_{CH_3} is the number of CH_3 groups in the aggregate [6]. The surface area, A , of each aggregate was computed geometrically based on the volume of the aggregate and the assumption of a perfectly smooth aggregate surface. The core-minor radius, or planar half-width, l_c , of each aggregate was estimated geometrically using the same assumption. The periodic length, PL , applies only in the case of the cylindrical and the planar aggregates, and refers to the periodic simulation cell length of the simulated infinite cylinders, as well as to the periodic simulation cell width and length of the simulated infinite planar layers. Each of the five different geometries simulated for each oil molecule has a different curvature, C , which we have defined using the convention used in the Gibbs-Tolman-Koenig-Buff equation [36–39]:

$$C = \frac{(S - 1)}{l_c} \quad (6.14)$$

where S is a shape factor that is equal to 3 for spheres, 2 for cylinders, and 1 for planar interfaces. As discussed in Section 6.3.6, although the actual dimensions of the simulated aggregates were chosen arbitrarily, they cover a range of aggregate shapes and sizes that are frequently encountered in modeling micellar systems. Representative spherical, cylindrical, and planar aggregate geometries have been simulated, with values of l_c ranging from 0.81 to 1.17 nm and curvature values ranging from zero to 1.74 nm^{-1} .

Spherical Oil Aggregates Each large spherical oil aggregate was prepared by first allowing oil molecules distributed randomly in a simulation cell to self-assemble into a spherical aggregate in vacuum (which is much less computationally expensive

Aggregate Type	n	V	A	l_c	PL	C
		[nm ³]	[nm ²]	[nm]	[nm]	[nm ⁻¹]
small sphere	17	6.42	16.70	1.15	N/A	1.73
large sphere	33	12.46	25.99	1.44	N/A	1.39
small cylinder	36	13.59	25.66	1.06	3.85	0.94
large cylinder	36	13.59	22.04	1.23	2.85	0.81
slab	128	48.33	28.88	0.84	3.80	0.0

Table 6.2: Geometric characteristics of each of the five dodecane aggregates simulated, including the aggregation number (n), the aggregate volume (V), the aggregate surface area (A), the aggregate core-minor radius (l_c), the periodic length (PL) of each cylinder and slab, and the degree of curvature (C , as defined in Eq. ??).

to simulate than their self-assembly in water). After self-assembly, which was driven by van der Waals attractions between the oil molecules, sufficient water molecules were added to the simulation cell to ensure that each oil aggregate was at least 2 nm away from its periodic image. An extended NPT simulation was then performed during which the x , y , and z -dimensions of the simulation cell were allowed to change subject to an applied pressure of 1 bar. During this equilibration period, which was 5 ns for octane and 10 ns for dodecane and hexadecane, both the system potential energy and the solvent accessible surface area (SASA) of each oil aggregate reached a constant value. We consider SASA to be the most important metric to measure equilibration, because this property is directly proportional to the degree of hydration of the oil aggregate, and obtaining accurate hydration information is the key objective of our computer simulations. After equilibration, a 5 ns data-gathering simulation was conducted.

Each small spherical oil aggregate was prepared by first starting from the post-equilibration conformation of a large spherical oil aggregate and then removing half of the oil molecules. An NPT equilibration run was subsequently done under these new conditions for 5 ns until both the system potential energy and the SASA of the oil aggregate became constant. During equilibration, the simulation cell dimensions quickly decreased to compensate for the volume of oil that was removed, forming a new simulation cell of approximately the same density as the initial one. Each new

Aggregate Type	n	V	A	l_c	PL	C
		[nm ³]	[nm ²]	[nm]	[nm]	[nm ⁻¹]
small sphere	13	6.31	16.51	1.15	N/A	1.74
large sphere	25	12.13	25.53	1.43	N/A	1.40
small cylinder	27	13.1	25.19	1.04	3.85	0.96
large cylinder	27	13.1	21.67	1.21	2.85	0.83
slab	96	46.58	28.88	0.81	3.80	0.0

Table 6.3: Geometric characteristics of each of the five hexadecane aggregates simulated, including the aggregation number (n), the aggregate volume (V), the aggregate surface area (A), the aggregate core-minor radius (l_c), the periodic length (PL) of each cylinder and slab, and the degree of curvature (C , as defined in Eq. ??).

oil aggregate constructed in this manner had a radius which was approximately 20% smaller than the original radius. After equilibration, each oil aggregate was simulated for an additional 5 ns under NPT conditions during which data was gathered.

Cylindrical Oil Aggregates Each cylindrical oil aggregate was prepared by first allowing oil molecules distributed randomly in a simulation cell to self-assemble into a cylindrical aggregate in vacuum. After self-assembly, the aggregate was in contact with the periodic boundaries on two sides of the simulation cell (which we define as the two sides perpendicular to the z -axis). Next, sufficient water molecules were added to ensure that the cylindrical oil aggregate was always at least 2 nm away from its periodic image in the x - and y -directions. An extended constant pressure simulation was then performed in which only the x - and y -dimensions of the simulation cell were allowed to change subject to an applied pressure of 1 bar, and during which both the system potential energy and SASA became constant. This equilibration continued for 5 ns for octane and for 10 ns for dodecane and hexadecane. Equilibration was followed by a 5 ns data-gathering simulation.

Initially, the three types of oil molecules were simulated in a simulation cell whose z -dimension was 3.85 nm in length. We will refer to this distance as the cylinder “length,” although one should keep in mind that because of the use of periodic boundary conditions, the cylinder is actually infinitely long. To investigate the effect of curvature on the simulation results and to evaluate the effectiveness of the CS-MT

modeling approach for cylinders of different curvature, a new simulation cell was constructed for octane, dodecane, and hexadecane by simulating the original simulation cell at constant pressure but without fixing the z -dimension. During these constant-pressure simulations, the length of the z -dimension of each simulation cell gradually contracted in response to the new boundary conditions. These simulations were continued for 1 to 2 ns until each simulation cell attained a cylinder length of 2.85 nm. At this point, the length of the z -dimension of each simulation cell was again fixed. Although each of the three new cylinders formed using this approach had the same volume as the original cylinders, each cylinder core radius was approximately 16% larger than the original cylinder core radius. We will refer to the cylinders that are 3.85 nm in length as the “small” cylinders because they are comparatively thin, and to the cylinders that are 2.85 nm in length as the “large” cylinders because they are comparatively thick. After additional equilibration in the new geometry for 100 ps to ensure that the system potential energy and SASA were stable, each cylindrical oil aggregate was simulated for an additional 5 ns during which data was gathered.

Planar Oil Aggregates Each planar oil aggregate was prepared by first placing a pre-equilibrated slab of octane, of dodecane, or of hexadecane within a simulation cell surrounded on two sides by water molecules. After construction, each simulation cell contained two oil/water interfaces perpendicular to what we define as the z -axis. For each oil slab, an NPT simulation was performed, in which only the z -dimension of the simulation cell was allowed to change. This prevented contraction of the simulation cell in the x - and y -dimensions to reduce the interfacial free energy. Equilibration was evaluated by monitoring the total potential energy of the system and the SASA of each oil slab, and ensuring that both properties had stabilized. For octane, a total of 5 ns of equilibration was found to be sufficient. However, for dodecane and for hexadecane, a total of 10 ns was required. After equilibration, a 5 ns data-gathering simulation was conducted.

Equilibration Results For the three types of oil molecules considered and for each of the five aggregate geometries simulated, we observed that the timescales associated with potential energy and SASA equilibration and fluctuation were much shorter than the total simulation time, although SASA fluctuation was found to occur on a much longer timescale than potential energy fluctuation. The total simulation time for each system was sufficient to ensure adequate sampling of both properties. To demonstrate this, in Figure 6-3, we plot SASA results from the 5 ns data-gathering simulation run for three representative octane aggregate geometries: the small spherical octane aggregate, the large cylindrical octane aggregate, and the planar octane aggregate. As can be seen, the SASA values are stable with time and exhibit no noticeable upward or downward drift during the data-gathering simulation.

Snapshots of the post-equilibration configurations corresponding to: (i) the large and the small dodecane spherical aggregates, (ii) the large and the small dodecane cylindrical aggregates, and (iii) the planar dodecane aggregate are shown in Figure 6-4. The snapshots of the octane and the hexadecane aggregates appear very similar. Each oil molecule is depicted using the van der Waals radius of each atom. For clarity, the water molecules are not shown.

6.4.5 Data Analysis Method

Definition of “Hydration”

In Sections 6.1 and 6.3, we discussed the importance of quantifying the degree of hydration of solutes in the bulk water and in the aggregate states. Before implementing the new CS-MT modeling approach described in Section 6.3, we describe below our specific methodology for determining the extent of hydration from the simulation data. In particular, our definition of hydration is based on the number of contacts with “hydrating” atoms, where a hydrating atom is defined as an atom that: (i) is capable of forming hydrogen bonds, or (ii) is capable of coordinate (dative covalent) bonding. Based on this definition, if a hydrophobic CH_2 group is in

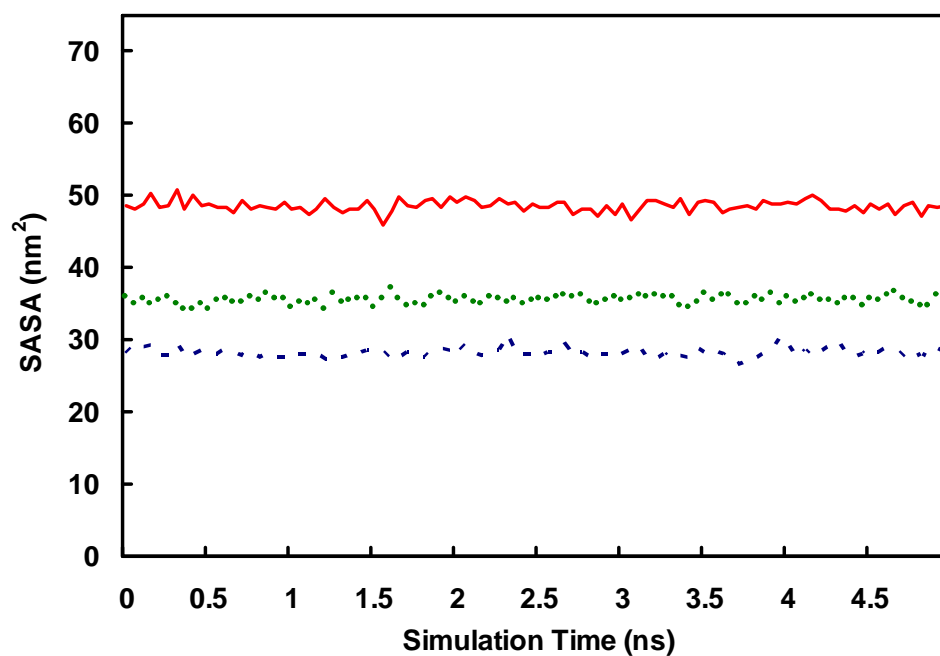


Figure 6-3: Solvent accessible surface area (SASA) as a function of simulation time for three representative simulated oil aggregates: a small octane sphere ($\square \square \square$), a large octane cylinder ($\bullet \bullet \bullet$), and an octane slab (—). The timescales involved in the SASA fluctuations are much shorter than the total simulation time.

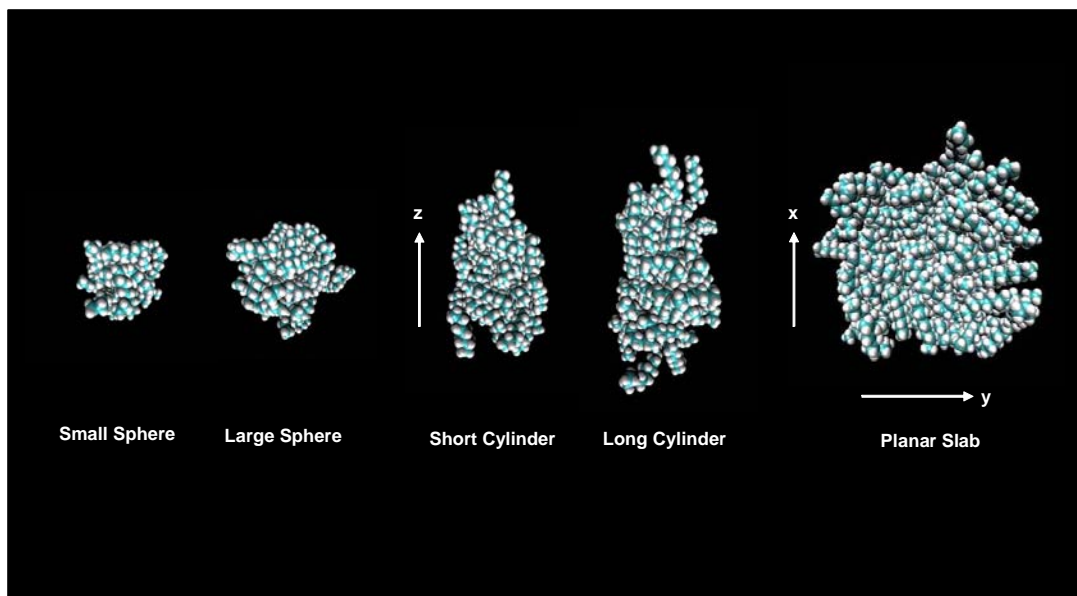


Figure 6-4: Snapshots of the post-equilibration structures of: (i) two dodecane spherical aggregates (of aggregation numbers 17 and 33), (ii) two dodecane cylindrical aggregates (of periodic lengths 2.85 nm and 3.85 nm), and (iii) a dodecane slab. The water molecules are not shown for clarity.

contact with any atom in a water molecule, with a positively-charged or negatively-charged ion, or with a hydrophilic group in the surfactant head that is capable of hydrogen bonding, then, that contact is considered “hydrating.” We adopt this definition because the hydrophobic effect arises from changes in the hydrogen-bonding or coordinate-bonding network of the aqueous solution that are induced by the presence of nonpolar, hydrophobic moieties [42]. Contact between a hydrophobic group and water, hydrogen-bonding groups in a surfactant head, or a negatively-charged ion in solution may break or perturb the hydrogen bonding network. Similarly, contact between a hydrophobic group and a positively-charged ion in aqueous solution may disrupt coordinate bonds between water and the ion. In the CS-MT model, we approximate all hydrating contacts as having the same free energy. The implications of this approximation for modeling nonionic surfactant micellization will be discussed in greater detail here and in subsequent chapters on micellization and micellar solubilization.

Analysis of the Bulk Water and the Aggregate Simulation Results

To quantify the degree of hydration of each atom (or group of atoms) in the solute molecule during a bulk water simulation, the number of contacts with hydrogen-bonding or with coordinate bonding atoms experienced by different atoms in the solute must be counted during the course of a simulation run. For the oil molecules in water considered here, the only contacts that need to be counted as contributing to hydration are contacts with the oxygen and the hydrogen atoms in water. However, for an ionic surfactant in aqueous solution, contacts with water atoms, ions, and hydrogen-bonding groups in the surfactant head should each be counted as contributing to hydration. In analyzing our simulation data, a contact was defined as two atoms being separated by less than a set distance (the “cutoff” distance) at any time during the simulation. It is important to note that the average number of contacts counted using this method of analysis is directly proportional to the average number of hydrating atoms located within the specified cutoff distance.

Quantifying the degree of hydration of the solute molecules during the aggregate simulations was done in the same manner (and using the same cutoff distance used to identify contacts) as was done in analyzing the results of the bulk water simulations. After counting the hydrating contacts in the bulk water and in the aggregate states, we analyzed the hydration data using the metric introduced to quantify hydration in Section 6.3. Recall that the relative degree of hydration, f , is defined as the extent of hydration in the aggregate environment divided by the extent of hydration in the bulk water environment (see Eq. 6.10). Based on this definition, f values for each solute molecule were computed from the simulation data as follows:

$$f = \frac{\text{number of hydrating contacts in the aggregate environment}}{\text{number of hydrating contacts in the bulk water environment}} \quad (6.15)$$

As expected intuitively, we found that f is significantly less than unity for a hydrophobic solute, because fewer contacts with hydrating atoms are experienced in the aggregate environment than in the bulk water environment.

Selecting the Cutoff Distance

In selecting the cutoff distance used to define contacts between atoms, we were guided by the realization that, in implementing the CS-MT model, we are interested only in quantifying the *local* environment of each hydrophobic atom or group of atoms. Accordingly, a cutoff distance should be selected such that only nearest-neighbor atoms contribute contacts to a hydrophobic group. However, to ensure that good contact statistics are obtained, the cutoff distance selected should be at least as large as the sum of the van der Waals radii of two hydrogen atoms (one that is bonded to a CH₂ or to a CH₃ group, and the other that is bonded to a water molecule), or 0.24 nm.

To determine the sensitivity of the CS-MT modeling results to the value of the cutoff distance selected, several different cutoff values were tested, including 0.25 nm, 0.3 nm, 0.4 nm, and 0.5 nm. Note that when computing f using Eq. 6.15, the same

cutoff value was used to count contacts in both the bulk water and the aggregate environments. The CS-MT modeling results were found to be weakly dependent on the value of the cutoff distance when modeling planar and curved oil aggregates. We found that by choosing the smallest value of the cutoff distance that yields good statistics, only nearest-neighbor contacts with hydrating atoms were included, and the dependence of f on curvature was minimized. As discussed in Section 6.3, the effect of curvature on g_{form} is accounted for theoretically in the CS-MT model, and need not be included by using a large cutoff distance that introduces curvature dependence into the calculated f values. We also computed radial distribution functions between the hydrophobic CH_2 and CH_3 groups and water using the bulk water simulation data to aid in determining an appropriate cutoff distance. Based on the results of our sensitivity and radial distribution function tests (results not reported), we selected a cutoff distance of 0.3 nm as being most appropriate when implementing the CS-MT model. All the CS-MT modeling results reported in this chapter were generated using this cutoff distance.

Error Analysis

An estimate of the standard error in f for each group of atoms in the solute molecules was obtained through the use of block averaging [59–61]. In block averaging, the standard error is computed from the variance between averages of blocks of data, and the block size is increased until the standard error estimate becomes constant. To assist in identifying this asymptotic value for the simulation data reported here, a two-exponential function was fit to the block average curve [59–61]. Block averaging is useful to analyze correlated data, such as the results obtained from a MD simulation. Data-gathering simulation runs for solute molecules in the bulk water and in the aggregate states were conducted for sufficient time to ensure that the uncertainty in each calculated value of f was sufficiently small — typically, less than 5%.

The block averaging approach described above provides an accurate estimate of the standard error of the results of a single simulation. However, typically, it is also

desirable to run multiple independent simulations to estimate the run-to-run variance. If the run-to-run variance is much larger than the variance estimated from a single simulation, it indicates that insufficient sampling has been done [50, 53, 55]. This problem has been commented upon in the context of free-energy calculations using computer simulation [52, 62]. Although the block averaged results for individual runs presented here indicate a high degree of statistical certainty, we conducted additional independent bulk water and aggregate simulations to determine the run-to-run variance. The run-to-run variance was found to be comparable in size to the block average estimates of the standard error for each solute (results not reported). Accordingly, and because of the high computational cost associated with conducting such simulations, independent simulations were not considered to be necessary for the surfactant systems simulated in Chapter 7.

6.5 Simulation Results and Discussion

6.5.1 Fractional Hydration Results

Simulations of a single molecule of octane, of dodecane, and of hexadecane in bulk water were conducted to determine the average number of contacts experienced by each of the CH_2 and the CH_3 groups in the oil molecules with water in the bulk aqueous state. Subsequently, aggregate simulations were conducted for each oil type and for the five different aggregate geometries discussed in Section 6.4.4.

The resulting average fractional degree of hydration, f , is plotted as a function of group number for octane in Figure 6-5, for dodecane in Figure 6-6, and for hexadecane in Figure 6-7. The error bars shown represent the standard error of the mean for each value of f , and are typically of the size of the various symbols shown or smaller. As discussed in Section 6.4.4, to the extent possible (given the requirement of an integer number of molecules), aggregation numbers were selected such that corresponding aggregates of octane, dodecane, and hexadecane have the same dimensions. Therefore, the simulation results presented here for each oil molecule can be compared directly

to evaluate the effect of the hydrocarbon chain length on f and on SASA.

As shown in Figures 6-5, 6-6, and 6-7, each of the three oil molecules considered has a symmetric degree of hydration profile in which each structurally equivalent CH_2 and CH_3 group has the same degree of hydration within the error of the simulation results. The CH_3 groups on both ends of each oil molecule have the highest f values, while the CH_2 groups near the middle of each oil molecule have the lowest f values. The average value of f for each oil aggregate is related to the exposed surface area per molecule, a . For a perfectly smooth oil aggregate, $a = S \cdot v_t / l_c$, where v_t is the volume of the solute tail [7]. Although the various oil aggregates simulated here are not perfectly smooth, we have found that the inverse relationship between a and l_c is still valid. The relatively low values of f for the planar oil aggregates (see the ✖ results in Figures 6-5, 6-6, and 6-7), for example, can be understood by noting that this aggregate has a value of a which is approximately 4.3 times larger than that of the small spherical aggregate (◆), 3.5 times larger than that of the large spherical aggregate (■), 3.2 times larger than that of the small cylindrical aggregate (▲), and 2.7 times larger than that of the large cylindrical aggregate (●).

It is interesting to note that although the average value of f for oil molecules in aggregates of the same shape and size are approximately the same for each of the three oil molecules, the magnitude of the difference between the highest and the lowest f value in each molecule is different for the three oil molecules. For example, the average magnitude of this difference for all five hexadecane geometries is 73% larger than the average magnitude of this difference for all five octane geometries, it is 53% larger for all five dodecane geometries than for all five octane geometries, and it is 43% larger for all five hexadecane geometries than for all five dodecane geometries. Visual inspection of the trajectories for each aggregate simulation revealed that these differences are due to a packing effect. More specifically, both dodecane and hexadecane exhibited relatively high degrees of hydrocarbon chain alignment after equilibration. This alignment resulted in a disproportionate number of CH_3 groups being adjacent to

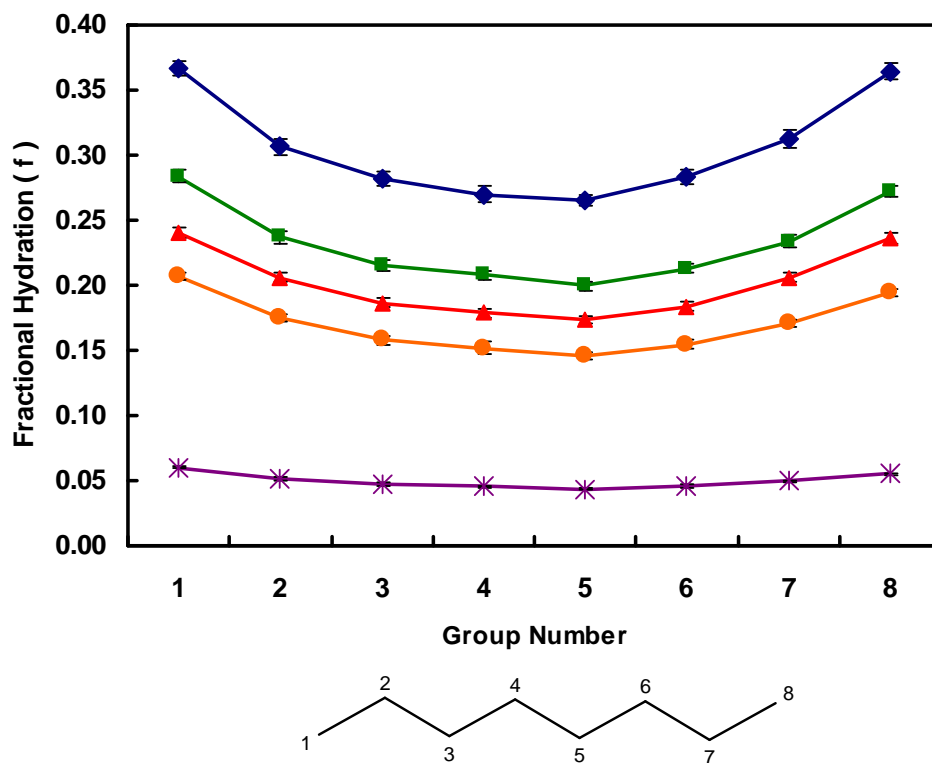


Figure 6-5: The average fractional degree of hydration (f), as defined in Eq. 6.15, corresponding to each of the groups in octane for each of the five simulated aggregate geometries. Results are presented for: (i) a small spherical aggregate (\blacklozenge), (ii) a large spherical aggregate (\blacksquare), (iii) a small cylindrical aggregate (\blacktriangle), (iv) a large cylindrical aggregate (\bullet), and (v) a planar slab (\ast). Group numbers are identified in the molecular structure shown below the fractional hydration plot. The error bars shown correspond to the standard error of the mean. The various lines are shown as a guide for the eye.

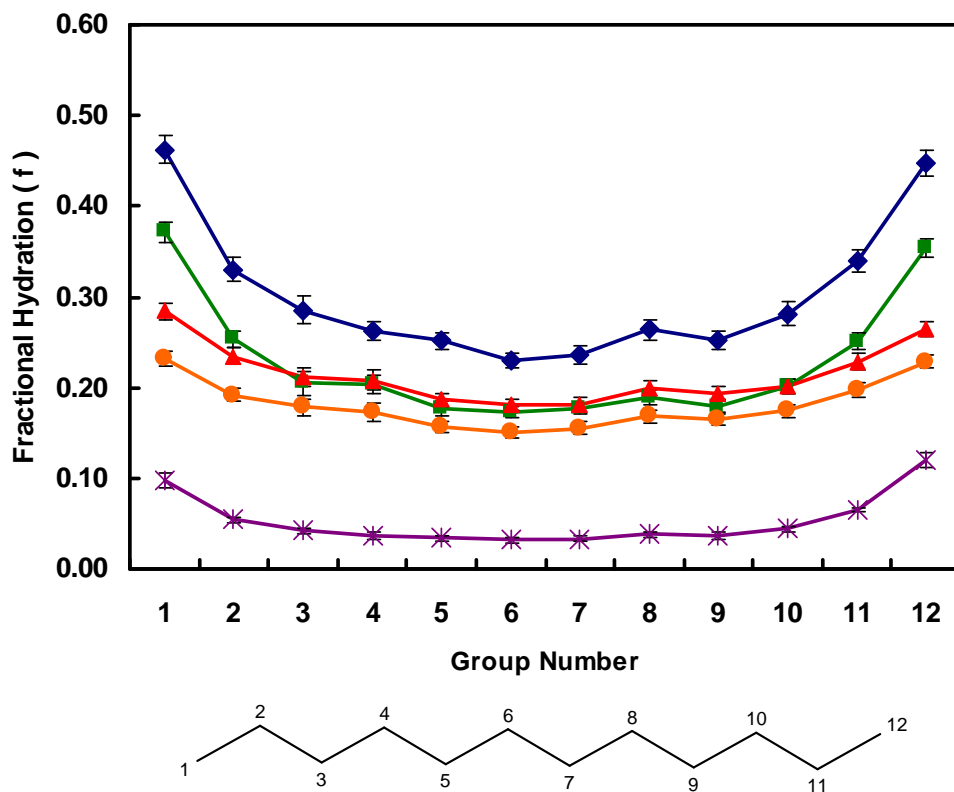


Figure 6-6: The average fractional degree of hydration (f), as defined in Eq. 6.15, corresponding to each of the groups in dodecane for each of the five simulated aggregate geometries. Results are presented for: (i) a small spherical aggregate (\blacklozenge), (ii) a large spherical aggregate (\blacksquare), (iii) a small cylindrical aggregate (\blacktriangle), (iv) a large cylindrical aggregate (\bullet), and (v) a planar slab (\ast). Group numbers are identified in the molecular structure shown below the fractional hydration plot. The error bars shown correspond to the standard error of the mean. The various lines are shown as a guide for the eye.

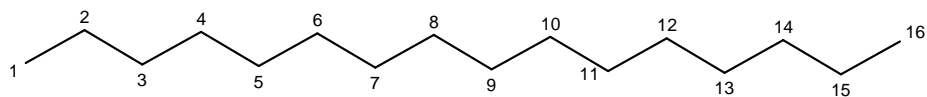
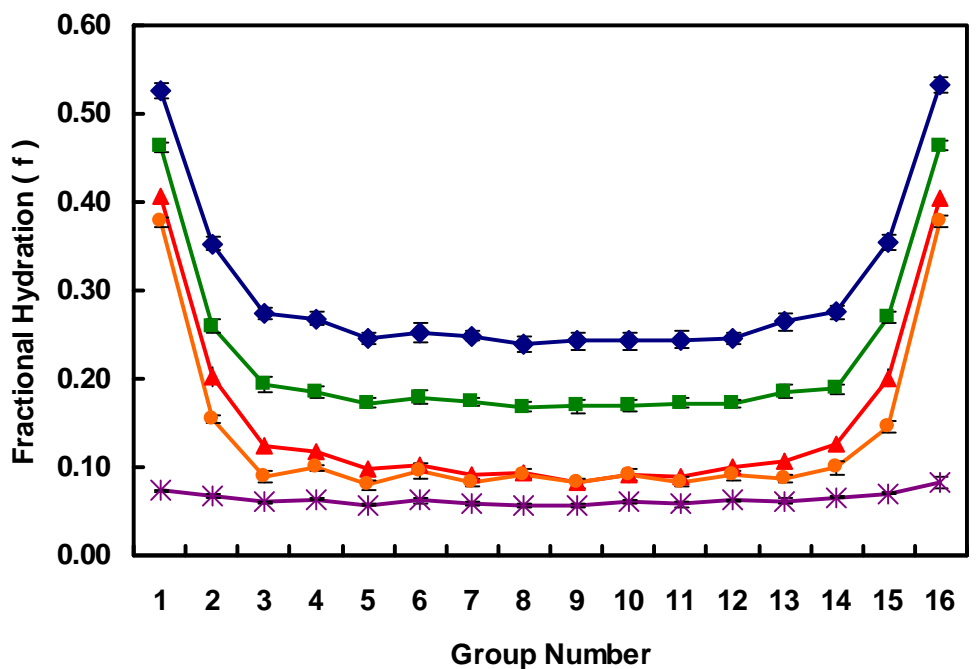


Figure 6-7: The average fractional degree of hydration (f), as defined in Eq. 6.15, corresponding to each of the groups in hexadecane for each of the five simulated aggregate geometries. Results are presented for: (i) a small spherical aggregate (\blacklozenge), (ii) a large spherical aggregate (\blacksquare), (iii) a small cylindrical aggregate (\blacktriangle), (iv) a large cylindrical aggregate (\bullet), and (v) a planar slab (\blackast). Group numbers are identified in the molecular structure shown below the fractional hydration plot. The error bars shown correspond to the standard error of the mean. The various lines are shown as a guide for the eye.

the aggregate core/water interface rather than being buried in the aggregate interior, which in turn imparts relatively high f values to the terminal CH_3 groups.

6.5.2 Solvent Accessible Surface Area (SASA) Results

The values of f computed for octane, for dodecane, and for hexadecane are intimately related to the average value of SASA associated with each oil aggregate interface. We have computed average values of SASA for each of the 15 oil aggregate geometries considered based on the simulation results. To calculate SASA, we used the double cubic lattice method as implemented in GROMACS. The solvent accessible surface was traced out by a probe sphere of radius 0.2 nm that was rolled around each molecule within the aggregate to identify the solvent accessible regions [54]. This probe sphere radius was selected based on the size of a water molecule (for which a probe radius of 0.14 nm is frequently used), and the requirement of preventing the probe from identifying any of the aggregate core region as being solvent accessible. The values of the time-averaged SASA divided by A , the “perfectly smooth” surface areas reported in Tables 6.1, 6.2, and 6.3, are shown in Figure 6-8. Note that the ratio, SASA/A , provides a convenient measure of surface roughness. The error bars shown in Figure 6-8 represent the standard error of the mean. As can be seen, the value of SASA/A for the 5 geometries considered is equal to 1.61 for octane (see the ■ results), 1.50 for dodecane (■), and 1.40 for hexadecane (■). It is interesting to note that for each geometry, SASA/A is lower for hexadecane than for dodecane, and for dodecane than for octane. Our results indicate that as the alkyl chain length decreases, the average roughness of the surface of the oil aggregate increases. In addition, a comparison of the results for the small and large spheres, and the results for the small and large cylinders, reveals that for each oil type considered, SASA/A is higher for the small aggregates and lower for the large aggregates.

As discussed in Section 6.3.4, to calculate g_{hydr} , we proposed a theoretical approach to estimate Δg_{wc} using Eq. 6.13. Recall that Δg_{wc} is equal to $\sigma_{\text{core}} - \sigma_{\text{bulk}}$. As such, it represents the free-energy difference (on a per unit SASA basis) associated

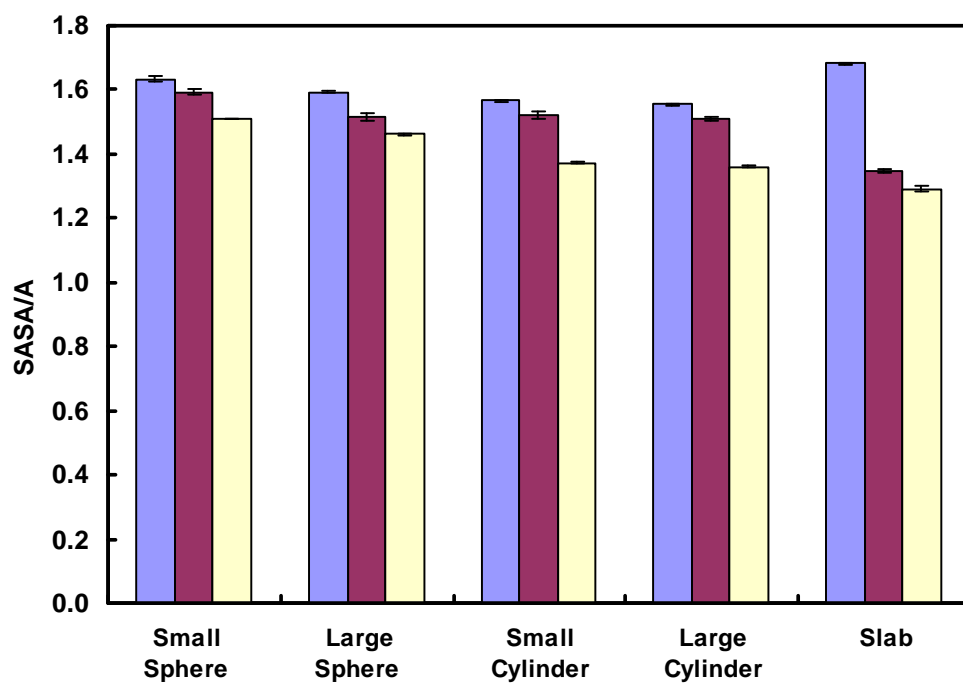


Figure 6-8: The ratio of the solvent accessible surface area (SASA) to the geometrically-defined surface area (A , see text) for each of the octane (■), dodecane (■), and hexadecane (■) oil aggregates simulated, grouped according to geometry. The error bars correspond to the standard error of the mean.

with hydrating contacts in the aggregate state and in the bulk water state. The value of σ_{core} is a function of both the alkyl tail length and the hydrophobic core curvature (see Section 6.3.4). We can estimate $\sigma_{\text{core}} = \sigma A_{\text{core}}/SASA_{\text{core}}$ using a value of σ corresponding to an oil molecule of type j ($j = \text{octane, dodecane, or hexadecane}$) calculated using Eq. 6.7. The ratio, $A_{\text{core}}/SASA_{\text{core}}$, is simply equal to the inverse of the SASA/ A ratios reported in Figure 6-8. We note that because $SASA_{\text{core}}$ is significantly larger than A_{core} , σ_{core} is significantly smaller than σ . We have performed a linear regression on the data to describe $SASA_{\text{core}}/A_{\text{core}}$ (or the “roughness” of the oil aggregate/water interface) as a function of linear alkyl chain length (n_t) and oil aggregate curvature (C , as defined in Eq. 6.14). The resulting expression, which has been fit with an R^2 value of 0.76, is given by:

$$SASA_{\text{core}}/A_{\text{core}} = 1.740 - 0.026n_t + 0.078C \quad (6.16)$$

Although σ_{core} is different for each oil aggregate, σ_{bulk} is approximately constant (see Section 6.3.4). Using a 0.2 nm probe for water (to be consistent with the SASA estimates for the oil aggregates), we computed $SASA_i$ values for octane, for dodecane, and for hexadecane, and then used these values to compute $\sigma_{\text{bulk}} = -g_{\text{tr}_i}/SASA_i$ using known values of g_{tr_i} (see Section 6.3.3). Our computed values of σ_{bulk} for octane, for dodecane, and for hexadecane are within 6% of each other, demonstrating that modeling the hydration free energy as being proportional to SASA for solutes of the same size as that of typical surfactant tails is a reasonable approximation. In addition, the average estimate of σ_{bulk} that we obtained for octane, for dodecane, and for hexadecane is 26.84 cal/mol/Å² (using a 0.2 nm probe for water to be consistent with the SASA estimates presented for the oil aggregate). As such, our result for σ_{bulk} is similar to σ_{bulk} estimates given by Tanford that are between 20 and 25 cal/mol/Å² [43].

We have predicted Δg_{wc} using: (i) the actual $SASA_{\text{core}}/A_{\text{core}}$ values obtained from our computer simulation results, and (ii) using the correlation for $SASA_{\text{core}}/A_{\text{core}}$

given in Eq. 6.16 for each of the 15 oil aggregates considered. Both predicted values of Δg_{wc} are plotted versus the oil aggregate curvature in Figure 6-9, where the curvature is defined in Eq. 6.14. As can be seen, the agreement between the two theoretical estimates of Δg_{wc} is reasonable. In general, our results indicate that Δg_{wc} decreases with increasing curvature. In addition, the change in Δg_{wc} with respect to curvature is smallest for octane (see the \blacklozenge results) and largest for hexadecane (\blacktriangle).

6.6 Molecular-Thermodynamic Modeling Based on Computer Simulation Inputs

We next use the CS-MT model to calculate g_{form} for each of the 15 oil aggregates discussed in Section 6.5. As discussed in Section 6.3.6, we have chosen oil aggregates as a starting point to evaluate the validity and accuracy of the CS-MT model because these structures do not require dealing with the computational challenges posed by the presence of the surfactant heads. Because experimental data are not available for the oil aggregates considered (since they are not thermodynamically stable except at infinite dilution), we compare our CS-MT model predictions with the predictions of the traditional MT model.

As discussed in Section 6.3.6, for each of the simulated oil aggregates, there are only two non-zero contributions to the free energy of aggregate formation, g_{form} . These contributions are g_{tr} and g_{int} in the traditional MT modeling approach, and g_{dehydr} and g_{hydr} in the CS-MT modeling approach.

CS-MT model predictions for g_{form} were made using Eq. 6.9 (where g_{pack} , g_{st} , g_{elec} , and g_{ent} are all equal to zero) and a 0.3 nm cutoff for the identification of the water contacts. The free energy of dehydration, g_{dehydr} , and the free energy of hydration, g_{hydr} , were computed using Eqs. 6.11 and 6.12, respectively. In computing g_{hydr} , we used the theoretical model for Δg_{wc} given in Eq. 6.13 and the correlation for $SASA_{core}/A_{core}$ given in Eq. 6.16. Traditional MT model predictions for g_{form} were

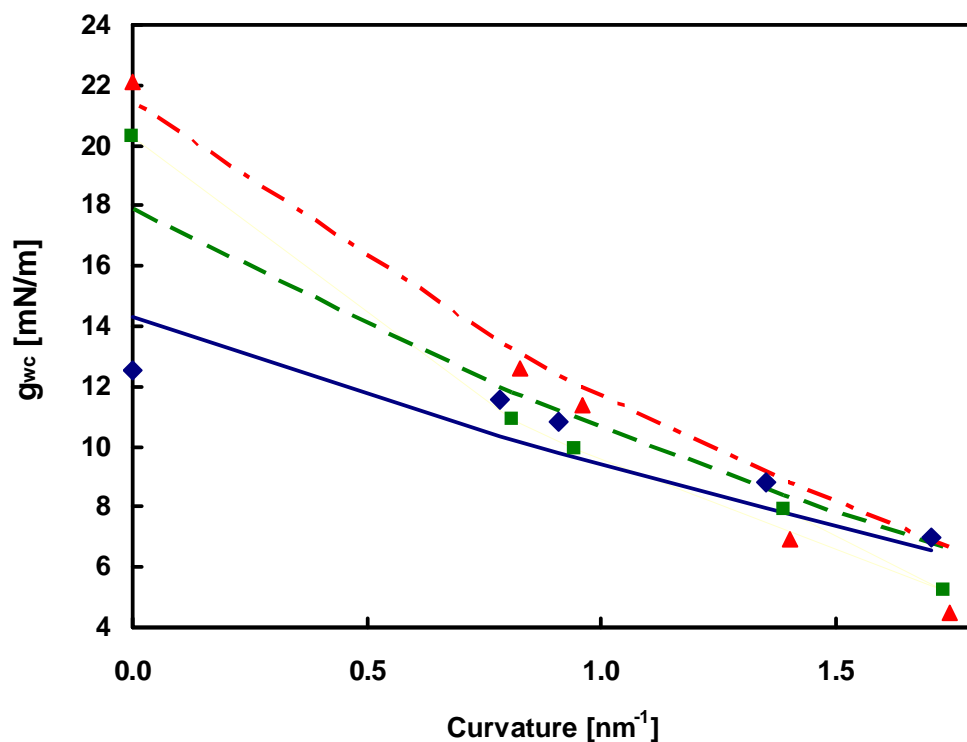


Figure 6-9: Theoretical predictions of the hydration free energy difference (Δg_{wc} [mN/m]) associated with hydrating contacts in the aggregate state and in the bulk water state are shown as a function of curvature [nm^{-1}], where the curvature, C , is defined using Eq. ???. Theoretical predictions based on values of $SASA_{core}/A_{core}$ computed from the simulation results are reported for octane (\blacklozenge), for dodecane (\blacksquare), and for hexadecane (\blacktriangle). Theoretical predictions based on values of $SASA_{core}/A_{core}$ obtained using the correlation given in Eq. 6.16 are also reported for octane (—), for dodecane (-- --), and for hexadecane (- . - .).

made using Eq. 6.4 (where g_{pack} , g_{st} , g_{elec} , and g_{ent} are all equal to zero) and by combining Eqs. 6.5, 6.6, and 6.7 to obtain the following expression:

$$g_{\text{form}} = \sum_{i=1}^{n_{\text{core}}} g_{\text{tr}_i} + a \left[\frac{\sigma_{0,j}}{\left(1 + \frac{(S-1)\delta}{l_c}\right)} \right] \quad (6.17)$$

In Table 6.4, we report predictions of the CS-MT model and of the traditional MT model for g_{form} , g_{dehydr} , and g_{hydr} corresponding to each of the five octane, dodecane, and hexadecane aggregate geometries simulated and modeled in this chapter. Each of the reported errors for the CS-MT model predictions corresponds to the standard error of the mean, and were computed through block averaging of the simulation results in the manner described in Section 6.4.5. Each reported Δ value corresponds to the percent difference between the CS-MT model and the MT model predictions for g_{form} . The estimated uncertainty in the CS-MT model predictions is comparable in magnitude to the difference between the predictions of the CS-MT model and those of the traditional MT model.

The average absolute discrepancy between the predictions of the CS-MT model and those of the traditional MT model for g_{form} , or the average of the absolute value of the 15 Δ values reported in Table 6.4, is only 1.04%. The best agreement between the predictions of the CS-MT model and those of the traditional MT model is for the small cylinders, with an average Δ value of only -0.05%. This is followed by the large sphere results (average Δ value = -0.56%), the large cylinder results (average Δ value = 0.74%), the slab results (average Δ value = 1.03%), and finally the small sphere results (average Δ value = -1.53%). On average, the differences are negative for the spheres and positive for the cylinders and the slabs, but in all cases, the errors are small. It is interesting to note that although, in all cases, the magnitude of g_{hydr} is much smaller than that of g_{dehydr} , it must be included in the CS-MT model for g_{form} in order to yield such a high level of agreement between the CS-MT model and the traditional MT model. Given the fact that the value of Δg_{wc} used to compute g_{hydr} in the CS-MT modeling approach was predicted theoretically using Eqs. 6.13

Octane					
Aggregate Type	$g_{\text{dehydr}} [k_B T]$	$g_{\text{hydr}} [k_B T]$	$g_{\text{form}} [k_B T]$		
			CS-MT	MT	Δ (%)
small sphere	-10.86 ± 0.04	1.82 ± 0.01	-9.04 ± 0.04	-9.13	-1.08
large sphere	-12.09 ± 0.03	1.74 ± 0.01	-10.35 ± 0.03	-10.31	0.42
small cylinder	-12.63 ± 0.02	2.03 ± 0.02	-10.60 ± 0.03	-10.59	0.06
large cylinder	-13.16 ± 0.02	1.66 ± 0.01	-11.5 ± 0.02	-11.27	1.97
slab	-15.14 ± 0.01	0.60 ± 0.00	-14.53 ± 0.01	-14.12	2.84
Dodecane					
Aggregate Type	$g_{\text{dehydr}} [k_B T]$	$g_{\text{hydr}} [k_B T]$	$g_{\text{form}} [k_B T]$		
			CS-MT	MT	Δ (%)
small sphere	-14.69 ± 0.09	1.94 ± 0.02	-12.75 ± 0.09	-12.85	-0.74
large sphere	-16.42 ± 0.07	2.23 ± 0.03	-14.19 ± 0.07	-14.24	-0.37
small cylinder	-17.01 ± 0.06	2.52 ± 0.03	-14.49 ± 0.07	-14.41	0.56
large cylinder	-17.80 ± 0.05	2.33 ± 0.03	-15.47 ± 0.06	-15.32	0.96
slab	-20.59 ± 0.04	1.41 ± 0.04	-19.18 ± 0.06	-19.09	0.46
Hexadecane					
Aggregate Type	$g_{\text{dehydr}} [k_B T]$	$g_{\text{hydr}} [k_B T]$	$g_{\text{form}} [k_B T]$		
			CS-MT	MT	Δ (%)
small sphere	-18.62 ± 0.06	2.14 ± 0.01	-16.48 ± 0.07	-16.94	-2.78
large sphere	-20.73 ± 0.05	2.56 ± 0.02	-18.17 ± 0.05	-18.48	-1.72
small cylinder	-22.68 ± 0.04	3.28 ± 0.02	-18.31 ± 0.05	-18.45	-0.78
large cylinder	-23.24 ± 0.04	2.92 ± 0.02	-19.39 ± 0.05	-19.53	-0.73
slab	-26.12 ± 0.02	2.10 ± 0.03	-24.01 ± 0.03	-24.06	-0.19

Table 6.4: Computer simulation/molecular-thermodynamic (CS-MT) and traditional molecular-thermodynamic (MT) modeling results for g_{dehydr} , g_{hydr} , and g_{form} corresponding to each of the five octane, dodecane, and hexadecane aggregate geometries simulated and modeled in this article. The uncertainties reported for the CS-MT model results corresponds to the standard error of the mean. Each Δ value presented in the table represents the percent difference between the CS-MT model and the traditional MT model predictions for g_{form} .

and 6.16, rather than through any type of fitting procedure, the very high level of agreement between the predictions of the CS-MT model and the traditional MT model further supports the validity of the proposed CS-MT modeling approach. In addition, it supports the validity of the procedure that we adopted to define and count hydrating contacts as well as to compute SASA values in implementing the new CS-MT modeling approach.

For the completely hydrophobic solutes (oils) modeled in this chapter, the equivalence of the CS-MT model and the traditional MT model for the hydrophobic effect can be demonstrated mathematically if the following two conditions are met: (i) each f_i value must be defined so that it only conveys information about the *local* environment of group i (i.e. the environment immediately surrounding the solvent accessible surface of group i), and (ii) the approach used to determine $SASA_i$ and $SASA_{\text{core}}$ must yield physically realistic results, where the same solute probe size must be used to quantify both values. A demonstration of the mathematical equivalence of the CS-MT model and the traditional MT model is given in Appendix B, along with a discussion of the criteria that must be met for the two models to be equivalent. The close agreement between the results of the CS-MT model and the traditional MT model for the 15 oil aggregates considered here demonstrates that criteria (i) and (ii) above are indeed satisfied, and that the simulation times used to gather hydration data were sufficient to provide highly accurate values of f_i . It is important to note that for amphiphilic solutes such as surfactants (which possess both a head and a tail), the CS-MT model and the traditional MT model are not equivalent even if criteria (i) to (ii) are met. The reasons behind this lack of equivalence are discussed in detail in Appendix B. We believe that the CS-MT model yields more realistic estimates of the hydrophobic driving force for micelle formation in the case of complex amphiphilic solutes. With this expectation in mind, in Chapter 7, we implement the CS-MT model in the case of nonionic surfactants, and will also compare predictions made by the CS-MT model with those made by the traditional MT model for these surfactants.

Using the data reported in Table 6.4, it is possible to evaluate the validity of a computational approach that we detail in Appendix A to extend the applicability of the CS-MT model to allow the prediction of g_{form} as a function of aggregate shape and size, rather than only for a specific simulated aggregate geometry. Briefly, in Appendix A, we will show that the CS-MT model can be used to predict the optimal shape and size of solute aggregates based on fractional hydration information obtained from simulation of a *single* aggregate.

6.7 Conclusions

We have developed a novel computer simulation/molecular-thermodynamic (CS-MT) modeling approach that allows one to eliminate many of the simplifying assumptions which were needed to quantify the magnitude of the hydrophobic effect in the traditional MT modeling approach. This was accomplished by making use of detailed hydration data obtained through atomistic computer simulations. The detailed hydration information was used in a new theoretical framework to quantify the hydrophobic free-energy contributions associated with the self-assembly of hydrophobic solutes. In this model, g_{form} is computed using the expression $g_{\text{form}} = g_{\text{dehydr}} + g_{\text{hydr}} + g_{\text{pack}} + g_{\text{st}} + g_{\text{elec}} + g_{\text{ent}}$, where g_{dehydr} is the dehydration free-energy contribution and g_{hydr} is the hydration free-energy contribution. These two free-energy contributions replace the transfer, g_{tr} , and the interfacial, g_{int} , free-energy contributions which quantify the hydrophobic effect in the traditional MT modeling approach. The remaining free-energy contributions (g_{pack} , g_{st} , g_{elec} , and g_{ent}) are calculated in the context of the new CS-MT modeling approach in the same manner that they are calculated in the traditional MT modeling approach. However, it is important to stress that computer simulation information obtained on the aggregate structure may be used to improve the estimation of g_{pack} and g_{st} . Work along these lines is in progress.

The free-energy contribution associated with dehydration, g_{dehydr} , is modeled using

the concept of a transfer free energy for each individual hydrophobic group in a solute. These transfer free energies can be obtained from experimental solubility data, or estimated theoretically using group-contribution methods. The free-energy contribution associated with hydration, g_{hydr} , accounts for the change in free energy associated with water contacts in the aggregate and in the bulk water states. In this chapter, we have proposed a specific method to theoretically calculate this free-energy difference in the case of oil molecules. However, the CS-MT model was formulated in a general way, and may be used to model single nonionic and ionic surfactant micellization, the micellization of mixtures of nonionic and ionic surfactants, and micellar solubilization in addition to the self-assembly of oil aggregates. Although the theoretical model for Δg_{wc} presented in this chapter was formulated based only on data obtained from oil aggregate simulations, we anticipate that it may be successfully used to model the self-assembly of a variety of solutes and solute mixtures. The free energy per unit SASA in the bulk water reference state, σ_{bulk} , for a hydrophobic group in a surfactant molecule should be very similar to σ_{bulk} for a hydrophobic group in an oil molecule. In addition, the success of the traditional MT modeling approach in modeling the aggregate core/water interface using an oil/water interfacial tension (see Section 6.2.3), does indicate that approximating the free energy per unit SASA in the aggregate reference state, σ_{core} , as being equal to σ_{core} for an oil aggregate should yield reasonable results.

In this chapter, we have demonstrated the validity and the accuracy of the new CS-MT model by using it to model spherical, cylindrical, and planar oil aggregates, each containing three different types of oil molecules and having different degrees of curvature. Excellent agreement between the predictions of the CS-MT model and those of the traditional MT model for g_{form} was obtained for each of the 15 oil aggregates considered, with an average absolute error of only 1.04% between the two theoretical approaches. Our results also demonstrate that the CS-MT model can be used to predict g_{form} for aggregates of arbitrary shapes and sizes by using hydration information obtained using only two independent molecular dynamics simulations.

Because the hydrophobic effect is the primary driving force for micelle formation in aqueous solution, and it is also the largest free-energy contribution to g_{form} , the modeling approach presented in this chapter provides an important new approach to more accurately model the self-assembly of hydrophobic and amphiphilic solutes in aqueous solution. By quantifying the actual hydration changes that occur upon self-assembly for various moieties within a solute, and by subsequently using this information in a new theoretical model to quantify the hydrophobic effect, the CS-MT modeling approach has the potential to improve our ability to model the micellization and the micellar solubilization behavior of complex surfactants and solubilizates in aqueous solution. In Chapter 7 [26], we use the CS-MT modeling approach presented here to model the micellization behavior of nonionic surfactants in aqueous solution. In Chapter 8 [27,63], we report modeling results for the aqueous micellization of ionic and zwitterionic surfactants.

6.8 Appendix A: Extension of the CS-MT Model to Predict Aggregate Shape and Size

As discussed in Section 6.3.5, a key capability of traditional MT modeling is that it enables prediction of g_{form} as a function of aggregate shape and size. From this functional dependence, the optimal aggregate shape and size can be predicted. In this appendix, we outline a computational approach to extend the CS-MT modeling approach to enable prediction of g_{form} as a function of aggregate shape and size. It is important to note that the MD simulations conducted as part of the CS-MT modeling approach do *not* allow direct prediction of the optimal aggregate shape and size because the simulation timescales are too short to permit the exchange of solute monomers between the aggregate phase and the aqueous phase.

With the exception of the transfer free-energy contribution, g_{tr} , the other five free-energy contributions to g_{form} in Eq. 6.4 are all functions of the micelle shape and size [14]. Note that g_{tr} is independent of the structural characteristics of the aggregate because it corresponds to the free-energy change associated with transferring a solute tail from infinite dilution in aqueous solution to an infinite bulk phase composed of solute tails. In order for the CS-MT model to be able to predict micelle shape and size, we will exploit this property of g_{tr} . Specifically, we combine the traditional MT model for the hydrophobic effect ($g_{\text{tr}} + g_{\text{int}}$) with the CS-MT model for the hydrophobic effect ($g_{\text{dehydr}} + g_{\text{hydr}}$) to obtain a CS-MT model prediction for the transfer free energy of a solute. Specifically,

$$g_{\text{tr,CS-MT}} = g_{\text{dehydr}} + g_{\text{hydr}} - \hat{g}_{\text{int}} \quad (6-A1)$$

where $g_{\text{tr,CS-MT}}$ is the transfer free energy computed using the CS-MT modeling approach, and \hat{g}_{int} is the MT prediction of the interfacial free energy of the *simulated* micellar aggregate. The free energy of aggregate formation, g_{form} , for micelles of a different shape and size than those for which the computer simulation data was col-

lected can then be calculated using Eq. 6.4 in the context of the traditional MT modeling approach:

$$g_{\text{form}} = g_{\text{tr,CS-MT}} + g_{\text{int}} + g_{\text{pack}} + g_{\text{st}} + g_{\text{elec}} + g_{\text{ent}} \quad (6\text{-A2})$$

After computing g_{form} using Eq. 6-A2, the optimal values of S , l_c , α , and β can be obtained in a computationally-efficient manner by minimizing g_{form} with respect to each of these variables (see Section 6.2.2). Using this strategy, the CS-MT modeling approach can be used to predict g_{form} for micelles of any shape and size using only two independent computer simulations: one simulation of the solute in the bulk water environment and a second simulation of the solute in an aggregate environment of arbitrary shape and size.

We would like to stress that for the proposed computational approach to be implemented successfully, during the aggregate simulation, the aggregate must remain stable and not break apart into monomers or into several smaller aggregates. This stability, of course, is not guaranteed when a micelle is pre-formed and simulated at a non-optimal shape and size. Fortunately, based on our experience, surfactant micelles in a somewhat non-optimal geometry (for example, a spherical instead of a cylindrical geometry, or at a non-optimal aggregation number) do remain stable during the 10 to 25 ns simulations conducted in the context of the CS-MT modeling approach. As discussed in Chapter 7, each nonionic surfactant micelle that we simulated remained stable on these timescales, even when pre-formed at a non-optimal shape and size. In addition, we note that all the 15 oil aggregates that we simulated in this chapter remained stable during the equilibration and the data gathering simulation runs.

Using the CS-MT model predictions for g_{form} presented in Table 6.4, we computed values of $g_{\text{tr,CS-MT}}$ for octane, for dodecane, and for hexadecane by evaluating Eq. 6-A1 using hydration information obtained from each of the five simulated aggregate geometries. Results for $g_{\text{tr,CS-MT}}$ calculated in this manner are reported in Table 6.5. For the computational approach outlined here to be successful, similar estimates of

	Octane	Dodecane	Hexadecane
small sphere	-15.90 ± 0.04	-21.88 ± 0.09	-27.49 ± 0.07
large sphere	-16.04 ± 0.03	-21.92 ± 0.07	-27.64 ± 0.05
small cylinder	-16.01 ± 0.03	-22.06 ± 0.07	-27.81 ± 0.05
large cylinder	-16.23 ± 0.02	-22.13 ± 0.06	-27.81 ± 0.05
slab	-16.41 ± 0.01	-22.06 ± 0.06	-27.91 ± 0.03
mean ± SD	-16.12 ± 0.20	-22.01 ± 0.10	-27.73 ± 0.16

Table 6.5: Predicted values of $g_{\text{tr,CS-MT}}$ for octane, dodecane, and hexadecane. The results (in $k_B T$) were obtained using Eq. 6-A1 and computer simulation data obtained for each of the five aggregate geometries considered. The uncertainty reported for each value of $g_{\text{tr,CS-MT}}$ corresponds to the standard error of the mean, as obtained through block averaging (see Section 6.4.5). The “mean” values reported for octane, for dodecane, and for hexadecane in the last row of the table are the average estimates for $g_{\text{tr,CS-MT}}$ obtained from the results for each oil type, and the standard deviation (SD) values are the standard deviations in the five $g_{\text{tr,CS-MT}}$ estimates obtained for each oil type.

$g_{\text{tr,CS-MT}}$ should be obtained for octane, for dodecane, and for hexadecane regardless of which aggregate simulation was used to obtain the hydration data.

As Table 6.5 shows, the predicted values of $g_{\text{tr,CS-MT}}$ for octane, for dodecane, and for hexadecane are quite consistent. The mean and standard deviation of the $g_{\text{tr,CS-MT}}$ values predicted for each oil type are reported in the last row of Table 6.5. The standard deviations reported for each oil type are quite small (between 0.10 and 0.20 $k_B T$), a result that supports the validity of the computational approach presented here to predict g_{form} for aggregates of arbitrary shapes and sizes.

To illustrate the manner in which Eq. 6-A2 may be used to reduce the number of simulations required in the CS-MT modeling approach, we have used it to predict g_{form} for each of the five dodecane aggregates considered in this chapter. The results are reported in Table 6.6. The first column of predictions in Table 6.6 for the free energy of formation (reported as g_{form}), is identical to what is reported in Table 6.4 as the CS-MT model predictions of g_{form} for dodecane. As discussed in Section 6.3, these CS-MT model predictions of g_{form} were made using Eq. 6.9, with g_{dehydr} and g_{hydr} computed using Eqs. 6.11 and 6.12, respectively. A total of five bulk water and five aggregate simulations were required to generate these results. The

	$g_{\text{form}} [k_{\text{B}}T]$	$g_{\text{form,max}} [k_{\text{B}}T]$	$g_{\text{form,min}} [k_{\text{B}}T]$	$\ \Delta (\%)\ [k_{\text{B}}T]$
small sphere	-12.75 ± 0.09	-12.75 ± 0.09	-12.93 ± 0.09	1.43
large sphere	-14.19 ± 0.07	-14.14 ± 0.07	-14.33 ± 0.07	1.29
small cylinder	-14.49 ± 0.07	-14.32 ± 0.07	-14.50 ± 0.07	1.27
large cylinder	-15.47 ± 0.06	-15.22 ± 0.06	-15.40 ± 0.06	1.19
slab	-19.18 ± 0.06	-19.00 ± 0.06	-19.18 ± 0.06	0.96

Table 6.6: Predicted values of g_{form} for the five simulated geometries of dodecane. CS-MT modeling results obtained using Eq. 6.9 are reported as g_{form} (in $k_{\text{B}}T$). CS-MT modeling results obtained using Eq. 6-A2 and the maximum value of $g_{\text{tr,CS-MT}}$ for dodecane reported in Table 4 are reported as $g_{\text{form,max}}$ (in $k_{\text{B}}T$). CS-MT modeling results obtained using Eq. 6-A2 and the minimum value of $g_{\text{tr,CS-MT}}$ for dodecane reported in Table 4 are reported as $g_{\text{form,min}}$ (in $k_{\text{B}}T$). The uncertainty reported for each value corresponds to the standard error of the mean, as obtained through block averaging (see Section 6.4.5).

second column of predictions for the free energy of formation (reported as $g_{\text{form,max}}$ in Table 6.6) were computed using the maximum value of $g_{\text{tr,CS-MT}}$ for dodecane given in Table 6.5 and using Eq. 6-A2. As a result, only one bulk water and one aggregate simulation were required to generate these results. The maximum value of $g_{\text{tr,CS-MT}}$ obtained using the CS-MT model in Table 6.5 corresponds to the small spherical dodecane aggregate ($-21.88 k_{\text{B}}T$). The third column of predictions for the free energy of formation (reported as $g_{\text{form,min}}$ in Table 6.6) were computed using the minimum value of $g_{\text{tr,CS-MT}}$ for dodecane given in Table 6.5 and using Eq. 6-A2. Like the $g_{\text{form,max}}$ predictions, only one bulk water and one aggregate simulation were required to generate the $g_{\text{form,min}}$ predictions. As shown in Table 6.5, the minimum value of $g_{\text{tr,CS-MT}}$ was obtained based on simulation results for the dodecane slab ($-22.06 k_{\text{B}}T$). The absolute values of the percent differences between $g_{\text{form,max}}$ and $g_{\text{form,min}}$ (reported as $\|\Delta (\%)\|$) are also reported in Table 6.6.

The level of agreement between g_{form} , $g_{\text{form,max}}$, and $g_{\text{form,min}}$ is very high. The average value of $\|\Delta(\%)\|$ for the five aggregate geometries considered in Table 6.6 is only 1.23%. In addition, the reduction in computational cost associated with the use of Eq. 6-A2 is very significant. Accordingly, we use Eq. 6-A2 in Chapter 7 to predict: (i) optimal micelle shapes and sizes, (ii) the corresponding values of g_{form} ,

and (iii) CMC's of nonionic surfactants.

6.9 Appendix B: Mathematical Demonstration of the Equivalence of the CS-MT Model and the Traditional MT Model for Completely Hydrophobic Solutes

The CS-MT model and the traditional MT model for the hydrophobic effect are equivalent for completely hydrophobic solutes such as the oil molecules considered in this chapter. In this Appendix, this equivalence will be demonstrated mathematically. For oil molecules, g_{dehydr} and g_{hydr} may be combined to obtain an expression analogous to the expression used to calculate g_{tr} and g_{int} in the traditional MT modeling approach. Recall that:

$$g_{\text{dehydr}} = \sum_{i=1}^{n_{\text{hyd}}} (1 - f_i) g_{\text{tr}_i} \quad (6-B1)$$

and

$$g_{\text{hydr}} = \sum_{i=1}^{n_{\text{core}}} SASA_i f_i \left(\frac{\sigma A_{\text{core}}}{SASA_{\text{core}}} + \frac{g_{\text{tr}_i}}{SASA_i} \right) \quad (6-B2)$$

as introduced and discussed in Section 6.3 (see Eqs. 6.11 and 6.12). For oil molecules, the sum of these two free energies represents the total contribution to g_{form} due to the hydrophobic effect (HE). We will refer to this free-energy contribution as g_{HE} . The CS-MT model for g_{HE} may be expressed and manipulated as follows:

$$g_{\text{HE}} = \sum_{i=1}^{n_{\text{hyd}}} (1 - f_i) g_{\text{tr}_i} + \sum_{i=1}^{n_{\text{core}}} SASA_i f_i \left(\frac{\sigma A_{\text{core}}}{SASA_{\text{core}}} + \frac{g_{\text{tr}_i}}{SASA_i} \right) \quad (6-B3)$$

or

$$g_{\text{HE}} = \sum_{i=1}^{n_{\text{hyd}}} g_{\text{tr}_i} - \sum_{i=1}^{n_{\text{hyd}}} f_i g_{\text{tr}_i} + \frac{\sigma A_{\text{core}}}{SASA_{\text{core}}} \sum_{i=1}^{n_{\text{core}}} SASA_i f_i + \sum_{i=1}^{n_{\text{core}}} f_i g_{\text{tr}_i} \quad (6-B4)$$

For the oil molecules considered in this chapter, $n_{\text{hyd}} = n_{\text{core}}$ because every hydrophobic group in each oil molecule is incorporated into the aggregate core upon aggregate self-assembly. As a result, the second term and the last term on the right-

hand side of Eq. 6-B4 cancel out. We note that this is not the case for amphiphilic solutes such as surfactants. For oil molecules, Eq. 6-B4 reduces to:

$$g_{\text{HE}} = \sum_{i=1}^{n_{\text{core}}} g_{\text{tr}_i} + \frac{\sigma A_{\text{core}}}{SASA_{\text{core}}} \sum_{i=1}^{n_{\text{core}}} SASA_i f_i \quad (6-B5)$$

or to:

$$g_{\text{HE}} = \sum_{i=1}^{n_{\text{core}}} g_{\text{tr}_i} + \sigma_{\text{core}} \langle SASA^{\text{hydr}} \rangle \quad (6-B6)$$

where $\sigma_{\text{core}} = \sigma A_{\text{core}}/SASA_{\text{core}}$ was introduced in Section 6.3.4 and represents the free energy of the hydrophobic core/water interface on a per unit SASA basis. Note that in Eq. 6-B5 we have replaced the term $\sum_{i=1}^{n_{\text{core}}} SASA_i f_i$ with $\langle SASA^{\text{hydr}} \rangle$ to emphasize that the product of $SASA_i$ and the average value of f_i obtained through computer simulations should be equal to the average value of SASA that is exposed to hydrating contacts. For $SASA_i f_i$ to be equal to $\langle SASA^{\text{hydr}} \rangle$ and for the CS-MT model to yield valid results, one requires that: (i) each f_i value must be defined so that it conveys information about only the *local* environment of group i (i.e. the environment immediately surrounding the solvent accessible surface of group i), and (ii) the approach used to determine $SASA_i$ and $SASA_{\text{core}}$ must give physically realistic results, where the same solute probe size must be used to quantify both SASA values. The close agreement between the CS-MT and the traditional MT modeling results obtained in this chapter demonstrate that both conditions (i) and (ii) above are satisfied for the analysis approach that we have presented.

The expression for g_{HE} in Eq. 6-B6 in the context of the CS-MT model is directly analogous to the g_{HE} expression in the traditional MT model of the hydrophobic effect for aggregates containing solutes that are completely hydrophobic (i.e. aggregates where no solute heads are present):

$$g_{\text{HE}} = g_{\text{tr}} + g_{\text{int}} \quad (6-B7)$$

or

$$g_{\text{HE}} = \sum_{i=1}^{n_{\text{core}}} g_{\text{tr}_i} + \sigma a \quad (6\text{-B8})$$

where σ is the interfacial tension of the aggregate core/water interface, and a is the area of the hydrophobic core per solute molecule as computed geometrically based on the volume of the aggregate under the assumption of a perfectly smooth aggregate surface (see Section 6.3.4). Comparison of Eqs. 6-B6 and 6-B8 shows that, in the absence of solute heads, the CS-MT and the traditional MT models both include a term that quantifies the free-energy contribution associated with transferring each hydrophobic group from bulk water to a bulk phase of group i ($\sum_{i=1}^{n_{\text{core}}} g_{\text{tr}_i}$), as well as a term that quantifies the free-energy contribution associated with the formation of a hydrophobic core/water interface. In the CS-MT model, this free-energy contribution is computed using SASA and σ_{core} , while in the traditional MT model it is computed using a and σ .

The CS-MT model and the traditional MT model are not equivalent, however, for amphiphilic solutes possessing a head and a tail. For such solutes, n_{hyd} is not equal to n_{core} , and the CS-MT and traditional MT estimates for the free-energy contribution associated with transferring each solute from the bulk water state to the aggregate state will differ. In the CS-MT model, each of the hydrophobic groups in a solute contributes its transfer free energy to g_{HE} to the extent that it is dehydrated, whereas in the traditional MT model only the hydrophobic groups in the surfactant tail contribute their transfer free energies to g_{HE} . The CS-MT modeling approach avoids the “all-or-nothing” approximation implicit in the traditional MT modeling approach shown in Eq. 6-B8, in which groups in the head do not contribute at all to g_{tr} , while groups in the tail contribute fully their individual transfer free energies.

CS-MT and traditional MT model estimates of the free-energy contribution associated with the formation of the aggregate core/water interface are also not equivalent for amphiphilic solutes, because the two models account differently for the presence of the solute heads at the aggregate core/water interface. For aggregates containing

amphiphilic solutes, the CS-MT modeling approach provides a way to directly calculate the hydrated SASA for each solute molecule, even when the solute heads are present, including using this SASA to compute the interfacial free energy. In Section 6.4.5, we argued that when the CS-MT model is used to model amphiphilic solutes, both contacts with water and with hydrogen-bonding atoms in the solute head should be counted as hydrating contacts in computing each f_i value. On the other hand, when using the traditional MT model, an assumption must be made about the extent to which the solute heads shield the aggregate core/water interface from water contacts. The area screened by a surfactant head is traditionally approximated as being equal to the cross-sectional area of a single carbon-carbon bond, or approximately 21 \AA^2 [14]. The validity of this assumption is discussed in greater detail in Chapter 7. Another difference between the CS-MT model and the traditional MT model estimates of the free-energy contribution associated with the formation of the aggregate core/water interface is that the CS-MT modeling approach permits estimation of the ensemble average of this free-energy contribution. This may be implemented in the CS-MT modeling approach by analyzing micelle microstructure and hydration at every snapshot in the molecular dynamics trajectory, and determining the hydrophobic groups in each amphiphilic solute that are part of the aggregate core at each instant in time. For solute groups that are part of the aggregate core, g_{hydr} is calculated using Eq. 6-B2. Determining the hydrophobic groups in each solute that are part of the aggregate core at any given time may be done in a number of ways, including comparing each group’s f_i value to a cutoff value of f used to identify groups that are part of the aggregate core, or determining each group’s position relative to the aggregate core/water interface. An estimate of g_{HE} can then be made by averaging the g_{hydr} values obtained over the course of the simulation run. In this manner, the CS-MT model avoids the “all-or-nothing” approximation implicit in the traditional MT modeling approach to compute g_{int} , in which head and tail assignments must be made, the aggregate core is assumed to contain only tails, and Eq. 6-B8 is invoked. A final difference between the way in which the free-energy

contribution associated with forming the aggregate core/water interface is estimated in the CS-MT and in the traditional MT modeling approaches is that by using the results from computer simulations, the CS-MT modeling approach enables estimation of the free-energy contribution associated with the formation of the aggregate core/water interface over an ensemble average of many different physically realistic micellar configurations, rather than of the three idealized, static configurations (a perfect sphere, a perfect cylinder, or a perfect bilayer) that can be successfully modeled in the traditional MT modeling approach [14]. The manner in which the traditional MT modeling results for these three idealized geometries are combined to model: (i) finite cylinders with hemispherical endcaps, and (ii) finite disklike micelles is discussed in detail in Ref. 32.

Bibliography

- [1] Elworthy, P. H., Florence, A. T., and Macfarlane, C. B., *Solubilization by Surface Active Agents*, Chapman and Hall, London, 1968.
- [2] Dunaway, C. S., Christian, S. D., and Scamehorn, J. F., *Solubilization in Surfactant Aggregates. Surfactant Science Series 55*, Marcel Dekker, New York, 1995.
- [3] Nagarajan, R., “Solubilization in aqueous solutions of amphiphiles,” *Current Opinion in Colloid and Interface Science*, Vol. 1, 1996, pp. 391–401.
- [4] Nagarajan, R., “Solubilization by amphiphilar aggregates,” *Current Opinion in Colloid and Interface Science*, Vol. 2, 1997, pp. 282–293.
- [5] Srinivasan, V., *Theoretical Modeling of Micellization and Solubilization in Ionic Surfactant Systems*, Ph.D. thesis, Massachusetts Institute of Technology, 2003, and references cited therein.
- [6] Tanford, C., *The Hydrophobic Effect: Formation of Micelles and Biological Membranes*, John Wiley and Sons, New York, 1991.
- [7] Israelachvili, J. N., *Intermolecular and Surface Forces*, Academic Press, 2nd ed., 1991.
- [8] Nagarajan, R. and Ruckenstein, E., “Theory of surfactant self-assembly: A predictive molecular thermodynamic approach,” *Langmuir*, Vol. 7, 1991, pp. 2934–2969.

- [9] Shiloach, A. and Blankschtein, D., “Predicting micellar solution properties of binary surfactant mixtures,” *Langmuir*, Vol. 14, 1998, pp. 1618–1636.
- [10] Gunnarsson, G., Jonsson, B., and Wennerstrom, H., “Surfactant association into micelles - An electrostatic approach,” *The Journal of Physical Chemistry*, Vol. 84, 1980, pp. 3114–3121.
- [11] Jonsson, B. and Wennerstrom, H., “Thermodynamics of ionic amphiphile-water systems,” *Journal of Colloid and Interface Science*, Vol. 80, 1981, pp. 482–496.
- [12] Evans, D. F., Mitchell, D. J., and Ninham, B. W., “Ion binding and dressed micelles,” *The Journal of Physical Chemistry*, Vol. 88, 1984, pp. 6344–6348.
- [13] Hayter, J. B., “A self-consistent theory of dressed micelles,” *Langmuir*, Vol. 8, 1992, pp. 2873–2876.
- [14] Puvvada, S. and Blankschtein, D., “Molecular thermodynamic approach to predict micellization, phase behavior and phase separation of micellar solutions. 1. Application to nonionic surfactants,” *The Journal of Chemical Physics*, Vol. 92, 1990, pp. 3710–3724, and references cited therein.
- [15] Srinivasan, V. and Blankschtein, D., “Effect of counterion binding on micellar solution behavior: 1. Molecular-thermodynamic theory of micellization of ionic surfactants,” *Langmuir*, Vol. 19, 2003, pp. 9932–9945.
- [16] Srinivasan, V. and Blankschtein, D., “Effect of counterion binding on micellar solution behavior: 2. Prediction of micellar solution properties of ionic surfactant-electrolyte systems,” *Langmuir*, Vol. 19, 2003, pp. 9946–9961.
- [17] Reif, I., Mulqueen, M., and Blankschtein, D., “Molecular-thermodynamic prediction of critical micelle concentrations of commercial surfactants,” *Langmuir*, Vol. 17, 2001, pp. 5801–5812.

- [18] Shiloach, A. and Blankschtein, D., “Measurement and prediction of ionic/nonionic mixed micelle formation and growth,” *Langmuir*, Vol. 14, 1998, pp. 7166–7182.
- [19] Shiloach, A. and Blankschtein, D., “Prediction of critical micelle concentrations of nonideal ternary surfactant mixtures,” *Langmuir*, Vol. 14, 1998, pp. 4105–4114.
- [20] Shiloach, A. and Blankschtein, D., “Prediction of critical micelle concentrations and synergism of binary surfactant mixtures containing zwitterionic surfactants,” *Langmuir*, Vol. 13, 1997, pp. 3968–3981.
- [21] Zoeller, N., Lue, L., and Blankschtein, D., “A statistical-thermodynamic framework to model nonionic micellar solutions,” *Langmuir*, Vol. 13, 1997, pp. 5258–5275.
- [22] Goldsipe, A. and Blankschtein, D., “Modeling counterion binding in ionic-nonionic and ionic-zwitterionic binary surfactant mixtures,” *Langmuir*, Vol. 22, 2005, pp. 9850–9865.
- [23] ChemSW, Inc., Fairfield, CA., *Molecular Modeling Pro version 3.2*, 2003.
- [24] Stephenson, B. C., Beers, K., and Blankschtein, D., “Complementary use of simulations and molecular-thermodynamic theory to model micellization,” *Langmuir*, Vol. 22, 2006, pp. 1500–1513.
- [25] Stephenson, B. C., Rangel-Yagui, C. O., Pessoa, A., Tavares, L. C., Beers, K. J., and Blankschtein, D., “Experimental and theoretical investigation of the micellar-assisted solubilization of ibuprofen in aqueous media,” *Langmuir*, Vol. 22, 2006, pp. 1514–1525.
- [26] Stephenson, B. C., Goldsipe, A., Beers, K. J., and Blankschtein, D., “Quantifying the hydrophobic effect: II. A computer simulation/molecular-thermodynamic

- model for the micellization of nonionic surfactants,” *The Journal of Physical Chemistry B*, 2006, pp. (submitted).
- [27] Stephenson, B. C., Beers, K. J., and Blankschtein, D., “Quantifying the hydrophobic effect: III. A computer simulation/molecular-thermodynamic model for the micellization of ionic and zwitterionic surfactants,” *The Journal of Physical Chemistry B*, 2006, pp. (submitted).
- [28] Ben-Shaul, A. and Szleifer, I., “Chain organization and thermodynamics in micelles and bilayers. I. Theory,” *The Journal of Chemical Physics*, Vol. 83, 1985, pp. 3597–3611.
- [29] Szleifer, I., Ben-Shaul, A., and Gelbart, W. M., “Chain organization and thermodynamics in micelles and bilayers. II. Model calculations,” *The Journal of Chemical Physics*, Vol. 83, 1985, pp. 3612–3620.
- [30] Szleifer, I., Ben-Shaul, A., and Gelbart, W. M., “Statistical thermodynamics of molecular organization in mixed micelles and bilayers,” *The Journal of Chemical Physics*, Vol. 86, 1987, pp. 7094–7109.
- [31] Srinivasan, V. and Blankschtein, D., “Prediction of conformational characteristics and micellar solution properties of fluorocarbon surfactants,” *Langmuir*, Vol. 21, 2004, pp. 1647–1660.
- [32] Puvvada, S. and Blankschtein, D., “Theoretical and experimental investigations of micellar properties of aqueous solutions containing binary mixtures of nonionic surfactants,” *The Journal of Physical Chemistry*, Vol. 96, 1992, pp. 5579–5592.
- [33] Maibaum, L., Dinner, A. R., and Chandler, D., “Micelle formation and the hydrophobic effect,” *The Journal of Physical Chemistry B*, Vol. 108, 2004, pp. 6778–6781.

- [34] Smith, R. and Tanford, C., “Hydrophobicity of long chain n-alkyl carboxylic acids, as measured by their distribution between heptane and aqueous solutions,” *Proceedings of the National Academy of Sciences*, Vol. 70, 1973, pp. 289–293.
- [35] Carale, T. R., Pham, Q. T., and Blankschtein, D., “Salt effects on intramolecular interactions and micellization of nonionic surfactants in aqueous solutions,” *Langmuir*, Vol. 10, 1994, pp. 109–121.
- [36] Gibbs, J. W., *The Scientific Papers of J.W. Gibbs*, Vol. 1, Dover, New York, 1961.
- [37] Koenig, F. O., “On the thermodynamic relation between surface tension and curvature,” *The Journal of Chemical Physics*, Vol. 18, 1950, pp. 449.
- [38] Buff, F. P., “The spherical interface. I. Thermodynamics,” *The Journal of Chemical Physics*, Vol. 19, 1951, pp. 1591.
- [39] Tolman, R. C., “Consideration of the Gibbs theory of surface tension,” *The Journal of Chemical Physics*, Vol. 16, 1948, pp. 758.
- [40] Aveyard, R., Briscoe, B. J., and Chapman, J., “Adhesion at the alkane/water and ester/water interfaces,” *Journal of the Chemical Society, Faraday Transactions*, Vol. 68, 1972, pp. 10.
- [41] Lum, K., Chandler, D., and Weeks, J. D., “Hydrophobicity and small and large length scales,” *The Journal of Physical Chemistry B*, Vol. 103, 1999, pp. 4570–4577.
- [42] Chandler, D., “Interfaces and the driving force of hydrophobic assembly,” *Nature*, Vol. 437, 2005, pp. 640–647.
- [43] Reynolds, J. A., Gilbert, D. B., and Tanford, C., “Empirical correlation between hydrophobic free energy and aqueous cavity surface area,” *Proceedings of the National Academy of Sciences*, Vol. 71, 1974, pp. 2925–2927.

- [44] Hermann, “Theory of hydrophobic bonding. II. The correlation of hydrocarbon solubility in water with solvent cavity surface area,” *The Journal of Physical Chemistry*, Vol. 76, 1972, pp. 2754–2759.
- [45] Pool, R. and Bolhuis, P. G., “Accurate free energies of micelle formation,” *The Journal of Physical Chemistry B*, Vol. 109, 2005, pp. 6650–6657.
- [46] Jorgensen, W. L., Maxwell, D. S., and Tirado-Rives, J., “Development and testing of the OPLS all-atom force field on conformational energetics and properties of organic liquids,” *Journal of the American Chemical Society*, Vol. 118, 1996, pp. 11225–11236.
- [47] Berendsen, H. J. C., Grigera, J. R., and Straatsma, T. P., “The missing term in effective pair potentials,” *The Journal of Physical Chemistry*, Vol. 91, 1987, pp. 6269–6271.
- [48] Darden, T., York, D., and Pedersen, L., “Particle mesh Ewald: An N-log(N) method for Ewald sums in large systems,” *The Journal of Chemical Physics*, Vol. 98, 1993, pp. 10089–10092.
- [49] Essmann, U., Perera, L., Berkowitz, M. L., Darden, T., Lee, H., and Pedersen, L. G., “A smooth particle mesh Ewald potential,” *The Journal of Chemical Physics*, Vol. 103, 1995, pp. 8577–8592.
- [50] Bader, J. S. and Chandler, D., “Computer-simulation study of the mean forces between ferrous and ferric ions in water,” *The Journal of Physical Chemistry*, Vol. 96, 1992, pp. 6423–6427.
- [51] Shirts, M. R., Pitner, J. W., Swope, W. C., and Pande, V. S., “Extremely precise free energy calculations of amino acid side chain analogs: Comparison of common molecular mechanics force fields for proteins,” *The Journal of Chemical Physics*, Vol. 119, 2003, pp. 5740–5760.

- [52] Shirts, M. R. and Pande, V. S., “Solvation free energies of amino acid side chain analogs for common molecular mechanics water models,” *The Journal of Chemical Physics*, Vol. 122, 2005, pp. 134508.
- [53] Shirts, M., *Calculating Precise and Accurate Free Energies in Biomolecular Systems*, Ph.D. thesis, Stanford, 2005, and references cited therein.
- [54] van der Spoel, D., Lindahl, E., Hess, B., van Buuren, A., Apol, E., Meulenhoff, P., Tieleman, D., Sijbers, A., Feenstra, K., van Drunen, R., and Berendsen, H., *Gromacs User Manual version 3.2*, www.gromacs.org, 2004.
- [55] van Gunsteren, W. F. and Berendsen, J. J. C., “A leap-frog algorithm for stochastic dynamics,” *Journal of Computational Chemistry*, Vol. 18, 1997, pp. 1463–1472.
- [56] Berendsen, H. J. C., van der Spoel, D., and van Drunen, R., “GROMACS: A message-passing parallel molecular dynamics implementation,” *Computational Physics Community*, Vol. 91, 1995, pp. 43–56.
- [57] Lindahl, E., Hess, B., and van der Spoel, D., “Gromacs 3.0: A package for molecular simulation and trajectory analysis,” *Journal of Molecular Modeling*, Vol. 7, 2001, pp. 306–317.
- [58] Jedlovsky, P., “Adsorption of apolar molecules at the water liquid-vapor interface: A Monte Carlo simulations study of the water-n-octane system,” *The Journal of Chemical Physics*, Vol. 119, 2003, pp. 1731–1740.
- [59] Flyvbjerg, H. and Petersen, H. G., “Error estimates on averages of correlated data,” *The Journal of Chemical Physics*, Vol. 91, 1989, pp. 461–466.
- [60] Hess, B., *Stochastic Concepts in Molecular Simulation*, Ph.D. thesis, Rijksuniversiteit Groningen, Groningen, 1999.

- [61] Hess, B., “Determining the shear viscosity of model liquids from molecular dynamics simulations,” *The Journal of Chemical Physics*, Vol. 116, 2001, pp. 209–217.
- [62] Pearlman, D. A. and Kollman, P. A., “The lag between the hamiltonian and the system configuration in free-energy perturbation calculations,” *The Journal of Chemical Physics*, Vol. 91, 1989, pp. 7831–7839.
- [63] Stephenson, B. C., Mendenhall, J., Beers, K. J., and Blankschtein, D., “Quantifying the hydrophobic effect: IV. A computer simulation/molecular-thermodynamic model for micellar solubilization,” *The Journal of Physical Chemistry B*, 2006, pp. (to be submitted).

Chapter 7

Quantifying the Hydrophobic Effect: II. A Computer Simulation/Molecular-Thermodynamic Model for the Micellization of Nonionic Surfactants in Aqueous Solution

7.1 Introduction

In Chapter 6, [1] we developed a computer simulation/molecular-thermodynamic (CS-MT) modeling approach to better understand and quantify the hydrophobic driving force for solute (surfactant and solubilizate) aggregate formation in aqueous solution. As discussed in Chapter 6, a significant body of literature on traditional MT modeling has demonstrated its ability to model the micellization behavior of structurally simple surfactants with quantitative or semi-quantitative accuracy [2–7]. In the traditional

MT modeling approach, the free-energy change associated with the formation of the surfactant aggregate in aqueous solution is expressed as the sum of several free-energy contributions, all of which can be computed molecularly given the chemical structures of the various micellar components and the solution conditions. To date, traditional MT models of micellization and micellar solubilization have relied on relatively simple approximations for the micellar hydration states of the surfactants and the solubilizates. To extend the applicability of the traditional MT modeling approach to more chemically and structurally complex surfactants and solubilizates, there is a need to accurately estimate the hydration states of these solutes in the micellar state. The CS-MT model represents a novel approach to obtain and analyze this type of hydration data. With the above in mind, in this chapter, we use the CS-MT model to predict the micellization behavior of nonionic surfactants that are both simple and challenging to model using the traditional MT modeling approach.

7.1.1 Review of the CS-MT Model

In the CS-MT model, the free energy of aggregate formation, g_{form} , is computed as the sum of the following six free-energy contributions [1]:

$$g_{\text{form}} = g_{\text{dehydr}} + g_{\text{hydr}} + g_{\text{pack}} + g_{\text{st}} + g_{\text{elec}} + g_{\text{ent}} \quad (7.1)$$

The physical origin of each of these free-energy contributions can be understood by representing the process of aggregate formation as a thermodynamic cycle consisting of three separate steps (see Figure 6-2 in Chapter 6). Two of the free-energy contributions in Eq. 7.1, g_{dehydr} and g_{hydr} , reflect the hydrophobic free-energy change associated with aggregate formation, or the hydrophobic driving force for micelle formation. In the CS-MT modeling approach, both g_{dehydr} and g_{hydr} are computed using hydration data obtained from computer simulations. The remaining four free-energy contributions (g_{pack} , g_{st} , g_{elec} , and g_{ent}) in Eq. 7.1 are computed in the CS-MT model in the same manner as they are computed in the traditional MT modeling ap-

proach [8]. However, the way in which g_{pack} and g_{st} are computed could, in principle, be informed by the molecular dynamics simulation data. In Chapter 6, we proposed and validated theoretical models to evaluate g_{dehydr} and g_{hydr} . The free-energy contribution, g_{dehydr} , is computed as follows [1]:

$$g_{\text{dehydr}} = \sum_{i=1}^{n_{\text{hyd}}} (1 - f_i) g_{\text{tr}_i} \quad (7.2)$$

where n_{hyd} is the total number of hydrophobic groups in the solute, f_i is the fractional hydration of group i , and g_{tr_i} is the free-energy change associated with transferring group i from the aqueous solution to a bulk phase of solute tails. In Chapter 6, we justified computing f for each group i as follows:

$$f = \frac{\text{number of hydrating contacts in the aggregate}}{\text{number of hydrating contacts in bulk water}} \quad (7.3)$$

where a ‘‘hydrating contact’’ is defined as a contact with an atom that: (i) forms hydrogen bonds, or (ii) is capable of co-ordinate (dative-covalent) bonding. Based on this definition, if a hydrophobic CH_2 group is in contact with the oxygen, or with the hydrogen, atoms of a water molecule, with a positively-charged or a negatively-charged ion, or with a hydrophilic group in the solute head that is capable of hydrogen bonding, then the contact is considered ‘‘hydrating.’’ In Chapter 6, we also justified the use of a 0.3 nm cutoff distance to count the hydrating contacts that occur during MD simulation.

The free-energy contribution, g_{hydr} , is computed as follows [1]:

$$g_{\text{hydr}} = \sum_{i=1}^{n_{\text{core}}} \text{SASA}_i f_i \Delta g_{\text{wc}_i} \quad (7.4)$$

where n_{core} is the total number of hydrophobic groups in the solute that adsorb onto, or penetrate into, the aggregate core, SASA_i is the solvent accessible surface area of group i , and Δg_{wc_i} is defined as the difference in the free energy per unit of solvent accessible surface area associated with the hydration of group i in the micellar state

and in the aqueous solution.

In Chapter 6, the CS-MT model was used to calculate the free-energy change associated with the formation of aggregates of octane, of dodecane, and of hexadecane having various shapes (spheres, cylinders, and slabs) and sizes. In total, five different aggregate geometries were considered for each oil type. To compute g_{form} , f_i data was calculated using information on water contacts obtained by simulating a single oil molecule in bulk water and by simulating the same oil molecule in an oil aggregate. Values of g_{tr_i} were estimated for the CH_2 and the CH_3 groups in each oil molecule from aqueous solubility data of linear alkanes. Values of $SASA_i$ for the CH_2 and the CH_3 groups were estimated using the double cubic lattice method as implemented in GROMACS and a solvent probe of radius 0.2 nm [9]. We also developed an approach to theoretically calculate Δg_{wc_i} for oil molecules, in which Δg_{wc_i} is calculated as the difference between two “microscopic interfacial tensions,” or free energies per unit SASA. For oil molecules, Δg_{wc_i} does not depend on i , and is given by [1]:

$$\Delta g_{\text{wc}} = \sigma_{\text{core}} - \sigma_{\text{bulk}} = \frac{\sigma A_{\text{core}}}{SASA_{\text{core}}} - \frac{g_{\text{tr}_i}}{SASA_i} \quad (7.5)$$

where σ_{core} is the microscopic “interfacial tension” (interfacial free energy per unit SASA) associated with the aggregate core/water interface, σ_{bulk} is the microscopic “interfacial tension” (interfacial free energy per unit SASA) associated with the group i (CH_2 or CH_3)/water interface in the aqueous solution, σ is the macroscopic interfacial tension of the aggregate core/water interface, A_{core} is the surface area of the hydrophobic aggregate core as computed geometrically based on the volume of the aggregate subject to the assumption of a perfectly smooth aggregate surface, and $SASA_{\text{core}}$ is the solvent accessible surface area of the hydrophobic aggregate core.

The ratio $A_{\text{core}}/SASA_{\text{core}}$ in Eq. 7.5 was estimated using the following correlation that was fitted based on our computer simulation results for the various oil aggregates considered [1]:

$$SASA_{\text{core}}/A_{\text{core}} = 1.740 - 0.026n_t + 0.078C \quad (7.6)$$

where n_t is the total number of hydrophobic groups in the solute that are part of the hydrophobic aggregate core, and C is the curvature of the micellar aggregate, which is defined as $2/l_c$ for spheres, $1/l_c$ for cylinders, and zero for planar interfaces, where l_c is the core-minor radius or planar half-width. In Chapter 6, excellent agreement between the predictions of the CS-MT model and the traditional MT model was obtained for g_{form} for each of the 15 oil aggregates modeled, with an average absolute error of only 1.04% between the two modeling approaches. The very high level of agreement between the CS-MT and the traditional MT modeling results demonstrates the ability of the CS-MT model to quantify the hydrophobic effect for completely hydrophobic solutes, as well as to calculate g_{form} with a high degree of accuracy.

In Appendix A of Chapter 6, we showed that by combining elements of the CS-MT model and the traditional MT model, g_{form} can be computed as a function of aggregate shape and size after performing *only two computer simulations*: the first of the solute in a bulk water environment and the second of the same solute in an aggregate environment (where the aggregate can have arbitrary shape and size). Specifically, we showed that [1]:

$$g_{\text{tr,CS-MT}} = g_{\text{dehydr}} + g_{\text{hydr}} - \hat{g}_{\text{int}} \quad (7.7)$$

where $g_{\text{tr,CS-MT}}$ is the transfer free-energy contribution computed using the CS-MT modeling approach, and \hat{g}_{int} is the traditional MT prediction for the interfacial free-energy contribution of the simulated micellar aggregate. The free energy of aggregate formation, g_{form} , for a micelle of a different shape and size than that at which the computer simulation data was gathered is then calculated using the following equation [1]:

$$g_{\text{form}} = g_{\text{tr,CS-MT}} + g_{\text{int}} + g_{\text{pack}} + g_{\text{st}} + g_{\text{elec}} + g_{\text{ent}} \quad (7.8)$$

In Chapter 6, we demonstrated that consistent values of $g_{\text{tr,CS-MT}}$ based on hydration information obtained through computer simulation of oil aggregates of different curvatures can be estimated using Eq. 7.7. Using the computed value of $g_{\text{tr,CS-MT}}$,

we also demonstrated that highly accurate values of g_{form} could be obtained using Eq. 7.8 for each of the 15 oil aggregates considered.

For a micelle of the optimum shape, size, composition (in the case of mixed micelles), and degree of counterion binding (in the case of ionic surfactants), g_{form} has a minimum value, which we denote as g_{form}^* . By solving for g_{form}^* , the optimal aggregate shape, S^* , the optimal core-minor radius, l_c^* , the optimal composition, α^* , and the optimal degree of counterion binding, β^* , can be predicted. In addition, the CMC in mole fraction units is computed as follows [10]:

$$\text{CMC} \approx \exp \left(\frac{g_{\text{form}}^*(S^*, l_c^*, \alpha^*, \beta^*)}{k_{\text{B}}T} \right) \quad (7.9)$$

where k_{B} is the Boltzmann constant and T is the absolute temperature.

7.1.2 Modeling Nonionic Surfactant Micellization

In this chapter, we will use the CS-MT modeling approach introduced in Chapter 6 to model the micellization behavior of nonionic surfactants. Although the CS-MT model enables the prediction of a wide range of solution properties, the CMC has been selected for prediction and comparison with the experimental CMC data because the CMC depends exponentially on g_{form} , and as such, it provides a stringent test with which to evaluate the predictive accuracy of the CS-MT model. We have selected the following seven nonionic surfactants in order to test and validate the CS-MT model: octyl glucoside (OG), dodecyl maltoside (DM), octyl sulfinyl ethanol (OSE), decyl methyl sulfoxide (C_{10}SO), decyl dimethyl phosphine oxide (C_{10}PO), dodecyl octa(ethylene oxide) (C_{12}E_8), and decanoyl-*n*-methylglucamide (MEGA-10). These seven nonionic surfactants have varying degrees of structural and chemical complexity, and as such, have allowed us to thoroughly gauge the validity and predictive accuracy of the CS-MT modeling approach.

In order to use the CS-MT modeling approach in the case of the nonionic surfactants considered here, we have made three approximations to calculate g_{dehydr} and

g_{hydr} in a relatively simple manner. The first approximation involves the way in which we estimate g_{tr_i} to enable the evaluation of g_{dehydr} using Eq. 7.2. The second approximation involves introducing an approach to determine which surfactant groups are adsorbed onto, or incorporated within, the micelle core to enable the evaluation of g_{hydr} using Eq. 7.4. The third approximation involves using the theoretical model for Δg_{wc} , given in Eqs. 7.5 and 7.6, which was developed for oil molecules, in the case of nonionic surfactants (which are amphiphilic solutes). The validity of these three approximations will be discussed in Section 7.4.

In addition to determining the validity of the CS-MT model in the case of nonionic surfactants, we will use the detailed hydration information obtained through computer simulation of nonionic surfactant micelles to quantitatively evaluate several of the approximations underlying the traditional MT modeling approach. Specifically, we will evaluate: (i) the accuracy of computing the transfer free-energy contribution, g_{tr} , using the head and tail approximations made in the context of the traditional MT modeling approach [1], and (ii) the extent to which the surfactant heads shield the micelle hydrophobic core from hydrating contacts.

The remainder of this chapter is organized as follows. Section 7.2 describes the computer simulation approach that we have used, including an overview of the modeling approach (Section 7.2.1), the simulation methods and parameters (Section 7.2.2), and a description of how each system has been prepared and equilibrated (Section 7.2.3). The data analysis method used to analyze the molecular dynamics trajectories is described in Section 7.2.4. In Sections 7.3.1 to 7.3.7, computer simulation results are presented for each of the seven nonionic surfactants modeled in this chapter. In Section 7.3.8, the accuracy of several approximations made in the traditional MT modeling approach is determined based on the computer simulation results. In Section 7.4, the CS-MT model and the traditional MT model are used to model the micellization behavior of each of the seven nonionic surfactants considered. Finally, concluding remarks are presented in Section 7.5.

7.2 Molecular Dynamics Simulations

7.2.1 Modeling Approach

To quantify the hydrophobic driving force associated with the formation of nonionic surfactant micelles, we have used atomistic-level computer simulations to determine the change in hydration for each atom (or group of atoms, such as a CH₂ group) upon being transferred from the aqueous solution to the aggregate environment. As described in Chapter 6, this is accomplished by performing two simulations. The first simulation is of a single nonionic surfactant in a simulation cell of water, which we will refer to hereafter as the “bulk water” simulation. The second simulation is of the same nonionic surfactant in a micellar environment, which we will refer to hereafter as the “aggregate” simulation. Each aggregate simulation was prepared by performing a nonionic micelle at an arbitrary aggregation number. The nonionic micelle was simulated for 10 to 15 ns, which provides sufficient time for the surfactant molecules within the micelle to rearrange and come to local equilibrium, but does not provide sufficient time for the surfactant molecules to exit the aggregate environment and enter the aqueous solution. As a result, the computer simulation results do not permit direct prediction of the optimal micelle shape and size that would be observed experimentally. However, as shown in Appendix A of Chapter 6, by using the CS-MT modeling approach, obtaining information about the hydration state of a micelle of a single shape and size is sufficient to allow prediction of the *optimal* micelle shape and size.

7.2.2 Simulation Methods and Parameters

The simulation methods and parameters used here are identical to those described in Chapter 6, where we provided a detailed description of the simulation methodology [1]. Each of the nonionic surfactants was modeled using the fully atomistic OPLS-AA force field [11], and water was modeled using the simple extended point-charge (SPC/E) model. For the nonionic surfactants OG, DM, and C₁₂E₈, atomic charges

were assigned based on the default atomic charge values recommended in OPLS-AA. However, because the OSE, C₁₀SO, C₁₀PO, and MEGA-10 surfactant head structures did not have suggested charges in the OPLS-AA force field, we estimated the atomic charges for these heads using the CHelpG algorithm (as implemented in Gaussian 98), in which atomic charges are assigned to fit electrostatic potentials at a number of points on the van der Waals surface [12]. We note that CHelpG was *not* used to assign atomic charges for the hydrophobic tails of these four surfactants. In a separate study, we determined that assigning atomic charges to the CH₂ and the CH₃ groups in a linear alkyl chain using CHelpG yields simulation results that are less physically realistic than those obtained by assigning atomic charges with the recommended OPLS-AA charges (results not shown).

In two recent publications, we investigated the sensitivity of the head and tail assignments obtained through computer simulation to the method used to assign atomic charges [13,14]. In general, we found that the results are sensitive to the atomic charges used, and that the charge assignments recommended within the OPLS-AA force field yield more reasonable results than those obtained using the CHelpG algorithm. However, if a specific surfactant or solubilize does not have suggested charges in the OPLS-AA force field, we found that applying the CHelpG approach to determine charges yields reasonably accurate results.

van der Waals interactions were treated using a cutoff distance of 0.9 nm, and Coulombic interactions were described using 3D particle mesh Ewald (PME) summation [15,16]. A long-range dispersion correction was implemented to more accurately calculate the energy and the pressure of the system. In modeling short-ranged, non-bonded interactions, a neighbor list with a cutoff of 0.9 nm was maintained and updated every 10 simulation steps. Each simulation was carried out with fixed bond lengths using the SHAKE algorithm as implemented in GROMACS [17], which allowed for an increase in simulation timestep from 1 fs to 2 fs.

In each simulation, the cell temperature was maintained at 298.15 K using a Berendsen temperature coupling algorithm, which mimics weak coupling to an exter-

nal heat bath with first-order kinetics [9]. A Berendsen pressure coupling algorithm was used to maintain each simulation cell at the desired pressure of 1.0 bar [9]. All simulations were conducted using a 2006 developers' version of the GROMACS software package [18,19].

7.2.3 System Preparation and Equilibration

Bulk Water Simulation

The bulk water simulation for each of the nonionic surfactants considered was initialized by placing a single surfactant molecule in a simulation cell and surrounding it with water molecules. The simulation cell was selected to be sufficiently large that there was always at least 2.0 nm of water separating the surfactant molecule from its periodic image, where this simulation cell size was justified in Chapter 6 [1]. After brief equilibration under *NPT* conditions until the system volume had stabilized, a 2 to 5 ns data-gathering simulation was carried out.

Aggregate Simulation

The method used to carry out each of the surfactant aggregate simulations was more complex. Each nonionic surfactant micelle was preformed as a spherical aggregate by placing a number of surfactant molecules in close proximity with each surfactant head oriented radially outwards from the micelle center. The surfactant molecules were placed such that the surfactant heads were approximately uniformly spaced at the micelle surface. Next, sufficient water molecules were added around each micelle such that it was separated by at least 2 nm from its periodic image. A relatively large simulation cell size was required for C₁₂E₈ because of the large size of its polymeric E₈ head. The number of surfactant and water molecules, and the total number of atoms included in the simulation cell for each nonionic surfactant micelle are listed in Table 7.1.

Surfactant	No. of Surfactant Molecules	No. of Water Molecules	Total No. of Atoms
OG	29	3695	12477
DM	45	4283	16494
OSE	25	3750	12125
C ₁₂ E ₈	41	15256	49663
C ₁₀ PO	50	6708	22174
C ₁₀ SO	50	3510	12380
MEGA-10	42	3351	12531

Table 7.1: The number of surfactant and water molecules and the total number of atoms corresponding to each of the seven simulated nonionic surfactant micelles.

Selection of the Simulation Geometry At this point, it is worth discussing why spherical, rather than cylindrical or bilayer, micelles were selected for simulation. As shown in Appendix A of Chapter 6, any aggregation number and aggregate geometry (whether spherical, cylindrical, or planar) may be used to obtain hydration information for input to the CS-MT modeling approach [1]. An infinite cylinder or bilayer can be modeled in a computationally efficient manner by simulating only a small cross section of the cylinder or the bilayer. We have selected spherical geometries for simulation, however, because carrying out physically realistic cylindrical and bilayer simulations requires that each surfactant molecule has a physically realistic area available to it at the micelle core/water interface (which we will refer to hereafter as a) for the simulated micelles to remain stable. The equilibrium area per surfactant head in a micelle results from a complex interplay of forces (including steric, electrostatic, van der Waals, and hydrogen bonding interactions). If a for a preformed spherical micelle is too small, then, the micelle will simply become somewhat ellipsoidal during simulation. On the other hand, if a for a preformed cylindrical or bilayer micelle is too small, the simulation cell dimensions must either be allowed to expand or the micelle will buckle during the simulation and may break apart. If a is much larger than the experimental value, a spherical micelle will remain stable on the simulation timescales involved in CS-MT modeling, but a cylindrical micelle or bilayer may break up to form smaller spherical or ellipsoidal aggregates during simulation. In addition

to these stability concerns, we note that if a is very different from the experimental value, we expect that Eqs. 7.7 and 7.8, in which $g_{\text{tr,CS-MT}}$ is assumed to be constant and not to be a function of micelle shape and size, may not be valid.

An appropriate value of a for each surfactant molecule in a cylindrical or planar aggregate can be determined through computer simulation by performing constant volume simulations of a number of cylindrical or planar aggregates performed with different a values, and using the computer simulation results to identify the value of a that yields the minimum energy of interface formation. Such an approach was implemented recently by Jang et al. in determining an appropriate a value for simulation of Newton black films [20]. An alternative approach to ensure that cylindrical or bilayer micelles are simulated with a reasonable value of a for each surfactant head is to preform the micelle at an arbitrary value of a per surfactant molecule, but then allow the simulation cell dimensions to change during simulation subject to physically realistic boundary conditions. Unfortunately, such boundary conditions are difficult to determine. The appropriate boundary condition to use parallel to the axis of a cylindrical micelle, or parallel to the surface of a bilayer micelle, is a surface tension that provides a post-equilibration value of a which is similar to the one that would be observed experimentally. Particularly in the case of bilayer simulations, one might assume that macroscopic surface tension data could be used to infer the appropriate surface tension value for use during simulation. However, it is known that macroscopically observed surface tensions are difficult to predict accurately from a microscopic simulation [21, 22]. A major reason for this is that long (micron) wavelength undulations are not included in nanometer-scale simulation results. Other researchers have commented on this limitation, and used it to justify applying non-zero surface tensions in flaccid lipid bilayer simulations where the appropriate macroscopic surface tension is arguably zero [22]. Accordingly, a macroscopic surface tension is not likely to be appropriate for use as a boundary condition during cylindrical or bilayer micelle simulation.

Clearly, the simulation of cylindrical or bilayer aggregates introduces complica-

tions that are not present during simulation of spherical aggregates. With these complications in mind, we chose to preform each surfactant micelle in a spherical geometry in aqueous solution. Each of the nonionic surfactant micelles was constructed with an aggregation number sufficiently small to ensure that it would exist as a spherical aggregate during simulation. For several surfactants (OG, DM, C₁₂E₈, and MEGA-10), this was accomplished by estimating the expected aggregation number of a spherical micelle given the head area and tail volume of each surfactant molecule [23]. For other surfactants (OSE, C₁₀PO, and C₁₀SO), the surfactant head area is sufficiently small that we would expect them to form cylindrical micelles with a potentially large aggregation number [23]. Therefore, for each of these three surfactants, spherical micelles were preformed with an aggregation number that was selected arbitrarily.

Micelle Equilibration After preforming each spherical micelle, an energy minimization was conducted to remove close contacts. Next, an extended equilibration run under *NPT* conditions was conducted for 10 ns. Results by other researchers when conducting atomistic-level simulations of micelles in aqueous solution suggest that a simulation time of 10 ns should be more than adequate to equilibrate a spherical micelle [24]. One measure of equilibration for micellar systems is whether or not each group in a surfactant molecule has come to an equilibrium distance from the micelle center-of-mass. Bruce et al. have reported that sodium counterions are the slowest component of an SDS surfactant/water system to come to an equilibrium distance from the SDS micelle center-of-mass, taking only about 1 ns to equilibrate [24]. For the nonionic surfactants considered here, no counterions were present. Equilibration was confirmed from our simulation results by monitoring the total potential energy (which became stable during a small fraction of the total simulation time) and the solvent accessible surface area (SASA) of the micelle, where SASA was computed using the double cubic lattice method as implemented in GROMACS. The solvent accessible surface was traced out by a probe sphere of radius 0.2 nm (as justified in

Chapter 6) [1] that was rolled around each molecule within the aggregate to identify the solvent accessible region [9]. We consider SASA to be the most important metric to measure equilibration because this property is directly proportional to the degree of hydration of the micelle, and obtaining accurate hydration information is the central objective of our computer simulations. Plots of the SASA profiles for three representative nonionic surfactants (DM, C₁₂E₈, and MEGA-10) during equilibration are shown in Figure 7-1. The SASA values reported in Figure 7-1 for each surfactant have been normalized by the average SASA value for that surfactant to facilitate comparison of the results. The lack of noticeable drift in SASA towards the end of the 10 ns equilibration simulation run confirms that water contact data gathered during the subsequent 5 ns of data gathering should be representative of the hydration state of the micelle in its equilibrium configuration. Plots of the normalized SASA values over the course of the 5 ns data-gathering simulation runs for each surfactant are presented in Appendix A.

Snapshots of the post-equilibration configurations of each simulated nonionic micelle are shown in Figure 7-2. Each surfactant molecule is depicted using the van der Waals radius of each atom. For clarity, the water molecules are not shown.

7.2.4 Data Analysis Method

To quantify the degree of hydration of each atom (or group of atoms) in the surfactant molecule during the bulk water simulation, the number of contacts with hydrogen-bonding or with co-ordinate (dative-covalent) bonding atoms per timestep experienced by each atom was counted over the course of a simulation run, as justified in Chapter 6 [1]. For the nonionic surfactants considered in this chapter, contacts with both water atoms and with hydrogen-bonding surfactant headgroups have been counted as contributing to hydration. In analyzing our simulation data, a contact was defined as two atoms separated by less than 0.3 nm (the “cutoff” distance) at any time during the simulation. The average number of contacts is directly proportional to the average number of hydrogen or coordinate bonding atoms located within

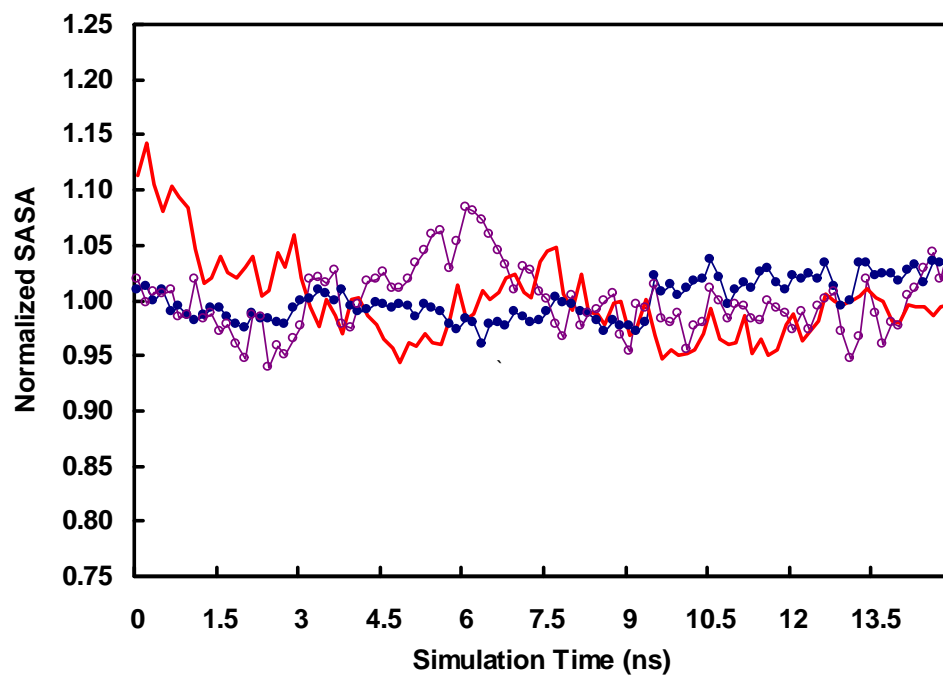


Figure 7-1: Solvent accessible surface area (SASA) normalized by the average value of SASA as a function of simulation time for micelles of three representative non-ionic surfactants: dodecyl maltoside (DM, \bullet), dodecyl octa(ethylene oxide) ($C_{12}E_8$, \circ), and decanoyl-*n*-methylglucamide (MEGA-10, —).

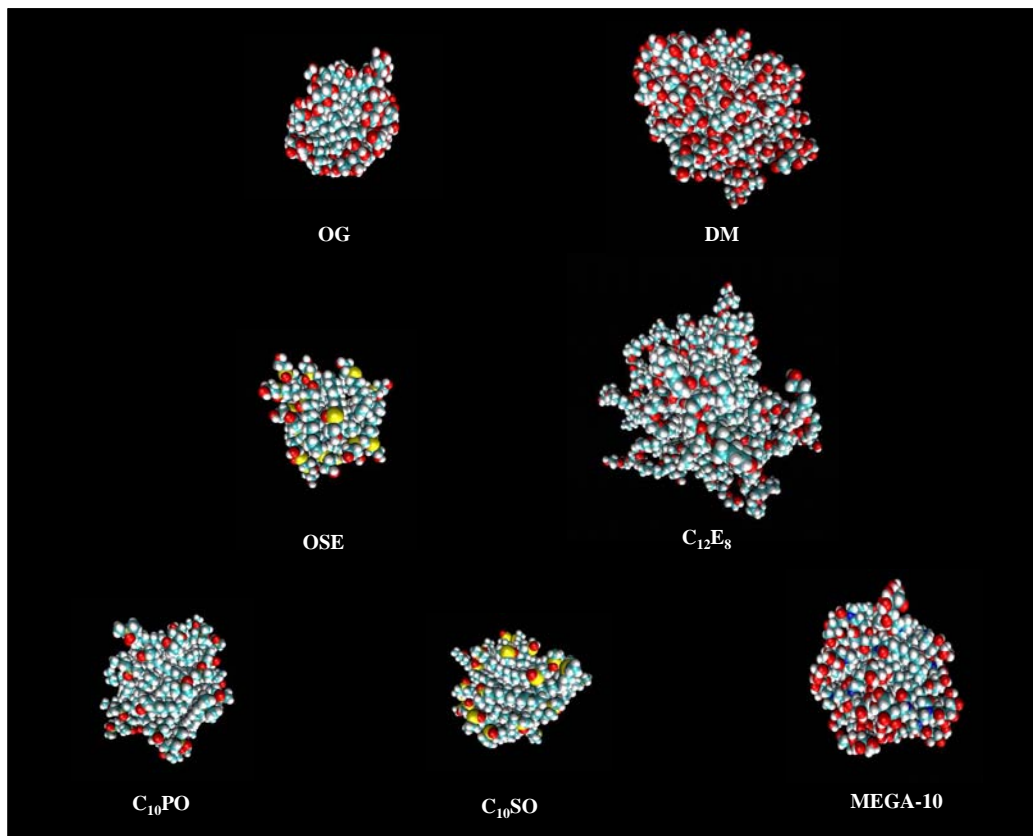


Figure 7-2: Snapshots of the post-equilibration structures of the seven simulated micelles considered here. The water molecules are not shown for clarity.

the cutoff distance. The degree of hydration of the surfactant molecules during the aggregate simulations was quantified in the same manner and with the same 0.3 nm cutoff distance used in analyzing the results of the bulk water simulation. From the contacts data obtained in this manner, we computed f , the fractional degree of hydration of each surfactant atom (or group of atoms), which is the key computer simulation input to the CS-MT model (see Eq. 7.3).

Although a cutoff of 0.3 nm was used to determine the hydration data for CS-MT modeling (which includes only f values for CH, CH₂, and CH₃ groups), a cutoff of 0.5 nm was used to generate the hydration plots presented in Section 7.3. Using a larger cutoff when generating the hydration plots improved the statistics of the f values obtained for several of the large atoms present in the surfactant heads (including nitrogen, sulfur, phosphorous, and oxygen).

An estimate of the standard error in f for each group of atoms in the surfactant molecule was made through block averaging, a useful approach to analyze correlated data [25–27]. A detailed discussion of this error analysis approach was presented in Chapter 6 [1]. Data-gathering simulation runs for each surfactant molecule in the bulk water and in the aggregate states were conducted for sufficient time to ensure that the uncertainty in each calculated value of f was small — typically less than 5%.

7.3 Simulation Results and Discussion


In this section, computer simulation results for fractional hydration are presented for each of the seven nonionic surfactants considered in this chapter. In addition to the f values computed using Eq. 7.3, two other fractional hydration values were computed: (i) f values in which the only contacts in the aggregate state that were counted as hydrating were water contacts (denoted as f_{water}), and (ii) f values in which the only contacts in the aggregate state that were counted as hydrating were contacts with

hydrogen-bonding groups in the surfactant heads (denoted as f_{head}), where:

$$f = f_{\text{water}} + f_{\text{head}} \quad (7.10)$$

We have computed values of f_{water} and f_{head} to gain insight into: (i) the extent to which contacts with hydrophilic groups in the head contribute to the hydration of hydrophobic atoms in each surfactant head and tail, and (ii) to determine whether f or f_{water} values are most appropriate to use in the CS-MT modeling approach. We can evaluate (i) based on the hydration results for each surfactant presented in this section (see Figures 7-3 to 7-9). We will discuss (ii) in greater detail in Section 7.4.10, where CS-MT modeling results obtained using f and f_{water} values will be compared.

7.3.1 Octyl Glucoside (OG)

The fractional degree of hydration of OG is plotted as a function of group number in Figure 7-3. Three different fractional hydration profiles (f , f_{water} , and f_{head}) are shown in the figure. Hydrophilic and hydrophobic groups that are considered to be part of the OG head in traditional MT modeling (groups 1 to 12) have f values (see the  results) that are much larger than the f values of groups in the OG tail (groups 13 to 20). However, to some extent, each group in the OG head is partially dehydrated and has an f value that is less than 1.0. The average f value of the groups in the OG head is 0.69. Clearly, the approximation made in traditional MT modeling that the surfactant head remains completely hydrated is not very accurate, although we note that for simple surfactants, the traditional MT modeling approach yields quantitatively, or semi-quantitatively, accurate predictions of the micellization behavior [2, 3, 8, 10].

The f results in Figure 7-3 show that the degree of dehydration of the groups in the surfactant head is a function of their distance from the surfactant tail. For example, oxygen atom 12 (closest to the tail) has an f value of 0.4, while oxygen atom 10 has an f value of 0.7. Similarly, the degree of dehydration of the groups

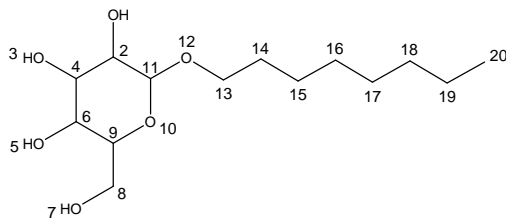
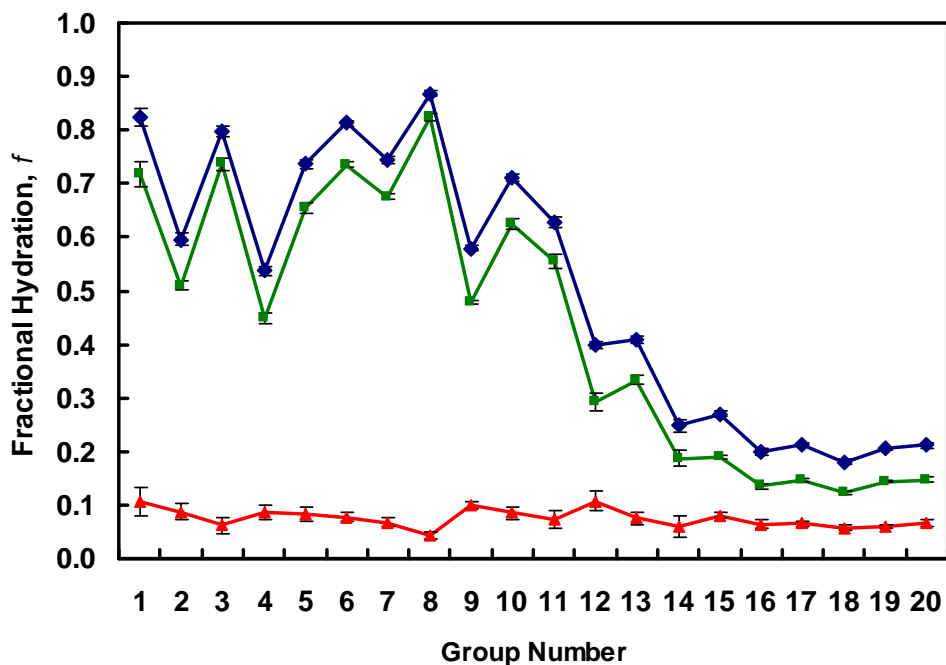







Figure 7-3: The average fractional degree of hydration, f , as defined in Eq. 7.3, for each of the groups in octyl glucoside (OG). Results are reported for fractional hydration values computed based on counting contacts with water and with hydrogen-bonding groups in the surfactant head in the aggregate state (f , \blacklozenge), for fractional hydration values based on counting contacts only with water in the aggregate state (f_{water} , \blacksquare), and for fractional hydration values based on counting contacts only with hydrogen-bonding groups in the surfactant head in the aggregate state (f_{head} , \blacktriangle). The chemical structure associated with each group is identified in the schematic of the molecule shown below the fractional hydration plot. The error bars shown correspond to the standard error of the mean.

in the surfactant tail is a function of their distance from the surfactant head. For example, the CH₂ group closest to the head (group 13) has an f value of 0.41, while the next CH₂ group (group 14) has an f value of 0.25. The average f value of the groups in the OG tail is 0.24.

Although most of the hydrating contacts experienced by the atoms in the OG tail are made with water, these atoms also make a significant number of contacts with hydrogen-bonding atoms in the OG head (groups 1, 3, 5, 7, 10, and 12). The average value of f_{water} () of the groups in the OG tail is 0.18, while the average value of f_{head} () of the groups in the OG tail is 0.07. Clearly, the value of $g_{\text{tr,CS-MT}}$ that is computed in the CS-MT model will depend strongly on whether or not hydrogen bonding atoms in the surfactant head are modeled as contributing to hydration, or in other words, on whether f or f_{water} are used in Eqs. 7.2 and 7.4.

7.3.2 Dodecyl Maltoside (DM)

The fractional degree of hydration of DM is plotted as a function of group number in Figure 7-4. Three different fractional hydration profiles (f , f_{water} , and f_{head}) are shown in the figure. The same general trends in f (see the  results), in f_{water} (), and in f_{head} () that are observed for OG are observed for DM. It is interesting to note, however, that the average f value of the groups in the DM tail (groups 24 to 35) is 0.19, which is significantly lower than the average f value of the groups in the OG tail (0.24). The DM tail is most likely less hydrated than the OG tail, on average, because the simulated DM micelle has a larger l_c value than the OG micelle, imparting to the hydrophobic core a lower surface area to volume ratio. The average f value of the groups in the DM head (groups 1 to 20) is 0.71, which is very similar to that of the OG head (0.69).

An interesting difference between the f_{head} profiles for OG and DM is that the average value of f_{head} for groups in the second ring structure in the DM head (groups 13 to 22), at 0.16, is significantly larger than the average value of f_{head} in the first ring of the DM head (groups 1 to 11), at 0.09. It is also significantly larger than

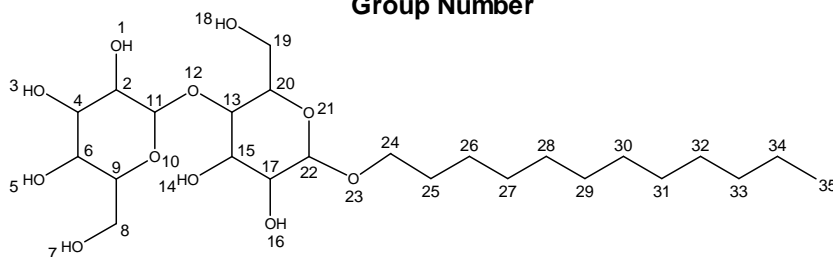
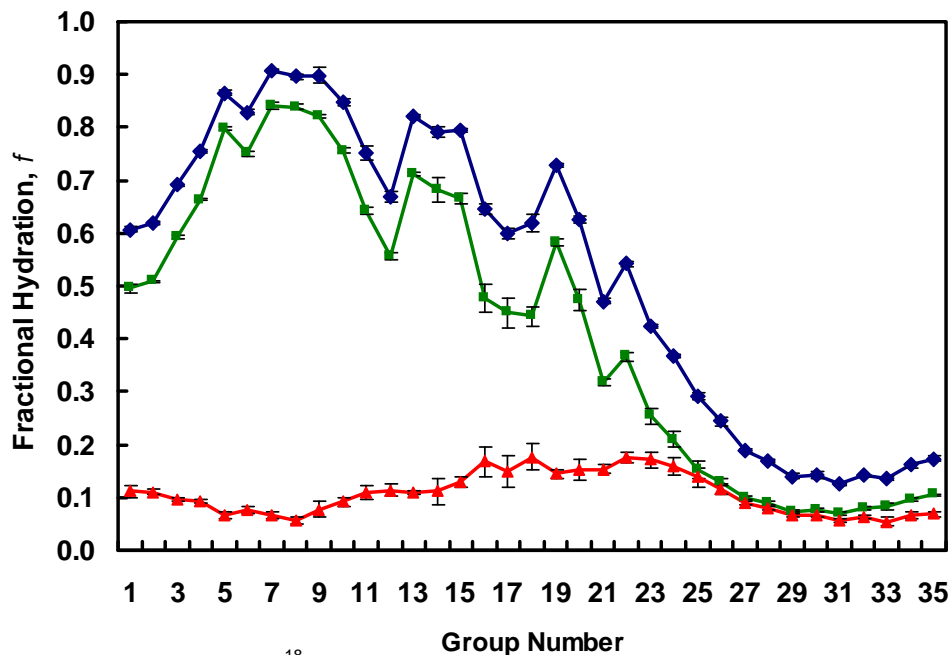




Figure 7-4: The average fractional degree of hydration, f , as defined in Eq. 7.3, for each of the groups in dodecyl maltoside (DM). Results are reported for fractional hydration values computed based on counting contacts with water and with hydrogen-bonding groups in the surfactant head in the aggregate state (f , \blacklozenge), for fractional hydration values based on counting contacts only with water in the aggregate state (f_{water} , \blacksquare), and for fractional hydration values based on counting contacts only with hydrogen-bonding groups in the surfactant head in the aggregate state (f_{head} , \blacktriangle). The chemical structure associated with each group is identified in the schematic of the molecule shown below the fractional hydration plot. The error bars shown correspond to the standard error of the mean.

the average value of f_{head} for the ring structure of the OG head (groups 1 to 11), at 0.08. The larger values of f_{head} experienced by groups 13 to 22 is most likely due to these groups being exposed to a higher concentration of hydrogen-bonding head groups than groups 1 to 11 in OG or in DM. Inspection of the contacts data shows that although head contacts account for only 28% of the total hydrating contacts in OG, they account for 35% of the total hydrating contacts in DM. From these observations, the use of f_{water} values, rather than of f values, in Eqs. 7.2 and 7.4 for CS-MT modeling is expected to have an even greater effect on the modeling results for DM than for OG.

7.3.3 Octyl Sulfinyl Ethanol (OSE)

Fractional degree of hydration results (f , f_{water} , and f_{head}) for OSE are plotted as a function of group number in Figure 7-5. The average value of f (see the  results) for the OSE head (0.73), is similar to that for the OG and the DM heads (0.69 and 0.71, respectively). However, the average value of f_{head} () for OSE (0.04) is smaller than that for OG (0.08) and for DM (0.11). This could be due to a lower concentration of hydrogen bonding groups at the OSE micelle surface and/or to a lower affinity of the hydrogen bonding groups for each other. The average value of f for the OSE tail groups (0.33) is more similar to that of OG (0.24) than to that of DM (0.19). It is interesting to note that the average value of f for the OSE tail groups is higher than that for the OG tail groups, indicating that the OSE micelle core is more hydrated than the OG micelle core, despite the fact that the simulated OSE micelle has a slightly smaller micelle core ($l_c = 1.13$ nm) than the simulated OG micelle ($l_c = 1.19$ nm). This comparatively high degree of hydration is due to the relatively large f values observed for hydrophobic groups 5, 6, and 7 in OSE relative to groups 13, 14, and 15 in OG.

It is interesting to note that the f values of groups 2 and 3, which are hydrophobic, are larger than that of group 4, which is hydrophilic. Clearly, the position of a group within a surfactant molecule (and therefore, relative to the micelle core), in addition

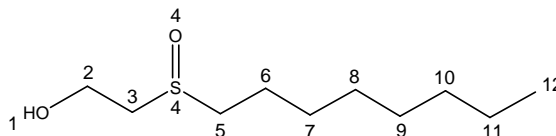
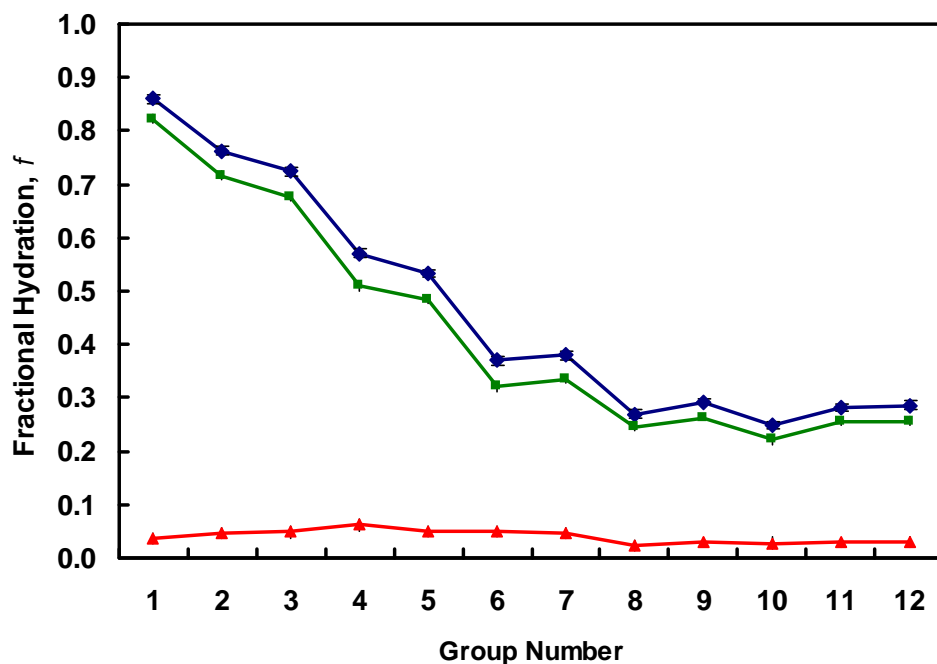




Figure 7-5: The average fractional degree of hydration, f , as defined in Eq. 7.3, for each of the groups in octyl sulfinyl ethanol (OSE). Results are reported for fractional hydration values computed based on counting contacts with water and with hydrogen-bonding groups in the surfactant head in the aggregate state (f , \blacklozenge), for fractional hydration values based on counting contacts only with water in the aggregate state (f_{water} , \blacksquare), and for fractional hydration values based on counting contacts only with hydrogen-bonding groups in the surfactant head in the aggregate state (f_{head} , \blacktriangle). The chemical structure associated with each group is identified in the schematic of the molecule shown below the fractional hydration plot. The error bars shown correspond to the standard error of the mean.

to its chemical identity, is of importance in determining the degree of dehydration that it experiences upon micelle formation.

7.3.4 Decyl Dimethyl Phosphine Oxide (C₁₀PO)

Fractional degree of hydration results (f , f_{water} , and f_{head}) for C₁₀PO are plotted as a function of group number in Figure 7-6. The average f values of the C₁₀PO head groups (groups 1 to 3) and of the C₁₀PO tail groups (groups 4 to 13) are 0.84 and 0.26, respectively (see the  results). The degree of hydration of the C₁₀PO head is higher than that observed in OG, DM, and OSE. It is interesting to note that groups 1, 2, and 3 have similar f values despite the hydrophobic character of groups 1 and 2. In addition, the average f value of the C₁₀PO tail groups (0.26) is significantly larger than that of the DM tail groups (0.19), despite the fact that the simulated C₁₀PO micelle is somewhat smaller ($l_c = 1.52$) than the simulated DM micelle ($l_c = 1.56$). This comparatively high degree of hydration is due to the relatively large f values observed for hydrophobic groups 4, 5, and 6 in C₁₀PO relative to groups 24, 25, and 26 in DM.

7.3.5 Decyl Methyl Sulfoxide (C₁₀SO)

Fractional degree of hydration results (f , f_{water} , and f_{head}) for C₁₀SO are plotted as a function of group number in Figure 7-7. The average f values (see the  results) of the C₁₀SO head groups (groups 1 and 2) and of the C₁₀SO tail groups (groups 3 to 12) are 0.76 and 0.29, respectively. In contrast to the results obtained for CH₃ groups 1 and 2 in C₁₀PO, the hydrophobic CH₃ group 1 in C₁₀SO has a lower f value than the hydrophilic groups in the head (groups 3 and 2 for C₁₀PO and C₁₀SO, respectively). This difference between C₁₀PO and C₁₀SO may reflect differences in the atomic charges of the two surfactant heads. Despite the superficial chemical similarity of these two head groups, the atomic charges predicted using the CHelpG algorithm for the two heads are quite different, with C₁₀PO having a charge

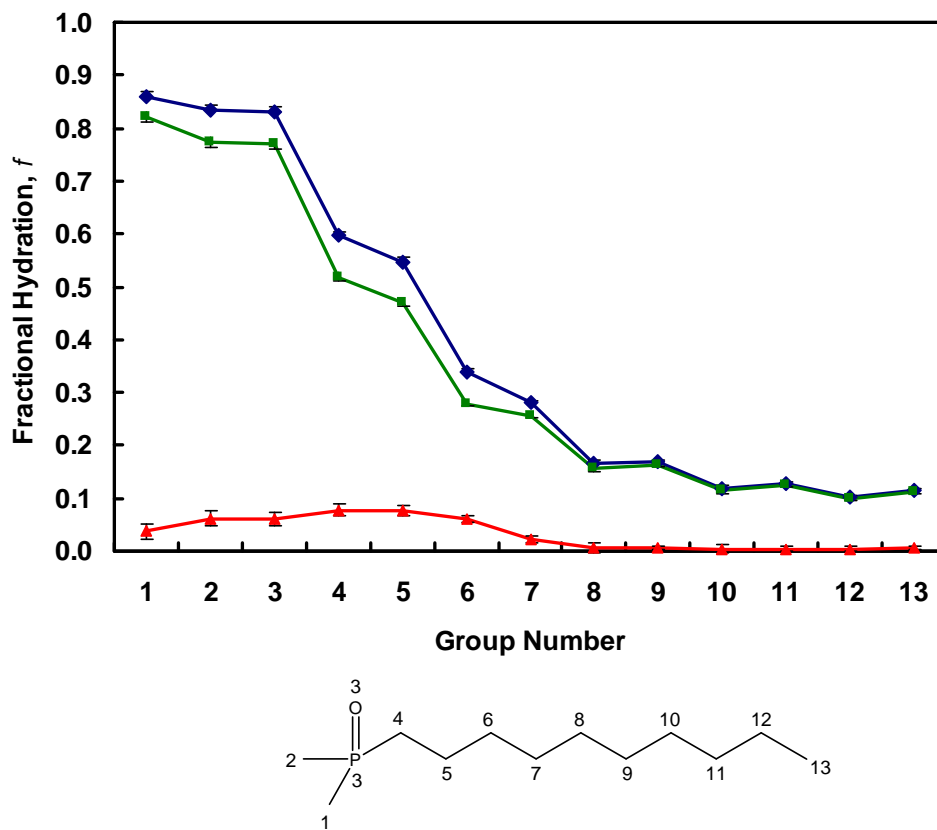


Figure 7-6: The average fractional degree of hydration, f , as defined in Eq. 7.3, for each of the groups in decyl dimethyl phosphine oxide (C_{10}PO). Results are reported for fractional hydration values computed based on counting contacts with water and with hydrogen-bonding groups in the surfactant head in the aggregate state (f , \blacklozenge), for fractional hydration values based on counting contacts only with water in the aggregate state (f_{water} , \blacksquare), and for fractional hydration values based on counting contacts only with hydrogen-bonding groups in the surfactant head in the aggregate state (f_{head} , \blacktriangle). The chemical structure associated with each group is identified in the schematic of the molecule shown below the fractional hydration plot. The error bars shown correspond to the standard error of the mean.

distribution that makes its dipole moment roughly twice as large as that of $C_{10}SO$. Differences in the hydration profiles of the $C_{10}PO$ and the $C_{10}SO$ tails could be due both to differences in the head atomic charges and to differences in the shape and size of the two surfactant heads.

7.3.6 Dodecyl Octa(Ethylene Oxide) ($C_{12}E_8$)

Fractional degree of hydration results (f , f_{water} , and f_{head}) for $C_{12}E_8$ are plotted as a function of group number in Figure 7-8. The average f values (see the \blacklozenge results) of the $C_{12}E_8$ head groups (groups 1 to 25) and of the $C_{12}E_8$ tail groups (groups 26 to 37) are 0.81 and 0.17, respectively. The small average degree of hydration of the hydrophobic core can be explained by the relatively large size of the micelle hydrophobic core ($l_c = 1.51$ nm), which is similar to that of the simulated DM micelle ($l_c = 1.56$ nm).

Because $C_{12}E_8$ and DM both have relatively large heads and the same hydrocarbon tail length, it is instructive to compare the fractional hydration results for $C_{12}E_8$ and DM. The most striking difference between the fractional hydration profiles of $C_{12}E_8$ and DM is the relatively low f_{head} values (\blacktriangle) observed for the $C_{12}E_8$ head groups. The average value of f_{head} for the $C_{12}E_8$ head groups (groups 1 to 25), which have an average value of 0.04, is significantly smaller than the average value of f_{head} for the DM head groups (0.12). A possible explanation for this difference is that the hydrogen-bonding groups in the $C_{12}E_8$ head are not as attracted to each other as are the head groups in DM. The DM head contains both hydrogen bond donors and acceptors, while the $C_{12}E_8$ head contains several hydrogen bond acceptors but only a single hydrogen bond donor (OH group 1). Therefore, a DM head is capable of forming hydrogen bonds with both water and with other DM heads, while a $C_{12}E_8$ head primarily forms hydrogen bonds with water, a difference which is expected to lower the average value of f_{head} of $C_{12}E_8$ relative to that of DM.

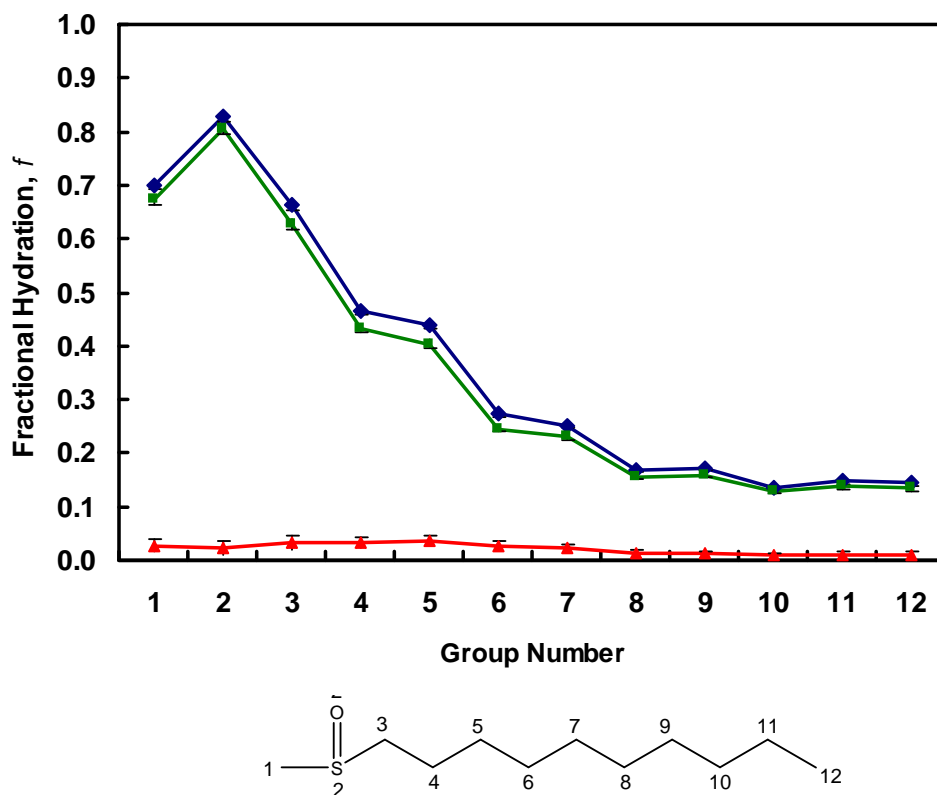


Figure 7-7: The average fractional degree of hydration, f , as defined in Eq. 7.3, for each of the groups in decyl ethyl sulfoxide (C_{10}SO). Results are reported for fractional hydration values computed based on counting contacts with water and with hydrogen-bonding groups in the surfactant head in the aggregate state (f , \blacklozenge), for fractional hydration values based on counting contacts only with water in the aggregate state (f_{water} , \blacksquare), and for fractional hydration values based on counting contacts only with hydrogen-bonding groups in the surfactant head in the aggregate state (f_{head} , \blacktriangle). The chemical structure associated with each group is identified in the schematic of the molecule shown below the fractional hydration plot. The error bars shown correspond to the standard error of the mean.

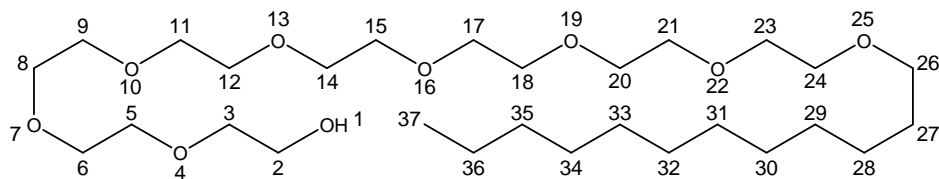
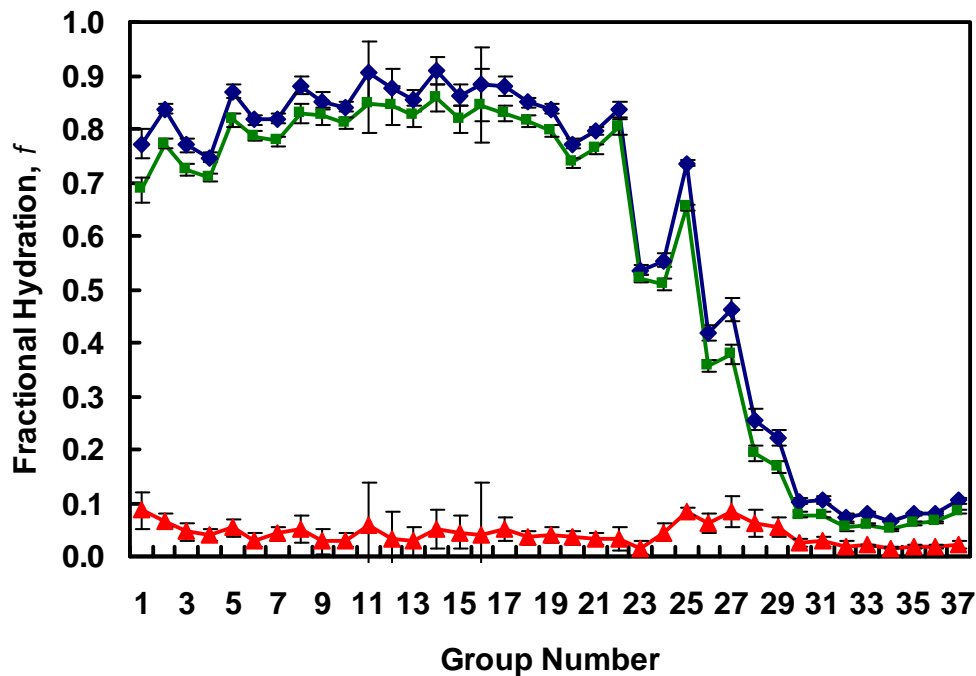




Figure 7-8: The average fractional degree of hydration, f , as defined in Eq. 7.3, for each of the groups in dodecyl octa(ethylene oxide) (C_{12}E_8). Results are reported for fractional hydration values computed based on counting contacts with water and with hydrogen-bonding groups in the surfactant head in the aggregate state (f , \blacklozenge), for fractional hydration values based on counting contacts only with water in the aggregate state (f_{water} , \blacksquare), and for fractional hydration values based on counting contacts only with hydrogen-bonding groups in the surfactant head in the aggregate state (f_{head} , \blacktriangle). The chemical structure associated with each group is identified in the schematic of the molecule shown below the fractional hydration plot. The error bars shown correspond to the standard error of the mean.

7.3.7 Decanoyl-*n*-Methylglucamide (MEGA-10)

Fractional degree of hydration results (f , f_{water} , and f_{head}) for MEGA-10 are plotted as a function of group number in Figure 7-9. The average f value (see the  results) of the groups in the MEGA-10 tail (groups 16 to 24) is 0.21, which is somewhat smaller than those in OG (0.24) and in OSE (0.33). The average f value of the remaining groups in MEGA-10 (1 to 15) is 0.66. In general, the values of f_{head} () observed for the MEGA-10 head groups are more similar to those of OG and DM than to that of C₁₂E₈. This can be understood by noting that the head structure of MEGA-10, like those of OG and DM, contains both hydrogen bond donors and acceptors.

MEGA-10 is difficult to model using the traditional MT modeling approach because it has a hydrophilic nitrogen atom (group 15) surrounded by three hydrophobic groups (CH₂ group 11, CH₃ group 12, and carbonyl groups 13 and 14). A logical starting point for traditional MT modeling would be to identify groups 16 to 24 to be the MEGA-10 tail, and to model each of the remaining groups as being part of the MEGA-10 head. By so doing, of course, the approximation is made that all the MEGA-10 head groups (including groups 11, 12, 13, and 14) remain fully hydrated in the micellar state. The hydration results presented in Figure 7-9 clearly show that this is indeed an approximation, and that because of their hydrophobic nature and location within the molecule, groups 11, 12, and 13 are significantly more dehydrated than other hydrophilic or hydrophobic groups in the MEGA-10 head. In Section 7.4.9, we will compare the CMC predicted with the CS-MT model with the CMC predicted by the traditional MT model, and test the assumption that groups 16 to 24 are part of the MEGA-10 tail.

7.3.8 Evaluation of Approximations Made in Traditional Molecular-Thermodynamic Modeling

The accuracy of two approximations made in traditional MT modeling to quantify the hydrophobic driving force for micelle formation can be evaluated using the computer

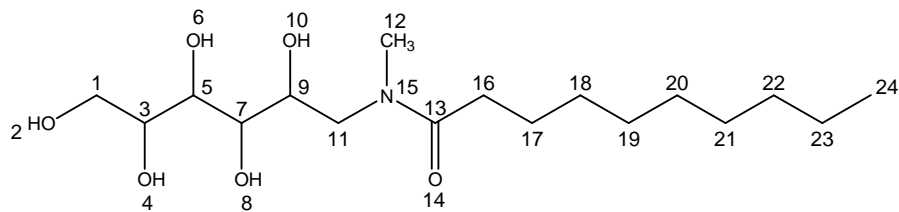
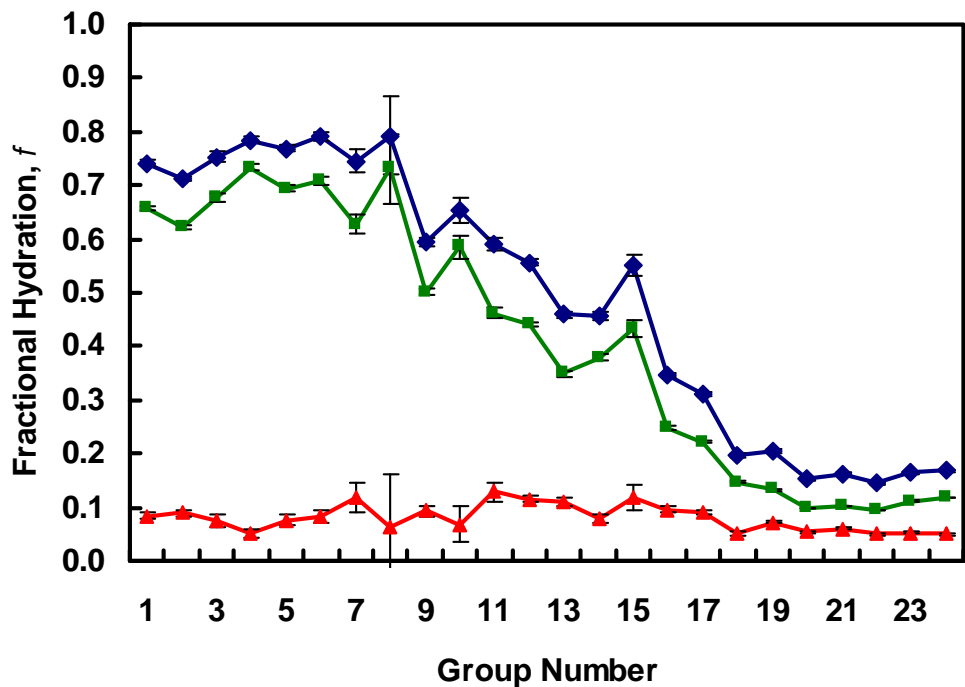

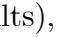
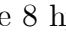





Figure 7-9: The average fractional degree of hydration, f , as defined in Eq. 7.3, for each of the groups in decanoyl- n -methylglucamide (MEGA-10). Results are reported for fractional hydration values computed based on counting contacts with water and with hydrogen-bonding groups in the surfactant head in the aggregate state (f , \blacklozenge), for fractional hydration values based on counting contacts only with water in the aggregate state (f_{water} , \blacksquare), and for fractional hydration values based on counting contacts only with hydrogen-bonding groups in the surfactant head in the aggregate state (f_{head} , \blacktriangle). The chemical structure associated with each group is identified in the schematic of the molecule shown below the fractional hydration plot. The error bars shown correspond to the standard error of the mean.

simulation data presented above. These include: (i) the accuracy of using surfactant head and tail assignments to compute g_{tr} , and (ii) the extent to which surfactant heads shield the micelle core from hydrating contacts.

Accuracy of Computing g_{tr} using the Head and Tail Approximation

As discussed in detail in Chapter 6 [1], in traditional MT modeling, the hydrophobic contribution to micelle formation is computed as the sum of two free-energy contributions: the transfer free-energy contribution, g_{tr} , and the interfacial free-energy contribution, g_{int} . A key assumption underlying the traditional MT modeling approach to compute g_{tr} is that the presence of the surfactant head at one end of the surfactant tail does not affect the change in hydration experienced by each group in the surfactant tail as it is transferred from the aqueous solution to a bulk solution of surfactant tails. By making this approximation, g_{tr} may be computed as if the surfactant heads are not present.

However, in practice, changes in the hydration state of the surfactant tail that occur upon its transfer to a bulk phase of tails are affected by the nature of the surfactant head attached to it. This can be shown by comparing hydration data for an oil molecule in bulk water to that of a surfactant tail in bulk water. We have computed the average number of hydrating contacts (as defined in Section 7.2.4) in bulk aqueous solution for each CH_2 and CH_3 group in hexadecane, as well as for those in the linear alkyl tails of several representative nonionic surfactants with tails containing either 8 or 12 CH_x ($x = 2$ or 3) groups. A cutoff of 0.3 nm was used to define hydrating contacts. In Figure 7-10, plots of hydrating contacts as a function of group number in the bulk aqueous solution are shown for 8 hexadecane groups (see the  results), for the 8 hydrophobic tail groups of OG (), and for the 8 hydrophobic tail groups of OSE (). In Figure 7-10, group 1 for OG and OSE is defined as the CH_2 group adjacent to the surfactant head, and group 8 for OG, OSE, and hexadecane corresponds to the terminal CH_3 group of each alkyl chain. In Figure 7-11, plots of hydrating contacts as a function of group number in the bulk aqueous

solution are shown for 12 hexadecane groups (), for the 12 hydrophobic tail groups of DM (), and for the 12 hydrophobic tail groups of C₁₂E₈ (). In Figure 7-11, group 1 for the surfactants is defined as the CH₂ group adjacent to the surfactant head, and group 12 for the surfactants and for hexadecane corresponds to the terminal CH₃ group of each alkyl chain. Note that we have not compared the OG and the OSE results with octane hydration data, or the DM and the C₁₂E₈ results with dodecane hydration data, because group 1 for each surfactant is a CH₂ group, rather than a CH₃ group. The hydration data presented in Figures 7-10 and 7-11 for the surfactants and hexadecane enable us to compare the hydration of chemically identical hydrophobic groups. The error bars shown in Figures 7-10 and 7-11 represent standard errors of the mean.

A comparison of the hydration profiles for OG, OSE, DM, and C₁₂E₈ with corresponding groups in hexadecane clearly shows that the surfactant head type has an effect on the hydration state of the adjacent CH₂ group in aqueous solution. In addition, our results show that the presence of the surfactant head affects the hydration states of a significant number of hydrophobic groups further down each linear alkyl chain (groups 2 and 3 for OG, DM, and C₁₂E₈, and groups 2 to 6 for OSE). The total number of hydrating contacts experienced by groups 1 to 8 of OG and OSE is 6.3% larger and 5.16% smaller, respectively, than those experienced by the 8 corresponding groups in hexadecane. The total number of hydrating contacts experienced by groups 1 to 12 of DM and C₁₂E₈ is 4.2% larger and 10.1% greater, respectively, than those experienced by the 12 corresponding groups in hexadecane.

Because the extent of hydration of the surfactant tail in the bulk water reference state is affected by the type of surfactant head, it follows that the change in hydration incurred upon transfer of the surfactant tail to a bulk phase of tails is affected by the type of surfactant head. The assumption made in traditional MT modeling in computing g_{tr} that every tail group is dehydrated to the same degree as a tail with no attached head is clearly an approximation [2, 8]. Nevertheless, it is important to point out that traditional MT modeling has been shown to yield quantitatively,

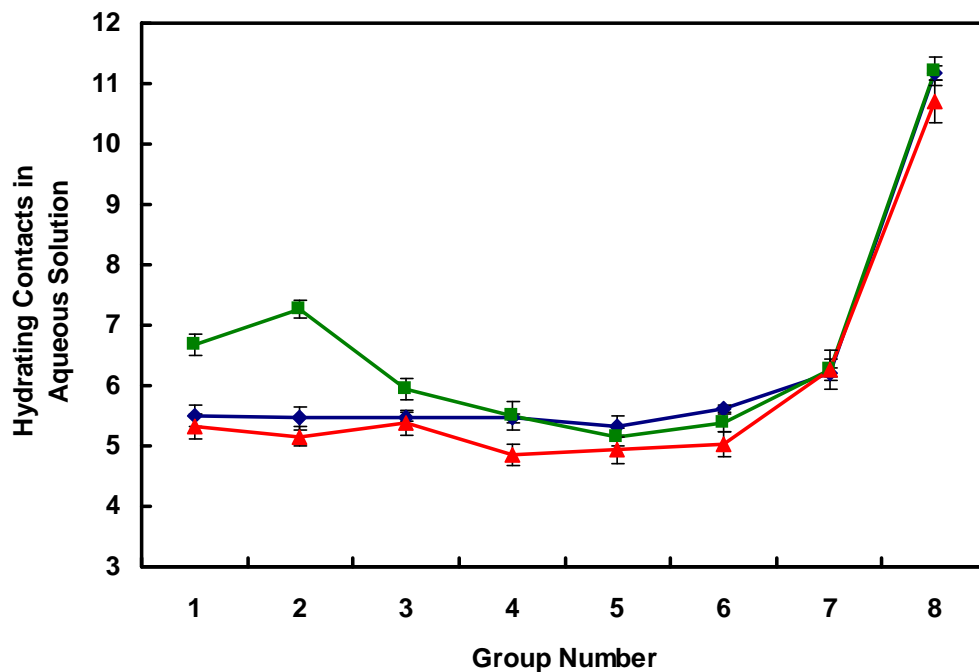


Figure 7-10: The number of hydrating contacts, as defined in the text, experienced in bulk water for 8 hydrophobic CH_2 or CH_3 groups in hexadecane ($\text{—}\blacklozenge\text{—}$), in octyl glucoside (OG, $\text{—}\blacksquare\text{—}$), and in octyl sulfinyl ethanol (OSE, $\text{—}\blacktriangle\text{—}$). The first group listed for each surfactant corresponds to the CH_2 group adjacent to the tail's point of attachment to the surfactant head, and the last group listed for all three alkyl chains corresponds to the terminal CH_3 group. The error bars shown correspond to the standard error of the mean.

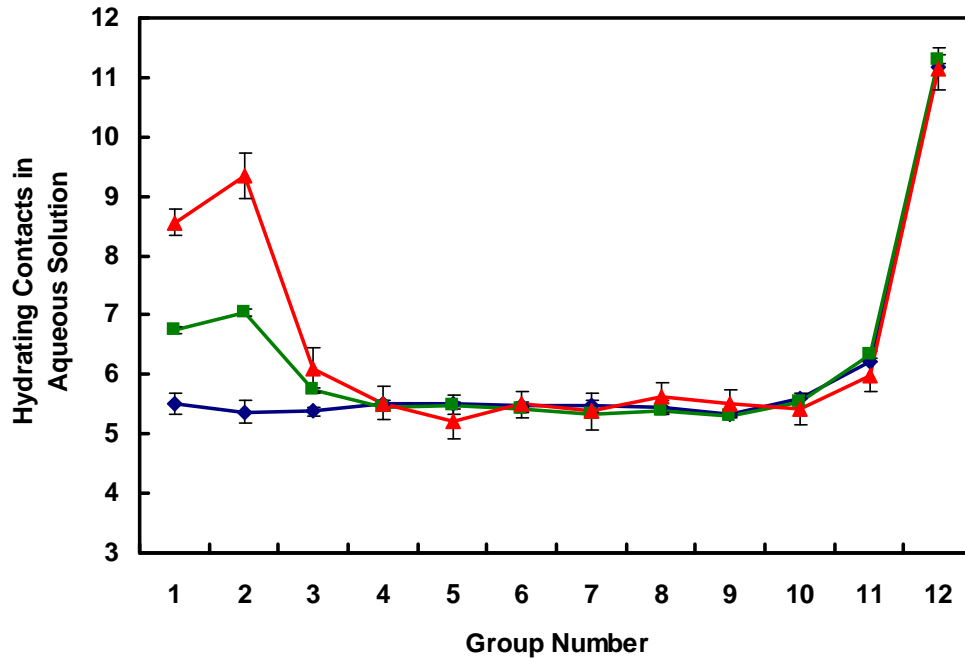


Figure 7-11: The number of hydrating contacts, as defined in the text, experienced in bulk water for 12 hydrophobic CH₂ or CH₃ groups in hexadecane (\blacklozenge), in dodecyl maltoside (DM, \blacksquare), and in dodecyl octa(ethylene oxide) (C₁₂E₈, \blacktriangle). The first group listed for each surfactant corresponds to the CH₂ group adjacent to the tail's point of attachment to the surfactant head, and the last group listed for all three alkyl chains corresponds to the terminal CH₃ group. The error bars shown correspond to the standard error of the mean.

or semi-quantitatively, accurate predictions of the micellization behavior of relatively simple nonionic surfactants [2, 8]. Accordingly, the hydration approximations that are made in traditional MT modeling to compute g_{tr} appear reasonable in the absence of detailed hydration data. The CS-MT modeling approach, however, eliminates the need to make such approximations by computing the changes in hydration that occur upon micelle formation directly from molecular dynamics simulation results.

Effect of the Surfactant Heads on Aggregate Core Hydration

The interfacial free-energy contribution, g_{int} , reflects the free-energy penalty associated with forming the micelle core/water interface, and is computed in the context of traditional MT modeling using a micelle core/water interfacial tension. Specifically, g_{int} is computed as follows [1]:

$$g_{\text{int}} = (a - a_0)\sigma \quad (7.11)$$

where a is the area per surfactant molecule at the micelle core/water interface, a_0 is the interfacial area that is screened by each surfactant head, and σ is a composition-weighted average of the curvature-corrected interfacial tension between water and a bulk phase of hydrophobic tails (for complete details, see Chapter 6). In our past work, we have estimated a_0 as being equal to 21 \AA^2 for every surfactant head in the micelle [8], an area which is equal to the cross-sectional area of a linear alkyl chain. Nagarajan et al. have modeled a_0 as being equal to the smaller of two areas — the cross-sectional area of a linear alkyl chain (21 \AA^2) or the cross-sectional area of the surfactant head.

The curvature-dependent interfacial tension of a surfactant tail of type j in the micelle has been estimated using the Gibbs-Tolman-Koenig-Buff equation [28–31]:

$$\sigma_j = \frac{\sigma_{0,j}}{\left(1 + \frac{(S-1)\delta}{l_c}\right)} \quad (7.12)$$

where $\sigma_{0,j}$ is the interfacial tension of component j at a flat interface with water (typically around 50 mN/m for hydrocarbons), δ is the Tolman distance, and S is a shape factor that is equal to 3 for spheres, 2 for cylinders, and 1 for disks or bilayers. The estimation of $\sigma_{0,j}$ for alkyl chains of varying length and as a function of temperature, as well as the estimation of the Tolman distance, δ , were discussed in detail in Chapter 6 [1].

The simulation data reported in Sections 7.3.1 to 7.3.7 can be used to evaluate how

physically reasonable Eq. 7.11 is as implemented in the context of the traditional MT modeling approach. By comparing simulation results for the small spherical octane aggregate (see Chapter 6) [1] with those for the OG and the OSE micelles, as well as simulation results for the large spherical dodecane aggregate (see Chapter 6) [1] with those for the DM and the C₁₂E₈ micelles, it is possible to comment on the extent to which the surfactant heads shield the micelle hydrophobic core from hydrating contacts. These two oil aggregates have been selected for comparison because their surface areas are similar to those of the simulated micelles. Table 7.2 reports the total number of hydrating contacts, N_{cont} , for octane, OG, OSE, dodecane, DM, and C₁₂E₈ in the aggregate state on a per molecule basis. To allow direct comparison of the results for the oil aggregates and for the micelles, N_{cont} for OG and OSE were computed by scaling the OG and the OSE hydrating contact results by $\left(\frac{A_{\text{core,mic}}}{A_{\text{core,oct agg}}}\right)$, where $A_{\text{core,mic}}$ is the surface area of the surfactant micelle core and $A_{\text{core,oct agg}}$ is the surface area of the octane aggregate, to correct for differences in aggregate surface area. We consider scaling based on surface area to be appropriate because hydrating contacts should be approximately proportional to the exposed surface area. Similarly, N_{cont} for DM and C₁₂E₈ were computed by scaling the DM and the C₁₂E₈ hydrating contact results by $\left(\frac{A_{\text{core,mic}}}{A_{\text{core,dod agg}}}\right)$, where $A_{\text{core,dod agg}}$ is the surface area of the dodecane aggregate. Table 7.2 also reports the difference between the number of hydrating contacts for OG or OSE and the number of hydrating contacts for octane, as well as the difference between the number of hydrating contacts for DM or C₁₂E₈ and the number of hydrating contacts for dodecane, as $(N_{\text{cont}} - N_{\text{cont,oil agg}})$. The decrease in the number of hydrating contacts observed for each surfactant micelle relative to the corresponding value for each oil aggregate can be used to infer the area at the micelle core/water interface that is effectively shielded from hydrating contacts by the surfactant heads. These results are reported in Table 7.2 as the “shielded area” values. The average of these shielded area values (21.85 Å²) is very similar to the shielded area value used in traditional MT modeling (21 Å²). However, inspection of the shielded area results reveals that the shielded area varies significantly among the

	N_{cont}	$N_{\text{cont}} - N_{\text{cont,oil agg}}$	Shielded Area [\AA^2]
Octane	18.25	0.00	N/A
OG	10.65	-7.61	31.22
OSE	15.28	-2.97	12.19
Dodecane	18.97	0.00	N/A
DM	12.14	-6.83	26.99
C₁₂E₈	14.66	-4.31	17.03

Table 7.2: Simulation results for the number of hydrating contacts (N_{cont}) on a per oil or surfactant molecule basis experienced by: octane, octyl glucoside (OG), octyl sulfinyl ethanol (OSE), dodecane, dodecyl maltoside (DM), and dodecyl octa(ethylene oxide) (C₁₂E₈) in the aggregate environment. The octane results correspond to the results for a spherical octane aggregate of aggregation number 25 (see article I) [1]. The dodecane results correspond to a spherical dodecane aggregate of aggregation number 33 (see article I) [1]. As described in the text, hydrating contacts results for each micelle have been scaled by the ratio of the micelle core area to the area of either the octane or the dodecane oil aggregate. The change in the number of hydrating contacts relative to the corresponding oil aggregate ($\Delta N_{\text{cont}} - \Delta N_{\text{cont,oil agg}}$) is also listed, again on a per oil or per surfactant molecule basis. The “Shielded Area” reported for the surfactant micelles corresponds to the area at the micelle core/water interface that is effectively shielded from hydrating contacts by the surfactant heads.

surfactants considered. The shielded area calculated for OSE, for example, at 12.19 \AA^2 , is less than half of the shielded area calculated for OG (31.22 \AA^2). An advantage of the CS-MT modeling approach is that it permits estimation of the hydrophobic contribution to g_{form} (as reflected in $g_{\text{dehyd}} + g_{\text{hyd}}$) without making any assumptions about the effect of the surfactant heads on the hydration state of the micelle core.

7.4 Molecular-Thermodynamic Modeling Based on Computer Simulation Inputs

7.4.1 Using the CS-MT Modeling Approach to Predict Surfactant Micellization Behavior

As stressed in Chapter 6, using the CS-MT modeling approach to quantify the hydrophobic effect for oil aggregates in water is less challenging than using it to model

surfactant micellization. Indeed, in surfactant micellization, the presence of the surfactant heads at the aggregate core/water interface introduces several complications that are absent in the oil aggregate case. To deal with these complications, we will make a number of simplifying approximations. Following a description of these approximations in Sections 7.4.1 and 7.4.1, we will use the CS-MT model to predict g_{form} and the CMC for each of the seven nonionic surfactants discussed in Section 7.3. Although the CS-MT model enables the prediction of a variety of micellar solution properties from g_{form} (including micelle shape, size, and composition), the surfactant CMC was selected for prediction and comparison with experimental CMC data because the CMC depends exponentially on g_{form} , and as such, it provides a stringent quantitative test with which to evaluate the predictive accuracy of the CS-MT model. The CMCs predicted by the CS-MT model will be compared both with the CMCs predicted by the traditional MT model and with the experimental CMC values. In addition, the accuracy of the approximations made in implementing the CS-MT model will be discussed in the context of the CS-MT and the traditional MT modeling results.

Estimation of g_{dehydr}

When using the CS-MT model to quantify the hydrophobic effect, Eq. 7.2 is used for every hydrophobic group in the surfactant molecule, regardless of whether the hydrophobic group is part of the surfactant head or the surfactant tail. Accordingly, every hydrophobic group in the surfactant molecule contributes to the hydrophobic driving force for micelle formation to the extent that the group is dehydrated upon micelle formation. To implement Eq. 7.2, therefore, suitable values of g_{tr_i} must be estimated for every hydrophobic group in the surfactant molecule.

In traditional MT modeling, only the surfactant tails are considered to be dehydrated upon micelle formation. In that case, the transfer free-energy contribution, g_{tr} , of these tails can be estimated in a straightforward manner using experimental tail solubility data, or a theoretical estimate of tail solubility made using a group-

contribution approach (see Chapter 6 for a detailed discussion) [1]. Similarly, in CS-MT modeling, g_{tr_i} values of hydrophobic groups in the surfactant tail can be determined from an estimate of the solubility of group i in water. Suitable g_{tr_i} values of hydrophobic groups in the surfactant head are more difficult to estimate. Dehydration of the surfactant heads upon micelle formation may result from solvent exclusion by other surfactant heads, from contact with hydrophobic groups in other surfactant heads, and from contact with the micelle hydrophobic core. Due to the highly anisotropic nature of the micelle core/water interfacial region, it is difficult to assign suitable g_{tr_i} values associated with transfer from bulk water to this interfacial environment because the required experimental solubility data is not available. To the best of our knowledge, there are no simple theoretical approaches to predict g_{tr_i} between bulk water and such a complex, anisotropic environment. A second complication in estimating g_{tr_i} values for groups in the surfactant head results from the fact that the hydrophobicity of hydrophobic groups in the surfactant head may be affected by their being bonded to hydrophilic groups. In molecular mechanics forcefields, the chemical effect of being bonded to a hydrophilic group is captured by the fact that the atomic charge of each atom in a molecule is a function of its adjacent atoms [11]. For example, in the OPLS-AA forcefield, the net atomic charge assigned to the CH₂ group in poly(ethylene oxide) is 0.1 $|e|$ (where e is the charge of an electron), which differs from the net charge of 0 $|e|$ assigned to a CH₂ group bonded to alkyl groups.

With the above complications in mind, in order to implement the CS-MT model in a straightforward manner, in this chapter, we make the approximation that the g_{tr_i} values of hydrophobic groups in the surfactant head are identical to the g_{tr_i} values of the same hydrophobic groups in the surfactant tail. We anticipate that implementing the CS-MT model in this approximate way should yield an improvement over the traditional MT modeling approach for many surfactants. In the traditional MT modeling approach, hydrophobic groups in the surfactant head do not contribute at all to the hydrophobic driving force for micelle formation. However, it is important to note that obtaining better estimates of g_{tr_i} for hydrophobic groups in the surfactant

head represents an important area for future research in order to improve the accuracy of the CS-MT model.

For the seven nonionic surfactants modeled here, we only need to consider CH, CH₂, and CH₃ hydrophobic groups. Accordingly, to implement the CS-MT model, g_{tri} values for CH₂ and CH₃ were estimated using the same solubility correlations for linear alkyl tails that are used in traditional MT modeling [32]. The g_{tri} value for CH was estimated using solubility data for branched alkyl tails [33].

Estimation of g_{hydr}

In Chapter 6, we presented an approach to theoretically estimate g_{hydr} for oil molecules. In our model for g_{hydr} , we calculated Δg_{wc} using Eqs. 7.5 and 7.6. In estimating g_{hydr} for each of the hydrophobic groups in a surfactant molecule, two complications arise: (i) g_{hydr} is nonzero only for those hydrophobic groups in the surfactant molecule that are adsorbed onto, or that penetrate into, the micelle hydrophobic core, and (ii) for those hydrophobic groups that are adsorbed onto, or that penetrate into, the micelle hydrophobic core, Δg_{wc} may be affected by the presence of the surfactant heads at the micelle core/water interface.

Note that the free-energy contribution, g_{hydr} , is zero for those hydrophobic groups that are not part of the micelle hydrophobic core, because g_{hydr} accounts for the difference in free energy associated with hydrating contacts in the bulk water and in the aggregate environment. Fundamentally, the origin of g_{hydr} is the size dependence of hydration thermodynamics. An isolated hydrophobic chain in water is much smaller in size than a typical aggregate core/water interface. Therefore, the hydrophobic chain disrupts the hydrogen bonding and coordinate bonding network of the aqueous solution to a different extent. Hydrophobic groups in a surfactant molecule that are not part of the micelle hydrophobic core continue to disrupt this hydrogen bonding and coordinate bonding network in the aggregate state in much the same way that they do in the bulk water state. Consequently, g_{hydr} for such groups is zero. With this in mind, we will consider any hydrophobic group that has an f value equal to,

or less than, 0.60 to be part of the micelle hydrophobic core (see below), and to have a nonzero value of g_{hydr} .

The selection of $f = 0.60$ as the appropriate cutoff value was motivated both by physical intuition and by our computer simulation results. For a hydrophobic group located precisely at a flat oil/water interface (with half of its surface in oil and the other half in water), the average value of f computed through molecular dynamics simulation would be 0.5. For a hydrophobic group adsorbed at a curved, rough oil/water interface, we would expect the average value of f to be greater than 0.5. We note that for the small, spherical hexadecane oil aggregate simulated in Chapter 6, the average value of f for the two terminal CH_3 groups was found to be 0.53, even though each of the CH_3 and the CH_2 groups in the hexadecane molecules are part of the aggregate core. We selected $f = 0.6$ as a suitable cutoff value after considering simulation results for the seven nonionic surfactants modeled here, as well as simulation results for a number of simple, ionic surfactants, including sodium dodecyl sulfate (SDS), cetyltrimethylammonium bromide (CTAB), and decyltrimethylammonium bromide (DTAB). CS-MT modeling results for these three ionic surfactants is presented in Chapter 8 [34]. For each of the nonionic and ionic surfactants that we simulated, groups that would be considered to be part of the surfactant head in traditional MT modeling had an f value greater than 0.60, and groups that would be considered to be part of the surfactant tail in traditional MT modeling had an f value that is less than, or equal to, 0.60. In traditional MT modeling, all the atoms in the surfactant tail are considered to be part of the micelle core, and such an assignment yields quantitatively, or semi-quantitatively, accurate predictions of the micellar solution behavior of simple surfactants [8]. In this chapter, therefore, we treat any hydrophobic groups in a surfactant molecule with an f value that is less than, or equal to, 0.60 as being part of the micelle hydrophobic core.

For those hydrophobic groups that are identified as being part of the micelle hydrophobic core, a reasonable value of Δg_{wc} must be estimated in order to compute g_{hydr} using Eq. 7.4. We propose that, to a first approximation, Δg_{wc} can be evaluated

as being equal to the value calculated for oil molecules in Chapter 6 [1]. As shown in Eq. 7.5, Δg_{wc} is the difference between the free energy per unit SASA in the aggregate core state (σ_{core}) and in the bulk water state (σ_{bulk}). The value of σ_{bulk} for a hydrophobic group in a surfactant molecule is very similar to that of σ_{bulk} for a hydrophobic group in an oil molecule. Furthermore, the success of the traditional MT approach in modeling the aggregate core/water interface using an oil/water interfacial tension (see Chapter 6) indicates that assuming that σ_{core} in a micelle is equal to σ_{core} of an oil/water interface is a reasonable approximation. This approximation has been made in modeling each of the seven nonionic surfactants considered in this chapter, which we discuss below.

7.4.2 Modeling Results for Octyl Glucoside (OG)

Using the simplifying approximations discussed in Sections 7.4.1 and 7.4.1, we used the CS-MT model to predict the micellization behavior for OG in aqueous solution at 25 °C. In Table 7.3, we report CS-MT modeling results for the *simulated* OG micelle, including: (i) g_{dehydr} , (ii) g_{hydr} , (iii) \hat{g}_{int} , and (iv) $g_{\text{tr,CS-MT}}$. The reported uncertainty for the CS-MT modeling results corresponds to the standard error of the mean, as computed through block averaging. The CS-MT modeling results for g_{dehydr} and g_{hydr} were generated using f values, which as discussed in Section 7.3.1, are based on contacts with water and with hydrogen-bonding groups in the surfactant head. The value of g_{dehydr} ($-12.11 k_{\text{B}}T$) is much larger in magnitude than that of g_{hydr} ($1.51 k_{\text{B}}T$). However, as shown in Table 7.4 and Table 7.5 (see below), if g_{hydr} is not included in the CS-MT model, accurate CS-MT modeling results would not be obtained. Equation 7.7 was used to compute $g_{\text{tr,CS-MT}}$ from g_{dehydr} , g_{hydr} , and \hat{g}_{int} . In Table 7.3, we also report the traditional MT model prediction of g_{tr} for comparison with $g_{\text{tr,CS-MT}}$. We note that the CS-MT model prediction for the transfer free-energy contribution ($g_{\text{tr,CS-MT}} = -14.61 k_{\text{B}}T$) is $0.63 k_{\text{B}}T$ more negative than the traditional MT model prediction ($g_{\text{tr}} = -13.98 k_{\text{B}}T$).

In Table 7.4 and Table 7.5, we report CS-MT and traditional MT modeling results

Surfactant	$g_{\text{dehydr}} [k_B T]$	$g_{\text{hydr}} [k_B T]$	$\hat{g}_{\text{int}} [k_B T]$	$g_{\text{tr,CS-MT}} [k_B T]$	$g_{\text{tr}} [k_B T]$
OG	-12.11 ± 0.06	1.51 ± 0.02	4.01	-14.61 ± 0.06	-13.98
DM	-17.90 ± 0.05	2.25 ± 0.02	4.71	-20.36 ± 0.06	-20.06
OSE	-10.53 ± 0.10	1.31 ± 0.02	4.34	-13.55 ± 0.10	-13.98
C₁₀PO	-14.34 ± 0.05	1.44 ± 0.03	3.86	-16.75 ± 0.06	-16.96
C₁₀SO	-13.08 ± 0.12	1.38 ± 0.04	3.86	-15.56 ± 0.12	-16.96
C₁₂E₈, all hyd. groups	-21.04 ± 0.22	1.29 ± 0.06	4.90	-24.65 ± 0.23	-19.95
C₁₂E₈, tail hyd. groups	-16.76 ± 0.09	0.55 ± 0.05	4.90	-21.10 ± 0.10	-19.95
MEGA-10	-14.91 ± 0.16	1.36 ± 0.06	3.81	-17.36 ± 0.17	-15.47

Table 7.3: Modeling results for the simulated micelles. Computer simulation/molecular-thermodynamic (CS-MT) and traditional molecular-thermodynamic (MT) modeling results for each of the seven simulated nonionic surfactant micelles considered in this article. CS-MT model predictions of g_{dehydr} , g_{hydr} , \hat{g}_{int} , and $g_{\text{tr,CS-MT}}$ were made as described in Section 7.1.1. The uncertainties reported for the CS-MT model predictions correspond to the standard error of the mean. Traditional MT modeling results for g_{tr} are presented for comparison with $g_{\text{tr,CS-MT}}$. For C₁₂E₈, CS-MT modeling results generated by summing in Eq. 7.2 over all the hydrophobic (hyd) groups in the C₁₂E₈ molecule, as well as over only the C₁₂E₈ tail hydrophobic groups, are reported separately (see Section 7.4.8).

for micelles of the *optimal* shape and size. The optimal micelle shape and size are predicted to be the values that minimize g_{form} [8]. Although the CS-MT model predicts a different g_{form} value than that obtained using the traditional MT model, both models yield identical predictions for the optimal micelle shape and size. This equivalence arises because the only contribution to g_{form} that differs in the two models (the transfer free-energy contribution) does not depend on the micelle shape and size, and therefore, does not affect the minimization procedure used to determine the optimal micelle properties. As discussed in Section 7.2.3, the computer simulation of the OG micelles was conducted for a spherical micelle with an aggregation number of 29, but both the CS-MT model and the traditional MT model predict that the optimal micelles are cylindrical with a number-average micelle aggregation number of 43. In Table 7.4, we report predictions of the CS-MT model and of the traditional MT model for: (i) the optimal micelle shape, (ii) the number-average aggregation number (n), (iii) g_{int} , (iv) g_{pack} , and (v) g_{st} . In Table 7.5 we report predictions of

Surfactant	Shape	n	$g_{\text{int}} [k_B T]$	$g_{\text{pack}} [k_B T]$	$g_{\text{st}} [k_B T]$
OG	cyl.	43	3.23	2.17	1.54
DM	cyl.	58	4.31	2.23	1.91
OSE	cyl.	535	2.71	2.39	1.07
C₁₀PO	cyl.	45	4.08	2.16	1.87
C₁₀SO	cyl.	12802	2.94	2.50	1.0
C₁₂E₈	cyl.	54	4.41	2.23	1.95
MEGA-10	sph.	22	4.96	2.39	1.97

Table 7.4: Modeling results for the optimal micelles. Computer simulation/molecular-thermodynamic (CS-MT) and traditional molecular-thermodynamic (MT) modeling results for each of the seven nonionic surfactants considered in this article. Both the CS-MT model and the traditional MT model yield identical predictions for the optimal micelle shape, the number-average aggregation number (n), g_{int} , g_{pack} , and g_{st} (see Section 7.4.2).

the CS-MT and of the traditional MT model for (i) the CS-MT model predictions of g_{form} and of the CMC, (ii) the traditional MT model prediction of g_{form} and of the CMC, and (iii) the experimental values of g_{form} and of the CMC [35]. The reported uncertainty for the CS-MT modeling results is the standard error of the mean, as computed through block averaging. The CS-MT and the traditional MT model predictions for g_{form} were obtained by using $g_{\text{tr,CS-MT}}$ and g_{tr} , respectively, as an input to Eq. 7.8. In applying the CS-MT model and the traditional MT model, the surfactant head area, a_{h} , was modeled as being equal to 40 \AA^2 [8]. Note that the molecular parameter, a_{h} , is used to calculate the steric free-energy contribution, g_{st} [8, 36]. Traditional MT modeling results were generated using the traditional MT modeling approach reviewed in Chapter 6 [1]. In generating the traditional MT modeling results, each OG surfactant was modeled as having 7 CH_2 groups and 1 CH_3 group in the surfactant tail (groups 13-20 in Figure 7-3). The CS-MT and the traditional MT model predictions of the CMC and the value of g_{form} inferred using the experimental CMC data were calculated using Eq. 7.9.

Because the shape and size of the optimal micelles predicted by the CS-MT model and the traditional MT model are identical, the values of g_{int} , g_{pack} , and g_{st} predicted

Surfactant	$g_{\text{form}} [k_B T]$ (CMC [mM])		
	CS-MT Model	MT Model	Experimental
OG	-8.67 ± 0.06 (9.52 ± 0.57)	-8.04 (17.97)	-7.74 (24.1)
DM	-12.89 ± 0.06 (0.14 ± 0.01)	-12.60 (0.19)	-12.87 (0.14)
OSE	-8.39 ± 0.10 (12.59 ± 1.27)	-8.81 (8.26)	-7.62 (27)
C₁₀PO	-9.64 ± 0.06 (3.61 ± 0.23)	-9.85 (2.93)	-9.58 (3.8)
C₁₀SO	-10.13 ± 0.12 (2.23 ± 0.28)	-11.53 (0.54)	-10.38 (1.7)
C₁₂E₈	all hyd. grps: -17.06 ± 0.23 (0.002 ± 0.0)	-12.36 (0.24)	-13.22 (0.1)
	tail hyd. grps: -13.51 ± 0.10 (0.08 ± 0.01)		
MEGA-10	-9.05 ± 0.17 (6.55 ± 1.15)	-8.12 (43.33)	-9.31 ± 0.01 (5)

Table 7.5: Modeling results for the optimal micelles. The CS-MT and the traditional MT model predictions of g_{form} were obtained using the values of $g_{\text{tr,CS-MT}}$ and g_{tr} reported in Table 3, respectively, as an input to Eq. 7.8. The CS-MT and the traditional MT model predictions of the CMC, and the value of g_{form} inferred using the experimental CMC data were calculated using Eq. 7.9. The uncertainties reported for the CS-MT model predictions correspond to the standard error of the mean. For C₁₂E₈, CS-MT modeling results generated by summing in Eq. 7.2 over all the hydrophobic (hyd) groups in the C₁₂E₈ molecule, as well as over only the C₁₂E₈ tail hydrophobic groups, are reported separately (see Section 7.4.8).

by each model are also identical [8]. Although the predicted value of g_{int} is the same in both the CS-MT model and the traditional MT model, as shown in Tables 7.3 and 7.4, the value of g_{int} computed for the optimal micelle ($3.23 k_{\text{B}}T$) is significantly lower than the value of \hat{g}_{int} computed for the simulated micelle ($4.01 k_{\text{B}}T$). The free-energy contributions, g_{st} ($1.54 k_{\text{B}}T$) and g_{pack} ($2.17 k_{\text{B}}T$), while smaller than g_{int} , both contribute significantly to g_{form} . Values of g_{ent} and g_{elec} are not reported because they are equal to zero for this nonionic, single-surfactant system. The CS-MT model, the MT model, and the experimental values of g_{form} are all within $0.63 k_{\text{B}}T$ of each other. The CS-MT and the traditional MT model predictions of the CMC, as well as the value of g_{form} inferred using the experimental CMC data, were calculated using Eq. 7.9. Both the CS-MT model and the traditional MT model predict CMC values that are somewhat lower than the experimental CMC value of 24.1 mM [35]. The CMC predicted by the CS-MT model is 61% lower than the experimental CMC value, while the CMC predicted by the traditional MT model is 25% lower than the experimental CMC value. This discrepancy reflects the different estimates of the hydrophobic driving force for micelle formation obtained using the two models ($g_{\text{tr,CS-MT}}$ and g_{tr} , as reported in Table 7.3). Although the traditional MT model result for the CMC is closer to the experimental CMC value than the CS-MT result for the CMC, we consider both the CS-MT model and the traditional MT model CMC predictions shown in Table 7.3 to be in reasonable agreement with the experimental data, given the exponential dependence of the CMC on g_{form} (see Eq. 7.9).

7.4.3 Modeling Results for Dodecyl Maltoside (DM)

CS-MT modeling results for the simulated DM micelle are reported in Table 7.3, where each free-energy contribution was calculated as described in Section 7.4.2. Theoretical predictions for the optimal micelles obtained using the CS-MT model and the traditional MT model, as well as the experimental data [37] for the micellization behavior of DM in aqueous solution at 25 °C with 0.1 M of added NaCl, are reported

in Table 7.4 and Table 7.5. The approach described in Section 7.4.2 was used to calculate each free-energy contribution, the g_{form} values, and the CMC values. In using the CS-MT model and the traditional MT model, the surfactant head area, a_{h} , was modeled as being equal to 52 \AA^2 [8].

Although computer simulation of DM was conducted in a micelle with an aggregation number of 45, the optimal DM micelles that are predicted to form in solution by the CS-MT model and by the traditional MT model are small cylinders with a number-average aggregation number of 58. The predicted value of g_{int} ($4.31 k_{\text{B}}T$) is slightly lower than that of \hat{g}_{int} ($4.71 k_{\text{B}}T$) due to this aggregation number difference. The predicted value of g_{st} is slightly larger for the optimal DM micelle ($1.91 k_{\text{B}}T$) than the predicted value for the optimal OG micelle ($1.54 k_{\text{B}}T$), because the DM head (groups 1 to 23) is modeled as being 12 \AA^2 larger in cross-sectional area than the OG head (groups 1 to 12) [8]. As in OG, the CS-MT model prediction of the transfer free-energy contribution ($g_{\text{tr,CS-MT}} = -20.36 k_{\text{B}}T$) is slightly more negative than that of the traditional MT model prediction ($g_{\text{tr}} = -20.06 k_{\text{B}}T$). This leads to the CS-MT model predicting a lower CMC (0.14 mM) than that predicted by the traditional MT model (0.19 mM). In this case, the CS-MT model prediction of the CMC agrees remarkably well with the experimental value (0.14 mM).

7.4.4 Modeling Results for Octyl Sulfinyl Ethanol (OSE)

CS-MT modeling results for the simulated OSE micelle are reported in Table 7.3, where each free-energy contribution was calculated as described in Section 7.4.2. Theoretical predictions for the optimal micelles obtained using the CS-MT model and the traditional MT model, as well as the experimental data [38] for the micellization behavior of OSE in aqueous solution at $25 \text{ }^\circ\text{C}$, are reported in Table 7.4 and Table 7.5. The approach described in Section 7.4.2 was used to calculate each free-energy contribution, the g_{form} values, and the CMC values listed in 7.5. In applying the CS-MT model and the traditional MT model, the surfactant head area, a_{h} , was modeled as being equal to 30 \AA^2 [8].

Although computer simulation of an OSE micelle was conducted at an aggregation number of 25, the optimal OSE micelles that are predicted using the CS-MT model are cylinders with a number-average aggregation number of 535. The predicted value of g_{int} ($2.71 k_{\text{B}}T$) is significantly lower than that of \hat{g}_{int} ($4.34 k_{\text{B}}T$) due to this large aggregation number difference. The g_{int} value for OSE is $1.60 k_{\text{B}}T$ lower than that for DM and $0.52 k_{\text{B}}T$ lower than that for OG due to the large aggregation number of the OSE micelle, which lowers the interfacial area per surfactant molecule [8]. For OSE, $g_{\text{tr,CS-MT}}$ ($-13.55 k_{\text{B}}T$) is slightly less negative than g_{tr} computed using the traditional MT modeling approach ($-13.98 k_{\text{B}}T$). As a result, the CS-MT model prediction of the CMC is higher than the MT model prediction of the CMC, and it is also slightly closer to the experimental CMC value. As shown in Figure 7-5, groups 2 and 3 in OSE both have relatively high f values. However, the net effect of using Eqs. 7.2 and 7.4 to determine the contribution of both of these groups to the hydrophobic driving force for micelle formation is still significant, at $-0.71 k_{\text{B}}T$. Allowing all the hydrophobic groups in the surfactant molecule (and not just those in the surfactant tail) to contribute to g_{form} shifts the CS-MT model prediction of the CMC for OSE closer to the experimental CMC value.

7.4.5 Modeling Results for Decyl Dimethyl Phosphine Oxide (C_{10}PO)

CS-MT modeling results for the simulated C_{10}PO micelle are reported in Table 7.3. Theoretical predictions for the optimal micelles obtained using the CS-MT model and the traditional MT model, as well as the experimental data [39] for the micellization behavior of C_{10}PO in aqueous solution at $24\text{ }^{\circ}\text{C}$ with 0.1 mM of added Na_2CO_3 , are reported in Table 7.4 and Table 7.5. All the free-energy contributions, the g_{form} values, and the CMC values listed in Tables 7.3, 7.4, and 7.5 were computed using the approach described in Section 7.4.2. In applying the CS-MT model and the traditional MT model, the surfactant head area, a_{h} , was modeled as being equal to

50 Å² [8].

Although computer simulation of C₁₀PO was done in a micelle with an aggregation number of 50, the optimal micelles predicted by the CS-MT model and by the traditional MT model are small cylindrical micelles with a number-average aggregation number of 45. The predicted value of g_{int} (4.08 $k_{\text{B}}T$) is slightly higher than that of \hat{g}_{int} (3.86 $k_{\text{B}}T$) because the optimal micelle is predicted to have a slightly larger aggregation number than that of the simulated micelle. For this surfactant, the predictions of the CS-MT model and the traditional MT model for g_{form} and the CMC are quite similar. Our estimate of $g_{\text{tr,CS-MT}}$ (-16.75 $k_{\text{B}}T$) is only 0.21 $k_{\text{B}}T$ less negative than our estimate of g_{tr} (-16.96 $k_{\text{B}}T$), but nevertheless, this leads to a CMC prediction that is closer to the experimental CMC value than the CMC predicted using traditional MT modeling. In the CS-MT model, it is interesting to note that despite their high f values, groups 1 and 2 (as defined in Figure 7-6) contribute a total of -0.65 $k_{\text{B}}T$ to the hydrophobic driving force for micelle formation. Despite this negative free-energy contribution from the C₁₀PO head, the CMC predicted by the CS-MT model is higher than the CMC predicted by the MT model. This can be explained by the fact that the CS-MT modeling approach models the hydration of the surfactant tail and its contribution to $g_{\text{tr,CS-MT}}$ in a different manner than the traditional MT model.

7.4.6 Modeling Results for Decyl Methyl Sulfoxide (C₁₀SO)

CS-MT modeling results for the simulated C₁₀SO micelle are reported in Table 7.3. Theoretical predictions for the optimal micelles obtained using the CS-MT model, as well as the traditional MT model and the experimental data [39] for the micellization behavior of C₁₀SO in aqueous solution at 24 °C with 0.1 mM of added Na₂CO₃, are reported in Table 7.4 and Table 7.5. The results reported in Tables 7.3, 7.4, and 7.5 for C₁₀SO were computed using the approach described in Section 7.4.2. In applying the CS-MT model and the traditional MT model, the surfactant head area, a_{h} , was modeled as being equal to 30 Å² [8].

Like C₁₀PO, the C₁₀SO micelle was simulated with an aggregation number of 50. However, the CS-MT model prediction for the optimal aggregation number was found to correspond to large cylindrical micelles with a number-average aggregation number of 12,802. The predicted value of g_{int} for C₁₀SO ($2.94 k_{\text{B}}T$) is significantly lower than the predicted value of g_{int} for C₁₀PO ($4.08 k_{\text{B}}T$). For C₁₀SO, the CS-MT model estimate of $g_{\text{tr,CS-MT}}$ ($-15.56 k_{\text{B}}T$) is $1.4 k_{\text{B}}T$ larger than the traditional MT model estimate of g_{tr} ($-16.96 k_{\text{B}}T$), making the CS-MT model estimate of the CMC significantly larger than that of the traditional MT model and closer to the experimental CMC value. Group 1 of C₁₀SO (see Figure 7-7) contributes $-0.66 k_{\text{B}}T$ to $g_{\text{tr,CS-MT}}$, but the overall hydrophobic driving force for micelle formation is predicted to be higher using the CS-MT model than using the traditional MT model. In the next section, the CMC predicted by the CS-MT model and by the traditional MT model for binary mixtures of C₁₀PO and C₁₀SO will be presented, and the similarities and differences between the various free-energy contributions to g_{form} for these two surfactants will be discussed in greater detail.

7.4.7 Modeling Results for Binary Mixtures of C₁₀PO and C₁₀SO

In Figure 7-12, we present both CS-MT model predictions (see the — results) and traditional MT model predictions (■ ■ ■) for CMCs of binary mixtures of C₁₀PO and C₁₀SO in aqueous solution at 24 °C with 0.1 mM of added Na₂CO₃. Experimental mixture CMC data (◆) are presented for comparison [39]. CMC values are reported in mM on the y -axis, and the mole fraction of C₁₀PO is reported on the x -axis. The mixture CMC values increase monotonically as the mole fraction of C₁₀PO is increased. Both the CS-MT model and the traditional MT model capture this increase, and yield reasonable estimates of the slope associated with this increase. However, the CMCs predicted by the CS-MT model are clearly in better agreement with the experimental CMC values than the CMCs predicted by the traditional MT

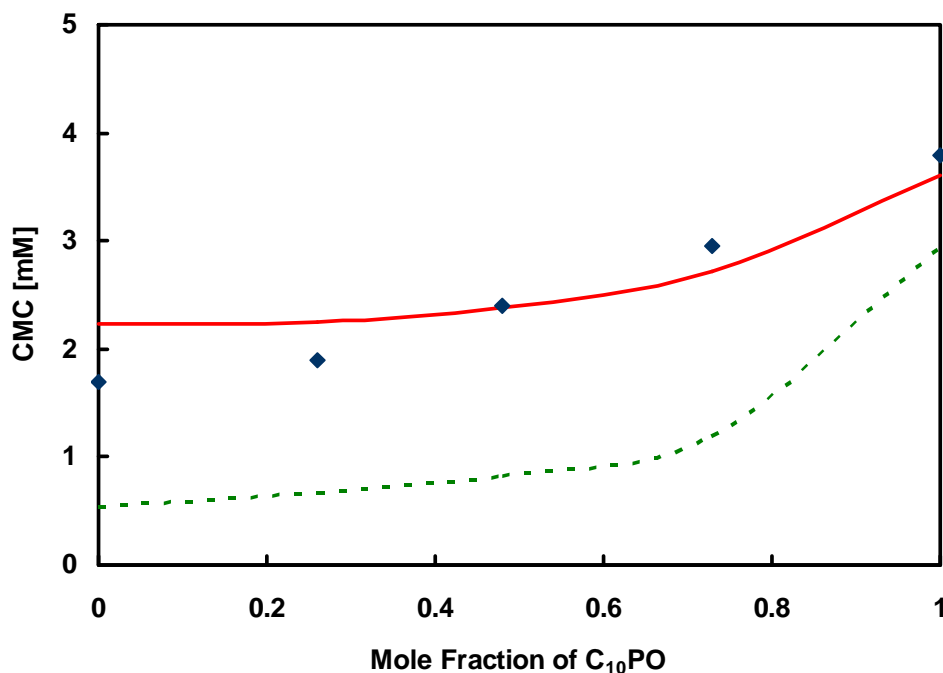


Figure 7-12: Predicted (— and - - -) and experimental (◆) CMCs of mixtures of C₁₀PO and C₁₀SO, where the full line corresponds to CMCs predicted by the CS-MT model, and the dashed line corresponds to CMCs predicted by the traditional MT model.

model.

It is instructive to compare each of the free-energy contributions to g_{form} for C₁₀PO and C₁₀SO, as estimated using the CS-MT model and the traditional MT model (see Tables 7.3, 7.4, and 7.5). The discrepancy between predictions made using the CS-MT model and the traditional MT model can be explained in terms of the difference between the CS-MT model estimates of $g_{\text{tr,CS-MT}}$ and the traditional MT model estimates of g_{tr} for these two surfactants (see Table 7.3). For C₁₀PO, $g_{\text{tr,CS-MT}} = -16.75 k_{\text{B}}T$ and $g_{\text{tr}} = -16.96 k_{\text{B}}T$, while for C₁₀SO, $g_{\text{tr,CS-MT}} = -15.56 k_{\text{B}}T$ and $g_{\text{tr}} = -16.96 k_{\text{B}}T$. As can be seen, the traditional MT model predictions for g_{tr} are the same for both C₁₀PO and C₁₀SO, because both surfactants have the same number of hydrophobic groups in their tails. The CS-MT model predictions for the transfer free-energy contribution are less negative than those of the traditional MT

model, making the CMC predicted using the CS-MT modeling approach higher for both surfactants and closer to the experimental CMC values (see Table 7.5).

Although the CS-MT model yields more accurate CMC predictions than the traditional MT model for C₁₀PO and C₁₀SO, both the CS-MT model and the traditional MT model correctly predict that C₁₀PO has a higher CMC than C₁₀SO. In the traditional MT model, the only molecular difference between C₁₀PO and C₁₀SO is their different head sizes (as captured in a_h). Therefore, the physical origin of the difference in CMC predictions for C₁₀PO and C₁₀SO made by the traditional MT model is due to steric effects (g_{st}). However, since the various free-energy contributions are coupled through the minimization of g_{form} , the influence of these steric effects is also manifested in the predicted values of g_{int} and g_{pack} . In the CS-MT modeling approach, the predicted CMCs also differ because of the different $g_{tr,CS-MT}$ values of C₁₀PO and C₁₀SO. The steric effects arising from differences in head size, however, more than compensate for the more negative $g_{tr,CS-MT}$ value of C₁₀PO ($-16.75 k_B T$) relative to that of C₁₀SO ($-15.56 k_B T$) predicted using the CS-MT model, making the predicted CMC of C₁₀PO 1.38 mM higher than that of C₁₀SO. In traditional MT modeling, g_{tr} for both surfactants is predicted to be the same, and therefore, the predicted CMC of C₁₀PO is 2.39 mM larger than the predicted CMC of C₁₀SO. The experimental CMC difference for these two surfactants is 2.1 mM, which is closer to the CS-MT model prediction for the difference in the CMCs than to the traditional MT prediction for the difference in the CMCs.

7.4.8 Modeling Results for Dodecyl Octa(Ethylene Oxide) (C₁₂E₈)

CS-MT modeling results for the simulated C₁₂E₈ micelle are reported in Table 7.3. Theoretical predictions for the optimal micelles obtained using the CS-MT model and the traditional MT model, as well as the experimental data [40] for the micellization behavior of C₁₂E₈ in aqueous solution at 25 °C, are reported in Table 7.4 and Table

7.5. The same computational approach described in Section 7.4.2 was used to generate each of the free-energy contributions to g_{form} , and the CMC values listed in Table 7.3, although for this surfactant, the CS-MT model predictions were made using two different approaches. In the first approach, reported under the heading “all hyd. groups” in Table 7.3, the CS-MT model for g_{dehyd} (given in Eq. 7.2) was used to compute the free-energy contribution of every hydrophobic group in the surfactant molecule, regardless of whether the group is part of the surfactant head or tail. This is the modeling approach that has been used to model each of the other nonionic surfactants considered in this chapter. However, we also implemented CS-MT modeling of C_{12}E_8 in an alternate way, reported under the heading “tail hyd. groups” in Table 7.3. In this alternate approach, only the hydrophobic groups in the surfactant tail (i.e., groups 26 to 37 listed in Figure 7-8) are included in the sum given in Eq. 7.2 to calculate g_{dehyd} . In both implementations of the CS-MT model, as well as in the implementation of the traditional MT model, the surfactant head area, a_{h} , was modeled as being equal to 53 \AA^2 [8].

C_{12}E_8 differs from the other six nonionic surfactants considered in this chapter in that the traditional MT model CMC prediction (0.24 mM) and the experimental CMC (0.1 mM) are in reasonable agreement, but the “all hyd. groups” CS-MT modeling approach severely underestimates the CMC (0.002 mM). The regular CS-MT modeling approach fails in this case because of the simplistic manner in which we have used Eq. 7.2 for C_{12}E_8 . As discussed in Section 7.4.2, the values of g_{tr_i} used in Eq. 7.2 are strictly accurate only for the transfer of a hydrophobic oil group (CH , CH_2 , or CH_3) from bulk water to a bulk phase of tails. For Eq. 7.2 to yield reasonable results, an accurate estimate of g_{tr_i} must first be made for each of the CH_2 groups in the E_8 head of C_{12}E_8 . As discussed in Section 7.4.1, we have made the approximation that for each of the nonionic surfactants modeled here, the g_{tr_i} values corresponding to hydrophobic groups in the surfactant head are equal to the g_{tr_i} values for the corresponding groups in the surfactant tail. For C_{12}E_8 , however, we believe that this approximation is not sufficiently accurate for the following reasons: (i) using a water-

to-oil transfer free energy for the process of transferring a CH_2 group in E_8 from bulk water to the corona region of a C_{12}E_8 micelle (which has a high concentration of water and other ethylene oxide groups) is a poor approximation, (ii) each of the hydrophobic groups in the surfactant head is bonded to a hydrophilic oxygen atom, thus affecting its hydrophobicity and g_{tr_i} value, and (iii) the large number of hydrophobic groups in the E_8 head (a total of 16) amplifies the effect of errors inherent in (i) and (ii) to a greater extent than that observed in the case of the other six nonionic surfactants considered in this chapter, which have relatively small, non-polymeric heads.

The CS-MT model “tail hyd. groups” approach actually yields the most accurate prediction of the CMC when compared with the experimental CMC. Clearly, for C_{12}E_8 , approximating each of the hydrophobic groups in the E_8 head of C_{12}E_8 as not contributing at all to the hydrophobic driving force for micelle formation is more appropriate than modeling them as contributing to the hydrophobic driving force with the same g_{tr_i} values as those corresponding to the CH_2 groups in the C_{12}E_8 tail. Based on the modeling results presented here, we conclude that care must be taken in applying the CS-MT model to surfactants with relatively long, polymeric heads. Without an accurate estimate of the appropriate g_{tr_i} values to use for the hydrophobic groups in the surfactant head, application of Eq. 7.2 to quantify the hydrophobic effect may not yield accurate results.

Although we do not explore these here, a number of approaches could be used to obtain more accurate estimates of g_{tr_i} values for the C_{12}E_8 head. Perhaps, the most straightforward approach would involve using an experimental or computational method to estimate the transfer free energy of an ethylene oxide monomer from bulk aqueous solution to a bulk phase of water and poly(ethylene oxide) molecules that serves as a reasonable proxy for the anisotropic corona region of the micelle. After obtaining the g_{tr_i} value of an ethylene oxide monomer, Eq. 7.2 could be used to calculate g_{dehyd} , albeit with the summation given in Eq. 7.2 extended to include all the hydrophobic groups in the C_{12}E_8 tail as well as all the ethylene oxide groups in the C_{12}E_8 head. To estimate g_{tr_i} of an ethylene oxide monomer, the solvation

free energy of an ethylene oxide group in water and the solvation free energy of an ethylene oxide group in a bulk phase of water and poly(ethylene oxide) molecules could be determined experimentally. Alternatively, a theoretical approach could be used to estimate the transfer free energy or solvation free energies, for example, by using the Flory-Huggins approach with appropriate χ parameters, or using a computer simulation approach which uses a realistic forcefield to describe interactions between the system components [2, 41].

7.4.9 Modeling Results for Decanoyl-*n*-Methylglucamide (MEGA-10)

CS-MT modeling results for the simulated MEGA-10 micelle are reported in Table 7.3, and theoretical predictions made using the CS-MT model and the traditional MT model for the micellization behavior of MEGA-10 are reported in Table 7.4 and Table 7.5. Experimental data is also reported in 7.5 for comparison [42]. All data were generated for MEGA-10 in aqueous solution at 30 °C with 0.1 M of added NaCl. Each value reported in Tables 7.3, 7.4, and 7.5 for MEGA-10 was computed using the approach described in Section 7.4.2. In applying the CS-MT model and the traditional MT model, the surfactant head area, a_h , was modeled as being equal to 62 Å² [8].

Computer simulation of MEGA-10 was conducted for a micelle with an aggregation number of 42. However, the optimal MEGA-10 micelle shape and size predicted by the CS-MT model is small spheres with a number-average aggregation number of only 22. As a result, the predicted value of g_{int} ($4.96 k_B T$) is significantly higher than the predicted value of \hat{g}_{int} ($3.81 k_B T$). The low predicted aggregation number of MEGA-10 is due in part to its large head area, which at 62 Å² is larger than that of any of the other nonionic surfactants modeled here. This large head area, in turn, results in MEGA-10 having the highest value of g_{st} ($1.97 k_B T$) among all the nonionic surfactants modeled. For MEGA-10, $g_{\text{tr,CS-MT}}$ ($-17.36 k_B T$) is significantly

more negative than g_{tr} ($-15.47 k_{\text{B}}T$) computed using the traditional MT modeling approach. This is due primarily to the hydrophobic free-energy contributions calculated in the CS-MT modeling approach for groups 11 and 12 (see Figure 7-9). In the traditional MT modeling approach, the most reasonable estimate of the head and tail of MEGA-10 would be to include only groups 16 to 24 in the linear alkyl chain as part of the tail. Based on this tail assignment, the traditional MT model prediction of g_{tr} is less negative than the CS-MT model prediction of $g_{\text{tr,CS-MT}}$. As a result, the CMC predicted by the CS-MT model (6.55 mM) is much closer to the experimental CMC (5 mM) than the CMC predicted by the traditional MT model (43.33 mM). Clearly, only the CS-MT model predictions are reasonable for MEGA-10.

7.4.10 Effect of the Definition of Hydrating Contacts on the Modeling Results

In Chapter 6, we stated that in the context of CS-MT modeling, an atom in contact with a hydrophobic group is considered “hydrating” if the atom: (i) is capable of forming hydrogen bonds, or (ii) is capable of coordinate (dative covalent) bonding. Based on this definition, both water and hydrogen-bonding groups in surfactant heads contribute hydrating contacts when computing f , and therefore, one should use f values, rather than f_{water} values, in implementing the CS-MT modeling approach.

The effect of the way in which hydrating contacts are defined on our modeling results can be evaluated by comparing the CS-MT model predictions for the CMC using f values in Eqs. 7.2 and 7.4 with the CS-MT model predictions of the CMC using f_{water} values in Eqs. 7.2 and 7.4. Figure 7-13 compares the CMC predictions for OG, DM, OSE, C₁₀PO, C₁₀SO, and MEGA-10 using both approaches with the experimental CMC values. Results for C₁₂E₈ are not shown because the CS-MT model does not yield sufficiently accurate CMC predictions for this surfactant (for reasons discussed in Section 7.4.8). CMC results are reported on a log scale because of the large range spanned by the predicted and the experimental CMC values. With the

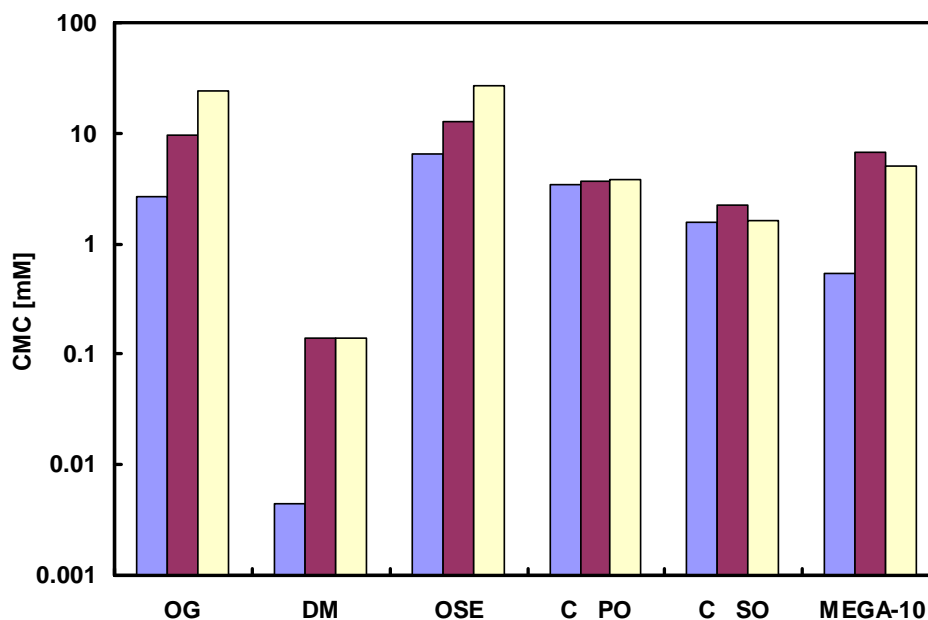


Figure 7-13: Comparison of CMCs predicted by the CS-MT model using f (■) and f_{water} (■) values (see Section 7.4.10) in Eqs. 7.2 and 7.4 to compute g_{dehydr} and g_{hydr} , respectively. The definitions of f and f_{water} are given in Section 7.3.1. The experimental CMCs (■) are also reported for comparison with the theoretical predictions. The CMC values are reported on a log scale.

exception of C_{10}SO , using f values (see the ■ results) in Eqs. 7.2 and 7.4 yields better CMC predictions than using f_{water} values (■) in Eq. 7.2 and 7.4. If only water molecules are considered to be hydrating, the degree of dehydration of the micelle core is overestimated, resulting in a prediction of g_{form} that is often significantly more negative than that predicted using the traditional MT model. As expected intuitively, the discrepancy between the f and f_{water} modeling results is largest for surfactants with many hydrogen-bonding groups in the surfactant head. For example, for OG, by defining hydration using f_{water} instead of using f , the predicted CMC is reduced by a factor of 3.6. For DM, defining hydration using f_{water} instead of using f has an even greater effect and reduces the predicted CMC by a factor of 31.

Modeling contacts with hydrogen-bonding groups in the surfactant head as being

hydrating is consistent with the approximation made in traditional MT modeling that the surfactant heads at the micelle core/water interface shield only 21 \AA^2 of the interface from hydrating contacts, an area corresponding to the cross-sectional area of the linear alkyl chain connected to the surfactant head, rather than to the cross-sectional area of the surfactant head. In traditional MT modeling, if the surfactant head is modeled as shielding its cross-sectional area, implying that the head itself does not provide hydrating contacts, less accurate predictions of micellization behavior would be obtained.

7.5 Conclusions

In this chapter, we have demonstrated the validity and accuracy of the CS-MT model by using it to model seven nonionic surfactants. To implement the CS-MT model, we have conducted two independent MD simulations for each nonionic surfactant to determine information about the changes in hydration that occur upon micelle formation. Changes in hydration were quantified by computing a fractional hydration value, f , for each group. The f values obtained for each surfactant through MD simulation were used as an input in a new model presented in Chapter 6 that computes the magnitude of the hydrophobic free-energy contribution as the sum of g_{dehydr} and g_{hydr} . In this chapter, we have used a simple computational strategy to estimate g_{dehydr} and g_{hydr} for each nonionic surfactant modeled. To calculate g_{dehydr} , g_{tr_i} values were estimated using the same solubility correlations for linear alkyl tails that our group has used in the past in traditional MT modeling [32]. To calculate g_{hydr} , we have made the simple approximation that this contribution is equal to zero for any hydrophobic group with a value of f greater than 0.60. For hydrophobic groups with a value of f less than 0.60, g_{hydr} was calculated using Eq. 7.4 and an expression for Δg_{wc} derived for oil molecules in Chapter 6. By combining elements of the CS-MT model and the traditional MT model, the hydrophobic driving force for micelle formation was quantified as a transfer free energy ($g_{\text{tr,CS-MT}}$). After determining this

input, the free energy of micelle formation, g_{form} , and the CMC were calculated for each surfactant for micelles of the optimal shape and size.

Reasonable agreement between the CS-MT model predictions and the experimental data for g_{form} and the CMC were obtained for OG, DM, OSE, C₁₀PO, C₁₀SO, and MEGA-10. For C₁₂E₈, the CS-MT model predictions were not in good agreement with the experimental data because the simple approximations that were made in this chapter to estimate g_{dehydr} were not sufficiently accurate for this surfactant. For the 16 hydrophobic CH₂ groups in the E₈ head of C₁₂E₈, we believe that more accurate values of g_{tr_i} must be used to obtain accurate modeling results. Consequently, we recommend that the simple approximations that we have made to compute g_{dehyd} only be used for surfactants with relatively small, non-polymeric heads.

The predictions of the CS-MT and the traditional MT modeling approaches were found to be in reasonable agreement for OG, DM, OSE, C₁₀PO, and C₁₀SO. For four of these surfactants (DM, OSE, C₁₀PO, and C₁₀SO), the CMCs predicted by the CS-MT model were closer to the experimental CMC values than the CMCs predicted by the traditional MT model. In addition, CMCs predicted for binary mixtures of C₁₀PO and C₁₀SO using the CS-MT modeling approach were significantly closer to the experimental CMCs than those predicted using the traditional MT modeling approach. The CMC predicted by the CS-MT model for MEGA-10 (6.55 mM) was significantly closer to the experimental CMC value (5 mM) than the CMC predicted by the traditional MT model (43.3 mM).

Using the relatively simple approach to estimate g_{dehydr} and g_{hydr} presented in this chapter, the CS-MT model was found to yield similar, or superior, predictions of the CMCs of nonionic surfactants with relatively small, non-polymeric heads when compared to the traditional MT model. The results obtained for the relatively complex surfactant MEGA-10 highlight the strengths of the CS-MT modeling approach: for surfactants where it is difficult to make accurate head and tail assignments for traditional MT modeling, and for surfactants where a significant number of hydrophobic groups are located near the aggregate core/water interface and are partially hydrated,

the CS-MT modeling approach is expected to yield better results than the traditional MT modeling approach. Clearly, the more accurate predictions of the CS-MT model come at the cost of greater computational expense. Nevertheless, given the relatively small fraction of surfactants with sufficient structural and chemical simplicity to be easily modeled using the traditional MT model, we conclude that the CS-MT modeling approach represents a very promising alternative. In the next chapter, Chapter 8, the CS-MT modeling approach will be used to model the micellization of nine anionic, zwitterionic, and cationic surfactants in aqueous solution.

7.6 Appendix A: Normalized SASA Profiles

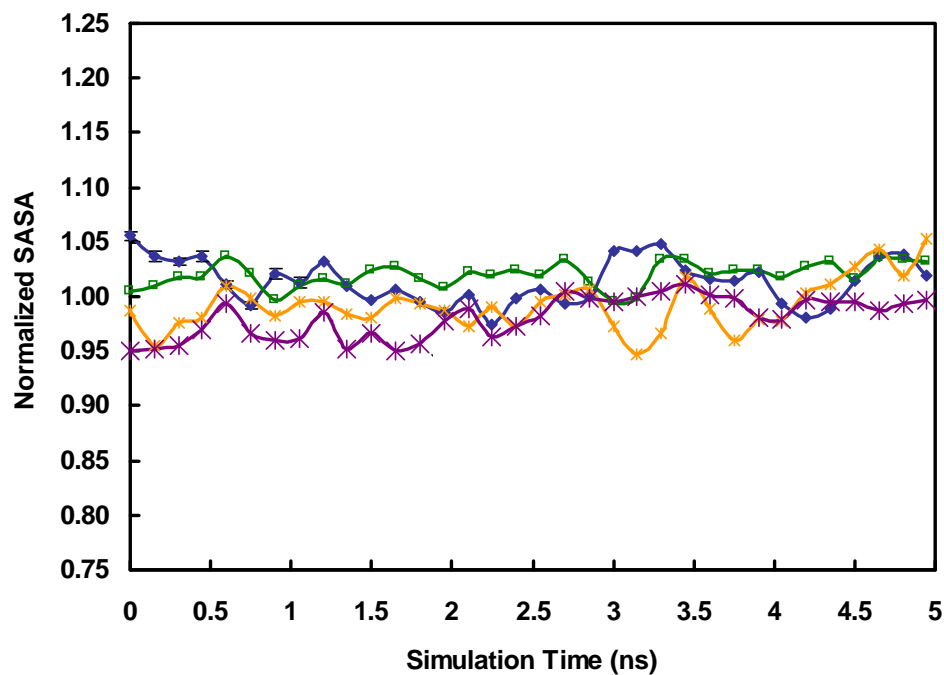


Figure 7-A1: Solvent accessible surface area (SASA) normalized by the average value of SASA as a function of simulation time for: octyl glucoside (OG, $\text{—}\blacklozenge\text{—}$), dodecyl maltoside (DM, $\text{—}\blacksquare\text{—}$), dodecyl octa(ethylene oxide) (C_{12}E_8 , $\text{—}\ast\text{—}$), and decanoyl-*n*-methylglucamide (MEGA-10, $\text{—}\ast\text{—}$) during the 5 ns data-gathering simulation run (see text).

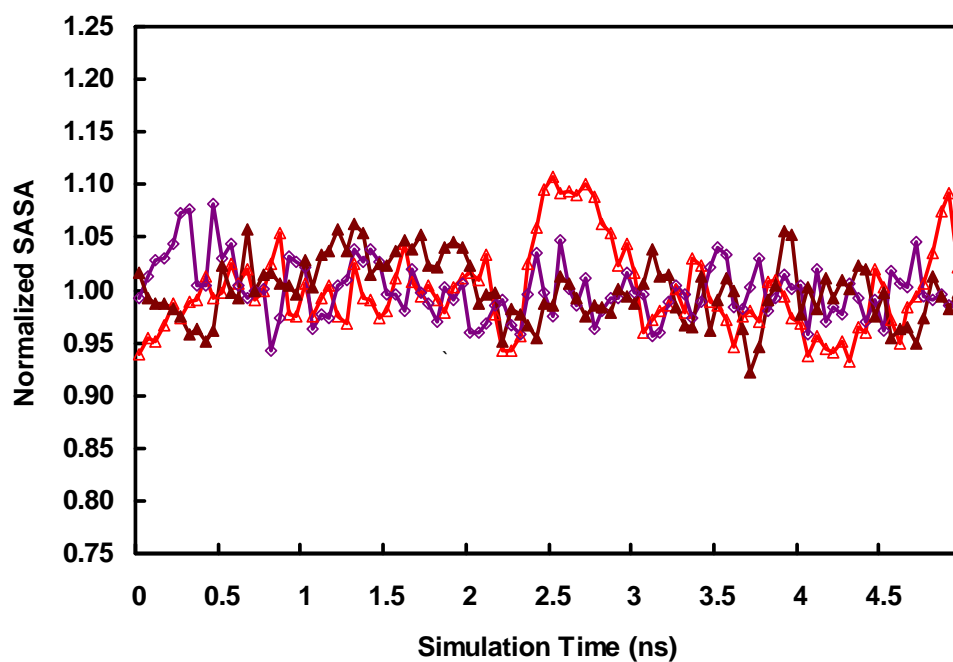


Figure 7-A2: Solvent accessible surface area (SASA) normalized by the average value of SASA as a function of simulation time for: octyl sulfinyl ethanol (OSE, \blacktriangle), decyl dimethyl phosphine oxide (C₁₀PO, \blacklozenge), and decyl methyl sulfoxide (C₁₀SO, \blacktriangle) during the 5 ns data-gathering simulation run (see text).

Bibliography

- [1] Stephenson, B. C., Goldsipe, A., Beers, K. J., and Blankschtein, D., “Quantifying the hydrophobic effect: I. A computer simulation/molecular-thermodynamic model for the aqueous self-assembly of hydrophobic and amphiphilic solutes,” *The Journal of Physical Chemistry B*, 2006, pp. (submitted).
- [2] Nagarajan, R. and Ruckenstein, E., “Theory of surfactant self-assembly: A predictive molecular thermodynamic approach,” *Langmuir*, Vol. 7, 1991, pp. 2934–2969.
- [3] Shiloach, A. and Blankschtein, D., “Predicting micellar solution properties of binary surfactant mixtures,” *Langmuir*, Vol. 14, 1998, pp. 1618–1636.
- [4] Gunnarsson, G., Jonsson, B., and Wennerstrom, H., “Surfactant association into micelles - An electrostatic approach,” *The Journal of Physical Chemistry*, Vol. 84, 1980, pp. 3114–3121.
- [5] Jonsson, B. and Wennerstrom, H., “Thermodynamics of ionic amphiphile-water systems,” *Journal of Colloid and Interface Science*, Vol. 80, 1981, pp. 482–496.
- [6] Evans, D. F., Mitchell, D. J., and Ninham, B. W., “Ion binding and dressed micelles,” *The Journal of Physical Chemistry*, Vol. 88, 1984, pp. 6344–6348.
- [7] Hayter, J. B., “A self-consistent theory of dressed micelles,” *Langmuir*, Vol. 8, 1992, pp. 2873–2876.

- [8] Puvvada, S. and Blankschtein, D., “Molecular thermodynamic approach to predict micellization, phase behavior and phase separation of micellar solutions. 1. Application to nonionic surfactants,” *The Journal of Chemical Physics*, Vol. 92, 1990, pp. 3710–3724, and references cited therein.
- [9] van der Spoel, D., Lindahl, E., Hess, B., van Buuren, A., Apol, E., Meulenhoff, P., Tieleman, D., Sijbers, A., Feenstra, K., van Drunen, R., and Berendsen, H., *Gromacs User Manual version 3.2*, www.gromacs.org, 2004.
- [10] Goldsipe, A. and Blankschtein, D., “Modeling counterion binding in ionic-nonionic and ionic-zwitterionic binary surfactant mixtures,” *Langmuir*, Vol. 22, 2005, pp. 9850–9865.
- [11] Jorgensen, W. L., Maxwell, D. S., and Tirado-Rives, J., “Development and testing of the OPLS all-atom force field on conformational energetics and properties of organic liquids,” *Journal of the American Chemical Society*, Vol. 118, 1996, pp. 11225–11236.
- [12] Chirlian, L. E. and Francl, M. M., “Atomic charges derived from electrostatic potentials: A detailed study,” *Journal of Computational Chemistry*, Vol. 8, 2004, pp. 894–905.
- [13] Stephenson, B. C., Beers, K., and Blankschtein, D., “Complementary use of simulations and molecular-thermodynamic theory to model micellization,” *Langmuir*, Vol. 22, 2006, pp. 1500–1513.
- [14] Stephenson, B. C., Rangel-Yagui, C. O., Pessoa, A., Tavares, L. C., Beers, K. J., and Blankschtein, D., “Experimental and theoretical investigation of the micellar-assisted solubilization of ibuprofen in aqueous media,” *Langmuir*, Vol. 22, 2006, pp. 1514–1525.

- [15] Darden, T., York, D., and Pedersen, L., "Particle mesh Ewald: An N-log(N) method for Ewald sums in large systems," *The Journal of Chemical Physics*, Vol. 98, 1993, pp. 10089–10092.
- [16] Essmann, U., Perera, L., Berkowitz, M. L., Darden, T., Lee, H., and Pedersen, L. G., "A smooth particle mesh Ewald potential," *The Journal of Chemical Physics*, Vol. 103, 1995, pp. 8577–8592.
- [17] van Gunsteren, W. F. and Berendsen, J. J. C., "A leap-frog algorithm for stochastic dynamics," *Journal of Computational Chemistry*, Vol. 18, 1997, pp. 1463–1472.
- [18] Berendsen, H. J. C., van der Spoel, D., and van Drunen, R., "GROMACS: A message-passing parallel molecular dynamics implementation," *Computational Physics Community*, Vol. 91, 1995, pp. 43–56.
- [19] Lindahl, E., Hess, B., and van der Spoel, D., "Gromacs 3.0: A package for molecular simulation and trajectory analysis," *Journal of Molecular Modeling*, Vol. 7, 2001, pp. 306–317.
- [20] Jang, S. S. and Goddard III, W. A., "Structures and properties of Newton black films characterized using molecular dynamics simulations," *The Journal of Physical Chemistry B*, Vol. 110, 2006, pp. 7992–8001.
- [21] Stephenson, B. C. and Beers, K. J., "Determination of the interfacial characteristics series of bolaamphiphilic poly(fluorooxetane) surfactants through molecular dynamics simulation," *The Journal of Physical Chemistry B*, 2006, pp. (submitted).
- [22] Feller, S. and Pastor, R., "On simulating lipid bilayers with an applied surface tension: Periodic boundary conditions and undulations," *Biophysical Journal*, Vol. 71, 1996, pp. 1350–1355.

- [23] Israelachvili, J. N., *Intermolecular and Surface Forces*, Academic Press, 2nd ed., 1991.
- [24] Bruce, C., Berkowitz, M., Perera, L., and Forbes, M., “Molecular dynamics simulation of sodium dodecyl sulfate micelle in water: Micellar structural characteristics and counterion distribution,” *The Journal of Physical Chemistry B*, Vol. 106, 2002, pp. 3788–3793.
- [25] Flyvbjerg, H. and Petersen, H. G., “Error estimates on averages of correlated data,” *The Journal of Chemical Physics*, Vol. 91, 1989, pp. 461–466.
- [26] Hess, B., *Stochastic Concepts in Molecular Simulation*, Ph.D. thesis, Rijksuniversiteit Groningen, Groningen, 1999.
- [27] Hess, B., “Determining the shear viscosity of model liquids from molecular dynamics simulations,” *The Journal of Chemical Physics*, Vol. 116, 2001, pp. 209–217.
- [28] Gibbs, J. W., *The Scientific Papers of J.W. Gibbs*, Vol. 1, Dover, New York, 1961.
- [29] Koenig, F. O., “On the thermodynamic relation between surface tension and curvature,” *The Journal of Chemical Physics*, Vol. 18, 1950, pp. 449.
- [30] Buff, F. P., “The spherical interface. I. Thermodynamics,” *The Journal of Chemical Physics*, Vol. 19, 1951, pp. 1591.
- [31] Tolman, R. C., “Consideration of the Gibbs theory of surface tension,” *The Journal of Chemical Physics*, Vol. 16, 1948, pp. 758.
- [32] Smith, R. and Tanford, C., “Hydrophobicity of long chain n-alkyl carboxylic acids, as measured by their distribution between heptane and aqueous solutions,” *Proceedings of the National Academy of Sciences*, Vol. 70, 1973, pp. 289–293.

- [33] Reynolds, J. A., Gilbert, D. B., and Tanford, C., “Empirical correlation between hydrophobic free energy and aqueous cavity surface area,” *Proceedings of the National Academy of Sciences*, Vol. 71, 1974, pp. 2925–2927.
- [34] Stephenson, B. C., Beers, K. J., and Blankschtein, D., “Quantifying the hydrophobic effect: III. A computer simulation/molecular-thermodynamic model for the micellization of ionic and zwitterionic surfactants,” *The Journal of Physical Chemistry B*, 2006, pp. (submitted).
- [35] Mukerjee, P. and Chan, C. C., “Effects of high salt concentrations on the micellization of octyl glucoside: Salting-out of monomers and electrolyte effects on the micelle-water interfacial tension,” *Langmuir*, Vol. 14, 2002, pp. 5375–5381.
- [36] Srinivasan, V. and Blankschtein, D., “Effect of counterion binding on micellar solution behavior: 1. Molecular-thermodynamic theory of micellization of ionic surfactants,” *Langmuir*, Vol. 19, 2003, pp. 9932–9945.
- [37] Rosen, M. J. and Sulthana, S. B., “The interaction of alkylglucosides with other surfactants,” *Journal of Colloid and Interface Science*, Vol. 239, 2001, pp. 528–534.
- [38] Aratono, M., Kanda, T., and Motomura, K., “Study on the adsorption and the micelle formation of a (decylsulfinyl)ethanol and (octylsulfinyl)ethanol mixture,” *Langmuir*, Vol. 6, 1990, pp. 843–846.
- [39] Holland, P. M. and Rubingh, D. N., “Nonideal multicomponent mixed micelle model,” *The Journal of Physical Chemistry*, Vol. 87, 1983, pp. 1984–1990.
- [40] Alargova, R. G., Kochijashky, I. I., Sierra, M. L., and Zana, R., “Micelle aggregation numbers of surfactants in aqueous solutions: A comparison between the results from steady-state and time-resolved fluorescence quenching,” *Langmuir*, Vol. 14, 1998, pp. 5412–5418.

- [41] Carale, T. R., Pham, Q. T., and Blankschein, D., “Salt effects on intramicellar interactions and micellization of nonionic surfactants in aqueous solutions,” *Langmuir*, Vol. 10, 1994, pp. 109–121.
- [42] Hierrezuelo, J. M., Aguiar, J., and Ruiz, C. C., “Stability, interaction, size, and microenvironmental properties of mixed micelles of decanoyl-N-methylglucamide and sodium dodecyl sulfate,” *Langmuir*, Vol. 20, 2004, pp. 10419–10426.

Chapter 8

Quantifying the Hydrophobic Effect: III. A Computer Simulation/Molecular-Thermodynamic Model for the Micellization of Ionic and Zwitterionic Surfactants in Aqueous Solution

8.1 Introduction

The CS-MT model combines hydration data obtained through computer simulation with a free-energy model for the hydrophobic driving force for micelle formation to model surfactant micellization and micellar solubilization in aqueous solution. This new modeling approach was introduced in Chapter 6 and tested by modeling oil

aggregates [1]. The primary motivation for the development of the CS-MT model is to extend the traditional MT model to increasingly chemically and structurally complex surfactants and solubilizates. In Chapter 7 [2], the CS-MT model was extended to model the micellization behavior of nonionic surfactants by outlining a simple computational strategy to estimate g_{dehydr} , the free-energy change associated with dehydration, and g_{hydr} , the change in the hydration free energy, when non-charged hydrophilic head groups are present at the micelle core/water interface. In Chapter 7, the CS-MT model was used to predict the micellization behavior of seven nonionic surfactants with varying degrees of structural complexity. In this chapter, we use the CS-MT model to predict the micellization behavior of ionic and zwitterionic surfactants that are both simple and challenging to model using the traditional MT modeling approach. The most complex of the surfactants considered in this chapter are too complex to model accurately using the traditional MT model.

8.1.1 Overview of the CS-MT Model

The free energy of aggregate formation, g_{form} , is computed in the CS-MT model as the sum of the following six free-energy contributions [1,2]:

$$g_{\text{form}} = g_{\text{dehydr}} + g_{\text{hydr}} + g_{\text{pack}} + g_{\text{st}} + g_{\text{elec}} + g_{\text{ent}} \quad (8.1)$$

Two of the free-energy contributions to g_{form} , g_{dehydr} and g_{hydr} , reflect the hydrophobic free-energy change associated with aggregate formation, or the hydrophobic driving force for aggregate formation. In the CS-MT modeling approach, computer simulation data on surfactant hydration in the bulk water and in the micellar states are used to compute both g_{dehydr} and g_{hydr} . They are computed using the following two equations [1, 2]:

$$g_{\text{dehydr}} = \sum_{i=1}^{n_{\text{hyd}}} (1 - f_i) g_{\text{tr}_i} \quad (8.2)$$

$$g_{\text{hydr}} = \sum_{i=1}^{n_{\text{core}}} SASA_i f_i \Delta g_{\text{wc}_i} \quad (8.3)$$

where n_{hyd} is the total number of hydrophobic groups in the solute, f_i is the fractional hydration of group i , g_{tr_i} is the free-energy change associated with transferring group i from the aqueous solution to a bulk solution composed of solute tails, n_{core} is the total number of hydrophobic groups in the solute that adsorb onto, or penetrate into, the aggregate core, $SASA_i$ is the solvent accessible surface area of group i , and Δg_{wc_i} is defined as the difference in the free energy per unit of solvent accessible surface area associated with the hydration of group i in the micellar state and in the aqueous solution. In Chapters 6 and 7, we justified computing f for each group i as follows [1, 2]:

$$f = \frac{\text{number of hydrating contacts in the aggregate}}{\text{number of hydrating contacts in bulk water}} \quad (8.4)$$

where a “hydrating contact” is defined as a contact with an atom that: (i) hydrogen bonds, or (ii) is capable of co-ordinate (dative-covalent) bonding. In Chapter 6, we justified the use of a 0.3 nm cutoff distance to count the hydrating contacts that occur during MD simulation. This cutoff distance was shown to be appropriate in the context of modeling nonionic surfactant micellization in Chapter 7. In Chapter 6, we developed a theoretical model to estimate Δg_{wc_i} for oil molecules. For oil molecules, Δg_{wc_i} does not depend on i , and is given by [1]:

$$\Delta g_{\text{wc}} = \sigma_{\text{core}} - \sigma_{\text{bulk}} = \frac{\sigma A_{\text{core}}}{SASA_{\text{core}}} - \frac{g_{\text{tr}_i}}{SASA_i} \quad (8.5)$$

where σ_{core} is the microscopic “interfacial tension” (interfacial free energy per unit SASA) associated with the aggregate core/water interface, σ_{bulk} is the microscopic “interfacial tension” (interfacial free energy per unit SASA) associated with the group i (CH_2 or CH_3)/water interface in the aqueous solution, σ is the macroscopic interfacial tension of the aggregate core/water interface, A_{core} is the area of the hydrophobic aggregate core as computed geometrically from the volume of the aggregate and the

assumption of a perfectly smooth aggregate surface, and $SASA_{\text{core}}$ is the solvent accessible surface area of the hydrophobic aggregate core. The ratio $A_{\text{core}}/SASA_{\text{core}}$ in Eq. 8.5 was estimated using the following correlation [1]:

$$SASA_{\text{core}}/A_{\text{core}} = 1.740 - 0.026n_t + 0.078C \quad (8.6)$$

where n_t is the total number of hydrophobic groups in the solute that are part of the hydrophobic aggregate core and C is the curvature of the micellar aggregate, which is defined as $2/l_c$ for spheres, $1/l_c$ for cylinders, and zero for planar interfaces, where l_c is the core-minor radius or planar half-width. In Chapter 7, we demonstrated that the model for Δg_{wc} given by Eqs. 8.5 and 8.6 can be used to model the change in hydration free energy experienced by the hydrophobic CH, CH₂, and CH₃ groups present in the hydrophobic core of a nonionic surfactant micelle.

We note that the remaining four free-energy contributions appearing in Eq. 8.1 (g_{pack} , g_{st} , g_{elec} , and g_{ent}) are computed in the CS-MT model in the same way that they are computed in the traditional MT modeling approach [3]. However, as noted in Chapter 6, the way in which g_{pack} and g_{st} are computed may be informed by molecular dynamics simulation data. With this in mind, in this chapter, we explore an approach to use computer simulation data to accurately estimate g_{st} for surfactants with complex head structures.

In Appendix A of Chapter 6, we showed that by combining elements of the CS-MT model and the traditional MT model, g_{form} can be computed as a function of aggregate shape and size after only two computer simulations — one simulation of the solute in bulk water and one simulation of the solute in an aggregate of arbitrary shape and size. The free energy of aggregate formation, g_{form} , for micelles of a different shape and size than the simulated micelle is computed using the following equation [1]:

$$g_{\text{form}} = g_{\text{tr,CS-MT}} + g_{\text{int}} + g_{\text{pack}} + g_{\text{st}} + g_{\text{elec}} + g_{\text{ent}} \quad (8.7)$$

where $g_{\text{tr,CS-MT}}$ is the transfer free-energy contribution obtained using the CS-MT

modeling approach. The term $g_{\text{tr,CS-MT}}$ is computed using the relationship $g_{\text{tr,CS-MT}} = g_{\text{dehydr}} + g_{\text{hydr}} - \hat{g}_{\text{int}}$, where \hat{g}_{int} is the traditional MT model prediction for the interfacial free-energy contribution of the *simulated* micellar aggregate.

As discussed in Chapter 6 and 7, for a micelle of the optimum shape, size, composition, and degree of counterion binding, g_{form} has a minimum value, which we denote as g_{form}^* . By determining g_{form}^* , the optimal aggregate shape, S^* , the optimal core-minor radius, l_c^* , the optimal composition, α^* , and the optimal degree of counterion binding, β^* , can be predicted. In addition, the CMC in mole fraction units is computed as follows [4]:

$$\text{CMC} \approx \exp \left(\frac{g_{\text{form}}^*(S^*, l_c^*, \alpha^*, \beta^*)}{k_B T} \right) \quad (8.8)$$

where k_B is the Boltzmann constant and T is the absolute temperature.

The CS-MT model was used in Chapter 6 to calculate the free-energy change associated with the formation of aggregates of octane, of dodecane, and of hexadecane having various shapes (spheres, cylinders, and slabs) and sizes. Excellent agreement between the predictions of the CS-MT model and of the traditional MT model was obtained for g_{form} for the 15 oil aggregates considered, with an average absolute error of only 1.04% between the two modeling approaches.

In Chapter 7, the validity and accuracy of the CS-MT model was demonstrated for nonionic surfactants by using it to model the micellization behavior of seven nonionic surfactants: octyl glucoside (OG), dodecyl maltoside (DM), octyl sulfinyl ethanol (OSE), decyl methyl sulfoxide ($C_{10}\text{SO}$), decyl dimethyl phosphine oxide ($C_{10}\text{PO}$), dodecyl poly(ethylene oxide) ($C_{12}\text{E}_8$), and decyl decanoyl-n-methylglucamide (MEGA-10). To use the CS-MT model for nonionic surfactants, f values obtained from MD simulation were used as an input to compute g_{dehydr} and g_{hydr} . To enable straightforward estimation of both of these free-energy contributions, a number of simplifying approximations were introduced in Chapter 7. For each surfactant, g_{dehydr} was calculated by estimating g_{tr_i} values using solubility correlations for linear alkyl tails [5].

The approximation was made that g_{tr_i} values could be estimated in this manner for hydrophobic groups in both the surfactant head and tail, although this is only approximately correct for hydrophobic groups in the surfactant head [2]. The free-energy contribution, g_{hydr} , was calculated for each surfactant by: (i) approximating g_{hydr} as being equal to zero for any hydrophobic group which is not adsorbed onto, or incorporated within, the micelle core, and (ii) estimating g_{hydr} for hydrophobic groups in the micelle core using the expression for Δg_{wc} given in Eqs. 8.5 and 8.6. As justified in Chapter 7, any hydrophobic group with a value of f greater than 0.60 was not considered to be part of the micelle core. In computing Δg_{wc} using Eqs. 8.5 and 8.6, the approximation is made that the change in hydration free energy experienced by hydrophobic groups as they are transferred from the bulk aqueous solution to the micelle core is unaffected by the presence of the surfactant heads at the micelle core/water interface.

In Chapter 7, the CS-MT model was found to yield similar, or superior, estimates of the CMCs of nonionic surfactants with relatively small, non-polymeric heads as compared to the traditional MT model. In addition, the CS-MT model predictions for the micellization behavior of the most complex nonionic surfactant modeled in Chapter 7, MEGA-10, were found to be in significantly better agreement with the experimental data than the traditional MT model predictions.

8.1.2 Modeling Ionic and Zwitterionic Surfactant Micellization

In this chapter, we use the CS-MT modeling approach to model the micellization behavior of nine ionic and zwitterionic surfactants in aqueous solution. The surfactants selected for modeling include three anionic surfactants (sodium dodecyl sulfate, or SDS, and two 3-hydroxy sulfonate surfactants with different hydrophobic tail lengths, or AOS-12 and AOS-16), one zwitterionic surfactant (dodecylphosphocholine, or DPC), and five cationic surfactants (cetyltrimethylammonium bromide, or

CTAB, and a homologous series of four DC_NA bromide surfactants with a positively charged dimethylammonium head attached to a dodecyl tail and to an alkyl sidechain of length C_N , having the chemical formula $\text{C}_{12}\text{H}_{25}\text{C}_N\text{H}_{2N+1}\text{N}(\text{CH}_3)_2\text{Br}$, where $N = 1$ for what we will refer to as DC_1AB , $N = 2$ for DC_2AB , $N = 4$ for DC_4AB , and $N = 6$ for DC_6AB).

To use the CS-MT modeling approach to model ionic and zwitterionic surfactant micellization, a number of approximations must be made to account for the presence of charged or dipolar hydrophilic groups at the micelle core/water interface. The validity of the approximations proposed in Chapter 7 to model nonionic surfactant micellization with the CS-MT model is discussed and evaluated in this chapter for ionic and zwitterionic surfactant micellization. The CS-MT model is first used to predict the micellization behavior of a simple anionic surfactant (SDS), a simple zwitterionic surfactant (DPC), and a simple cationic surfactant (CTAB). The CMCs predicted using the CS-MT model for these surfactants are compared with the CMCs predicted using the traditional MT model as well as with the experimental CMCs taken from the literature. Based on the modeling results, we discuss whether the theoretical approach used to derive Eqs. 8.5 and 8.6 can be used to calculate Δg_{wc} in the case of ionic and zwitterionic surfactants, or whether Δg_{wc} must be fit for these surfactants.

After determining the applicability of the CS-MT model for three simple ionic and zwitterionic surfactants, we use it to model six complex ionic surfactants (AOS-12, AOS-16, and the homologous series of DC_NAB surfactants). The CMCs predicted using the CS-MT model for these six surfactants are compared with the CMCs predicted using the traditional MT model as well as with the experimental CMCs taken from the literature.

The remainder of this chapter is organized as follows. Section 8.2 describes the computer simulation approach used in this chapter, including an overview of the modeling approach (Section 8.2.1), the simulation methods and parameters (Section 8.2.2), a description of how each system was prepared and equilibrated (Section 8.2.3),

and the data analysis method used to analyze the molecular dynamics trajectories (Section 8.2.4). Computer simulation results are presented in Section 8.3. The CS-MT model is used to predict the micellization behavior of the nine surfactants considered in Section 8.4. Concluding remarks are presented in Section 8.5.

8.2 Molecular Dynamics Simulations

8.2.1 Modeling Approach

As discussed in Chapter 6 and 7, the CS-MT model requires fractional hydration data as an input. This fractional hydration data is obtained by performing two simulations. The first simulation is of a single surfactant molecule in a simulation cell of water (the “bulk water” simulation), and the second simulation is of the same surfactant molecule in a micellar environment (the “aggregate” simulation). As shown in Appendix A of Chapter 6, obtaining information about the hydration state of a surfactant molecule in a micelle of a single shape and size is sufficient to allow prediction of the *optimal* micelle shape and size.

8.2.2 Simulation Methods and Parameters

The simulation methods and parameters used in this study are identical to those introduced in Chapter 6 and Chapter 7. Surfactants were modeled using the fully atomistic OPLS-AA force field [6], and water molecules were modeled using the simple extended point-charge (SPC/E) model for water. Some additional parameters to describe angles and angle vibrations were taken from the literature to model the sulfate (SO_4^-) group in SDS [7]. Dodecylphosphocholine (DPC) was modeled using the GROMACS forcefield using the same parameters that were used by Tieleman et al. [8]. The GROMACS forcefield models methylene (CH_2) groups and methyl (CH_3) groups as unified atoms [9].

The atoms in the surfactant head for each ionic surfactants considered did not have

suggested charges in the OPLS-AA force field, so the atomic charges for the heads of these surfactants were estimated using the CHelpG algorithm (as implemented in Gaussian 98) [10]. We note that CHelpG was not used to assign atomic charges for the hydrophobic tail of each surfactant, for reasons discussed in Chapter 7. The atomic charges used by Tieleman et al. were used in modeling DPC.

During simulation, van der Waals interactions were described using a cutoff distance of 0.9 nm, and Coulombic interactions were described using 3D particle mesh Ewald (PME) summation [11,12]. Long-range dispersion corrections for energy and pressure were implemented. Each simulation was carried out with fixed bond lengths, permitting a simulation timestep of 2 fs. The simulation cell temperature was maintained at 298.15 K, and the simulation cell pressure was maintained at 1.0 bar using the Berendsen temperature and pressure coupling algorithm, respectively [13]. All simulations were conducted using a 2006 developers' version of the GROMACS software package [14,15].

8.2.3 System Preparation and Equilibration

Bulk Water Simulation

The bulk water simulation for each surfactant considered was initialized by placing a single surfactant molecule in a simulation cell and surrounding it with sufficient water molecules to approximation infinite dilution (see Chapter 6 and Chapter 7). A single ion (which we will refer to hereafter as the counterion) was introduced into the simulation cell by replacing the water molecule experiencing the greatest electrostatic potential after initial energy minimization. After a brief *NPT* simulation to equilibrate the cell volume, data was gathered over the course of an additional 3 ns of *NPT* simulation.

Surfactant	No. of Surfactant Molecules	No. of Water Molecules	Total No. of Atoms
SDS	44	3,347	11,933
DPC	48	10,453	10,453
CTAB	49	10,304	33,999
AOS-12	32	3,555	12,041
AOS-16	40	6,119	20,557
DC ₁ AB	25	3,522	11,841
DC ₂ AB	20	3,771	12,393
DC ₄ AB	18	3,734	12,282
DC ₆ AB	16	3,711	12,189

Table 8.1: The geometry, the number of surfactant and water molecules, and the total number of atoms corresponding to each of the ionic and zwitterionic micelle simulations.

Aggregate Simulation

Each surfactant micelle was performed as a spherical aggregate in the manner discussed in Chapter 7. To preserve electroneutrality, equal numbers of counterions and ionic surfactant molecules were added to each simulation cell. To speed equilibration, counterions were added by replacing water molecules experiencing the greatest electrostatic potential after initial energy minimization, with the potential being recalculated after every counterion insertion. In Table 8.1, we report the number of surfactant and water molecules and the total number of atoms included in each simulation cell.

Each micelle was built with a sufficiently small aggregation number to ensure that it would be spherical during simulation by estimating the expected spherical aggregation number based on the head area and tail volume of each surfactant [16]. As shown in Appendix A of Chapter 6, a micelle of any aggregation number and geometry (whether spherical, cylindrical, or planar) may be simulated to obtain hydration information for the CS-MT modeling approach. However, as discussed in Chapter 7, it is most convenient computationally to simulate spherical aggregates because this removes the need to either: (i) specify a physically realistic area for each surfactant molecule within a cylindrical micelle or bilayer, or (ii) specify a poorly defined in-

terfacial tension perpendicular to the axis of a cylindrical micelle or the plane of a bilayer.

After performing each spherical micelle, a 15 ns equilibration run was conducted under *NPT* conditions. For reasons discussed in Chapter 7, we believe that this equilibration time is more than adequate to thoroughly equilibrate each micelle [17]. Plots of the equilibration profile of the solvent accessible surface area (SASA) for three representative surfactants (SDS, DPC, and AOS-12) are shown in Figure 8-1. The SASA values reported in Figure 8-1 for each surfactant were normalized by the average value of SASA for that surfactant to facilitate comparison of the results. SASA was computed using a probe sphere of radius 0.2 nm (for a justification of this choice, see Chapter 6) and using the double cubic lattice method as implemented in GROMACS [13]. Since obtaining accurate hydration information is the primary objective of our computer simulations, we consider SASA to be an important metric to evaluate equilibration, because this property is directly proportional to the degree of hydration of the micelle. As shown in Figure 8-1, after the first 5 ns of simulation, there is no apparent drift in SASA for these three surfactants. Plots of the normalized values of SASA during the 5 ns data gathering simulation runs for the remaining six surfactants considered are presented in Appendix A. All the equilibration SASA profiles indicate that the hydration data obtained during the data gathering simulations are representative of the equilibrium hydration state of the micelle.

Snapshots of the post-equilibration configurations of each simulated ionic and zwitterionic micelle are shown in Figure 8-2 (water molecules and counterions have been omitted for clarity). Each surfactant molecule is depicted using the van der Waals radius of each atom.

8.2.4 Data Analysis Method

The fractional hydration of each atom (or group of atoms) in the surfactant molecule during the bulk water simulation and the aggregate simulation was quantified by counting hydrating contacts using a cutoff distance of 0.3 nm, and by determining

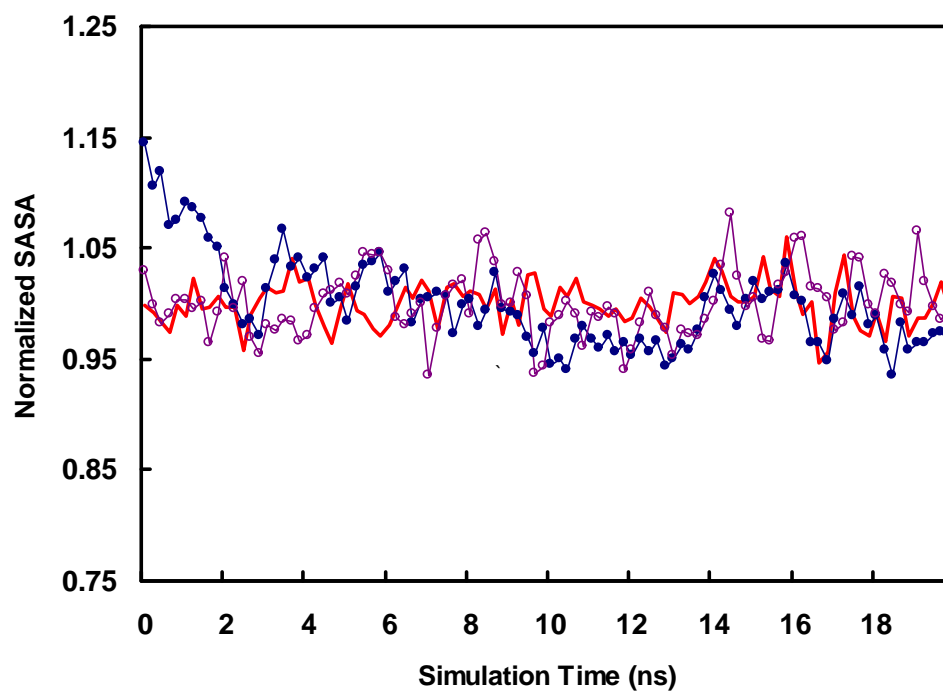


Figure 8-1: Solvent accessible surface area (SASA) normalized by the average value of SASA as a function of simulation time for micelles of three representative ionic and zwitterionic surfactants: sodium dodecyl sulfate (SDS, —), dodecylphosphocholine (DPC, —●—), and 3-hydroxy dodecyl sulfonate (AOS-12, —○—).

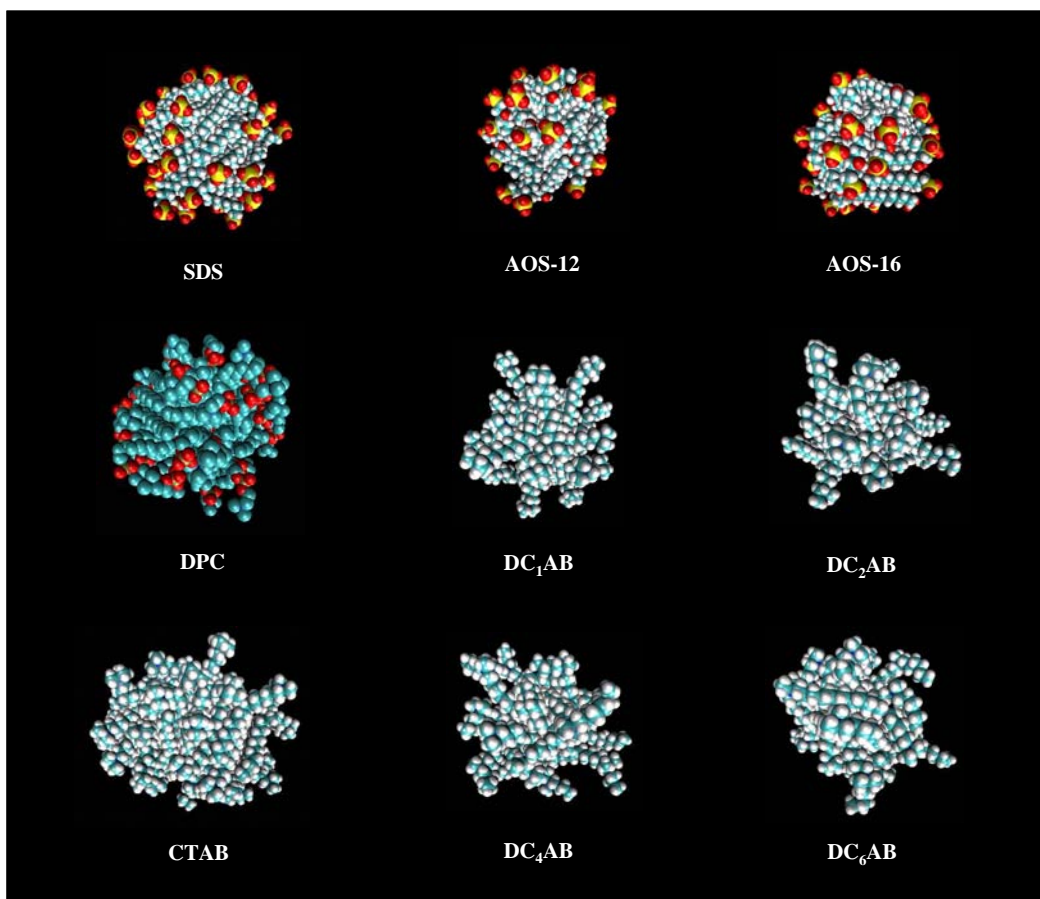


Figure 8-2: Snapshots of the post-equilibration structures of the simulated micelles corresponding to each of the nine ionic and zwitterionic surfactants considered here. The water molecules are not shown for clarity.

f from the contact data using Eq. 8.4 (for details, see Chapter 6 and Chapter 7). For the ionic surfactants simulated in this chapter, contacts with water atoms, with hydrogen bonding surfactant heads, and with counterions were each included as contributing to hydration. For the zwitterionic surfactant DPC, only contacts with water atoms and with hydrogen bonding surfactant heads were counted as being hydrating, since no counterions were present in the simulation cell.

Although a cutoff of 0.3 nm was used in determining the f values for the CS-MT model, we note that to obtain estimates of f for some of the large atoms present in some of the surfactant heads considered (including nitrogen, sulfur, and oxygen), it was necessary to use a larger cutoff of 0.5 nm in order to obtain good statistics for f . Accordingly, a cutoff of 0.5 nm was used to generate all the hydration plots presented in Section 8.3.

An estimate of the standard error in f for each group of atoms in the surfactant molecule was obtained through the use of block averaging (for details, see Chapter 6) [18–20]. Data-gathering simulation runs were conducted for sufficient time to ensure that the uncertainty in each calculated value of f was small (typically less than 5%).

8.3 Simulation Results and Discussion

8.3.1 Sodium Dodecyl Sulfate (SDS)

SDS is a widely used and extensively studied anionic surfactant. The fractional degree of hydration, f , of SDS is plotted as a function of group number in Figure 8-3. Groups in SDS that are considered to be part of the SDS head in traditional MT modeling (groups 1 and 2) have f values that are much larger than the f values of groups in the SDS tail (groups 3 to 13). However, even groups in the SDS head are partially dehydrated, with group 1 having an f value of 0.89 and group 2 having an f value of 0.63. The average f value of the groups in the SDS tail is 0.24.

The f results shown in Figure 8-3 reveal that the degree of dehydration of the

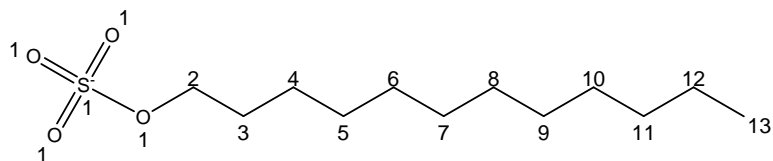
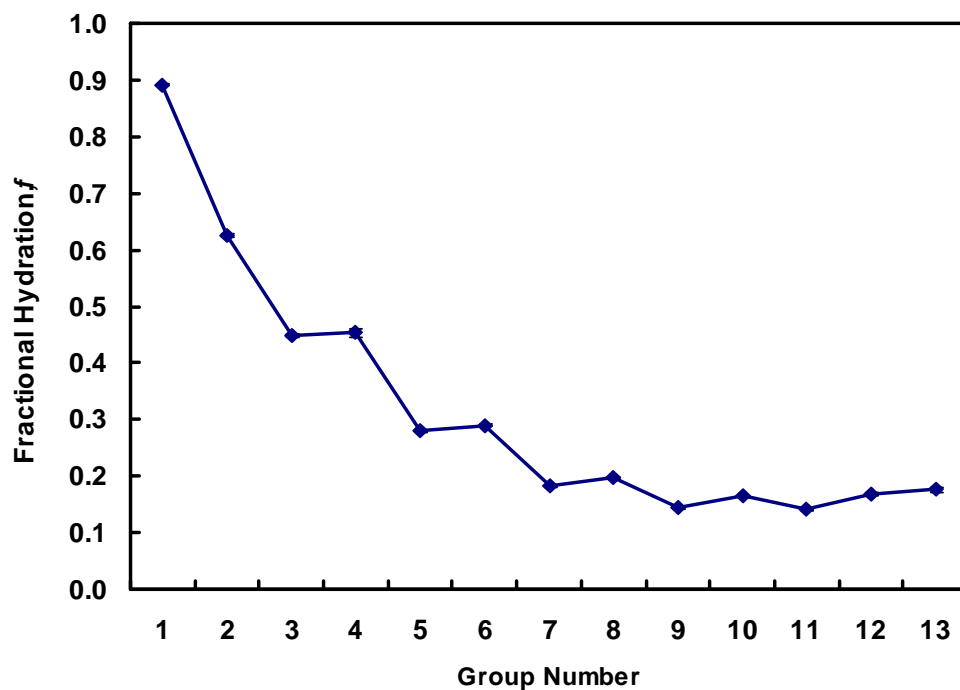


Figure 8-3: The average fractional degree of hydration, f , as defined in Eq. 8.4, of each of the groups in sodium dodecyl sulfate (SDS). The chemical structure of each group is identified in the schematic of the molecule shown below the fractional hydration plot. The error bars shown correspond to the standard error of the mean.

groups in the SDS tail is a function of their distance from the SDS head. For example, group 3 in the tail (closest to the head) has an f value of 0.45, while group 13 (furthest from the head) has an f value of 0.18. We note that each of the groups in the SDS head has an f value greater than 0.60, and each of the groups in the SDS tail has an f value less than 0.60. As discussed in Chapter 7, only hydrophobic surfactant groups with an f value below 0.60 are considered to be part of the micelle core and to have a nonzero value of g_{hydr} .

8.3.2 Dodecylphosphocholine (DPC)

DPC is a zwitterionic surfactant frequently used as a model membrane lipid to study lipid-bound peptides and proteins [21]. DPC has been widely studied both experimentally and through computer simulations [8, 21]. As discussed in Section 8.2.2, the forcefield parameters used to model this surfactant are the same as those used by Tieleman et al. [8, 21, 22].

The fractional degree of hydration, f , of DPC is plotted as a function of group number in Figure 8-4. The average f value of the groups in the DPC head (groups 1 to 8) is 0.70, while that of the groups in the DPC tail (groups 9 to 19) is 0.18. It is interesting to note that most of the hydrophobic groups in the DPC head (1 to 3, 5, and 6) are very hydrated, with f values of 0.69 or greater. As discussed in Chapter 7, such groups do not contribute to g_{hydr} because they are not incorporated into the micelle core. However, they do contribute significantly to g_{dehydr} . It is interesting to note that the hydrophobic CH_2 group adjacent to the DPC tail (group 8), has an f value of 0.40, which as discussed in Chapter 7, is sufficiently low that it is modeled as being part of the micelle hydrophobic core in CS-MT modeling. The low f value for this group is closer to the f value that would be expected if the group were adjacent to a nonionic surfactant head (for details, see Chapter 7) than to an ionic surfactant head (see the f values of group 2 in SDS and of group 5 in CTAB).

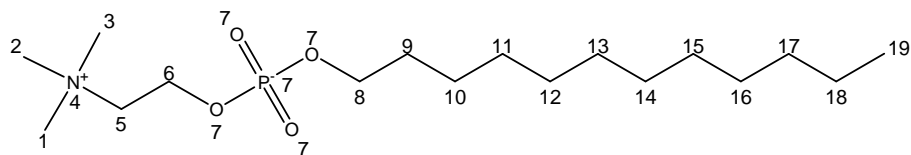
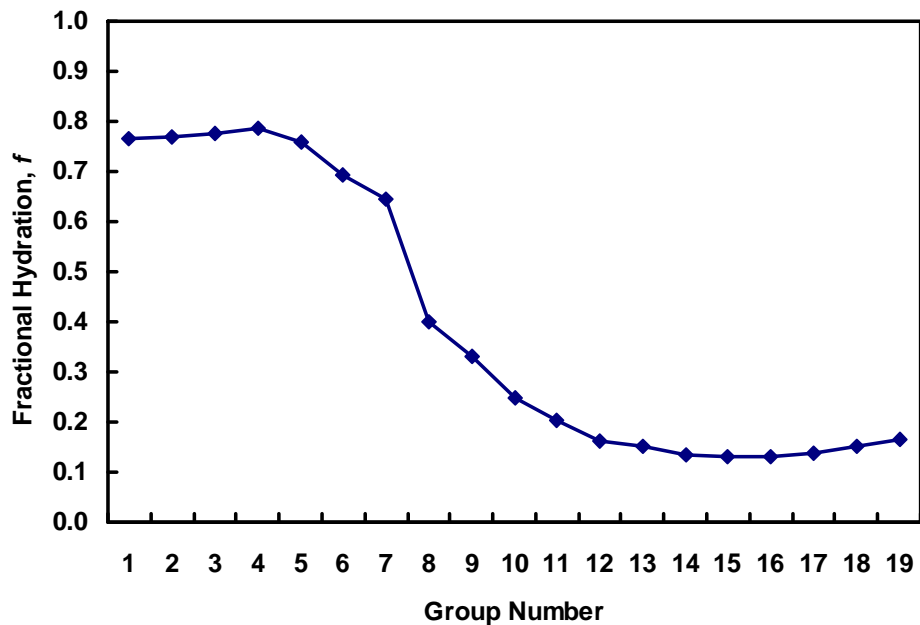


Figure 8-4: The average fractional degree of hydration, f , as defined in Eq. 8.4, of each of the groups in dodecylphosphocholine (DPC). The chemical structure of each group is identified in the schematic of the molecule shown below the fractional hydration plot. The error bars shown correspond to the standard error of the mean.

8.3.3 Cetyltrimethylammonium Bromide (CTAB)

CTAB is a commonly used cationic surfactant for which extensive experimental micellization data is available. The fractional degree of hydration, f , of CTAB is plotted as a function of group number in Figure 8-5. The average f value of the groups in the CTAB head (groups 1 to 5) is 0.85, while that of the groups in the CTAB tail (groups 6 to 20) is 0.20. As in the case of SDS and DPC, the hydrophobic groups in the CTAB head (1 to 3 and 5) are highly hydrated, with f values of 0.71 or greater. In general, the hydration profile observed for the anionic surfactant SDS is similar to the hydration profile observed for the cationic surfactant CTAB. For example, the average f value of the groups in the SDS head is 0.85, while the average f value of the groups in the CTAB head is also 0.85. In addition, the first CH₂ group in the SDS tail (group 3) and in the CTAB tail (group 6) have f values of 0.45 and 0.57, respectively. In contrast, the zwitterionic surfactant DPC exhibits significant differences in the hydration of its head groups relative to those in SDS and in CTAB (see Section 8.3.2).

8.3.4 Sodium 3-Hydroxy Sulfonates (AOS-12 and AOS-16)

Sodium α -olefinsulfonates (AOS) are anionic surfactants frequently used in household and industrial formulations [23]. These surfactants are useful because of their wetting and detergency attributes, and because of their tolerance for hard water ions. AOS, as it is used industrially, is a mixture of several chemical species, including: 60-70% sodium alkenesulfonate, 30% hydroxyalkanesulfonate, and 0-10% sodium disulfonate. The hydroxyalkanesulfonate fraction is present in both the 3-hydroxy sulfonate and the 4-hydroxy sulfonate forms, and the hydroxyalkanesulfonate backbone may contain between 12 and 18 carbon atoms [23]. We have selected two hydroxyalkanesulfonates for modeling to determine if computer simulations can be used to correctly identify the “head” and “tail” portions of surfactants with two hydrophilic groups (SO₃⁻ and OH) connected by hydrophobic CH₂ groups: sodium 3-hydroxydodecyl-1-sulfonate

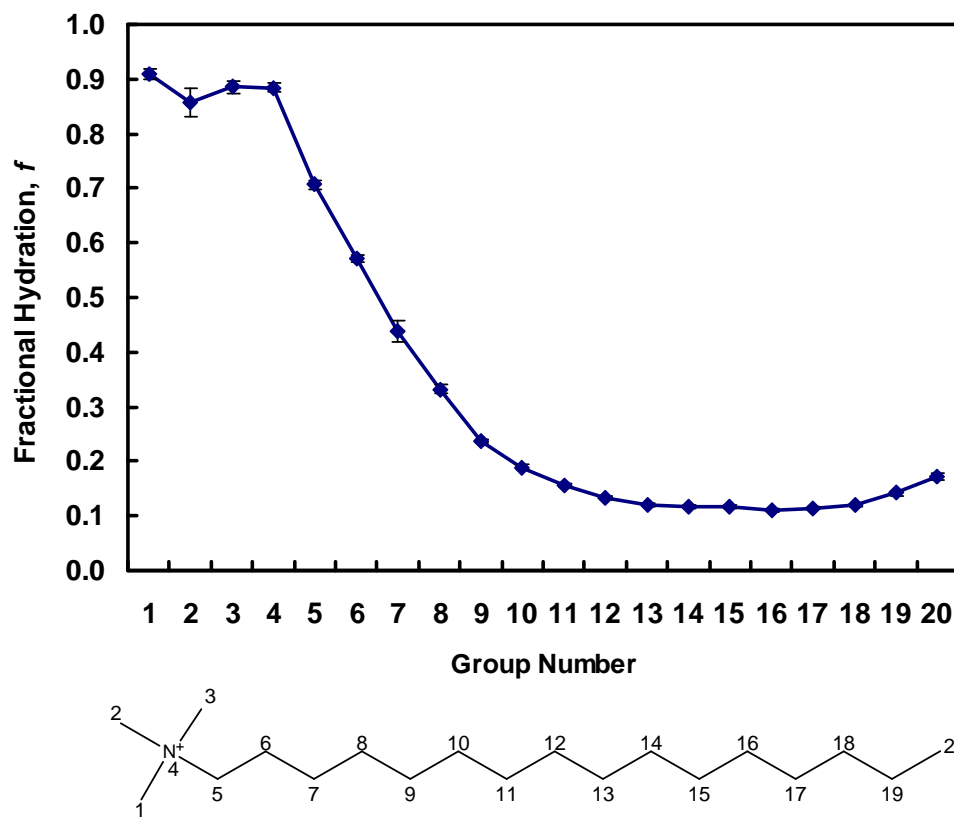


Figure 8-5: The average fractional degree of hydration, f , as defined in Eq. 8.4, of each of the groups in cetyltrimethylammonium bromide (CTAB). The chemical structure of each group is identified in the schematic of the molecule shown below the fractional hydration plot. The error bars shown correspond to the standard error of the mean.

(AOS-12) and sodium 3-hydroxyhexadecyl-1-sulfonate (AOS-16).

The fractional degree of hydration, f , of AOS-12 and AOS-16 is plotted as a function of group number in Figures 8-6A and 8-6B, respectively. The non-monotonic nature of the fractional hydration plots of both surfactants is due to the presence of the 3-hydroxy group (group 5). The f results shown in Figure 8-6 reveal that groups 1, 2, 3, and 5 in both surfactants have f values greater than 0.60. The average value of f for these four groups in AOS-12 and in AOS-16 is 0.79 and 0.75, respectively. With an f value of 0.60 and 0.56 in AOS-12 and AOS-16, respectively, group 4 is considered to be part of the micelle hydrophobic core for both surfactants. As such, group 4 is modeled as contributing to g_{hydr} in the CS-MT modeling approach (for details, see Chapter 7). The average f value of the tail groups in AOS-12 and in AOS-16 are 0.27 and 0.21, respectively.

8.3.5 $\text{C}_{12}\text{H}_{25}\text{C}_N\text{H}_{2N+1}\text{N}(\text{CH}_3)_2\text{Br}$ Surfactants (DC_1AB - DC_6AB)

The micellization behavior of the DC_NAB cationic surfactants is very interesting from a theoretical perspective. The experimental CMCs of each of the four DC_NAB surfactants are ranked as follows: $\text{DC}_1\text{AB} > \text{DC}_2\text{AB} > \text{DC}_4\text{AB} > \text{DC}_6\text{AB}$ [24]. This CMC ranking is difficult to rationalize using the traditional MT model (see discussion in Section ??). Because of the structural complexity of the DC_NAB surfactants, the CS-MT model is expected to provide more accurate predictions of the micellization behavior of these surfactants than the traditional MT modeling approach.

The fractional degree of hydration, f , of DC_1AB , DC_2AB , DC_4AB , and DC_6AB are plotted as a function of group number in Figures 8-7A, 8-7B, 8-7C, and 8-7D, respectively. The non-monotonic nature of the fractional hydration plots of the DC_2AB , DC_4AB , and DC_6AB surfactants reflects the fact that the C_N group in each of these surfactants (group 1 in DC_1AB , groups 1 to 2 in DC_2AB , groups 1 to 4 in DC_4AB , and groups 1 to 6 in DC_6AB) is less hydrated than the dimethylammonium group.

The f values of DC_1AB shown in Figure 7A are very similar to the f values shown

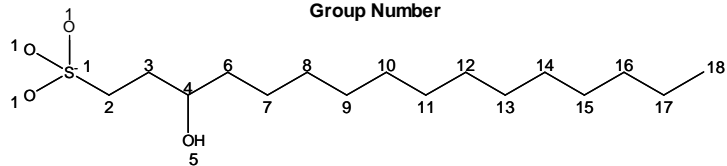
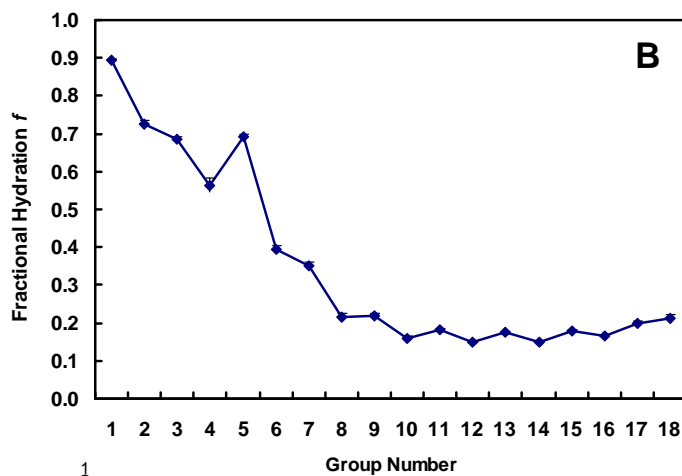
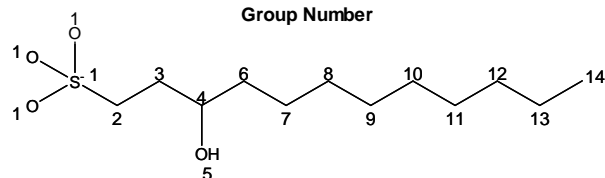
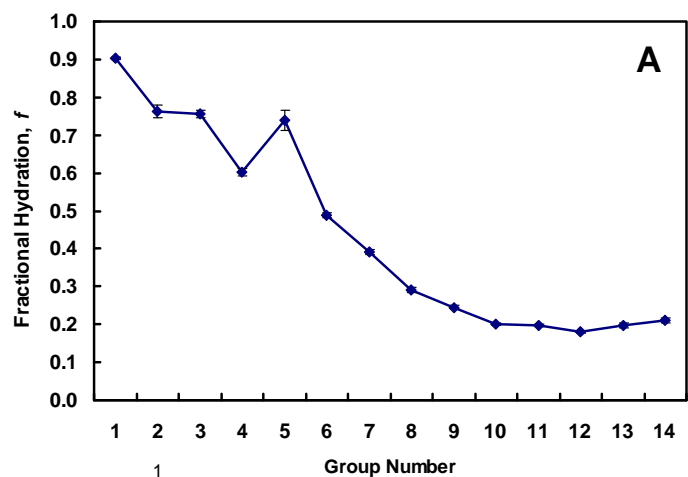


Figure 8-6: The average fractional degree of hydration, f , as defined in Eq. 8.4, of each of the groups in 3-hydroxy dodecyl sulfonate (AOS-12, see A) and 3-hydroxy hexadecyl sulfonate (AOS-16, see B). The chemical structure of each group is identified in the schematic of the molecule shown below each of the fractional hydration plot. The error bars shown correspond to the standard error of the mean.

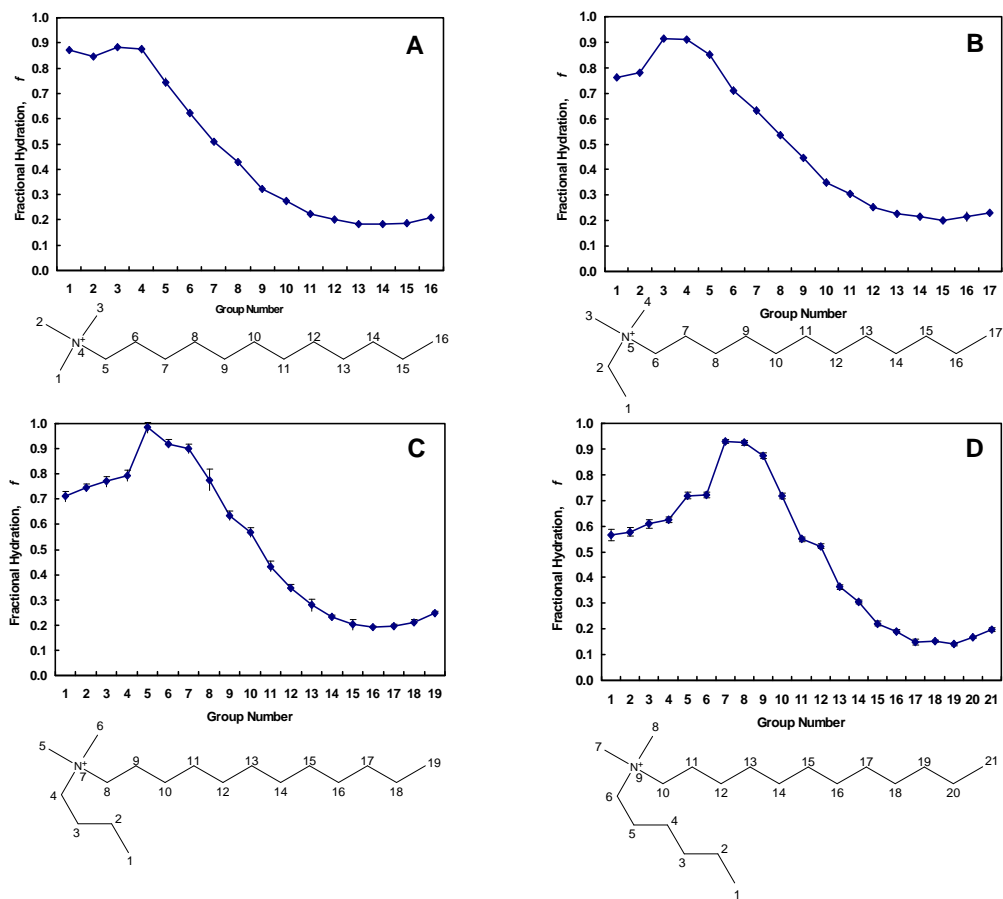


Figure 8-7: The average fractional degree of hydration, f , as defined in Eq. 8.4, of each of the groups in decyltrimethylammonium bromide (DC₁AB, see A), C₁₂H₂₅C₂H₅N(CH₃)₂Br (DC₂AB, see B), C₁₂H₂₅C₄H₉N(CH₃)₂Br (DC₄AB, see C), and C₁₂H₂₅C₆H₁₃N(CH₃)₂Br (DC₆AB, see D). The chemical structure of each group is identified in the schematic of the molecule shown below the fractional hydration plot. The error bars shown correspond to the standard error of the mean.

in Figure 8-5 for CTAB. This is not surprising given the chemical similarity of these two surfactants. The average f value of the groups in the DC₁AB head (groups 1 to 5) is 0.84. By comparison, the average f value of the groups in the CTAB head (groups 1 to 5) is 0.85.

The fractional hydration profiles of DC₂AB, DC₄AB, and DC₆AB (shown in Figures 8-7B, 8-7C, and 8-7D, respectively) are more complex. Comparison of the hydration profiles of DC₁AB and DC₂AB reveals that the additional CH₂ in the C_N group of DC₂AB has a significant impact on hydration. The f value of group 1 in DC₂AB (0.76) is significantly lower than the f value of group 1 in DC₁AB (0.87). The f value of group 2 in DC₂AB (0.78) is also relatively low compared to the average f value of the groups in the DC₁AB head (0.84). The f values of groups 1 to 4 in DC₄AB range from 0.71 to 0.79. The f values of groups 1 to 6 in DC₆AB range from 0.57 to 0.92. Our results suggest that, as the length of the C_N group increases, the C_N group is increasingly incorporated within the micelle hydrophobic core. Groups 1 and 2 in DC₆AB both have f values that are below 0.60. Consequently, both of these groups will be modeled as being part of the micelle hydrophobic core using the CS-MT model.

It is interesting to note that the D group (the C₁₂H₂₅ group) present in each of the four DC_NAB surfactants is hydrated to a similar extent in each of the four simulated micelles. The average f value of the D group in DC₁AB, DC₂AB, DC₄AB, and DC₆AB is 0.34, 0.36, 0.36, and 0.31, respectively.

8.4 Molecular-Thermodynamic Modeling Based on Computer Simulation Inputs

8.4.1 Using the CS-MT Modeling Approach to Predict the Micellization Behavior of Ionic and Zwitterionic Surfactants

As discussed in Chapter 7, to use the CS-MT modeling approach to model surfactant micellization, a number of simplifying approximations must be made to enable the straightforward evaluation of g_{dehydr} and g_{hydr} . With this in mind, we make the same approximations discussed in Chapter 7 to evaluate g_{dehydr} and g_{hydr} for ionic and zwitterionic surfactants. In so doing, we will evaluate the validity of these approximations in the case of ionic and zwitterionic surfactants.

After using the CS-MT model to predict the micellization behavior of two simple ionic and one simple zwitterionic surfactants in Section 8.4.2, we use it to model more complex surfactants in Section 8.4.3. To evaluate the CS-MT model, the surfactant CMC was selected for prediction and comparison with the experimental CMC data, as well as with the CMC predictions of the traditional MT model, because the CMC is exponentially dependent on g_{form} , and therefore, provides a rigorous quantitative test for the predictive accuracy of the CS-MT model. However, we would like to stress that the CS-MT model enables the prediction of a variety of micellar solution properties in addition to the CMC (including micelle shape, size, composition, and the degree of counterion binding).

As discussed in Chapter 6, to implement the traditional MT model to predict the micellization behavior of ionic and zwitterionic surfactants, it is necessary to identify a head and a tail for each surfactant. The head and tail assignments made for traditional MT modeling are reported in Table 8.2, where the group numbers listed correspond to the group numbers shown in the surfactant diagrams given in Figures 8-3 to 8-7. For reasons that will be discussed in Section 8.4.3, the head and tail

assignments for DC₂AB, DC₄AB, and DC₆AB may be made in a number of ways in the traditional MT modeling approach. Based on the head and tail assignments, three geometric parameters were estimated for each surfactant and used as inputs for traditional MT modeling [3, 4, 25–27]. These geometric parameters are also reported in Table 8.2, and were determined based on the surfactant chemical structures and the head and tail assignments made. The first geometric parameter is a_h — the cross-sectional area of the surfactant head. The second geometric parameter is d_{charge} — the distance from the location of the charge in the surfactant head to the beginning of the surfactant tail. The third geometric parameter is l_{hg} — the length of the surfactant head, or the distance from the tip of the surfactant head to the start of the surfactant tail. Note that a_h is needed to calculate g_{st} , and both d_{charge} and l_{hg} are needed to calculate g_{elec} [3, 25]. The a_h , d_{charge} , and l_{hg} values listed in Table 8.2 were also used to determine g_{st} and g_{elec} in the CS-MT model (see Eq. 8.1). Values of a_h , d_{charge} , and l_{hg} computed based on three traditional MT modeling limits (see Section 8.4.3) are also listed in Table 8.2 for DC₂AB, DC₄AB, and DC₆AB. An additional parameter which is not listed in Table 8.2 but that is needed to compute g_{elec} in the case of zwitterionic surfactants is d_{sep} — the distance between the two charges in the zwitterionic surfactant head. The d_{sep} value for DPC was estimated to be 4.3 Å.

8.4.2 Modeling Results for Simple Surfactants

Sodium Dodecyl Sulfate (SDS)

We have used the CS-MT model to predict the micellization behavior of SDS in aqueous solution at 25 °C. In Table 8.3, we report CS-MT modeling results for the *simulated* SDS micelle, including: (i) g_{dehydr} , (ii) g_{hydr} , (iii) \hat{g}_{int} , and (iv) $g_{\text{tr,CS-MT}}$. The reported uncertainty for the CS-MT modeling results is the standard error of the mean, as computed through block averaging of the computer simulation data. CS-MT modeling results for g_{dehydr} and g_{hydr} were obtained using the simulated f values and Eqs. 8.2 and 8.3. As can be seen, the value of g_{dehydr} ($-15.04 k_{\text{B}}T$) is

Surfactant	Head Groups	Tail Groups	a_h [\AA^2]	d_{charge} [\AA]	l_{hg} [\AA]
SDS	1-2	3-13	25	3.7	6.3
DPC	1-8	9-19	32	5.3	4.3
CTAB	1-5	6-20	32	3.8	6.4
AOS-12	1-5	6-14	23	5.3	7.2
AOS-16	1-5	6-18	23	5.3	7.2
DC₁AB	1-5	6-16	32	3.8	6.4
DC₂AB					
Limit 1	1-6	7-17	42	3.8	6.4
Limit 2	1-6	7-17	37.4	3.8	6.4
Limit 3	2-6	1 & 7-17	32	3.8	6.4
DC₄AB					
Limit 1	1-8	9-19	62	3.8	6.4
Limit 2	1-8	9-19	38.3	3.8	6.4
Limit 3	4-8	1-3 & 9-19	32	3.8	6.4
DC₆AB					
Limit 1	1-10	11-21	82	3.8	6.4
Limit 2	1-10	11-21	39.3	3.8	6.4
Limit 3	6-10	1-5 & 10-21	32	3.8	6.4

Table 8.2: Molecular parameters used in modeling each surfactant. The traditional MT model identifications of heads and tails are reported, along with molecular parameters used to model each surfactant using the CS-MT model and the traditional MT model. These molecular parameters were estimated geometrically based on the structure of each surfactant molecule, and include: a_h , the cross-sectional area of the surfactant head, d_{charge} , the distance between the beginning of the surfactant tail and the location of the charge in the surfactant head, and l_{hg} , the length of the surfactant head.

Surfactant	$g_{\text{dehydr}} [k_B T]$	$g_{\text{hydr}} [k_B T]$	$\hat{g}_{\text{int}} [k_B T]$	$g_{\text{tr,CS-MT}} [k_B T]$	$g_{\text{tr}} [k_B T]$
SDS	-15.04 ± 0.03	1.73 ± 0.01	4.38	-17.69 ± 0.04	-18.46
DPC	-15.98 ± 0.34	1.93 ± 0.04	4.26	-18.32 ± 0.34	-18.46
CTAB	-20.67 ± 0.20	2.39 ± 0.04	5.44	-23.73 ± 0.21	-24.43
AOS-12	-12.74 ± 0.01	1.60 ± 0.05	4.30	-15.44 ± 0.05	-15.37
AOS-16	-18.50 ± 0.10	1.95 ± 0.03	5.26	-21.81 ± 0.10	-21.27
DC₁AB	-14.80 ± 0.07	1.44 ± 0.03	5.10	-18.46 ± 0.07	-18.46
DC₂AB	-14.96 ± 0.10	1.44 ± 0.04	5.54	-19.06 ± 0.11	-18.46 to -21.98
DC₄AB	-15.44 ± 0.10	1.10 ± 0.03	5.87	-20.21 ± 0.11	-18.46 to -24.96
DC₆AB	-18.41 ± 0.11	2.71 ± 0.07	6.55	-22.24 ± 0.13	-18.46 to -27.95

Table 8.3: Modeling results for the simulated micelles. Computer simulation/molecular-thermodynamic (CS-MT) and traditional molecular-thermodynamic (MT) modeling results for each of the nine simulated ionic and zwitterionic surfactant micelles considered in this article. CS-MT model predictions of g_{dehydr} , g_{hydr} , \hat{g}_{int} , and $g_{\text{tr,CS-MT}}$ were made as described in Section 8.1.1. The uncertainties reported for the CS-MT model predictions correspond to the standard error of the mean. Traditional MT modeling results for g_{tr} are presented for comparison with $g_{\text{tr,CS-MT}}$.

much larger in magnitude than that of g_{hydr} ($1.73 k_B T$). In Table 8.3, we also report the traditional MT model prediction of g_{tr} for comparison with $g_{\text{tr,CS-MT}}$. We note that the transfer free-energy contribution predicted by the CS-MT model ($g_{\text{tr,CS-MT}} = -17.69 k_B T$) is $0.77 k_B T$ more positive than the prediction of the traditional MT model ($g_{\text{tr}} = -18.46 k_B T$).

In Table 8.4 and Table 8.5, we report CS-MT and traditional MT modeling results for micelles of the *optimal* shape and size. As discussed in Section 8.1, at the optimal micelle shape and size, g_{form} attains a minimum value [3]. Both the CS-MT model and the traditional MT model yield identical predictions for the optimal micelle shape and size. As discussed in Chapter 7, this equivalence arises because the only contribution to g_{form} that differs in the two models (the transfer free-energy contribution) does not depend on micelle shape and size. The simulated SDS micelle had an aggregation number of 44, but both the CS-MT model and the tradition MT model predict that

Surf.	Shape	n	$g_{\text{int}} [k_B T]$	$g_{\text{pack}} [k_B T]$	$g_{\text{st}} [k_B T]$	$g_{\text{elec}} [k_B T]$	$g_{\text{ent}} [k_B T]$
SDS	sph.	47	4.33	2.51	1.10	3.56	-0.99
DPC	sph.	39	4.61	2.47	0.65	0.48	0.00
CTAB	sph.	49	5.35	2.57	1.07	5.54	-0.93
AOS-12	sph.	21	4.95	1.28	0.61	2.59	-0.71
AOS-16	sph.	45	4.83	2.53	0.77	4.82	-0.87
DC₁AB	sph.	47	4.24	2.87	1.45	3.67	-0.97
DC₂AB	sph.	47	4.24	2.83	1.78	3.85	-0.93
DC₄AB	sph.	47	4.24	2.85	1.82	4.30	-0.92
DC₆AB	sph.	41	4.49	2.92	1.67	4.97	-0.88

Table 8.4: Modeling results for the optimal micelles. Computer simulation/molecular-thermodynamic (CS-MT) and traditional molecular-thermodynamic (MT) modeling results for each of the nine ionic and zwitterionic surfactants considered in this article. Both the CS-MT model and the traditional MT model yield identical predictions of the optimal micelle shape, the number-average micelle aggregation number (n), g_{int} , g_{pack} , and g_{st} (see Section 8.4.2).

the optimal SDS micelle is spherical with a number-average aggregation number of 47. In Table 8.4, we report predictions using the CS-MT model and the traditional MT model of: (i) the micelle shape, (ii) the number-average micelle aggregation number (n), (iii) g_{int} , (iv) g_{pack} , (v) g_{st} , (vi) g_{elec} (including the discharging, the charging, and the counterion binding free-energy contributions [25,28]), and (vii) g_{ent} . In Table 8.5 we report predictions of (i) g_{form} and the CMC predicted by the CS-MT model, (ii) g_{form} and the CMC predicted by the traditional MT model, and (iii) the experimental values of g_{form} and of the CMC [16]. The reported uncertainty in the CS-MT modeling results corresponds to the standard error of the mean. Note that because the shape and size of the optimal micelles predicted by the CS-MT model and by the traditional MT model are identical, free-energy contributions (iii) to (vii) are also identical. Traditional MT modeling results were generated using the approach reviewed in Chapter 6. The CMCs predicted by the CS-MT model and by the traditional MT model and the value of g_{form} inferred using the experimental CMC data were calculated using Eq. 8.8.

For SDS, the value of g_{int} computed for the optimal micelle (4.33 $k_B T$) is slightly

Surf.	$g_{\text{form}} [k_B T]$ (CMC [mM])		
	CS-MT Model	Traditional MT Model	Expt.
SDS	-8.20 ± 0.04 (15.28 ± 0.58)	-8.66 (9.62)	-8.83 (8.1)
DPC	-11.11 ± 0.34 (0.83 ± 0.29)	-11.25 (0.72)	-10.92 (1.0)
CTAB	-11.14 ± 0.21 (0.81 ± 0.17)	-11.55 (0.54)	-11.03 (0.9)
AOS-12	-7.87 ± 0.05 (21.29 ± 1.02)	-7.83 (22.18)	-7.71 (24.8)
AOS-16	-10.74 ± 0.10 (1.21 ± 0.13)	-10.42 (1.66)	-10.55 (1.45)
DC₁AB	-8.18 ± 0.07 (15.51 ± 1.13)	-8.22 (12.59)	-8.16 (15.90)
DC₂AB	-8.29 ± 0.11 (13.99 ± 1.52)	-9.85 to -7.65 (2.93 to 26.42)	-8.23 (14.80)
DC₄AB	-8.92 ± 0.11 (7.44 ± 0.80)	-11.56 to -6.33 (0.53 to 51.66)	-8.82 (8.20)
DC₆AB	-10.08 ± 0.13 (2.33 ± 0.30)	-13.73 to -5.06 (0.06 to 354.08)	-9.59 (3.80)

Table 8.5: Modeling results for the optimal micelles. The CS-MT and the traditional MT model predictions of g_{form} were obtained using the values of $g_{\text{tr,CS-MT}}$ and g_{tr} reported in Table 4, respectively, as an input to Eq. 8.7. The CS-MT and the traditional MT model predictions of the CMC and the value of g_{form} inferred from the experimental CMC data were computed using Eq. 8.8. The uncertainties reported for the CS-MT model predictions correspond to the standard error of the mean.

lower than the value of \hat{g}_{int} computed for the simulated micelle ($4.38 k_B T$) because of the difference between the simulated and the optimal micelle aggregation numbers. The free-energy contributions, g_{pack} ($2.51 k_B T$), g_{st} ($1.10 k_B T$), g_{elec} ($-0.45 k_B T$), and g_{ent} ($-0.99 k_B T$), while all smaller in magnitude than g_{int} , each contribute significantly to g_{form} . For this surfactant, the CMC predicted by the CS-MT model is 15.28 mM, which is roughly a factor of two larger than the experimental CMC (8.1 mM). The traditional MT model predicts a CMC of 9.62 mM, which is very close to the experimental CMC value of 8.1 mM [16]. Given the exponential dependence of the CMC on g_{form} (see Eq. 8.8), we consider both the CS-MT and the traditional MT results shown in Table 8.5 to be in reasonable agreement with the experimental data.

Dodecylphosphocholine (DPC)

CS-MT and traditional MT modeling results for the simulated DPC micelle are reported in Table 8.3. Each free-energy contribution has been calculated as described

in Section 8.4.2. Theoretical predictions for the optimal micelles obtained using the CS-MT model and the traditional MT model as well as experimental data [21] for the micellization behavior of DPC in aqueous solution at 25 °C are reported in Table 8.4 and Table 8.5.

The optimal DPC micelles that are predicted to form in solution by the CS-MT model and by the traditional MT model are somewhat smaller ($n = 39$) than the simulated DPC micelle ($n = 48$). The predicted value of g_{int} ($4.61 k_{\text{B}}T$) is slightly larger than that of \hat{g}_{int} ($4.26 k_{\text{B}}T$) because of this difference in aggregation numbers. Note that g_{ent} for this surfactant is equal to zero because there is no counterion binding for this zwitterionic surfactant. The CS-MT model prediction of the transfer free-energy contribution ($g_{\text{tr,CS-MT}} = -18.32 k_{\text{B}}T$) is slightly less negative than that of the traditional MT prediction ($g_{\text{tr}} = -18.46 k_{\text{B}}T$). The traditional MT estimate of g_{tr} for DPC is identical to the g_{tr} estimate for SDS because both surfactants have identical tails. In contrast, the CS-MT model estimate of $g_{\text{tr,CS-MT}}$ for DPC is $0.63 k_{\text{B}}T$ more negative than the estimate of $g_{\text{tr,CS-MT}}$ for SDS. As discussed in Chapter 7, the nature of the surfactant head can have a significant effect on the degree of hydration of the surfactant tail in bulk aqueous solution, and this is further confirmed by the difference in the $g_{\text{tr,CS-MT}}$ values obtained for DPC and SDS. The difference between the CS-MT estimate of $g_{\text{tr,CS-MT}}$ and the traditional MT estimate of g_{tr} for DPC leads to the CS-MT model predicting a higher CMC (0.83 mM) than that predicted by the traditional MT model (0.72 mM). In this case, the CMC predicted by the CS-MT model is closer to the experimental CMC (1.0 mM) [21].

Cetyltrimethylammonium Bromide (CTAB)

CS-MT and traditional MT modeling results for the simulated CTAB micelle are reported in Table 8.3. Theoretical predictions for the optimal micelles obtained using the CS-MT model and the traditional MT model as well as experimental data [29] for the micellization behavior of CTAB in aqueous solution at 25 °C are reported in Table 8.4 and Table 8.5.

Computer simulation of CTAB was conducted in a micelle with an aggregation number of 49, which is identical (after rounding to the nearest integer value) to the CS-MT and the traditional MT number-average aggregation number predictions for the optimal CTAB micelles. The predicted value of g_{int} ($5.35 k_{\text{B}}T$) is very close to the predicted value of \hat{g}_{int} ($5.44 k_{\text{B}}T$), while the transfer free-energy contribution ($g_{\text{tr,CS-MT}} = -23.73 k_{\text{B}}T$) predicted by the CS-MT model is slightly less negative than that predicted by the traditional MT model ($g_{\text{tr}} = -24.43 k_{\text{B}}T$). The difference between the CS-MT estimate of $g_{\text{tr,CS-MT}}$ and the traditional MT estimate of g_{tr} for CTAB leads to the CS-MT model predicting a higher CMC (0.81 mM) than that predicted by the traditional MT model (0.54 mM). In this case, the CMC predicted by the CS-MT model is closer to the experimental CMC (0.9 mM) [29].

Applicability of the CS-MT Modeling Approach to Ionic and Zwitterionic Surfactants

Based on the modeling results obtained for the simple anionic, zwitterionic, and cationic surfactants discussed in Sections 8.4.2 to 8.4.2, it is possible to evaluate the applicability of the CS-MT modeling approach to model the micellization behavior of surfactants with charged hydrophilic heads. For the three surfactants considered, the CMCs predicted by the CS-MT model are in reasonable agreement with the experimental CMCs. For DPC and CTAB, the CMCs predicted using the CS-MT model are more accurate than those predicted using the traditional MT model. Based on these results, we conclude that the approximations introduced in Chapter 7 to enable straightforward calculation of g_{dehydr} and g_{hydr} are reasonably accurate for non-polymeric, small-head ionic and zwitterionic surfactants.

For the three simple, small-head surfactants modeled above, three key approximations were made to enable straightforward implementation of the CS-MT model. The first approximation involves estimating g_{tr_i} for hydrophobic groups in the surfactant head and tail using solubility data for linear alkyl chains. This approximation has already been shown in Chapter 7 to yield reasonable modeling results for small-head

nonionic surfactants, and we believe that it should also be reasonably accurate (and physically realistic) in the case of small-head ionic and zwitterionic surfactants. The second approximation involves identifying hydrophobic groups in each surfactant as being adsorbed onto, or incorporated within, the micelle hydrophobic core if they have an f value which is less than 0.60. It is reasonable to make this approximation for ionic and zwitterionic surfactants because the selection of this f value in Chapter 7 was informed by data for both nonionic and ionic surfactants. The third approximation involves using the expression for Δg_{wc} given in Eqs. 8.5 and 8.6 to evaluate g_{hydr} . This model for Δg_{wc} was originally developed in Chapter 6 for oil aggregates. In using such a model in the case of ionic and zwitterionic surfactant micelles, the approximation is made that the change in hydration free energy experienced by hydrophobic groups in being transferred from the bulk aqueous solution to the micelle hydrophobic core is unaffected by the presence of the charged surfactant heads and the charged counterions (if present) at the micelle core/water interface. It was not clear *a priori* whether Δg_{wc} could be evaluated for ionic and zwitterionic surfactants using Eqs. 8.5 and 8.6, or whether it would be necessary to fit a value of Δg_{wc} to obtain accurate predictions of the micellization behavior. Fortunately, the results for SDS, DPC, and CTAB suggest that evaluating Δg_{wc} using a model developed for oil aggregates is reasonably accurate even for ionic and zwitterionic surfactant micelles. As a result, when modeling each of the complex surfactants considered next in Section 8.4.3 we will calculate Δg_{wc} using Eqs. 8.5 and 8.6.

8.4.3 Modeling Results for Complex Surfactants

Sodium 3-Hydroxy Sulfonates (AOS-12 and AOS-16)

CS-MT and traditional MT modeling results for the simulated AOS-12 and AOS-16 micelles are reported in Table 8.3. Theoretical predictions for the optimal micelles obtained using the CS-MT model and the traditional MT model as well as experimental data [30] for the micellization behavior of AOS-12 and AOS-16 in aqueous

solution at 30 °C are reported in Table 8.4 and Table 8.5.

The CS-MT and the traditional MT model predictions of the optimal number-average micelle aggregation numbers of AOS-12 ($n = 21$) and of AOS-16 ($n = 45$) are somewhat different than the aggregation numbers of the simulated AOS-12 ($n = 32$) and AOS-16 ($n = 40$) micelles. The predicted value of g_{int} for AOS-12 ($4.95 k_{\text{B}}T$) is significantly larger than that of \hat{g}_{int} ($4.30 k_{\text{B}}T$) because of this difference in aggregation numbers. In contrast, g_{int} for AOS-16 ($4.83 k_{\text{B}}T$) is predicted to be significantly smaller than \hat{g}_{int} ($5.26 k_{\text{B}}T$). For both AOS-12 and AOS-16, the CS-MT model predictions of the transfer free-energy contribution ($g_{\text{tr,CS-MT}} = -15.44$ and $-21.81 k_{\text{B}}T$, respectively) are slightly more negative than the traditional MT model predictions of the transfer free-energy contribution ($g_{\text{tr}} = -15.37$ and -21.27 , respectively). This leads to the CS-MT model predicting lower CMCs for both surfactants (21.29 mM and 1.21 mM for AOS-12 and AOS-16, respectively) than those predicted by the traditional MT model (22.18 mM and 1.66 mM, respectively). The CMCs predicted by the CS-MT model and by the traditional MT model are both in reasonable agreement with the experimental CMCs (24.8 mM and 1.45 mM, respectively). However, it is important to note that the groups in AOS-12 and in AOS-16 that should be modeled as being part of the surfactant head and as part of the surfactant tail in traditional MT modeling are not entirely clear. As a result, we have used head and tail assignments for these surfactants determined through computer simulation in a previous study [26]. Without such information, it would not have been possible to make such accurate predictions using the traditional MT model.

For these two surfactants, our results indicate that although computer simulation inputs are necessary, reasonably accurate predictions of their micellization behavior can be made using computer simulations to make head and tail identifications for use in traditional MT modeling (as was done in Reference 26), or to obtain fractional hydration data for use in the CS-MT model (as was done in this chapter). In Reference 26, head and tail identifications for both of these surfactants were made in a computationally efficient way by simulating both surfactants at a water/oil interface

(serving as a proxy for the micelle core/water interface), and comparably accurate modeling results were obtained. The four computer simulations used here to obtain fractional hydration information for these two surfactants for input in the CS-MT model required approximately an order of magnitude more computational expense.

$C_{12}H_{25}C_NH_{2N+1}N(CH_3)_2Br$ Surfactants (DC₁AB-DC₆AB)

CS-MT and traditional MT modeling results for the simulated DC₁AB, DC₂AB, DC₄AB, and DC₆AB micelles are reported in Table 8.3. Theoretical predictions for the optimal micelles obtained using the CS-MT model and the traditional MT model as well as experimental data [30] for the micellization behavior of each surfactant in aqueous solution at 25 °C are reported in Table 8.4 and Table 8.5. The approach described in Section 8.4.2 was used to calculate each free-energy contribution, the values of g_{form} , and the CMC values reported in Table 8.4 and Table 8.5.

As shown in Tables 8.3, 8.4, and 8.5, although only one value of $g_{\text{tr,CS-MT}}$, g_{form} , and the CMC are reported for DC₂AB, DC₄AB, and DC₆AB using the CS-MT model, a range of g_{tr} , g_{form} , and CMC values are reported for these surfactants using the traditional MT modeling approach because it is difficult to determine the head and tail of each surfactant. As discussed in Chapter 6, for simple surfactants and solubilizates, simple guidelines can be used for head and tail identification. For ionic and zwitterionic surfactants, the approximation is made that $n_t = n_c - 1$, where n_c is the total number of CH₂ and CH₃ groups in the hydrocarbon chain and n_t is the number of CH₂ and CH₃ groups that should be modeled as being part of the surfactant tail [3,31]. In other words, a hydrophobic group bonded to a charged hydrophilic group is modeled as being part of the surfactant head, while other hydrophobic groups are modeled as being part of the surfactant tail. Unfortunately, these guidelines are inadequate to provide accurate head and tail identifications for DC₂AB, DC₄AB, and DC₆AB because it is unclear how to model each C_N group. Because of this uncertainty, we have implemented the traditional MT modeling approach based on three different modeling limits. The first limit (which we will refer to as Limit 1) involves modeling

each atom in the C_N groups as being part of the surfactant head, with the remaining groups in each surfactant being modeled as being part of the head or the tail according to the $n_t = n_c - 1$ guideline. Using this approach, groups 1 to 6 of DC₂AB are modeled as being part of the head, while groups 7-17 are modeled as being part of the tail (see the group numbers defined in Figure 8-7 and the a_h values listed in Table 8.2). Based on the structure of the selected head, the area of the surfactant head (a_h) was computed geometrically by assuming that the entire C_N group lies parallel to the micelle core/water interface and contributes to the surfactant head area at the interface. The second limit (Limit 2) is based on the same assignment of head and tail made in Limit 1. However, in Limit 2, an accurate value of a_h for each surfactant has been determined from the computer simulation data by measuring the projected area of each surfactant head at the micelle core/water interface. The same values of a_h used in Limit 2 of traditional MT modeling were also used in CS-MT modeling. It is important to note that the estimation of a_h using the computer simulation data is expected to yield significantly more accurate results for complex surfactants such as DC₂AB, DC₄AB, and DC₆AB than attempting to approximate a_h based on an assumption of what portions of the surfactant are present at the micelle core/water interface. In the third limit (Limit 3), the head and tail portions of DC₂AB, DC₄AB, and DC₆AB were estimated using the $n_t = n_c - 1$ guideline for both the C_N chain and each of the remaining groups in the surfactant. Using this approach, groups 2 to 6 of DC₂AB were assigned as being part of the head, while groups 1 and 7 to 17 were assigned as being part of the tail (see the group numbers defined in Figure 8-7 and the a_h values listed in Table 8.2). Similarly, groups 4 to 8 of DC₄AB were assigned as being part of the head, while groups 1 to 3 and 9 to 19 were assigned as being part of the tail. Based on this assignment of heads and tails, the values of a_h for DC₂AB, DC₄AB, and DC₆AB are identical and are equal to the value of a_h for DC₁AB. Limits 1 and 3 yield upper-bound and lower-bound estimates of the CMC using the traditional MT modeling approach, respectively. As demonstrated by the results shown in Table 8.5, the range of CMC values encompassed by these two limits

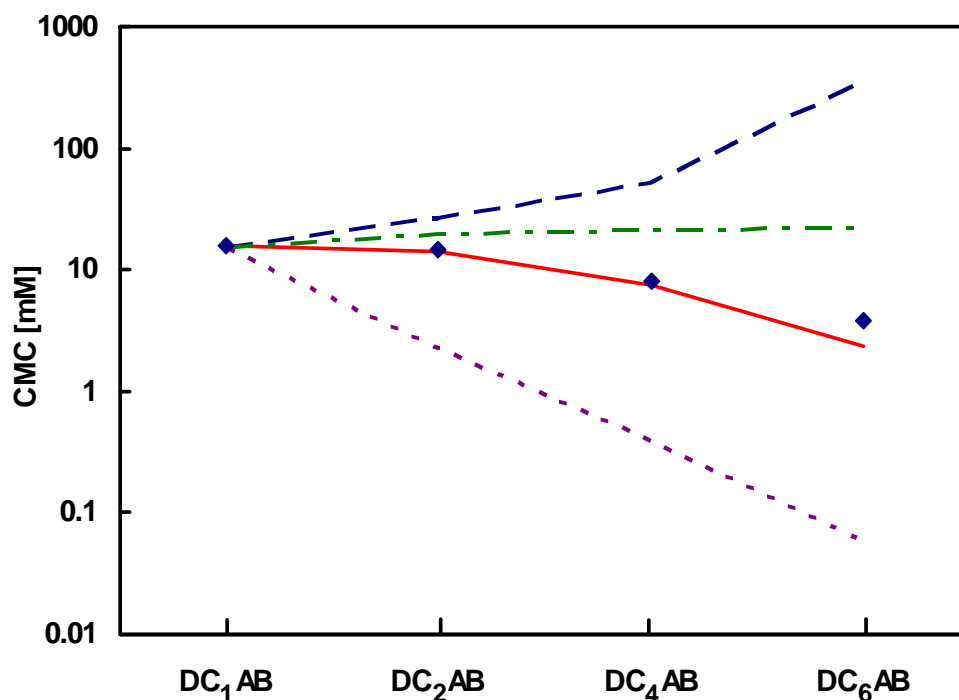


Figure 8-8: Comparison of the CMCs predicted using the CS-MT model (—) and the CMCs predicted using the three traditional MT modeling limits discussed in Section 8.4.3 (Limit 1 : ---, Limit 2 : -.-, and Limit 3 : ····) for decyltrimethylammonium bromide (DC₁AB), C₁₂H₂₅C₂H₅N(CH₃)₂Br (DC₂AB), C₁₂H₂₅C₄H₉N(CH₃)₂Br (DC₄AB), and C₁₂H₂₅C₆H₁₃N(CH₃)₂Br (DC₆AB). The lines are shown as a guide for the eye. The experimental CMC data is shown for comparison (◆).

is very large, and the range of values increases in magnitude as the length of the C_N group increases.

The CMCs predicted using the CS-MT model and the traditional MT model are reported graphically in Figure 8-8 on a log scale. Not only are the CMCs predicted using the CS-MT model in remarkably good agreement with the experimental CMCs, but they are also much more accurate than any of the CMCs predicted using the three traditional MT modeling limits.

The traditional MT model fails to accurately model the DC₂AB, DC₄AB, and DC₆AB surfactants for several reasons. Limit 1 is in poor agreement with the exper-

imental CMC data because: (i) computing a_h geometrically based on the assumption that the entire C_N group is part of the surfactant head and lies flat at the micelle core/water interface overestimates a_h , and consequently, leads to an overestimation of g_{st} , and (ii) making the approximation that the C_N group is part of the surfactant head (and therefore remains fully hydrated upon micelle formation) leads to a severe overprediction of g_{tr} . Limit 2 is in poor agreement with the experimental CMC data because of (ii). It is interesting to note, however, that using a computer simulation estimate of a_h significantly improves the traditional MT model CMC predictions. Limit 3 is in poor agreement with the experimental CMC data because: (i) the head and tail assignments made in this limit imply that a_h for DC₂AB, DC₄AB, and DC₆AB are each equal to 32 \AA^2 , which underestimates the value of a_h , and (ii) the large number of groups included in the surfactant tail leads to an overly negative estimate of g_{tr} .

The length of the C_N group in each DC_{*N*}AB surfactant influences the CS-MT model estimate of g_{form} in several interesting ways. First, as the length of the C_N group increases, the computer simulation estimate of a_h increases. This serves to increase the steric free-energy contribution, g_{st} . At the same time, however, the transfer free-energy contribution, $g_{tr,CS-MT}$, of the C_N group becomes increasingly negative. In addition, the C_N group in DC₆AB has two hydrophobic groups (1 and 2) that are sufficiently dehydrated that they are modeled as being part of the micelle core and that therefore affect g_{pack} . As shown in Table 8.5, the experimental CMC values of the four DC_{*N*}AB surfactants are ranked as follows: DC₁AB > DC₂AB > DC₄AB > DC₆AB [24]. Consequently, the net effect of increasing the length of the C_N group is to lower g_{form} , which in turn lowers the value of the CMC. Not only is this ranking of g_{form} and CMC values correctly predicted by the CS-MT model, but the values of g_{form} and of the CMC predicted by the CS-MT model are in very close agreement with the experimental data.

In Chapter 7, we concluded that care must be taken in computing g_{dehyd} for surfactants with large, polymeric heads using the simplifying approximations discussed

in Section 8.4.2. It is important to note that the DC_NAB surfactants modeled here do not fall into this category of surfactants for the following reasons: (i) the maximum size of the DC_NAB surfactant heads is relatively small, and (ii) hydrophobic groups in the DC_NAB heads are transferred (to the extent that they are dehydrated) to an environment that is chemically similar to a bulk solution of surfactant tails (see additional discussion in Chapter 7).

Evaluation of the majority of the free-energy contributions that appear in Eq. 8.7 for the DC_NAB surfactants is relatively straightforward. However, accurate estimation of the packing free-energy contribution, g_{pack} , for Limit 3 of the traditional MT modeling and for the CS-MT modeling of DC₂AB, DC₄AB, and DC₆AB has required the development and implementation of a modified packing model that is capable of accurately estimating g_{pack} for surfactants with two tails separated by a head. The packing free-energy contribution, g_{pack} , represents the free-energy change required to fix one end of the surfactant tail(s) at the micelle core/water interface. This free-energy contribution is typically estimated using a mean-field model first introduced by Ben-Shaul, Szleifer, and Gelbart [32–34], and requires sampling each important conformation and orientation of the surfactant tail subject to the constraint that the micelle hydrophobic core has a uniform density. As shown in Table 8.3, in Limit 3 of the traditional MT modeling of DC₂AB, tail groups 1 and 7-17 are separated by head groups 2-6. A similar separation of head and tail groups is also present in DC₄AB and DC₆AB. To maintain consistency between the CS-MT model for the hydrophobic effect (g_{dehydr} and g_{hydr}) and the evaluation of g_{pack} for the CS-MT model, head and tail assignments used in computing g_{pack} for the CS-MT model were made using the criterion that any group with an f value greater than 0.60 was modeled as a group in the head, and any group with an f value less than 0.60 was modeled as a group in the tail. Using this approach, each of the C_N groups in DC₂AB and DC₄AB was identified as being part of the head. Groups 3-6 in the C_N group in DC₆AB were identified as being part of the head, while groups 1-2 were identified as being part of the tail.

The mean-field approach that was implemented to determine g_{pack} for Limit 3 of the traditional MT model and the CS-MT model was modified to be more physically realistic by relaxing the constraint that groups in the surfactant tail cannot exit the micelle core. In the modified approach, each important conformation and orientation of the C_N group was sampled, and the C_N group was modeled as contributing to the volume of the micelle core for conformations where atoms in C_N the group entered the micelle core. For conformations where atoms in the C_N group did enter the micelle core, they affect the lateral pressures present in the micelle core and the value of g_{pack} . This packing approach allowed sampling of each of the conformations that were actually observed during the molecular dynamics simulation, where each C_N group was found to adopt a wide variety of conformations both inside and outside the micelle core. Complete details of the modified packing approach used to compute g_{pack} for DC₂AB, DC₄AB, and DC₆AB will be presented in a future publication.

Although not explored in this chapter, the predictions of the traditional MT model may be improved by using computer simulations to determine the appropriate head and tail assignments for the DC₂AB, DC₄AB, and DC₆AB surfactants. Such an approach (with data taken from a previous publication) [26] was used in modeling AOS-12 and AOS-16 in Section 8.4.3. Although computer simulation determination of head and tail groups might improve the traditional MT model predictions, this approach is unlikely to yield predictions that are as accurate as those obtained using the CS-MT model. This is due to the fact that the traditional MT model is limited by the simplistic modeling approximation that groups in the surfactant head remain fully hydrated in the micellar state. The effect of this approximation can be understood by closely examining the traditional MT modeling results for DC₂AB. In Limit 2, the entire C_N group (CH₂-CH₃) is modeled as being part of the head, while in Limit 3, the CH₂ group in C_N is modeled as being part of the head and the CH₃ group in C_N is modeled as being part of the tail. These two limits represent the only physically plausible head and tail assignments for the C_N group in DC₂AB that could be obtained from computer simulation. As shown in Figure 8-8, both limits yield

predicted CMCs that are less accurate than the CMC predicted using the CS-MT model.

8.5 Conclusions

In this chapter, we have demonstrated the validity and accuracy of the CS-MT model by using it to model nine ionic and zwitterionic surfactants of varying structural complexity. To implement the CS-MT model, we have used molecular dynamics computer simulations to determine quantitative information about the changes in hydration that occur upon micelle formation. This detailed hydration information was then used to quantify the hydrophobic driving force for micelle self-assembly ($g_{\text{tr,CS-MT}}$). After determining this input, the free energy of micelle formation, g_{form} , and the CMC were calculated for each surfactant for micelles of the optimal shape and size.

To quantify the hydration changes that occur upon micelle formation, we conducted two independent molecular dynamics simulations for each of the nine ionic surfactants modeled. Changes in hydration were quantified by computing a fractional hydration value, f , for each group. The f values obtained for each surfactant through MD simulation were used as an input in a free-energy model to compute the magnitude of the hydrophobic driving force for micelle formation (g_{dehydr} and g_{hydr}). In this chapter, we have used the approximations discussed in Chapter 7 to estimate g_{dehydr} and g_{hydr} . These approximations were found to be reasonably accurate in modeling ionic and zwitterionic surfactants. In particular, we found that Δg_{wc} could be modeled using Eq. 8.2 and 8.3, and need not be fitted to obtain accurate results for ionic and zwitterionic surfactants.

Reasonable agreement between the CS-MT model predictions and the experimental data for g_{form} and the CMC were obtained for each of the nine ionic and zwitterionic surfactants modeled in this chapter. For five of these surfactants (SDS, DPC, CTAB, AOS-12, AOS-16, and DC₁AB) the CMCs predicted using the CS-MT

model were found to be in reasonable agreement with the CMCs predicted using the traditional MT model. However, for DC₂AB, DC₄AB, and DC₆AB, the predictions of the CS-MT model were in much closer agreement with the experimental data than the predictions of the traditional MT model.

The results obtained for the relatively complex surfactants DC₂AB, DC₄AB, and DC₆AB highlight the strengths of the CS-MT modeling approach: for surfactants where a significant number of hydrophobic groups are located near the aggregate core/water interface and remain partially hydrated upon micelle formation, the CS-MT modeling approach eliminates the guesswork involved in traditional MT modeling. Furthermore, because the CS-MT modeling approach uses a more realistic free-energy model to quantify the hydrophobic driving force for micelle formation, it yields more accurate predictions of the micellization behavior than the traditional MT modeling approach. Obviously, the additional accuracy of the CS-MT model comes at the expense of greater computational effort. Nevertheless, given the relatively small fraction of surfactants with sufficient structural and chemical simplicity to be accurately modeled using the traditional MT modeling approach, we believe that the CS-MT model represents a very attractive and useful alternative.

In Part I of this thesis, I have described several approaches to use molecular dynamics simulations to obtain inputs for molecular thermodynamic modeling. In Chapters 2 and 3, computer simulations were used to identify surfactant and solubilize heads and tails. In Chapters 4 and 5, computer simulations were used to identify solubilize heads, tails, and neutral groups. Finally, in Chapters 6, 7, and 8, computer simulations were used to obtain fractional hydration information. In Part II of this thesis, the application of computer simulation free-energy methods to evaluate the free-energy change associated with mixed micelle formation will be explored. In Chapter 9, an introduction to computer simulation free-energy methods and the theoretical framework underlying what will be referred to as the CS-FE (computer simulation-free-energy)/MT modeling approach will be introduced. In Chapter 10, implementation of the CS-FE/MT model will be discussed and CS-FE/MT modeling

results will be presented for a total of 5 mixed surfactant/solubilize and surfactant/cosurfactant systems. In Part III of this thesis, direct prediction of surfactant solution properties using molecular dynamics simulations will be explored.

8.6 Appendix A: Normalized SASA Profiles

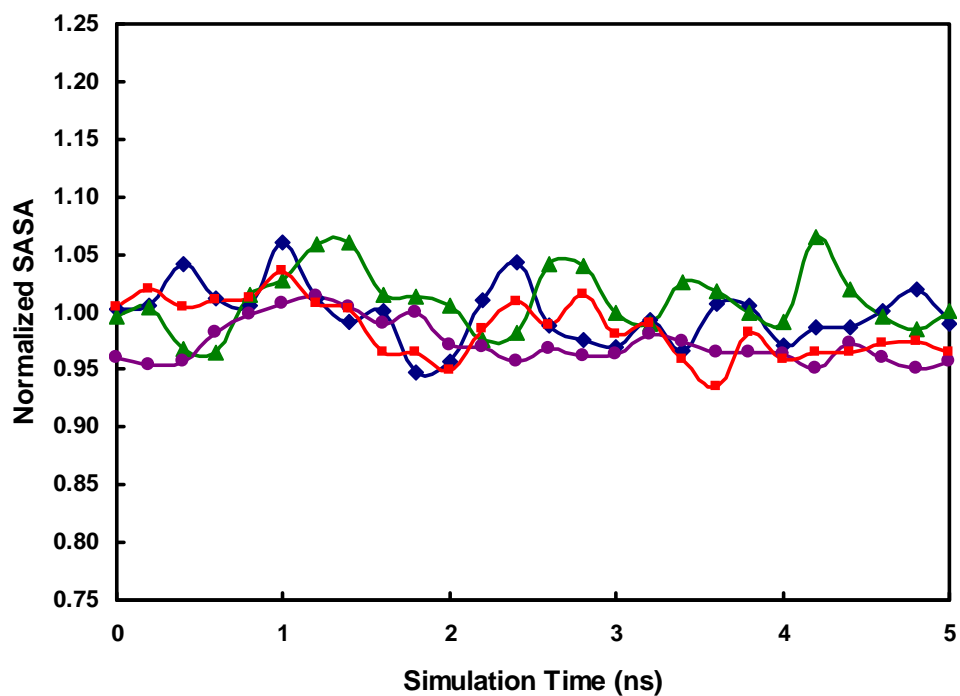

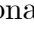




Figure 8-A1: Solvent accessible surface area (SASA) normalized by the average value of SASA as a function of simulation time for: sodium dodecyl sulfate (SDS, ) , 3-hydroxy dodecyl sulfonate (AOS-12, ) , 3-hydroxy hexadecyl sulfonate (AOS-16, ) , and dodecylphosphocholine (DPC, ) during the 5 ns data-gathering simulation run (see text).

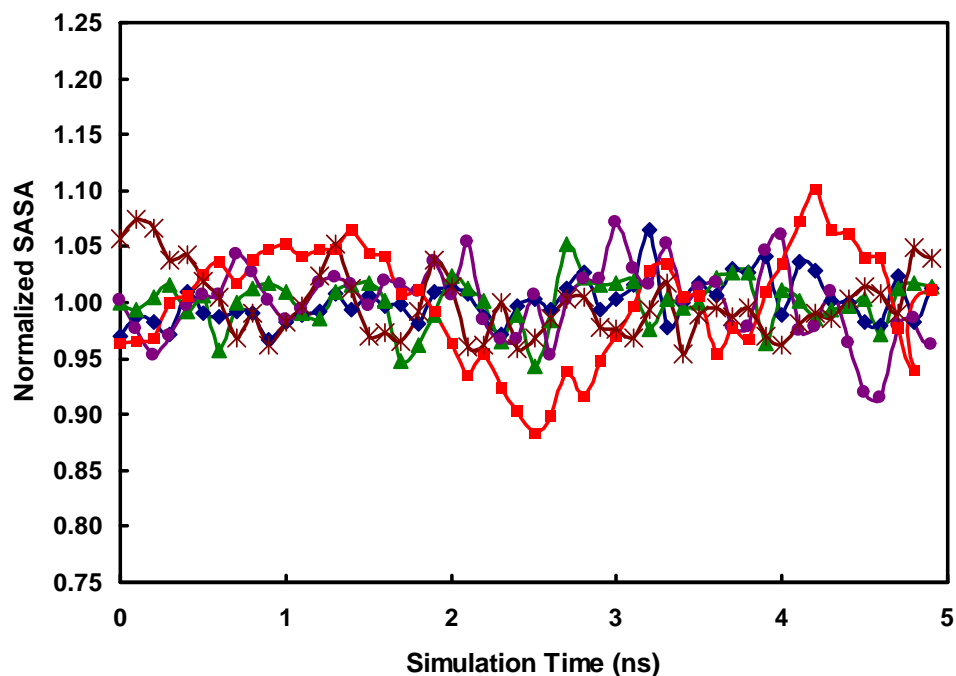


Figure 8-A2: Solvent accessible surface area (SASA) normalized by the average value of SASA as a function of simulation time for: cetyltrimethylammonium bromide (CTAB, \blacklozenge), decyltrimethylammonium bromide (DC₁AB, \blacktriangle), C₁₂H₂₅C₂H₅N(CH₃)₂Br (DC₂AB, \bullet), C₁₂H₂₅C₄H₉N(CH₃)₂Br (DC₄AB, \blacksquare), and C₁₂H₂₅C₆H₁₃N(CH₃)₂Br (DC₆AB, \blackast) during the 5 ns data-gathering simulation run (see text).

Bibliography

- [1] Stephenson, B. C., Goldsipe, A., Beers, K. J., and Blankschtein, D., “Quantifying the hydrophobic effect: I. A computer simulation/molecular-thermodynamic model for the aqueous self-assembly of hydrophobic and amphiphilic solutes,” *The Journal of Physical Chemistry B*, 2006, pp. (submitted).
- [2] Stephenson, B. C., Goldsipe, A., Beers, K. J., and Blankschtein, D., “Quantifying the hydrophobic effect: II. A computer simulation/molecular-thermodynamic model for the micellization of nonionic surfactants,” *The Journal of Physical Chemistry B*, 2006, pp. (submitted).
- [3] Puvvada, S. and Blankschtein, D., “Molecular thermodynamic approach to predict micellization, phase behavior and phase separation of micellar solutions. 1. Application to nonionic surfactants,” *The Journal of Chemical Physics*, Vol. 92, 1990, pp. 3710–3724, and references cited therein.
- [4] Goldsipe, A. and Blankschtein, D., “Modeling counterion binding in ionic-nonionic and ionic-zwitterionic binary surfactant mixtures,” *Langmuir*, Vol. 22, 2005, pp. 9850–9865.
- [5] Smith, R. and Tanford, C., “Hydrophobicity of long chain n-alkyl carboxylic acids, as measured by their distribution between heptane and aqueous solutions,” *Proceedings of the National Academy of Sciences*, Vol. 70, 1973, pp. 289–293.
- [6] Jorgensen, W. L., Maxwell, D. S., and Tirado-Rives, J., “Development and testing of the OPLS all-atom force field on conformational energetics and properties

- of organic liquids,” *Journal of the American Chemical Society*, Vol. 118, 1996, pp. 11225–11236.
- [7] Schweighofer, K. J., Essmann, U., and Berkowitz, M., “Simulation of sodium dodecyl sulfate at the water-vapor and water-carbon tetrachloride interfaces at low surface coverage,” *The Journal of Physical Chemistry B*, Vol. 101, 1997, pp. 3793–3799.
- [8] Tieleman, D. P. and Berendsen, H. J. C., “Molecular dynamics simulations of a fully hydrated dipalmitoyl phosphatidylcholine bilayer with different macroscopic boundary conditions and parameters,” *The Journal of Chemical Physics*, Vol. 105, 1996, pp. 4871–4880.
- [9] van der Spoel, D., Lindahl, E., Hess, B., van Buuren, A. R., Apol, E., Meulenhoff, P. J., Tieleman, D. P., Sijbers, A. L. T. M., Feenstra, K. A., van Drunen, R., and Berendsen, H. J. C., *Gromacs User Manual*, www.gromacs.org, 2004.
- [10] Chirlian, L. E. and Francl, M. M., “Atomic charges derived from electrostatic potentials: A detailed study,” *Journal of Computational Chemistry*, Vol. 8, 2004, pp. 894–905.
- [11] Darden, T., York, D., and Pedersen, L., “Particle mesh Ewald: An N-log(N) method for Ewald sums in large systems,” *The Journal of Chemical Physics*, Vol. 98, 1993, pp. 10089–10092.
- [12] Essmann, U., Perera, L., Berkowitz, M. L., Darden, T., Lee, H., and Pedersen, L. G., “A smooth particle mesh Ewald potential,” *The Journal of Chemical Physics*, Vol. 103, 1995, pp. 8577–8592.
- [13] van der Spoel, D., Lindahl, E., Hess, B., van Buuren, A., Apol, E., Meulenhoff, P., Tieleman, D., Sijbers, A., Feenstra, K., van Drunen, R., and Berendsen, H., *Gromacs User Manual version 3.2*, www.gromacs.org, 2004.

- [14] Berendsen, H. J. C., van der Spoel, D., and van Drunen, R., "GROMACS: A message-passing parallel molecular dynamics implementation," *Computational Physics Community*, Vol. 91, 1995, pp. 43–56.
- [15] Lindahl, E., Hess, B., and van der Spoel, D., "Gromacs 3.0: A package for molecular simulation and trajectory analysis," *Journal of Molecular Modeling*, Vol. 7, 2001, pp. 306–317.
- [16] Israelachvili, J. N., *Intermolecular and Surface Forces*, Academic Press, 2nd ed., 1991.
- [17] Bruce, C., Berkowitz, M., Perera, L., and Forbes, M., "Molecular dynamics simulation of sodium dodecyl sulfate micelle in water: Micellar structural characteristics and counterion distribution," *The Journal of Physical Chemistry B*, Vol. 106, 2002, pp. 3788–3793.
- [18] Flyvbjerg, H. and Petersen, H. G., "Error estimates on averages of correlated data," *The Journal of Chemical Physics*, Vol. 91, 1989, pp. 461–466.
- [19] Hess, B., *Stochastic Concepts in Molecular Simulation*, Ph.D. thesis, Rijksuniversiteit Groningen, Groningen, 1999.
- [20] Hess, B., "Determining the shear viscosity of model liquids from molecular dynamics simulations," *The Journal of Chemical Physics*, Vol. 116, 2001, pp. 209–217.
- [21] Kallick, D. A., Tessmer, M. R., Watts, C. R., and Li, C.-Y., "The use of dodecylphosphocholine micelles in solution NMR," *Journal of Magnetic Resonance*, Vol. 109, 1995, pp. 60–65.
- [22] Tieleman, D. P., van der Spoel, D., and Berendsen, H. J. C., "Molecular dynamics simulations of dodecylphosphocholine micelles at three different aggregate sizes: Micellar structure and lipid chain relaxation," *The Journal of Physical Chemistry B*, Vol. 104, 2000, pp. 6380–6388.

- [23] Van Os, N. M., Van Ginkel, R., Van Zon, A., Heywood, F. W., Berryman, E. L., and Borchardt, J. K., *Solubilization in Surfactant Aggregates. Surfactant Science Series 56*, Marcel Dekker, New York, 1996.
- [24] Bai, G., Wang, J., Yan, H., Li, Z., and Thomas, R. K., “Thermodynamics of molecular self-assembly of two series of double-chain singly charged cationic surfactants,” *The Journal of Physical Chemistry B*, Vol. 105, 2001, pp. 9576–9580.
- [25] Srinivasan, V. and Blankschtein, D., “Effect of counterion binding on micellar solution behavior: 1. Molecular-thermodynamic theory of micellization of ionic surfactants,” *Langmuir*, Vol. 19, 2003, pp. 9932–9945.
- [26] Stephenson, B. C., Beers, K., and Blankschtein, D., “Complementary use of simulations and molecular-thermodynamic theory to model micellization,” *Langmuir*, Vol. 22, 2006, pp. 1500–1513.
- [27] Stephenson, B. C., Rangel-Yagui, C. O., Pessoa, A., Tavares, L. C., Beers, K. J., and Blankschtein, D., “Experimental and theoretical investigation of the micellar-assisted solubilization of ibuprofen in aqueous media,” *Langmuir*, Vol. 22, 2006, pp. 1514–1525.
- [28] Srinivasan, V. and Blankschtein, D., “Effect of counterion binding on micellar solution behavior: 2. Prediction of micellar solution properties of ionic surfactant-electrolyte systems,” *Langmuir*, Vol. 19, 2003, pp. 9946–9961.
- [29] Hansson, P., Jonsson, B., Strom, C., and Soderman, O., “Determination of micellar aggregation numbers in dilute surfactant systems with the fluorescence quenching method,” *The Journal of Physical Chemistry B*, Vol. 104, 2000, pp. 3496–3506.
- [30] Van Os, N. M., Rupert, L. A. M., and Haak, J. R., *Physico-Chemical Properties of Selected Anionic, Cationic and Nonionic Surfactants*, Elsevier, Amsterdam, 1993.

- [31] Srinivasan, V., *Theoretical Modeling of Micellization and Solubilization in Ionic Surfactant Systems*, Ph.D. thesis, Massachusetts Institute of Technology, 2003, and references cited therein.
- [32] Ben-Shaul, A. and Szleifer, I., “Chain organization and thermodynamics in micelles and bilayers. I. Theory,” *The Journal of Chemical Physics*, Vol. 83, 1985, pp. 3597–3611.
- [33] Szleifer, I., Ben-Shaul, A., and Gelbart, W. M., “Chain organization and thermodynamics in micelles and bilayers. II. Model calculations,” *The Journal of Chemical Physics*, Vol. 83, 1985, pp. 3612–3620.
- [34] Szleifer, I., Ben-Shaul, A., and Gelbart, W. M., “Statistical thermodynamics of molecular organization in mixed micelles and bilayers,” *The Journal of Chemical Physics*, Vol. 86, 1987, pp. 7094–7109.

PART II

FREE-ENERGY CALCULATIONS USING COMPUTER SIMULATION

Chapter 9

Free-Energy Calculations Using Computer Simulations: Theory

In Part I of this thesis, several modeling approaches were described in which computer simulations are used to determine input parameters for molecular-thermodynamic (MT) modeling. These input parameters are determined from microstructural information obtained through molecular dynamics (MD) simulation, including information about the average local environment of different surfactant/solubilize groups or about the average fractional hydration of different surfactant/solubilize groups. Using this information, the free energy associated with micelle formation, or g_{form} , was determined. A thermodynamic description of the surfactant and solubilize solution was used to make predictions of solution properties such as the CMC, the shape and size distribution of micelles, the micelle composition, the degree of counterion binding, and the locus and the extent of solubilization from the calculated value of g_{form} . In Part II of this thesis, a different modeling strategy is explored in which computer simulation free-energy methods are used to predict g_{form} . The new modeling approach will be referred to as the computer simulation-free energy/molecular thermodynamic (CS-FE/MT) model to reflect the fact that computer simulations are used to estimate free energies. Part II of this thesis is divided into two chapters. In Chapter 9, the theoretical basis for the CS-FE/MT model is described, including a description of

the thermodynamic framework underlying the CS-FE/MT model and the computer simulation approach that will be used to estimate free-energy differences. In Chapter 10, predictions of surfactant micellization and micellar solubilization behavior made using the CS-FE/MT model will be presented and discussed.

9.1 Background

Two different approaches may be used to estimate the free energy of micelle formation through computer simulation. The first approach involves simulating hundreds to thousands of surfactant monomers, solubilizates, counterions, and water molecules distributed randomly within a simulation cell until self-assembly occurs and all the simulation cell components come to equilibrium. Unfortunately, such an approach can be extremely computationally expensive because of the large system size and the long simulation times involved. This approach is particularly intractable if the surfactant/solubilizate system of interest has a low CMC value. To correctly identify the CMC from simulations of self-assembly, a number of simulations must be performed at low concentrations of surfactant and solubilizate, implying that the total number of water molecules that must be included in the simulation cell is very large. The high ratio of water molecules to surfactant and solubilizate molecules required for such simulations leads to large system sizes and long timescales associated with the self-assembly process.

The second approach to determine the free energy of micelle formation involves using computer simulation free-energy methods to determine g_{form} as a function of the number of surfactant and solubilizate molecules located in a micelle (i.e., as a function of the micelle aggregation number and composition). Determination of g_{form} as a function of micelle size and composition may be accomplished by using computer simulations alone, or by using a hybrid modeling approach.

Only a few computer simulation studies have been reported in the literature in which computer simulation free-energy methods are used to determine g_{form} . Mo-

hanty et al. described a hybrid modeling approach where computer simulations are combined with MT modeling [1]. They used their model to predict the CMC and the sphere-to-wormlike micelle shape transition for the cationic surfactant cetyltrimethylammonium bromide (CTAB) and the partially hydrophobic counterion sodium salicylate (Sal^-) [1]. In their modeling approach, which they refer to as the “Complementary Model,” Monte Carlo (MC) simulations are used to evaluate the free-energy contribution associated with forming the head-shell region of the micelle, and MT theory is used to calculate the free-energy contribution associated with forming the micelle core. The core of the micelle is modeled in the same way as in the traditional MT model, except that the core radius is assumed to correspond only to the core region where no solubilizates are present. The extent of penetration of Sal^- into the micelle core was determined by Mohanty et al. by performing isobaric MC simulations (constant NPT) of an entire spherical micelle, or of a section of a cylindrical micelle, having various CTAB and Sal^- compositions. The core region of the micelle was defined as the spherical, or the cylindrical, region around the aggregate center that had zero concentration of salicylate counterions. The head-shell region of the micelle was defined as the remaining portion of the micelle, which contained a high concentration of CTA^+ heads, Sal^- counterions, and two CH_2 groups in the cetyl alkyl chain. It is important to note that to reduce computational expense, Mohanty et al. used a mean-field approach to model water and the counterions. The free-energy contribution associated with the head-shell region was calculated with respect to a pure CTA^+ head shell through the use of semi-grand-canonical (constant N_{tot} , P , T , and μ_{Sal^-}) MC simulation. The free energy of the head-shell region was added to that of the core region to obtain g_{mic} , or the free-energy change associated with transferring the surfactant monomers and the Sal^- counterions from bulk aqueous solution to the micelle head-shell region. The computed value of g_{mic} was then combined with a thermodynamic description of self-assembly to predict the CMC, the micelle shape, the micelle aggregation number, and the degree of counterion binding.

Pool et al. recently described the use of a computer simulation approach to

calculate g_{form} as a function of aggregation number using free-energy methods [2]. In their approach, MC simulation was conducted in a semi-grand ensemble (constant $N_{\text{tot}}PT\mu$) in which solvent and surfactant molecules were exchanged. Configurational bias MC was used to improve insertion probability, and surfactants were only inserted in the region adjacent to the simulated micelle to improve acceptance statistics. Iso-baric hybrid MC was used to efficiently reach thermal equilibrium. Determination of the CMC was facilitated by using umbrella sampling to obtain statistically significant results in unlikely regions of the micelle size distribution. Pool et al. conclude that their approach is more computationally efficient than identification of the CMC by direct simulation of surfactant self-assembly. Although, to date, this computer simulation approach has been implemented only to estimate the CMC for simple Lennard Jones surfactants, Pool et al. assert that their simulation approach opens up the way to perform similar calculations using a realistic, atomistic-level forcefield.

The remainder of this chapter is organized as follows. In Section 9.2, an overview of the CS-FE/MT modeling approach is presented, including a description of the inputs and outputs of the model. In Section 9.3, a thermodynamic framework is developed to enable predictions of micellar solution properties using the free-energy values obtained in CS-FE/MT modeling. Although presented in the context of modeling two-component micelles (binary surfactant micellization and micellar solubilization), the framework presented in Section 9.3 may be generalized in a straightforward manner to describe the micellization and micellar solubilization behavior of n -component systems. In Section 9.4, an introduction to computer simulation free-energy methods is presented, including an introduction to the approach used in the CS-FE/MT model to determine the free-energy change associated with changing micelle composition. In Section 9.5, a description of the free-energy calculations made in the context of the CS-FE/MT model is presented.

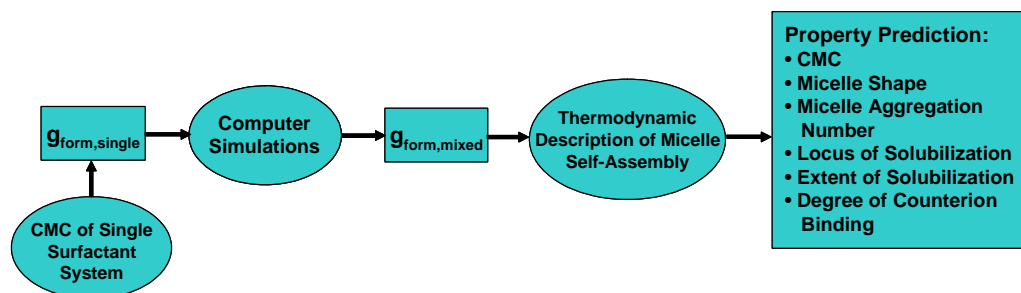


Figure 9-1: Computational strategy used in the CS-FE/MT model.

9.2 Overview of the CS-FE/MT Modeling Approach

The proposed CS-FE/MT model is a hybrid approach in which computer simulations are used to find the free-energy change associated with changing micelle composition from a single (pure) surfactant micelle reference state. A flowchart outlining the computational approach applied in the CS-FE/MT model is shown in Figure 9-1.

As shown in Figure 9-1, the CMC of a single surfactant system is taken as the starting point for the CS-FE/MT model. This CMC may be determined experimentally or predicted using the MT model. In the next step shown in Figure 9-1, the CMC is converted to the free energy associated with single surfactant micelle formation ($g_{\text{form,single}}$). Next, computer simulations are used to find the free-energy change associated with changing the micelle composition. When added to $g_{\text{form,single}}$, the computer simulation result enables determination of the free energy associated with mixed micelle formation ($g_{\text{form,mixed}}$). The computed value of $g_{\text{form,mixed}}$ is then used in a thermodynamic description of micelle self-assembly to make predictions of all relevant micellization properties, including the CMC, the micelle shape, the micelle aggregation number, the locus and the extent of solubilization, and the degree of counterion binding.

Direct computer simulation determination of g_{form} using free-energy methods is very computationally expensive (requiring months of simulation time on today's computers) [2]. In contrast, using MT modeling it is possible to predict g_{form} with very little computational expense (requiring only seconds using today's computers). However, the traditional MT model is capable of making quantitatively or semi-quantitatively accurate predictions of g_{form} only for relatively simple surfactants and solubilizates. It was hoped that the CS-FE/MT modeling approach, by combining an experimental or an MT value of $g_{\text{form, single}}$ with computer simulation free-energy methods to find the free-energy change associated with changing micelle composition, would enable evaluation of $g_{\text{form, mixed}}$ in a computationally efficient way. Furthermore, it was hoped that successful implementation of the CS-FE/MT model would: (i) improve our fundamental understanding of multicomponent surfactant micellization and of micellar solubilization phenomena by providing additional insight into the thermodynamics associated with changes in micelle composition, and (ii) advance the current state-of-the-art in computer simulation free-energy methods. To the best of our knowledge, the CS-FE/MT modeling approach presented here represents the first attempt to evaluate the free energy associated with mixed micelle formation using atomistic-level computer simulations.

9.3 Formulation of the Thermodynamic Framework Used in the CS-FE/MT Model

A thermodynamic framework to describe single and mixed surfactant systems in the context of traditional MT modeling has been described in detail elsewhere [3,4]. Here, nevertheless, the essential elements of this framework are briefly reviewed to provide the proper context to understand the CS-FE/MT model. The thermodynamic framework described in this section is formulated in the context of two-component surfactant micellization and two-component micellar solubilization. To simplify notation, the thermodynamic framework is formulated only for nonionic surfactants and solu-

bilizates. However, the framework can be reformulated in a straightforward manner to describe n -component surfactant micellization and micellar solubilization, as well as the micellization and micellar solubilization of ionic surfactants and solubilizates. As discussed in Section 9.2, in the CS-FE/MT modeling approach, the free-energy change associated with changing the composition of a single (pure) surfactant micelle is evaluated using computer simulations. Throughout the remainder of this section, the surfactant present in the single surfactant micelle is denoted as component A , and the surfactant or solubilizate that is added through computer simulation is denoted as component B .

At thermodynamic equilibrium, the chemical potential of a micelle of aggregation number n and composition α ($\mu_{n\alpha}$) can be related to the the chemical potential of the monomers of component A (μ_A) and of component B (μ_B) in bulk aqueous solution as follows:

$$n_A\mu_A + n_B\mu_B = \mu_{n\alpha} \quad (9.1)$$

where n_A is the number of component A molecules in the micelle, n_B is the number of component B molecules in the micelle, n is equal to $n_A + n_B$, and $\alpha = n_A/n$. Each chemical potential appearing in Eq. 9.1 can be expressed as follows:

$$\mu_i = \mu_i^{\circ} + k_B T \ln(a_i) \quad (9.2)$$

where μ_i° is the standard-state chemical potential of component i , where the standard state is infinite dilution in the bulk aqueous solution, k_B is Boltzmann's constant, T is the absolute temperature, and a_i is the activity of component i in the aqueous solution. Because the CS-FE/MT model will only be used to model micellization and micellar solubilizate at low monomer and micelle concentrations, the term $\ln(a_i)$ in Eq. 9.2 may be replaced by $\ln(X_i)$, where X_i is the mole fraction of component i in the aqueous solution.

Substituting the expression for μ_i given in Eq. 9.2 for each component i in Eq.

9.1 yields the following expression:

$$n_A[\mu_A^\circ + k_B T \ln(X_A)] + n_B[\mu_B^\circ + k_B T \ln(X_B)] = n[\mu_{n\alpha}^\circ + k_B T \ln(X_{n\alpha})] \quad (9.3)$$

which can be rearranged as follows:

$$X_{n\alpha} = X_{1A}^{n_A} X_{1B}^{n_B} \exp\left[-\frac{G_{\text{form}}}{k_B T}\right] \quad (9.4)$$

where $G_{\text{form}} = \mu_{n\alpha}^\circ - n_A \mu_A^\circ - n_B \mu_B^\circ$, and represents the total free-energy change associated with transferring component A and B monomers from their standard states in bulk aqueous solution to form a micelle of aggregation number n and composition α . Eq. 9.4 can be reformulated in terms of α as follows:

$$X_{n\alpha} = \left(\frac{X_1 X_{1A}}{X_1}\right)^{\alpha n} \left(\frac{X_1 X_{1B}}{X_1}\right)^{(1-\alpha)n} \exp\left[-\frac{G_{\text{form}}}{k_B T}\right] \quad (9.5)$$

$$= X_1^{\alpha n} \alpha_1^{\alpha n} X_1^{(1-\alpha)n} (1 - \alpha_1)^{(1-\alpha)n} \exp\left[-\frac{G_{\text{form}}}{k_B T}\right] \quad (9.6)$$

where $\alpha n = n_A$, $(1 - \alpha)n = n_B$, $\alpha_1 = X_{1A}/X_1$, and $(1 - \alpha_1) = X_{1B}/X_1$, where α_1 is the monomer composition. Equation 9.6 can be rearranged to move the entropic free-energy contribution associated with the composition of the monomeric phase ($\alpha_1^{\alpha n} (1 - \alpha_1)^{(1-\alpha)n}$) into the Boltzmann factor as follows:

$$X_{n\alpha} = X_1^n \exp\left[-\frac{G_{\text{form}}}{k_B T} + \alpha n \ln \alpha_1 + (1 - \alpha)n \ln(1 - \alpha_1)\right] \quad (9.7)$$

or

$$X_{n\alpha} = X_1^n \exp\left[-\frac{G_f}{k_B T}\right] \quad (9.8)$$

where $G_f = G_{\text{form}} - k_B T[\alpha n \ln \alpha_1 + (1 - \alpha)n \ln(1 - \alpha_1)]$ and is referred to as the modified free energy of mixed micellization [5]. Note that in Chapter 2, G_{form} was expressed as an intensive quantity (on a per surfactant molecule basis) and was denoted as g_{form} . In this chapter, intensive free-energy contributions are represented with a

lower-case g , and extensive free-energy contributions are represented with an upper-case G . The free-energies G_f and G_{form} in Eqs. 9.7 and 9.8, respectively, are given as extensive quantities because it is most intuitive to develop the CS-FE/MT model on an extensive basis.

In the traditional MT model, G_{form} is modeled as a series of reversible steps, each of which is computed molecularly based on the chemical structures of components A and B . This series of steps was reviewed in detail in Chapter 4. In the traditional MT model, G_f is computed using the following expression:

$$G_f = n [g_{\text{tr}} + g_{\text{int}} + g_{\text{pack}} + g_{\text{st}} + g_{\text{elec}} + g_{\text{ent}}] - k_B T [\alpha n \ln \alpha_1 + (1 - \alpha) n \ln(1 - \alpha_1)] \quad (9.9)$$

where each of the six free-energy contributions appearing in Eq. 9.9, whose sum is equal to g_{form} introduced in Chapter 4, is multiplied by n because they are expressed on a per surfactant molecule basis.

In the CS-FE/MT model, in contrast, G_f is formulated in terms of variables which can be determined through computer simulation. In the CS-FE/MT modeling approach, computer simulations are used to find the free-energy change associated with exchanging molecules of component A with molecules of component B . This free-energy change will be referred to hereafter as $\Delta\Delta G_i$, where $\Delta\Delta G_i$ is the free-energy change associated with the i th exchange of component B with component A , and i is an index which ranges from 1 to $n_B = n(1 - \alpha)$ (the number of component B molecules in the micelle). The free-energy change is referred to as $\Delta\Delta G_i$ rather than as ΔG_i because (as will be discussed in Section 9.5), in implementing the CS-FE/MT model, exchanging molecules of component A with molecules of component B in the micelle also requires a corresponding transformation in bulk aqueous solution, and it is the difference between these two transformation free energies that is used in CS-FE/MT modeling. Accordingly, G_f is computed using the following expression:

$$G_f = G_{\text{form, single}}(\alpha = 0) + \sum_{i=1}^{n(1-\alpha)} \Delta\Delta G_i + G_{\text{ent1}} + G_{\text{ent}} \quad (9.10)$$

or

$$G_f = G_{\text{form,mixed}} + G_{\text{ent1}} + G_{\text{ent}} \quad (9.11)$$

where $G_{\text{form,single}}(\alpha = 0)$ is equal to $n \cdot g_{\text{form,single}}$ (see Figure 9-1), and is determined from the experimental CMC value or is computed using the traditional MT model, $G_{\text{form,mixed}}$ is equal to $n \cdot g_{\text{form,mixed}}$ (see Figure 9-1), $G_{\text{ent1}} = -k_B T[\alpha n \ln \alpha_1 + (1 - \alpha)n \ln(1 - \alpha_1)]$ and represents the entropic contribution to G_f associated with the monomer composition, and $G_{\text{ent}} = -k_B T[\alpha n \ln \alpha + (1 - \alpha)n \ln(1 - \alpha)]$ and represents the entropic contribution to G_f associated with the micelle composition. Note that the free-energy contribution G_{ent} must be included because all molecules modeled during a MD computer simulation are distinguishable; hence, the entropic effect associated with changing n indistinguishable (identical) molecules of component A into n_A molecules of component A and n_B molecules of component B , where molecules of type A are distinguishable from molecules of type B , gives rise to an entropy of mixing free-energy contribution that is not accounted for in the computer simulation result for $\Delta\Delta G_i$. Therefore, by adding G_{ent} to G_f , this entropy of mixing free-energy contribution is accounted for. A detailed description of the manner in which $\Delta\Delta G_i$ is obtained using computer simulations is presented in Section 9.4.

To use the CS-FE/MT model to make predictions of surfactant solution properties, an iterative procedure is required to determine the optimum (minimum) value of G_f , which we denote hereafter as G_f^* . From G_f^* , the surfactant solution properties of interest can be obtained. For example, the size and composition of the micelles that will be observed experimentally are determined as the size and composition of the micelles that yield the optimal value of G_f , or G_f^* . In addition, the CMC can be estimated using the expression $\exp(G_f^*/nk_B T)$. The sequence of steps that are required to implement the CS-FE/MT model include:

1. Guess a value of α_1 .
2. At the specified value of α_1 , solve for the value of α that yields the minimum value of G_f (or equivalently, solve for the value of α that yields the maximum

- value of $X_{n\alpha}$, see Eq. 9.8). This value of α represents the most thermodynamically favorable micelle composition at the specified value of α_1 .
3. After solving for the optimal value of α at the specified value of α_1 , update α_1 by evaluating Eq. 9.7 with the current estimate of G_f and by solving a mass balance for the solution [6, 7]. The implementation of this mass balance has been discussed by previous researchers in the context of the traditional MT modeling approach [3, 4, 6, 7].
 4. Repeat steps 2 and 3 until the value of α_1 becomes constant.
 5. Compute G_f^* using Eq. 9.11.

For reasons that will be discussed in detail in Section 9.4, steps 1 to 5 outlined above are sufficient to determine the optimal aggregation number for a cylindrical or a discoidal micelle because the value of l_c (the core-minor radius of a cylindrical micelle or the half width of a bilayer) is free to come to an equilibrium value at any micelle composition given the $N\gamma T$ (constant N , interfacial tension, and T) periodic boundary conditions that are applied during simulation. On the other hand, to determine the optimal value of l_c for spherical micelles, the iterative procedure outlined above must be modified slightly to permit changes in the aggregation number (because l_c for spherical micelles can only change if the aggregation number changes). In Step 1, a value must be guessed for both α_1 and n . In Step 2, the computer simulation procedure used to compute $\Delta\Delta G_i$ must be modified to evaluate the free-energy change associated with exchanging one component A molecule with one component B molecule (a process that keeps n constant), one component A molecule with two component B molecules (a process that increases that value of n), and two component A molecules with one component B molecule (a process that decreases the value of n). By evaluating the free-energy change associated with these three exchanges, Eq. 9.11 can be used to solve for G_f for the optimal value of α and n associated with a specified value of α_1 . In Step 3, α_1 would be updated by solving a mass balance

for the solution. In Step 4, Steps 2 and 3 would be repeated until the value of α_1 becomes constant, and in Step 5, G_f^* would be computed using Eq. 9.11.

To reduce the computational expense associated with determining the optimal value of α (Step 2 of the iterative procedure outlined above), it may be possible to express $\Delta\Delta G_i$ as an analytical function of α . If the dependence of $\Delta\Delta G_i$ on α is found to be smooth and monotonic, it may be necessary to perform only a few exchanges of molecules of component A with molecules of component B to determine the dependence of $\Delta\Delta G$ on α . Once this dependence is determined, identifying the value of α that minimizes G_f in Eq. 9.11 may be accomplished by taking the derivative of Eq. 9.11 with respect to α , and solving for the value of α for which the derivative is equal to zero. Specifically,

$$\frac{\partial G_f}{\partial \alpha} = \frac{\partial \left(\sum_{i=1}^{n(1-\alpha)} \Delta\Delta G_i(\alpha) \right)}{\partial \alpha} + \frac{\partial G_{\text{ent}1}}{\partial \alpha} + \frac{\partial G_{\text{ent}}}{\partial \alpha} = 0 \quad (9.12)$$

9.4 Introduction to Computer Simulation Free-Energy Methods

Calculation of free-energy changes for physical and chemical systems is one of the most important applications of computer simulations. All molecular behavior, from the self-assembly of surfactants to form micelles to protein-ligand binding, can be directly linked to free energy and free-energy changes. Consequently, an accurate computer simulation approach to determine free energy and free-energy changes would allow the prediction of any molecular property of interest. Computer simulation estimates of free energy have been made in many different contexts, including protein folding [8], protein stability [9], enzyme reaction paths [10], ligand binding [11], ion transport [12], solvation processes [13,14], and conformational equilibria [15]. In this section, I discuss methods for the evaluation of free-energy differences (Section 9.4.1),

as well as the thermodynamic integration free-energy method (Section 9.4.2).

9.4.1 Methods for the Evaluation of Free-Energy Differences

There are only two methods which may be used to determine the free-energy difference between two states I and II from either experiment or computer simulation: (i) evaluation of the probability of finding the system in state I or state II, and (ii) evaluation of the reversible work required to move from state I to state II [?]. Free energy perturbation and thermodynamic integration are two of the most generally applicable and accurate free-energy methods developed to date [16]. In free energy perturbation, the free-energy difference between two states is evaluated with approach (i), while in thermodynamic integration, it is evaluated with approach (ii). The equations involved in free energy perturbation and thermodynamic integration are exact [16], and the two methods yield the same solution in the limit of infinite sampling of phase space (coordinate and momentum space) [17]. However, a number of other methods have been developed to estimate free-energy differences, including quantum mechanical methods [18–20], Poisson-Boltzmann based continuum methods [21, 22], integral equation methods [23–25], and linear response theory [26–28]. Quantum mechanical methods can be used to determine free-energy changes only for very small systems because of the computational expense associated with solving Schrödinger’s equation. To model larger systems, quantum mechanical methods must be combined with molecular dynamics simulations [29, 30]. Poisson-Boltzmann based continuum methods are relatively computationally inexpensive, but because they do not model the solvent explicitly, they are approximate and are not well-suited for capturing the free-energy changes involved in hydrophobic interactions [28]. Integral equation methods [31] and linear response theory [26–28] also involve a number of approximations, and linear response theory requires parameterization for specific systems.

With the above in mind, we have chosen thermodynamic integration as the free-energy method to implement the CS-FE/MT model because we expect it to be well

sited for determining the free-energy changes involved in changing micellar composition. Because surfactant micellization and micellar solubilization are driven by the hydrophobic effect, explicit simulation of water molecules is expected to be necessary to accurately predict G_f^* . As a result, continuum free-energy methods are not suitable. Similarly, integral equation methods and linear response theory are expected to be too approximate. Implementation of quantum mechanical methods would be much too computationally expensive, because explicit simulation of water implies that simulations of several thousand atoms will be required to implement the CS-FE/MT model. The thermodynamic integration method is discussed in detail in the next section.

9.4.2 Thermodynamic Integration

In thermodynamic integration, the free-energy difference between two states of a system is computed from the integrated work required to move from one state to the other along a reversible path [32]. The path between the two states may be physical or non-physical. In thermodynamic integration, the two states of the system are connected by an artificial coordinate referred to as the coupling parameter λ which ranges from 0 to 1 [33].

The Hamiltonian H of a molecular system describes the total energy of the system in terms of coordinates, \mathbf{q} , and their conjugated momenta, \mathbf{p} , (where the bolded variables denote vectorial quantities):

$$H(\mathbf{p}^N, \mathbf{q}^N) = \sum_{i=1}^N \frac{\mathbf{p}_i^2}{2m_i} + V(\mathbf{q}^N) \quad (9.13)$$

where $\mathbf{p}^N \equiv (\mathbf{p}_1, \mathbf{p}_2, \dots, \mathbf{p}_N)$ represents the momenta of each of the N atoms, $\mathbf{q}^N \equiv (\mathbf{q}_1, \mathbf{q}_2, \dots, \mathbf{q}_N)$ represents the coordinates of the N atoms, m_i is the mass of atom i , and $V(\mathbf{q}^N)$ is the potential energy function, which depends on the coordinates of each atom in the system [34].

In thermodynamic integration, the Hamiltonian (which includes the kinetic energy,

$K(\mathbf{p}^N) = \sum_{i=1}^N \frac{\mathbf{p}_i^2}{2m_i}$, and the potential energy, $V(\mathbf{q}^N)$, is made an analytical function of λ as follows:

$$H(\mathbf{p}^N, \mathbf{q}^N, \lambda) = K(\mathbf{p}^N, \lambda) + V(\mathbf{q}^N, \lambda) \quad (9.14)$$

such that $H_{\text{I}} = H(\mathbf{p}^N, \mathbf{q}^N, \lambda = 0)$ and $H_{\text{II}} = H(\mathbf{p}^N, \mathbf{q}^N, \lambda = 1)$, where the Hamiltonians H_{I} and H_{II} characterize states I and II.

For the isothermal, isobaric systems that are simulated in the CS-FE/MT modeling approach, the partition function, Ξ , can be expressed as a function of λ as follows [35]:

$$\Xi(\lambda) = \frac{1}{h^{3N} N!} \iiint \exp \left\{ -\frac{H(\mathbf{p}^N, \mathbf{q}^N, \lambda) + PV}{k_{\text{B}}T} \right\} dV d\mathbf{p}^N d\mathbf{q}^N \quad (9.15)$$

where h is Planck's constant, $H(\lambda)$ is the λ -dependent Hamiltonian, P is the pressure, and V is the volume.

The Gibbs free energy can be expressed as a function of this partition function as follows:

$$G(\lambda) = -k_{\text{B}}T \ln \Xi(\lambda) \quad (9.16)$$

Differentiation of $G(\lambda)$ with respect to λ results in the following expression:

$$\begin{aligned} \frac{\partial G(\lambda)}{\partial \lambda} &= -\frac{k_{\text{B}}T}{\Delta(\lambda)} \left[\frac{\partial \Delta(\lambda)}{\partial \lambda} \right] \quad (9.17) \\ &= \frac{\iiint (\partial H(\mathbf{p}^N, \mathbf{q}^N, \lambda) / \partial \lambda) \exp\{-[H(\mathbf{p}^N, \mathbf{q}^N, \lambda) + PV/k_{\text{B}}T]\} dV d\mathbf{p}^N d\mathbf{q}^N}{\iiint \exp\{-[H(\mathbf{p}^N, \mathbf{q}^N, \lambda) + PV/k_{\text{B}}T]\} dV d\mathbf{p}^N d\mathbf{q}^N} \\ &= \left\langle \frac{\partial H(\lambda)}{\partial \lambda} \right\rangle_{\lambda} \quad (9.18) \end{aligned}$$

where $\langle \partial H(\lambda) / \partial \lambda \rangle_{\lambda}$ represents the ensemble average of the quantity $\partial H(\lambda) / \partial \lambda$ at a specific value of λ . Equation 9.18 is referred to as the thermodynamic integration formula [33]. The ensemble average given in Eq. 9.18 can be obtained directly through molecular simulation results and used to determine the free-energy difference

between two states:

$$\Delta G = G(\lambda = 1) - G(\lambda = 0) = \int_0^1 \left[\frac{\partial G(\lambda)}{\partial \lambda} \right]_{\lambda} d\lambda = \int_0^1 \left\langle \frac{\partial H(\lambda)}{\partial \lambda} \right\rangle_{\lambda} d\lambda \quad (9.19)$$

In Cartesian coordinates, the kinetic energy term in the Hamiltonian ($K(\mathbf{p}^N, \lambda)$ in Eq. 9.14) depends only on \mathbf{p}^N , and therefore, can be separately integrated and eliminated from Eq. 9.19. If the masses of the simulated atoms are not altered during simulation, the kinetic energy makes no contribution to ΔG . However, if the masses are altered, the contribution to ΔG is given by $-\frac{3}{2}k_B T \ln(\frac{m_{\text{II}}}{m_{\text{I}}})$ (in the absence of constraints), where m_{I} is the mass in state I and m_{II} is the mass in state II [34]. Upon elimination of the kinetic-energy contribution, Eq. 9.19 can be expressed as follows:

$$\Delta G = G(\lambda = 1) - G(\lambda = 0) = \int_0^1 \left\langle \frac{\partial V(\lambda)}{\partial \lambda} \right\rangle_{\lambda} d\lambda \quad (9.20)$$

where $H(\lambda)$ is now replaced by $V(\lambda)$, which is the potential energy function expressed as a function of the coupling parameter λ .

In multiconfiguration thermodynamic integration (MCTI), ΔG is evaluated numerically from $\langle \partial V(\lambda)/\partial \lambda \rangle_{\lambda}$ results gathered at discrete values of lambda, as follows [35]:

$$\Delta G = \sum_i \left\langle \frac{\partial V(\lambda)}{\partial \lambda} \right\rangle_{\lambda} \Delta \lambda_i \quad (9.21)$$

On the other hand, in single-configuration thermodynamic integration (SCTI), the approximation is made that the sum over ensemble averages can be replaced by the sum over single configuration values of the $\partial V(\lambda)/\partial \lambda$ derivative [35]:

$$\Delta G = \sum_i \left(\frac{\partial V(\lambda)}{\partial \lambda} \right)_{\lambda} \Delta \lambda_i \quad (9.22)$$

9.5 Free-Energy Calculations Made in the CS-FE/MT Model

As discussed in Section 9.3, the starting point for the CS-FE/MT model is a micelle containing only surfactant (component) A . The free-energy change associated with exchanging molecules of surfactant A with molecules of a cosurfactant or solubilizate (component) B , or $\Delta\Delta G_i$, must be determined through computer simulation, where $\Delta\Delta G_i$ refers to the free-energy change associated with the i th exchange of component A with component B . As discussed in Section 9.4.2, thermodynamic integration will be used to compute $\Delta\Delta G_i$. To implement thermodynamic integration, a free-energy pathway must be chosen to move between state I and state II. The free-energy pathway that was selected to implement the CS-FE/MT model was inspired by a thermodynamic cycle that has proven useful in performing substrate-enzyme binding calculations in aqueous media.

In Figure 9-2A, we present a typical thermodynamic cycle used to find the difference in binding free energies between two different substrates and an enzyme, or $\Delta\Delta G_{\text{bind}}$. Experimentally, the difference in binding free energies for the two substrates can be determined by measuring the free energies $G_{\text{bind},1}$ and $G_{\text{bind},2}$ associated with the physical binding processes represented by the two horizontal arrows. $\Delta\Delta G_{\text{bind}}$ would then simply be evaluated as $G_{\text{bind},2} - G_{\text{bind},1}$. However, computer simulation determinations of $G_{\text{bind},1}$ and $G_{\text{bind},2}$ may be difficult for two reasons: (i) the process of bringing a substrate and an enzyme together may lead to conformational rearrangements of the substrate and/or the enzyme, which may require extended simulation time to adequately sample, and (ii) choosing an efficient reaction coordinate for binding can be difficult, and the free-energy changes experienced along this coordinate may require significant sampling in order to converge. Even if conformational rearrangements of the substrate and/or the enzyme do not occur, many of the water molecules associated with the substrate and the enzyme in the bulk aqueous state must be displaced for binding to occur, which may require significant computational

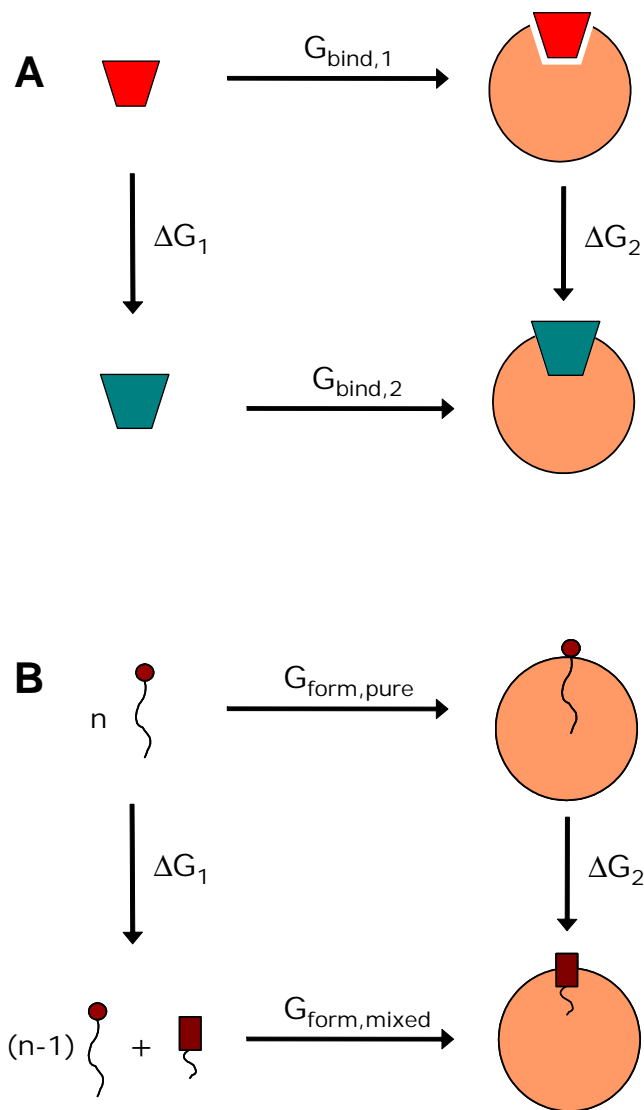


Figure 9-2: Comparison of alchemical pathways used to determine $\Delta\Delta G$ for substrate-enzyme binding (A), and for composition change in a micelle (B).

expense to sample adequately.

Instead of following the physical pathways represented by the two horizontal arrows labeled $G_{\text{bind},1}$ and $G_{\text{bind},2}$ in Figure 9-2A, it is much more computationally efficient in practice to determine the free-energy changes associated with the non-physical processes ΔG_1 and ΔG_2 , as represented by the vertical arrows in Figure 9-2A [16]. Note that ΔG_1 represents the free-energy change associated with chemically modifying a substrate in aqueous solution, and ΔG_2 represents the free-energy change associated with chemically modifying a substrate that is bound to an enzyme in aqueous solution. In contrast to the two physical processes associated with the free-energy changes $G_{\text{bind},1}$ and $G_{\text{bind},2}$, the non-physical processes associated with the free-energy changes ΔG_1 and ΔG_2 typically: (i) do not involve significant conformational rearrangements of the substrate and/or the enzyme, (ii) do not require the definition of a reaction coordinate, and (iii) do not require displacement of large numbers of water molecules, thus greatly reducing the computational expense associated with making accurate free-energy estimates [16]. Since the thermodynamic cycle in Figure 9-2A satisfies: $G_{\text{bind},1} + \Delta G_2 - G_{\text{bind},2} - \Delta G_1 = 0$, it follows that $\Delta\Delta G_{\text{bind}} = G_{\text{bind},2} - G_{\text{bind},1} = \Delta G_2 - \Delta G_1$. In the limit of infinite sampling of phase space, the value of $\Delta\Delta G_{\text{bind}}$ computed as $G_{\text{bind},2} - G_{\text{bind},1}$ or as $\Delta G_2 - \Delta G_1$ are identical because free energy is a state function. Consequently, the computed free-energy difference does not depend on the reversible path taken to move from one state to the other. The type of unphysical path associated with the evaluation of ΔG_1 or ΔG_2 is referred to as an “alchemical” path or as “computer alchemy” because of the chemical transformations involved [36, 37].

The thermodynamic cycle proposed for use in the CS-FE/MT model of micellization or micellar solubilization is shown in Figure 9-2B. Determining the free-energy changes associated with transferring a surfactant A molecule from aqueous solution to the micellar environment, or with transferring a surfactant/solubilizate B molecule from aqueous solution to the micellar environment, are expected to require long simulation times to give accurate free-energy estimates because such transi-

tions involve: (i) structural rearrangements within the micelle, and (ii) significant rearrangement of the water molecules surrounding the surfactant or solubilizate and the micelle. Therefore, we propose an alternative path involving alchemical transformations, as shown by the two non-physical processes ΔG_1 and ΔG_2 in Figure 9-2B. Note that ΔG_1 represents the free-energy change associated with chemically modifying one surfactant A molecule (represented by the brown circular head) into a surfactant/solubilizate B molecule (represented by the brown rectangular head) in aqueous solution, and ΔG_2 represents the free-energy change associated with chemically modifying a surfactant A molecule into a surfactant/solubilizate B molecule in a simulated micelle. Since the thermodynamic cycle in Figure 9-2B satisfies: $G_{\text{form,single}} + \Delta G_2 - G_{\text{form,mixed}} - \Delta G_1 = 0$, it follows that $\Delta\Delta G = G_{\text{form,mixed}} - G_{\text{form,single}} = \Delta G_2 - \Delta G_1$.

To compute the free-energy differences involved in the thermodynamic cycle shown in Figure 9-2B, computer simulations of surfactant to cosurfactant, or surfactant to solubilizate, transformations must be conducted in bulk aqueous solution and in a micellar environment. Because differences in Gibbs free energy are being computed, all bulk aqueous solution simulations should be conducted in the NPT ensemble [34]. When implementing the CS-FE/MT model to determine G_{f}^* for spherical micelles, simulations in the micellar environment will also be conducted in the NPT ensemble. However, when implementing the CS-FE/MT model to determine G_{f}^* for cylindrical or discoidal micelles, simulation in the NPT ensemble in the micellar environment is not appropriate because only a “slice” of an infinite cylinder or a “plug” of an infinite bilayer are simulated. The appropriate boundary condition to use parallel to the axis of a cylindrical micelle, or parallel to the surface of a bilayer, during micellar simulation is a surface tension that provides a post-equilibration value of area per surfactant/solubilizate head that is similar to the area that would be observed experimentally [38]. Therefore, for cylindrical and discoidal micelles, simulation in the $N\gamma T$ ensemble is required, where γ is the appropriate surface tension (see additional discussion in Chapters 4 and 6).

9.6 Conclusions

In this chapter, a theoretical approach was introduced to use computer simulation free-energy methods to evaluate the free-energy change associated with changing micelle composition (as reflected in $\Delta\Delta G_i$). In this approach, experimental CMC data, or the traditional MT model, is first used to evaluate the free energy associated with single (pure) surfactant micelle formation, $g_{\text{form, single}}$, where the single surfactant micelle contains only surfactant A molecules. An iterative approach was proposed to combine the estimated value of $G_{\text{form, single}}$ with free-energy computer simulation estimates of $\Delta\Delta G_i$ to determine the optimal free energy of mixed micelle formation, the optimal micelle aggregation number and composition, and the optimal bulk solution composition. A variety of free-energy methods were briefly reviewed, and the selection of the thermodynamic integration free-energy method was justified for implementing the CS-FE/MT model and subsequently discussed in some detail. An alchemical free-energy pathway was proposed to allow evaluation of the free-energy change associated with exchanging a surfactant A molecule with a surfactant/solubilizate B molecule through thermodynamic integration. In Chapter 10, the implementation of the CS-FE/MT model to make predictions of surfactant micellization and micellar solubilization for several surfactant/solubilizate systems will be discussed, and the predictions of the CS-FE/MT model will be compared with the predictions of the traditional MT model as well as with appropriate experimental data.

Bibliography

- [1] Mohanty, S., Davis, H. T., and McCormick, A. V., “Complementary use of simulations and free energy models for CTAB/NaSal systems,” *Langmuir*, Vol. 17, 2001, pp. 7160–7171.
- [2] Pool, R. and Bolhuis, P. G., “Accurate free energies of micelle formation,” *The Journal of Physical Chemistry B*, Vol. 109, 2005, pp. 6650–6657.
- [3] Shiloach, A. and Blankschtein, D., “Predicting micellar solution properties of binary surfactant mixtures,” *Langmuir*, Vol. 14, 1998, pp. 1618–1636.
- [4] Puvvada, S. and Blankschtein, D., “Molecular thermodynamic approach to predict micellization, phase behavior and phase separation of micellar solutions. 1. Application to nonionic surfactants,” *The Journal of Chemical Physics*, Vol. 92, 1990, pp. 3710–3724, and references cited therein.
- [5] Goldsipe, A. and Blankschtein, D., “Modeling counterion binding in ionic-nonionic and ionic-zwitterionic binary surfactant mixtures,” *Langmuir*, Vol. 22, 2005, pp. 9850–9865.
- [6] Srinivasan, V. and Blankschtein, D., “Effect of counterion binding on micellar solution behavior: 1. Molecular-thermodynamic theory of micellization of ionic surfactants,” *Langmuir*, Vol. 19, 2003, pp. 9932–9945.
- [7] Srinivasan, V., *Theoretical Modeling of Micellization and Solubilization in Ionic Surfactant Systems*, Ph.D. thesis, Massachusetts Institute of Technology, 2003, and references cited therein.

- [8] Roux, B. and Karplus, M., “Ion transport in a gramicidin-like channel: Structure and thermodynamics,” *Biophysical Journal*, Vol. 59, 1991, pp. 961–981.
- [9] Tidor, B. and Karplus, M., “Simulation analysis of the stability mutant R96H of T4 lysozyme,” *Biochemistry*, Vol. 30, 1991, pp. 3217–3228.
- [10] Schweins, T., Langen, R., and Warshel, A., “Why have mutagenesis studies not located the general base in ras p21?” *Nature Structural Biology*, Vol. 1, 1994, pp. 476–484.
- [11] Kollman, P., “Free energy calculations: Applications to chemical and biochemical phenomena,” *Chemical Reviews*, Vol. 93, 1993, pp. 2395.
- [12] Gao, J., Kuczera, K., Tidor, B., and Karplus, M., “Hidden thermodynamics of mutant proteins: A molecular dynamics analysis,” *Science*, Vol. 244, 1989, pp. 1069–1072.
- [13] Miller, J. L. and Kollman, P. A., “Solvation free energies of the nucleic acid bases,” *The Journal of Physical Chemistry*, Vol. 100, 1996, pp. 8587.
- [14] Henchman, R. H. and Essex, J. W., “Free energies of hydration using restrained electrostatic potential derived charges via free energy perturbations and linear response,” *Journal of Computational Physics*, Vol. 20, 1998, pp. 499.
- [15] Koichi, T. and Shimizu, K., “Molecular dynamics simulations in aqueous solution: Application to the free energy calculation of oligopeptides,” *The Journal of Physical Chemistry B*, Vol. 102, 1998, pp. 6419.
- [16] Pearlman, D. A. and Rao, B. G., *Free Energy Calculations: Methods and Applications*, John Wiley & Sons, Ltd., New York, 1998.
- [17] Danciulescu, C., *Investigation of the relative conformational stability of protein mutants by molecular dynamics simulation*, Ph.D. thesis, Rheinisch-Westfälischen Technischen Hochschul Aachen zur Erlangung, 2004.

- [18] Schaefer III, H. F., editor, *Modern Theoretical Chemistry. Vol. 3: Method of Electronic Structure Theory*, Plenum, 1977.
- [19] Schaefer III, H. F., editor, *Modern Theoretical Chemistry. Vol. 4: Method of Electronic Structure Theory*, Plenum, 1977.
- [20] Segal, G., editor, *Modern Theoretical Chemistry. Vols. 7-8: Semiempirical Methods of Electronic Structure Calculation*, Plenum, 1977.
- [21] Gilson, M., Sharp, K. A., and Honig, B., “Calculating the electrostatic potential of molecules in solution: Method and error assessment,” *Journal of Computational Chemistry*, Vol. 9, 1988, pp. 327–335.
- [22] Honig, B., Sharp, K. A., and Yang, A. S., “Macroscopic models of aqueous solutions: Biological and chemical applications,” *The Journal of Physical Chemistry*, Vol. 97, 1993, pp. 1101–1109.
- [23] Chandler, D. and Andersen, H. C., “Optimized cluster expansions for classical fluids. II. Theory of molecular liquids,” *The Journal of Chemical Physics*, Vol. 57, 1972, pp. 1930–1937.
- [24] Pettitt, B. M., Karplus, M., and Rossky, P. J., “Integral equation model for aqueous solvation of polyatomic solutes: Application to the determination of the free energy surface for the internal motion of biomolecules,” *The Journal of Physical Chemistry*, Vol. 90, 1986, pp. 6335–6345.
- [25] Yu, H. A., Roux, B., and Karplus, M., “Solvation thermodynamics: An approach from analytic temperature derivatives,” *The Journal of Chemical Physics*, Vol. 92, 1990, pp. 5020–5032.
- [26] King, G. and Barford, R., “Calculation of electrostatic free energy differences with a time-saving approximate method,” *The Journal of Physical Chemistry*, Vol. 97, 1993, pp. 8798–8802.

- [27] Aqvist, J., Medina, C., and Samuelsson, J. E., “A new method for predicting binding affinity in computer-aided drug design,” *Protein Engineering*, Vol. 7, 1994, pp. 385–391.
- [28] Dejaegere, A. and Karplus, M., “Analysis of coupling schemes in free energy simulations: A unified description nonbonded contributions to solvation free energies,” *The Journal of Physical Chemistry*, Vol. 100, 1996, pp. 11148–11164.
- [29] Field, M. J., Bash, P. A., and Karplus, M., “A combined quantum mechanical and molecular mechanical potential for molecular dynamics simulations,” *Journal of Computational Chemistry*, Vol. 11, 1990, pp. 700–733.
- [30] Gao, J. L. and Xia, X. F., “A priori evaluation of aqueous polarization effects through Monte Carlo QM-MM simulations,” *Science*, Vol. 258, 1992, pp. 631–635.
- [31] Kitao, A., Hirata, F., and Go, N., “Effects of solvent on the conformation and the collective motions of a protein. 3. Free energy analysis by the extended RISM theory,” *The Journal of Physical Chemistry*, Vol. 97, 1993, pp. 10231–10235.
- [32] van Gunsteren, W. F., Billeter, S. R., Eising, A. A., Hunenberger, P. H., Kruger, P., Mark, A. E., Scott, W. R. P., and Tironi, I. G., *Biomolecular Simulation: The GROMOS96 Manual and User Guide*, Hochschulverlag AG an der ETH Zurich, 1996.
- [33] van Gunsteren, W. F., Daura, X., and Mark, A. E., “Computation of free energy,” *Helvetica Chimica Acta*, Vol. 85, 2002, pp. 3113–3129.
- [34] van der Spoel, D., Lindahl, E., Hess, B., van Buuren, A., Apol, E., Meulenhoff, P., Tieleman, D., Sijbers, A., Feenstra, K., van Drunen, R., and Berendsen, H., *Gromacs User Manual version 3.2*, www.gromacs.org, 2004.
- [35] Straatsma, T. P. and McCammon, J. A., “Multiconfiguration thermodynamic integration,” *The Journal of Chemical Physics*, Vol. 2, 1991, pp. 1175–1188.

- [36] Zwanzig, R., “High-temperature equation of state by a perturbation method. I. Nonpolar gases,” *The Journal of Chemical Physics*, Vol. 22, 1954, pp. 1420.
- [37] Straatma, T. P. and McCammon, J. A., “Computational alchemy,” *Annual Review of Physical Chemistry*, Vol. 43, 1992, pp. 407–435.
- [38] Stephenson, B. C., Goldsipe, A., Beers, K. J., and Blankschtein, D., “Quantifying the hydrophobic effect: I. A computer simulation/molecular-thermodynamic model for the aqueous self-assembly of hydrophobic and amphiphilic solutes,” *The Journal of Physical Chemistry B*, 2006, pp. (submitted).

Chapter 10

Free-Energy Calculations Using Computer Simulation: Implementation and Results

In Chapter 9, the CS-FE/MT model, a theoretical approach that uses computer simulations to evaluate the free-energy change associated with changing micelle composition, was formulated. In the CS-FE/MT model, experimental CMC data or the traditional MT model is used to evaluate the free energy associated with single surfactant micelle formation, or $G_{\text{form,single}}$. An iterative approach is then used to combine the estimated value of $G_{\text{form,single}}$ with free-energy estimates obtained through computer simulation for the exchange of a surfactant of type A with a cosurfactant or solubilize of type B to determine the optimal micelle aggregation number, the optimal micelle and bulk solution composition, and the optimal free energy of mixed micelle formation, or $G_{\text{form,mixed}}$. In Chapter 9, the thermodynamic integration free-energy method was discussed, and an alchemical free-energy pathway was proposed to allow evaluation of the free energy associated with exchanging a surfactant molecule of type A with a surfactant/solubilize molecule of type B . This alchemical free-energy pathway is reviewed in Figure 10-1. In this chapter, the CS-FE/MT model is used to make predictions of the free-energy change associated with the alchemical transforma-

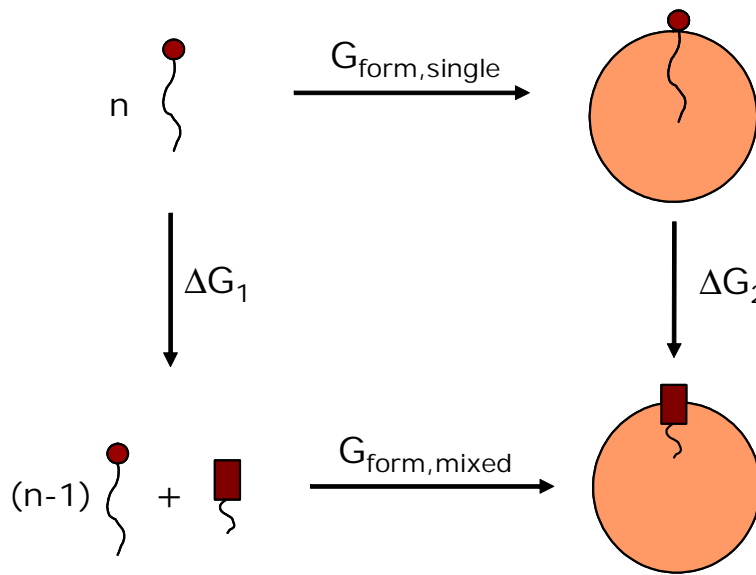


Figure 10-1: Alchemical free-energy pathway used in the CS-FE/MT model.

tion of several surfactants into cosurfactants or solubilizates. The systems selected for study include: sodium dodecyl sulfate (SDS)/ibuprofen (IBU) mixed micelles, octyl glucoside (OG)/*p*-aminobenzoate (PAB) mixed micelles, *n*-decyl dimethyl phosphine oxide (C₁₀PO)/*n*-decyl methyl sulfoxide (C₁₀SO) mixed micelles, octylsulfanyl ethanol (C₈SE)/decylsulfanyl ethanol (C₁₀SE) mixed micelles, and *n*-decyl methyl sulfoxide (C₁₀SO)/*n*-octyl methyl sulfoxide (C₈SO) mixed micelles. Each system was selected for investigation because of the availability of experimental mixture CMC data. Taken collectively, these systems permit evaluation of the accuracy of the CS-FE/MT model for a wide range of surfactant to cosurfactant and surfactant to solubilizate structural transformations. To evaluate the accuracy and validity of the CS-FE/MT model, free-energy predictions made with the model will be compared with the predictions of a traditional MT model that has been fit to experimental CMC data in order to yield highly accurate free-energy predictions.

10.1 Implementation of Alchemical Free-Energy Calculations

10.1.1 Selection of λ -Dependent Energy Functions

The thermodynamic integration method discussed in Chapter 9 is implemented in the open source MD software GROMACS [1, 2], the same software package used to perform the MD simulations discussed in Parts I and III of this thesis. The λ dependence of the potentials used for the free-energy calculations made in this chapter is discussed in this section. All bonded interactions have been modified during alchemical transformation as a function of the coupling parameter λ through linear interpolation of the interaction potentials. The harmonic bonded potential used for alchemical transformations was modified as a function of λ as follows [3]:

$$V_{\text{bonded}} = \frac{1}{2} \left((1 - \lambda) k_{\text{b}}^{\text{A}} + \lambda k_{\text{b}}^{\text{B}} \right) \left(r - (1 - \lambda) b_0^{\text{A}} - \lambda b_0^{\text{B}} \right)^2 \quad (10.1)$$

where V_{bonded} is the potential energy associated with the bonded interaction, k_{b}^{A} is the bond spring constant in state A , k_{b}^{B} is the bond spring constant in state B , r is the distance between the two bonded atoms, b_0^{A} is the equilibrium bond distance in state A , and b_0^{B} is the equilibrium bond distance in state B . The derivative of V_{bonded} with respect to λ , and its free-energy contribution (see Chapter 9), is given by [3]:

$$\frac{\partial V_{\text{bonded}}}{\partial \lambda} = \frac{1}{2} \left(k_{\text{b}}^{\text{B}} - k_{\text{b}}^{\text{A}} \right) \left(r - (1 - \lambda) b_0^{\text{A}} - \lambda b_0^{\text{B}} \right)^2 + \left(b_0^{\text{A}} - b_0^{\text{B}} \right) \left(r - (1 - \lambda) b_0^{\text{A}} - \lambda b_0^{\text{B}} \right) \left[(1 - \lambda) k_{\text{b}}^{\text{A}} + \lambda k_{\text{b}}^{\text{B}} \right] \quad (10.2)$$

The angle potential and the Ryckaert-Bellemans dihedral potential used during simulation have more complex functional forms than the harmonic bonded potential (V_{bonded}), and therefore, these will not be presented here [3]. For the systems modeled in this chapter, bond constraints have been used in order to remove bond vibrations, which represent the highest frequency motions present in the system, in

order to enable taking a larger simulation timestep. A detailed description of the constraint algorithm used during our simulations and the free-energy contribution of these constraints, is given in [3]. Bond constraints have been implemented by changing the unconstrained coordinates to a set of coordinates that satisfy all of the distance constraints. This change in coordinates is accomplished by solving a set of Lagrange multipliers. Bond and angle constraints imposed on a simulated system affect the Hamiltonian of the system, and hence, they affect the system free energy. With bond constraints implemented, the equations of motion fulfill a set of constraint equations g_k , defined as:

$$g_k = r_k - d_k \quad (10.3)$$

where r_k is the distance vector between two atoms and d_k is the constraint distance between the two atoms. Because d_k may be different in states A and B , it is expressed as a function of λ , and the λ -dependent constraint distance can be expressed as follows [3]:

$$g_k = r_k - ((1 - \lambda)d_k^A + \lambda d_k^B) \quad (10.4)$$

and the contribution C_λ to the Hamiltonian using Lagrange multipliers λ_k is equal to [3]:

$$C_\lambda = \sum_k \lambda_k g_k \quad (10.5)$$

The derivative of C_λ with respect to λ is given by [3]:

$$\frac{\partial C_\lambda}{\partial \lambda} = \sum_k \lambda_k (d_k^B - d_k^A) \quad (10.6)$$

In contrast to the bonded interactions, nonbonded interactions have not been linearly interpolated in order to avoid problems which can occur when growing atoms out of nothing (i.e., changing a dummy atom into an interacting atom, see Section 10.1.3) or when making atoms disappear (changing from an interacting atom to a dummy atom). Linear interpolation of van der Waals potentials can be particularly problematic because, at short distances, the repulsive term (r^{-12}) in the Lennard-

Jones potential yields very large potential energies. This problem is referred to as the “end-point catastrophe” [4, 5]. Two approaches used to resolve this problem include: (i) the “bond-shrink” approach [6], in which dummy atoms are initially modeled as being bonded with a very short bond length to an interacting atom, and (ii) the gradual increase of the bond length as a function of λ , and the use of “separation-shifted scaling” or “soft-core” potentials [7, 8]. For the alchemical simulations implemented in this chapter, soft-core potentials (V_{sc}) were used to avoid the end-point catastrophe. The functional form of the soft-core potential used during alchemical transformation to switch interactions from those consistent with being in state A to those consistent with being in state B is as follows [3]:

$$V_{\text{sc}}(r) = (1 - \lambda)V_{\text{A}}(r_{\text{A}}) + \lambda V_{\text{B}}(r_{\text{B}}) \quad (10.7)$$

$$r_{\text{A}} = (\alpha\sigma_{\text{A}}^6\lambda^2 + r^6)^{1/6} \quad (10.8)$$

$$r_{\text{B}} = (\alpha\sigma_{\text{B}}^6(1 - \lambda)^2 + r^6)^{1/6} \quad (10.9)$$

where V_{A} and V_{B} are the normal, “hard-core” potentials in state A and state B , α is the soft-core parameter, which controls the height of the potential $V_{\text{sc}}(r)$ around $r = 0$ (for our simulations, it was set equal to 1.51 [3]), σ is the radius of the interactions, which is equal to $(C_{12}/C_6)^{1/6}$. The two parameters C_6 and C_{12} correspond to the two parameters characterizing the shape of the Lennard-Jones potential: $V(r) = C_{12}/r^{12} - C_6/r^6$. When C_{12} or C_6 are equal to zero, which occurs when computing the interactions between dummy atoms and interacting atoms (see Section 10.1.2), σ is set equal to a predefined value (in our simulations, it was set equal to 0.3 nm [3]). When r is less than $\alpha^{1/6}\sigma$, r_{A} and r_{B} switch V_{sc} to a nearly constant value, while when r is greater than $\alpha^{1/6}\sigma$, r_{A} and r_{B} have little affect on the nonbonded interactions and V_{sc} resembles a simple linear interpolation of the V_{A} and V_{B} van der Waals or Lennard-Jones potential energies. The derivative of V_{sc} with respect to λ , and therefore, its

contribution to free energy, is equal to [3]:

$$\frac{\partial V_{\text{sc}}(r)}{\partial \lambda} = -V_{\text{A}}(r_{\text{A}}) + V_{\text{B}}(r_{\text{B}}) + \frac{1}{3}\alpha\lambda(1 - \lambda) \left[-F_{\text{A}}(r_{\text{A}})\sigma_{\text{A}}^6 r_{\text{A}}^{-5/6} + F_{\text{B}}(r_{\text{B}})\sigma_{\text{B}}^6 r_{\text{B}}^{-5/6} \right] \quad (10.10)$$

where $F_{\text{A}} = -\partial V_{\text{A}}(r_{\text{A}})/\partial r_{\text{A}}$ and $F_{\text{B}} = -\partial V_{\text{B}}(r_{\text{B}})/\partial r_{\text{B}}$ are the “hard-core” forces. A detailed description of the soft-core algorithm implemented in GROMACS can be found in [3].

10.1.2 Single versus Dual Topology Approaches

For the alchemical simulations that are performed in the CS-FE/MT model, the state corresponding to $\lambda = 0$ is defined as a surfactant molecule of type *A*, and the state corresponding to $\lambda = 1$ is defined as a surfactant or a solubilizate molecule of type *B*. Generally speaking, there are two approaches that are used to interpolate between two states *A* and *B* in alchemical free-energy simulations. These two approaches are the single topology approach [9, 10] and the dual topology approach, which are discussed next [11, 12].

10.1.3 Description of Alchemical Topologies

In the single topology approach, alchemical changes are accomplished by changing nonbonded (van der Waals and electrostatic) and bonded (bond, angle, dihedral) interactions as a function of the coupling parameter λ . Frequently, the total numbers of atoms present in state *A* and state *B* are different. If this is the case, “dummy” atoms — or atoms which have no nonbonded interactions — are used to represent atoms which exist in one state but have no counterpart in the other state [13]. Dummy atoms are modeled as having the same mass as the physical atoms that they represent when they interact with other components in the simulation cell.

In the dual topology approach, two complete versions of any atoms that are dif-

ferent in the initial and the final states are simulated. These two versions exist simultaneously during alchemical simulation and both interact with the other system components, but not with each other. The atom types and the bonded (bond, angle, and dihedral) interactions do not change during simulation. Using the dual topology approach, dummy atoms are present in the simulation cell in both state *A* and state *B*. In state *A*, each of the atoms in the version of the topology that corresponds to state *B* are modeled as dummy atoms, and in state *B*, each of the atoms in the version of the topology that corresponds to state *A* are modeled as dummy atoms.

Dummy atoms interact with other simulated atoms through nonbonded van der Waals or electrostatic interactions, but until recently, it was not well understood whether, or how, bonded interactions to dummy atoms should be modeled. Boresch and Karplus [14,15] recently conducted a detailed study of such bonded interactions. These authors concluded that vibrational and Jacobian factor contributions to the free energy, G , are not included in certain dual topology approaches that are included when using single topology approaches. As a result, ΔG values associated with moving from state *A* to state *B* obtained using the two approaches frequently cannot be compared directly. Nevertheless, identical $\Delta\Delta G$ values should be obtained in all cases using both approaches. In the CS-FE/MT model, one is interested only in calculating a $\Delta\Delta G$ value (i.e. the value of $\Delta G_2 - \Delta G_1$ shown in Figure 10-1), and therefore, artificial free-energy contributions associated with using the dual topology approach are not a concern. Due to convergence issues which arise when removing bonds and angle terms during an alchemical simulation, Boresch and Karplus suggest that it is most appropriate to keep the harmonic bond and angle terms in the nonbonded interaction potentials for dummy atoms unaltered during alchemical transformation. However, these authors recommend that the nonharmonic dihedral interaction potentials for these atoms be changed to zero so that no dihedral potentials are present in the dummy state. In alchemical simulations reported in the literature, bond and angle terms for dummy atoms are typically kept constant, but the treatment of proper (nonharmonic) dihedral and improper (harmonic) dihedral

terms varies [14, 15].

Pearlman et al. conducted a detailed study to evaluate the convergence rates associated with using the single topology and dual topology approaches by investigating the “self-transformation” of ethane into ethane [16]. These authors found that the single topology approach yields more rapid convergence than the dual topology approach. The main advantage associated with using the single topology approach is that fewer atoms are simulated and modified during alchemical simulation, and therefore, the magnitude of the free-energy change at a given value of λ is lower. This leads to faster convergence of the free energy results. The main advantage associated with the dual topology approach is that it can be used to model any two endpoints, including endpoints where a ring structure is present in one state but not in the other state.

The single topology and dual topology approaches are contrasted in Figure 10-2, which depicts two alternative pathways to transform an alkyl sulfate surfactant with a linear alkyl tail into an alkyl sulfate surfactant with a branched alkyl tail. Note that the dual topology approach involves separate representation of the two tails, while the single topology approach involves modification of a single representation. In Figure 10-2, DUM represents dummy groups.

Topologies for Surfactant to Solubilize Transformation

The state *A* and state *B* topologies associated with the transformation of sodium dodecyl sulfate (SDS) into ibuprofen (IBU) and with the transformation of octyl glucoside (OG) into *p*-aminobenzoate (PAB) are shown in Figure 10-3. The SDS (see groups 1-18 in the figure) and IBU (groups 1-7 and 19-27) topologies are shown on the left, and the OG (groups 1-12 and 15-22) and PAB (groups 12-14 and 23-33) topologies are shown on the right. For atoms whose identity is changed during alchemical simulation, the atom type present in state *A* is listed first, followed by the atom type present in state *B*. For example, for the SDS/IBU topology shown in Figure 10-3, group 5 is an oxygen atom in state *A* and a carbon atom in state

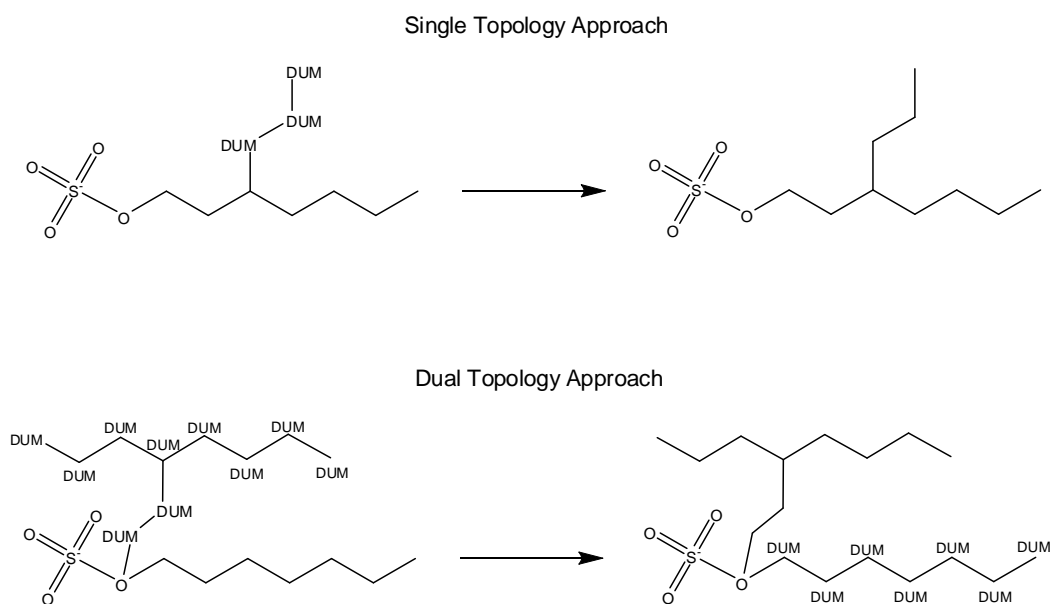


Figure 10-2: Comparison of the single and dual topology approaches.

B. Oxygen atoms are labeled as “O,” carbon atoms are labeled as “C,” sulfur atoms are labeled as “S,” and atoms labeled as “DUM” are dummy atoms that have no nonbonded interactions with their environment.

The approach selected here to morph SDS into IBU cannot be categorized simply as either single topology or dual topology. In morphing SDS into IBU, two separate versions of the tail atoms in the two molecules (groups 7-18 in SDS and groups 7 and 19-27 in IBU) are simulated. The tail portions of the two molecules may therefore be considered as being modeled using the dual topology approach. This dual topology approach was needed because SDS possesses a linear alkyl tail while IBU possesses a benzene ring. The head atoms present in SDS and IBU (groups 1-6 in SDS and IBU), however, were modeled using a single topology approach to minimize the total number of atoms simulated and the magnitude of the free-energy change which will be experienced at each λ value [16]. The single topology approach was used only for atoms that are head atoms (implying that they extend into the aqueous phase at the micelle core/water interface) in both the *A* and the *B* states.

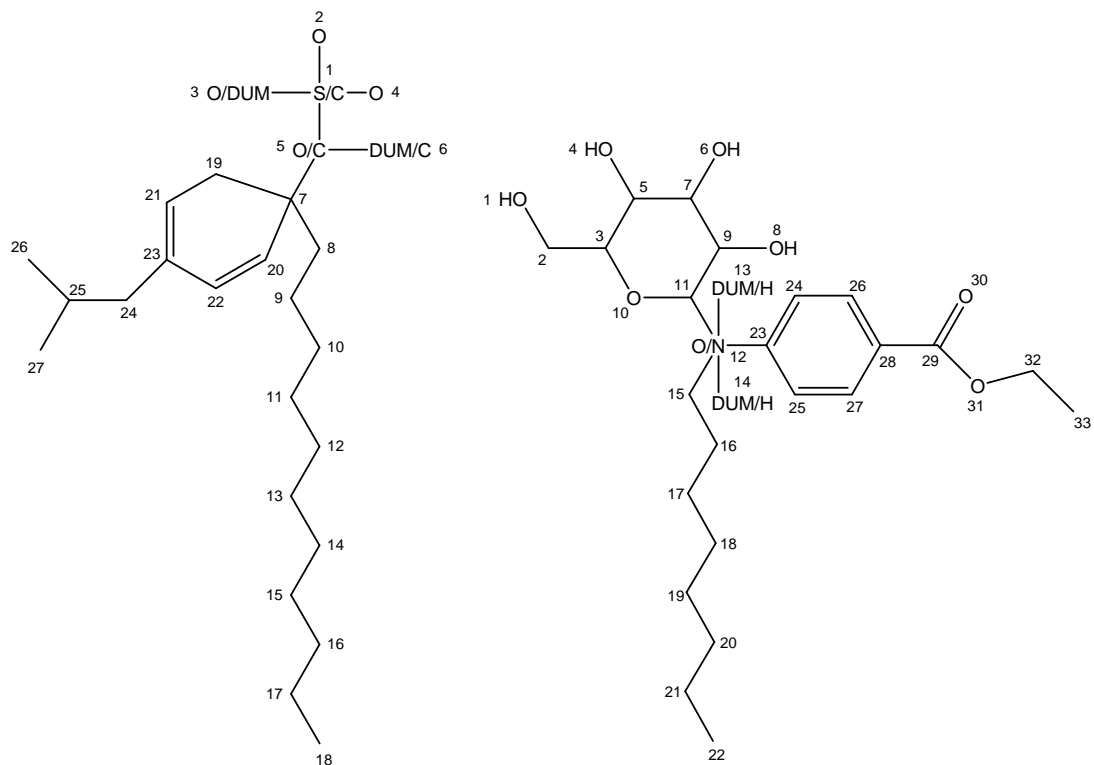


Figure 10-3: Topologies for surfactant to solubilize transformation. The sodium dodecyl sulfate (SDS)/ibuprofen (IBU) topology is shown on the left, where SDS corresponds to state *A* and IBU corresponds to state *B*. The octyl glucoside (OG)/*p*-aminobenzoate (PAB) topology is shown on the right, where OG corresponds to state *A* and PAB corresponds to state *B*. For an explanation of notation, see the text.

As a result, the simulated SDS/IBU molecule will not have change its position or orientation significantly within the micelle during alchemical transformation to come to equilibrium. This is expected to improve the rate of free-energy convergence during alchemical transformation.

The approach used to morph OG into PAB is a dual topology approach. Selection of the dual topology approach was needed because the head and tail structures of both of these molecules are quite different, and because OG possesses a linear alkyl tail while PAB possesses a benzene ring. Apart from group 12, which is an oxygen atom that is part of OG in state *A* and is a nitrogen atom that is part of PAB in state *B*, there is no overlap between the topologies used to model both molecules. To improve the rate of free-energy convergence for this alchemical transformation, the atom that was selected as the common atom for both OG and PAB (group 12) is a head atom in states *A* and *B*. This assignment is expected to improve the rate of free-energy convergence.

Topologies for Surfactant to Cosurfactant Transformation

The state *A* and state *B* topologies associated with the transformation of C₁₀PO into C₁₀SO, with the transformation of C₈SE into C₁₀SE, and with the transformation of C₁₀SO into C₈SO are shown in Figure 10-4. The C₁₀PO (see groups 1-14 in the figure) and C₁₀SO (groups 1 and 3-14) topologies are shown on the left, the C₈SE (groups 1-11) and C₁₀SE (groups 1-13) topologies are shown in the center, and the C₁₀SO (groups 1-13) and C₈SO (groups 1-11) topologies are shown on the right. For atoms whose identity is changed during the alchemical simulation, the atom type present in state *A* is listed first, followed by the atom type present in state *B*. Oxygen atoms are labeled as “O,” carbon atoms are labeled as “C,” sulfur atoms are labeled as “S,” phosphorous atoms are labeled as “P,” and atoms labeled as “DUM” are dummy atoms that have no nonbonded interactions with their environment.

A single topology approach was used to morph each of these three surfactants into their respective cosurfactants. This approach is expected to minimize the total

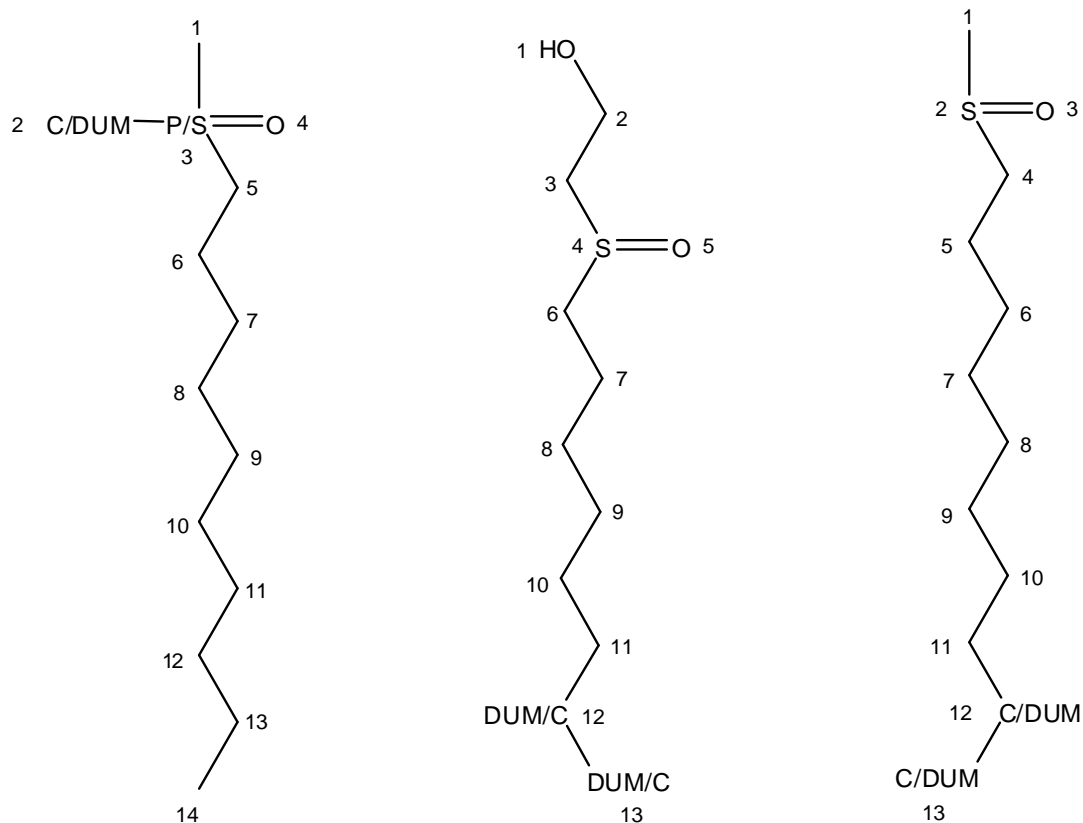


Figure 10-4: Topologies for surfactant to cosurfactant transformation. The *n*-decyl dimethyl phosphine oxide ($C_{10}PO$)/*n*-decyl methyl sulfoxide ($C_{10}SO$) topology is shown on the left, the octylsulfinyl ethanol (C_8SE)/decylsulfinyl ethanol ($C_{10}SE$) topology is shown in the center, and the *n*-decyl methyl sulfoxide ($C_{10}SO$)/*n*-octyl methyl sulfoxide (C_8SO) topology is shown on the right. For an explanation of the notation used, see text.

number of atoms simulated, the magnitude of the free-energy change which will be experienced at each λ value, and the rate of free-energy convergence. The transformation of $C_{10}PO$ into $C_{10}SO$ involves changing the identity of group 3 from a phosphorus to a sulfur atom and the transformation of group 2 from an interacting methyl group to a non-interacting group of dummy atoms. The transformation of C_8SE into $C_{10}SE$ involves adding two additional CH_2 groups to the original surfactant (groups 12 and 13). The transformation of $C_{10}SO$ into C_8SO involves removing two CH_2 groups from the original surfactant (groups 12 and 13). The transformations of C_8SE into $C_{10}SE$ and $C_{10}PO$ into $C_{10}SO$ are expected to have a negative free-energy change, because the CMCs of both cosurfactants of type *B* are lower than the CMCs of the surfactants of type *A* (recall that the CMC is exponentially related to the free-energy associated with micelle formation). The transformation of $C_{10}SO$ into C_8SO is expected to have a positive free-energy change because the CMC of C_8SO is higher than the CMC of $C_{10}SO$.

10.2 Simulation Methods and Parameters

All the surfactants, cosurfactants, and solubilizates considered in this chapter were modeled using the bonded and nonbonded interaction potentials included in the fully-atomistic OPLS-AA force field [17]. Some additional parameters needed to describe angles and angle vibrations were taken from the literature to model the sulfate (SO_4^-) group in SDS [18]. For molecules undergoing alchemical transformation, λ -dependent bonded and nonbonded interaction potentials were computed as described in Section 10.1.1. Water was modeled using the simple extended point-charge (SPC/E) model for water. SPC/E represents an improvement over SPC in which a correction is implemented to account for the self-polarization of water [19]. Atomic charges were assigned to each surfactant and solubilizate molecule based on the default atomic charge values recommended in OPLS-AA. Van der Waals interactions were modeled using a cutoff distance of 1.2 nm, and Coulombic interactions were described using the

reaction field method and a cutoff distance of 1.4 nm. In the reaction field method, electrostatic interactions between molecules within a specified cutoff distance are modeled explicitly, and molecules located beyond the cutoff distance are modeled as a continuous dielectric [5]. In our simulations, long-range dispersion corrections were implemented to more accurately model the energy and the pressure of the system. Both dispersion corrections are negative, and while the energy correction is small, the pressure correction is significant and must be included to yield accurate results [3]. In modeling short-range, nonbonded interactions, a neighbor list with a cutoff of 0.9 nm was maintained and updated every 5 simulation steps. Each simulation was carried out with fixed bond lengths using the SHAKE algorithm as implemented in GROMACS [20], which allowed an increase in simulation timestep from 1 fs to 2 fs. The effect of these bond constraints on the free energy was taken into account using the approach discussed in Section 10.1.1.

In each simulation, the cell temperature was maintained at 300 K using a Berendsen temperature coupling algorithm, which mimics weak coupling to an external heat bath with first-order kinetics [3]. A Berendsen pressure coupling algorithm was used to maintain each simulation cell at the desired pressure of 1.0 bar [3]. All simulations were conducted using a 2006 developers' version of the GROMACS software package [1, 2].

10.3 Simulation Preparation and Equilibration

10.3.1 Aqueous Simulations

Each alchemical simulation in aqueous solution in the CS-FE/MT modeling approach was initialized by placing a single alchemical topology in a simulation cell and surrounding it with water molecules. The simulation cell was selected to be sufficiently large that there would always be at least 2.0 nm separating the alchemical topology from its periodic image. Computer simulation studies of the propagation of water ordering away from an interface suggest that such a separation distance should

be sufficient to prevent the molecule from interacting with itself through the periodic boundary conditions [21]. Brief equilibration was then conducted under NPT conditions until the system simulation volume had stabilized.

10.3.2 Micellar Simulations

The starting point for each alchemical simulation in the micellar environment in the CS-FE/MT modeling approach is an equilibrated surfactant A micelle surrounded by water molecules. To evaluate the accuracy and the applicability of the CS-MT model, which is the goal of the present study, any micelle aggregation number could have been selected to construct the single surfactant micelles. Consequently, an arbitrary aggregation number was selected to form micelles composed of $C_{10}PO$, C_8SE , and C_8SO . These aggregation numbers were 50, 25, and 50, respectively. From previous studies (see Chapters 7 and 8), the post-equilibration configuration of an SDS and of an OG micelle of aggregation numbers 44 and 29, respectively, were available and were used as the starting point for the surfactant to solubilize transformations studied in this chapter. Both aggregation numbers correspond to the optimal aggregation numbers predicted by the molecular-thermodynamic theory for SDS and OG micelles that form in solution at the CMC.

Each surfactant micelle was preformed as a spherical aggregate, which was constructed by placing a number of surfactant molecules in close proximity with each surfactant head oriented radially outwards from the micelle center. The surfactant molecules were placed such that the surfactant heads were approximately uniformly spaced at the micelle surface. Next, sufficient water molecules were added around each micelle such that it was separated by at least 2 nm from its periodic image. Counterions were added to the simulation cell in equal proportion to the number of ionic surfactant molecules in order to maintain electroneutrality. To speed equilibration, these counterions were added by replacing water molecules experiencing the greatest electrostatic potential after initial energy minimization, with the potential being recalculated after every counterion insertion [3]. In Table 10.1, we report the

Surfactant	Surfactant Molecules	Water Molecules	Total Atoms
SDS	44	3,347	11,960
OG	29	6,611	21,247
C₁₀PO	50	6,708	22,174
C₈SE	25	3,750	12,131
C₈SO	50	3,510	12,380

Table 10.1: The number of surfactant molecules, water molecules, and the total number of atoms corresponding to the starting point for each alchemical simulation in the micellar environment.

number of surfactant and water molecules and the total number of atoms included in each simulation cell.

After performing each spherical micelle, a 10 ns equilibration run was conducted under *NPT* conditions. Results obtained by other researchers conducting atomistic-level simulations of micelles in aqueous solution and results presented in Chapter 4 suggest that a simulation time of 10 ns should be more than adequate to equilibrate a spherical micelle [22]. Bruce et al. reported that although the sodium counterions are the slowest components to equilibrate, they take only 1 ns to come to an equilibrium distance from the micelle center of mass after beginning simulation of a preformed SDS micelle [22]. In addition, the simulation time required to equilibrate each of the surfactant/solubilizate micelles discussed in Chapter 4 (where the simulation parameters and methodology are the same as those used in the present study) was significantly less than 10 ns. Equilibration of surfactant/solubilizate micelles was confirmed in Chapter 4 by: (i) monitoring the system potential energy (which stabilized very quickly), (ii) computing the micelle solvent accessible surface area (SASA) as a function of equilibration time, and (iii) computing the distance between several system components and the micelle center of mass as a function of equilibration time. These three metrics indicated that equilibration occurred in less than 10 ns.

Equilibration was confirmed for each single component surfactant micelle simulated in this chapter by monitoring the total potential energy (which became stable within a small fraction of the total simulation time) and by monitoring the micelle solvent accessible surface area (SASA). Plots of SASA for the SDS and OG micelles

are shown in Figure 10-5, and plots of SASA for the C₈SE, C₁₀SO, and C₁₀PO micelles are shown in Figure 10-6. The solvent accessible surface areas reported in both figures were determined using the double cubic lattice method implemented in GROMACS [3]. A probe sphere of radius 0.14 nm was rolled around each surfactant molecule comprising the micelle to identify the micelle solvent accessible region.

As shown in Figures 10-5 and 10-6, after the first 1 ns of simulation, there is no apparent upwards or downwards drift in SASA for the five simulated micelles. However, significant fluctuations in SASA occur even after the first nanosecond of simulation. For example, after the first nanosecond of simulation, the computed values of SASA for the SDS micelle range from 89 nm² to 77 nm² (a range which represents 15% of the average micelle SASA value). Similarly, after the first nanosecond of simulation, the OG, C₁₀PO, C₈SE, and C₁₀SO micelles have fluctuations in SASA that represent 24%, 16%, 25%, and 29% of their respective average SASA values.

Snapshots of the post-equilibration configurations of each of the simulated surfactant *A* micelles are shown in Figure 10-7 (note that the water molecules have been omitted for clarity). Each surfactant molecule is depicted using the van der Waals radius of each atom.

After equilibrating each surfactant *A* micelle, a single molecule of surfactant *A* was removed and replaced with one of the alchemical topologies shown in Figures 10-3 and 10-4. To prevent perturbation of the system from its equilibrium state, atoms in the alchemical topology corresponding to atoms in the surfactant *A* molecule being replaced were placed in the same position as the atoms present in the original surfactant *A* molecule. For example, all the SDS atoms in the alchemical topology representation of SDS/IBU were placed in the same location as the atoms in the SDS molecule that were being removed. The inserted topology was then transformed from a surfactant *A* molecule into a surfactant *B* molecule as a function of the coupling parameter λ . Details of this alchemical transformation and of the alchemical transformation conducted in aqueous solution are provided in the next section.

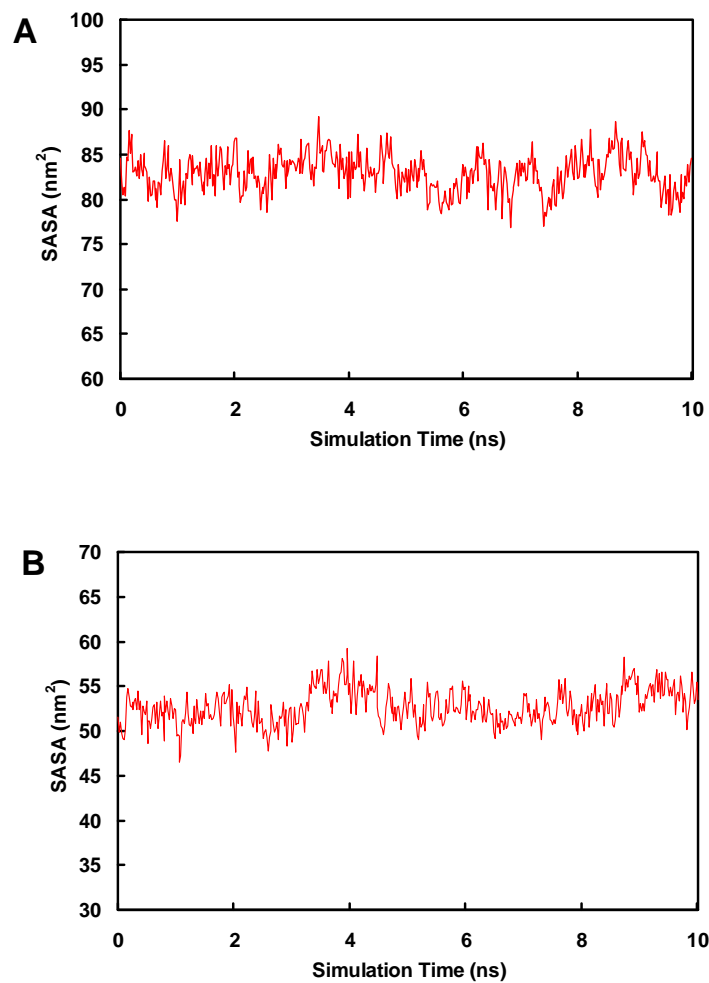


Figure 10-5: Solvent accessible surface area (SASA) as a function of simulation time for the sodium dodecyl sulfate (A) and octyl glucoside (B) micelles during the 10 ns of equilibration conducted prior to beginning alchemical transformations.

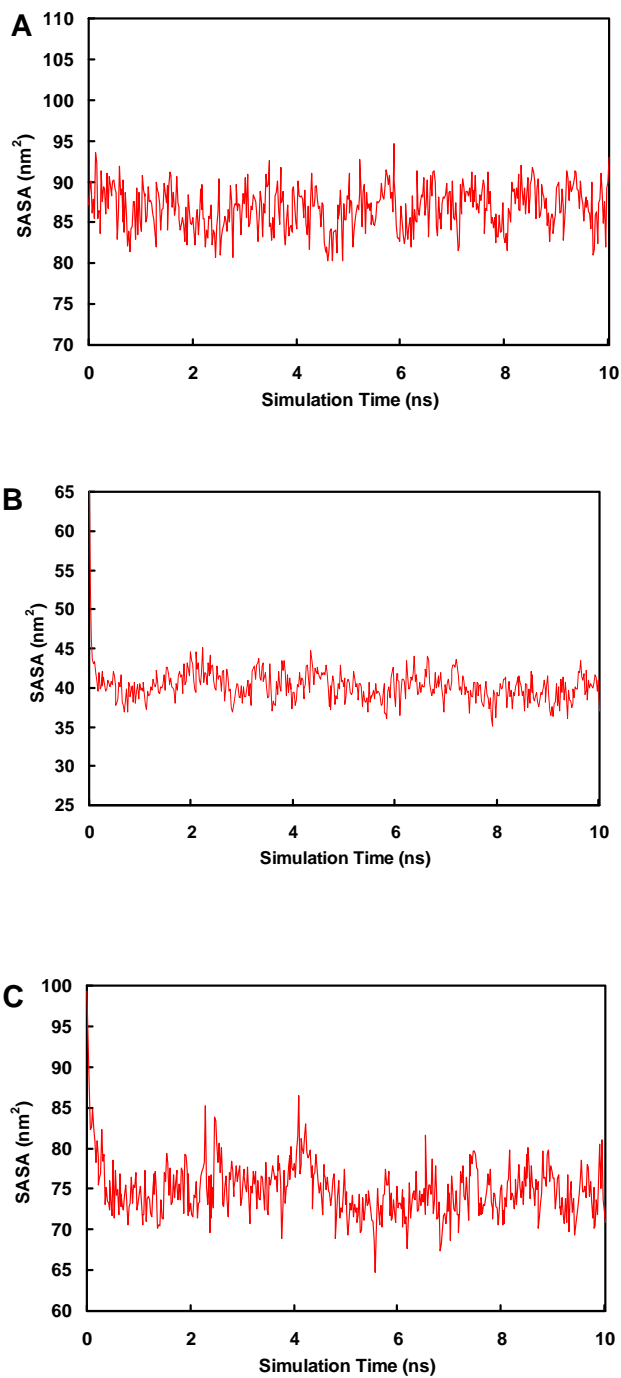


Figure 10-6: Solvent accessible surface area (SASA) as a function of simulation time for the C₁₀PO (A), C₈SE (B), and C₁₀SO (C) micelles during the 10 ns of equilibration conducted prior to beginning alchemical transformations.

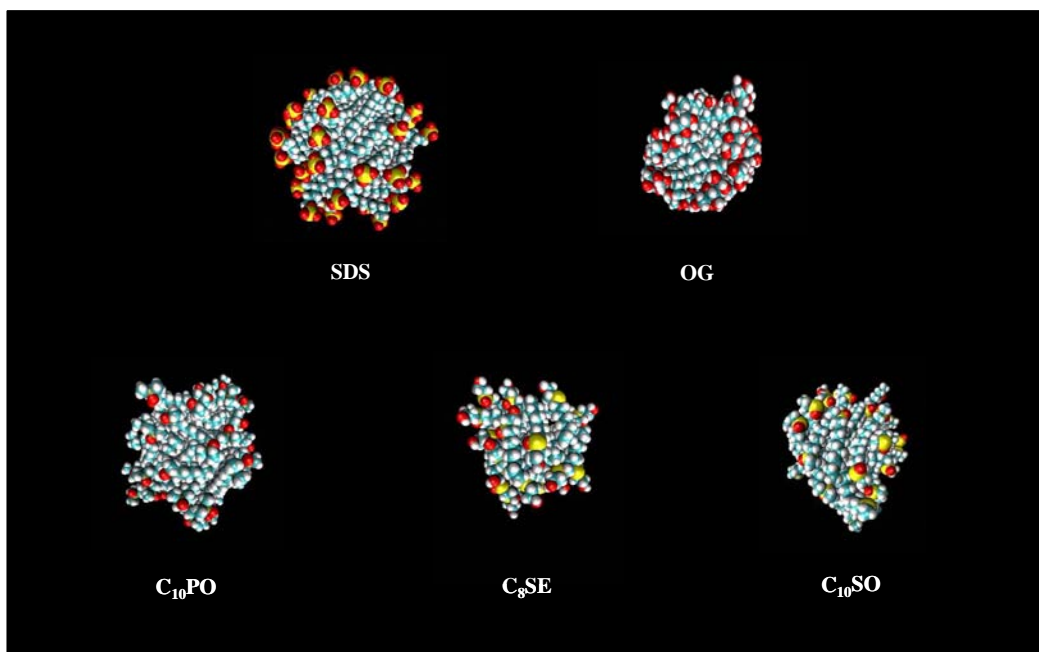


Figure 10-7: Snapshots of the post-equilibration structures of the SDS, OG, C₁₀PO, C₈SE, and C₁₀SO micelles used as the starting point for free-energy calculations. The water molecules are not shown for clarity.

10.4 Alchemical Simulations and Results

To evaluate the accuracy and applicability of the CS-FE/MT modeling approach, the free-energy changes associated with transforming a single surfactant of type A into a single surfactant/solubilizate of type B in the aqueous solution (ΔG_1 in Figure 1) and in the micellar environment (ΔG_2 in Figure 1) were determined. Note that the difference between these two free-energy changes ($\Delta G_2 - \Delta G_1$) is equal to the difference in the free-energy change associated with forming a mixed micelle and the free-energy change associated with forming a single surfactant micelle ($G_{\text{form,mixed}} - G_{\text{form,single}}$). To simplify notation, throughout the remainder of this chapter $G_{\text{form,mixed}} - G_{\text{form,single}}$, or $\Delta G_2 - \Delta G_1$, will be referred to as $\Delta\Delta G$.

10.4.1 Evaluation of $\Delta\Delta G$ from ΔG_1 and ΔG_2

To determine ΔG_1 and ΔG_2 for each surfactant to cosurfactant or surfactant to solubilizate transformation, the ensemble average of $\partial G/\partial\lambda$, $\langle\partial G/\partial\lambda\rangle_\lambda$, was computed at a number of different λ values and numerically integrated to determine the area under the $\langle\partial G/\partial\lambda\rangle_\lambda$ versus λ curve [23] (see discussion in Chapter 9). At each value of λ , equilibration was conducted prior to recording the $\partial G/\partial\lambda$ results.

To assess the rate of convergence in the free-energy results, $\langle\partial G/\partial\lambda\rangle_\lambda$ values were determined based on several different equilibration and data-gathering simulation times. Results for each surfactant A to surfactant/solubilizate B transformation in aqueous solution (ΔG_1) and in the micellar environment (ΔG_2) are presented in Table 10.2 along with the equilibration time (E.T.), data-gathering time (D.G.T.), and the number of different values of λ at which $\langle\partial G/\partial\lambda\rangle_\lambda$ was evaluated. Each of the λ values selected was evenly spaced between 0 and 1. Values of $\Delta\Delta G$, or $\Delta G_2 - \Delta G_1$, are also reported in Table 10.2. The free-energy results are discussed in detail in Section 10.4.1.

SDS \rightarrow IBU (aqueous)				SDS \rightarrow IBU (micelle)				$G_{\text{form,mixed}} - G_{\text{form,single}}$
E.T. [ps]	D.G.T. [ps]	λ	$\Delta G_1 [k_B T]$	E.T. [ps]	D.G.T. [ps]	λ	$\Delta G_2 [k_B T]$	$(=\Delta\Delta G = \Delta G_2 - \Delta G_1)$
100	200	30	-19.6 ± 1.48	100	200	20	21.4 ± 1.92	41.0 ± 2.43
200	200	30	-19.4 ± 1.47	200	200	20	22.6 ± 1.99	42.0 ± 2.47
200	500	30	-24.6 ± 1.68	200	200	20	25.4 ± 1.54	50.0 ± 2.27
OG \rightarrow PAB (aqueous)				OG \rightarrow PAB (micelle)				
200	400	30	-19.7 ± 0.64	200	400	30	-68.6 ± 0.88	-49.0 ± 1.09
600	800	30	-19.6 ± 0.58	600	800	30	-74.9 ± 0.76	-55.3 ± 0.96
1400	1600	30	-18.8 ± 0.57	1400	1600	30	-81.3 ± 0.89	-62.5 ± 1.06
3000	3200	30	-20.2 ± 0.33	3000	2700	30	-78.0 ± 0.54	-57.8 ± 0.64
$C_{10}PO \rightarrow C_{10}SO$ (aqueous)				$C_{10}PO \rightarrow C_{10}SO$ (micelle)				
200	200	20	87.6 ± 0.92	100	100	20	92.7 ± 53.5	5.08 ± 53.54
400	200	20	82.7 ± 0.36	200	200	20	88.8 ± 1.05	6.10 ± 1.11
600	400	20	86.9 ± 0.28	400	400	20	87.5 ± 0.87	0.60 ± 0.91
$C_8SE \rightarrow C_{10}SE$ (aqueous)				$C_8SE \rightarrow C_{10}SE$ (micelle)				
200	200	20	6.29 ± 0.25	40	100	20	6.32 ± 0.75	0.03 ± 0.79
200	400	20	6.44 ± 0.19	400	400	20	5.45 ± 0.37	-0.99 ± 0.42
600	800	20	6.45 ± 0.11	800	800	20	5.00 ± 0.31	-1.45 ± 0.33
$C_{10}SO \rightarrow C_8SO$ (aqueous)				$C_{10}SO \rightarrow C_8SO$ (micelle)				
100	100	20	-5.05 ± 0.20	200	400	20	-4.74 ± 0.33	0.32 ± 0.39
200	400	20	-5.17 ± 0.20	600	800	20	-4.07 ± 0.38	1.10 ± 0.43
600	800	20	-4.98 ± 0.19	1400	1600	20	-1.81 ± 0.30	3.18 ± 0.35

Table 10.2: Transformation free energies computed using the CS-FE/MT model.

Error Analysis

Each error in ΔG_1 and ΔG_2 reported in Table 10.2 corresponds to the standard deviation of the reported value. To determine this standard deviation, (i) block averaging was used to determine the standard error of the mean of $\langle \partial G / \partial \lambda \rangle_\lambda$ at each value of λ , and (ii) the computed standard errors of the mean were used to estimate the error associated with the integral of the $\langle \partial G / \partial \lambda \rangle_\lambda$ vs. λ curve. In block averaging, the standard error is computed from the variance between averages of blocks of data, and the block size is increased until the standard error estimate becomes constant. To assist in identifying this asymptotic value for the simulation data reported here, a two-exponential function was fit to the block average curve [24–26]. To convert the standard error of the mean determined for each $\langle \partial G / \partial \lambda \rangle_\lambda$ value to an estimate of the error associated with the integral of the $\langle \partial G / \partial \lambda \rangle_\lambda$ vs. λ curve, a Monte Carlo approach was used in which 10,000 $\langle \partial G / \partial \lambda \rangle_\lambda$ values were generated at each value of λ . Each $\langle \partial G / \partial \lambda \rangle_\lambda$ value was selected randomly from a Gaussian distribution centered around the simulation value of $\langle \partial G / \partial \lambda \rangle_\lambda$, and with a standard deviation equal to the block averaging estimate of the standard error in $\langle \partial G / \partial \lambda \rangle_\lambda$. After generating the $\langle \partial G / \partial \lambda \rangle_\lambda$ values, 10,000 ΔG_1 or ΔG_2 estimates were made by numerically integrating each of the 10,000 generated $\langle \partial G / \partial \lambda \rangle_\lambda$ vs. λ curves. The standard deviation of the distribution of computed ΔG_1 and ΔG_2 values is reported in Table 10.2 as the uncertainty in the free-energy results. The error reported in $G_{\text{form,mixed}} - G_{\text{form,single}}$, or $\Delta \Delta G = \Delta G_2 - \Delta G_1$, was evaluated by propagating the errors calculated for ΔG_1 and ΔG_2 .

It is important to note that the computed errors reported in Table 10.2 for ΔG_1 , ΔG_2 , and $\Delta \Delta G$ should be regarded as lower bound estimates of the standard deviation associated with the free-energy estimates, because they have been computed from a single data-gathering simulation conducted at each value of λ . Results obtained from a single simulation are generally not statistically relevant [23, 27]. It is usually necessary to run multiple independent simulations to determine whether phase space has been sampled adequately and whether the uncertainty determined based

on a single simulation is reasonable. Additional insight into the statistical significance of the free-energy results can therefore be gained by comparing the free-energy results obtained using different equilibration and data-gathering times reported in Table 10.2, and by comparing the results presented in Table 10.2 with the independent micellar simulation results reported in Table 10.3 (see Section 10.3). The $\Delta\Delta G$ results reported in Table 10.2 exhibit a large amount of variation as a function of the total length of equilibration and simulation time, an effect which will be discussed in greater detail in subsequent sections.

Discussion of the $\Delta\Delta G$ Free-Energy Results Reported in Table 10.2

Surfactant to Solubilizate $\Delta\Delta G$ Results The value of $\Delta\Delta G$ for the SDS to IBU transformation obtained using the longest simulation times (200 ps E.T. and 500 ps D.G.T. at each λ value in aqueous solution, and 200 ps E.T. and 200 ps D.G.T. at each λ value in the micelle, for a total of 29 ns of simulation) is $50.0 \pm 2.27 k_B T$, a value which is too positive to be physical. Indeed, the exchange of one surfactant molecule for one solubilizate molecule should have a $\Delta\Delta G$ value of no more than a few $k_B T$ (as shown by experimental data on changes in CMC that accompany changes in solution composition, see Section 10.4.1). One possible reason for this poor free-energy result is that the systems simulated in determining ΔG_1 and ΔG_2 for the transformation of SDS into IBU are charged, and it is possible that the reaction field approach used to model electrostatic interactions may have led to errors in the evaluation of ΔG_1 and ΔG_2 that did not cancel when computing $\Delta\Delta G$. Indeed, as discussed in Appendix A, poor free-energy results were obtained in a validation study in which alchemical and non-alchemical free-energy methods were used to determine the difference in the hydration free energies associated with the charged species benzoate and propionate. In contrast, reasonable free-energy results were obtained in a similar validation study in which alchemical and non-alchemical free-energy methods were used to determine the difference in hydration free energies associated with the uncharged species benzene and hexane.

Another possible reason for the poor estimate of $\Delta\Delta G$ obtained for the SDS to IBU transformation is insufficient sampling of phase space. The possibility that inadequate sampling of phase space is responsible for the poor $\Delta\Delta G$ estimate is supported by the observation that there are large variations in the computed values of $\Delta\Delta G$ for the transformation of SDS into IBU as a function of the total simulation time (ranging from $41.0 \pm 2.43 k_B T$ for the shortest simulation time to $50.0 \pm 2.27 k_B T$ for the longest simulation time). We note that if the simulation time was adequate but more values of λ were needed to accurately estimate $\Delta\Delta G$, the computed $\Delta\Delta G$ values would not be a strong function of the total simulation time. The observed level of variation suggests that the poor estimates of $\Delta\Delta G$ obtained are not due only to performing simulations at an insufficient number of λ values to allow an accurate numerical integration of the $\langle \partial G / \partial \lambda \rangle_\lambda$ versus λ profile. The extent to which the electrostatics model and inadequate sampling of phase space are responsible for the poor estimate of $\Delta\Delta G$ can be better understood by examining the $\Delta\Delta G$ results obtained for the OG to PAB transformation, which involves only uncharged species.

The calculated value of $\Delta\Delta G$ for the OG to PAB transformation obtained using the longest simulation times (3,000 ps of E.T. and 3,200 ps of D.G.T. at each λ value in aqueous solution, and 3,000 ps of E.T. and 2,700 ps of D.G.T. at each λ value in the micelle, for a total of 414 ns of simulation) is $-57.8 \pm 0.64 k_B T$, a result which is too negative to be physical. For the OG to PAB transformation, very long simulation times were used in an attempt to determine whether or not the computed value of $\Delta\Delta G$ would converge to a reasonable value with sufficient simulation time. The OG and PAB results demonstrate that accurate estimates of $\Delta\Delta G$ are not obtained even for uncharged species, indicating that insufficient phase space sampling is the most probable source of the poor free-energy results. The data presented in Table 10.2, which shows that the computed values of $\Delta\Delta G$ range from $-49.0 \pm 1.09 k_B T$ to $-62.5 \pm 1.06 k_B T$ for different total simulation times suggests that the poor estimates of $\Delta\Delta G$ obtained are not due only to performing simulations at an insufficient number of λ values. As discussed in the context of the SDS to IBU transformation results,

if simulation at an insufficient number of λ values was the only source of the poor $\Delta\Delta G$ estimates, the computed $\Delta\Delta G$ values should not be a strong function of the total simulation time.

As shown in Figure 10-3, the structural transformations involved in morphing SDS into IBU and OG into PAB are quite large. Because of the large structural changes being made, it is likely that relevant regions of phase space associated with surfactant, solubilizate, and each of the intermediate λ states in which both surfactant and solubilizate interact to some extent with the environment, may not be sampled adequately even after 29 ns of simulation in the case of the SDS to IBU transformation and 414 ns of simulation in the case of the OG to PAB transformation. The fact that even very lengthy simulation of the OG to PAB transformation fails to yield accurate (and consistent) estimates of $\Delta\Delta G$ suggests that the structural transformations which were made in morphing these two surfactants into solubilizates are too large to permit adequate sampling of relevant regions of phase space and thereby obtain accurate estimates of $\langle \partial G / \partial \lambda \rangle_\lambda$. In general, when large structural changes are attempted, free-energy calculations may not converge even after long simulation times [23]. In this respect, it is instructive to compare the surfactant to solubilizate $\Delta\Delta G$ estimates with the surfactant to cosurfactant $\Delta\Delta G$ estimates, where much smaller structural changes are made during alchemical transformation. This comparison is presented next.

Surfactant to Cosurfactant $\Delta\Delta G$ Results In contrast to the surfactant to solubilizate $\Delta\Delta G$ predictions, which were unphysically large, the surfactant to cosurfactant $\Delta\Delta G$ values reported in Table 10.2 range between $6.10 \pm 1.11 k_B T$ and $-1.45 \pm 0.33 k_B T$ in magnitude. Specifically, the computed value of $\Delta\Delta G$ for the C₁₀PO to C₁₀SO transformation based on the longest simulations conducted (600 ps E.T. and 400 ps D.G.T. at each λ value in aqueous solution, and 400 ps E.T. and 400 ps D.G.T. at each λ value in the micelle, for a total of 36 ns of simulation) is $0.60 \pm 0.91 k_B T$, which has the wrong sign based on the experimental observation that, in

general, surfactants with smaller heads have lower CMCs than surfactants with larger heads and the same tail, and the fact that C₁₀SO has a head which is smaller than that of C₁₀PO. The calculated value of $\Delta\Delta G$ for the C₈SE to C₁₀SE transformation from the longest simulations conducted (600 ps E.T. and 800 ps D.G.T. at each λ value in aqueous solution, and 800 ps E.T. and 800 ps D.G.T. at each λ value in the micelle, for a total of 60 ns of simulation) is $-1.45 \pm 0.33 k_B T$, which has the correct sign based on the experimental observation that surfactants with longer alkyl tails have lower CMCs than surfactants with shorter alkyl tails and the same head, which is the case for C₁₀SE and C₈SE. The computed value of $\Delta\Delta G$ for the C₁₀SO to C₈SO transformation based on the longest simulations conducted (600 ps E.T. and 800 ps D.G.T. at each λ value in aqueous solution and 1,400 ps E.T. and 1,600 ps D.G.T. at each λ value in the micelle, for a total of 88 ns of simulation) is $3.18 \pm 0.35 k_B T$, which again has the correct sign based on the experimental observations for surfactants having the same head and longer (C₁₀) and shorter (C₈) alkyl tails.

Comparison of CS-FE/MT Model Predictions with MT Model Predictions of $\Delta\Delta G$ To enable quantitative evaluation of the accuracy of the $\Delta\Delta G$ predictions of the CS-FE/MT model presented in Table 10.2, experimental CMC data for C₁₀PO/C₁₀SO, C₈SE/C₁₀SE, and C₁₀SO/C₈SO surfactant mixtures were used in conjunction with MT theory to determine the $\Delta\Delta G$ values for each of these three systems. Note that a theoretical model was needed to determine $\Delta\Delta G$ using the experimental CMC data because the experimental CMC data for the mixed surfactant/cosurfactant systems considered is complicated by the fact that the aggregation numbers of the micelles that form in aqueous solution are not known and are unlikely to correspond to the aggregation numbers of the simulated micelles (50 for the C₁₀PO/C₁₀SO system, 25 for the C₈SE/C₁₀SE system, and 50 for the C₁₀SO/C₈SO system) for which $\Delta\Delta G$ was evaluated using the CS-FE/MT model. With the above in mind, to determine values of $\Delta\Delta G$ for the C₁₀PO/C₁₀SO, C₈SE/C₁₀SE, and C₁₀SO/C₈SO systems which are consistent with the experimental CMC data,

the following procedure was adopted:

- Experimental CMC data for mixtures of C₁₀PO/C₁₀SO [28], C₈SE/C₁₀SE [29], and C₁₀SO/C₈SO [30] was obtained from the literature.
- A molecular-thermodynamic (MT) model of single surfactant micellization was used to predict the CMCs of the single surfactants C₁₀PO, C₁₀SO, C₈SE, C₁₀SE, C₁₀SO, and C₈SO [31].
- The head areas of C₁₀PO, C₁₀SO, C₈SE, C₁₀SE, C₁₀SO, and C₈SO were adjusted such that the CMCs predicted by the MT model for each single surfactant considered matched the experimental CMC values. The fitted head areas of C₁₀PO, C₁₀SO, C₈SE, C₁₀SE, and C₈SO were 52.4 Å², 44.9 Å², 44.2 Å², 46.4 Å², 43.8 Å², respectively. As expected, the fitted head areas for C₁₀SO and C₈SO, and the fitted head areas for C₈SE and C₁₀SE, are quite similar because these surfactants have the same heads.
- Next, the MT model based on the fitted head areas was used to predict the mixture CMCs of C₁₀PO/C₁₀SO, C₈SE/C₁₀SE, and C₁₀SO/C₈SO at several different compositions corresponding to solutions for which experimental data was available. The mixture CMC predictions made by the MT model and the experimental mixture CMCs were found to be nearly identical. The observed level of agreement is not surprising because the MT model was fit to experimental CMC data at both single surfactant limits, and each of the surfactant/cosurfactant systems modeled are quite simple (the surfactant and cosurfactant only differ in the length of their linear alkyl tails or in the size of their heads).
- Having developed an accurate MT model to model the mixed micellization behavior of C₁₀PO/C₁₀SO, C₈SE/C₁₀SE, and C₁₀SO/C₈SO, the model was used to predict $\Delta\Delta G$ for each surfactant/cosurfactant system. The CS-FE/MT model prediction of $\Delta\Delta G$ for the C₁₀PO/C₁₀SO system corresponds to the difference between the free energy associated with forming a micelle containing 49 C₁₀PO

surfactants and 1 C₁₀SO surfactant and the free energy associated with forming a micelle containing 50 C₁₀PO surfactants. Similarly, the CS-FE/MT model prediction of $\Delta\Delta G$ for the C₈SE/C₁₀SE system corresponds to the difference between the free energy associated with forming a micelle containing 24 C₈SE surfactants and 1 C₁₀SE surfactant and the free energy associated with forming a micelle containing 25 C₈SE surfactants, and the CS-FE/MT model prediction of $\Delta\Delta G$ for the C₁₀SO/C₈SO system corresponds to the difference between the free energy associated with forming a micelle containing 49 C₁₀SO surfactants and 1 C₈SO surfactant and the free energy associated with forming a micelle containing 50 C₁₀SO surfactants. The MT models of single and mixed surfactant micellization were used to make free-energy predictions for each of these six micellar systems, thereby allowing determination of the three free-energy differences corresponding to the $\Delta\Delta G$ predictions of the CS-FE/MT model. It is important to note that to allow direct comparison of the CS-FE/MT and the MT model estimates of $\Delta\Delta G$, when evaluating $\Delta\Delta G$ using the MT model, the ideal mixing entropy between the surfactants and the cosurfactants, or between the surfactants and solubilizates (the g_{mix} free-energy contribution discussed in Chapter 4), were set equal to zero. As discussed in Chapter 9, each of the molecules in an MD simulation is distinguishable, and therefore, the ideal mixing entropy is not accounted for in the computer simulation estimate of $\Delta\Delta G$.

- The predicted values of $\Delta\Delta G$ for C₁₀PO/C₁₀SO, C₈SE/C₁₀SE, and C₁₀SO/C₈SO using the MT model following the procedure outlined above are: $-0.60 k_{\text{B}}T$, $-1.70 k_{\text{B}}T$, and $2.74 k_{\text{B}}T$, respectively.

Comparison of the CS-FE/MT model estimates of $\Delta\Delta G$ for the transformation of C₁₀PO into C₁₀SO ($0.60 k_{\text{B}}T$ based on the longest computer simulation results) is $1.2 k_{\text{B}}T$ larger than the MT model estimate of $\Delta\Delta G$ ($-0.60 k_{\text{B}}T$) for the same transformation. The discrepancy between the CS-FE/MT model and MT model estimates in this case is sufficiently large that the sign of $\Delta\Delta G$ predicted by the CS-

FE/MT model is incorrect. Consequently, while the CS-FE/MT model predicts that the exchange of C₁₀SO with C₁₀PO is thermodynamically unfavorable, the MT model predicts that it is thermodynamically favorable. The experimental CMC data for mixtures of C₁₀PO and C₁₀SO clearly demonstrates that the exchange of C₁₀SO with C₁₀PO is thermodynamically favorable, because adding C₁₀SO to a solution of C₁₀PO reduces the mixture CMC. Comparison of the CS-FE/MT model estimate of $\Delta\Delta G$ for the transformation of C₈SE into C₁₀SE ($-1.45 k_B T$ based on the longest computer simulation results) with the MT model estimate of $\Delta\Delta G$ ($-1.70 k_B T$) for the same transformation shows that the two predictions are in reasonable agreement. The CS-FE/MT model overestimates the $\Delta\Delta G$ associated with the exchange of a C₁₀SE molecule with a C₈SE molecule by approximately $0.25 k_B T$. Finally, the CS-FE/MT model estimate of $\Delta\Delta G$ for the transformation of C₁₀SO into C₈SO ($3.18 k_B T$ based on the longest computer simulation results) is also in reasonable agreement with the MT model estimate of $\Delta\Delta G$ ($2.74 k_B T$) for the same transformation. In this case, the CS-FE/MT model prediction of $\Delta\Delta G$ overestimates the MT model prediction of $\Delta\Delta G$ by approximately $0.44 k_B T$.

Characteristics of the $\partial G/\partial\lambda$ Profiles

To provide insight into the convergence rate associated with the computed values of $\langle\partial G/\partial\lambda\rangle_\lambda$, in Figures 10-8A and 10-9A, we plot $\partial G/\partial\lambda$ as a function of data-gathering time for the transformation of SDS into IBU and OG into PAB in aqueous solution, respectively. In Figures 10-8B and 10-9B, we plot $\partial G/\partial\lambda$ as a function of data-gathering time for the transformation of SDS into IBU and OG into PAB in the micellar environment. In each figure, results are presented for three λ values: 0.0 (the black profile), 0.5 (the red profile), and 1.0 (the green profile). Each reported $\partial G/\partial\lambda$ profile has been taken from the longest simulation reported in Table 10.2 (for example, the $\partial G/\partial\lambda$ profile presented in Figure 10-8A was taken from the 500 ps data-gathering simulation run in which SDS is transformed into IBU in aqueous solution).

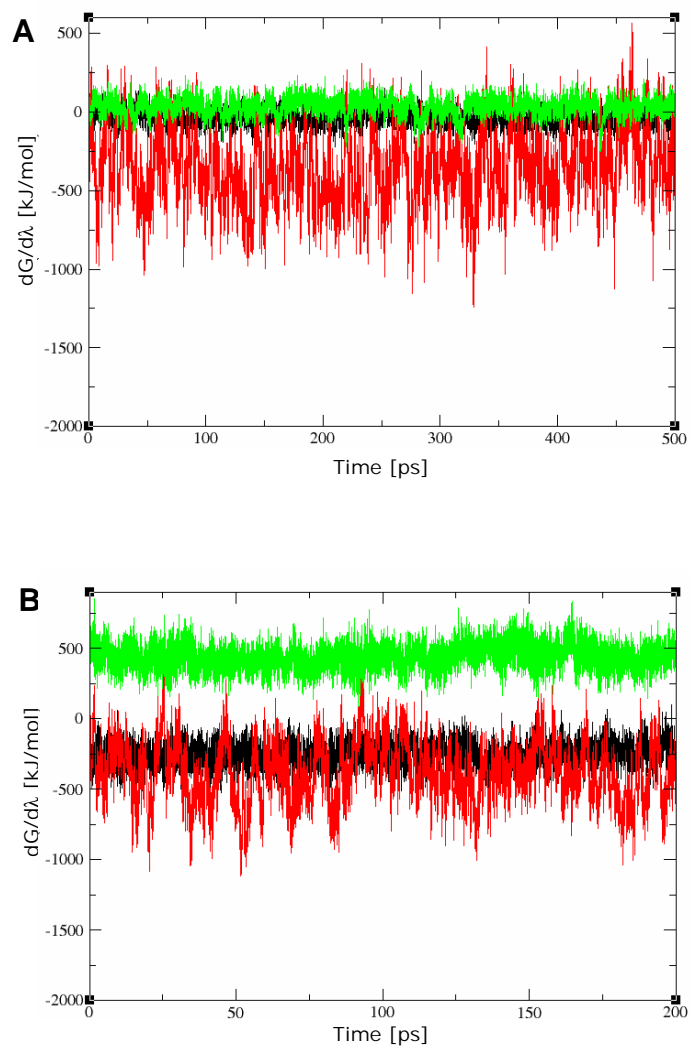


Figure 10-8: Computed values of $\partial G/\partial\lambda$ as a function of data gathering time for the transformation of SDS into IBU in aqueous solution (A) and in the micellar environment (B). Results are presented for simulation at three values of λ : 0.0 (the black profile), 0.5 (the red profile), and 1.0 (the green profile).

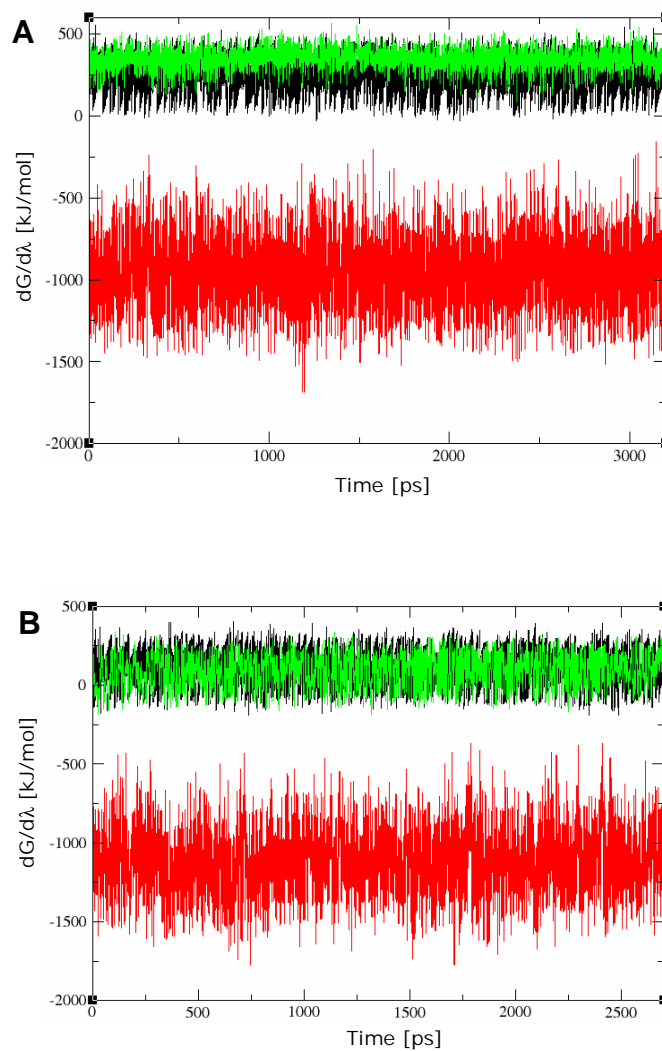


Figure 10-9: Computed values of $\partial G/\partial\lambda$ as a function of data gathering time for the transformation of OG into PAB in aqueous solution (A) and in the micellar environment (B). Results are presented for simulation at three values of λ : 0.0 (the black profile), 0.5 (the red profile), and 1.0 (the green profile).

The noise in the $\partial G/\partial\lambda$ profiles reported in Figures 10-8 and 10-9 is quite high, particularly for the $\partial G/\partial\lambda$ results computed at $\lambda = 0.5$ (the red profiles, where both the surfactant and the solubilizate atoms interact to some extent with their environment). In addition, the magnitude of the $\partial G/\partial\lambda$ values is quite large, ranging from approximately 500 to -1750 kJ/mol. The high levels of noise present in the $\partial G/\partial\lambda$ profiles suggest that, phase space sampling issues aside, a significant amount of simulation time is required to obtain an accurate estimate of both ΔG_1 and ΔG_2 . This reality is reflected in the large uncertainties in the $\Delta\Delta G$ values reported in Table 10.2. However, none of the $\partial G/\partial\lambda$ profiles exhibit any noticeable upwards or downwards drift over the course of the data-gathering simulation, suggesting that each system is adequately equilibrated and that the $\partial G/\partial\lambda$ data obtained should be representative of the equilibrium state of the system at each λ value examined.

In Figures 10-10A, 10-11A, and 10-12A, we plot $\partial G/\partial\lambda$ as a function of data-gathering time for the $C_{10}PO$ to $C_{10}SO$ transformation, the C_8SE to $C_{10}SE$ transformation, and the $C_{10}SO$ to C_8SO transformation in aqueous solution, respectively. In Figures 10-10B, 10-11B, and 10-12B, we plot $\partial G/\partial\lambda$ as a function of data-gathering time for the same three transformations in the micellar environment. In each figure, results are presented for three λ values: 0.0 (the black profiles), 0.5 (the red profiles), and 1.0 (the green profiles). Like the surfactant to solubilizate transformation results reported in Figures 10-8 and 10-9, each $\partial G/\partial\lambda$ profile reported for the surfactant to cosurfactant transformation was taken from the longest simulations reported for each system in Table 10.2.

Each of the 18 $\partial G/\partial\lambda$ profiles shown in Figures 10-10 to 10-12 show a significant level of noise. The highest level of noise in the $\partial G/\partial\lambda$ profiles is observed for $\lambda = 0.5$. No noticeable upwards or downwards trends in the $\partial G/\partial\lambda$ profiles is noticeable for the surfactant to cosurfactant transformations in either the aqueous or the micellar environments. In general, although the level of noise in the profiles shown is quite high, the general shape of each $\partial G/\partial\lambda$ profile is quite flat.

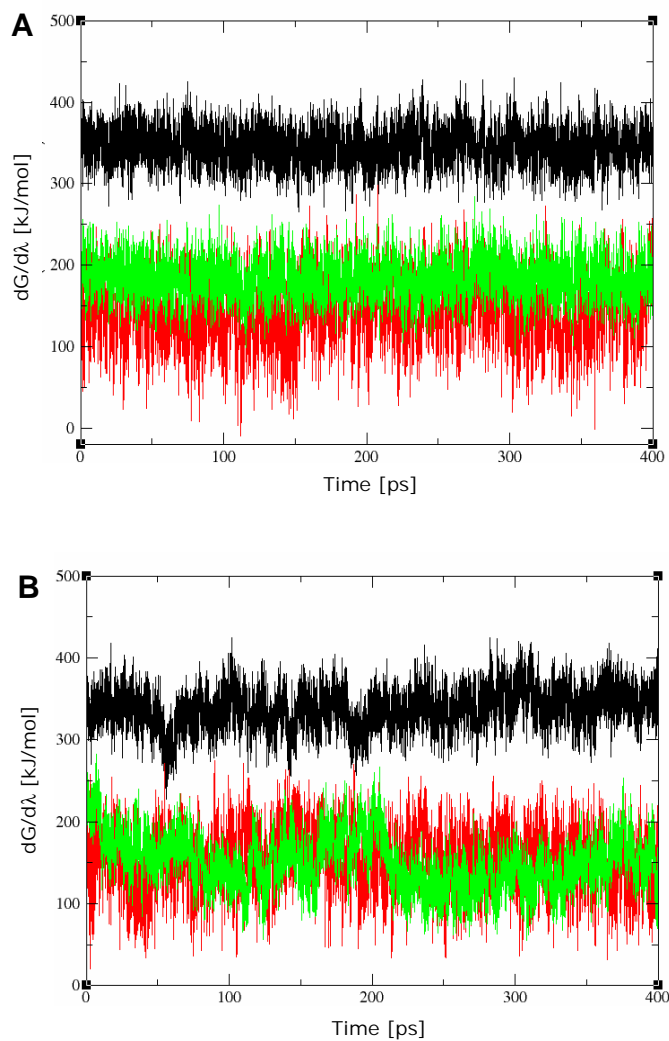


Figure 10-10: Computed values of $\partial G/\partial \lambda$ as a function of data gathering time for the transformation of $C_{10}PO$ into $C_{10}SO$ in aqueous solution (A) and in the micellar environment (B). Results are presented for simulation at three values of λ : 0.0 (the black profile), 0.5 (the red profile), and 1.0 (the green profile).

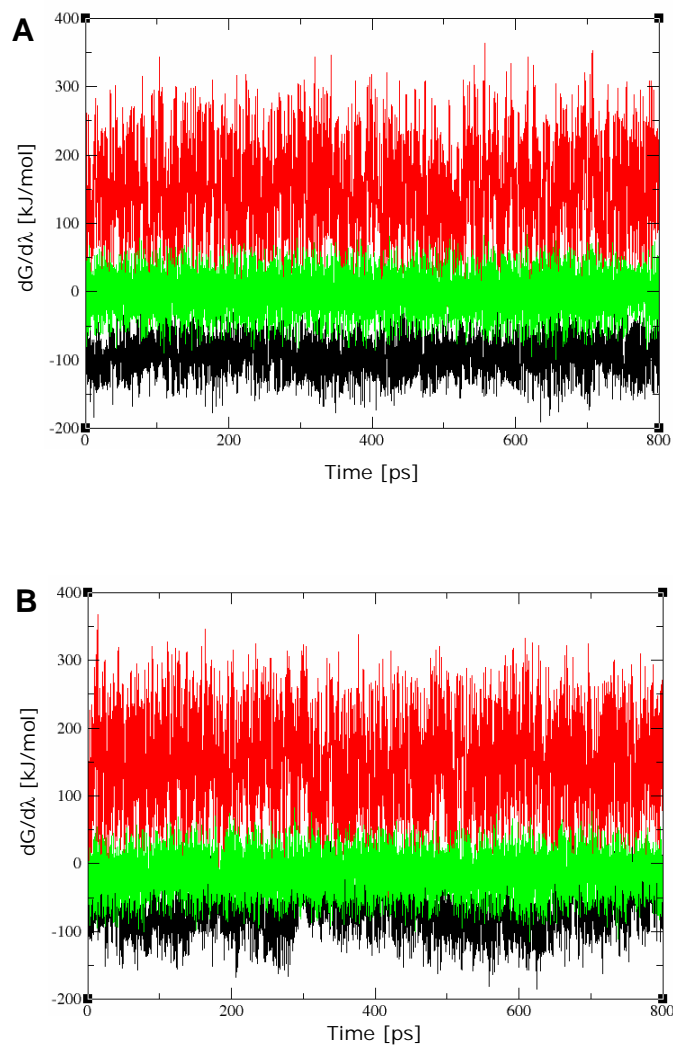


Figure 10-11: Computed values of $\partial G/\partial\lambda$ as a function of data gathering time for the transformation of C_8SE into $C_{10}SE$ in aqueous solution (A) and in the micellar environment (B). Results are presented for simulation at three values of λ : 0.0 (the black profile), 0.5 (the red profile), and 1.0 (the green profile).

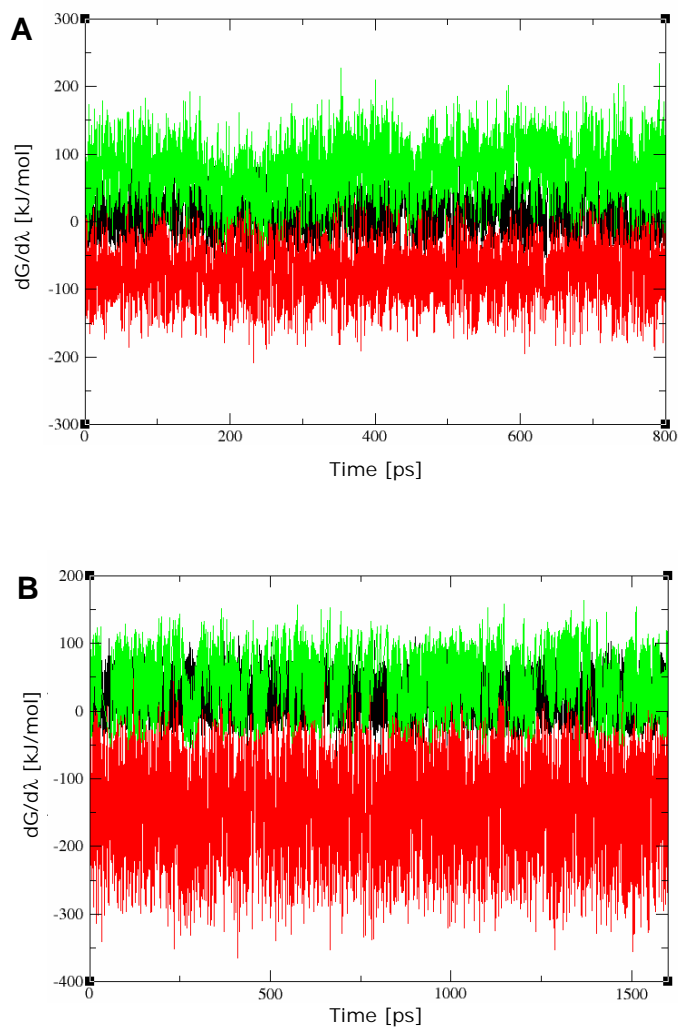


Figure 10-12: Computed values of $\partial G/\partial\lambda$ as a function of data gathering time for the transformation of $C_{10}SO$ into C_8SO in aqueous solution (A) and in the micellar environment (B). Results are presented for simulation at three values of λ : 0.0 (the black profile), 0.5 (the red profile), and 1.0 (the green profile).

Characteristics of the $\langle \partial G / \partial \lambda \rangle_\lambda$ Profiles

In Figures 10-13 and 10-14, we report $\langle \partial G / \partial \lambda \rangle_\lambda$, or the ensemble average of $\partial G / \partial \lambda$ at a constant value of λ , as a function of λ in aqueous solution (the black profiles) and in the micellar environment (the red profiles) for the transformation of SDS to IBU and OG to PAB, respectively. Each reported $\langle \partial G / \partial \lambda \rangle_\lambda$ versus λ profile corresponds to the longest simulations reported in Table 10.2, and reflects the time averaged value of $\partial G / \partial \lambda$ measured at each λ value. Therefore, the $\langle \partial G / \partial \lambda \rangle_\lambda$ values reported for $\lambda = 0$, $\lambda = 0.5$, and $\lambda = 1.0$ were obtained by averaging the $\partial G / \partial \lambda$ versus time profiles presented in Figures 10-8 and 10-9.

The $\langle \partial G / \partial \lambda \rangle_\lambda$ profiles for the SDS to IBU transformation in both aqueous solution and in the micellar environment are rough and irregular, suggesting that simulation at additional values of λ may be necessary to accurately estimate the area under the $\langle \partial G / \partial \lambda \rangle_\lambda$ versus λ curve and accurately determine ΔG_1 and ΔG_2 . In addition, the magnitudes of the $\langle \partial G / \partial \lambda \rangle_\lambda$ values are quite large, ranging from approximately 750 kJ/mol to -500 kJ/mol.

Although not as irregular, the $\langle \partial G / \partial \lambda \rangle_\lambda$ profiles for the OG to PAB transformation exhibit sharp discontinuities at $\lambda = 0.47$ and 0.5 in both the aqueous solution and in the micellar environment. The lack of a smooth $\langle \partial G / \partial \lambda \rangle_\lambda$ versus λ profile in both cases suggests that simulation at additional values of λ may be necessary to obtain an accurate estimate of ΔG_1 and ΔG_2 . The magnitudes of the $\langle \partial G / \partial \lambda \rangle_\lambda$ values for the OG to PAB transformations range from approximately 500 kJ/mol to -1100 kJ/mol, a range of values that is even larger than that measured for the SDS to IBU transformations.

In Figures 10-15, 10-16, and 10-17 the same information presented in Figures 10-13 and 10-14 is reported for the surfactant to cosurfactant transformations of $C_{10}PO$ to $C_{10}SO$, C_8SE to $C_{10}SE$, and $C_{10}SO$ to C_8SO , respectively. Calculated values of $\langle \partial G / \partial \lambda \rangle_\lambda$ are reported for transformation in aqueous solution (the black profiles) and transformation in the micellar environment (the red profiles). Each reported $\langle \partial G / \partial \lambda \rangle_\lambda$ versus λ profile corresponds to the longest aqueous and micellar

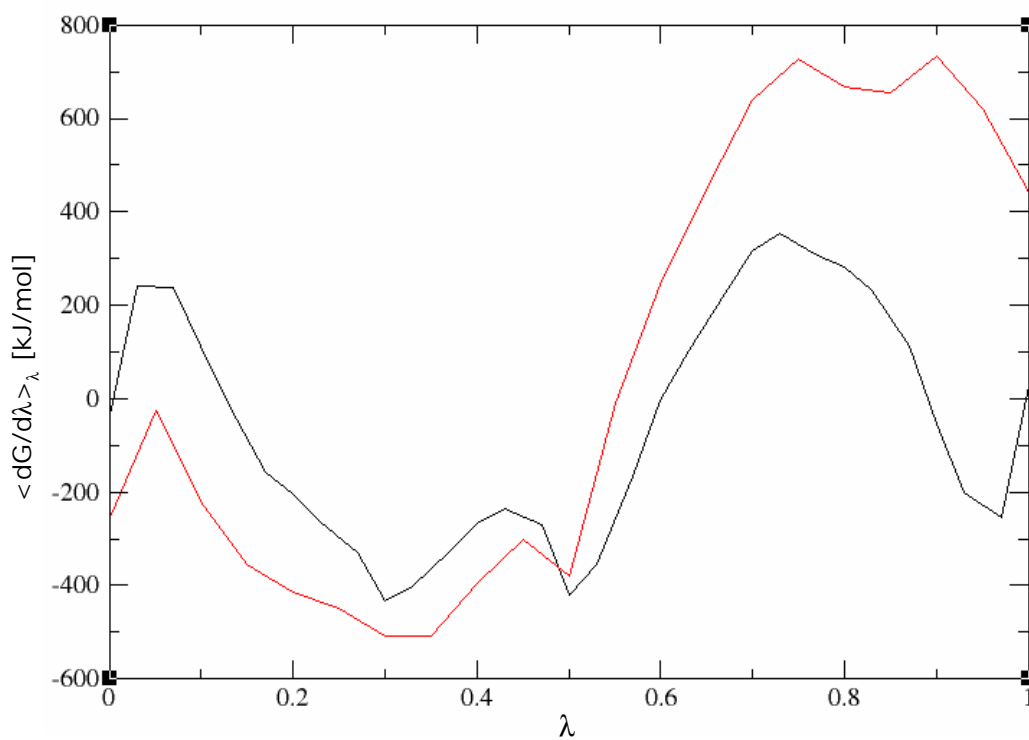


Figure 10-13: Computed values of $\langle \partial G / \partial \lambda \rangle_\lambda$ as a function of λ for the transformation of SDS into IBU in aqueous solution (the black line) and in the micellar environment (the red line).

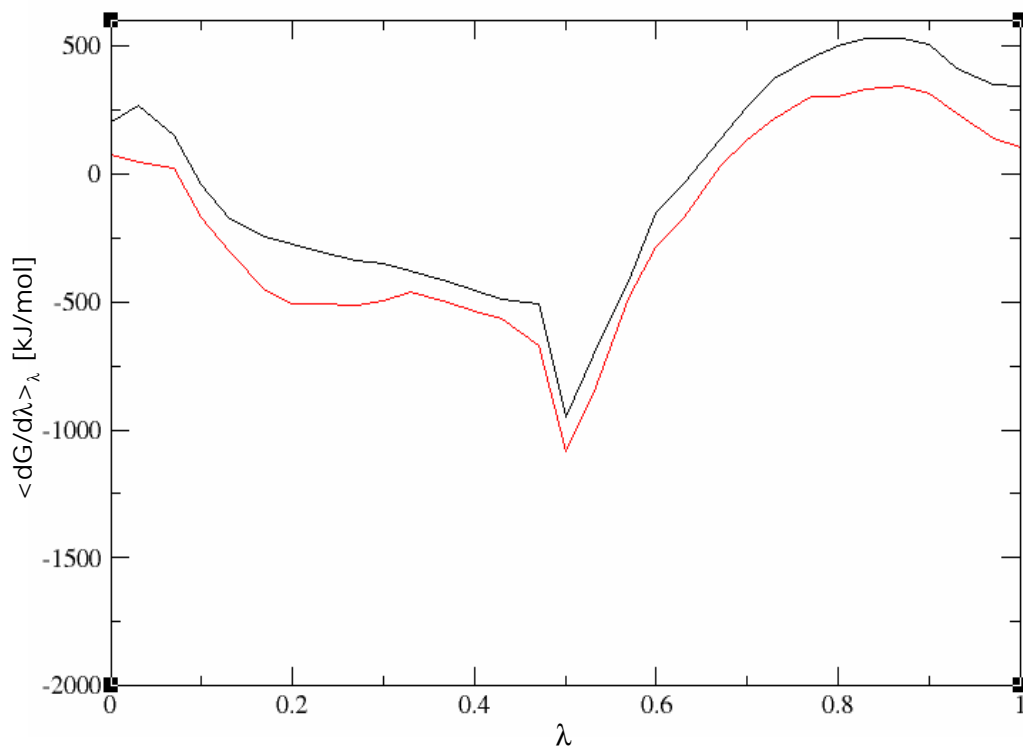


Figure 10-14: Computed values of $\langle \partial G / \partial \lambda \rangle_\lambda$ as a function of λ for the transformation of OG into PAB in aqueous solution (the black line) and in the micellar environment (the red line).

simulations reported in Table 10.2.

The $C_{10}PO$ to $C_{10}SO$ $\langle \partial G / \partial \lambda \rangle_\lambda$ versus λ profile is quite rough and irregular (similar to the profiles associated with the SDS to IBU and with the OG to PAB transformations). In particular, the profiles associated with the $C_{10}PO$ to $C_{10}SO$ transformation exhibit sharp discontinuities at $\lambda = 0.05$ and 0.95 in both the aqueous solution and in the micellar environment. Like the free-energy results presented in Figures 10-13 and 10-14, the free-energy results presented in Figure 10-15 suggests that simulation at additional values of λ may be necessary to accurately estimate the area under the $\langle \partial G / \partial \lambda \rangle_\lambda$ versus λ curve. The C_8SE to $C_{10}SE$ and the $C_{10}SO$ to C_8SO $\langle \partial G / \partial \lambda \rangle_\lambda$ versus λ profiles are comparatively smooth and well-behaved, although they also exhibit a discontinuity in the $\langle \partial G / \partial \lambda \rangle_\lambda$ profile at around $\lambda = 0.05$. It is interesting to note that the free-energy results obtained for the C_8SE to $C_{10}SE$ and the $C_{10}SO$ to C_8SO transformations in aqueous solution are significantly smoother than the results obtained for transformations in the micellar environment.

The magnitude of the $\langle \partial G / \partial \lambda \rangle_\lambda$ values calculated for the $C_{10}PO$ to $C_{10}SO$ transformations are significantly larger than those calculated in transforming C_8SE into $C_{10}SE$ and $C_{10}SO$ into C_8SO , and range from approximately 550 kJ/mol to -50 kJ/mol. The larger magnitude of the $\langle \partial G / \partial \lambda \rangle_\lambda$ values calculated for the $C_{10}PO$ to $C_{10}SO$ transformations reflects the larger structural changes associated with the exchange of $C_{10}SO$ for $C_{10}PO$; namely, changing both the identity of phosphorus to sulfur and the removal of a CH_3 group within the surfactant head. The magnitude of the $\langle \partial G / \partial \lambda \rangle_\lambda$ values calculated for the C_8SE to $C_{10}SE$ transformations range from approximately 150 kJ/mol to -100 kJ/mol. The magnitude of the $\langle \partial G / \partial \lambda \rangle_\lambda$ values calculated for the $C_{10}SO$ to C_8SO transformations range from approximately 100 kJ/mol to -150 kJ/mol. The $\langle \partial G / \partial \lambda \rangle_\lambda$ profiles calculated for the C_8SE to $C_{10}SE$ and for the $C_{10}SO$ to C_8SO transformations appear to be roughly the inverse of each other, a result that would be intuitively expected because the chemical modification made to C_8SE (the addition of two CH_2 groups) is the inverse of the chemical modification made to $C_{10}SO$ (the removal of two CH_2 groups). One should keep in

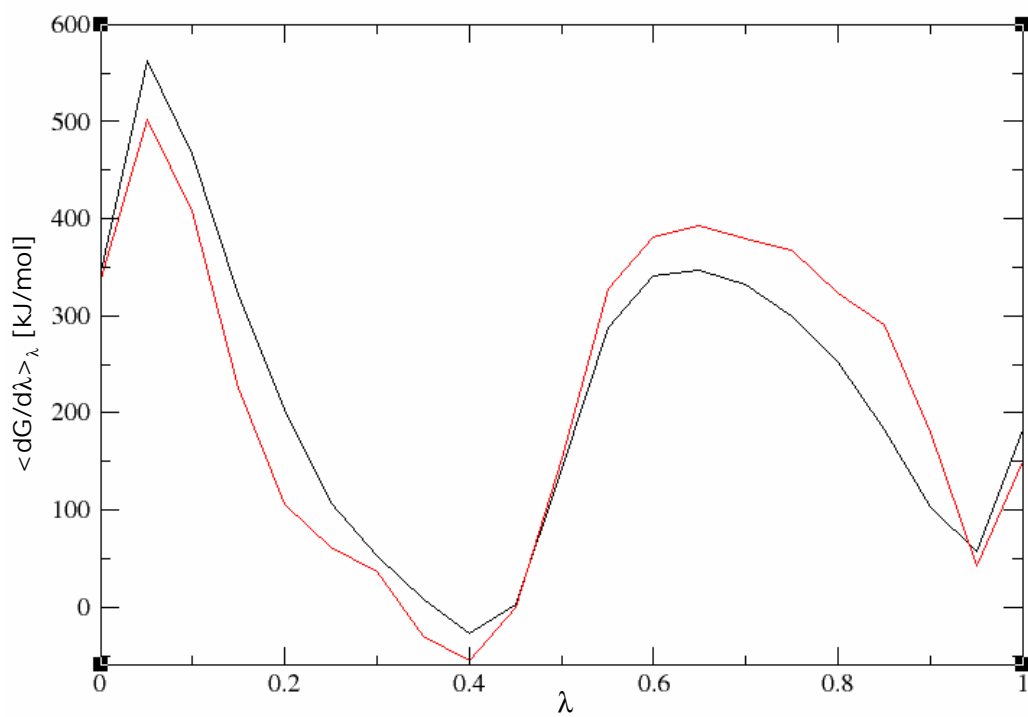


Figure 10-15: Computed values of $\langle \partial G / \partial \lambda \rangle_\lambda$ as a function of λ for the transformation of C₁₀PO into C₁₀SO in aqueous solution (the black line) and in the micellar environment (the red line).

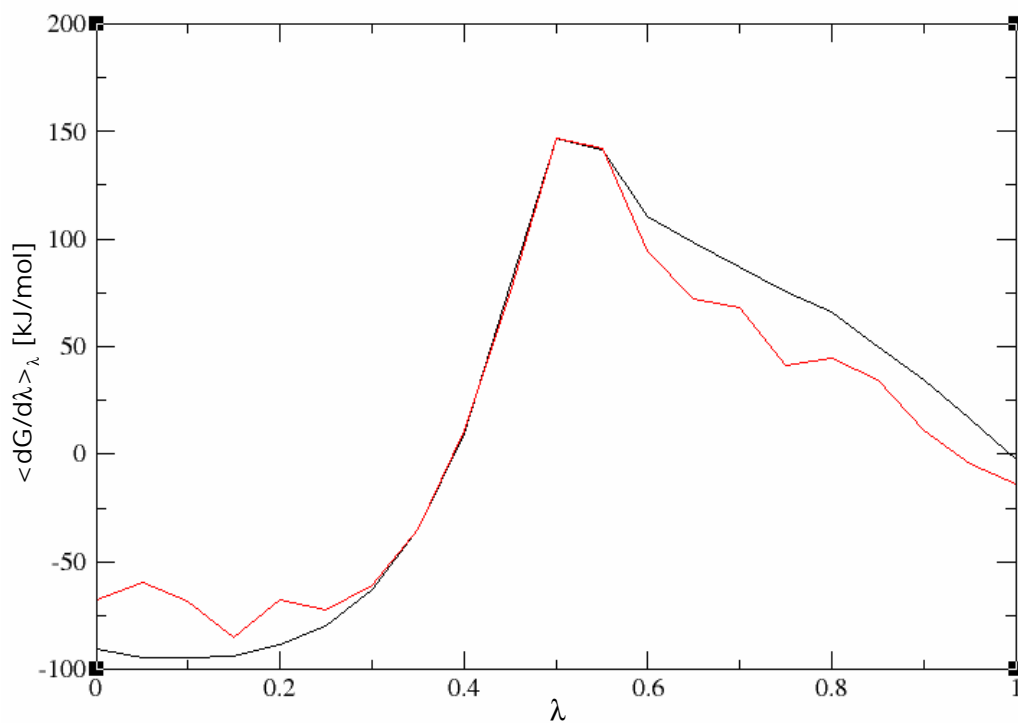


Figure 10-16: Computed values of $\langle \partial G / \partial \lambda \rangle_\lambda$ as a function of λ for the transformation of C₈SE into C₁₀SE in aqueous solution (the black line) and in the micellar environment (the red line).

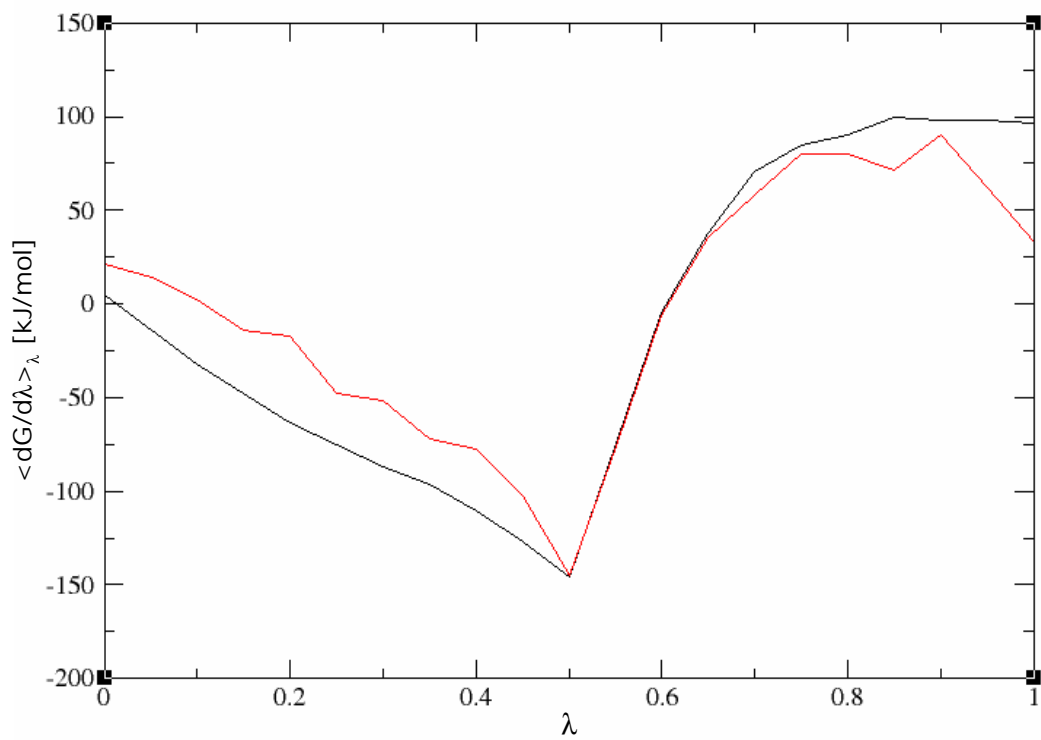


Figure 10-17: Computed values of $\langle \partial G / \partial \lambda \rangle_\lambda$ as a function of λ for the transformation of $C_{10}SO$ into C_8SO in aqueous solution (the black line) and in the micellar environment (the red line).

mind, however, that: (i) the heads of the two surfactants are different (SE versus SO), and (ii) when transforming C₈SE into C₁₀SE, the transformation occurs in a micelle composed of surfactants with eight carbon tails and an aggregation number of 25, while when transforming C₁₀SO into C₈SO, the transformation occurs in a micelle composed of surfactants with ten carbon tails and an aggregation number of 50. Consequently, the free-energy profiles shown in Figures 10-15 and 10-16 are not expected to be exactly inversely related.

In comparison with the SDS to IBU and OG to PAB transformations, the C₁₀PO to C₁₀SO, C₈SE to C₁₀SE, and C₈SO to C₁₀SO transformations involve relatively small structural transformations. The ΔG_1 and ΔG_2 results for the C₁₀PO to C₁₀SO, C₈SE to C₁₀SE, and C₈SO to C₁₀SO transformations reported in Table 10.2 exhibit less variation as a function of the length of equilibration and simulation time than the ΔG_1 and ΔG_2 results reported for the SDS to IBU and OG to PAB transformations. In addition, the ΔG_1 and ΔG_2 results for the C₈SE to C₁₀SE and the C₁₀SO to C₈SO transformations exhibit less variation as a function of the length of equilibration and simulation time than the C₁₀PO to C₁₀SO transformation.

10.4.2 $\Delta\Delta G$ Results Based on Simulations at Additional λ Values

As discussed in Section 10.4.1, the $\langle\partial G/\partial\lambda\rangle_\lambda$ versus λ profiles for each surfactant to solubilize and for one of the surfactant to cosurfactant transformations are relatively rough and irregular, suggesting that simulation at additional values of λ may result in a more accurate determination of the area under the $\langle\partial G/\partial\lambda\rangle_\lambda$ versus λ curve. With this in mind, the number of λ values at which the $\partial G/\partial\lambda$ data was gathered for the transformations of C₁₀PO into C₁₀SO, C₈SE into C₁₀SE, and C₁₀SO into C₈SO in the micellar environment was increased from 20 to 40 to evaluate the effect of increasing the number of λ values on the accuracy of the CS-FE/MT model estimates of $\Delta\Delta G$. Each of the λ values selected were evenly spaced between 0 and 1. In Table 10.3, we

C ₁₀ PO \rightarrow C ₁₀ SO (micelle)				$G_{\text{form,mixed}} - G_{\text{form,single}}$
E.T. [ps]	D.G.T. [ps]	λ	$\Delta G_2 [k_B T]$	($=\Delta\Delta G = \Delta G_2 - \Delta G_1^*$)
50	50	40	88.9 ± 0.80	2.02 ± 0.84
100	200	40	87.9 ± 0.73	1.09 ± 0.78
300	600	40	86.9 ± 0.69	0.05 ± 0.74
C ₈ SE \rightarrow C ₁₀ SE (micelle)				
50	50	40	3.98 ± 0.35	-2.47 ± 0.37
100	200	40	4.24 ± 0.52	-2.21 ± 0.53
300	600	40	4.63 ± 0.31	-1.82 ± 0.33
C ₁₀ SO \rightarrow C ₈ SO (micelle)				
25	25	40	-2.38 ± 0.31	2.60 ± 0.36
50	50	40	-3.11 ± 0.47	1.87 ± 0.50
100	200	40	-3.23 ± 0.57	1.75 ± 0.60
300	600	40	-2.12 ± 0.32	2.86 ± 0.37

Table 10.3: Transformation free energies computed using the CS-FE/MT model with additional λ values.

report the equilibration simulation time (E.T.), the data-gathering simulation time (D.G.T.), the number of λ values at which simulations were conducted, ΔG_2 , and $G_{\text{form,mixed}} - G_{\text{form,single}}$ (evaluated as the difference between the computed value of ΔG_2 and the value of ΔG_1 reported in Table 10.2, denoted as ΔG_1^* , determined from the longest aqueous state transformation of each surfactant into its cosurfactant). The values of $\Delta G_1^* = \Delta\Delta G - \Delta G_2$ for the C₁₀PO to C₁₀SO, the C₈SE to C₁₀SE, and the C₈SO to C₁₀SO transformations are equal to $86.9 k_B T$, $6.45 k_B T$, and $-4.98 k_B T$, respectively (see Table 10.3).

The surfactant to cosurfactant $\Delta\Delta G$ predictions reported in Table 10.3 range between $2.86 \pm 0.37 k_B T$ and $-2.47 \pm 0.37 k_B T$. The computed value of $\Delta\Delta G$ for the C₁₀PO to C₁₀SO transformation based on the longest simulations conducted (1,000 ps of simulation at each λ value in aqueous solution, as shown in Table 10.2, and 300 ps E.T. and 600 ps D.G.T. at each λ value in the micelle (see Table 10.3), for a total of 56 ns of simulation) is $0.05 \pm 0.74 k_B T$, which is within $0.65 k_B T$ of the MT model prediction for $\Delta\Delta G$ ($-0.60 k_B T$, see Section 10.4.1). The computed value of

$\Delta\Delta G$ for the C₈SE to C₁₀SE transformation from the longest simulation conducted in aqueous solution and in the micelle (1,400 ps of simulation at each λ value in aqueous solution, and 300 ps E.T. and 600 ps D.G.T. at each λ value in the micelle, for a total of 64 ns of simulation) is $-1.82 \pm 0.33 k_B T$. This estimate is only $0.12 k_B T$ more negative than the MT model prediction of $\Delta\Delta G$ ($-1.70 k_B T$, see Section 10.4.1). Finally, the computed value of $\Delta\Delta G$ for the C₁₀SO to C₈SO transformation based on the longest simulations conducted (1,400 ps of simulation at each λ value in aqueous solution, and 300 ps E.T. and 600 ps D.G.T. at each λ value in the micelle, for a total of 64 ns of simulation) is $2.86 \pm 0.37 k_B T$. The CS-FE/MT model prediction of $\Delta\Delta G$ for this surfactant to cosurfactant transformation is within $0.12 k_B T$ of the MT model prediction for $\Delta\Delta G$ ($2.74 k_B T$, see Section 10.4.1). Each of these $\Delta\Delta G$ predictions are in better agreement with the MT model prediction of $\Delta\Delta G$ than the $\Delta\Delta G$ values obtained based on micellar simulation at only twenty values of λ .

10.5 Conclusions

In this chapter, the CS-FE/MT modeling approach introduced in Chapter 9 was implemented to predict the free-energy change associated with surfactant to solubilize and surfactant to cosurfactant transformations (as reflected in $\Delta\Delta G$) through alchemical computer simulation. As discussed in Chapter 9, to make predictions of solution behavior using the CS-FE/MT modeling approach, it would be necessary to evaluate $\Delta\Delta G$ for multiple surfactant to solubilize or surfactant to cosurfactant transformations. The goal of the research presented in this chapter, however, has simply been to evaluate the ability of the alchemical computer simulation method used in the CS-FE/MT modeling approach to evaluate $\Delta\Delta G$ for a single surfactant to solubilize or a single surfactant to cosurfactant transformation. For the three surfactant to cosurfactant transformations considered in this chapter, the theoretical predictions of the CS-FE/MT model for $\Delta\Delta G$ were compared with $\Delta\Delta G$ predictions made by an accurate MT model developed by fitting to experimental CMC data.

In implementing the CS-FE/MT model, a number of decisions must be made about the way in which the alchemical transformations should be performed. Such decisions can have a significant impact on the computational expense required to obtain accurate free-energy estimates [16, 23]. For the alchemical simulations implemented in this chapter, soft-core potentials (V_{sc}) were used to avoid the end-point catastrophe. The advantages and limitations associated with using single topology and dual topology approaches in implementing alchemical transformations was discussed. A hybrid single/dual topology approach was used to morph SDS into IBU, a dual topology approach was used to morph OG into PAB, and a single topology approach was used to morph C₁₀PO into C₁₀SO, C₈SE into C₁₀SE, and C₁₀SO into C₈SO. The alchemical topology used for each surfactant to solubilize transformation, or for each surfactant to cosurfactant transformation, was selected based on: (i) the extent of structural changes required to morph one molecule into the other, and (ii) the desire to minimize the total number of atoms simulated and the total number of atoms whose interactions with the environment are altered.

For each alchemical transformation, thermodynamic integration was used to evaluate the difference in free energy associated with forming a micelle composed of $n - 1$ surfactant A molecules and one surfactant/solubilize B molecule, and with forming a micelle composed of n surfactant A molecules. This free-energy difference, referred to as $G_{\text{form,mixed}} - G_{\text{form,single}}$ (or $\Delta\Delta G$), is a necessary input to the CS-FE/MT model that ultimately allows prediction of the solution behavior of mixed surfactant/solubilize or surfactant/cosurfactant micelles (see Chapter 9). Each $\Delta\Delta G$ value was computed by determining the difference in free energy associated with: (i) transforming a surfactant molecule of type A into a cosurfactant/solubilize molecule of type B in a micellar environment (referred to as ΔG_2), and (ii) transforming a surfactant molecule of type A into a cosurfactant/solubilize molecule of type B in aqueous solution (referred to as ΔG_1).

CS-FE/MT model predictions of $\Delta\Delta G$ for SDS to IBU, OG to PAB, C₁₀PO to C₁₀SO, C₈SE to C₁₀SE, and C₁₀SO to C₈SO transformations were made at a

number of simulation conditions, including: (i) different equilibration times at each λ value, (ii) different data-gathering times at each λ value, (iii) simulation at a different number of λ values.

Even after performing lengthy equilibration and data gathering at each λ value, physically unrealistic values of $\Delta\Delta G$ were predicted by the CS-FE/MT model for the transformation of SDS into IBU and the transformation of OG into PAB. The predictions of the CS-FE/MT model were unphysically large for the transformation of SDS into IBU, and they were unphysically small for the transformation of OG into PAB. The $\Delta\Delta G$ results for these two surfactant to solubilizate transformations, which involved significant structural changes, suggests that with the alchemical approach discussed in this chapter and present-day computational resources, the CS-FE/MT model cannot be used to accurately compute free-energy changes that are associated with large structural transformations.

The $\Delta\Delta G$ predictions of the CS-FE/MT model were more physically realistic for the transformations of $C_{10}PO$ into $C_{10}SO$, C_8SE into $C_{10}SE$, and $C_{10}SO$ into C_8SO , which each involved significantly less extensive structural changes than the surfactant to solubilizate transformations considered above. To enable quantitative evaluation of the $\Delta\Delta G$ predictions of the CS-FE/MT model for these three surfactant to cosurfactant transformations, experimental CMC data for $C_{10}PO/C_{10}SO$, $C_8SE/C_{10}SE$, and $C_{10}SO/C_8SO$ surfactant/cosurfactant mixtures were used to develop a highly accurate MT model of the micellization behavior of each surfactant/cosurfactant mixture by adjusting the head area of each surfactant as a fitted parameter until the MT model predictions matched the pure surfactant and pure cosurfactant CMCs. This MT model was then used to predict a value of $\Delta\Delta G$ corresponding to the same change in micelle composition accomplished alchemically through computer simulation in the CS-FE/MT model. For each surfactant to cosurfactant transformation, the resulting MT model was used to predict the free-energy difference associated with forming a micelle containing $n - 1$ surfactant A molecules and 1 surfactant B molecule and with forming a micelle containing n surfactant A molecules. Because the MT model was

fit to experimental CMC data, we believe that it provides an excellent prediction of the true physical value of $\Delta\Delta G$, and also serves as an excellent quantitative indicator with which to evaluate the accuracy of the $\Delta\Delta G$ predictions of the CS-FE/MT model.

The CS-FE/MT model estimate of $\Delta\Delta G$ for the C₁₀PO to C₁₀SO transformation based on simulation at 20 different λ values in the micellar environment (0.60 $k_B T$ for the longest computer simulations conducted) was found to be 1.2 $k_B T$ larger than the MT model estimate of $\Delta\Delta G$ (-0.60 $k_B T$) for this system. The CS-FE/MT model estimate of $\Delta\Delta G$ for the C₁₀PO to C₁₀SO transformation based on simulation at 40 different λ values in the micellar environment was found to be $0.05 \pm 0.74 k_B T$ based on the longest simulations conducted, a prediction which is 0.65 $k_B T$ larger than the MT model prediction of $\Delta\Delta G$ for this system. Unfortunately, the sign of $\Delta\Delta G$ predicted by the CS-FE/MT model for the C₁₀PO to C₁₀SO transformation is incorrect for both the 20 and 40 λ value simulation results. Consequently, the CS-FE/MT model predicts that exchange of C₁₀SO with C₁₀PO is thermodynamically unfavorable when it is actually favorable. The CS-FE/MT model estimate of $\Delta\Delta G$ for the C₈SE/C₁₀SE system based on simulation at 20 different λ values in the micellar environment (-1.45 $k_B T$ for the longest computer simulations conducted) and the MT model estimate of $\Delta\Delta G$ (-1.70 $k_B T$) were found to be in reasonable agreement. The CS-FE/MT model estimate of $\Delta\Delta G$ for the C₈SE/C₁₀SE system based on simulation at 40 different λ values in the micellar environment was found to be $-1.82 \pm 0.33 k_B T$ for the longest simulations conducted, a prediction that is only 0.12 $k_B T$ more negative than the MT model estimate of $\Delta\Delta G$ for this system. Finally, the CS-FE/MT model estimate of $\Delta\Delta G$ for the C₁₀SO to C₈SO transformation based on simulation at 20 different λ values in the micellar environment (3.18 $k_B T$ for the longest computer simulations conducted) was also found to be in reasonable agreement with the MT model estimate of $\Delta\Delta G$ (2.74 $k_B T$) for this system. The CS-FE/MT model estimate of $\Delta\Delta G$ based on simulation at 40 different λ values in the micellar environment for the C₁₀SO to C₈SO transformation was found to be $2.86 \pm 0.37 k_B T$ for the longest

simulations conducted, which is only $0.12 k_B T$ greater than the MT model prediction of $\Delta\Delta G$ for this system.

All three $\Delta\Delta G$ predictions for the surfactant to cosurfactant transformations are in better agreement with the MT model predictions of $\Delta\Delta G$ when simulations are conducted at 40 values of λ to evaluate ΔG_2 than when simulations are conducted at 20 values of λ to evaluate ΔG_2 , suggesting that further improvement in the predictions of the CS-FE/MT model may be obtained by simulating at additional λ values in both the micellar environment and the aqueous solution to obtain more accurate estimates of the $\langle\partial G/\partial\lambda\rangle_\lambda$ versus λ integrals.

It is interesting to point out that the accuracy of the $\Delta\Delta G$ predictions obtained using the CS-FE/MT model can be correlated with the magnitude of the $\langle\partial G/\partial\lambda\rangle_\lambda$ values calculated during each alchemical transformation. The magnitude of the $\langle\partial G/\partial\lambda\rangle_\lambda$ values calculated during SDS to IBU, OG to PAB, and C₁₀PO to C₁₀SO transformations are all quite large (see Figures 10-13, 10-14, and 10-17), indicating that additional simulation time (and possibly simulation at many more λ values) may be necessary to accurately determine $\Delta\Delta G$ for these systems. As discussed in Section 10.4.1, the range of $\langle\partial G/\partial\lambda\rangle_\lambda$ values calculated for the transformation of SDS into IBU is approximately 1,250 kJ/mol. The range of $\langle\partial G/\partial\lambda\rangle_\lambda$ values calculated for the transformation of OG into PAB is 1,600 kJ/mol. For the transformations of C₁₀PO into C₁₀SO, C₈SE into C₁₀SE, and C₁₀SO into C₈SO, the range of $\langle\partial G/\partial\lambda\rangle_\lambda$ values calculated are approximately 600 kJ/mol, 250 kJ/mol, and 250 kJ/mol, respectively. Not surprisingly, the largest $\langle\partial G/\partial\lambda\rangle_\lambda$ values calculated are for the alchemical transformations that involve that largest structural changes (see Figures 10-3 and 10-4). The three transformations with the largest $\langle\partial G/\partial\lambda\rangle_\lambda$ values were each poorly modeled using the CS-FE/MT modeling approach, while the two transformations with the smallest $\langle\partial G/\partial\lambda\rangle_\lambda$ values were modeled with reasonable accuracy using the CS-FE/MT model.

The statistical uncertainties in ΔG_1 and ΔG_2 determined based on the error analysis approach discussed in Section 10.4.1 are ranked as follows for each alchemical

transformation (from largest to smallest, and as ranked based on the longest computer simulation result): SDS into IBU, OG into PAB, C₁₀PO into C₁₀SO, C₁₀SO into C₈SO, and C₈SE into C₁₀SE. Close examination of the $\Delta\Delta G$ values obtained for the three alchemical transformations for which poor $\Delta\Delta G$ predictions were obtained (SDS into IBU, OG into PAB, and C₁₀PO into C₁₀SO) shows that the predicted value of $\Delta\Delta G$ varies significantly depending on the length of the equilibration and the data-gathering simulations conducted, suggesting that phase space was insufficiently sampled and more simulation is required to obtain an accurate estimate of $\Delta\Delta G$. For the free-energy results to be accurate, a large fraction of the phase space states that contribute significantly to the overall free-energy change associated with surfactant/solubilize morphing must be sampled adequately [32]. Most alchemical free-energy studies reported in the literature describe successful results for relatively modest structural changes. The larger the structural changes attempted, the more difficult it is to adequately sample phase space and to obtain an accurate estimate of the free-energy change [23]. Determining the free-energy change associated with large structural modifications could be particularly difficult within a micellar environment due to slow dynamics and conformational sampling within the micelle core. It is instructive to note that there are fluctuations in SASA shown in Figures 10-5 and 10-6 that occur on relatively long, nanosecond time scales. Simulation over extended periods of time may be required to thoroughly sample the configurations adopted by a micelle fluctuating at equilibrium and to observe convergence in the free-energy results when large structural changes are attempted.

The CS-FE/MT modeling results presented in this chapter suggest that with present-day computational resources, it may not be possible to make accurate predictions of the free-energy changes (and therefore, of the micelle and the micellar solution properties) associated with forming mixed surfactant/cosurfactant and surfactant/solubilize micelles where the chemical structures of the surfactant and the cosurfactant or the solubilize are significantly different. However, the CS-FE/MT modeling approach appears to yield reasonably accurate results for $\Delta\Delta G$ when it is

used to evaluate the free-energy change associated with relatively small structural transformations, such as the transformation of C₈SE into C₁₀SE and the transformation of C₁₀SO into C₈SO.

To the best of our knowledge, the free-energy results presented in this chapter represent the first attempt to use alchemical free-energy methods to model the micellization behavior of mixed surfactant/cosurfactant and surfactant/solubilizate systems. While certainly of interest from an academic perspective, and although this approach may become practical in the future as the computational power of computers increases, at the present time, more accurate estimates of $G_{\text{form,mixed}}$ can be obtained with less computational expense using traditional MT modeling with computer simulation estimates of surfactant/solubilizate heads and tails (see Chapters 2-5), or using the CS-MT modeling approach (see Chapters 6-8). As computer power increases and as advances in alchemical free-energy methods are made, the computational expense of the CS-FE/MT model may no longer pose a significant barrier to its use. In addition, it may become possible to apply the CS-FE/MT model to make accurate predictions of the free-energy changes associated with forming multicomponent surfactant and solubilizate micelles where the chemical structures of the surfactants, the cosurfactants, and/or the solubilizates differ significantly.

In Part I of this thesis, several approaches were introduced to use molecular dynamics simulations to obtain inputs for molecular thermodynamic modeling. In Part II of this thesis, the application of computer simulation free-energy methods to evaluate the free-energy change associated with mixed micelle formation has been explored. In Part III of this thesis, direct prediction of surfactant solution properties using molecular dynamics simulations is investigated through the exploration of: (i) the interfacial characteristics of surfactant monolayers, and (ii) the self-assembly behavior of complex surfactants in aqueous solution. In Chapter 11, results are presented for the simulation of monolayers of a series of bolaamphiphilic poly(fluorooxetane) surfactants at an air/water interface. In this study, properties such as the saturated interfacial area per surfactant molecule, the interfacial area per surfactant molecule

as a function of surface tension, density profiles, order parameters, the degree of hydration of various atoms in each surfactant molecule, and the degree of counterion binding were determined directly through molecular dynamics simulation. In Chapter 12, molecular dynamics simulations to investigate the self-assembly behavior of the triterpenoids asiatic acid (AA) and madecassic acid (MA) in aqueous solution are described. In this study, properties such as the kinetics of micelle formation, structural characteristics of the self-assembled micellar aggregates, the local environment of atoms in AA and MA in the micellar environment, the degree of counterion binding, and the thermodynamics of AA and MA micelle formation were each determined directly through molecular dynamics simulation.

10.6 Appendix: Validation of Alchemical Free-Energy Methods Used to Implement the CS-FE/MT Model

To evaluate the accuracy of the free-energy methods discussed in this chapter that were used to implement the CS-FE/MT modeling approach, free-energy calculations were made for several starter systems. These validation studies include computer simulation determinations of hydration free energies (ΔG_{hyd}), and computer simulation determinations of alchemical transformation free energies (ΔG_{al}).

Using the bonded and the nonbonded λ -dependent interaction potentials described in Section 10.1.1, a single topology approach, and the simulation methods and parameters described in Section 10.2, ΔG_{hyd} for methane and hexane were computed by transforming each of the atoms in both molecules into dummy (non-interacting) particles in vacuum (ΔG_{vacuo}), transferring the dummy particles into a simulation cell of water molecules ($\Delta G = 0$), and transforming each of the dummy particles into interacting atoms in aqueous solution (ΔG_{water}). The computed value of ΔG_{hyd} using 20 values of λ , 200 ps of equilibration and data gathering at each λ value, and the data analysis approach discussed in Section 10.4 was found to be 8.21 kJ/mol for methane and 9.67 J/mol for hexane. These results are in good agreement with the experimental data, which is 8.08 kJ/mol for methane [33] and 10.40 kJ/mol for hexane [34]. Ashbaugh et al. report ΔG_{hyd} values of 10.97 kJ/mol and 16.41 J/mol for methane and hexane, respectively, estimated using computer simulations and a united atom OPLS forcefield [33]. The $\langle \partial G / \partial \lambda \rangle_{\lambda}$ values computed for hexane are shown in Figure A1.

To evaluate the accuracy and the free-energy convergence behavior of the alchemical methods described in Section 10.1.1, the “self-transformation” of ethane into ethane ($\Delta G_{\text{eth} \rightarrow \text{eth}}$) and propane into propane ($\Delta G_{\text{pro} \rightarrow \text{pro}}$) were implemented and simulated in the same manner described in a study by Pearlman et al [16], but using

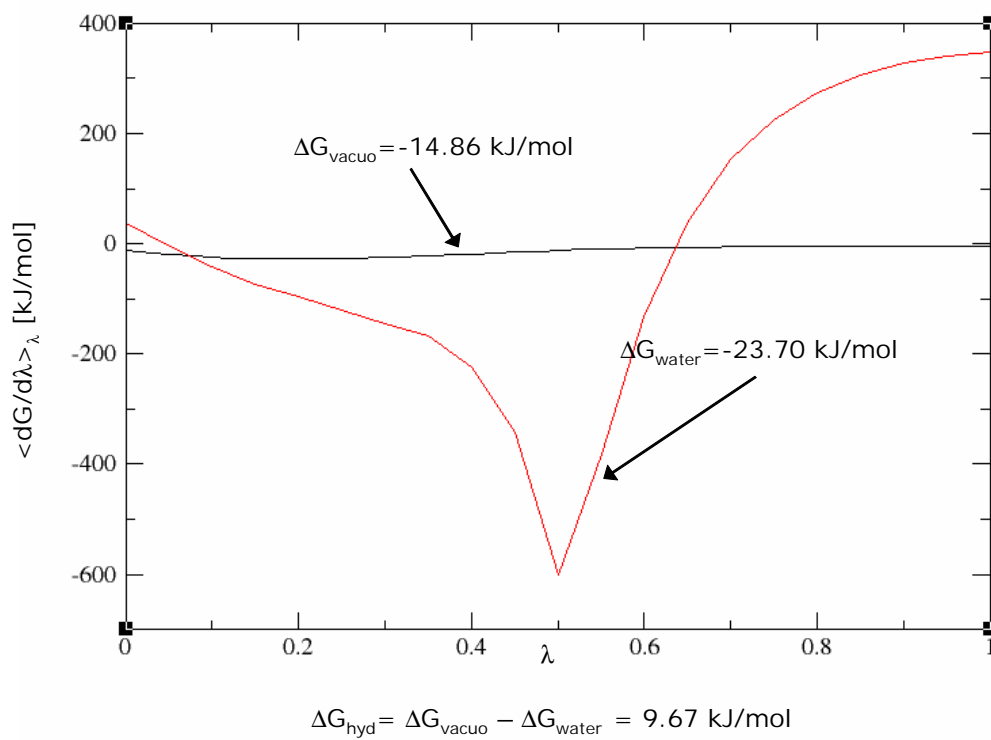


Figure 10-A1: Profiles of $\langle \partial G / \partial \lambda \rangle_\lambda$ versus λ calculated for hexane in vacuum (the black line) and in water (the red line) as a function of the value of the coupling parameter λ . The values of ΔG_{vacuo} and ΔG_{water} were obtained by integrating the corresponding $\langle \partial G / \partial \lambda \rangle_\lambda$ versus λ profiles.

the OPLS-AA forcefield. Values of $\langle \partial G / \partial \lambda \rangle_\lambda$ were obtained at 50 values of λ . A total of 12 ps of equilibration and 12 ps of data gathering was performed at each λ value. Numerical integration of the $\langle \partial G / \partial \lambda \rangle_\lambda$ results gave an estimate of $\Delta G_{\text{eth} \rightarrow \text{eth}}$ equal to 0.24 kJ/mol, and an estimate of $\Delta G_{\text{pro} \rightarrow \text{pro}}$ equal to 0.33 kJ/mol. Because the starting and ending states of the simulated molecules are identical, the computer simulation estimate of $\Delta G_{\text{eth} \rightarrow \text{eth}}$ and $\Delta G_{\text{pro} \rightarrow \text{pro}}$ should converge to 0 kJ/mol in the limit of infinite sampling of phase space. We found that the ΔG results converged toward 0 kJ/mol roughly as fast as the ethane to ethane self-transformation results reported by Pearlman et al. [16].

To evaluate the free-energy convergence behavior and the self-consistency of the alchemical and the nonalchemical free-energy methods, the free-energy differences present in two thermodynamic cycles were determined through computer simulation and are shown in Figures A3 and A4. The free-energy changes represented by the horizontal lines are determined through alchemical transformation (ΔG_{al}), while those represented by the vertical lines are determined by changing each interacting molecule into dummy particles in vacuum, transferring the dummy particles into water, and changing the dummy particles into an interacting molecule in water ($\Delta G_{\text{hyd,DUM}}$). In Figure A3, results are presented for the hydration free energies of benzene and hexane and for the alchemical transformations of benzene into hexane in vacuum and in water. Simulation results were generated using 50 values of λ , with 50 ps of equilibration and 100 ps of data gathering at each λ value. Results for each ΔG value are given in units of kJ/mol. The sum of the four free-energy differences, which in the limit of infinite sampling of phase space would equal 0 kJ/mol, was computed to be -3.19 kJ/mol. The computer simulation prediction of $\Delta G_{\text{hyd,DUM}}$ for benzene is -4.52 kJ/mol, while the experimental value is -3.64 kJ/mol (an error of 24.1%). The computer simulation prediction of $\Delta G_{\text{hyd,DUM}}$ for hexane is 9.67 kJ/mol, while the experimental value is 10.40 kJ/mol (an error of -7.00%) [34]. Below the schematic of the thermodynamic cycle, the difference in the hydration free energies of the two molecules is reported. The computer simulation prediction for this difference in

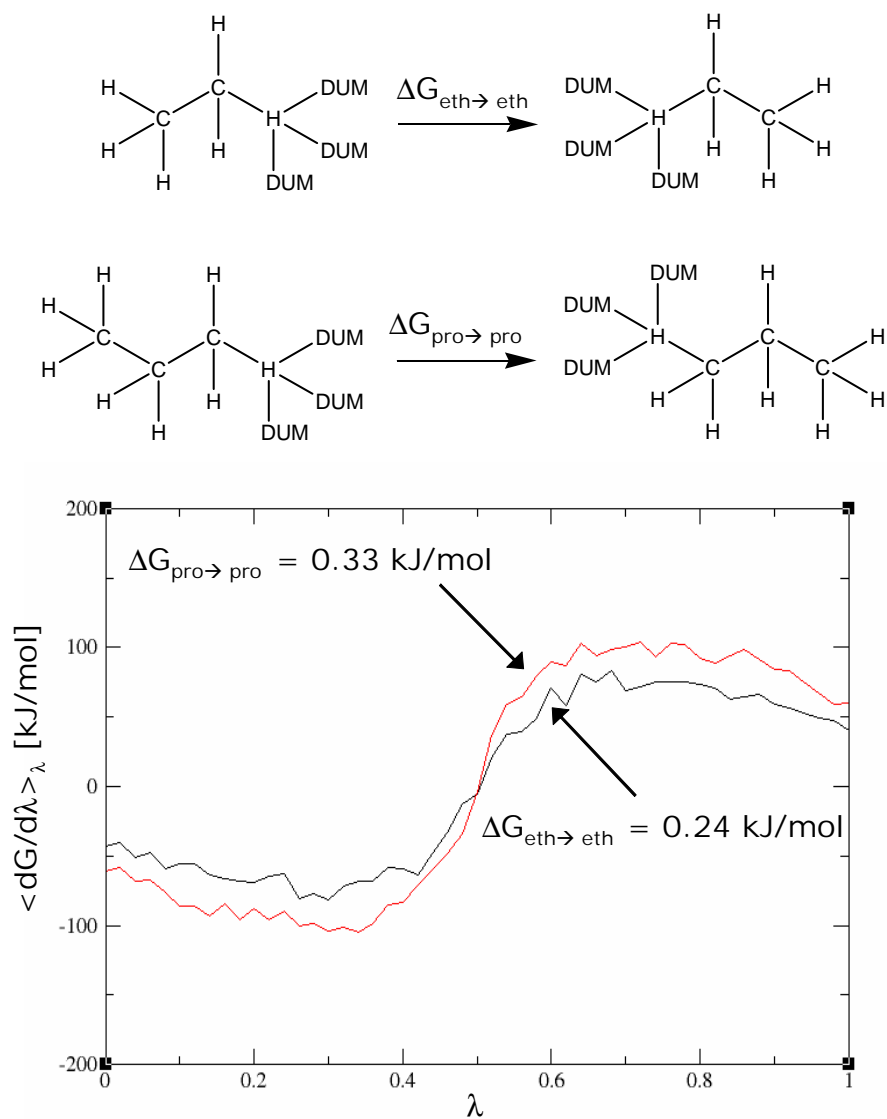


Figure 10-A2: Schematic representations of the ethane into ethane “self-transformation” ($\Delta G_{\text{eth} \rightarrow \text{eth}}$) and the propane into propane “self-transformation” ($\Delta G_{\text{pro} \rightarrow \text{pro}}$). Below the schematics, profiles of $\langle \partial G / \partial \lambda \rangle_\lambda$ versus λ calculated for the ethane into ethane and for the propane into propane “self-transformations” (the red and the black profiles, respectively) are shown as a function of the value of the coupling parameter λ . The values of $\Delta G_{\text{eth} \rightarrow \text{eth}}$ and $\Delta G_{\text{pro} \rightarrow \text{pro}}$ were obtained by integrating the corresponding $\langle \partial G / \partial \lambda \rangle_\lambda$ versus λ profiles.

hydration free energies using dummy atoms ($\Delta G_{\text{hyd,DUM}}$) is equal to 14.19 kJ/mol, while the prediction for this difference using alchemical methods ($\Delta G_{\text{hyd,al}}$) is equal to 17.42 kJ/mol. The experimental value ($\Delta G_{\text{hyd,expt.}}$) is equal to 14.32 kJ/mol. The average of the two computer simulation predictions for the difference in hydration free energy is 10.37% larger than the experimental value. These results suggest that: (i) the alchemical methods used to calculate $\Delta G_{\text{hyd,al}}$ and the free-energy methods used to calculate $\Delta G_{\text{hyd,DUM}}$ are thermodynamically consistent (because they yield similar results for the difference in the hydration free energies of benzene and hexane), and (ii) the number of λ values, the equilibration simulation time used at each value of λ , and the data-gathering simulation time used at each value of λ were sufficient to obtain a reasonably accurate estimate of each free-energy difference.

In Figure A4, results are presented for the hydration free energies of benzoate and propionate and for the alchemical transformation of benzoate into propionate in vacuum and in water. Simulation results were generated using 50 values of λ , with 50 ps of equilibration and 100 ps of data gathering at each λ value. Results for each ΔG value are given in units of kJ/mol. The sum of the four free-energy differences, which in the limit of infinite sampling of phase space would equal 0 kJ/mol, was computed to be 0.3 kJ/mol. The computer simulation prediction of $\Delta G_{\text{hyd,DUM}}$ for benzoate is -289.4 kJ/mol, while the experimental value is -318.2 kJ/mol (an error of -9.07%). The computer simulation prediction of $\Delta G_{\text{hyd,DUM}}$ for propionate is -252.9 kJ/mol, while the experimental value is -331.2 kJ/mol (an error of -23.6%). Below the schematic of the thermodynamic cycle, the difference in the hydration free energies of the two molecules is reported. The computer simulation prediction for this difference in hydration free energies using dummy atoms ($\Delta G_{\text{hyd,DUM}}$) is equal to 36.47 kJ/mol, while the prediction for this difference using alchemical methods ($\Delta G_{\text{hyd,al}}$) is equal to 36.17 kJ/mol. The experimental value ($\Delta G_{\text{hyd,expt.}}$) is equal to -12.98 kJ/mol. The average of the two computer simulation predictions for the difference in hydration free energy is 380% larger than the experimental value. Similar to the benzene/hexane free-energy calculations, the results obtained for benzoate/propionate

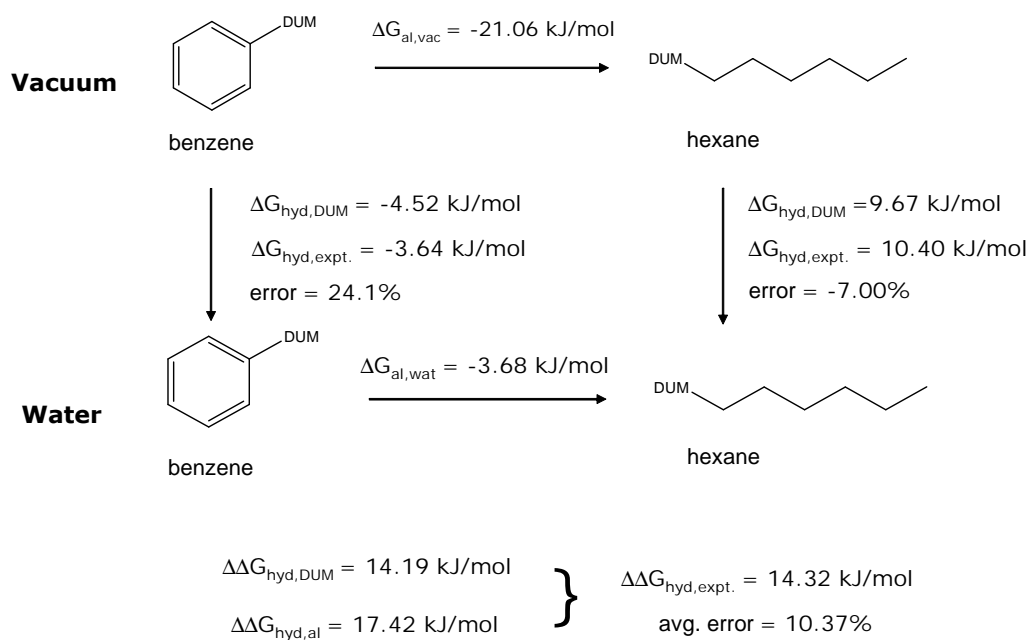


Figure 10-A3: Schematic representation of the alchemical and the non-alchemical free-energy paths used to evaluate the difference in the hydration free energies of benzene and hexane (see text).

suggest that the alchemical methods used to calculate $\Delta G_{\text{hyd,al}}$, and the free-energy methods used to calculate $\Delta G_{\text{hyd,DUM}}$ are thermodynamically consistent because they yield similar results for the difference in the hydration free energies of benzoate and propionate. However, the predictions made using both free energy approaches for benzoate/propionate are in poor agreement with the experimental data. The most likely explanation for this poor agreement is that the reaction field method was used to evaluate electrostatic interactions, an approach which involves approximations and which is not expected to yield as accurate results as those obtained using Ewald summation [35]. Another possible explanation for the poor agreement is that the large magnitude of the free-energy changes associated with the hydration of ionic species such as benzoate and propionate causes these simulations to require longer simulation times to properly converge, although this explanation is not consistent with the high degree of agreement between the $\Delta G_{\text{hyd,expt.}}$ and the $\Delta G_{\text{hyd,al}}$ free-energy results. Additional independent simulations would be required to determine conclusively why the computer simulation results are not in good agreement with the experimental values.

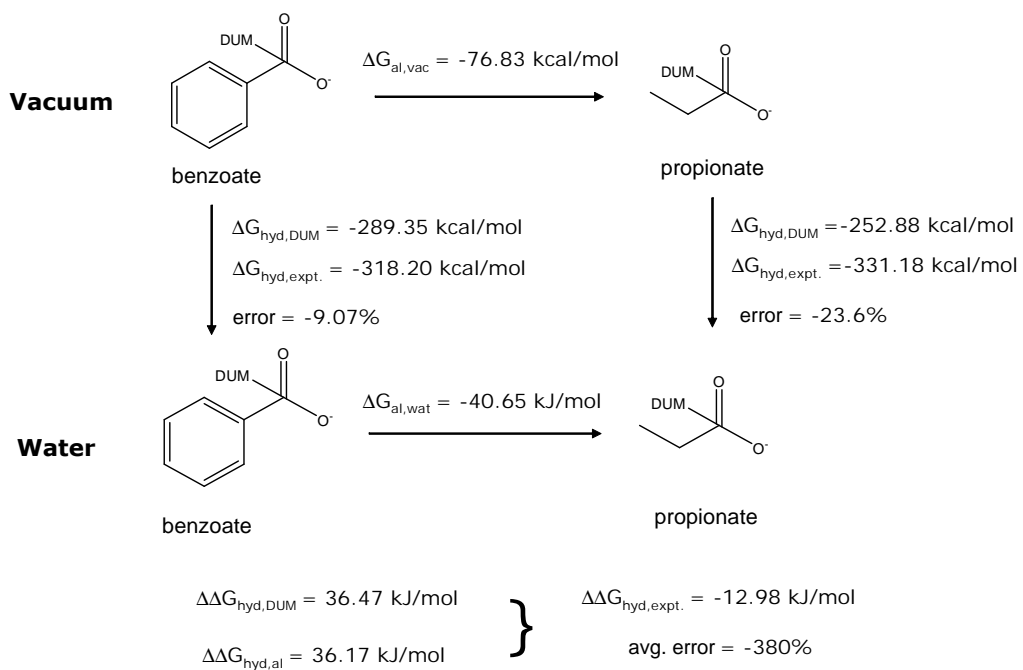


Figure 10-A4: Schematic representation of the alchemical and the non-alchemical free-energy paths used to evaluate the difference in the hydration free energies of benzoate and propionate (see text).

Bibliography

- [1] Berendsen, H. J. C., van der Spoel, D., and van Drunen, R., “GROMACS: A message-passing parallel molecular dynamics implementation,” *Computational Physics Community*, Vol. 91, 1995, pp. 43–56.
- [2] Lindahl, E., Hess, B., and van der Spoel, D., “Gromacs 3.0: A package for molecular simulation and trajectory analysis,” *Journal of Molecular Modeling*, Vol. 7, 2001, pp. 306–317.
- [3] van der Spoel, D., Lindahl, E., Hess, B., van Buuren, A., Apol, E., Meulenhoff, P., Tieleman, D., Sijbers, A., Feenstra, K., van Drunen, R., and Berendsen, H., *Gromacs User Manual version 3.2*, www.gromacs.org, 2004.
- [4] van Gunsteren, W. F., Beutler, T. C., Fraternali, F., King, P. M., Mark, A. E., and Smith, P. E., *Computer Simulation of Biomolecular Systems: Theoretical and Experimental Applications. Volume 2*, Escom Science Publishers, 1993.
- [5] Leach, A., *Molecular Modeling: Principles and Applications*, Prentice Hall, 2nd ed., 2001.
- [6] Straatsma, T. P., Zacharias, M., and McCammon, J. A., “Holonomic constraint contributions to free energy differences from thermodynamic integration molecular dynamics simulations,” *Chemical Physics Letters*, Vol. 196, 1992, pp. 297–302.
- [7] Beutler, T. C., Mark, A. E., van Schaik, R. C., Gerber, P. R., and van Gunsteren, W. F., “Avoiding singularities and numerical instabilities in free energy calcula-

- tions based on molecular simulations,” *Chemical Physics Letters*, Vol. 222, 1994, pp. 529–539.
- [8] Zacharias, M., Straatsma, T. P., and McCammon, J. A., “Separation-shifted scaling, a new scaling method for Lennard-Jones interactions in thermodynamic integration,” *The Journal of Chemical Physics*, Vol. 100, 1994, pp. 9025–9031.
- [9] Pearlman, D. A., Case, D. A., Caldwell, J. C., and Ross, W. S., “AMBER, a package of computer programs for applying molecular mechanics, normal mode analysis, molecular dynamics and free energy calculations to simulate the structural and energetic properties of molecules,” *Computational Physics Community*, Vol. 91, 1995, pp. 1–41.
- [10] van Gunsteren, W. and Berendsen, H. J. C., *GRONINGEN MOlecular Simulation (GROMOS) Library Manual*, Laboratory of Physical Chemistry, University of Groningen, 1987.
- [11] Gao, J., Kuczera, K., Tidor, B., and Karplus, M., “Hidden thermodynamics of mutant proteins: A molecular dynamics analysis,” *Science*, Vol. 244, 1989, pp. 1069–1072.
- [12] Brooks, B. R., Bruccoleri, R. E., Olafson, B. D., States, D. J., Swaminathan, S., and Karplus, M., “CHARMM: a program for macromolecular energy, minimization, and dynamics calculations,” *Journal of Computational Chemistry*, Vol. 4, 1983, pp. 187–217.
- [13] van Gunsteren, W. F., *Computer Simulation of Biomolecular Systems: Theoretical and Experimental Applications*, Escom Science, 1989.
- [14] Boresch, S. and Karplus, M., “The role of bonded terms in free energy simulations: 1. Theoretical analysis,” *The Journal of Physical Chemistry A*, Vol. 103, 1999, pp. 103–118.

- [15] Boresch, S. and Karplus, M., “The role of bonded terms in free energy simulations. 2. Calculation of their influence on free energy differences of solvation,” *The Journal of Physical Chemistry A*, Vol. 103, 1999, pp. 119–136.
- [16] Pearlman, D. A., “A comparison of alternative approaches to free energy calculations,” *The Journal of Physical Chemistry*, Vol. 98, 1994, pp. 1487–1493.
- [17] Jorgensen, W. L., Maxwell, D. S., and Tirado-Rives, J., “Development and testing of the OPLS all-atom force field on conformational energetics and properties of organic liquids,” *Journal of the American Chemical Society*, Vol. 118, 1996, pp. 11225–11236.
- [18] Schweighofer, K. J., Essmann, U., and Berkowitz, M., “Simulation of sodium dodecyl sulfate at the water-vapor and water-carbon tetrachloride interfaces at low surface coverage,” *The Journal of Physical Chemistry B*, Vol. 101, 1997, pp. 3793–3799.
- [19] Berendsen, H. J. C., Grigera, J. R., and Straatsma, T. P., “The missing term in effective pair potentials,” *The Journal of Physical Chemistry*, Vol. 91, 1987, pp. 6269–6271.
- [20] van Gunsteren, W. F. and Berendsen, J. J. C., “A leap-frog algorithm for stochastic dynamics,” *Journal of Computational Chemistry*, Vol. 18, 1997, pp. 1463–1472.
- [21] Jedlovsky, P., “Adsorption of apolar molecules at the water liquid-vapor interface: A Monte Carlo simulations study of the water-n-octane system,” *The Journal of Chemical Physics*, Vol. 119, 2003, pp. 1731–1740.
- [22] Bruce, C., Berkowitz, M., Perera, L., and Forbes, M., “Molecular dynamics simulation of sodium dodecyl sulfate micelle in water: Micellar structural characteristics and counterion distribution,” *The Journal of Physical Chemistry B*, Vol. 106, 2002, pp. 3788–3793.

- [23] Pearlman, D. A. and Rao, B. G., *Free Energy Calculations: Methods and Applications*, John Wiley & Sons, Ltd., New York, 1998.
- [24] Flyvbjerg, H. and Petersen, H. G., “Error estimates on averages of correlated data,” *The Journal of Chemical Physics*, Vol. 91, 1989, pp. 461–466.
- [25] Hess, B., *Stochastic Concepts in Molecular Simulation*, Ph.D. thesis, Rijksuniversiteit Groningen, Groningen, 1999.
- [26] Hess, B., “Determining the shear viscosity of model liquids from molecular dynamics simulations,” *The Journal of Chemical Physics*, Vol. 116, 2001, pp. 209–217.
- [27] Shirts, M. R., Pitner, J. W., Swope, W. C., and Pande, V. S., “Extremely precise free energy calculations of amino acid side chain analogs: Comparison of common molecular mechanics force fields for proteins,” *The Journal of Chemical Physics*, Vol. 119, 2003, pp. 5740–5760.
- [28] Holland, P. M. and Rubingh, D. N., “Nonideal multicomponent mixed micelle model,” *The Journal of Physical Chemistry*, Vol. 87, 1983, pp. 1984–1990.
- [29] Aratono, M., Kanda, T., and Motomura, K., “Study on the adsorption and the micelle formation of a (decylsulfinyl)ethanol and (octylsulfinyl)ethanol mixture,” *Langmuir*, Vol. 6, 1990, pp. 843–846.
- [30] Clint, J. H., “Micellization of mixed nonionic surface active agents,” *Journal of the Chemical Society, Faraday Transactions I*, Vol. 71, 1975, pp. 1327–1334.
- [31] Puvvada, S. and Blankschtein, D., “Molecular thermodynamic approach to predict micellization, phase behavior and phase separation of micellar solutions. 1. Application to nonionic surfactants,” *The Journal of Chemical Physics*, Vol. 92, 1990, pp. 3710–3724, and references cited therein.
- [32] Frenkel, D. and Smit, B., *Understanding Molecular Simulation*, Academic Press, 2nd ed., 2002.

- [33] Ashbaugh, H. S., Kaler, E. W., and Paulaitis, M. E., "A "universal" surface area correlation for molecular hydrophobic phenomem," *Journal of the American Chemical Society*, Vol. 121, 1999, pp. 9243–9244.
- [34] Privalov, P. L. and Makhatadze, G. I., "Contribution of hydration to protein folding thermodynamics. II. The entropy and Gibbs energy of hydration," *Journal of Molecular Biology*, Vol. 232, 1993, pp. 660–679.
- [35] Bader, J. S. and Chandler, D., "Computer-simulation study of the mean forces between ferrous and ferric ions in water," *The Journal of Physical Chemistry*, Vol. 96, 1992, pp. 6423–6427.

PART III

DIRECT PREDICTION OF SURFACTANT SOLUTION PROPERTIES USING COMPUTER SIMULATIONS

Chapter 11

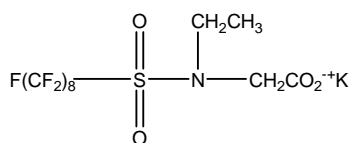
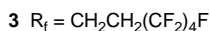
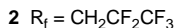
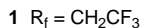
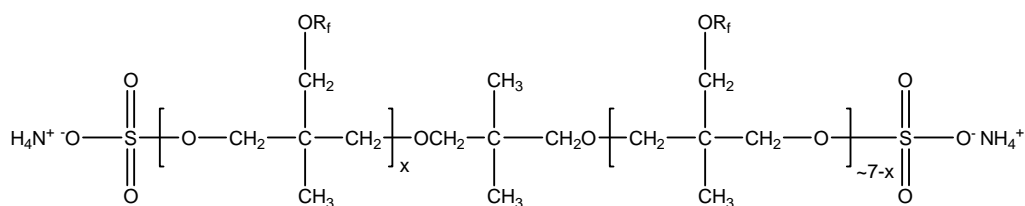
Determination of the Interfacial Characteristics of a Series of Bolaamphiphilic Poly(fluorooxetane) Surfactants through Molecular Dynamics Simulation

11.1 Introduction

Fluorosurfactants play important technological roles in many industries [1]. They are used in the polymerization of fluoropolymers, as repellents in clothing, and to reduce surface tension and level irregularities in microelectronics coatings, paints, and floor polishes. These surfactants typically contain a cationic, anionic, or nonionic hydrophilic group and a relatively long fluorocarbon tail. Many studies have shown that given a series of such fluorosurfactants with different tail lengths, the minimum

surface tension is attained with C_8F_{17} [1]. Serious environmental and health concerns have arisen in recent years as tests have shown that traditional C_8F_{17} fluorosurfactants are pervasive throughout the environment [2]. Traditional fluorosurfactants are degraded in the environment by enzymes to perfluorooctanoic acid ($F(CF_2)_7COOH$, or PFOA) or perfluorooctane sulfonic acid ($F(CF_2)_8SO_3H$, or PFOS), but no further, making them highly persistent [3, 4]. The lipophilicity of PFOA and PFOS makes bioaccumulation in fatty tissue a concern, and the detection of these compounds in the tissue of wild animals demonstrates their persistence in the environment. In addition, studies conducted by 3M beginning in the mid 1990s show that PFOA is present in the blood of more than 90 percent of Americans [5]. Recently, the EPA has announced a new level of emphasis on PFOA toxicity due to these concerns and in response to laboratory studies showing it causes developmental toxicity in rats [3]. In addition, the EPA has been investigating PFOS more closely since late 1999, and recently released a significant new use rule for perfluoroalkyl sulfonates [6].

When the perfluoroalkyl chain length is four or less, bioaccumulation in fatty tissue is reduced significantly; however, a single-chain surfactant such as $F(CF_2)_4CH_2COO^-$ does not yield sufficient reductions in surface tension and coating irregularities to make it commercially viable. A novel approach to synthesize fluorosurfactants has recently been developed in which short perfluoroalkyl chains are attached as side-chains to an oligomeric poly(fluorooxetane) backbone [7]. The cyclic molecule $CH_2 - CH_2 - O - C(CH_3)Br$ is substituted to yield a monomer, $CH_2 - CH_2 - O - C(CH_3) - O - CH_2 - (CF_2)_x F$ that undergoes cationic ring-opening polymerization to produce short backbone chains of approximately seven monomer units [7]. These chains are then end-terminated with SO_3^- groups to yield molecules that have hydrophilic groups at the ends as well as oxygen atoms spaced regularly along a backbone chain. Short perfluoroalkyl chains are attached to this backbone. Although such chains are poor surfactants as single molecules, when linked together in this manner onto an oligomeric backbone, experimental studies conducted by Kausch et al. have demonstrated technologically-useful reductions in surface tension and



4 3M Fluorad FC-129

Figure 11-1: Chemical structures of three poly(fluoroacetate)s and 3M Fluorad FC-129.

favorable interfacial rheological properties that make for good flow-and-leveling performance [1, 8]. The structures of the surfactants Kausch et al. characterized are shown in Figure 11-1. Surfactant **4**, as a typical long perfluoroalkyl chain surfactant, was included in the Kausch et al. study for comparison with surfactants **1-3**.

Kausch et al. report that the target degree of polymerization for surfactants **1-3** was 7. Preliminary matrix-assisted laser desorption ionization (MALDI) mass spectroscopy indicated that the polydispersities obtained were in the 1-2 range. Surfactants **1-3** were found to reach approximately the same minimum surface tension of ≈ 28 mN/m in a pH 8 buffered water solution. When tested under the same conditions, surfactant **4** decreased the surface tension to a minimum of ≈ 17 mN/m. The surface tension data was fit parametrically to the Davies adsorption isotherm, which takes into account the effect of double-layer charging, giving an estimate of molecular interfacial area ($\text{\AA}^2/\text{molecule}$) for each surfactant. A pseudo-single-surfactant approach was used to analyze the adsorption isotherm. Values regressed by Kausch

Surfactant	Molecular Area ($\text{\AA}^2/\text{molecule}$) from Davies Isotherm Fit	Molecular Area ($\text{\AA}^2/\text{molecule}$) from Gibbs Adsorption Equation
1	47.4 ± 2	46.0 ± 1
2	48.8 ± 1	35.1 ± 0.7
3	68.7 ± 1	64.4 ± 2
4	24.3 ± 1	31.5 ± 2

Table 11.1: Values of the interfacial area per surfactant molecule at saturation reported by Kausch et al. based on fitting experimental surface tension data to the Davies and Gibbs adsorption isotherms [1].

et al. from a fit to the Davies and Gibbs adsorption isotherms are shown in Table 11.1 [1].

The molecular interfacial areas reported for surfactants **1-3** are quite small given these surfactants' sizes. Kausch et al. speculated that this might be due to the surfactants adopting a "bent" conformation with the SO_4^- head groups buried in the solvent and some of the fluorocarbon chains being oriented as a "loop" in the vapor phase [1]. However, prior to the research presented here, no study had been conducted to determine the structure of these surfactants at a water/air interface. To better understand the properties of these novel surfactants and explore the origin of their ability to reduce surface tension, constant surface tension molecular dynamics simulations have been performed on surfactants **1-4** to determine the equilibrium interfacial area of each of these fluorosurfactants at different applied surface tensions. The interfacial structure of these surfactants was also visualized at the infinite dilution and saturation limits. Density profiles as a function of distance from the interface have been generated for water, surfactant, and groups of surfactant atoms. The results allow quantitative comparison of the ability of each surfactant to shield water from air, a key factor in determining surface tension. A "penetration parameter" based on a study by Stone et al. has been defined to characterize the ability of each surfactant to separate air from water [9]. The degree of hydration of various atoms in each surfactant was calculated to gain quantitative information about local environment. Finally, order parameters for the perfluoroalkyl side chains of surfactants **1-3** were calculated and compared with the order parameters for surfactant **4** to gain

insight into the average structure of these compounds at the water/air interface.

A number of computer simulation studies of surfactant monolayers at water/air, oil/water, and water/ CCl_4 interfaces has been reported in the literature [9–21]. da Rocha et al. have applied NPT and NVT simulations to study the behavior of a perfluoropolyether ammonium carboxylate surfactant monolayer at a high-pressure CO_2 /water interface [18]. Stone et al. have reported constant normal pressure simulations of dichain hydrocarbon and fluorocarbon phosphate surfactants and have analyzed structural information they obtained about the CO_2 /surfactant/water interface to explore the molecular origins of differences in the ability of hydrocarbon and fluorocarbon surfactants to lower surface tension [9]. They defined an interfacial parameter, which they refer to as the penetration parameter (P), which characterizes the ability of a surfactant at an interface to separate two bulk phases and thereby reduce surface tension. Molecular dynamics simulations have been conducted on the fluorosurfactants $\text{F}(\text{CF}_2)_{11}\text{COOH}$ and $\text{F}(\text{CF}_2)_{10}\text{CH}_2\text{COOH}$ at a water/air interface [22–24]. Other computer simulation studies of surfactants at interfaces include the work of Berkowitz et al., who simulated sodium dodecyl sulfate at the water/vapor and water/ CCl_4 interface [12,13]. Dominguez has applied molecular dynamics simulations to study sodium dodecyl sulfate at the water/ CCl_4 interface and investigated the effect of surfactant charge and surfactant concentration on interfacial structure [14,21]. Tarek et al. have simulated cetyltrimethylammonium bromide at the water/air interface [10]. Rehage et al. have studied a monododecyl pentaethylene glycol monolayer at a water/air and oil/water interface to determine its orientational behavior and dynamics [15–17]. As computer power increases, computer simulations are playing an increasingly important role in providing detailed information about the structure and dynamics of surfactant monolayers at interfaces.

The results obtained from simulation studies complement a number of experimental techniques which can also be used to probe surfactant interfacial behavior. These experimental approaches include X-ray diffraction [22–25], surface pressure-area isotherm analysis [22–25], vibrational sum frequency spectroscopy [26–28], time-

resolved quasi-elastic laser scattering studies [29], second-harmonic-generation studies [30], neutron reflection [31], fluorescence [32], resonance Raman spectra [33], and ellipsometric measurements [34].

The remainder of this chapter is organized as follows. In Section 11.2 we present the simulation methodology, including a discussion of the simulation parameters (Section 11.2.1) and system preparation and equilibration (11.2.2). In Section 11.3 we present and discuss our simulation results, including the saturated interfacial area per surfactant molecule (Section 11.3.1), interfacial area as a function of surface tension (Section 11.3.2), visualization of surfactant conformation (Section 11.3.3), interfacial density profiles (Section 11.3.4), a discussion of the degree of hydration and extent of counterion binding for each surfactant (Section 11.3.5), and order parameters for each surfactant chain (Section 11.3.6).

11.2 Simulation Methodology

11.2.1 Simulation Parameters

All simulations were done with the GROMACS software package, version 3.2 [35, 36]. Surfactants **1-4** were simulated with a force field based on the OPLS-AA framework [37, 38] with additional parameters added both for the perfluoroalkanes [39] and SO_4^- head groups [40]. NH_4^+ counterions for each poly(fluorooxetane) and the K^+ counterion for Fluorad FC-129 were also modeled using the OPLS-AA force field [41]. Water was treated explicitly using the simple extended point-charge model (SPC/E) [42]. The SPC/E model for water was used because it was found to give excellent estimates of the water/air surface tension at 300 K (68 mN/m in our tests compared to an experimental value of 73 mN/m). For initial equilibration, long-range interactions were treated with a Coulombic and van der Waals cut-off distance of 11 Å to decrease simulation time. Later, the Particle Mesh Ewald (PME) summation technique was implemented to describe electrostatic interactions more accurately. During constant surface tension ($N\gamma T$) simulation, a relatively small timestep (0.5

fs) was required by the Berendsen pressure scaling algorithm [43] to retain stability. After equilibration, data was gathered in constant-volume (NVT) simulations. In these data-gathering runs, a van der Waals cut-off of 11 Å and PME were used to describe nonbonded interactions and bond constraints were applied with the SHAKE algorithm to allow a larger simulation timestep of 2 fs [43].

11.2.2 System Preparation and Equilibration

The boundary conditions for each $N\gamma T$ and NVT simulation were selected to ensure that the results from our simulations would permit direct comparison with the experimental results for surface tension and area per surfactant molecule reported by Kausch et al [1]. Several different boundary conditions for computer simulation of surfactant monolayers have been reported in the literature. In simulations of phosphatidylcholine and sodium dodecyl sulfate at water/air and CCl_4 /water interfaces, Dominguez and Berkowitz report placing surfactant between two bulk phases and then placing reflecting walls at opposite sides of the simulation box parallel to the interface to prevent the two bulk phases from contacting [14]. Such a configuration permits use of 3D periodic boundary conditions and hence the use of 3D Ewald summation for treatment of electrostatics. In simulations of a fluorosurfactant at a CO_2 /water interface, da Rocha et al. also applied 3D periodic boundary conditions, but instead chose to simulate a CO_2 /water and CO_2 /fluorosurfactant/water interface within their simulation cell [18]. An alternative to the approach of da Rocha et al. is to simulate two separate monolayers located on opposite sides of a continuous layer of water. We have chosen to use the approach of da Rocha et al. during initial equilibration of our simulation cell (to minimize simulation time), but to create two separate monolayers separated by water for final equilibration and data gathering. Such an approach permits application of 3D periodic boundary conditions and 3D Ewald summation treatment of electrostatics during both initial equilibration and final equilibration and data gathering.

The approach used to construct simulation cells containing monolayers of surfac-

tants **1-4** is shown in Figure 11-2, with surfactant **3** being shown as a representative example. Simulation cells for surfactants **1-3** were constructed by first placing a uniform monolayer of 16 surfactant molecules parallel to the x - y plane. The simulation cell for surfactant **4** was constructed by placing 25 surfactant molecules parallel to the x - y plane. Next, an energy minimization was performed to remove high energy contacts. To break the symmetry of the system, a 25 ps simulation at 400 K was done with the surfactant heads fully constrained. Berendsen temperature coupling [43] was used to maintain the simulation cell at the desired temperature, and van der Waals and electrostatic interactions were modeled with a 11 Å cut-off. Note that a cut-off method to model electrostatics was used for initial equilibration because tests showed that the cutoff method was over three times faster than Particle Mesh Ewald Summation (PME). Two 10 ps simulations were performed at $T = 350$ K and 300 K to gradually cool the surfactants to the final simulation temperature. Next, 32 NH_4^+ counterions were added randomly in the vicinity of the surfactant **1-3** head groups to make the simulation cell electrically-neutral. Similarly, 25 K^+ counterions were added in the vicinity of the surfactant **4** head groups. These counterions were chosen to match the surfactant solutions studied by Kausch et al. At this point each simulation cell resembled the snapshot shown in frame 1 of Figure 11-2.

Next, a layer of ≈ 20 Å of SPC/E water molecules was added to the hydrophilic side of the surfactant interface, and a short equilibration run of 10 ps was performed with the surfactant heads fixed to allow the water molecules and counterions to relax around the surfactant heads. A number of nitrogen molecules were added to the simulation cell to give a pressure in the vapor phase of ≈ 1 atm. At this point each simulation cell was composed of a layer of air, a ≈ 20 Å thick layer of water, 16-25 surfactant molecules, and a final layer of air. Our initial guess for the optimal surface area per molecule (which determined the spacing in the uniform monolayer constructed within the simulation cell) was based on the surfactant molecular areas parametrically fitted from the Davies isotherm data reported in Table 11.1. However, it quickly became clear that this did not allow sufficient area for the molecules to

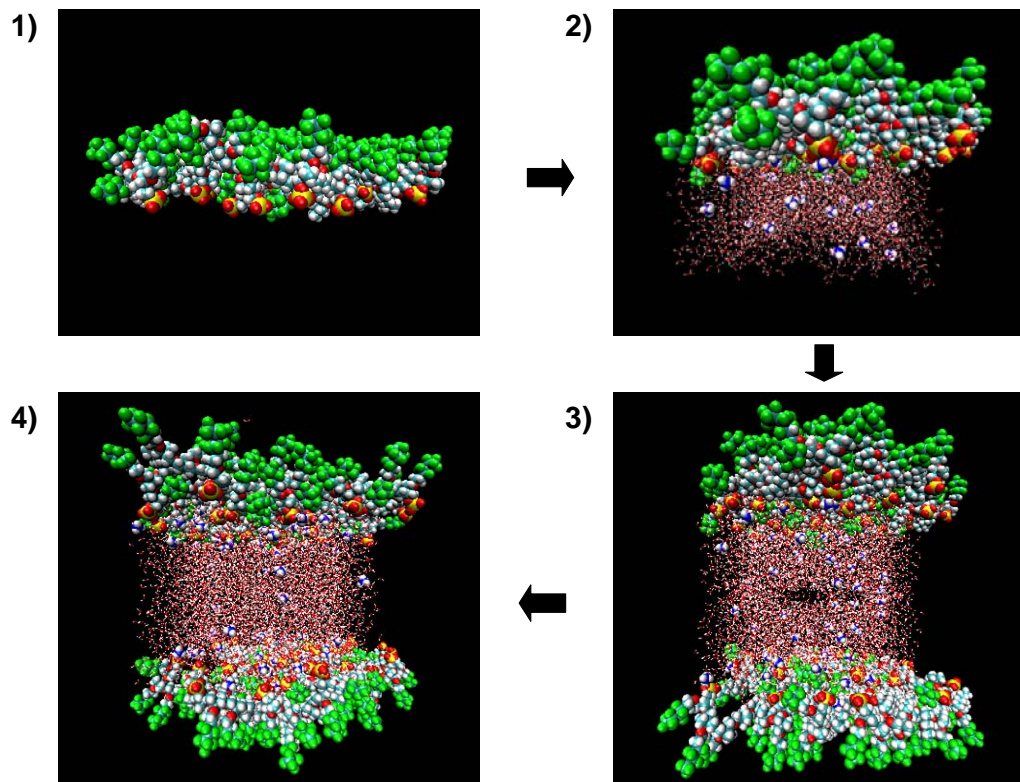


Figure 2

Figure 11-2: Sequence of steps followed to form and equilibrate simulation cells containing monolayers of surfactants 1-4.

fit at the interface, particularly for surfactants **1-3**. Even after repeated energy minimization runs, the resulting interfaces were too closely packed to be stable and quickly buckled and twisted during the simulation runs. To create a stable interface, the Davies isotherm areas estimated by Kausch et al. were tripled for surfactants **1-3** and doubled for surfactant **4** as an initial guess for the surface area per molecule. This increased area per surfactant head was found to be both a stable initial configuration for the interface and reasonably close to the final equilibrated area per headgroup. Each simulation cell was reconstructed and equilibrated in the manner described above using this increased surface area for each surfactant.

Constant surface tension ($N\gamma T$) simulations were then performed for 3,000 ps on each simulation cell. Because each simulation cell at this point contained both a water/air and a water/surfactant/air interface (see Figure 11-2, frame 2), the applied surface tension for these simulations was set equal to the sum of the minimum (saturated) surface tension values reported by Kausch et al. for the water/surfactant/air interface and the surface tension of the water/air interface (which was determined in a separate simulation for pure SPC/E water). Berendsen temperature coupling was used to maintain the cell temperature at 300 K. To prevent buckling of the interface, the surfactant head groups were constrained to remain within their original x - y plane during this simulation. This constraint permitted motion of the head groups in the x and y directions, but not in the z direction normal to the interface. A Berendsen pressure coupling algorithm implemented in GROMACS [43] was used to change the x and y cell dimensions, while enforcing the constraint that the x and y cell dimensions remain equal. At the end of the 3,000 ps run, the x and y dimensions of each cell were found to have equilibrated to the point that the applied surface tension roughly matched the internal surface tension of the simulation cell. After this initial equilibration each simulation cell resembled the snapshot shown in frame 2 of Figure 11-2, which depicts a roughly equilibrated monolayer of surfactant **3**.

At this point each simulation cell contained a water/surfactant/air and water/air interface. Such an asymmetric composition at two interfaces will impose a net shear

stress on the water molecules within the simulation cell because of the difference in surface tension on both sides of the water layer. Although simulations have been reported in the literature of interfaces with such an asymmetric composition [18], we decided instead to conduct simulations of two separate surfactant monolayers to remove the compositional asymmetry and eliminate any artificial effect shear stress from compositional asymmetry could have on the behavior of the surfactant monolayer. This was accomplished by making a copy of each simulation cell and rotating it 180° about the x axis. The copy was then translated and added to the original simulation cell to create two surfactant/air interfaces connected by a continuous layer of water, as shown in frame 3 of Figure 11-2. After forming the new interfaces, the simulation cell was equilibrated for 50 ps with the surfactant headgroups constrained to their original position in the x - y plane.

The advantages of this initialization and equilibration approach for constructing surfactant monolayers are two-fold: 1) it allows the simulator to improve the initial stability of the system by imposing an x - y constraint on the motion of the surfactant head groups until the simulation cell size has roughly equilibrated, and 2) it reduces simulation time significantly by allowing simulation of only half of the molecules present in the final simulation cell during initial equilibration.

After forming the two water/surfactant/air interfaces, position constraints on the surfactant headgroups were removed. Additional equilibration was done for 2.5 ns with van der Waals and electrostatic interactions modeled using an 11 Å cut-off to minimize simulation time. Further equilibration was then done using PME instead of a distance cut-off to describe electrostatic interactions. A snapshot of the fully equilibrated simulation cell structure for surfactant **3** is shown in frame 4 of Figure 11-2.

Figure 11-3 shows how the simulation cell x (or equivalently y) dimension changed over the course of these equilibration runs for surfactants **1-4**. Surfactants **1** and **3** were equilibrated for a total of 5 ns, and surfactant **2** was equilibrated for a total of 4.5 ns. Because surfactant **4** is much smaller than surfactants **1-3** it was possible to

simulate this surfactant system for a total of 12.5 ns. It is clear from Figure 11-3 that PME treatment of electrostatics has a significant effect on the simulation results—as soon as PME was initialized in place of an 11 Å cut-off for electrostatic interactions the simulation cells containing surfactants **1**, **3**, and **4** expanded significantly in the x and y directions.

The time scales involved in allowing each of the four surfactants to approach their equilibrium interfacial area were quite large. However, the plots of simulation cell dimension as a function of simulation time shown in Figure 11-3 suggest that each surfactant molecule has been simulated sufficiently long to come to an equilibrium configuration and interfacial area. Although it is never possible to prove that the results from a simulation are ergodic, each cell has been equilibrated until the cell size appears to be fluctuating about an equilibrium value.

After equilibration, a 1 ns data gathering run was conducted for each surfactant. During this data gathering run, pressure scaling was turned off and the simulation cell size was fixed. Simulation data from these NVT simulations have been used to analyze structural characteristics of the surfactant monolayers, such as density profiles, degrees of hydration, and fluorocarbon chain order parameters.

Surface tension was also set at several values below the saturated (minimum) values reported by Kausch et al. to determine the sensitivity of the surfactant molecular area to the applied surface tension. At each specified surface tension, the cell was allowed to come to a new equilibrium configuration. The equilibration curves for each externally-applied surface tension appear qualitatively the same as what is shown in Figure 11-3. As would be expected, the equilibrated x and y cell dimensions decreased as the applied surface tension was lowered.

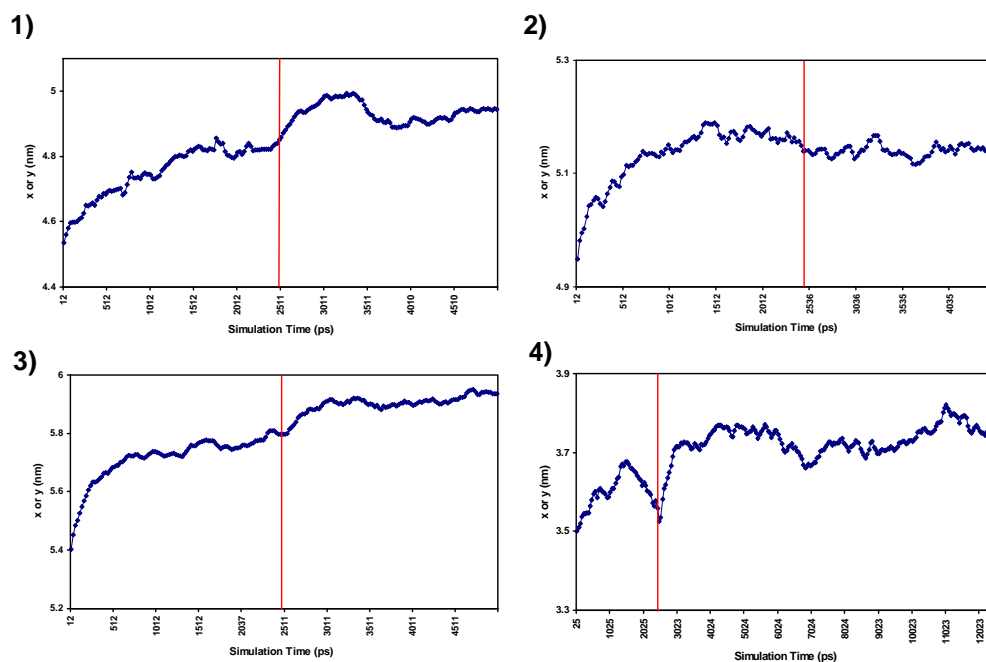


Figure 11-3: Simulation cell x (or equivalently y) dimension (nm) equilibration curves. The x - y plane is parallel to the water/air interface. Results are presented for 1) surfactant **1**, 2) surfactant **2**, 3) surfactant **3**, and 4) surfactant **4**. The vertical line in each figure indicates when electrostatic interactions were switched from being modeled using an 11 Å cut-off to using Particle Mesh Ewald summation.

Surfactant	Molecular Area ($\text{\AA}^2/\text{molecule}$)	Molecular Area ($\text{\AA}^2/R_f$ chain)	Molecular Area ($\text{\AA}^2/\text{molecule}$)
	from MD Results	from MD Results	from Davies Isotherm Fit
1	152.9	21.8	47.4 ± 2
2	164.6	23.5	48.8 ± 1
3	220.2	31.5	68.7 ± 1
4	55.2	55.2	24.3 ± 1

Table 11.2: Computer simulation estimates of the interfacial area per surfactant molecule at saturation for surfactants **1-4**.

11.3 Results and Discussion

11.3.1 Saturated Interfacial Areas per Surfactant Molecule

The final simulation cell dimensions after the extended equilibration runs shown in Figure 11-3 have been used to determine the saturated interfacial areas per surfactant molecule. The interfacial areas are presented in Table 11.2 for surfactants **1-4**, and are compared with the interfacial areas obtained by Kausch et al. through parametric fitting to the Davies adsorption isotherm. The areas per fluorocarbon chain (R_f) have also been calculated and are reported in Table 11.2.

There is significant discrepancy between the predictions obtained from this molecular dynamics study and the fitted results of Kausch et al. To check the validity of our MD results, it is instructive to look closely at the results for surfactant **4**. Although to our knowledge no studies have been published describing the saturated interfacial area for this specific surfactant, some studies have been done on related perfluoroalkyl chain surfactants. X-ray diffraction, surface pressure-area isotherm analysis with a Teflon trough, and molecular dynamics simulations have been conducted on $\text{F}(\text{CF}_2)_{11}\text{COOH}$ and $\text{F}(\text{CF}_2)_{10}\text{CH}_2\text{COOH}$ surfactants at an water/air interface [22–25]. These surfactants have a significantly smaller hydrophilic moiety than surfactant **4** and also lack an ethyl branch within the hydrophilic portion of the surfactant. MD simulations indicate the saturated interfacial head group area of $\text{F}(\text{CF}_2)_{10}\text{CH}_2\text{COOH}$ is $29.4 \pm 0.1 \text{ \AA}^2$ at 300 K and 8.0 dyn/cm of applied surface

tension and $29.7 \pm 0.2 \text{ \AA}^2$ at 300 K and 0.16 dyn/cm of applied surface tension, where the reported errors represent the standard deviations of the means [22,23]. MD simulations also indicate that the saturated interfacial head group area of $\text{F}(\text{CF}_2)_{11}\text{COOH}$ is $29.8 \pm 0.1 \text{ \AA}^2$ at 300 K and 8.0 dyn/cm of applied surface tension [22]. These values were in close agreement with experimental measurements [22, 24]. Saturated interfacial area per head group measurements have also been made for a series of perfluoroalkyl chain surfactants with the general structure $\text{F}(\text{CF}_2)_n-(\text{CH}_2)_m\text{COOH}$ at a pH of 8.6, giving the following areas per surfactant: 37.2 \AA^2 ($n = 10, m = 10$), 37.5 \AA^2 ($n = 8, m = 10$), and 37.0 \AA^2 ($n = 7, m = 10$) [44]. The measured and predicted saturated interfacial head group areas for these surfactants are all larger than those obtained by Kausch et al. ($24.3 \pm 1 \text{ \AA}^2$) for surfactant **4** by parametrically fitting to the Davies adsorption isotherm. The surfactants considered in each of these theoretical and experimental studies have smaller hydrophilic moieties than that of surfactant **4**, and therefore have a smaller cross-sectional area. The head group of surfactant **4** has a cross-sectional area of roughly 12.5 \AA^2 , which is a factor of three larger than the cross-sectional area of $\text{F}(\text{CF}_2)_{10}\text{CH}_2\text{COOH}$. Consequently, it would be surprising if surfactant **4** occupies only 24.3 \AA^2 at the water/air interface when $\text{F}(\text{CF}_2)_{10}\text{CH}_2\text{COOH}$ occupies 29-30 \AA^2 .

The cross-sectional area of each SO_4^- head group in poly(fluorooxetane) is 6.3 \AA^2 , meaning that the total interfacial area per surfactant (that contains two SO_4^- head groups) cannot be less than 12.6 \AA^2 . This is a factor of three larger than the cross-sectional area of $\text{F}(\text{CF}_2)_{10}\text{CH}_2\text{COOH}$. Making the rough approximation that interfacial area is directly proportional to surfactant cross-sectional area, the interfacial surface area of poly(fluorooxetane) would be approximately 87 \AA^2 at the interface. Although this estimate is below the interfacial area values determined from our MD simulations, it does suggest that the Kausch et al. surface area estimates for surfactants **1** and **2** (47.4 and 48.8 \AA^2) may be too small. In addition, as discussed earlier, our attempts to initialize surfactants **1-3** with the Kausch et al. values for surfactant interfacial area of 27.3 \AA^2 , 48.8 \AA^2 , and 68.7 \AA^2 , respectively,

resulted in interfaces that appeared much too closely packed and that were unstable. This analysis suggests that the Davies isotherm fit applied by Kausch et al. underestimates the interfacial area occupied by surfactants **1-4**. It is also possible that our MD simulation results overestimate the required interfacial area for each surfactant because the time scales involved in poly(fluorooxetane) movement and entwining at the water/air interface are larger than our simulation time, preventing adequate equilibration of the water/surfactant/air interface. To check for this possibility, surfactant **3** was equilibrated (under $N\gamma T$ conditions) for an additional 2 ns. However, during this additional simulation the simulation cell size continued to fluctuate about an equilibrium value and showed no upwards or downwards drift. The final x and y box dimensions after additional simulation were only 0.09 % larger than the initial dimensions.

11.3.2 Interfacial Areas per Surfactant Molecule as a Function of Applied Surface Tension

Macroscopically-observed surface tensions are difficult to predict properly from a microscopic simulation. A major reason for this is that long (micron) wavelength undulations are not included in nanometer-scale simulation results. Other researchers have commented on this limitation, and used it to justify applying non-zero surface tensions in flaccid lipid bilayer simulations where the appropriate macroscopic surface tension is arguably zero [45]. Although the SPC/E water model was chosen for this study specifically because the surface tension measured from a microscopic simulation compares well with the macroscopic surface tension of water, it would be surprising if the OPLS forcefield parameters implemented to describe surfactants **1-4** were to give excellent predictions of macroscopic surface tension from nanometer-scale simulations.

To ensure that the applied surface tension in our simulations is not the source of the discrepancy between the surfactant interfacial areas fitted by Kausch et al.

Surfactant	$\sigma = 0$	$\sigma = \left(\frac{1}{3}\right) \sigma_{Expt.}$	$\sigma = \left(\frac{2}{3}\right) \sigma_{Expt.}$
1	130.46 Å ² (3 ns)	141.76 Å ² (3 ns)	148.09 Å ² (3 ns)
2	156.68 Å ² (3.5 ns)	158.93 Å ² (3.5 ns)	157.05 Å ² (3.5 ns)
3	201.31 Å ² (2.25 ns)	203.59 Å ² (2.25 ns)	206.33 Å ² (2.25 ns)
4	50.05 Å ² (6.5 ns)	51.77 Å ² (6.5 ns)	52.66 Å ² (6.5 ns)

Table 11.3: Effect of applied surface tension on the interfacial area per surfactant molecule for surfactants **1-4**.

and our simulation results, several $N\gamma T$ simulations have been run at different values of surface tension to probe the sensitivity of our simulation results to the applied surface tension. The initial configuration for each $N\gamma T$ simulation was the same as configuration used to initialize the equilibration runs shown in Figure 11-3. Simulations were conducted for each surfactant at two-thirds of the saturated (minimum) surface tension measured by Kausch et al., one-third of the saturated surface tension, and no applied surface tension. Each simulation was run until the simulation cell appeared roughly to equilibrate in size. Results are presented in Table 11.3, with the simulation times reported in parentheses.

The results suggest that the predicted interfacial area per surfactant is relatively insensitive to the applied surface tension, varying on average only 11% from the full applied surface tension to no applied surface tension. Other researchers have also found that surfactant interfacial area is not a strong function of the applied surface tension [22, 23, 46]. In particular, in MD simulations conducted on $F(CF_2)_{10}CH_2COOH$ the observed molecular interfacial area only changed by 1% as the applied surface tension decreased from 8.0 dyn/cm to 0.16 dyn/cm [22, 23]. Our results indicate that the value of the external surface tension applied during equilibration is not responsible for the discrepancy between our MD simulation results and the interfacial molecular area results reported by Kausch et al.

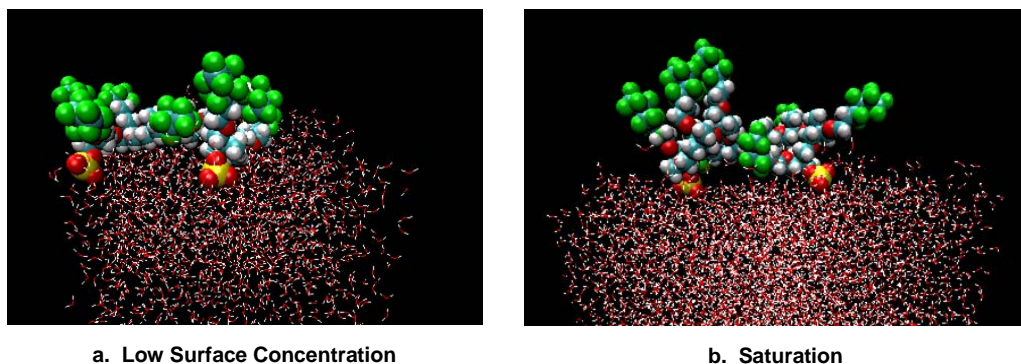


Figure 11-4: Representative snapshots of surfactant **3** at the water/air interface at (a) low surface concentration and (b) saturation. For clarity, only a single surfactant **3** molecule is shown in frame b, although other surfactant **3** molecules are also present at the water/air interface. The size of water atoms has been reduced for clarity.

11.3.3 Visualization of Surfactant Conformation

To better understand the relationship between surfactant interfacial area and surfactant conformation we have visualized surfactants **1-4** at low surface concentration and at saturation (based on simulation cell dimensions obtained from $N\gamma T$ simulation at the saturated surface tensions measured by Kausch et al.). Representative snapshots of surfactant **3** at (a) low surface concentration and (b) saturation are presented in Figure 11-4. In the figure, van der Waals radii are used to display each surfactant atom, but the size of each water atom has been reduced significantly to permit a clearer view of the surfactant.

It is clear from these snapshots that at high surface concentrations, the backbone connecting the SO_4^- head groups and the fluorocarbon chains attached along this backbone are forced into the air phase. This greatly reduces the area requirement of each surfactant, and is responsible for the low interfacial molecular area required by each poly(fluorooxetane), despite their high molecular weight.

Visualization of an entire monolayer of surfactants reveals that there is a significant amount of intertwining at the water/surfactant/air interface, i.e. that when viewed from above a significant number of the surfactant backbone “loops” cross each

Surfactant	1-D Sinusoidal Wave
1	0.123 nm
2	0.123 nm
3	0.127 nm
4	0.163 nm

Table 11.4: Estimates of the amplitude of fluctuations for surfactants **1-4** at the water/air interface expected based on $1 k_B T$ of energy.

other. Such visualization also reveals that there is a significant amount of fluctuation in the z direction (perpendicular to the water/surfactant/air interface). These fluctuations can be clearly seen in Figure 11-5 in the case of surfactant **2**, where the water molecules have been removed to allow a better view of the surfactant monolayer. The level of fluctuations observed in the surfactant **1**, **3**, and **4** monolayers was quite similar. Visualization of each surfactant monolayer showed that the amplitude of fluctuations occurring perpendicular to the water/air interface is approximately 0.19 nm (corresponding to the length an SO_4^- head group). These fluctuations are consistent in magnitude with those to be expected from random shape fluctuations of a fluid-fluid interface. Considering the lowest-energy fluctuation consistent with the periodic boundary conditions, a one-dimensional sinusoidal wave of the same length as the simulation cell, the amplitudes of waves that increase the contact free energy (through creating additional surface area) by $1 k_B T$ are reported in Table 11.4. These simple estimates neglect any steric effects, but the agreement between this primitive one-dimensional sine wave model based on $1 k_B T$ of energy fluctuation and the observed level of interfacial fluctuations perpendicular to the interface is reasonable. A two-dimensional sine wave model was also tested, but because a two-dimensional fluctuation results in a greater surface area than a one-dimensional fluctuation, the calculated maximum amplitude was lower than what was predicted with the one-dimensional model. Visualization of the MD trajectories showed that one-dimensional fluctuations appeared to dominate over two-dimensional fluctuations.

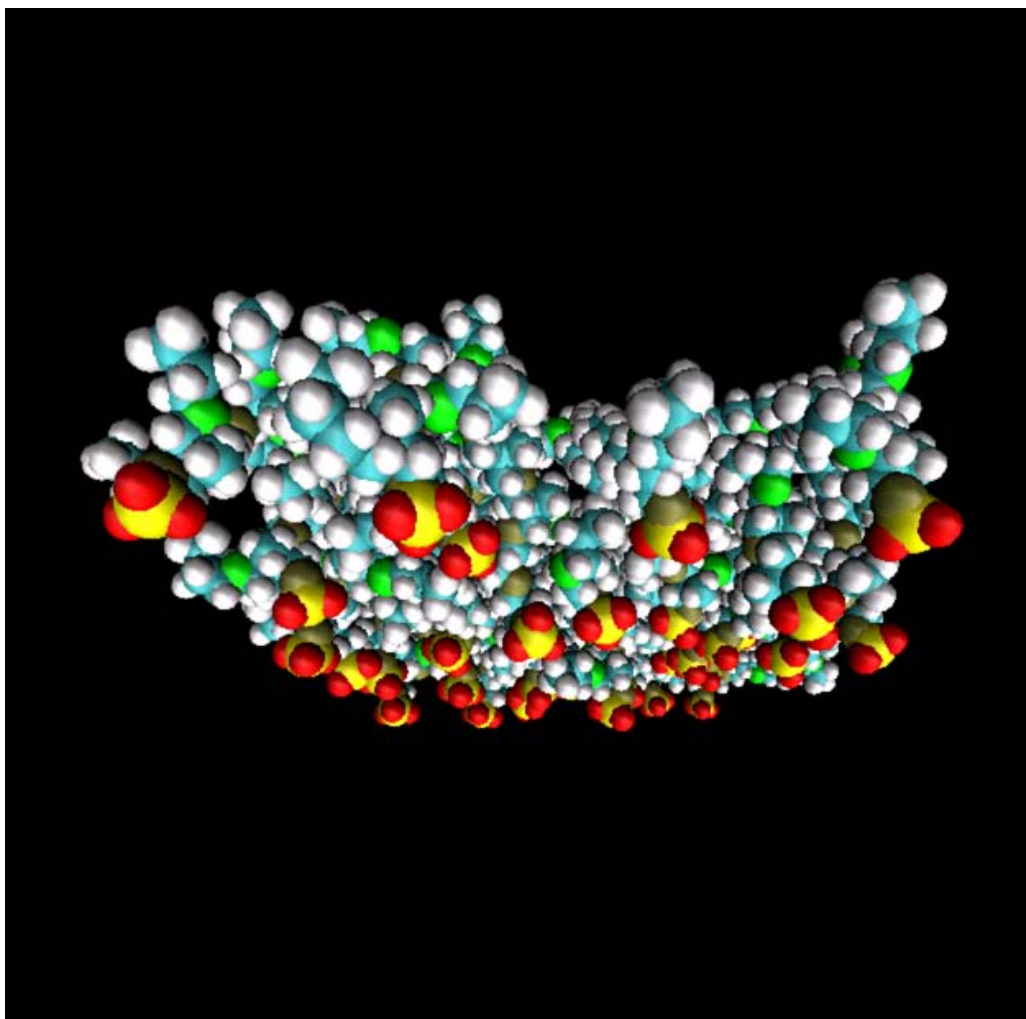


Figure 11-5: Representative snapshot (from below the water surface) of a monolayer of surfactant **2**. The degree of roughness present in the interface surface is typical of what was observed for surfactants **1-3** during *NVT* simulation. To permit a clear view of the surfactants, water molecules are not shown.

11.3.4 Interfacial Density Profiles

To quantitatively assess the average structure of each surfactant monolayer, atom number density profiles have been computed for each surfactant over the course of the post-equilibration, 1 ns *NVT* data-gathering runs described in Section 11.2.2. These density profiles, which have the units of number of atoms per nm^3 , are reported in Figures 11-6 to 11-9 for surfactants **1-4** as a function of the z simulation cell dimension (which is perpendicular to the water/surfactant/air interface). As indicated by the water density profile (the thick black line in each figure), the bulk air phase is located at the left side of each figure, and the bulk water phase is located at the right side. Because the density of atoms in the air phase is so low, only the density profiles of groups of surfactant atoms, the counterions, and water are shown in Figures 11-6 to 11-9. Note that the density profiles shown were generated based on density data from only one of the two surfactant monolayers present in each simulation cell. To facilitate comparison between the density profile results for each surfactant monolayer, the z axis of each figure has been centered about the peak of the overall density distribution for each surfactant. The location of this peak was determined by fitting the density profile for the surfactant monolayer to a Gaussian distribution (see Eq. 11.1).

Density profiles are reported for five groups of atoms in surfactants **1-3** to provide detailed information about organization within the monolayer and the extent of hydration of different atoms within each surfactant. The five groups reported include: the two sulfur atoms in each surfactant (S), each of the four oxygen atoms bonded to each sulfur atom (O-S), each oxygen atom present in the carbon-oxygen backbone of the surfactant (O-back), the average density of each carbon atom present in the carbon-oxygen backbone of the surfactant (C-back), and finally the average density of each carbon and fluorine atom in the R_f group (as defined in Figure 11-1) and the oxygen that connects the R_f sidechain to the surfactant backbone (O- R_f). Density profiles are reported for six groups of atoms in surfactant **4**. These include: the CO_2 group at the hydrophilic terminus of the surfactant (CO2), the CH_2 group attached to the CO_2 group (CH2-CO2), the nitrogen atom (N), the ethyl group attached to

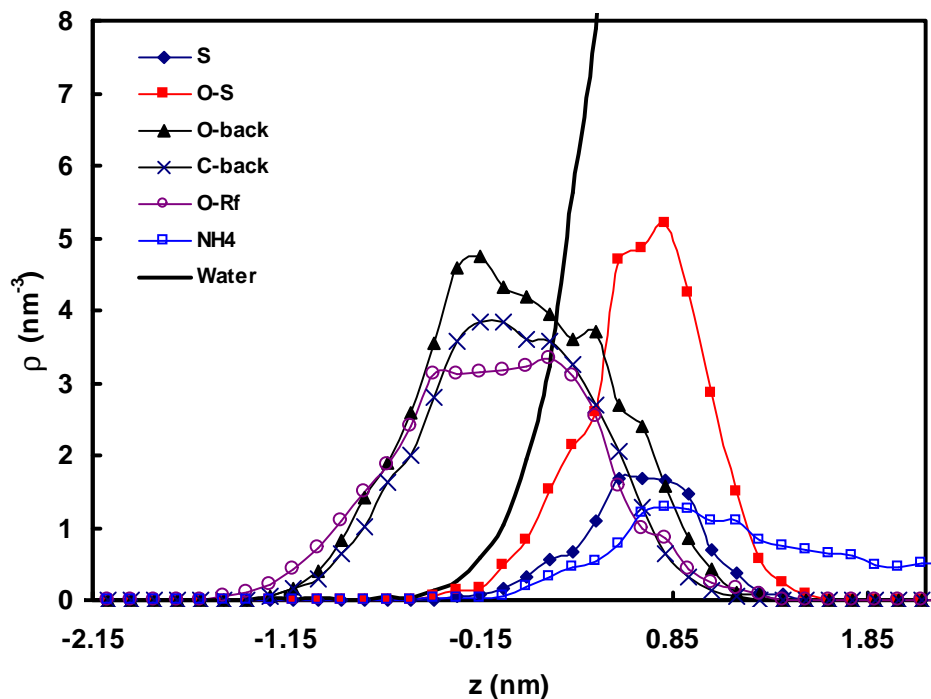


Figure 11-6: Number density profile for surfactant **1** at the water/air interface. S refers to the two sulfur atoms in each surfactant, O-S to each of the four oxygen atoms bonded to each sulfur atom, O-back to each oxygen atom present in the carbon-oxygen surfactant backbone, C-back to the average density of each carbon atom in the carbon-oxygen surfactant backbone, and O- R_f to the average density of each R_f group (as defined in Figure 1) and the oxygen atom connecting the R_f group to the surfactant backbone. Density profiles for NH_4^+ counterions and water are also shown.

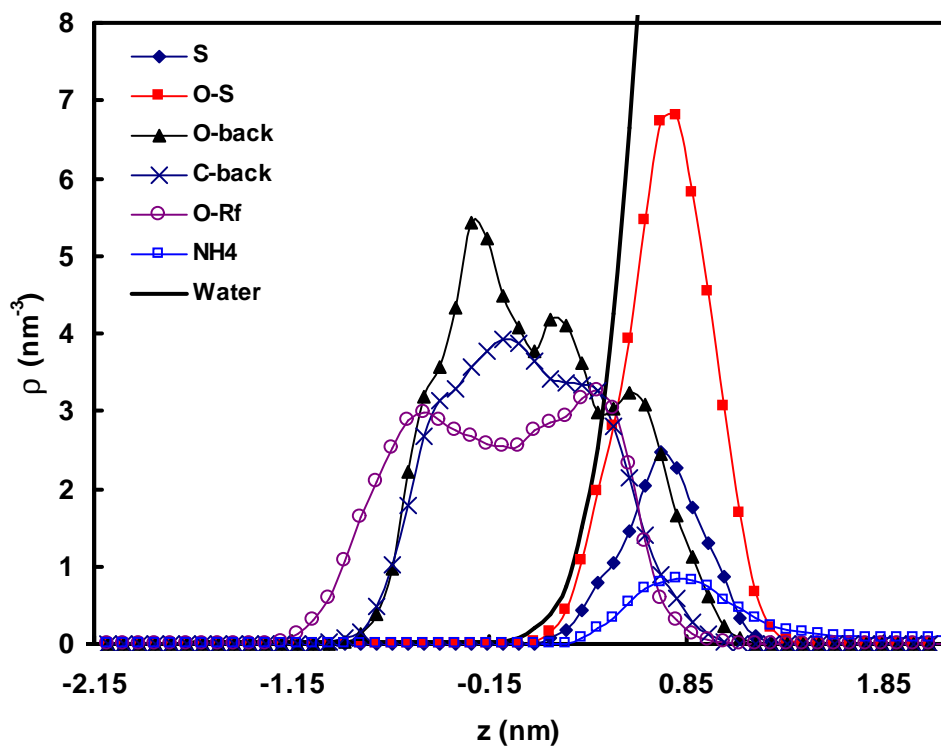


Figure 11-7: Number density profile for surfactant **2** at the water/air interface. S refers to the two sulfur atoms in each surfactant, O-S to each of the four oxygen atoms bonded to each sulfur atom, O-back to each oxygen atom present in the carbon-oxygen surfactant backbone, C-back to the average density of each carbon atom in the carbon-oxygen surfactant backbone, and O- R_f to the average density of each R_f group (as defined in Figure 1) and the oxygen atom connecting the R_f group to the surfactant backbone. Density profiles for NH_4^+ counterions and water are also shown.

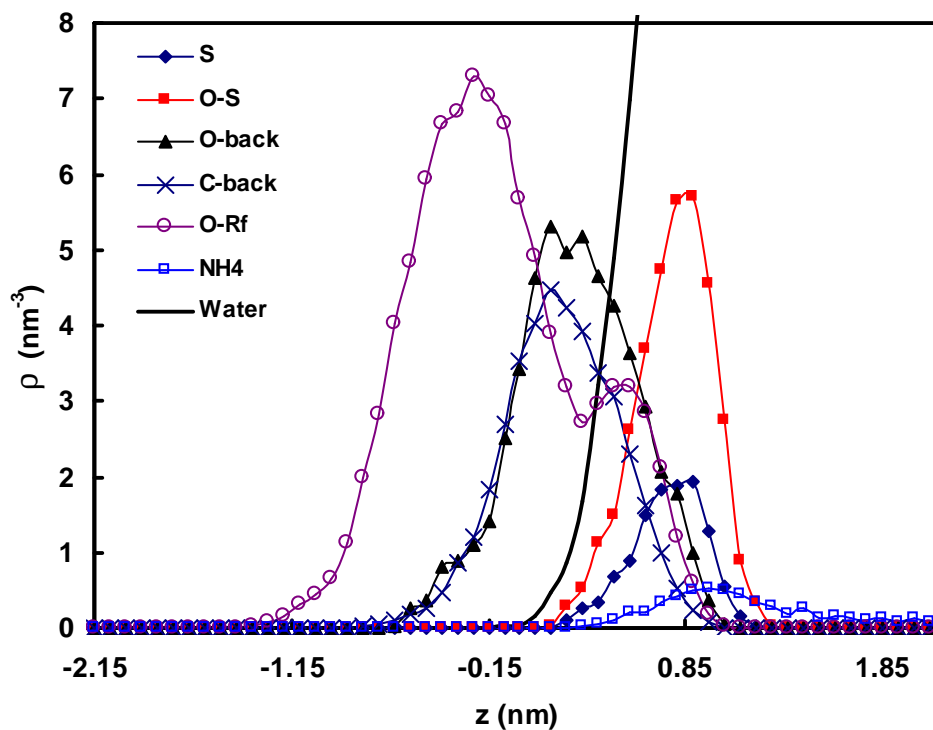


Figure 11-8: Number density profile for surfactant **3** at the water/air interface. S refers to the two sulfur atoms in each surfactant, O-S to each of the four oxygen atoms bonded to each sulfur atom, O-back to each oxygen atom present in the carbon-oxygen surfactant backbone, C-back to the average density of each carbon atom in the carbon-oxygen surfactant backbone, and O- R_f to the average density of each R_f group (as defined in Figure 1) and the oxygen atom connecting the R_f group to the surfactant backbone. Density profiles for NH_4^+ counterions and water are also shown.

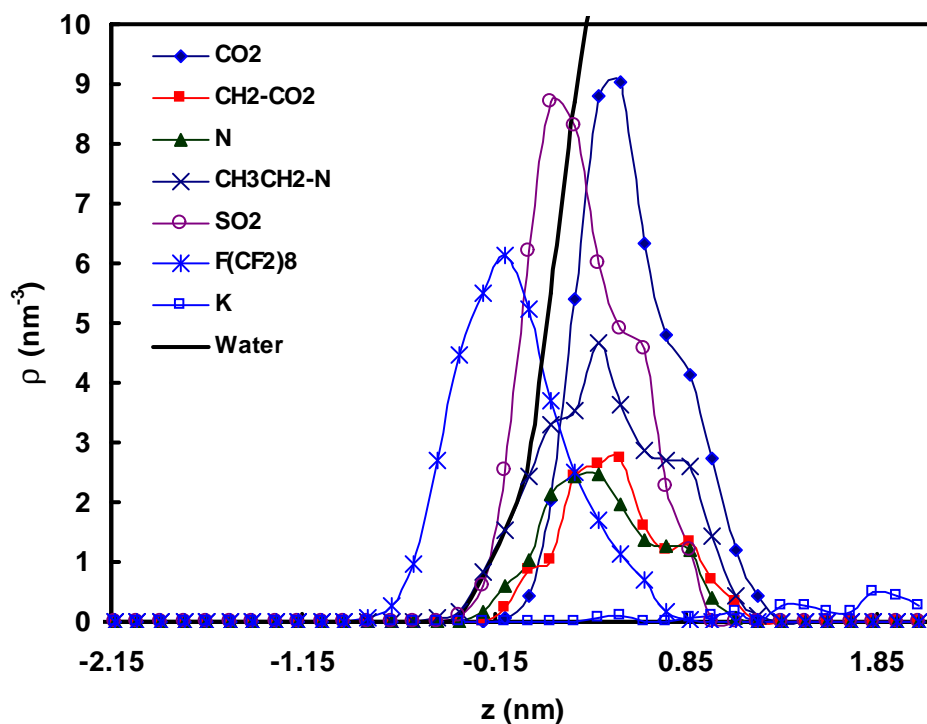


Figure 11-9: Number density profile for surfactant 4 at the water/air interface. CO₂ refers to the carboxylate group, CH₂-CO₂ to the CH₂ group attached to the CO₂ group, N to the nitrogen atom, CH₃CH₂-N to the ethyl group attached to the nitrogen atom, SO₂ to the sulfur atom and the two oxygen atoms attached to it, and F(CF₂)₈ to the average density of the carbon and fluorine groups comprising the linear fluorocarbon chain. Density profiles for K⁺ counterions and water are also shown.

this nitrogen (CH₃CH₂-N), the sulfur atom with two oxygen atoms attached to it (SO₂), and finally the average density of the eight carbon and 17 fluorine groups in the linear fluorocarbon chain comprising the hydrophobic portion of the surfactant (F(CF₂)₈).

The distribution of densities for each of the reported surfactant segments is in qualitative agreement with density profiles reported for a number of amphiphiles at water/air interfaces [10, 12, 13]. As would be expected, both the sulfur and oxygen atoms within each SO₄ group in surfactants **1-3** are largely surrounded by water. Similarly, for surfactant **4** the CO₂ group, the CH₂ group attached to the CO₂ group, the nitrogen atom, and even the ethyl group (CH₂CH₃) attached to the nitrogen atom appear largely within the water phase. For surfactant **4**, the peak of the density profile for the SO₂ group is just to the left of the density profile for the water phase.

As would be expected, the number density distribution of oxygen atoms and carbon atoms in each surfactant backbone for surfactants **1-3** is peaked at approximately the same value of z and mirror each other fairly closely. However, it is interesting to note that the oxygen and carbon atoms in the backbone are located predominantly within the air phase. This is in agreement with visual observation of the looped conformation of the surfactant backbone atoms, which force these atoms away from the water phase and into the air. The average density profile reported for each atom in the O-R_{*f*} group also indicates they spend the majority of their time in contact with the air phase. Similarly, each of the carbon and fluorine groups comprising the linear fluorocarbon chain in surfactant **4** remains primarily in the air phase.

To better understand and compare the average configuration of each surfactant at the water/air interface, we have scaled the surfactant density data by the peak surfactant density and fitted each surfactant profile to a Gaussian distribution of the form:

$$\rho'_{surf} = \frac{\rho_{surf}}{\rho^{peak}} = \exp \left[\frac{-(z - z_{surf}^o)^2}{2\sigma^2} \right] \quad (11.1)$$

where ρ'_{surf} is the surfactant density scaled by the peak surfactant density (ρ^{peak}),

z_{surf}^o is the center of the Gaussian distribution, and σ is the standard deviation of the Gaussian distribution. On this basis the density of surfactant ranges between 0 and 1. In addition, the scaled density profile of water was found by dividing each water density by the bulk density of water and fitting the resulting data to the following function:

$$\rho'_{water} = \frac{\rho_{water}}{\rho^{bulk}} = 0.5 \left(1 + \tanh \left(\frac{z - z_{water}^o}{w_{water}} \right) \right) \quad (11.2)$$

where ρ'_{water} is the water density scaled by the bulk density of water (ρ^{bulk}), z_{water}^o is the location of the water interface, and w_{water} is the width of the water interface. The scaled water density ranges between 0 and 1. For the purpose of analysis we would like to be able to define a similar function for the scaled density of the air phase which also ranges between 0 and 1. However, because of the low number of air molecules present in the simulation cell such an analysis approach gave results with poor statistics. Because of this, we have computed an “air density fraction” at each value of z from the density data gathered for both the surfactant and water phases using the following equation:

$$\rho'_{air} = 1 - \rho'_{surf} - \rho'_{water} \quad (11.3)$$

where ρ'_{air} is the “air density fraction,” ranging between 0 and 1, and ρ'_{surf} and ρ'_{water} are defined as given above. The ρ'_{air} “data” thus generated was then fitted to the following equation:

$$\rho'_{air} = 0.5 \left(1 - \tanh \left(\frac{z - z_{air}^o}{w_{air}} \right) \right) \quad (11.4)$$

where, as for water, z_{air}^o is the location of the air interface and w_{air} is the width of the air interface. A plot of each of these density profiles for surfactants **3** and **4** is shown in Figures 11-10 and 11-11, respectively. It is immediately apparent from the figures that surfactant **3** has a significantly wider distribution than surfactant **4** at the water/air interface. In addition, it is interesting to note that the decrease in the density of vacuum and water as they approach the surfactant monolayer is more

symmetric for surfactant **3** than surfactant **4**.

The average location of surfactant, the location of the air interface, and the location of the water interface has been determined by fitting the density data to the functional forms shown in Eq. 11.1, Eq. 11.2, and Eq. 11.4. Each of these values is reported in Table 11.5. The uncertainty reported in the table for each fitted parameter is the 95% confidence interval. Also reported in the table is the width of the surfactant density profile (w_{surf}), which has been estimated as $2 \cdot 1.96 \cdot \sigma = 3.92 \cdot \sigma$ (to include 95% of the area under the density profile), and the width of the air (w_{air}) and water (w_{water}) interfaces as determined by Eqs. 11.2 and 11.4. To better understand the ability of each surfactant to reduce surface tension, we also report the absolute value of the distance between the location of the air and water interfaces ($|z_{air}^o - z_{water}^o|$, or $|\Delta z|$). At a fundamental level, surface tension arises from the excess free energy present at an interface due to unfavorable contacts between two bulk phases. In so far as a surfactant reduces the number of unfavorable interactions between the two bulk phases and replaces it with favorable interactions it reduces the surface tension. The extent to which the number of unfavorable contacts between the bulk phases is reduced due to the presence of surfactant should be related to both (i) the distance between the location of the air and water interfaces, and (ii) the width of the air and water interfaces. To characterize differences between the ability of hydrocarbon and fluorocarbon surfactants to reduce the surface tension at a CO₂/water interface, Stone et al. reported $|\Delta z|$ values for both types of surfactants and also defined what they refer to as a penetration parameter (P), which reflects the degree to which the two bulk phases come into contact at the interface. The penetration parameter is directly proportional to the width of both interfaces and inversely proportional to the distance between both interfaces. It is defined as follows:

$$P = \frac{w_{air} + w_{water}}{|z_{air}^o - z_{water}^o|} \quad (11.5)$$

Values of the penetration parameter, P , are reported for surfactants **1-4** in Table

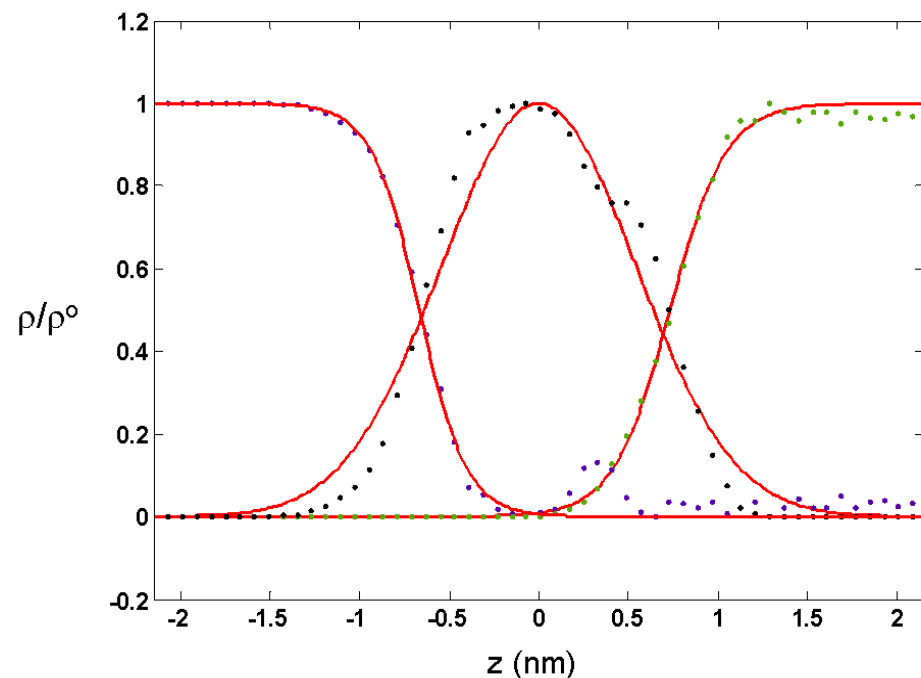


Figure 11-10: Scaled density profiles for surfactant **3** at the water/air interface. Simulation data is shown as points, and the curve fits generated by fitting Eqs. 11.1, 11.2, and 11.4 to the data are shown as solid lines. The air density “data” was determined from the water and surfactant density data as $\rho'_{air} = 1 - \rho'_{surf} - \rho'_{water}$. The bulk air phase is located on the left side of the plot, surfactant **3** is in the center, and the bulk water phase is located to the right side of the plot. The z axis has been centered based on the center of the Gaussian distribution fitted to the surfactant **3** density data.

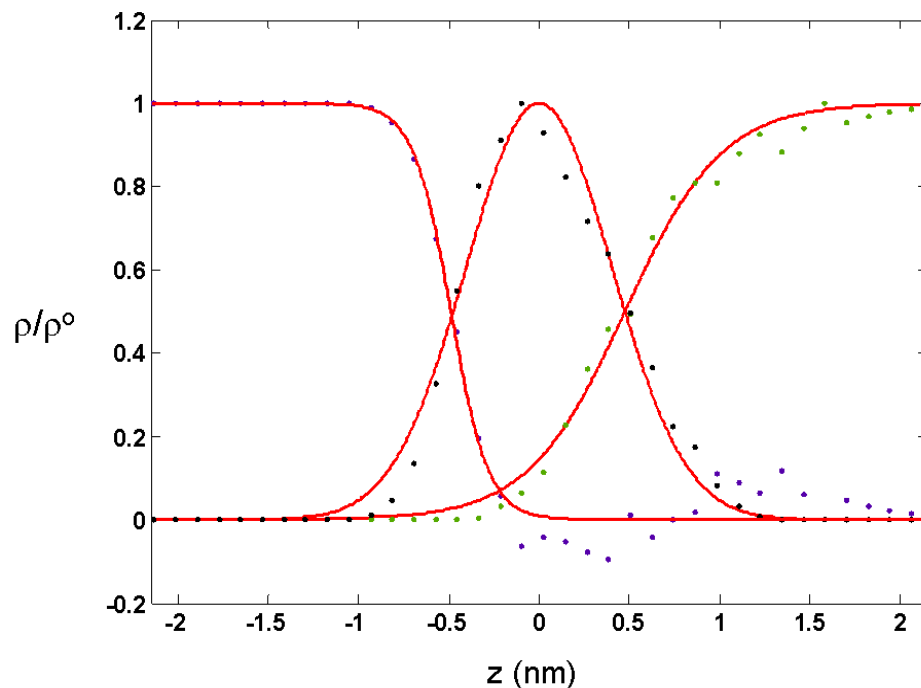


Figure 11-11: Scaled density profiles for surfactant **4** at the water/air interface. Simulation data is shown as points, and the curve fits generated by fitting Eqs. 11.1, 11.2, and 11.4 to the data are shown as solid lines. The air density “data” was determined from the water and surfactant density data as $\rho'_{air} = 1 - \rho'_{surf} - \rho'_{water}$. The bulk air phase is located on the left side of the plot, surfactant **4** is in the center, and the bulk water phase is located to the right side of the plot. The z axis has been centered based on the center of the Gaussian distribution fitted to the surfactant **4** density data.

Surf.	Air		Water		Surfactant		separation,	penetration
Type	w_{air} (nm)	z_{air}^o (nm)	w_{water} (nm)	z_{water}^o (nm)	w_{surf} (nm)	z_{surf}^o (nm)	$ \Delta z $ (nm)	parameter, P
1	0.34 ± 0.04	-0.69 ± 0.02	0.43 ± 0.02	0.63 ± 0.01	2.20 ± 0.04	0.0	1.33 ± 0.02	0.59 ± 0.03
2	0.29 ± 0.02	-0.74 ± 0.01	0.27 ± 0.01	0.66 ± 0.01	2.23 ± 0.08	0.0	1.40 ± 0.02	0.40 ± 0.02
3	0.26 ± 0.03	-0.67 ± 0.02	0.31 ± 0.02	0.73 ± 0.01	2.13 ± 0.05	0.0	1.40 ± 0.02	0.41 ± 0.02
4	0.21 ± 0.04	-0.49 ± 0.02	0.54 ± 0.05	0.48 ± 0.03	1.58 ± 0.07	0.0	0.97 ± 0.04	0.77 ± 0.07

Table 11.5: The width (w_{air}) and location (z_{air}^o) of the air interface in nanometers as determined by fitting scaled density profile data to Eq. 11.4. The width (w_{water}) and location (z_{water}^o) of the water interface in nanometers as determined by fitting the scaled density profile data to Eq. 11.2. The width of the Gaussian distribution of surfactant density (σ) (based on Eq. 11.1), and the location (z_{surf}^o) of the peak of the Gaussian distribution in nanometers. All distances are reported relative to z_{surf}^o . The separation distance between the location of the air and water interfaces, $|\Delta z|$, is reported in nanometers. Values of the penetration parameter, as defined in the text, are also listed for each surfactant.

11.5. Again, the uncertainty reported for each fitted parameter is the 95% confidence interval. In the study of Stone et al., it was found that the penetration parameter P is significantly larger for hydrocarbon surfactants than fluorocarbon surfactants, suggesting why fluorocarbon surfactants are better able to reduce interfacial surface tension between CO_2 and water than hydrocarbon surfactants. As can be seen in Table 11.5, of the four surfactants considered, surfactant **4** has the greatest value of the penetration parameter (0.77). Surfactant **1** has a penetration parameter which is significantly smaller (0.59), and surfactants **2** and **3** have virtually the same value of the penetration parameter (0.40 and 0.41, respectively).

The fact that surfactants **1-3** are capable of effectively separating the water from the air phase, as reflected in the relatively small values of the penetration parameter for these interfaces, suggests why they are so effective at reducing surface tension. Obviously, however, the penetration parameter does not completely explain the surface tension behavior of these surfactants. Despite having the largest penetration parameter, surfactant **4** actually reduces the surface tension to the greatest extent. Also, surfactants **1-3** are all roughly equally effective at reducing surface tension, despite the fact that the penetration parameter for surfactant **1** is greater than that of surfactants **2** and **3**. Other factors that could play an important role in determining surface

tension which are not taken into account in the penetration parameter (which only takes into account enthalpic interactions between the two bulk phases) include surfactant entropy and the degree to which the surfactant makes enthalpically-favorable contacts with both bulk phases.

11.3.5 Degree of Hydration and Counterion Binding

To quantitatively determine and compare the degree of hydration of the atoms in each surfactant monolayer, the average number of oxygen water atoms within 0.5 nm of groups of atoms in surfactants **1-4** has been computed. The results for each surfactant are shown in Figure 11-12. The trends in the hydration data shown in Figure 11-12 remain the same if this distance is increased to 0.6 nm or decreased to 0.4 nm. Results were averaged over similar atoms within each surfactant (for surfactants **1-3**) and over the surfactants in both monolayers. The degree of hydration was calculated using data from the same 1 ns, *NVT* molecular dynamics simulation described in Section 11.2.2.

The degree of hydration data matches what would be intuitively expected given the snapshots of surfactant conformation presented in Figure 11-4 b). The large SO_4^- head groups in surfactants **1-3**, which are buried within the solvent, have the greatest degree of hydration. However, the backbone oxygen atoms, the backbone carbon atoms, the oxygen atom at the base of each perfluoroalkyl chain, and the atoms in each perfluoroalkyl chain all experienced a similar degree of hydration for all three poly(fluorooxetane) surfactants. The fact that the degree of hydration data is very similar for surfactants **1-3** suggests why each of these surfactants are almost equally effective at reducing surface tension at the water/air interface.

Comparison of the hydration data for the single-chain surfactant **4** and the short-chain oligomeric surfactants **1-3** provides insight into the question of why short perfluoroalkyl chains (such as the $\text{CH}_2-(\text{CF}_2)_x$ groups attached to surfactants **1-3**) do not provide adequate surface tension reduction when attached directly to the surfactant head. For surfactants **1-3**, the backbone carbon, oxygen, and $\text{CH}_2-(\text{CF}_2)_x$

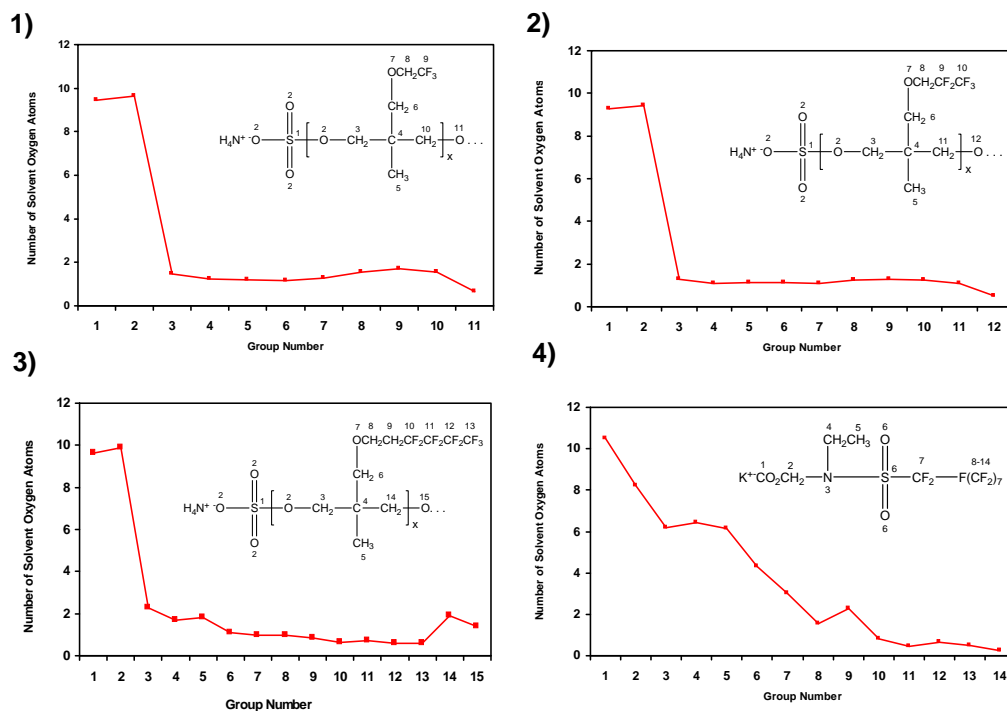


Figure 11-12: Average degree of hydration for surfactants **1-4**, as measured by the number of water oxygen atoms within 0.5 nm of selected groups of surfactant atoms. Results are presented for 1) surfactant **1**, 2) surfactant **2**, 3) surfactant **3**, and 4) surfactant **4**.

units are at positions 4 and higher, and the average degree of hydration for each of these groups is less than 2.0. By contrast, a comparably water-free environment is not experienced by the CF₂ units of surfactant **4** until group 10, or the fourth CF₂ unit. This difference is attributed to the “loop” configuration evident in Figure 11-4, which presents the backbone carbon and oxygen atoms and each CH₂–(CF₂)_x chain into the hydrophobic (air) phase and away from the water.

The degree of counterion binding has been determined for each surfactant by analyzing headgroup-counterion radial distribution functions. For surfactants **1-3**, the radial distribution function was computed between each sulfur atom and the nitrogen atom in NH₄⁺. For surfactant **4**, the radial distribution function was computed between the carbon atom in the carboxylate group and K⁺. Radial distribution function results were averaged over each surfactant in both monolayers. The number of counterions associated with each surfactant head, or the degree of counterion binding, can be computed by integrating the first peak of the radial distribution function. The degree of counterion binding was found to be 0.71 for surfactant **1**, 0.64 for surfactant **2**, 0.45 for surfactant **3**, and 0.66 for surfactant **4**. The results for surfactants **1-3** match what would be intuitively expected based on the average areas per headgroup reported in Table 11.2. The smaller the area per headgroup, the greater the electrostatic potential at the water/surfactant interface and the greater the driving force for counterion binding. The results for surfactant **4** do not fall neatly into this trend, but direct comparison is not possible because the headgroup and counterion of surfactant **4** is different than that of surfactants **1-3**.

11.3.6 Order Parameters

Average bond-bond order parameters have been calculated for the fluorocarbon chains in surfactants **1-4** based on the same *NVT* simulation data discussed in Section 11.2.2. The order parameter used in this analysis is defined as follows for atom *i*:

$$S_{z,i} = \frac{3}{2} \langle \cos^2 \theta_{z,i} \rangle - \frac{1}{2} \quad (11.6)$$

Surfactant 1			Surfactant 3			Surfactant 4		
(C-O-CH ₂ -CF ₃)			(C-O-CH ₂ -CH ₂ -CF ₂ -CF ₂ -CF ₂ -CF ₃)			(CF _{2,1} -CF _{2,7})		
x	y	z	x	y	z	x	y	z
0.086	0.019	-0.106	-0.062	-0.096	0.158	-0.251	0.049	0.202
0.062	0.013	-0.075	-0.072	-0.107	0.180	-0.226	0.030	0.196
Surfactant 2			-0.086	-0.094	0.180	-0.287	-0.186	0.473
(C-O-CH ₂ -CF ₂ -CF ₃)			-0.083	-0.091	0.174	-0.096	-0.066	0.162
0.066	-0.020	-0.046	-0.064	-0.095	0.159	-0.021	-0.077	0.097
0.049	-0.029	-0.021	-0.060	-0.027	0.087	-0.007	-0.095	0.102
0.036	-0.016	-0.020						

Table 11.6: Order parameters with respect to the x , y , and z -axis for the side chains of surfactants **1-3** and the fluorocarbon chain of surfactant **4**. The first x , y , and z order parameters listed for each surfactant correspond to the first three atoms adjacent to the chain’s point of attachment. Order parameters are listed starting from the left of the structure as drawn (for example, the first order parameters listed for Surfactant **1** are defined based on C-O-CH₂).

where θ_z is the angle between the z -axis of the simulation box and an axis defined by the vector connecting atoms $i - 1$ and $i + 1$ along the fluorocarbon chain. S_x and S_y are defined in a similar manner. Using the definition given in Eq. 11.6, S_z is equal to 1 when there is complete ordering along the z -axis, 0 when the system is isotropic, and $-\frac{1}{2}$ when there is complete ordering perpendicular to the z -axis. At each instant in time, the simulation data for $\cos^2 \theta_{z,i}$ was averaged over every i atom in each perfluoroalkyl chain. These results were averaged over the entire simulation timespan for surfactants **1-3**. With the order parameter defined in this way, $n - 2$ order parameters can be defined for a chain containing n atoms. Order parameter results are presented in Table 11.6, where the first order parameter listed corresponds to the first three atoms adjacent to the chain’s point of attachment to the surfactant backbone.

Our data indicates that there is very little ordering of the perfluoroalkyl chains for surfactants **1-3** with respect to the x , y , and z -axes. This is not surprising given the snapshots shown in Figure 11-4. The “loop” formed by the carbon and oxygen backbone that connects each SO_4^- head group does not support the fluorocarbon chains in any consistent x , y , or z orientation. The S_z values for surfactant **4** are not

atypical of chains packed in bilayers [47]. The data indicates that although ordering with respect to the z -axis is present in the carbons closest to the surfactant **4** head, carbons near the terminal CF_3 group are quite disordered.

11.4 Conclusions

Molecular dynamics simulations have been conducted at both constant surface tension (for equilibration) and constant volume (to gather equilibrium data) for a series of bolaamphiphilic poly(fluorooxetane)s with perfluoroalkyl chain lengths ranging from $-\text{CF}_3$ to $-(\text{CF}_2)_4\text{F}$. Similar MD simulations have been conducted for a typical small-molecule, long-fluorocarbon chain anionic surfactant. Relatively long simulations of 3-9 ns were required to observe approximate equilibration of the simulation cell geometry in the presence of an externally-applied surface tension. Accurate treatment of electrostatics was found to be quite important in determining the final simulation cell geometry.

The equilibrated values for interfacial area per surfactant molecule obtained in this study differ significantly from the fitted values obtained by Kausch et al. There are several possible reasons for this discrepancy, ranging from errors associated with fitting molecular areas using the Davies isotherm to insufficient simulation time to permit complete equilibration. An additional series of $N\gamma T$ simulations conducted at several reduced surface tension values revealed that the interfacial area of each surfactant is not a strong function of the applied surface tension. Direct visualization of typical conformations adopted by each surfactant at low surface concentration and at saturated surface concentration clearly reveal that upon packing with other surfactants, each bola amphiphile extends much of its carbon and oxygen backbone into the air phase. This allows each of these surfactants to occupy a relatively small area at the water/air interface despite their high molecular weight. Density profiles were generated for groups of atoms in each surfactant to investigate ordering and levels of hydration for each atom in surfactants **1-4**. In addition, scaled density

profiles for the water, surfactant, and a mathematically defined “air volume fraction” were fitted to mathematical expressions describing the density profile that allowed determination of the average location of the air and water interfaces. Based on these fits, we determined that surfactants **1-3** actually separate the air and water phases to a greater extent than surfactant **4**. In addition, the degree of penetration between the air and water phases, as revealed by a geometrical defined penetration parameter, is higher for surfactant **4** than for surfactants **1-3**. Degree of hydration data was obtained from *NVT* MD simulations, and the results corroborate the conformational information inferred from surfactant visualization. The surfactant SO_4^- head groups have a high degree of hydration in comparison with other atoms in the surfactant backbone and the fluorocarbon chains, confirming that these surfactants adopt a “looped” conformation at the water/air interface and that the fluorocarbon chains are forced into the vapor phase. When viewed in the context of the penetration parameter analysis, this hydration data suggests why each poly(fluorooxetane) is capable of significantly reducing surface tension when other fluorosurfactants with similarly short perfluoroalkyl moieties provide surface tension reduction that is inadequate for practical flow-and-leveling applications. Order parameters computed for surfactants **1-4** indicate a lower degree of ordering with respect to the x , y , and z -axes for each perfluoroalkyl chain in surfactants **1-3** in comparison with the fluorocarbon chain of surfactant **4**.

In the next chapter, Chapter 12, molecular dynamics simulations are used to investigate the self-assembly behavior of the triterpenoids asiatic acid (AA) and madecassic acid (MA) in aqueous solution. In that chapter, properties such as the kinetics of micelle formation, structural characteristics of the self-assembled micellar aggregates, the local environment of atoms in AA and MA in the micellar environment, and the degree of counterion binding are reported as determined directly through molecular dynamics simulation. In addition, a modified version of the CS-MT modeling approach described in Chapters 6, 7, and 8 (referred to as the MCS-MT model) is used in conjunction with computer simulation data on the hydrophobic solvent accessible

surface area of AA and MA micelles to quantify the thermodynamics of AA and MA micelle formation.

Bibliography

- [1] Kausch, C. M., Kim, Y., Russell, V. M., Medsker, R. E., and Thomas, R. R., "Surface tension and adsorption properties of a series of bolaamphiphilic poly(fluorooxetane)s," *Langmuir*, Vol. 19, 2003, pp. 7182–7187.
- [2] Hawthorne, M., "Marvel Chemicals Pop Up in Animals All Over World," *Chicago Tribune*, 2002, pp. July 27.
- [3] Hawthorne, M., "Marvel Chemicals Pop Up in Animals All Over World," *Chicago Tribune*, 2002, pp. July 27.
- [4] Ritter, S. K., Washington, C., and Washington, E., "Fluorine Persists," *Chemical and Engineering News*, Vol. 82, 2004, pp. 44–45.
- [5] Cortese, A., "Dupont, Now in the Frying Pan," *New York Times*, 2002, pp. August 8.
- [6] *Perfluoroalkyl Sulfonates: Significant New Use Rule*, Environmental Protection Agency, Federal Register, Office of Pollution Prevention and Toxics, Washington, DC., 2002.
- [7] Kausch, C. M., Kim, Y., Russell, V. M., Medsker, R. E., and Thomas, R. R., "Synthesis, characterization, and unusual surface activity of a series of novel architecture, water-dispersible poly(fluorooxetane)s," *Langmuir*, Vol. 18, 2002, pp. 5933–5938.

- [8] Kausch, C. M., Kim, Y., Russell, V. M., Medsker, R. E., and Thomas, R. R., “Interfacial rheological properties of a series of bolaamphiphilic poly(fluorooxetane)s,” *Langmuir*, Vol. 19, 2003, pp. 7354–7361.
- [9] Stone, M. T., da Rocha, S. R. P., Rossky, P. J., and Johnston, K. P., “Molecular differences between hydrocarbon and fluorocarbon surfactants at the CO₂/water interface,” *The Journal of Physical Chemistry B*, Vol. 107, 2003, pp. 10185–10192.
- [10] Tarek, M., Tobias, D. J., and Klein, M. L., “Molecular dynamics simulation of tetradecyltrimethylammonium bromide monolayers at the air-water interface,” *The Journal of Physical Chemistry*, Vol. 99, 1995, pp. 1393–1402.
- [11] Wijmans, C. M. and Linse, P., “Surfactant self-assembly at a hydrophilic surface. A Monte Carlo simulation study,” *The Journal of Physical Chemistry*, Vol. 100, 1996, pp. 12583–12591.
- [12] Schweighofer, K. J., Essmann, U., and Berkowitz, M., “Simulation of sodium dodecyl sulfate at the water-vapor and water-carbon tetrachloride interfaces at low surface coverage,” *The Journal of Physical Chemistry B*, Vol. 101, 1997, pp. 3793–3799.
- [13] Schweighofer, K. J., Essmann, U., and Berkowitz, M., “Structure and dynamics of water in the presence of charged surfactant monolayers at the water-CCl₄ interface. A molecular dynamics study,” *The Journal of Physical Chemistry*, Vol. 101, 1997, pp. 10775–10780.
- [14] Dominguez, H. and Berkowitz, M. L., “Computer simulations of sodium dodecyl sulfate at liquid/liquid and liquid/vapor interfaces,” *The Journal of Physical Chemistry B*, Vol. 104, 2000, pp. 5302–5308.

- [15] Kuhn, H. and Rehage, H., “Molecular dynamics computer simulations of surfactant monolayers: Monododecyl pentaethylene glycol at the surface between air and water,” *The Journal of Physical Chemistry B*, Vol. 103, 1999, pp. 8493–8501.
- [16] Kuhn, H. and Rehage, H., “Molecular orientation of monododecyl pentaethylene glycol (C12E5) surfactants at infinite dilution at the air/water interface. A molecular dynamics computer simulation study,” *Physical Chemistry Chemical Physics*, Vol. 2, 2000, pp. 1023–1028.
- [17] Kuhn, H. and Rehage, H., “Molecular orientation of monododecyl pentaethylene glycol at water/air and water/oil interfaces. A molecular dynamics computer simulation study,” *Colloid and Polymer Science*, Vol. 114-118, 2000, pp. 278.
- [18] da Rocha, S. R. P., Johnston, K. P., and Rosky, P. J., “Surfactant-modified CO₂-water interface: A molecular view,” *The Journal of Physical Chemistry*, Vol. 106, 2002, pp. 13250–13261.
- [19] Rekvig, L., Hafskjold, B., and Smit, B., “Simulating the effect of surfactant structure on bending moduli of monolayers,” *The Journal of Chemical Physics*, Vol. 120, 2004, pp. 4897–4905.
- [20] Rekvig, L., Hafskjold, B., and Smit, B., “Chain length dependencies of the bending modulus of surfactant monolayers,” *Physical Review Letters*, Vol. 92, 2004, pp. 116101.
- [21] Dominguez, H., “Computer simulations of surfactant mixtures at the liquid/liquid interface,” *The Journal of Physical Chemistry B*, Vol. 106, 2002, pp. 5915–5924.
- [22] Shin, S., Collazo, N., and Rice, S., “Comment on molecular dynamics simulations of monolayers of fluorinated amphiphiles,” *The Journal of Chemical Physics*, Vol. 98, 1993, pp. 3469–3474.

- [23] Shin, S., Collazo, N., and Rice, S., “A molecular dynamics study of the packing structures in monolayers of partially fluorinated amphiphiles,” *The Journal of Chemical Physics*, Vol. 96, 1992, pp. 1352–1366.
- [24] Barton, S. W., Goudot, A., Bouloussa, O., Rondelez, F., Lin, B., Novak, F., Acero, A., and Rice, S. A., “Structural transitions in a monolayer of fluorinated amphiphile molecules,” *The Journal of Chemical Physics*, Vol. 96, 1992, pp. 1343–1351.
- [25] Acero, A., Li, M., Lin, B., Rice, S., Goldmann, M., Azouz, I. B., Goudot, A., and Rondelez, F., “Molecular packing in water supported monolayers of FCF211COOH and FCF210CH2COOH,” *The Journal of Chemical Physics*, Vol. 99, 1993, pp. 7214–7220.
- [26] Gragson, D. E., McCarty, B. M., and Richmond, G. L., “Surfactant/water interactions at the air/water interface probed by vibrational sum frequency generation,” *The Journal of Physical Chemistry*, Vol. 100, 1996, pp. 14272–14275.
- [27] Conboy, J. C., Messmer, M. C., and Richmond, G. L., “Dependence of alkyl chain conformation of simple ionic surfactants on head group functionality as studied by vibrational sum-frequency spectroscopy,” *The Journal of Physical Chemistry B*, Vol. 101, 1997, pp. 6724–6733.
- [28] Conboy, J. C., Messmer, M. C., and Richmond, G. L., “Effect of alkyl chain length on the conformation and order of simple ionic surfactants adsorbed at the D2O/CCl4 interface as studied by sum-frequency vibrational spectroscopy,” *Langmuir*, Vol. 14, 1998, pp. 6722–6727.
- [29] Zhang, Z. H. H., Tsuyumoto, I., Kitamori, T., and Sawada, T., “Observation of the dynamic and collective behavior of surfactant molecules at a water/nitrobenzene interface by a time-resolved quasi-elastic laser-scattering method,” *The Journal of Physical Chemistry B*, Vol. 102, 1998, pp. 10284.

- [30] Grubb, S. G., Kim, M. W., Raising, T., and Shen, Y. R., "Orientation of molecular monolayers at the liquid liquid interface as studied by optical 2nd harmonic generation," *Langmuir*, Vol. 102, 1988, pp. 452–454.
- [31] Li, Z. X., Weller, A., Thomas, R. K., Rennie, A. R., and Webster, J. R. P., "Adsorption of the lamellar phase of aerosol-OT at the solid/liquid and air/liquid interfaces," *The Journal of Physical Chemistry B*, Vol. 103, 1999, pp. 10800–10806.
- [32] Piasecki, D. A. and Wirth, M. J., "Reorientation of acridine-orange in a sodium dodecyl sulfate monolayer at the water hexadecane interface," *The Journal of Physical Chemistry*, Vol. 97, 1993, pp. 7700–7705.
- [33] Tian, Y., Umemura, J., Takenaka, T., and Kunitake, T., "Ultraviolet visible absorption and resonance raman-spectra of azobenzene-containing amphiphile monolayers adsorbed at the acidic aqueous solution carbon tetrachloride interface," *Langmuir*, Vol. 4, 1988, pp. 1064–1066.
- [34] Kjellin, U. R. M., Claesson, P. M., and Linse, P., "Surface properties of tetra(ethylene oxide) dodecyl amide compared with poly(ethylene oxide) surfactants. 1. Effect of the headgroup on adsorption," *Langmuir*, Vol. 18, 2002, pp. 6745–6753.
- [35] Berendsen, H. J. C., van der Spoel, D., and van Drunen, R., "GROMACS: A message-passing parallel molecular dynamics implementation," *Computational Physics Community*, Vol. 91, 1995, pp. 43–56.
- [36] Lindahl, E., Hess, B., and van der Spoel, D., "Gromacs 3.0: A package for molecular simulation and trajectory analysis," *Journal of Molecular Modeling*, Vol. 7, 2001, pp. 306–317.
- [37] Jorgensen, W. L., Maxwell, D. S., and Tirado-Rives, J., "Development and testing of the OPLS all-atom force field on conformational energetics and properties

- of organic liquids,” *Journal of the American Chemical Society*, Vol. 118, 1996, pp. 11225–11236.
- [38] Watkins, E. K. and Jorgensen, W. L., “Perfluoroalkanes: Conformational analysis and liquid-state properties from ab initio and Monte Carlo calculations,” *Journal of Physical Chemistry A*, Vol. 105, 2001, pp. 4118–4125.
- [39] Padua, A. A. H., “Torsion energy profiles and force fields derived from ab initio calculations for simulations of hydrocarbon-fluorocarbon diblocks and perfluoroalkylbromides,” *The Journal of Physical Chemistry A*, Vol. 206, 2002, pp. 10116–10123.
- [40] Schweighofer, K. J., Essmann, U., and Berkowitz, M., “Simulation of sodium dodecyl sulfate at the water-vapor and water-carbon tetrachloride interfaces at low surface coverage,” *The Journal of Physical Chemistry B*, Vol. 101, 1997, pp. 3793–3799.
- [41] Aqvist, J., “Ion-water interaction potentials derived from free energy perturbation simulations,” *The Journal of Physical Chemistry*, Vol. 94, 1990, pp. 8021–8024.
- [42] Berendsen, H. J. C., Grigera, J. R., and Straatsma, T. P., “The missing term in effective pair potentials,” *The Journal of Physical Chemistry*, Vol. 91, 1987, pp. 6269–6271.
- [43] van der Spoel, D., Lindahl, E., Hess, B., van Buuren, A., Apol, E., Meulenhoff, P., Tieleman, D., Sijbers, A., Feenstra, K., van Drunen, R., and Berendsen, H., *Gromacs User Manual version 3.2*, www.gromacs.org, 2004.
- [44] Bennett, M. K. and Zisman, W. A., “The behavior of monolayers of progressively fluorinated fatty acids adsorbed on water,” *The Journal of Physical Chemistry*, Vol. 67, 1963, pp. 1534–1540.

- [45] Feller, S. and Pastor, R., “On simulating lipid bilayers with an applied surface tension: Periodic boundary conditions and undulations,” *Biophysical Journal*, Vol. 71, 1996, pp. 1350–1355.
- [46] Tieleman, D. and Berendsen, H., “Molecular dynamics simulations of a fully hydrated dipalmitoyl phosphatidylcholine bilayer with different macroscopic boundary conditions and parameters,” *Journal of Chemical Physics*, Vol. 105, 1996, pp. 4871–4880.
- [47] Berendsen, H. and Tieleman, D., *Encyclopedia of Computational Chemistry*, John Wiley and Sons, Ltd., New Jersey, 1998.

Chapter 12

Molecular Dynamics Simulation of the Self-Assembly of the Triterpenoids Asiatic Acid and Madecassic Acid in Aqueous Solution

12.1 Introduction

Asiatic acid (AA) and madecassic acid (MA) are two triterpenoids present in *Centella asiatica* and other tropical plants. Both compounds have recently been the subject of investigation because of their anti-cancer activity [1–4]. The chemical structures of AA and MA are related to the structures of bile salts found in animals, the principal difference being that AA and MA are pentacyclic in structure, while bile salts are tetracyclic [5]. The chemical structures of AA and MA are shown schematically in Figure 12-1. Like bile salts, AA and MA are surface active [6, 7]. Recently, the surface-active properties of these two triterpenoids have been characterized ex-

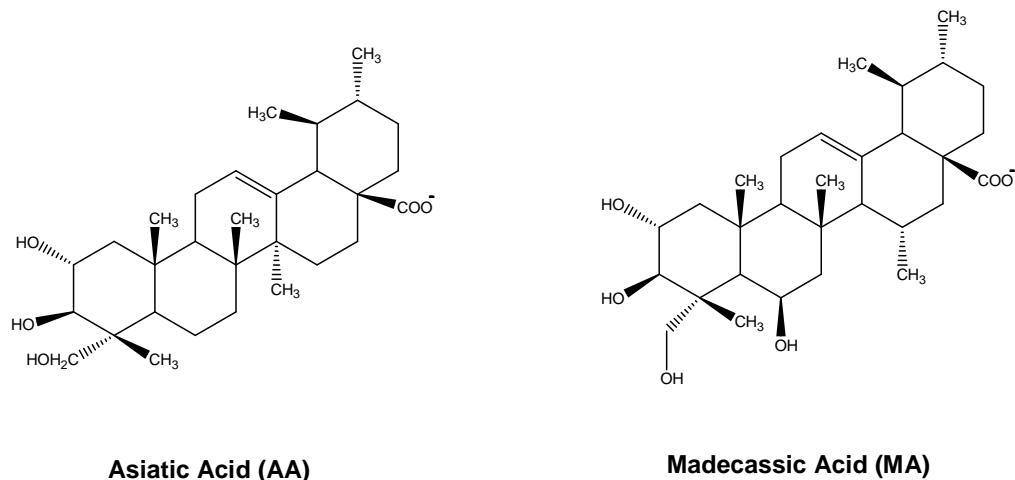


Figure 12-1: The chemical structures of asiatic acid (AA) and madecassic acid (MA).

perimentally through measurement of their critical micelle concentrations (CMCs) in water, phosphate buffered saline (PBS), and 1% dimethyl sulfoxide (DMSO)/ethanol in PBS [8]. In addition, a lower-bound estimate of the aggregation number of both AA and MA micelles was obtained experimentally through matrix-assisted laser desorption/ionization (MALDI), and was found to be approximately five for both molecules [8].

The self-assembly behavior of bile salts and bile salt analogues such as AA and MA is not well understood. Unlike more traditional surfactants, which typically possess a hydrophilic group bonded to a linear hydrocarbon or fluorocarbon chain [9,10], AA and MA possess multiple hydrophilic groups separated by ringed hydrophobic structures (see Figure 12-1). For relatively simple surfactants, it is possible to use molecular-thermodynamic theory [11–15] to make predictions of micellization behavior in aqueous solution (including the CMC, micelle shape, size, composition, and microstructure). However, the structural complexity of surfactants like AA and MA makes them difficult to model using the molecular-thermodynamic modeling approach. Computer simulations provide an alternative approach to model the self-assembly behavior of more complex surfactant systems and to gain insight into the

process of micelle formation. When conducted at an atomistic level of detail, computer simulations have the advantage, in principle, of being capable of modeling the self-assembly of arbitrarily complex surfactants in aqueous solution.

As computer power increases, computer simulations are playing an increasingly important role in providing detailed information about the self-assembly of surfactants in aqueous solution. Currently, simulations of micelle formation with atomistic-level detail are possible; however, because simulation time is severely limited by the size and density of micellar systems, such simulations have only been performed well above the CMC [16]. Several researchers have simulated spontaneous micelle, vesicle, and bilayer formation in water at an atomistic level of detail. Maillet et al. conducted large-scale molecular dynamics (MD) simulation of the self-assembly of short and long chain cationic surfactants [17]. In their studies, simulations of *n*-nonyltrimethylammonium chloride (C₉TAC) and erucyl *bis* [2-hydroxyethyl] methylammonium chloride (EMAC) surfactants were conducted for up to 3 ns. Starting from an isotropic distribution of surfactant molecules in solution, spontaneous micelle formation was observed and analyzed in terms of generalized classical nucleation theory. The authors concluded that for systems far from equilibrium, or for systems at high surfactant concentration, the basic aggregation and fragmentation mechanism is of Smoluchowski type (cluster-cluster coalescence and break up); however, for systems closer to equilibrium, or for systems at lower surfactant concentration, the aggregation and fragmentation mechanism followed a Becker-Döring process (stepwise addition or removal of surfactant monomers) [17]. Marrink et al. simulated the spontaneous aggregation of phospholipids into bilayers in simulations between 10 and 100 ns in duration. From the self-assembly results, the authors identified several time scales characterizing the aggregation process, and determined that the rate-limiting process in phospholipid bilayer formation is the gradual disappearance of hydrophilic, water-filled transmembrane pores [18]. Marrink et al. also simulated the self-assembly of 54 dodecylphosphocholine (DPC) surfactant molecules at high and low concentrations (both of which were above the CMC) in water, and observed self-assembly into

cylindrical and spherical micelles after 1 ns and 12 ns of simulation, respectively [19]. In a separate study, Marrink et al. simulated the formation, structure, and dynamics of small dipalmitoylphosphatidylcholine (DPPC) vesicles [20]. These authors found that by adding 25% dipalmitoylphosphatidylethanolamine (DPPE) or lysoPC to the DPPC solution, the aggregation process took less time to come to completion. From their results, Marrink et al. were able to shed light on the mechanism of vesicle fusion [21]. More recently, de Vries et al. studied the spontaneous formation of an oblong DPPC vesicle in water through 90 ns of MD simulation [22]. Starting from isotropically distributed SDS monomers in an aqueous solution, Braun et al. simulated the formation of a complete SDS micelle around glycophorin A (GpA) transmembrane helices over the course of 32 ns of MD simulation [23]. These authors found that the characteristics of the self-assembled SDS micelle around the GpA dimer were indistinguishable from those of an SDS micelle preformed around the GpA dimer and equilibrated for 2.5 ns.

To our knowledge, only one self-assembly study involving bile salt surfactants has been reported in the literature. Specifically, Marrink et al. studied the self-assembly and structure of micelles modeling human bile through MD simulation [24]. In their study, Marrink et al. compared results for the internal structure of mixed micelles composed of long-chain phosphatidylcholine lipids and bile salts with two proposed structures for the mixed micelles, the “stacked disk” micelle structure and the “radial shell” micelle structure. Their MD results, which included data gathered in simulations of up to 50 ns in duration, revealed that phospholipids were packed radially in the simulated micelles with bile salts wedged between the phospholipid headgroups, a result that supported the “radial shell” micelle structure. To our knowledge, to date, no computer simulation studies of the self-assembly behavior of pure bile salts has been reported in the literature. In addition, no computer simulation studies of pentacyclic bile salt analogues, such as the triterpenoids AA and MA, has been reported in the literature.

To better understand the dynamics of AA and MA micelle formation and the

structure of self-assembled AA and MA micelles, we have performed a series of extended MD simulations. Experimental data on the approximate aggregation number of the AA and MA micelles (≈ 5 [8]) suggested that simulating a relatively small number of AA and MA molecules in aqueous solution would be sufficient to realistically model the process of micelle self-assembly. In general, to realistically simulate micelle self-assembly, the number of simulated surfactant molecules must be significantly larger than the aggregation number of a single micelle so that an equilibrium can be established between monomers and a number of micellar aggregates of (potentially) different shapes and sizes [17–24]. In our simulations, molecules of AA and MA distributed randomly in aqueous solution and modeled at an atomistic level of detail were observed to aggregate into micelles during 75 ns of MD simulation. In this chapter, the dynamics of self-assembly, the structure of the self-assembled micelles, the local environment of the various micelle components, and a hybrid computer simulation/molecular-thermodynamic modeling approach to quantify AA and MA micellization thermodynamics are each characterized using the computer simulation results.

The remainder of the chapter is organized as follows. Methods are described in Section 12.2, including a discussion of the simulation methodology and parameters (Section 12.2.1) and a discussion of system preparation and equilibration (Section 12.2.2). Computer simulation results are presented in Section 12.3, including a general discussion of the AA and MA self-assembly behavior (Section 12.3.1), the number of micelles and micelle aggregation number (Section 12.3.2), monomer concentration (Section 12.3.3), micelle principal moments of gyration (Section 12.3.4), orientational order parameters (12.3.5), radial distribution functions (Section 12.3.6), the degree of hydration of selected atoms within AA and MA (Section 12.3.7), and the solvent accessible surface area (Section 12.3.8). A hybrid computer simulation/molecular-thermodynamic modeling approach to quantify micellization thermodynamics is introduced and discussed in Section 12.4, including a discussion of the thermodynamic framework used to describe the micellar solution (Section 12.4.1), a molecular model

of single-surfactant micellization (Section 12.4.2), and the implementation of the hybrid model to describe AA and MA micelle self-assembly (Section 12.4.3). Finally, concluding remarks are presented in Section 12.5.

12.2 Methods

12.2.1 Simulation Methodology and Parameters

All simulations were conducted using a 2006 developers' version of the GROMACS software package [25,26]. Both AA and MA were simulated at an atomistic level of detail using the OPLS-AA force field [27]. The carboxylate group of each molecule was modeled as being fully dissociated based on the pH of the solutions in which experimental CMC data was gathered, imparting to each AA and MA molecule a net charge of -1. Sodium ions were added as needed to preserve electroneutrality. Water was simulated explicitly using the simple extended point-charge model (SPC/E) [28]. Atomic charges were assigned to each AA and MA molecule based on the default atomic charge values specified in the OPLS-AA force field.

van der Waals interactions were modeled using a cutoff distance of 9.0 Å, and Coulombic interactions were evaluated using 3D particle mesh Ewald (PME) summation. A long-range dispersion correction was applied to more accurately estimate the energy and pressure of the system. The van der Waals cutoff selected has been shown to be accurate with the inclusion of long-range dispersion corrections for energy and pressure for the OPLS-AA forcefield by Shirts et al. [29–31]. In modeling short-ranged nonbonded interactions, a neighbor list of 9.0 Å was maintained and updated every 10 simulation timesteps. Each simulation was carried out using fixed bond lengths, which allowed an increase in simulation timestep from 1 fs to 2 fs. Bond lengths were constrained using the SHAKE algorithm [32].

Simulations were conducted in the *NPT* (constant number of particles, constant pressure, and constant temperature) ensemble. In each simulation, the cell temperature was maintained at 298.15 K using a Berendsen temperature coupling algorithm,

which mimics weak coupling to an external heat bath with first-order kinetics [33]. A Berendsen pressure coupling algorithm was applied to maintain each simulation cell at the specified pressure of 1.0 bar [33].

12.2.2 System Preparation and Equilibration

Two separate MD simulations were conducted to investigate AA and MA self-assembly — one simulation of AA molecules and sodium ions in water, and one simulation of MA molecules and sodium ions in water. The AA and MA simulations were initialized by randomly distributing the AA and MA molecules in water. To provide a more physically realistic initial configuration, the sodium ions were inserted into the simulation cell by replacing those water molecules experiencing the greatest electrostatic potential, with the electrostatic potential being recalculated after every ion insertion [33].

The AA simulation was initialized by placing 15 AA molecules randomly in a simulation cell with 6,147 water molecules and 15 sodium ions, yielding a total of 19,686 simulated atoms. Similarly, the MA simulation was initialized by placing 15 MA molecules randomly in a simulation cell with 6,171 water molecules and 15 sodium ions, yielding a total of 19,773 atoms. The initial size of the AA and MA simulation cells was 5.81 nm x 5.81 nm x 5.81 nm, yielding an initial concentration of AA and MA monomers in solution of 126 mM.

After energy minimization to remove close contacts, the AA and MA simulation cells were simulated under *NPT* conditions for 75 ns. Completion of these simulations was expedited by dividing the computational expense among multiple processors. In total, the two extended simulations required approximately 9,000 CPU hours.

12.3 Computer Simulation Results and Analysis

12.3.1 Self-Assembly Behavior

After beginning MD simulation, aggregation of the AA and the MA monomers commenced immediately, and dimers and trimers were observed to form within tens of picoseconds. Because of the relatively high concentration of AA and MA molecules (126 mM), individual AA and MA monomers only had to diffuse short distances before encountering other AA or MA molecules in the simulation cell. A quantitative analysis of the self-assembly process is presented in Sections 12.3.2 and 12.3.3.

Snapshots of the initial and final configurations of the AA and MA simulation cells are shown in Figures 12-2A and 12-2B, respectively. As suggested by the post-self-assembly snapshots shown in Figures 12-2A and 12-2B, the AA and MA micelles present in the aqueous solution exhibit a broad distribution of shapes and aggregation numbers. The micelle shapes observed range over the course of simulation from quite spherical (typical of micelles with small aggregation numbers) to rather cylindrical and elongated (typical of micelles with relatively large aggregation numbers). A quantitative analysis of the average shape of the self-assembled AA and MA micelles is presented in Section 12.3.4.

12.3.2 Number of Micellar Aggregates and Micelle Aggregation Number

Two criteria were examined to quantitatively analyze the simulation results and to identify the number of micellar aggregates present in the AA and MA simulation cells over the course of MD simulation. The simplest of the two criteria involved identifying two surfactants (AA or MA) as being in the same micellar aggregate if the centers of mass of the two molecules were within a specified cutoff distance. A range of cutoffs was tested and the micellar aggregates identified using each cutoff were compared with snapshots taken over the course of MD simulation to visually

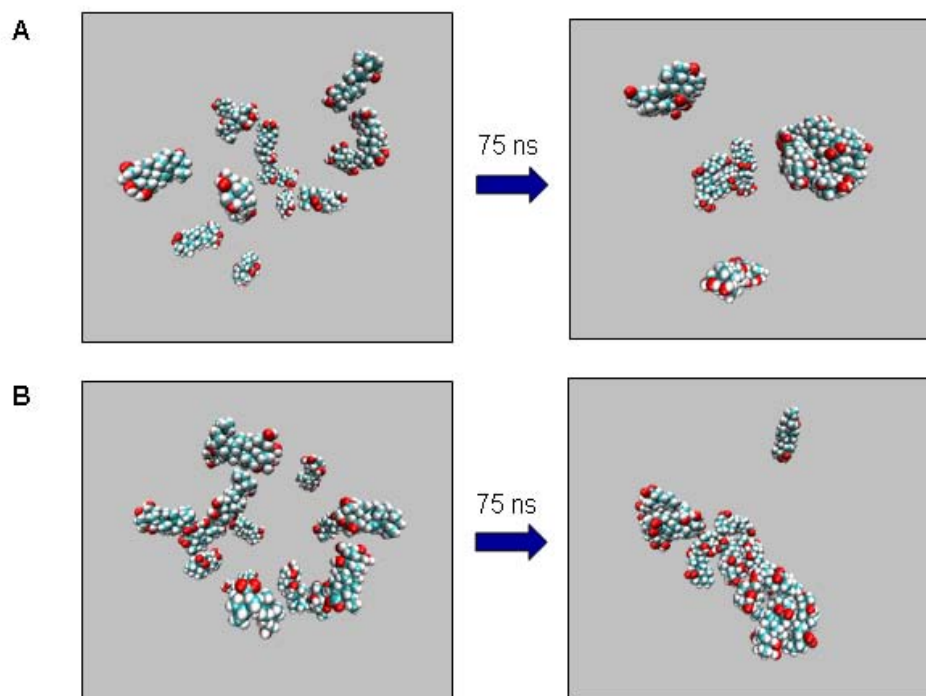




Figure 3

Figure 12-2: Starting and ending configurations of the AA (A) and MA (B) simulations (see Section 12.2.2).

assess the validity of this analysis approach. Although a range of cutoffs was tested, the center of mass criterion to identify micellar aggregates was found to be inadequate at the relatively high surfactant concentrations present in our simulation cells. In particular, direct visualization of the simulation snapshots revealed that even using the best possible cutoff, identification of micellar aggregates using molecular center of mass data occasionally resulted in two micelles being incorrectly categorized as being part of one larger micelle when the micelles were in close proximity but remained separated by a layer of water molecules.

The second criterion used to identify micellar aggregates was based on the premise that two surfactant molecules having hydrophobic contacts should be identified as being in the same micellar aggregate. A hydrophobic contact was defined as a hydrophobic atom in one surfactant molecule being located within a specified cutoff distance from a hydrophobic atom in another surfactant molecule. In our analysis, all carbon atoms except those in carboxylate (COO^-) moieties, as well as all hydrogen atoms except those in OH moieties, were identified as hydrophobic. Based on the van der Waals radii of the hydrophobic atoms, a cutoff distance of 3.0 Å was assumed to be adequate for identifying hydrophobic contacts, and was subsequently used to identify micellar aggregates. Direct visualization of the simulation results confirmed that identification of micellar aggregates based on hydrophobic contacts correctly identified separate micelles in cases where making micellar aggregate identifications based on center of mass data gave incorrect results. Since the criterion based on hydrophobic contacts appeared to be the most reliable of the two criteria considered, it is the criterion that is used to identify micellar aggregates throughout the remainder of this chapter.

The number of AA (see the  results) and MA () micellar aggregates identified using the hydrophobic contact criterion are reported in Figure 12-3 for the entire 75 ns of MD simulation. To make the results shown in Figure 12-3 more clear, the aggregation number data have been block averaged, with 10 data points recorded during simulation being averaged to generate one data point included in

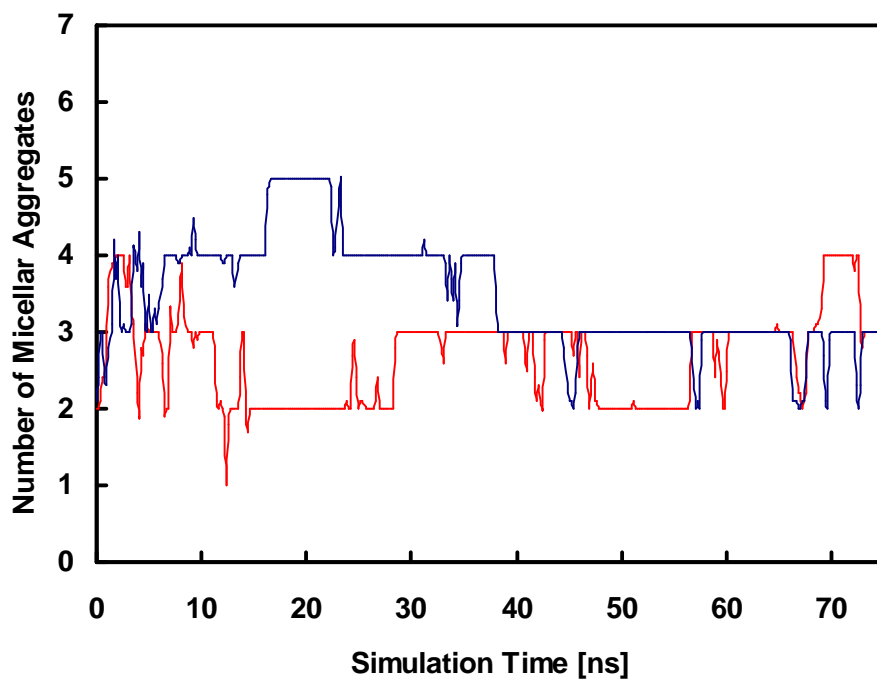




Figure 12-3: The number of micellar aggregates identified using the hydrophobic contact criterion (see the text) in the AA (—) and MA (—) simulation cells as a function of simulation time. Results have been block averaged as described in the text.

the figure (due to this block averaging, the number of identified aggregates is not always an integer value). Because even a dimer is identified as a micellar aggregate using the hydrophobic contact criterion, some micellar aggregates were identified immediately upon commencing MD simulation. The number of identified micellar aggregates approached what appears to be an equilibrium value very quickly for AA; specifically, the average number of micellar aggregates observed during the first 10 ns of simulation (3.02) is quite similar to the average number of micellar aggregates observed during the last 10 ns of simulation (3.26). In contrast, the number of identified micellar aggregates slowly decreased over a significant period of the MA simulation; the average number of micellar aggregates observed during the first 10 ns of simulation (3.52) is larger than the average number of micellar aggregates observed during the last 10 ns of simulation (2.75). Based on an average over the last 50 ns of simulation, the average number of identified micellar aggregates is 2.76 ± 0.04 for the AA simulation and 3.17 ± 0.03 for the MA simulation, where the uncertainties reported are the standard errors of the mean.

The number-average aggregation number of the identified AA (see the  results) and MA () micellar aggregates over the course of MD simulation is shown in Figure 12-4. The number-average aggregation number reported at each simulation time, which will be referred to hereafter as $\langle n \rangle_n$, represents an average of the number-average aggregation number associated with each micellar aggregate in the simulation cell. To make the results shown in Figure 12-4 more clear, values of $\langle n \rangle_n$ have been block averaged, with 10 data points recorded during simulation being averaged to generate one data point included in the figure. Upon beginning MD simulation, the value of $\langle n \rangle_n$ for both the AA and MA micellar aggregates increased rapidly from 2.15 and 2.38 at 0 ns for AA and MA, respectively, to 3.25 and 2.73 at 2.5 ns, to 4.4 and 3.32 at 5.0 ns. The average value of $\langle n \rangle_n$ for AA over the last 50 ns of simulation is 5.65 ± 0.08 , and the average value of $\langle n \rangle_n$ for MA over the same time period is 4.35 ± 0.05 , where the uncertainties reported for both aggregation numbers are the standard errors of the mean.

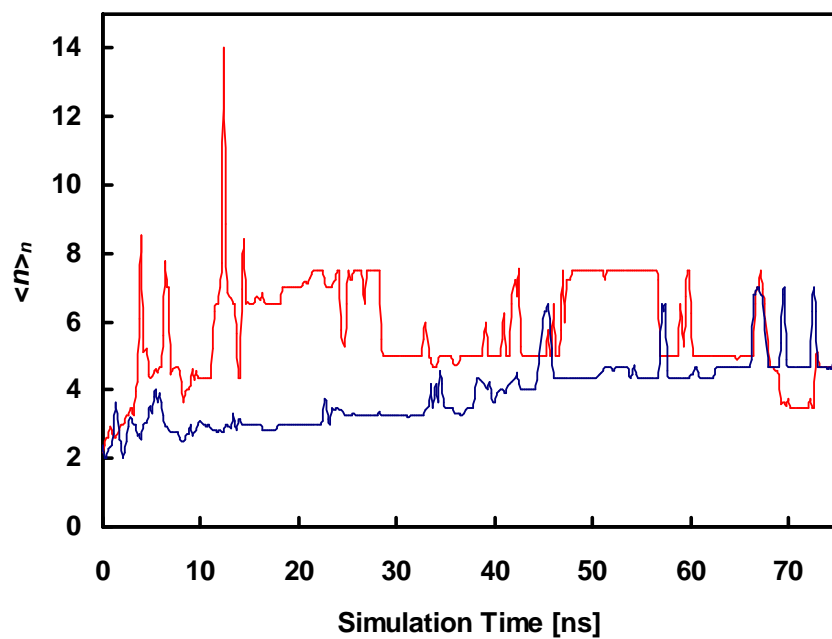




Figure 12-4: The number-average aggregation number, $\langle n \rangle_n$, of the AA (—) and MA (—) micelles identified using the hydrophobic contact criterion as a function of simulation time. Results have been block averaged as described in the text.

12.3.3 Monomer Concentration

Any surfactant molecule which was not identified as having hydrophobic contacts with another surfactant molecule (see Section 12.3.2) was identified as a monomer. The number of monomers present in the AA (see the  results) and MA () simulation cells is reported on the y -axis shown on the left in Figure 12-5 as a function of simulation time. To make the results shown in the figure more clear, the reported monomer data have been block averaged, with 10 data points being averaged to generate one data point included in the figure.

For single surfactant systems at equilibrium, above the CMC, the surfactant monomer concentration remains approximately constant at a concentration close to the CMC [10]. Making the approximation that the equilibrium surfactant monomer concentration is equal to the CMC, the CMC of AA and MA may be evaluated directly from the monomer concentrations observed during computer simulation. The CMC values (in units of mM) that would correspond to the observed number of surfactant monomers in the AA and MA simulation cells at each instant in time are reported on the y -axis on the right in Figure 12-5. Obviously, the observed monomer concentration is related to the CMC only after simulation has been conducted for a sufficiently long time that the surfactant monomer concentration is fluctuating about its equilibrium value. In addition, the simulation must be conducted for a sufficiently long time to obtain an accurate average value of the monomer concentration at equilibrium.

Based on the average number of surfactant monomers observed during the last 25 ns of AA and MA simulation (i.e., from 50 ns to 75 ns), the CMC of AA is equal to 2.39 mM, and the CMC of MA is equal to 11.3 mM. On the other hand, the experimental CMCs of AA and MA in pure aqueous solution are 17 μ M and 62 μ M, respectively [8]. Although the computer simulation results correctly predict that the monomer concentration of MA is higher than that of AA, and therefore that the CMC of MA is higher than that of AA, the computer simulation CMC estimates overestimate the experimental CMCs by a factor of 140 for AA and 182 for MA.

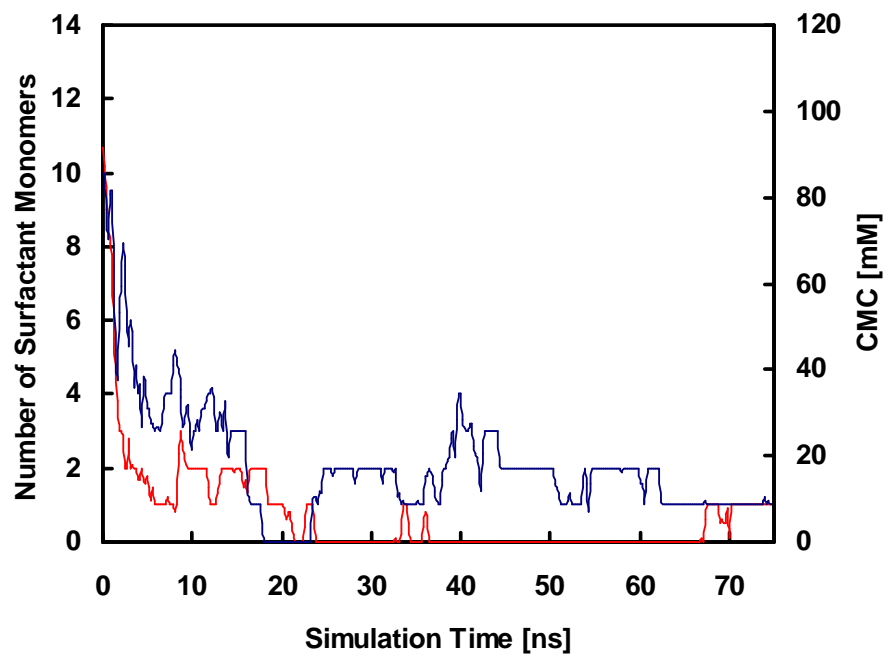


Figure 12-5: The number of surfactant monomers identified in the AA (—) and MA (—) simulation cells as a function of simulation time (see the y -axis on the left) and the critical micelle concentration (CMC) corresponding to that monomer concentration (see the y -axis on the right) as a function of simulation time. Results have been block averaged as described in the text.

The results reported in Figure 12-5, which show that the timescales associated with monomer entry and exit from the AA and MA micelles are quite long (on the order of tens of nanoseconds for AA and nanoseconds for MA, as shown by the characteristic lengths of time separating jumps in the monomer concentration profiles shown in the figure), suggest that simulation over a longer period of time would be necessary to obtain a statistically accurate estimate of the average monomer concentration at equilibrium and of the CMC. To avoid the high computational expense associated with performing additional MD simulation, I will instead use a hybrid computer simulation/molecular-thermodynamic modeling approach to quantify the free energy associated with AA and MA micelle formation, and use this estimated free energy to predict the CMCs of AA and MA. This hybrid modeling approach will be introduced and discussed in Section 12.4.

12.3.4 Micelle Principal Moments of Gyration

Micelle structure was characterized by computing the principal moments of the gyration tensor associated with each micelle identified using the hydrophobic contact criterion discussed in Section 12.3.2. The coordinates of each of the N atoms in the AA or MA molecules identified as being part of a single micelle were used to determine the gyration tensor, S_{mn} , which is defined as follows [34]:

$$S_{mn} \equiv \frac{1}{N} \sum_{i=1}^N (r_m^{(i)} - r_m^{(\text{com})}) (r_n^{(i)} - r_n^{(\text{com})}) \quad (12.1)$$

where $r_m^{(i)}$ denotes the m th Cartesian coordinate of atom i , $r_m^{(\text{com})}$ is the m th Cartesian coordinate of the micelle center of mass (com), $r_n^{(i)}$ denotes the n th Cartesian coordinate of atom i , and $r_n^{(\text{com})}$ is the n th Cartesian coordinate of the micelle center of mass. The eigenvalues of S_{mn} (λ_x^2 , λ_y^2 , and λ_z^2) are known as the principal moments of the gyration tensor. Following standard conventions, we have sorted the eigenvalues so that $\lambda_x^2 < \lambda_y^2 < \lambda_z^2$. The moments are related to the micelle radius of gyration,

Simulation Time [ns]	AA			
	λ_x [nm]	λ_y [nm]	λ_z [nm]	R_g [nm]
0 – 25	3.04 ± 0.01	4.03 ± 0.01	7.06 ± 0.05	8.68 ± 0.07
25 – 50	3.20 ± 0.01	4.00 ± 0.01	6.50 ± 0.04	8.28 ± 0.05
50 – 75	3.07 ± 0.01	3.97 ± 0.01	6.26 ± 0.04	8.03 ± 0.06
0 – 75	3.11 ± 0.00	4.00 ± 0.01	6.59 ± 0.02	8.31 ± 0.04
Simulation Time [ns]	MA			
	λ_x [nm]	λ_y [nm]	λ_z [nm]	R_g [nm]
0 – 25	2.47 ± 0.01	3.44 ± 0.01	5.74 ± 0.03	7.13 ± 0.05
25 – 50	2.67 ± 0.01	3.49 ± 0.01	4.83 ± 0.01	6.52 ± 0.03
50 – 75	2.94 ± 0.01	3.90 ± 0.01	5.39 ± 0.02	7.28 ± 0.04
0 – 75	2.70 ± 0.00	3.62 ± 0.01	5.31 ± 0.01	6.97 ± 0.02

Table 12.1: Principal moments of the gyration tensor (λ_x , λ_y , λ_z) and the radius of gyration (R_g) computed for the AA and MA micelles based on data obtained over 0-25 ns, 25-50 ns, 50-75 ns, and the entire 0-75 ns of MD simulation.

R_g , as follows [34]:

$$R_g = (\lambda_x^2 + \lambda_y^2 + \lambda_z^2)^{1/2} \quad (12.2)$$

Note that the micelle is approximately spherical if the three principal moments of the gyration tensor are nearly equal, while it is approximately cylindrical or discoidal if two of the three principal moments of the gyration tensor are nearly equal.

Principal moment of gyration and radius of gyration results are presented in Table 12.1 for AA and MA micelles based on data obtained over 0-25 ns, 25-50 ns, and 50-75 ns, and the entire 0-75 ns of MD simulation. Comparison of the 0-25 ns, 25-50 ns, and 50-75 ns results shows that the computed values of λ_x , λ_y , λ_z , and R_g do not exhibit any consistent upwards or downwards drift as the MD simulations progress. For all four periods of simulation time reported in Table 12.1, R_g of the AA micelles is computed to be larger than R_g of the MA micelles. The average values of R_g were 8.31 ± 0.04 nm and 6.97 ± 0.02 nm for the AA and MA micelles over the entire 75 ns of simulation, respectively.

Analysis of the radius of gyration values in Table 12.1 and the aggregation number data reported in Figure 12-4 suggests that both AA and MA exhibit one-dimensional growth. As the aggregation number increases, micelles change from being approxi-

mately spherical to being approximately cylindrical. However, the micelles are not perfectly cylindrical because the two smaller axes (λ_x and λ_y , see Table 12.1) are not equal. Therefore, the typical shape of a micelle with a large aggregation number could perhaps best be described as a “squashed cylinder.” Based on all the AA and MA simulation data, the following correlation between λ_z (in units of nm) and the number-average micelle aggregation number, $\langle n \rangle_n$, has been determined:

$$\lambda_z = 0.1 + 0.1\langle n \rangle_n \quad (12.3)$$

12.3.5 Orientational Order Parameters

The relative orientation of the surfactant molecules within each AA and MA micelle was examined by computing two different orientational order parameters. The orientation of each AA or MA molecule was characterized by defining a molecular axis for each molecule as the vector parallel to the longest axis of the AA or the MA molecule.

The first of the two orientational order parameters computed is the micelle orientational order parameter. For each surfactant pair ij in a micelle, the angle θ_{ij} between the molecular axis vectors of surfactant molecules i and j was calculated. The micelle orientational order parameter, P_{mic} , is then defined as follows:

$$P_{\text{mic}} \equiv \frac{1}{n(n-1)} \sum_{i=1}^{n-1} \sum_{j=i+1}^n \cos(2\theta_{ij}) \quad (12.4)$$

where n is the total number of AA or MA molecules in a single micelle. The order parameter P_{mic} provides information about orientational ordering averaged over an entire micelle. To quantify the extent to which local ordering exists between adjacent molecules within a micelle, the nearest neighbor of each AA or MA molecule in the micellar environment was identified and used to compute a nearest neighbor (n.n.) orientational order parameter. The nearest neighbor orientational order parameter,

Simulation Time [ns]	AA		MA	
	P_{mic}	$P_{\text{n.n.}}$	P_{mic}	$P_{\text{n.n.}}$
0 – 25	-0.11 ± 0.01	0.00 ± 0.00	-0.22 ± 0.01	-0.18 ± 0.01
25 – 50	0.03 ± 0.01	0.13 ± 0.01	-0.05 ± 0.01	0.01 ± 0.01
50 – 75	-0.02 ± 0.01	0.08 ± 0.01	-0.24 ± 0.01	-0.19 ± 0.01
0 – 75	-0.03 ± 0.00	0.07 ± 0.00	-0.17 ± 0.01	-0.12 ± 0.01

Table 12.2: Micelle (P_{mic}) and nearest neighbor ($P_{\text{n.n.}}$) orientational order parameters computed for AA and MA micelles based on data obtained over 0-25 ns, 25-50 ns, 50-75 ns, and the entire 0-75 ns of MD simulation.

$P_{\text{n.n.}}$, is defined as follows:

$$P_{\text{n.n.}} \equiv \cos(2\theta_{ij}) \quad (12.5)$$

where i and j refer to the indices of two AA or MA molecules identified as nearest neighbors.



Values of P_{mic} or $P_{\text{n.n.}}$ which are close to 1 indicate that surfactant molecules in the micelle, or nearest neighbor surfactant molecules in the micelle, are parallel to each other. Conversely, values of P_{mic} or $P_{\text{n.n.}}$ which are close to -1 indicate that surfactant molecules in the micelle, or nearest neighbor surfactant molecules in the micelle, are perpendicular to each other.

The computed values of P_{mic} and $P_{\text{n.n.}}$ were found to fluctuate significantly and rapidly about their average values, with large changes in P_{mic} and $P_{\text{n.n.}}$ being observed on nanosecond time scales (results not shown). Average orientational order parameter results are presented in Table 12.2 based on data averaged over 0-25 ns, 25-50 ns, 50-75 ns, and the entire 0-75 ns of MD simulation. The P_{mic} values reported in the table have been averaged over all micelles, and the $P_{\text{n.n.}}$ values reported have been averaged over all nearest neighbors identified in the surfactant micelles. As shown in Table 12.2, the computed P_{mic} and $P_{\text{n.n.}}$ values for all four simulation time periods are similar. In addition, most of the values are fairly close to zero, indicating that, on average, there is little orientational bias for the AA and MA molecules towards being oriented either parallel or perpendicular to each other in the micellar environment, either at the level of an entire micelle or at the level of adjacent molecules within a

micelle. However, it is interesting to note that each of the $P_{\text{n.n.}}$ values reported in Table 12.2 for AA and MA are more positive than the corresponding values of P_{mic} computed during the same time period. For example, based on an average of all the simulation data (0-75 ns), the average $P_{\text{n.n.}}$ value for AA is 0.07 ± 0.00 , while the average value of P_{mic} is -0.03 ± 0.00 . Similarly, the average value of $P_{\text{n.n.}}$ for MA is -0.12 ± 0.01 , while the average value of P_{mic} is -0.17 ± 0.01 . These results indicate that, as would be expected intuitively, on average nearest neighbor AA or MA molecules are oriented slightly more parallel to each other than AA or MA molecules that are not adjacent to each other within the micelle.

12.3.6 Radial Distribution Functions

To quantify the local environment of atoms in the AA and MA molecules following their self-assembly into micelles, radial distribution functions, $g(r)$, have been computed between each of the carboxylate oxygen atoms (O^- groups) in AA and MA (see Figure 12-1) and all the atoms in water ($g(r)_{\text{O}^--\text{H}_2\text{O}}$). Recall that the radial distribution function yields the probability of finding an atom at a distance r from a reference atom [35]. Each $g(r)_{\text{O}^--\text{H}_2\text{O}}$ profile was computed using data gathered over the last 50 ns of AA or MA simulation and represents an average over all the O^- groups present in the simulation cell. Radial distribution functions between the oxygen in the OH groups and the atoms in water ($g(r)_{\text{OH}-\text{H}_2\text{O}}$) have been computed using data taken from the last 50 ns of AA and MA simulation. Each $g(r)_{\text{OH}-\text{H}_2\text{O}}$ profile represents an average for the three OH groups present in each AA molecule and the four OH groups present in each MA molecule (see Figure 12-1), as well as over each of the AA or MA molecules in the simulation cell.

The $g(r)_{\text{O}^--\text{H}_2\text{O}}$ and $g(r)_{\text{OH}-\text{H}_2\text{O}}$ profiles for AA (see the  results) and MA () are shown in Figure 12-6. Both the $g(r)_{\text{O}^--\text{H}_2\text{O}}$ and $g(r)_{\text{OH}-\text{H}_2\text{O}}$ radial distribution functions exhibit a shell structure. The peaks in the $g(r)_{\text{O}^--\text{H}_2\text{O}}$ profile are significantly larger than the peaks in the $g(r)_{\text{OH}-\text{H}_2\text{O}}$ profile, indicating that, on average, more water molecules are coordinated around the charged O^- group in AA

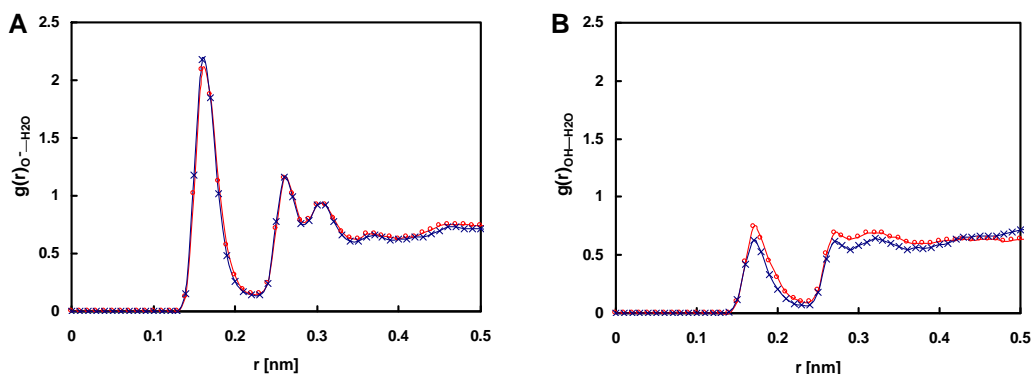


Figure 12-6: The radial distribution functions $g(r)_{O^- - H_2O}$ (A) and $g(r)_{OH - H_2O}$ (B) for AA ($\text{---}\circ\text{---}$) and MA ($\text{---}\times\text{---}$).

and MA than around the uncharged OH groups. However, the $g(r)_{O^- - H_2O}$ profiles for AA and MA, as well as the $g(r)_{OH - H_2O}$ profiles for AA and MA, are quite similar, indicating that the extent of hydration of chemically equivalent groups in the AA and MA molecules are quite similar.

To determine the number of sodium ions bound, or closely associated with, each O^- group (typically referred to as the degree of counterion binding) in AA and MA, radial distribution functions between the O^- atoms present in AA and MA and sodium counterions (Na^+) have been computed for AA and MA ($g(r)_{O^- - Na^+}$) using data taken from the last 50 ns of simulation. The $g(r)_{O^- - Na^+}$ profiles for AA and MA are shown in Figure 12-7 for AA (see the $\text{---}\circ\text{---}$ results) and MA ($\text{---}\times\text{---}$). The first peak in the $g(r)_{O^- - Na^+}$ profiles is very large. The highest value of $g(r)_{O^- - Na^+}$ for AA is 168, while the highest value of $g(r)_{O^- - Na^+}$ for MA is 66. Integration of this first peak in the radial distribution function (from $r = 0$ to 0.3 nm) allows evaluation of the degree of counterion binding, which is defined here as the number of Na^+ counterions in the first coordination shell associated with O^- . The degree of counterion binding computed for AA is 0.27 ± 0.05 , and the degree of counterion binding computed for MA is 0.14 ± 0.03 , where both uncertainties are standard errors of the mean. The degree of counterion binding results can be rationalized by recalling that: (i) the average

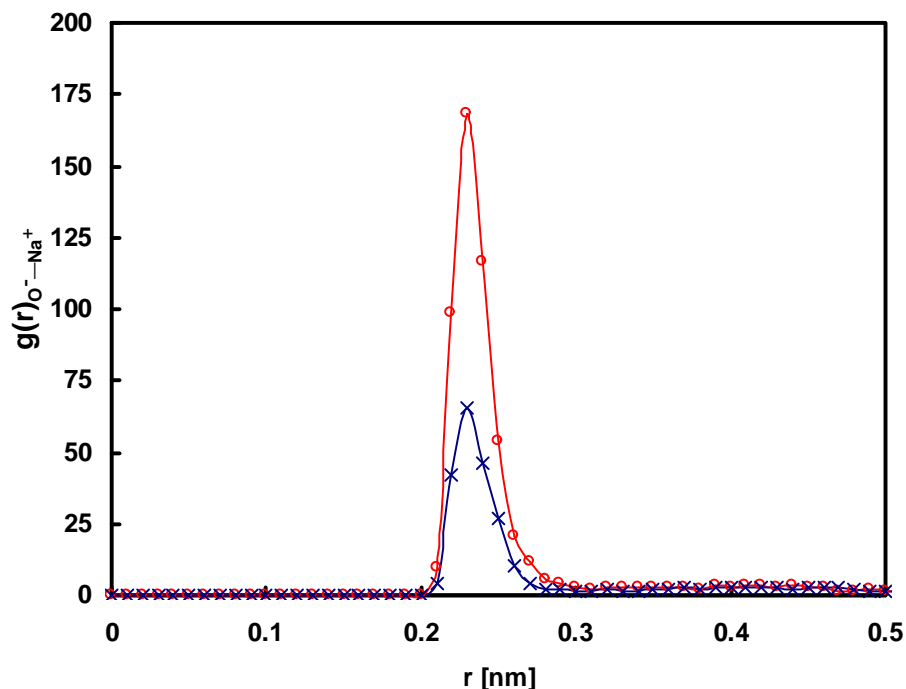


Figure 12-7: The radial distribution functions $g(r)_{O^- - Na^+}$ (see text) for AA ($\text{---}\circ\text{---}$) and MA ($\text{---}\times\text{---}$).

micelle aggregation number for AA is larger, on average, than that for MA (5.65 versus 4.35 averaged over the last 50 ns of simulation), and (ii) the average monomer concentration of AA is significantly lower than that of MA (1.39 mM versus 14.2 mM averaged over the last 50 ns of simulation). The electrostatic potential (which drives counterion binding) is higher for a surfactant molecule in a large micelle (having lower curvature) than in a small micelle (having higher curvature), and for a surfactant molecule in a micelle than for a surfactant monomer [14, 36].

12.3.7 Extent of Hydration

Although the radial distribution functions $g(r)_{O^- - H_2O}$ and $g(r)_{OH - H_2O}$ reported in Section 12.3.6 provide information about the average density and average number of

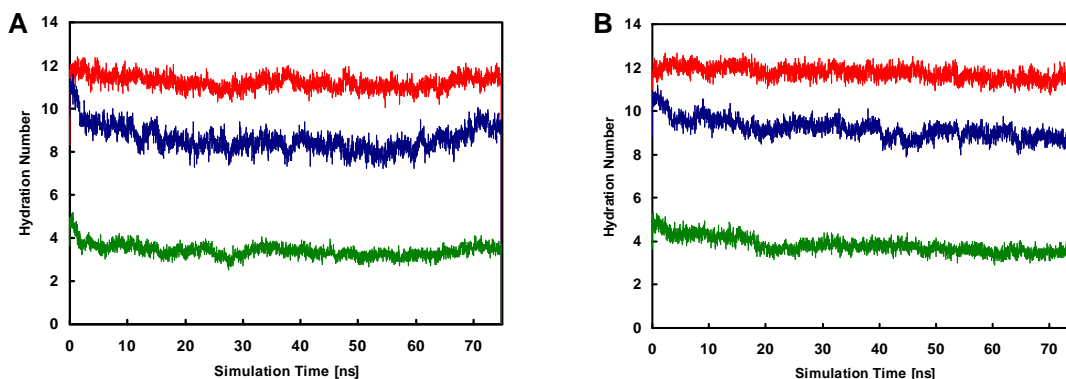


Figure 12-8: Degree of hydration for O^- (—), for OH (—), and for carbon ring atoms (—) measured during 75 ns of molecular dynamics simulation for AA (A) and MA (B).

water molecules surrounding O^- and OH groups during the last 50 ns of simulation, to better understand the local environment experienced by both hydrophilic and hydrophobic groups in the AA and MA molecules *as a function of simulation time*, we have computed the average number of water molecules (which we refer to as the “hydration number”) within 0.5 nm of each O^- atom, each OH group, and the carbon atoms in the central, six-membered ring of AA and MA (see Figure 12-1) at each moment of MD simulation. Hydration number results are presented in Figure 12-8 for O^- (see the — results), for OH (—), and for the carbon ring atoms (—) as a function of simulation time. The hydration numbers reported for O^- are an average of the hydration numbers determined for the two carboxylate oxygen atoms in each molecule, those reported for OH are an average of the hydration numbers determined for the OH groups in each molecule (3 for AA and 4 for MA), and those reported for the carbon ring atoms are an average of the hydration numbers determined for the six carbons in the central, six-membered ring in each molecule.

As shown in Figure 12-8, the hydration number of O^- decreased only slightly as AA and MA micelle self-assembly occurred. From approximately 60 to 75 ns, the hydration number of O^- in AA increased slightly and then began to decrease

again (trends that accompany an increase and subsequent decrease in the number of identified micellar aggregates, as shown in Figure 12-3). The average hydration number of O^- during the last 50 ns of simulation for AA is 11.16 ± 0.01 , while for MA it is 11.67 ± 0.01 , where the uncertainties reported represent the standard errors of the mean.

The hydration number of OH, in contrast to that of O^- , decreased significantly during simulation. A steep decrease in the hydration number of OH occurred within the first 5 ns of simulation for both AA and MA, after which the hydration number continued to decrease at a slower rate. The hydration number of AA increased after approximately 50 ns of simulation before beginning to decrease once again. The average hydration number of OH during the last 50 ns simulation is 8.42 ± 0.02 for AA and 9.00 ± 0.01 for MA.

The hydration number of the carbon ring atoms throughout MD simulation was much lower than the hydration number of O^- and OH at the beginning of simulation. However, the percent decrease in the extent of hydration of the ring carbons occurring during the entire 75 ns of simulation (-23.6% for AA and -23.7% for MA) is greater than the percent decrease in the extent of hydration of O^- (-5.12% for AA and -1.16% for MA) and of OH (-19.8% for AA and -14.2% for MA). Similar to the hydration number profiles for OH, the hydration number profiles for the ring carbons decreased sharply within the first 5 ns of simulation (particularly for AA), and then decreased more slowly.

12.3.8 Solvent Accessible Surface Area

The primary driving force for AA and MA micelle self-assembly in aqueous solution is unfavorable contacts between water and the hydrophobic atoms in AA and MA [37, 38]. The number of unfavorable contacts may be approximated reasonably well as being proportional to the solvent accessible surface area (SASA) (see Section 6.3 in Chapter 6). To calculate SASA, I used the double cubic lattice method as implemented in GROMACS [33]. The solvent accessible surface was traced out by

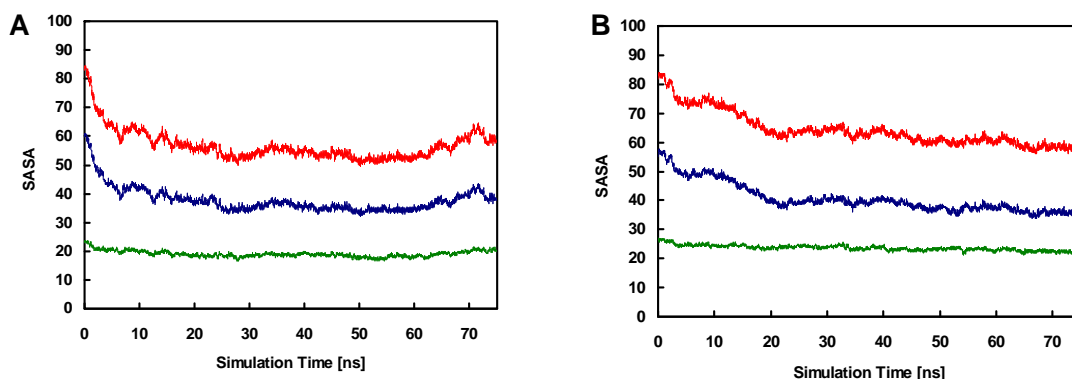


Figure 12-9: The total (—), hydrophobic (—), and hydrophilic (—) solvent accessible surface area (SASA) measured during molecular dynamics simulation for the 15 AA molecules (A) and the 15 MA molecules (B) in their respective simulation cells.

a probe sphere of radius 0.14 nm that was rolled around each of the 15 AA or MA molecules in the simulation cell to identify the total (all atoms), hydrophobic (carbon and hydrogen bonded to carbon), and hydrophilic (oxygen and hydrogen bonded to oxygen) solvent accessible regions at each simulation time [39–41].

As shown in Figure 12-9, the total (—), hydrophobic (—), and hydrophilic (—) SASA values began to decrease immediately upon the start of simulation as aggregation of the AA and MA molecules commenced. Only relatively small changes were observed in hydrophilic SASA values during MD simulation. Hydrophilic SASA decreased slightly during the first 5 ns of the AA and MA simulations and subsequently became relatively constant. The first 5 ns corresponds to the same amount of simulation time over which a sharp decrease in the hydration number of the OH groups is observed in Figure 12-8. For AA, hydrophilic SASA increased slightly during the last 10 ns of simulation before beginning to decrease again.

The hydrophobic SASA values measured for AA and MA decreased both to a greater extent and over longer timescales than the hydrophilic SASA values for these molecules. The hydrophobic SASA of AA decreased sharply within the first 20 ns of simulation, remained approximately constant for an additional 40 ns, and then

increased and began to decrease again during the last 15 ns of simulation. The hydrophobic SASA of MA decreased over a period of approximately 20 ns (though less sharply than what was observed for AA), and then became approximately constant, although a slight decrease in SASA continued for the remainder of the simulation. As will be discussed in Section 12.4, the reduction in hydrophobic SASA shown in Figure 12-7 may be used to quantify the hydrophobic driving force for micelle formation in aqueous solution using a modified version of the computer simulation/molecular-thermodynamic modeling approach presented in Chapters 6, 7, and 8 [38,42,43].

12.4 Computer Simulation/Molecular-Thermodynamic Model to Investigate Micellization Thermodynamics

Computer simulation studies of self-assembly provide considerable information on the kinetics of micelle formation (as reflected in the rate at which micelles form and the monomer concentration decreases), micelle structure, and the arrangement of surfactant molecules within a micelle. However, as illustrated by the results presented in Section 12.3.3, it can be very computationally expensive to obtain statistically accurate estimates of surfactant monomer concentration. Therefore, it is not possible to accurately determine the CMC of AA and MA in aqueous solution using the self-assembly simulation data reported in this chapter.

Instead, if a thermodynamic model of micelle self-assembly in aqueous solution is used to make CMC predictions, considerable computational expense that would otherwise be required to obtain a statistically accurate estimate of surfactant monomer concentration may be saved. Currently, the most accurate theoretical models of surfactant micellization make use of a molecular-thermodynamic approach [12]. Molecular-thermodynamic models combine thermodynamic descriptions of self-assembly with a molecular model to estimate the free energy of micellization. The free energy of mi-

cellization is calculated as the sum of several free-energy contributions, each of which can be computed molecularly given the chemical structures of the surfactants present in the aqueous solution and the solution conditions. The free energy of micellization can then be related in a straightforward manner to the surfactant CMC (see Section 2.2 in Chapter 2). Traditional molecular-thermodynamic models allow prediction of solution properties for relatively simple surfactants and solubilizates where it is possible to identify *a priori* what equilibrium position each component will adopt in a self-assembled micellar aggregate. Unfortunately, for many surfactants possessing more complex chemical structures (including AA and MA), it is not clear a priori how the system components will assemble and locate themselves within a micellar environment.

As part of this thesis, I have developed several theoretical approaches to use computer simulations and molecular-thermodynamic modeling in a complementary manner to enable the modeling of more complex surfactant systems than has been possible to date. Two main strategies to combine computer simulations with molecular-thermodynamic modeling include: i) using information determined from computer simulation of surfactants and solubilizates at a water/oil interface, or in a micellar environment, to identify head and tail input parameters for molecular-thermodynamic modeling [11, 15] (see also Chapters 2-5), ii) using fractional hydration information obtained from computer simulations of surfactants in a micellar environment in a thermodynamic model to quantify the hydrophobic driving force for micelle formation in aqueous solution [38, 42, 43] (see also Chapters 6-8). The second of these two approaches is referred to as the computer simulation/molecular-thermodynamic (CS-MT) modeling approach.

To investigate the thermodynamics associated with AA and MA micelle formation in aqueous solution, in this section I will formulate a modified CS-MT modeling approach (referred to as the MCS-MT modeling approach). This modified approach will make use of: (i) the aggregation number and hydrophobic SASA simulation results presented in Sections 12.3.2 and 12.3.8, respectively, (ii) experimental solubility

data, and (iii) experimental surface tension data to predict the CMCs of AA and MA in aqueous solution. The accuracy of the CMCs predicted using the MCS-MT modeling approach will be compared with the CMCs of AA and MA inferred from the computer simulation data on AA and MA monomer concentration (see Section 12.3.3). The thermodynamic framework and the molecular model of micellization used to predict the CMCs of AA and MA are presented in Sections 12.4.1 and 12.4.2, respectively. Note that both the thermodynamic framework and the molecular model of micellization will be formulated for single surfactants, because the objective here is to predict the CMCs of single-component AA and MA surfactant systems.

12.4.1 Thermodynamic Framework

In the multiple-chemical equilibrium model [12, 13], each micellar aggregate is considered as a distinct chemical species in equilibrium with other micellar aggregates and with individually-dispersed surfactant molecules (monomers) present in the aqueous solution. By relating the chemical potentials of the micellar aggregates, the surfactant monomers and the counterions, an expression is obtained that describes the population distribution (mole fractions) of micellar aggregates, $X_{n\beta}$, containing n surfactant (s) molecules and β bound counterions (c) per surfactant molecule in the micellar aggregate [11]. Specifically,

$$X_{n\beta} = \frac{1}{e} X_{1s}^n X_{1c}^{n\beta} \exp \left[-\frac{n}{k_B T} g_{\text{mic}}(S, l_c, \beta) \right] \quad (12.6)$$

where X_{1s} is the mole fraction of the surfactant monomers, X_{1c} is the mole fraction of the counterions, S is the micelle shape factor ($S = 3$ for spherical micelles, 2 for cylindrical micelles, and 1 for bilayers), l_c is the micelle core-minor radius (the radius of a spherical or cylindrical micelle and the planar half-width of a bilayer), β is the degree of counterion binding (the number of bound counterions divided by the number of surfactant molecules in the micelle), and the free energy of micellization,

g_{mic} , is defined as follows:

$$g_{\text{mic}} = \frac{1}{n} \mu_{n\beta}^{\circ} - \mu_{\text{s}}^{\circ} - \beta \mu_{\text{c}}^{\circ} - k_{\text{B}} T (1 + \beta) \quad (12.7)$$

In Eq. 12.7, $\mu_{n\beta}^{\circ}$ is the standard-state chemical potential of a micelle containing n surfactant molecules and $n\beta$ bound counterions, μ_{s}° is the standard-state chemical potential of the surfactant monomers, μ_{c}° is the standard-state chemical potential of the counterions, k_{B} is the Boltzmann constant, and T is the absolute temperature [11]. The free energy of micellization, g_{mic} , reflects the free-energy change associated with transferring the surfactant monomers and the counterions in their corresponding standard states from the aqueous solution to form a micellar aggregate in its standard state in the aqueous solution. As shown in Eq. 12.6, g_{mic} is a function of the aggregate shape, S , the aggregate core-minor radius, l_{c} , and the degree of counterion binding, β .

For the values of S , l_{c} , and β that minimize g_{mic} (denoted as S^* , l_{c}^* , and β^*), g_{mic} has a minimum value denoted as g_{mic}^* . Due to the exponential dependence of $X_{n\beta}$ on $n \cdot g_{\text{mic}}$ in Eq. 12.6, small deviations of g_{mic} from g_{mic}^* yield $X_{n\beta}$ values that are essentially zero. Note that the optimal aggregate shape, S^* , the optimal core-minor radius, l_{c}^* , and the optimal degree of counterion binding, β^* , characterize the micelles that form in aqueous solution at equilibrium. In addition, the CMC of the surfactant/counterion system is given by [12]:

$$\text{CMC} \approx \exp \left(\frac{g_{\text{mic}}^*(S^*, l_{\text{c}}^*, \beta^*)}{k_{\text{B}} T} \right) \quad (12.8)$$

Instead of using the molecular-thermodynamic modeling approach in the conventional way in which it is typically implemented (to predict S^* , l_{c}^* , β^* , and g_{mic}^*), in the modeling conducted in this chapter, I will take the equilibrium micelle shape, micelle size, and degree of counterion binding determined through computer simulation (see Section 12.3) as an input to the molecular-thermodynamic model. Using this computer simulation data as an input greatly simplifies the molecular-thermodynamic

modeling problem by reducing it from one of finding the global minimum of g_{mic} with respect to S , l_c , and β to one of simply evaluating g_{mic} for specified values of S , l_c , and β determined through computer simulation.

12.4.2 Molecular Model of Single-Surfactant Micellization

Molecular-thermodynamic models of single-surfactant micellization enable estimation of g_{mic} based on the chemical structures of the surfactants and the counterions present in the aqueous solution and the solution conditions [12]. The free energy associated with single-surfactant micellization, g_{mic} , can be expressed as the sum of the following five free-energy contributions [36]:

$$g_{\text{mic}} = g_{\text{tr}} + g_{\text{int}} + g_{\text{pack}} + g_{\text{st}} + g_{\text{elec}} \quad (12.9)$$

Each of the five contributions in Eq. 12.9 arises from a distinct step in a thermodynamic cycle used to model the process of micelle formation. The various steps involved are shown schematically in Figure 12-10, which depicts the micellization process for AA. An analogous thought process may be used to model the formation of the MA micelles. In the figure, AA molecules are depicted using the van der Waals radius of each atom. Oxygen atoms are shown in red, hydrogen atoms are shown in white, carbon atoms are shown in grey, and the sodium ions are shown in yellow. The blue background shown in frames (1), (2), (4), (5), and (6) represents the bulk aqueous solution (water molecules are not shown explicitly, and are modeled as a continuum), and the light grey background shown in frame (3) represents a bulk surfactant tail solution (the *bulk* surfactant tails are not shown explicitly, and are modeled as a continuum).

The free-energy change associated with transferring the surfactants (AA) and the counterions from their standard states in the aqueous solution to form a micelle in the aqueous solution (the transition from frame (1) to frame (6) shown in Figure 12-10) is equal to g_{mic} given in Eq. 12.9. To evaluate g_{mic} , it is computationally

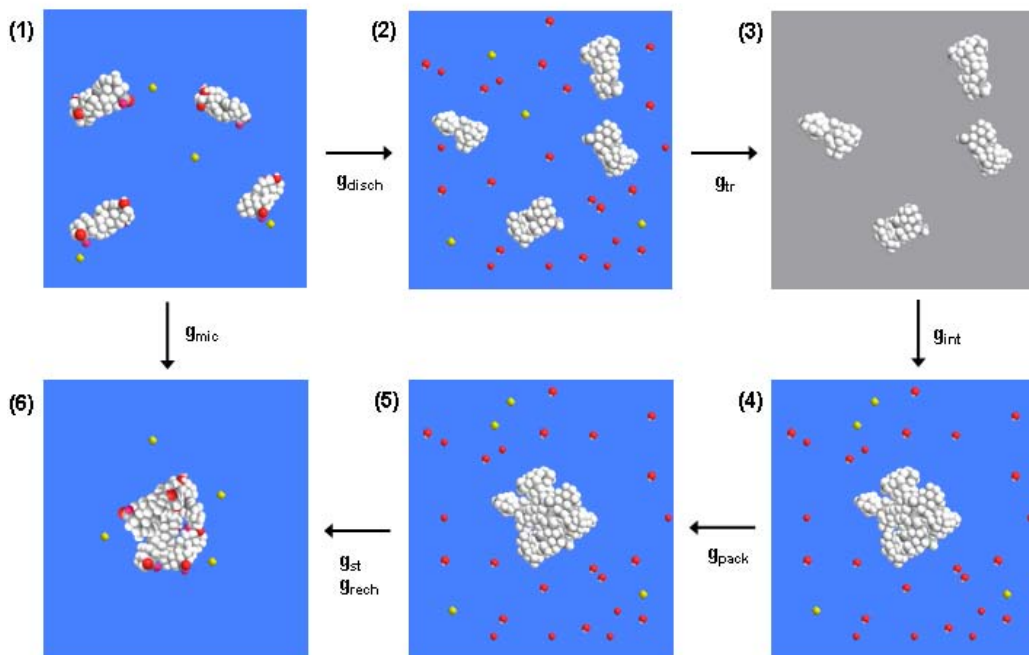


Figure 12-10: Illustrative thermodynamic cycle used to evaluate the free energy of micellization, g_{mic} , associated with AA micelle formation. Oxygen atoms are shown in red, hydrogen atoms are shown in white, carbon atoms are shown in grey, and the sodium ions are shown in yellow. The aqueous solution is shown as a blue background, and the bulk (continuum) solution of surfactant tails described in the text is shown as a grey background.

convenient to construct a thermodynamic cycle to move from frame (1) to frame (6). This cycle involves the following steps — (1) \rightarrow (2): separating the hydrophilic atoms (the “heads” — carboxylate oxygens, OH oxygens, and OH hydrogens) from hydrophobic atoms (the “tails” — carbon atoms and hydrogen atoms bonded to carbons) and discharging the charged oxygen atoms and the sodium counterions in aqueous solution; (2) \rightarrow (3): transferring the surfactant tails from aqueous solution to a bulk tail solution; (3) \rightarrow (4): transferring the surfactant tails in the micellar configuration from bulk tail solution to aqueous solution; (4) \rightarrow (5): arranging the surfactant tails in the configuration they adopt within a micelle; and (5) \rightarrow (6): attaching the surfactant heads at the micelle surface and recharging the carboxylate groups and the sodium counterions. The free-energy contributions associated with each step are as follows — (1) \rightarrow (2): the discharge free-energy contribution, g_{disch} [36]; (2) \rightarrow (3): the transfer free-energy contribution, g_{tr} [9]; (3) \rightarrow (4): the interfacial free-energy contribution, g_{int} [38]; (4) \rightarrow (5): the packing free-energy contribution, g_{pack} [12]; and (5) \rightarrow (6): the steric free-energy contribution, g_{st} [12], and the reversible work associated with recharging the surfactant heads at the micelle core/water interface in the presence of the counterions, g_{rech} [36]. The free-energy contributions g_{disch} and g_{rech} are traditionally added together and referred to as the electrostatic free-energy contribution, g_{elec} , that appears in Eq. 12.9 (see Section 4.4.3 in Chapter 4). Note that two free-contributions present in the thermodynamic cycle shown in Figure 12-10 — the free-energy contribution associated with separating the surfactant heads from the surfactant tail in the transition from frame (1) to frame (2), g_{sep} , and the free-energy contribution associated with connecting the surfactant heads to the surfactant tails in the transition from frame (5) to frame (6), g_{con} — are not shown in Figure 12-10, or listed in Eq. 12.9, because g_{sep} and g_{con} are identical in magnitude but opposite in sign, and therefore cancel out [12].

The transfer free-energy contribution, g_{tr} , captures the free-energy change associated with transferring the surfactant tails from the aqueous solution to a bulk solution of surfactant tails [9, 38]. The interfacial free-energy contribution, g_{int} , captures the

free-energy change associated with forming an interface between the surfactant tails and the aqueous solution [38]. It is important to stress that g_{int} does not account for the overall translational entropy loss associated with micelle formation, an entropic penalty which is accounted for in the thermodynamic framework used to describe micelle formation (given by the X_{Is}^n term in Eq. 12.6). The packing free-energy contribution, g_{pack} , captures the free-energy change associated with the translational constraints associated with pinning the surfactant tails at the micelle core/water interface (as required by each tail being chemically bonded to a surfactant head). The steric free-energy contribution, g_{st} , reflects the steric repulsions between the surfactant heads and the bound counterions at the micelle core/water interface [44]. The electrostatic free-energy contribution, g_{elec} , reflects the electrostatic repulsions between charged surfactant heads in the presence of counterions [14, 36].

AA and MA are significantly more structurally complex than surfactants that can be easily modeled using molecular-thermodynamic theory without computer simulation input. As shown in Figure 12-1, AA and MA contain five hydrophobic ringed groups as part of their chemical structure and several widely separated hydrophilic groups (the O^- and OH groups). Based on their chemical structures, we believe that it is physically justifiable to approximate two of the five free-energy contributions listed in Eq. 12.6 (specifically, g_{pack} and g_{st}) as being equal to zero (see below).

For traditional surfactants with a linear or branched alkyl tails, g_{pack} may be estimated using a mean-field model first introduced by Ben-Shaul, Szleifer, and Gelbart [45–47], and requires sampling each important conformation and orientation of a central surfactant tail in a micellar environment subject to the constraint that the hydrophobic micelle core has uniform density. Because of the relatively rigid nature of the AA and MA molecules, g_{pack} may reasonably be approximated as being equal to zero for the formation of AA and MA micelles (see Chapter 5). Reflecting this fact, frames (4) and (5) in Figure 12-10 are identical, reflecting the fact that *the configurations adopted by the surfactant tails after implementing packing constraints are modeled as being identical to the configurations adopted prior to implementing*

packing constraints. It is important to note that without *a priori* knowledge of the optimal micelle shape and size (knowledge available from computer simulation), making the approximation that $g_{\text{pack}} = 0$ would not be acceptable, because an inequality constraint is traditionally included in g_{pack} to ensure that l_c never exceeds l_{max} [12]. Recall that l_{max} is the maximum value of the core-minor radius that can be adopted by a micelle given the geometry of the surfactant tail (see Section 4.4.3 in Chapter 4). For the simple surfactants typically modeled using molecular-thermodynamic theory (surfactants with linear hydrocarbon or fluorocarbon chains), l_{max} can be computed from the maximum extended length of the surfactant tail. Because of the complex chemical structures of AA and MA, it is difficult to evaluate an appropriate value of l_{max} ; fortunately, however, because the shape and size of the micelles that form in solution are taken as an input from the computer simulation results, it is not necessary to impose a constraint on l_c in the modeling conducted here.

Like g_{pack} , it is reasonable to approximate the steric free-energy contribution, g_{st} , as being equal to zero because: (i) the O^- and OH heads are small in size, and (ii) the surfactant heads and counterions are present at the micelle surface at a low concentration, and therefore occupy only a small fraction of the total micelle core/water interfacial area. Both of these factors result in g_{st} being small in magnitude (see Section 4.4.3 in Chapter 4).

After setting g_{pack} and g_{st} equal to zero, Eq. 12.9 can be expressed as follows as it applies to the micelles observed to form in solution during computer simulation (which are assumed to be representative of the optimal micelles):

$$g_{\text{mic}}^* = g_{\text{tr}}^* + g_{\text{int}}^* + g_{\text{elec}}^* \quad (12.10)$$

$$= \ln \frac{S_{\text{aq}}}{S_{\text{aq}} + 55.6} + \frac{\sigma'' S A S A_{\text{core}}}{\langle n \rangle_n} + g_{\text{elec}}^* \quad (12.11)$$

where $g_{\text{tr}}^* = \ln \frac{S_{\text{aq}}}{S_{\text{aq}} + 55.6}$, $g_{\text{int}}^* = \sigma'' S A S A_{\text{core}}/n$, S_{aq} is the molar solubility limit of the hydrophobic tails, 55.6 corresponds to the molarity of pure water in molar units, σ'' is the interfacial tension of the micelle core/water interface expressed on a per unit SASA

basis, $SASA_{\text{core}}$ is the hydrophobic solvent accessible surface area of the micelle core, and $\langle n \rangle_n$ is the number-average micelle aggregation number [38, 42, 43]. As shown in Eqs. 12.10 and 12.11, g_{tr}^* can be related to the solubility of the hydrophobic tails in aqueous solution, and g_{int}^* can be related to the reversible work (on a per surfactant molecule basis) associated with forming an interface of area $SASA_{\text{core}}$ between the hydrophobic AA or MA tails and the aqueous solution against the interfacial tension σ'' . The interested reader is referred to Chapter 6 for a complete discussion of the CS-MT model, and to Chapters 4 and 6 for additional information on the molecular models used to evaluate g_{tr}^* , g_{int}^* , and g_{elec}^* .

12.4.3 Implementation of the MCS-MT Model

As discussed in Section 12.4.1, in the MCS-MT model implemented in this chapter, I will make the assumption that the equilibrium micelle shape, size, and degree of counterion binding can be taken as inputs from the computer simulation results presented in Section 12.3. Because the parameters S , l_c , β , and the value of $SASA_{\text{core}}$ (see Eq. 12.11) that must be known to implement the MCS-MT model vary from micelle to micelle and over time during simulation, MCS-MT modeling will be implemented here based on the average values of S , l_c , β , and $SASA_{\text{core}}$ observed during a suitable simulation timeframe. The computer simulation data reported in Figures 12-3 to 12-9 provide considerable information with which to identify an appropriate timeframe over which to evaluate the required average values of S , l_c , β , and $SASA_{\text{core}}$. Inspection of the results presented in Figures 12-3 to 12-9 reveals that each calculated property, ranging from the number of micelles in solution to the solvent accessible surface area, change most significantly during the first 25 ns of simulation. During the subsequent 50 ns of simulation, most of the measured properties change only slightly or appear to fluctuate about an equilibrium value. Consequently, the MCS-MT model will be implemented here using inputs taken from computer simulation data corresponding to the last 50 ns of simulation.

Evaluation of g_{tr}^*

To evaluate g_{tr}^* , a solubility estimate is required for the AA and MA tails. The tails of both molecules are identical, and were taken as the chemical structures shown in Figure 12-1 without the hydrophilic carboxylate oxygens and OH groups. Because experimental solubility data was not available for both tails, their solubility was estimated to be $S_{\text{aq}} = 4.7 \cdot 10^{-11}$ M in aqueous solution using a group-contribution approach implemented in the Advanced Chemistry Development Software v8.19 [48], resulting in g_{tr}^* evaluated using Eq. 12.11 being equal to $-27.8 k_{\text{B}}T$.

Evaluation of g_{int}^*

Evaluation of g_{int}^* for the AA and MA micelles which form in aqueous solution was carried out using Eq. 12.11 and average values of $SASA_{\text{core}}$ obtained through computer simulation. In so doing, the assumption is made that the hydrophobic SASA values measured during the last 50 ns of computer simulation provide an accurate estimate of the hydrophobic SASA values characterizing the micelles at equilibrium in the aqueous solution. The physical property σ'' , or the interfacial tension of the micelle core/water interface, was calculated using the following expression (see Section 6.3 in Chapter 6):

$$\sigma'' = \frac{\sigma A_{\text{core}}}{SASA_{\text{core}}} \quad (12.12)$$

where σ is the curvature-dependent interfacial tension between water and a bulk phase of surfactant tails, A_{core} is the area of the aggregate hydrophobic core computed geometrically based on the volume of the aggregate and the assumption of a perfectly smooth aggregate surface, and $SASA_{\text{core}}$ is the solvent accessible surface area of the aggregate hydrophobic core obtained through computer simulation. The physical property σ was estimated using experimental interfacial tension data for the cyclohexane/water interface (51 mN/m [49]), and by correcting for the curvature of the micelle core/water interface using the Gibbs-Tolman-Koenig-Buff equation [50–53], yielding values of 36.4 mN/m and 35.6 mN/m for the AA and MA micelles, respec-

tively. Note that experimental interfacial tension data for the cyclohexane/water interface has been used because experimental data for the interfacial tension of the AA and MA tail/water interface was not available, and because cyclohexane is similar in structure to the carbon rings present in the AA and MA surfactant tails. The quantity $SASA_{\text{core}}$, or the average hydrophobic solvent accessible surface area for a single self-assembled micelle, is equal to 19.48 nm^2 and 16.27 nm^2 for AA and MA, respectively. The σ'' values estimated using the σ , A_{core} , and $SASA_{\text{core}}$ values reported above in Eq. 12.12 are 25.5 mN/m for AA and 25.6 mN/m for MA. Note that the estimated σ'' values for AA and MA are different not because they have different tail structures (in fact, their tails are identical), but because the AA and MA micelles observed during computer simulation have different sizes and different average values of $SASA_{\text{core}}$. Using Eq. 12.11, along with the estimated values of σ'' , g_{int}^* was estimated to be $13.98 k_{\text{B}}T$ for the formation of an AA micelle and $13.94 k_{\text{B}}T$ for the formation of an MA micelle.

Evaluation of g_{elec}^*

The electrostatic free-energy contribution, g_{elec}^* , was computed using the following expression:

$$g_{\text{elec}}^* = g_{\text{disch}}^* + g_{\text{rech}}^* \quad (12.13)$$

$$= g_{\text{disch}}^* + \int_0^{q_f} \psi_0(q) dq \quad (12.14)$$

where $\psi_0(q)$ is the instantaneous micelle electrostatic surface potential, expressed as a function of the instantaneous micelle charge, q , and $\int_0^{q_f} \psi_0(q) dq$ is the work required to charge the micelle surface against this instantaneous electrostatic surface potential from an uncharged state ($q = 0$) to the final state of charge ($q = q_f$). Details about the electrostatic method used have been presented in previous publications, and therefore, are not discussed here [14, 36]. The g_{elec}^* value predicted using Eq. 12.14 associated with the formation of an AA micelle with the same average shape,

size, and degree of counterion binding observed during the last 50 ns of AA simulation is equal to $0.07 k_B T$. Similarly, the g_{elec}^* value predicted using Eq. 12.14 associated with the formation of a MA micelle with the same characteristics observed during the last 50 ns of MA simulation is equal to $0.59 k_B T$. Although the self-assembled MA micelles were smaller, on average, than the self-assembled AA micelles (which serves to decrease g_{elec}), the predicted value of g_{elec}^* is higher for MA than for AA because the degree of counterion binding observed for MA was lower than that observed for AA.

CMC Predictions

After determining g_{mic}^* using Eq. 12.11, the CMCs of AA and MA could be estimated using Eq. 12.8. The predicted CMC of AA is $59 \mu\text{M}$, compared with the experimentally measured CMC of $17 \mu\text{M}$ [8]. The predicted CMC of MA is $96 \mu\text{M}$, compared with the experimentally measured CMC of $62 \mu\text{M}$ [8]. Both predicted CMCs are larger than the experimental CMCs. Specifically, the predicted CMC of AA is a factor of 3.4 larger than the experimental CMC of AA and the predicted CMC of MA is a factor of 1.5 larger than the experimental CMC of MA. Nevertheless, we consider the predicted CMC accuracy to be very good, since as shown in Eq. 12.8, the CMC is exponentially dependent on g_{mic}^* . Consequently, small errors in the predicted g_{mic}^* value lead to large errors in the predicted CMC [38]. The predicted g_{mic}^* value for AA micelle formation ($-13.8 k_B T$) is only 8.1% smaller than the experimental value ($-15.0 k_B T$, as inferred from the experimental CMC value and Eq. 12.8), and the predicted g_{mic}^* value for MA micelle formation ($-13.3 k_B T$) is only 2.9% smaller than the experimental value ($-13.7 k_B T$). It is important to note that a number of assumptions were made in the theoretical approach used here to predict g_{mic}^* , ranging from approximations that are not expected to introduce a significant error (setting $g_{\text{pack}} = 0$ and $g_{\text{st}} = 0$ in Eq. 12.9), to more significant approximations (the use of a group-contribution approach to evaluate S_{aq} and the use of experimental cyclohexane/water interfacial tension data to estimate σ). Nevertheless, even

after making these approximations, it is important to stress that the CMCs predicted using the MCS-MT model formulated here are significantly more accurate than the CMCs inferred from the computer simulation results for the AA and MA monomer concentration.

12.5 Conclusions

A series of extended molecular dynamics (MD) simulations were performed to gain insight into the self-assembly behavior of the triterpenoids AA and MA in aqueous solution. AA and MA molecules initially distributed randomly in aqueous solution were observed to aggregate into micelles during 75 ns of MD simulation. Two criteria were examined to identify micellar aggregates during MD simulation. The first criterion tested was to identify two AA or MA molecules as being part of the same micellar aggregate if the centers of mass of the two molecules were within a specified cutoff distance. The second criterion tested was to identify micellar aggregates by determining which AA or MA molecules experienced hydrophobic contacts with other AA or MA molecules. Direct visualization of the computer simulation results revealed that identification of micelles using the hydrophobic contacts criterion yields the most reasonable micelle identifications. The average number of identified micelles over the last 50 ns of simulation using the hydrophobic contacts criterion is 2.76 ± 0.04 for the AA simulation and 3.17 ± 0.03 for the MA simulation. The average aggregation number of the AA micelles during the last 50 ns of simulation is 5.65 ± 0.08 , and the average aggregation number of the MA micelles during the same time period is 4.35 ± 0.05 .

Any AA or MA molecule that experienced no hydrophobic contacts with other AA or MA molecules was identified as a monomer. The CMCs of AA and MA were evaluated directly from the average monomer concentrations observed during the last 25 ns of AA and MA simulation. Using this approach, the predicted CMCs of both AA and MA were much larger than the experimental CMCs, although the CMC

of AA was correctly predicted to be lower than that of MA. Because of the large timescales associated with monomer entry and exit from micelles, simulation over a longer period of time would have been necessary to make a statistically accurate estimate of the CMCs directly from the computer simulation results on the AA and MA monomer concentrations. The poor convergence of the computer simulation results for the AA and MA monomer concentrations suggested that a hybrid computer simulation/molecular-thermodynamic modeling approach should be used instead to predict the CMCs of AA and MA.

To characterize the structure of the self-assembled AA and MA micelles, the principal moments of the radius of gyration tensor were computed for each identified micelle. Evaluation of the radius of gyration data and of the aggregation number data revealed that both AA and MA exhibit one-dimensional growth. The following relationship between the largest eigenvalue of the radius of gyration tensor, λ_z (in units of nm), and the number-average micelle aggregation number, $\langle n \rangle_n$, was determined: $\lambda_z = 0.1 + 0.1 \langle n \rangle_n$. As the micelle aggregation number increases, the AA and MA micelles were found to change from being spherical to resembling a “squashed cylinder.” To quantify the level of internal ordering present in each AA and MA micelle, two different orientational order parameters were computed: (i) P_{mic} , a measure of the orientational ordering present throughout an entire micelle, and (ii) $P_{\text{n.n.}}$, a measure of the orientational ordering that exists between nearest neighbor AA or MA molecules in a micelle. The computed values of P_{mic} and $P_{\text{n.n.}}$ were found to fluctuate significantly and rapidly about their average values, with large changes in P_{mic} and $P_{\text{n.n.}}$ being observed on nanosecond time scales. The computed value of P_{mic} , averaged over all micelles and over the entire 75 ns simulation, and the computed value of $P_{\text{n.n.}}$, averaged over all nearest neighbors and over the entire 75 ns of simulation, were found to be fairly close to zero, suggesting that, on average, the AA and MA molecules within the self-assembled micelles are not preferentially oriented either parallel or perpendicular to each other.

The local environment of atoms within the AA and MA molecules in micelles

was characterized by computing radial distribution functions between the O^- and water and between OH groups and water ($g(r)_{O^-H_2O}$ and $g(r)_{OH-H_2O}$, respectively), as well as between the O^- group and the sodium ions present in the simulation cell ($g(r)_{O^-Na^+}$). The extent of counterion binding was computed by integrating the first peak in the $g(r)_{O^-Na^+}$ profile, and was found to be 0.27 and 0.14 for AA and MA, respectively, based on data taken from the last 50 ns of simulation. The extent of hydration experienced by OH, O^- , and selected carbon atoms within the AA and MA molecules was quantified by measuring the degree of hydration, which was defined as the number of water atoms within 0.5 nm of the group in question. As would be expected intuitively, the extent of hydration of each group decreased as micelle self-assembly occurred, and the decrease in hydration was found to be the largest for the hydrophobic carbon atoms. The total, hydrophobic, and hydrophilic solvent accessible surface areas associated with all the AA and MA molecules present in the AA and MA simulation cells was also measured over the course of MD simulation. The hydrophobic SASA was found to decrease to a much greater extent than the hydrophilic SASA for both AA and MA, as well as to decrease more rapidly for the AA micelles than for the MA micelles.

Motivated by the high computational cost that would have been required to obtain an accurate estimate of the CMC from the average monomer concentration observed in the AA and MA simulation cells, a hybrid, modified computer simulation/molecular-thermodynamic model (referred to as the MCS-MT model) was formulated to quantify the free-energy change associated with AA and MA micelle formation (g_{mic}) in order to predict the CMCs of AA and MA. The theoretical model required as inputs: (i) the average micelle aggregation number at equilibrium, (ii) the average hydrophobic solvent accessible surface area of the self-assembled AA and MA micelles at equilibrium, (iii) solubility estimates of the hydrophobic portions of the AA and MA molecules, and (iv) an estimate of the interfacial tension at the micelle core/water interface to determine g_{mic}^* , and from it, to predict the CMCs of AA and MA. The predicted g_{mic}^* value for AA micelle formation ($-13.8 k_B T$) was found to be only 8.1% smaller than

the experimental g_{mic}^* value, and the predicted g_{mic}^* value for MA micelle formation ($-13.3 k_{\text{B}}T$) was found to be only 2.9% smaller than the experimental g_{mic}^* value. The predicted CMC of AA was found to be 59 μM , compared with the experimentally measured CMC of 17 μM , and the predicted CMC of MA was found to be 96 μM , compared with the experimentally measured CMC of 62 μM [8]. Although the theoretically predicted CMCs of AA and MA overestimate the experimentally measured CMCs of AA and MA by a factor of 3.4 and 1.5, respectively, both predicted CMCs are much more accurate than the CMCs inferred from the monomer concentrations of AA and MA found in the simulation cells after micelle self-assembly. The CMCs inferred directly from the computer simulation results for the AA and MA monomer concentrations resulted in predicted CMCs that are a factor of 140 and 182 larger than the experimentally measured CMCs of AA and MA, respectively. The theoretical modeling results obtained for AA and MA indicate that by combining computer simulation inputs with molecular-thermodynamic models of surfactant self-assembly in aqueous solution, reasonably accurate estimates of CMCs can be obtained with a fraction of the computational expense that would be required otherwise.

In the CS-MT modeling approach introduced in Chapters 6, 7, and 8, theoretical predictions of surfactant solution properties are made after performing two independent computer simulations: (i) simulation of a single surfactant molecule in aqueous solution, and (ii) simulation of a surfactant molecule in a micelle in aqueous solution (requiring equilibration of a *preformed* surfactant micelle in aqueous solution). From (i) and (ii), fractional hydration information is obtained that is subsequently used to quantify the hydrophobic driving force for micelle self-assembly. In comparison with the CS-MT model, the modified CS-MT (MCS-MT) model used in this chapter to predict g_{mic}^* and the CMC for AA and MA surfactants in aqueous solution is more computationally expensive because it involves simulation of micelle self-assembly. It is important to note, however, that the CS-MT model requires computer simulation fractional hydration inputs *in conjunction* with the application of a molecular-thermodynamic model in order to determine S^* , l_{c}^* , β^* , and g_{mic}^* — a complexity

that is not present in the MCS-MT model (see Section 12.4.1). In the MCS-MT modeling approach, S^* , l_c^* , and β^* are obtained directly from the computer simulation results rather than being predicted using a molecular-thermodynamic model. Consequently, the molecular-thermodynamic modeling problem is greatly reduced in complexity from one of finding the global minimum of g_{mic} with respect to S , l_c , and β to one of simply evaluating g_{mic}^* for specified values of S^* , l_c^* , and β^* obtained through computer simulation. To use the CS-MT model to predict the micellization behavior of structurally complex surfactants such as AA or MA, an accurate model for packing constraints would be required in order to allow prediction of S^* and l_c^* . For such structurally complex surfactants, using a mean-field modeling approach to evaluate g_{pack} (such as the approach described in Section 4.4.3 of Chapter 4) is not feasible because it is not possible to estimate l_{max} . Furthermore, it is not clear that applying a simple geometric constraint such as l_{max} in a mean-field packing model would be adequate to capture the physics involved in complex surfactant self-assembly and yield accurate predictions of S^* and l_c^* . As a result, the MCS-MT modeling approach formulated in this chapter is the only viable approach developed to date to model the micellization thermodynamics of highly structurally complex surfactants such as AA and MA.

Bibliography

- [1] Bunpo, P., Kataoka, K., Arimochi, H., Nakayama, H., Kuwahara, T., and Vinitketkummuen, U., “Inhibitory effects of asiatic acid and CPT-11 on growth of HT-29 cells,” *The Journal of Medical Investigation*, Vol. 52, 2005, pp. 65–73.
- [2] Soo Lee, Y., Jin, D. Q., Beak, S. M., Lee, E. S., and Kim, J. A., “Inhibition of ultraviolet-A-modulated signaling pathways by asiatic acid and ursolic acid in HaCaT human keratinocytes,” *European Journal of Pharmacology*, Vol. 476, 2003, pp. 173–178.
- [3] Park, B. C., Bosire, K. O., Lee, E. S., and Kim, J. A., “Asiatic acid induces apoptosis in SK-MEL-2 human melanoma cells,” *Cancer Letters*, Vol. 218, 2005, pp. 81–90.
- [4] Lee, Y. S., Jin, D. Q., Kwon, E. J., Park, S. H., Lee, E. S., Jeong, T. C., Nam, D. H., Huh, K., and Kim, J. A., “Asiatic acid, a triterpene, induces apoptosis through intracellular Ca²⁺ release and enhanced expression of p53 in HepG2 human hepatoma cells,” *Cancer Letters*, Vol. 186, 2002, pp. 83–91.
- [5] Setzer, W. N. and Setzer, M. C., “Plant-derived triterpenoids as potential anti-neoplastic agents,” *Mini- Reviews in Medicinal Chemistry*, Vol. 3, 2003, pp. 540–556.
- [6] Barrett, D. and Gellman, S. H., “Effect of amphiphile topology on aggregation properties: Distinctive behavior of contrafacial amphiphiles,” *Journal of the American Chemical Society*, Vol. 115, 1993, pp. 9343–9344.

- [7] Venkatesan, P., Cheng, Y., and Kahne, D., “Hydrogen bonding in micelle formation,” *Journal of the American Chemical Society*, Vol. 116, 1994, pp. 6955–6956.
- [8] Sambandan, T. B., Rafat, M., Lanza, A. M., Fong, K. W., Goldsipe, A., Stephenson, B. C., and Rha, C. K., “Surface activity of the triterpenoids asiatic and madecassic acid,” 2006, pp. (unpublished results).
- [9] Tanford, C., *The Hydrophobic Effect: Formation of Micelles and Biological Membranes*, John Wiley and Sons, New York, 1991.
- [10] Israelachvili, J. N., *Intermolecular and Surface Forces*, Academic Press, 2nd ed., 1991.
- [11] Stephenson, B. C., Rangel-Yagui, C. O., Pessoa, A., Tavares, L. C., Beers, K. J., and Blankschtein, D., “Experimental and theoretical investigation of the micellar-assisted solubilization of ibuprofen in aqueous media,” *Langmuir*, Vol. 22, 2006, pp. 1514–1525.
- [12] Puvvada, S. and Blankschtein, D., “Molecular thermodynamic approach to predict micellization, phase behavior and phase separation of micellar solutions. 1. Application to nonionic surfactants,” *The Journal of Chemical Physics*, Vol. 92, 1990, pp. 3710–3724, and references cited therein.
- [13] Shiloach, A. and Blankschtein, D., “Predicting micellar solution properties of binary surfactant mixtures,” *Langmuir*, Vol. 14, 1998, pp. 1618–1636.
- [14] Goldsipe, A. and Blankschtein, D., “Modeling counterion binding in ionic-nonionic and ionic-zwitterionic binary surfactant mixtures,” *Langmuir*, Vol. 22, 2005, pp. 9850–9865.
- [15] Stephenson, B. C., Beers, K., and Blankschtein, D., “Complementary use of simulations and molecular-thermodynamic theory to model micellization,” *Langmuir*, Vol. 22, 2006, pp. 1500–1513.

- [16] Pool, R. and Bolhuis, P. G., “Accurate free energies of micelle formation,” *The Journal of Physical Chemistry B*, Vol. 109, 2005, pp. 6650–6657.
- [17] Maillet, J. B., Lachet, V., and Coveney, P. V., “Large scale molecular dynamics simulation of self-assembly processes in short and long chain cationic surfactants,” *Physical Chemistry Chemical Physics*, Vol. 1, 1999, pp. 5277.
- [18] Marrink, S., Lindahl, E., Edholm, O., and Mark, A., “Simulation of the spontaneous aggregation of phospholipids into bilayers,” *Journal of the American Chemical Society*, Vol. 123, 2001, pp. 8638–8639.
- [19] Marrink, S. J., Tieleman, D. P., and Mark, A. E., “Molecular dynamics simulation of the kinetics of spontaneous micelle formation,” *The Journal of Physical Chemistry B*, Vol. 104, 2000, pp. 12165–12173.
- [20] Marrink, S. and Mark, A., “Molecular dynamics simulation of the formation, structure, and dynamics of small phospholipid vesicles,” *Journal of the American Chemical Society*, Vol. 125, 2003, pp. 15233–15242.
- [21] Marrink, S. J. and Mark, A. E., “The mechanism of vesicle fusion as revealed by molecular dynamics simulations,” *Journal of the American Chemical Society*, Vol. 125, 2003, pp. 11144–11145.
- [22] de Vries, A., Mark, A., and Marrink, S., “Molecular dynamics simulation of the spontaneous formation of a small DPPC vesicle in water in atomistic detail,” *Journal of the American Chemical Society*, Vol. 126, 2004, pp. 4488–4489.
- [23] Braun, R., Engelman, D. M., and Schulten, K., “Molecular dynamics simulations of micelle formation around dimeric glycoporphin A transmembrane helices,” *Biophysical Journal*, Vol. 87, 2004, pp. 754–763.
- [24] Marrink, S. J. and Mark, A. E., “Molecular dynamics simulations of mixed micelles modeling human bile,” *Biochemistry*, Vol. 41, 2002, pp. 5375–5382.

- [25] Berendsen, H. J. C., van der Spoel, D., and van Drunen, R., “GROMACS: A message-passing parallel molecular dynamics implementation,” *Computational Physics Community*, Vol. 91, 1995, pp. 43–56.
- [26] Lindahl, E., Hess, B., and van der Spoel, D., “Gromacs 3.0: A package for molecular simulation and trajectory analysis,” *Journal of Molecular Modeling*, Vol. 7, 2001, pp. 306–317.
- [27] Jorgensen, W. L., Maxwell, D. S., and Tirado-Rives, J., “Development and testing of the OPLS all-atom force field on conformational energetics and properties of organic liquids,” *Journal of the American Chemical Society*, Vol. 118, 1996, pp. 11225–11236.
- [28] Berendsen, H. J. C., Grigera, J. R., and Straatsma, T. P., “The missing term in effective pair potentials,” *The Journal of Physical Chemistry*, Vol. 91, 1987, pp. 6269–6271.
- [29] Shirts, M. R., Pitera, J. W., Swope, W. C., and Pande, V. S., “Extremely precise free energy calculations of amino acid side chain analogs: Comparison of common molecular mechanics force fields for proteins,” *The Journal of Chemical Physics*, Vol. 119, 2003, pp. 5740–5760.
- [30] Shirts, M. R. and Pande, V. S., “Solvation free energies of amino acid side chain analogs for common molecular mechanics water models,” *The Journal of Chemical Physics*, Vol. 122, 2005, pp. 134508.
- [31] Shirts, M., *Calculating Precise and Accurate Free Energies in Biomolecular Systems*, Ph.D. thesis, Stanford, 2005, and references cited therein.
- [32] van Gunsteren, W. F. and Berendsen, J. J. C., “A leap-frog algorithm for stochastic dynamics,” *Journal of Computational Chemistry*, Vol. 18, 1997, pp. 1463–1472.

- [33] van der Spoel, D., Lindahl, E., Hess, B., van Buuren, A., Apol, E., Meulenhoff, P., Tieleman, D., Sijbers, A., Feenstra, K., van Drunen, R., and Berendsen, H., *Gromacs User Manual version 3.2*, www.gromacs.org, 2004.
- [34] Mattice, W. L. and Suter, U. W., *Conformational Theory of Large Molecules: The Rotational Isomeric State Model in Macromolecular Systems*, Wiley, New York, 1994.
- [35] Leach, A., *Molecular Modeling: Principles and Applications*, Prentice Hall, 2nd ed., 2001.
- [36] Srinivasan, V. and Blankschtein, D., “Effect of counterion binding on micellar solution behavior: 1. Molecular-thermodynamic theory of micellization of ionic surfactants,” *Langmuir*, Vol. 19, 2003, pp. 9932–9945.
- [37] Chandler, D., “Interfaces and the driving force of hydrophobic assembly,” *Nature*, Vol. 437, 2005, pp. 640–647.
- [38] Stephenson, B. C., Goldsipe, A., Beers, K. J., and Blankschtein, D., “Quantifying the hydrophobic effect: I. A computer simulation/molecular-thermodynamic model for the aqueous self-assembly of hydrophobic and amphiphilic solutes,” *The Journal of Physical Chemistry B*, 2006, pp. (submitted).
- [39] Reynolds, J. A., Gilbert, D. B., and Tanford, C., “Empirical correlation between hydrophobic free energy and aqueous cavity surface area,” *Proceedings of the National Academy of Sciences*, Vol. 71, 1974, pp. 2925–2927.
- [40] Levy, R. M., Zhang, L. Y., Gallicchio, E., and Felts, A. K., “On the nonpolar hydration free energy of proteins: Surface area and continuum solvent models for the solute-solvent interaction energy,” *Journal of the American Chemical Society*, Vol. 125, 2003, pp. 9523–9530.

- [41] Hermann, “Theory of hydrophobic bonding. II. The correlation of hydrocarbon solubility in water with solvent cavity surface area,” *The Journal of Physical Chemistry*, Vol. 76, 1972, pp. 2754–2759.
- [42] Stephenson, B. C., Goldsipe, A., Beers, K. J., and Blankschtein, D., “Quantifying the hydrophobic effect: II. A computer simulation/molecular-thermodynamic model for the micellization of nonionic surfactants,” *The Journal of Physical Chemistry B*, 2006, pp. (submitted).
- [43] Stephenson, B. C., Beers, K. J., and Blankschtein, D., “Quantifying the hydrophobic effect: III. A computer simulation/molecular-thermodynamic model for the micellization of ionic and zwitterionic surfactants,” *The Journal of Physical Chemistry B*, 2006, pp. (submitted).
- [44] Puvvada, S. and Blankschtein, D., “Theoretical and experimental investigations of micellar properties of aqueous solutions containing binary mixtures of nonionic surfactants,” *The Journal of Physical Chemistry*, Vol. 96, 1992, pp. 5579–5592.
- [45] Ben-Shaul, A. and Szleifer, I., “Chain organization and thermodynamics in micelles and bilayers. I. Theory,” *The Journal of Chemical Physics*, Vol. 83, 1985, pp. 3597–3611.
- [46] Szleifer, I., Ben-Shaul, A., and Gelbart, W. M., “Chain organization and thermodynamics in micelles and bilayers. II. Model calculations,” *The Journal of Chemical Physics*, Vol. 83, 1985, pp. 3612–3620.
- [47] Szleifer, I., Ben-Shaul, A., and Gelbart, W. M., “Statistical thermodynamics of molecular organization in mixed micelles and bilayers,” *The Journal of Chemical Physics*, Vol. 86, 1987, pp. 7094–7109.
- [48] ACD/Labs, “Advanced chemistry development software v8.19 for Solaris,” 1994–2006.

- [49] Pomerantz, P., Clinton, W. C., and Zisman, W. A., “Spreading pressures and coefficients, interfacial tensions, and adhesion energies of the lower alkanes, alkenes, and alkyl benzenes on water,” *Journal of Colloid and Interface Science*, Vol. 24, 1967, pp. 16–28.
- [50] Gibbs, J. W., *The Scientific Papers of J.W. Gibbs*, Vol. 1, Dover, New York, 1961.
- [51] Koenig, F. O., “On the thermodynamic relation between surface tension and curvature,” *The Journal of Chemical Physics*, Vol. 18, 1950, pp. 449.
- [52] Buff, F. P., “The spherical interface. I. Thermodynamics,” *The Journal of Chemical Physics*, Vol. 19, 1951, pp. 1591.
- [53] Tolman, R. C., “Consideration of the Gibbs theory of surface tension,” *The Journal of Chemical Physics*, Vol. 16, 1948, pp. 758.

Chapter 13

Conclusions and Future Research Directions

The central objective of this thesis has been to develop modeling approaches to enable prediction of micellar solution properties based on the chemical structures of the solution components and the solution conditions. In addition to the obvious benefit that such prediction would provide to formulators in industry and scientists in academia, the development of such approaches will improve our fundamental, molecular-level understanding of self-assembly phenomena. With this objective in mind, this chapter is organized as follows. Section 13.1 summarizes the main results of the thesis. Section 13.2 discusses extensions that may be made to research described in Part I of this thesis, in which computer simulations were used to obtain input parameters for molecular-thermodynamic modeling. Section 13.3 discusses several future directions which may be explored to extend the research described in Part II of this thesis, in which computer simulations were used to compute free-energy changes. Section 13.4 describes future work which may be undertaken in the research areas described in Part III of this thesis, in which computer simulations were used to directly predict accessible surfactant solution properties. Finally, Section 13.5 contains concluding remarks.

13.1 Thesis Summary

The main results of this thesis are summarized below. In Chapter 2, a computer simulation/ molecular-thermodynamic modeling approach was described in which computer simulations were used to obtain head and tail input parameters for molecular-thermodynamic (MT) modeling. To identify heads and tails for MT modeling, simulations were conducted of a single surfactant molecule at infinite dilution at a flat water/oil interface (modeling the water/micelle core interface) to determine how the surfactant would locate itself between the two phases. From each water/oil interface simulation, the extent of hydration of different portions of each surfactant molecule was determined. A computational approach was developed to identify the head and tail groups of each surfactant using the hydration data. The approach was used to determine heads and tails for simple surfactants such as sodium dodecyl sulfate (SDS), cetyltrimethylammonium bromide (CTAB), dodecylphosphocholine (DPC), and octa(ethylene oxide) ($C_{12}E_8$), as well as of three more complex surfactants, 3- and 4-hydroxy sulfonate (AOS) and decanoyl-*n*-methylglucamide (MEGA-10). The sensitivity of the head and tail assignments obtained to the method used to assign atomic charges was evaluated and discussed. The modeling results presented in Chapter 2 demonstrate that computer simulations at a water/oil interface can be used to obtain reasonable head and tail input parameters for simple and complex surfactants in the context of MT modeling.

In Chapter 3, the micellar solubilization of the drug ibuprofen in aqueous solution was investigated theoretically and experimentally for three surfactants — the anionic surfactant SDS, the cationic surfactant dodecyltrimethylammonium bromide (DTAB), and the nonionic surfactant $C_{12}E_8$ — each having the same hydrocarbon tail length but differing in their hydrophilic heads. The goal of this research was to theoretically and experimentally determine the effect of changes in the surfactant head on the micellar solubilization capacity. Simulations of ibuprofen were conducted at a water/oil interface to identify the head and tail portions of this molecule. Using

the input parameters determined from computer simulation, MT theory was used to predict: (i) the micelle composition as a function of surfactant concentration, (ii) the aqueous solubility of ibuprofen as a function of surfactant concentration, and (iii) the micellar solubilization capacity. Theoretical predictions were compared with experimental solubilization data provided by our research collaborators at the University of São Paulo in Brazil [1]. For ibuprofen, the same head and tail identification was obtained using both OPLS-AA and CHelpG atomic charges. Without the computer simulation inputs, it would not have been possible to obtain the level of agreement with the experimental results that was obtained.

In Chapter 4, computer simulations were used to determine head and tail input parameters for 12 structurally diverse solubilizates (*o*-aminobenzoate, *m*-aminobenzoate, *p*-aminobenzoate, ibuprofen, benzene, chlorobenzene, acetophenone, naphthalene, benzophenone, benzonitrile, benzamide, and anthracene). To accomplish this, 36 extended molecular dynamics (MD) simulations of solubilizates in the following environments were performed: (i) a water/oil interface, (ii) a spherical SDS micelle, and (iii) a cylindrical SDS micelle. By identifying heads and tails using computer simulation data obtained from (i), (ii), and (iii), the effects of curvature, ordering of the surfactant tails, and the presence of the surfactant heads were thoroughly investigated. Micellar solubilization is a process that has not been widely investigated theoretically using the MT modeling approach. Consequently, significant effort was required to implement MT modeling for the 12 solubilizates considered in Chapter 4. Specifically, the evaluation of g_{tr} , g_{int} , and g_{pack} required generalization of the traditional MT modeling approach to estimate these free-energy contributions. A detailed description of the generalizations made to the MT model to permit accurate modeling of micellar solubilization was presented.

In Chapter 5, MT modeling results were presented for each of the 12 solubilizates considered in Chapter 4. MT modeling was implemented using each of the head and tail identifications made in Chapter 4. For the 12 solubilizates modeled, simulation at a water/oil interface was found in most cases to be adequate in providing

accurate hydration information for MT modeling. MT predictions of: (i) the micelle composition as a function of surfactant concentration, (ii) the aqueous solubility of the solubilize as a function of surfactant concentration, (iii) the micelle/water partition coefficient, and (iv) structural characteristics of the micelle were evaluated and reported. When possible, the theoretical predictions were compared with available experimental data. The predictions of the theoretical model were found to be in reasonable agreement with experimental data on micelle/water partition coefficients.

In Chapter 6, a computer simulation/molecular-thermodynamic (CS-MT) modeling approach was introduced. Although using computer simulations for head and tail identification improves the accuracy of the traditional MT modeling approach for complex solutes (surfactants and solubilizes) with a minimum of computational expense, the limitation remains that individual groups in the solute molecule are modeled as being in only one of two states — head or tail — while in reality, there is a continuous spectrum of hydration states between these two limits. In the CS-MT modeling approach, atomistic MD simulations were first used to quantify the hydration changes that take place during self-assembly. This hydration information was then used in a new MT model to quantify the hydrophobic effect, which is decomposed into two components: (1) the free-energy change associated with the dehydration of solute hydrophobic groups that accompanies aggregate self-assembly (as captured in g_{dehydr}), and (2) the change in hydration free energy experienced by these same hydrophobic groups during aggregate self-assembly (as captured in g_{hydr}). The CS-MT model was formulated to allow the prediction of the free-energy change associated with aggregate formation of solute aggregates of any shape and size by performing only two computer simulations — one of the solute in bulk water and the second of the solute in an aggregate of arbitrary shape and size. To test the validity and accuracy of the new CS-MT modeling approach, it was used to model the formation of 15 different oil aggregates of various shapes (spheres, cylinders, and slabs) and sizes in aqueous solution, where the additional complexities associated with the presence of the solute heads are absent. Excellent agreement was obtained between

the theoretically predicted values of g_{form} obtained using the CS-MT model and a traditional MT model of self-assembly. For the 15 oil aggregates modeled, the average discrepancy between the predictions of the CS-MT model and those of the traditional MT model was only 1.04%. The CS-MT modeling results also demonstrated that the model can accurately predict g_{form} for aggregates of any shape and size using hydration information obtained from only two independent MD simulations.

In Chapter 7, the validity and accuracy of the CS-MT model was evaluated by using it to predict the micellization behavior of seven different nonionic surfactants in aqueous solution. Detailed information about the changes in hydration that occur upon the self-assembly of each surfactant into micelles was obtained through MD simulation, and subsequently used to compute the hydrophobic driving force for micelle formation. To enable a relatively simple estimation of g_{dehydr} and g_{hydr} in the case of nonionic surfactants, a number of approximations were made. Although the CS-MT model enables the prediction of a rich variety of micellar solution properties from g_{form} (including micelle shape, size, and composition), the CMC was selected for prediction and comparison with available experimental data because the CMC depends exponentially on g_{form} , and as such, it provides a stringent quantitative test with which to evaluate the predictive accuracy of the CS-MT model. Reasonable agreement between the CMC predictions made using the CS-MT model and the experimental CMCs was obtained for octyl glucoside (OG), dodecyl maltoside (DM), octyl sulfinyl ethanol (OSE), decyl methyl sulfoxide (C_{10}SO), decyl dimethyl phosphine oxide (C_{10}PO), and decanoyl-*n*-methylglucamide (MEGA-10). For five of these surfactants, the CMCs predicted using the CS-MT model were closer to the experimental CMCs than the CMCs predicted using traditional MT modeling. In addition, the CMCs predicted for mixtures of C_{10}PO and C_{10}SO using the CS-MT modeling approach were significantly closer to the experimental CMCs than those predicted using the traditional MT modeling approach. For dodecyl octa(ethylene oxide) (C_{12}E_8), the CMC predicted using the CS-MT model was not in good agreement with the experimental CMC data or with the CMC predicted using the traditional MT model,

because the simplifying approximations made to estimate g_{dehydr} and g_{hydr} in this case were not sufficiently accurate. Consequently, it is recommended that these simplifying approximations only be used to model nonionic surfactants with relatively small, non-polymeric heads. For MEGA-10, which is the most structurally complex of the seven nonionic surfactants modeled, the CMC predicted by the CS-MT model (6.55 mM) was found to be in much closer agreement with the experimental CMC value (5 mM) than the CMC predicted by the traditional MT model (43.3 mM). For complex nonionic surfactants where it is difficult to accurately quantify the hydrophobic driving force for micelle formation using the traditional MT modeling approach, our results indicate that the CS-MT modeling approach yields better results than those obtained using the traditional MT modeling approach. In addition, the results suggest that even after making simplifying approximations to allow relatively straightforward estimation of g_{dehydr} and g_{hydr} , the CS-MT model is still capable of making reasonable predictions of the aqueous micellization behavior of nonionic surfactants possessing non-polymeric heads.

In Chapter 8, the validity and accuracy of the CS-MT model was further evaluated by utilizing it to model the micellization behavior of ionic and zwitterionic surfactants in aqueous solution. Both the CS-MT model and the traditional MT model were used to predict the micellization behavior of simple and complex ionic and zwitterionic surfactants. The most complex ionic surfactants considered included a homologous series of cationic surfactants with two tails attached to a single dimethylammonium head. Reasonable agreement between the CMCs predicted using the CS-MT model and the experimental CMCs were obtained for sodium dodecyl sulfate (SDS), dodecylphosphocholine (DPC), cetyltrimethylammonium bromide (CTAB), two 3-hydroxy sulfonate surfactants (AOS-12 and AOS-16), and a homologous series of four cationic DC_NA surfactants with a dimethylammonium bromide head attached to a dodecyl alkyl tail and to an alkyl sidechain of length C_N, having the chemical formula C₁₂H₂₅C_NH_{2N+1}N(CH₃)₂Br, with $N = 1$ (DC₁AB), 2 (DC₂AB), 4 (DC₄AB), and 6 (DC₆AB). For six of these surfactants, the CMCs predicted using the CS-

MT model were closer to the experimental CMCs than the CMCs predicted using the traditional MT model. For DC₂AB, DC₄AB, and DC₆AB, which are the most structurally complex of the ionic surfactants modeled, the CMCs predicted using the CS-MT model were in remarkably good agreement with the experimental CMCs, while the CMCs predicted using the traditional MT model were quite inaccurate. These results suggest that the CS-MT model accurately predicts the hydrophobic driving force for micelle formation for ionic and zwitterionic surfactants.

Chapter 9 discussed the development of a new computer simulation-free energy/molecular-thermodynamic (CS-FE/MT) modeling approach. In the CS-FE/MT model, traditional MT modeling, or experimental data, are used to determine the free energy of formation of a single-surfactant micelle and the aggregation number of a single-surfactant micelle. A micelle with the theoretically, or the experimentally, determined aggregation number is then built and equilibrated in aqueous solution in a simulation cell. At this point, alchemical computer simulations are used to compute the free-energy change associated with: (i) changing the identity of surfactant molecules of type *A* to solubilize molecules of type *B* (to model micellar solubilization) in the micellar environment and in bulk aqueous solution, and (ii) changing the identity of surfactant molecules of type *A* to cosurfactant molecules of type *B* (to model binary surfactant micellization) in the micellar environment and in bulk aqueous solution. The difference between the free-energy change associated with alchemical transformation in the micellar environment and the free-energy change associated with alchemical transformation in bulk aqueous solution is referred to as $\Delta\Delta G$. A theoretical framework was outlined to use computer simulation estimates of $\Delta\Delta G$ with the free energy of single-surfactant micelle formation to determine the free energy associated with mixed micelle formation.

In Chapter 10, the CS-FE/MT modeling approach was implemented to make predictions of $\Delta\Delta G$ for two surfactant to solubilize exchanges and for three surfactant to cosurfactant exchanges. The CS-FE/MT model was implemented using a dual-topology thermodynamic integration approach. Molecules of type *A* were

transformed into molecules of type B as a function of a coupling parameter, λ . To evaluate the accuracy of the CS-FE/MT model, MD simulation results for $\Delta\Delta G$ were compared with the predictions of a MT model developed by fitting to experimental CMC data. Reasonable predictions of $\Delta\Delta G$ were obtained for: (i) the exchange of octyl sulfoxide with decyl sulfoxide, and (ii) the exchange of octylsulfanyl ethanol with decylsulfanyl ethanol. However, the computational cost required to obtain even qualitatively correct modeling results was very high. Consequently, given present-day computational power, the CS-FE/MT modeling approach is not a practical method to model mixed surfactant micellization or micellar solubilization. Although computer simulation free-energy methods are certainly of interest from an academic perspective, and although these methods may enable the accurate prediction of surfactant solution properties as the computational power of computers increases, at the present time, more accurate estimates of g_{form} can be obtained with less computational expense using traditional MT modeling with computer simulation estimates of heads and tails, or using the CS-MT model.

In Chapter 11, atomistic-level MD simulations were used to determine and understand the interfacial behavior of a homologous series of structurally complex fluorosurfactants. Although the computational expense of atomistic-level MD simulations limits their use to the evaluation of a limited subset of surfactant solution properties, these simulations can provide a great deal of insight into the structural characteristics of surfactant assemblies, including surfactant monolayers. Constant surface tension ($N\gamma T$) and constant volume (NVT) MD simulations were conducted on a series of bolaamphiphilic α, ω -(diammonium disulfato)poly(fluorooxetane)s with several perfluoroalkyl chain lengths and a typical “long-chain” anionic fluorosurfactant used to improve the flow-and-leveling characteristics of aqueous coatings, in order to compare their behavior at a water/air interface. Recent research has shown that these poly(fluorooxetane) surfactants are an effective substitute for traditional fluorosurfactants used in flow-and-leveling applications [2]. From MD simulation, the saturated interfacial area per surfactant molecule, interfacial area per surfactant molecule as a

function of surface tension, density profiles, order parameters, the degree of hydration of various atoms in each surfactant molecule, and the degree of counterion binding were each determined. The simulation results shed light on experimental data which indicates that these surfactants occupy very low interfacial areas at the water/air interface. The low interfacial areas occupied by each poly(fluorooxetane) molecule result from their ability to adopt a “looped” conformation, in which the carbon and oxygen backbone of each surfactant molecule and the attached perfluoroalkyl chains are forced into the air phase. A geometrically defined penetration parameter was calculated from the density profiles, which revealed that each poly(fluorooxetane) surfactant is more effective at separating the air and water phases than a traditional “long-chain” anionic fluorosurfactant. The degree of hydration measured for different atoms in poly(fluorooxetane) during simulation also confirmed that a “looped” conformation is adopted in which the surfactant backbone and the perfluoroalkyl chains are lifted away from the water surface. When viewed in the context of the penetration parameter analysis, the hydration data suggests why each poly(fluorooxetane) molecule is capable of significantly reducing surface tension while other fluorosurfactants with similarly short perfluoroalkyl moieties provide inadequate surface tension reduction for practical flow-and-leveling applications.

In Chapter 12, extended MD simulations were used to study the self-assembly of the triterpenoids asiatic acid (AA) and madecassic acid (MA) in aqueous solution. The two initial configurations for the simulations reported in this chapter were a simulation cell containing 15 AA molecules distributed isotropically in water, and a simulation cell containing 15 MA molecules distributed isotropically in water. Self-assembly of the AA and the MA molecules into micelles began to occur almost immediately upon commencing MD simulation. However, approximate equilibration of micelle aggregation numbers and monomer concentrations was not observed until after 25 to 50 ns of simulation. The computer simulation results were used to obtain information about: i) the kinetics of micelle formation, ii) the average aggregation numbers of the self-assembled AA and MA micelles, iii) the AA and the MA monomer

concentrations, iv) structural characteristics of the AA and MA micelles, v) the local environments of hydrophobic and hydrophilic groups in AA and MA molecules in the micellar environment, and vi) the thermodynamics associated with AA and MA micelle formation (through application of a modified CS-MT modeling approach). Direct observation of the monomer concentrations of AA and MA after micelle self assembly and the CS-MT modeling results suggested that MA has a lower CMC than AA, an observation that is consistent with the experimental CMC data.

13.2 Future Research Directions: Application of Computer Simulation to Obtain Inputs for MT Theory

In this section, future research directions related to the modeling approaches developed in Part I of this thesis, in which computer simulations were used to determine input parameters for MT modeling, are discussed. The extensions discussed in this section are particularly significant in that the modeling approaches described in Part I represent the most quantitatively accurate approaches developed in this thesis to predict properties such as the critical micelle concentration, the shape and size of micelles that form in solution, and the extent of solubilization. Further exploration of the modeling approaches presented in Part I is expected to contribute significantly to both our ability to accurately predict complex surfactant and solubilizate self-assembly in aqueous solution, as well as to enhance our fundamental understanding of such self-assembly phenomena.

13.2.1 Head and Tail Identification through Water/Oil Interface Simulation

In this thesis, we have discussed several alternative approaches to make head and tail identifications for traditional MT modeling of surfactant micellization and micel-

lar solubilization in aqueous solution. The least computationally expensive of these approaches is to simulate a *single* surfactant or solubilizate molecule at a water/oil interface. Although such an interface lacks the curvature, the ordering of the surfactant/solubilizate tails, and the presence of the additional surfactant heads that characterizes the micelle core/water interface, results presented in Chapters 2, 3, and 4 indicate that, in many cases, water/oil interface simulations can provide accurate head and tail identifications for traditional MT modeling.

Having said that, additional investigation is warranted to identify the classes of surfactants and solubilizates for which water/oil interface simulations provide reasonable head and tail input parameters for MT modeling. Given the sensitivity of the head and tail identification to not only the atom types present in a surfactant or solubilizate, but also to the connectivity of those atoms, such an investigation will most likely require simulation of a large set of structurally diverse molecules as well as careful categorization of the molecules into classes exhibiting chemical and architectural similarity. To characterize the accuracy of the head and tail identifications obtained through water/oil interface simulation, it will be necessary to: i) compare the head and tail identifications made with identifications made through simulation in a micellar environment, and ii) to compare predictions of micellization and micellar solubilization behavior made using the head and tail identifications as inputs in the traditional MT model with the available experimental data.

To facilitate the generation of large amounts of head and tail data for many surfactants and solubilizates, it will be helpful to better characterize the minimum simulation time required for water/oil interface simulations to yield statistically significant identification of heads and tails. Because the results presented in Chapter 5 suggest that the minimum simulation time is a function of the surfactant and the solubilizate chemical structure, it may be most practical to continually evaluate the statistical significance of head and tail identifications as the computer simulation progresses, and to terminate the simulation as soon as a reasonable degree of certainty has been attained, where a “reasonable degree of certainty” might be defined as 95%

confidence in the head and tail assignments.

Results presented in Chapter 2 also demonstrated that head and tail identification through simulation at a water/oil interface is sensitive to the method used to assign atomic charges to each atom in a surfactant or solubilizate molecule. For atoms for which atomic charges were not suggested in the OPLS-AA forcefield, the CHelpG algorithm (as implemented in *Gaussian 98*) was used to estimate atomic charges [3,4]. Although reasonable head and tail assignments can be made using charges determined using the CHelpG algorithm, the default atomic charges recommended in OPLS-AA were found to give more accurate simulation results when they were available. Optimal selection of atomic charges for computer simulation is an important area of research with many outstanding issues. A recent publication by Heintz and Suter concludes that the assignment of atomic charges using electronic structure methods exhibits 5-fold variation from using different basis sets and 5-fold variation depending on the method used to partition the atomic charges among different atoms within a molecule [5]. In future work, it would be valuable to systematically test different approaches to assign atomic charges (for a discussion of possible approaches, see Ref. [5]), and to evaluate the accuracy of the traditional MT modeling results obtained using the head and tail identifications made with each set of atomic charges through comparison with the appropriate experimental data.

13.2.2 Head and Tail Identification through Micellar Simulation

Although simulation of a surfactant or a solubilizate in a micellar environment is more computationally expensive than simulation at a water/oil interface, results presented in Chapter 4 demonstrate that head and tail identifications obtained with the two methods are not always in agreement. Head and tail identifications made through simulation in a micellar environment are expected to be superior to head and tail identifications made through simulation at a water/oil interface, because simulation

in a micellar environment accounts explicitly for: (i) the curvature of the micelle, (ii) the ordering of the surfactant/solubilize tails in the micelle core, and (iii) the presence of the hydrophilic surfactant/solubilize heads.

Although micellar simulation is expected to yield the most accurate head and tail assignments, for classes of surfactants and solubilizes for which simulation in a micellar environment is necessary to accurately determine heads and tails, it is recommended that the CS-MT model be used for modeling and property prediction rather than the traditional MT model. As discussed in Chapter 6, implementing the CS-MT model requires two independent MD simulations — one of the surfactant/solubilize in bulk aqueous solution and the second of the surfactant/solubilize in a micellar environment. The first of these simulations requires very little computational expense relative to a micellar simulation because the total number of molecules that must be simulated is relatively small (see the discussion in Chapter 6). The second of these two simulations — simulation in a micellar environment — is also required to make head and tail identifications for traditional MT modeling. Consequently, implementing the CS-MT model is almost as computationally efficient as making head and tail identifications through simulation in a micellar environment. Because the CS-MT model is more physically realistic than the traditional MT model, the CS-MT model should be used in these cases.

13.2.3 CS-MT Modeling of Surfactants and Solubilizes

As discussed in Chapter 6, the CS-MT model is a powerful approach to accurately quantify the hydrophobic driving force associated with surfactant micellization and micellar solubilization. The primary advantage of the CS-MT model is that it allows one to eliminate several assumptions which must be made in the traditional MT modeling approach — most importantly, the assumption that the surfactant head remains fully hydrated in the micellar environment, and an assumption about the extent to which the surfactant heads shield the micelle core from being hydrated.

Minimization of Computational Expense

Because the CS-MT model requires only equilibration of a pre-formed micelle and adequate sampling of the hydration states of surfactants/solubilizates within the equilibrated micelle, implementation of the CS-MT model for a specific surfactant/solubilizate system requires significantly less computational expense than that required to directly simulate micelle self-assembly. Nevertheless, additional characterization of the minimum time required to obtain statistically significant fractional hydration data would be very valuable to minimize the computational expense associated with the CS-MT model. The minimum simulation time required to obtain accurate fractional hydration data is expected to be a function of the surfactant/solubilizate chemical structure. Consequently, it may be most convenient and computationally efficient to continually evaluate the statistical significance of the fractional hydration data gathered as the computer simulation progresses, and to terminate the simulation as soon as a reasonable degree of certainty has been attained in the fractional hydration results, where a “reasonable degree of certainty” might be defined as a standard error that is less than 5% of the fractional hydration value.

Improved Estimation of g_{dehydr}

As discussed in Chapter 6, in the CS-MT modeling approach, the hydrophobic driving force for micelle formation is decomposed into two free-energy contributions — g_{dehydr} , or the free-energy change associated with dehydration upon micelle formation, and g_{hydr} , or the change in hydration free energy experienced upon micelle formation. The first of these two contributions is estimated using the following expression:

$$g_{\text{dehydr}} = \sum_{i=1}^{n_{\text{hyd}}} (1 - f_i) g_{\text{tr}_i} \quad (13.1)$$

where n_{hyd} is the total number of hydrophobic groups in the solute, f_i is the fractional hydration of group i , and g_{tr_i} is the free-energy change associated with transferring group i from the aqueous solution to a bulk solution composed of solute tails. A key

approximation made in Chapters 6, 7, and 8 in evaluating g_{dehydr} was to estimate g_{tr_i} for hydrophobic groups in the surfactant head and tail using solubility data for linear alkyl chains. This approximation gave reasonable modeling results for small-head nonionic surfactants and for small-head ionic and zwitterionic surfactants. However, it did not give accurate modeling results for surfactants with large, polymeric heads, as shown in Chapter 7 for the nonionic surfactant C₁₂E₈. For surfactants with large, polymeric heads, computing g_{tr_i} for hydrophobic groups in the surfactant head using solubility data for those hydrophobic groups in aqueous solution is not sufficiently accurate for the following reasons: (i) using a water-to-oil transfer free energy for the process of transferring a hydrophobic group from bulk water to the corona region of a micelle (which has a high concentration of water and surfactant heads) is a poor approximation, (ii) in many cases, a large number of the hydrophobic groups present in large, polymeric surfactant heads are bonded to hydrophilic atom(s), thus affecting their hydrophobicity and associated g_{tr_i} values, and (iii) the number of hydrophobic groups which may be present in a surfactant with a polymeric head may be quite large, which serves to amplify the effect of the errors inherent in (i) and (ii) above.

In future work, it will be very instructive to explore a number of approaches to obtain more accurate estimates of the g_{tr_i} values. Such extension will be particularly important to accurately model the micellization and the micellar solubilization behavior of surfactants with large, polymeric heads. The general strategy that must underlie all such potential improvements is to approximate as accurately as possible the actual free-energy change associated with the transfer from a bulk aqueous phase to the environment experienced by group i in a micelle. Because the environment experienced in the micelle core and in the corona region are quite different, it is helpful to think about improving the estimate of g_{tr_i} for groups which localize in the micelle core and the corona region separately. Below, I propose possible ways to accomplish this.

Accurate Evaluation of Transfer Free Energies of Groups in the Micelle Core For groups which localize in the micelle core, a free-energy change must be estimated for each group which is transferred from bulk aqueous solution to a bulk, unordered phase of surfactant tails during self-assembly. In traditional MT modeling of surfactants with simple linear alkane tails, g_{tr} has historically been estimated using aqueous solubility data for each tail [6]. An equivalent approximation that one can make in the context of CS-MT modeling is to estimate g_{tr_i} from an estimate of the solubility of group i in aqueous solution. When modeling multicomponent surfactant micellization or micellar solubilization, however, such an approach is only accurate when the enthalpy of mixing is equal to zero for each component ($\Delta H_{\text{mix}} = 0$). If ΔH_{mix} is not equal to zero (which is expected to be the case when the surfactant/solubilize tails are chemically dissimilar), evaluation of ΔH_{mix} may be accomplished using regular solution theory [7] with the appropriate solubility parameters [8], or using Flory-Huggins theory with the appropriate χ parameters [9]. Some preliminary work in this direction has been described in Chapter 6 of this thesis.

Accurate Evaluation of Transfer Free Energies of Groups in the Corona Region For groups which localize in the corona region, a free-energy change must be estimated for each group which is transferred from bulk aqueous solution to an anisotropic, partially ordered phase of surfactant heads and water molecules during self-assembly. A number of approaches could be used to compute accurate transfer free energies for these groups. Perhaps, the most straightforward approach would be to use an experimental, or a computational, method to estimate the transfer free energy associated with transferring a monomeric head group unit from bulk aqueous solution to a bulk phase of water and head group units that serves as a reasonable proxy for the anisotropic corona region of the micelle. To estimate this contribution, the solvation free energy of the monomer in water and the solvation free energy of the monomer in a bulk phase of water and head group units could be determined experimentally, or a theoretical approach could be used to estimate the transfer free energies

or the solvation free energies (for example, by using Flory-Huggins theory with the appropriate χ parameters, or by using computer simulations and a realistic force field to describe interactions between the system components) [10, 11]. In this respect, Soda et al. have outlined a computer simulation strategy which enables the estimation of the transfer free energy from one phase to another using computer simulations and atomic transfer parameters (ATPs), or transfer free energies per unit of accessible surface area. Their approach, although formulated in the context of predicting the hydration free energy of biomolecules such as proteins, is also relevant in determining g_{tr_i} for groups in surfactant molecules. Their analysis decomposes the interactions which are relevant in determining the transfer free energy into two separate classes: (i) intramolecular interactions of solutes where the shielding effect of the solvent is included, and (ii) various solvation effects which are characteristic of the constituent atoms of each solute [12–15]. After obtaining g_{tr_i} for a surfactant head monomer, Eq. 13.1 can be used to calculate g_{dehyd} , but with the summation extended to include both the hydrophobic groups in the surfactant tail and the monomeric units in the surfactant head.

Improved Estimation of g_{hydr}

In the CS-MT model, the change in hydration free energy is computed using the following expression:

$$g_{\text{hydr}} = \sum_{i=1}^{n_{\text{core}}} SASA_i f_i \Delta g_{\text{wc}_i} \quad (13.2)$$

where n_{core} is the total number of hydrophobic groups in the solute that adsorb onto, or penetrate into, the aggregate core, $SASA_i$ is the solvent accessible surface area of group i , and Δg_{wc_i} is defined as the difference in free energy per unit of solvent accessible surface area associated with the hydration of group i in the micellar state and in the aqueous solution.

As discussed in Chapter 7, two main approximations are made in evaluating g_{hydr} for surfactants and solubilizates. The first approximation is related to the approach

used to determine which surfactant or solubilizate groups are part of the micelle core (note that the summation in Eq. 13.2 extends only from $i = 1$ to $i = n_{\text{core}}$). As it was implemented in this thesis, hydrophobic groups in each surfactant/solubilizate that have an f value which is less than 0.60 are modeled as being part of the micelle core. The selection of this cutoff value of f was justified in Chapter 7.

In the future, it would be instructive to investigate a number of different approaches to more accurately identify whether each group i is, or is not, part of the micelle core. One approach may involve evaluating the average location of each group i relative to the location of the micelle core/water interface. The location of the water/octane interface might be determined by first normalizing the water and the surfactant density profiles by the bulk densities of pure water and pure surfactant, respectively, and then by identifying the point at which the water and the surfactant densities are equal. With sufficient simulation time, the density profile for each surfactant atom should generate a smooth Gaussian curve [16–18]. However, preliminary density profile analysis results discussed in Chapter 2 suggest that noise in the density profile data may prevent accurate identification of whether or not each group i is part of the micelle core. It is not clear whether or not the increased simulation times used to generate the results reported in Chapters 6, 7, and 8 would provide sufficient averaging to reduce the noise in the density profile data to an acceptable level. An alternative approach to identify groups that are part of the micelle core involves characterizing the local environment of each group i by integrating the first coordination shell of the radial distribution function between group i and water and between group i and other surfactant/solubilizate atoms. Alternatively, the method of Voronoi polyhedra could be used to rigorously determine the local environment of group i . [19–24]

An improvement to the current implementation of the CS-MT modeling approach that should be implemented in future work is to calculate g_{hydr} using a “snapshot-by-snapshot” analysis approach in which Eq. 13.2 is evaluated at every snapshot of an MD simulation (or, in other words, at every set of coordinates recorded during an

MD simulation). By implementing such an approach, each group i would no longer be modeled as being part of the micelle core based on an average value of f_i . Instead, each group i would be identified as being part of the micelle core at a given instant in time if it satisfies the criteria selected to identify groups in the micelle core. For example, using the micelle core-identification criteria discussed in Chapters 7 and 8, each group i would be identified as being part of the micelle core in a given snapshot if its f_i value is less than 0.60, and its contribution to g_{hydr} would then be evaluated using Eq. 13.2. Implementation of a snapshot-by-snapshot analysis approach to determine g_{hydr} would yield an estimate of the ensemble average of g_{hydr} , which would be more physically realistic than the current approach in which g_{hydr} is evaluated based on an estimate of the ensemble average value of f_i . It is worth noting that a snapshot-by-snapshot analysis approach would not change the computed value of g_{dehydr} , because g_{dehydr} is a continuous function of f_i (recall that Eq. 13.1 is used to compute g_{dehydr} for every hydrophobic group i in a surfactant molecule regardless of the value of f_i for that group). In contrast, g_{hydr} is a noncontinuous function of f_i (recall that Eq. 13.2 is used to compute g_{hydr} only for hydrophobic groups i that are part of the micelle core).

One of the most significant approximations made in Chapters 7 and 8 in applying the CS-MT model was to estimate Δg_{wc} using a model derived in Chapter 6 for oil aggregates. In so doing, the approximation was made that the change in hydration free energy experienced by hydrophobic groups upon transfer from the bulk aqueous solution to the micelle core is unaffected by the presence of surfactant heads and (if present) charged counterions at the micelle core/water interface. Although reasonable modeling results for surfactants (including nonionic, zwitterionic, and ionic surfactants) and solubilizates were obtained using this approximation, further investigation into the accuracy of this approximation, as well as into the availability of other approaches that could be used to relax this approximation, would be valuable.

In Chapter 6, we noted that Δg_{wc} is a function of the chemical nature of group i . Although the approximation was made that Δg_{wc} is identical for each of the hy-

drophobic groups in a linear alkyl chain (CH_2 and CH_3 groups), Δg_{wc} will certainly be different for semipolar groups (such as phenyl groups) present in surfactant or solubilizate tails. To estimate Δg_{wc} for semipolar groups in a micelle, a theoretical approach that is similar to what was implemented to estimate Δg_{wc} for oil molecules could be utilized. First, a number of aggregates of different shapes and sizes composed of the semipolar tails would be pre-formed in aqueous solution and allowed to equilibrate. After equilibration, an extended computer simulation run would be conducted to determine the ensemble average value of $SASA_{\text{core}}/A_{\text{core}}$. In the case of oil aggregates, the $SASA_{\text{core}}/A_{\text{core}}$ results obtained from computer simulation were fitted to a mathematical expression describing $SASA_{\text{core}}/A_{\text{core}}$ as a function of the number of carbons in each oil molecule and the curvature of the oil aggregate. $SASA_{\text{core}}/A_{\text{core}}$ results for aggregates of semipolar tails could be fit to a similar expression. Next, Δg_{wc} would be evaluated using the following equation:

$$\Delta g_{\text{wc}} = \sigma_{\text{core}} - \sigma_{\text{bulk}} = \frac{\sigma A_{\text{core}}}{SASA_{\text{core}}} - \frac{g_{\text{tr}_i}}{SASA_i} \quad (13.3)$$

where σ_{core} is the microscopic “interfacial tension” (interfacial free energy per unit SASA) associated with the aggregate core/water interface, σ_{bulk} is the microscopic “interfacial tension” (interfacial free energy per unit SASA) associated with the group i /water interface in the aqueous solution, and σ is the curvature-corrected macroscopic interfacial tension of the aggregate core/water interface. To evaluate Eq. 13.3, an estimation of σ must be made, which would involve developing a theoretical approach to model the curvature dependence of the tail/water interfacial tension. As discussed in Chapter 6, for oil molecules the curvature-dependent interfacial tension, σ_j , is determined using the Gibbs-Tolman-Koenig-Buff equation [25–28]:

$$\sigma_j = \frac{\sigma_{0,j}}{\left(1 + \frac{(S-1)\delta}{l_c}\right)} \quad (13.4)$$

where $\sigma_{0,j}$ is the interfacial tension of component j at a flat interface, δ is the Tolman distance [28], and S is a shape factor (3 for spheres, 2 for cylinders, and 1 for disks

or bilayers). An estimate of $\sigma_{0,j}$ could be obtained from experimental data [29], and the Tolman distance for the semipolar tail could be inferred using an approach described in earlier work done in the Blankschtein group to evaluate this quantity for linear alkyl chains [6].

Improved Estimation of g_{int}

As discussed in Chapter 7, the CS-MT modeling approach can be used to evaluate the effective area at the micelle core/water interface shielded from hydrating contacts by each surfactant head (a_0). To improve the accuracy of both the traditional MT model and the CS-MT model, it would be valuable to build a library of a_0 values for different types of surfactant heads. As shown in Chapter 7, values of a_0 may vary significantly from surfactant to surfactant. In that chapter, the smallest estimate of a_0 (12.19 Å² for OSE) was less than half the value of the largest estimate of a_0 (31.22 Å² for OG).

13.3 Future Research Directions: Application of Computer Simulation to Determine Free-Energy Changes

In Part II of this thesis, the CS-FE/MT modeling approach was described to quantify the free-energy change associated with changing the composition of a single (pure) surfactant micelle through the addition of a cosurfactant or a solubilize. Because of the computationally expensive nature associated with determining alchemical free-energy changes, particularly in a constrained environment such as a micelle core, the CS-FE/MT modeling approach was shown to give qualitatively accurate results only when the chemical structure of the added surfactant or solubilize was very similar to the chemical structure of the original surfactant. The CS-FE/MT modeling approach nevertheless represents an interesting application of alchemical free-energy methods

in the case of micellar systems. As computing power increases, the quantitative accuracy of such free-energy methods will improve as it becomes more and more computationally feasible to adequately sample all the important regions of phase space. In addition, it may become possible to make quantitatively accurate estimates of the free-energy change associated with morphing a surfactant into a cosurfactant, or into a solubilizate, that is significantly different in structure than the original surfactant.

13.3.1 Selection of the Optimal Transition Path

In future work, a number of strategies may be investigated to reduce the computational expense associated with the CS-FE/MT modeling approach. Additional research should be conducted to identify the most computationally efficient alchemical path that may be taken to morph the original surfactant into a cosurfactant or a solubilizate. Identification of the most efficient path between two states A and B in an alchemical free-energy calculation is not trivial, and can make an enormous difference in the computational expense required to converge to an accurate estimate of the free-energy difference between the two states.

As discussed in Chapter 10, soft core potentials [30] have been used in the free-energy computer simulations conducted in this thesis to avoid the “end-point catastrophe,” and to improve convergence of the free-energy results obtained at large and small values of the coupling parameter, λ . In future work, alternative implementations of the soft-core potential could be investigated, as well as slow growth approaches in which atoms are gradually extended (or “grown”) from the atom(s) to which they are bonded in order to prevent excessive free-energy changes at large and small value of λ [31]. One potential area for improvement is making adjustments to the value of α (the soft core parameter) and σ (the radius of interaction) used in the soft-core potentials [32]. Some researchers suggest that the optimal value of the dimensionless parameter α is 0.5, but further testing is warranted [33–36].

In addition to implementing a strategy to avoid the end-point catastrophe, iden-

tification of the most efficient alchemical path to move between two states, A and B , will require selection of an optimal approach to alter the interactions of the morphing particles with their local environments. Some researchers have suggested that when evaluating the free-energy change associated with changing an atom into a dummy particle, it is most computationally efficient to first gradually remove the Coulombic interactions between the atom and its environment, and then to gradually remove the van der Waals interactions between the atom and its environment [33].

Additional research is also warranted to determine the optimal approach to construct the dual topology that is used to morph a system from state A to state B (see the discussion in Chapter 10). Although identifying the optimal dual topology to estimate the free-energy change associated with morphing one molecule into another is relatively simple if the two molecules are similar in structure, it is more difficult when the two molecules are quite different in structure. Information about the best approach to construct dual topologies is hard to find in the alchemical free-energy literature, and research contributions in this area could be of great value to researchers who seek to estimate free-energy changes through alchemical computer simulations. Trial-and-error experimentation will likely be required to identify the optimal dual-topology simulation approach.

13.3.2 Alternative Free-Energy Methods

In addition to further exploring the dual-topology, thermodynamic integration free-energy approach used in this thesis to estimate free-energy changes, in future work, alternative free-energy methods may be identified which could reduce the computational expense associated with determining the free-energy change associated with altering the micelle composition. Other free-energy methods that have been discussed in the literature include free energy perturbation, acceptance ratio techniques, weighted histogram analysis, particle insertion methods, and energy distribution approaches [37]. Improved free-energy methods for computer simulation are an active area of research, and are routinely published in the literature [38–50].

Using Monte Carlo (MC) computer simulations, rather than MD simulations, to determine the free-energy change associated with changes in micelle composition may permit better sampling of phase space with less computational expense, and its use should be explored. Recent research published by Pool and Bolhuis describes a promising MC simulation approach to calculate the free energy of micelle formation as a function of aggregation number [51]. In their approach, MC simulation in a semi-grand ensemble was conducted in which solvent and surfactant molecules were exchanged. Configurational bias MC was used to improve insertion probabilities, and surfactants were only inserted in the region around the micelle to improve the acceptance statistics. Isobaric hybrid MC was used to efficiently reach thermal equilibrium. In addition, determination of the CMC was accomplished by using umbrella sampling to obtain statistically significant results in unlikely regions of the micelle size distribution. Although the authors only described the implementation of this approach to estimate the CMC for simple Lennard-Jones surfactants, they conclude that their research opens up the way to perform similar calculations using a realistic atomistic-level forcefield.

13.4 Future Research Directions: Application of Computer Simulation to Make Direct Predictions of Surfactant Solution Properties

In Part III of this thesis (Chapters 11, 12, and 13), atomistic level MD simulations were used to make predictions of surfactant solution properties. Because the simulations reported in Chapters 11, 12, and 13 were done at an atomistic level, the length and timescales that could be modeled were limited. In Chapters 11 and 12, MD simulations were used to equilibrate and analyze the structure of pre-formed surfactant monolayers and pre-formed surfactant/solubilizate aggregates, respectively. In Chapter 13, MD simulations were used to investigate the self-assembly of triterpenoid

surfactants that form relatively small micelles in aqueous solution.

Despite the computational expense inherent in atomistic level simulation, it is difficult to accurately quantify surfactant monolayer and micelle microstructure in aqueous solution using a coarse-grained description of either the surfactant or the solubilizate. Surfactant micellization and micellar solubilization phenomena are very sensitive to the specific chemical structures of the surfactant and the solubilizate. For example, it is known experimentally that the CMC of a surfactant generally increases as the degree of branching in the surfactant tail increases [52, 53]. In addition, the solubilization capacity of a surfactant depends on the degree of branching in the surfactant tail [52, 53]. If such structural details of the surfactant are removed or obscured as a result of coarse graining, accurate prediction of surfactant solution properties will not be possible.

Coarse graining of water, or the use of an implicit solvent model, have the potential to greatly reduce the computational cost associated with simulation. Unfortunately, however, both approaches may remove or distort essential physics that must be captured in order to accurately model surfactant self-assembly and to obtain accurate predictions of surfactant monolayer and micelle microstructure. Lazaridis et al. have recently implemented an implicit solvent model to model DPC micelle formation which was originally developed as a solvation model for proteins [54]. In this implicit solvation model, the solvation free energy is modeled using the following expression:

$$\Delta G^{\text{slv}} = \sum_i \Delta G_i^{\text{slv}} = \sum_i \Delta G_i^{\text{ref}} - \sum_i \sum_{j \neq i} f_i(r_{ij}) V_j \quad (13.5)$$

where ΔG_i^{slv} is the solvation free energy of atom i , $f_i(r_{ij})$ is the solvation free-energy density (which is modeled as a Gaussian function) of group i at distance r_{ij} , and V_j is the volume of group j . In Eq. 13.5, the solvation free energy of atom i is computed as being equal to the solvation free energy of the atom when it is fully exposed to solvent (represented by ΔG_i^{ref}) minus the solvation free energy lost due to the presence of the surrounding atoms (represented by $\sum_{j \neq i} f_i(r_{ij}) V_j$). However, micelles

simulated using MD with this implicit solvent model were found to be more irregular than micelles simulated in explicit water [54]. Another implicit solvent model formulated by Morisada et al. accounts for the effect of the solvent using solvent-averaged interactions between the surfactant segments in water [55]. Langevin dynamics (LD) simulation has been used by Shinto et al. to simulate the self-assembly of *n*-decyltrimethylammonium chloride surfactants in aqueous solution [56]. In their LD simulations, the effect of the solvent was considered via a frictional and random force on the solute, and by computing effective forces between the solutes. The authors conclude that their simulation results are in fair agreement with those obtained using atomistic MD simulations and experimental measurements. Yamamoto et al. have described a dissipative particle dynamics simulation study of the spontaneous vesicle formation of amphiphilic molecules [57]. In their simulations, the surfactant molecules were modeled as containing one or two hydrophilic head beads and three to six hydrophobic tail beads, and water was modeled as a hydrophilic bead of the size of several water molecules. In the Brownian dynamics model of Bourov et al., the self-assembly of amphiphiles has also been investigated [58]. Amphiphilicity was introduced into their model system by introducing a repulsive cutoff distance for head-head and for head-tail interactions, and an attractive cutoff distance for tail-tail interaction.

The extent to which proper parameterization of a coarse-grained water model, or of an implicit solvent model, can permit accurate prediction of surfactant aggregate microstructure and free energy is poorly understood and represents an important area of future research. Valuable research contributions could be made by carefully reviewing each of the approaches described in the literature to determine the advantages and disadvantages of each approach in the context of predicting surfactant solution properties, and selecting the most promising approach for use and extension.

13.5 Concluding Remarks

This thesis has presented a detailed, atomistic-level computer simulation and molecular-thermodynamic investigation of the micellar solution behavior of nonionic, zwitterionic, and ionic surfactants in aqueous solutions, as well as of the aqueous micellar solubilization of solubilizates by surfactants. It is hoped that the approaches developed in this thesis to use computer simulations and molecular-thermodynamic theory in a complementary way will not only extend our ability to make accurate predictions of surfactant solution behavior, but will also contribute to our fundamental knowledge of the solution behavior of surfactants and solubilizates. It is further hoped that this thesis will provide a solid foundation for future research in the area of surfactant science, and, more generally, that it will assist future researchers working to connect atomistic-level computer simulation methods with continuum thermodynamic models.

Bibliography

- [1] Yagui et al., C. R., 2004., Ongoing Collaboration.
- [2] Kausch, C. M., Kim, Y., Russell, V. M., Medsker, R. E., and Thomas, R. R., “Surface tension and adsorption properties of a series of bolaamphiphilic poly(fluorooxetane)s,” *Langmuir*, Vol. 19, 2003, pp. 7182–7187.
- [3] Foresman, J. and Frisch, A., *Exploring Chemistry with Electronic Structure Methods*, Gaussian, Inc., Pittsburgh, Pennsylvania, 1996.
- [4] Chirlian, L. E. and Francl, M. M., “Atomic charges derived from electrostatic potentials: A detailed study,” *Journal of Computational Chemistry*, Vol. 8, 2004, pp. 894–905.
- [5] Heinz, H. and Suter, U., “Atomic charges for classical simulations of polar systems,” *The Journal of Physical Chemistry B*, Vol. 108, 2004, pp. 18341–18342.
- [6] Puvvada, S. and Blankschtein, D., “Molecular thermodynamic approach to predict micellization, phase behavior and phase separation of micellar solutions. 1. Application to nonionic surfactants,” *The Journal of Chemical Physics*, Vol. 92, 1990, pp. 3710–3724, and references cited therein.
- [7] Hildebrand, J. H., Prausnitz, J. M., and Scott, R. L., *Regular and Related Solutions*, Van Nostrand Reinhold Company, 1971.
- [8] Barton, A. F. M., *CRC Handbook of Solubility Parameters and Other Cohesion Parameters*, CRC Press, Inc., 1983.

- [9] Flory, P. J., *Principles of Polymer Chemistry*, Cornell University Press, 1953.
- [10] Carale, T. R., Pham, Q. T., and Blankschtein, D., “Salt effects on intramolecular interactions and micellization of nonionic surfactants in aqueous solutions,” *Langmuir*, Vol. 10, 1994, pp. 109–121.
- [11] Nagarajan, R. and Ruckenstein, E., “Theory of surfactant self-assembly: A predictive molecular thermodynamic approach,” *Langmuir*, Vol. 7, 1991, pp. 2934–2969.
- [12] Soda, K. and Hirashima, H., “Hydration thermodynamics of biomolecules. I. Transfer free energy of solutes with variable conformations,” *Journal of the Physical Society of Japan*, Vol. 59, 1990, pp. 4177–4185.
- [13] Hirashima, H. and Soda, K., “Hydration thermodynamics of biomolecules. II. Atomic transfer parameters of amino acids,” *Journal of the Physical Society of Japan*, Vol. 60, 1991, pp. 330–339.
- [14] Hirashima, H. and Soda, K., “Hydration thermodynamics of biomolecules. III. Transfer free energies of ionic amino acid derivatives,” *Journal of the Physical Society of Japan*, Vol. 60, 1991, pp. 2783–2790.
- [15] Soda, K. and Hirashima, H., “Hydration thermodynamics of biomolecules. IV. Hydration free energy of amino acid related molecules,” *Journal of the Physical Society of Japan*, Vol. 61, 1992, pp. 2992–3006.
- [16] Penfold, J. and Thomas, R. K., “Solvent distribution in non-ionic surfactant monolayers,” *Physical Chemistry Chemical Physics*, Vol. 4, 2002, pp. 2648–2652.
- [17] Bocker, J., Schlenkrich, M., Bopp, P., and Brinkmann, J., “Molecular dynamics simulation of a n-hexadecyltrimethylammonium chloride monolayer,” *The Journal of Chemical Physics*, Vol. 96, 1992, pp. 9915–9922.

- [18] Tarek, M., Tobias, D. J., and Klein, M. L., “Molecular dynamics simulation of tetradecyltrimethylammonium bromide monolayers at the air-water interface,” *The Journal of Physical Chemistry*, Vol. 99, 1995, pp. 1393–1402.
- [19] Montoro, J. C. G. and Abascal, J. L. F., “The Voronoi polyhedra as tools for structure determination in simple disordered systems,” *The Journal of Physical Chemistry*, Vol. 97, 1993, pp. 4211–4215.
- [20] Brostow, W., “Voronoi polyhedra and Delanay simplexes in the structural analysis of molecular-dynamics-simulated materials,” *Physical Review B*, Vol. 57, 1998, pp. 13448–13458.
- [21] Rustad, J. R. and Yuen, D. A., “Molecular dynamics of amorphous silica at very high pressures (135 GPa): Thermodynamics and extraction of structures through analysis of Voronoi polyhedra,” *Physical Reviews B*, Vol. 44, 1991, pp. 2108–2121.
- [22] Gerstein, M., Tsai, J., and Levitt, M., “The volume of atoms on the protein surface: Calculated from simulation, using Voronoi polyhedra,” *Journal of Molecular Biology*, Vol. 249, 1995, pp. 955–966.
- [23] Finney, Y. R., “A procedure for the construction of Voronoi polyhedra,” *Journal of Computational Physics*, Vol. 32, 1979, pp. 137143.
- [24] Bernal, J. D. and Finney, J. L., “Random close-packed hard-sphere model. II. Geometry of random packing of hard spheres,” *Discussions of the Faraday Society*, Vol. 43, 1967, pp. 62–69.
- [25] Gibbs, J. W., *The Scientific Papers of J.W. Gibbs*, Vol. 1, Dover, New York, 1961.
- [26] Koenig, F. O., “On the thermodynamic relation between surface tension and curvature,” *The Journal of Chemical Physics*, Vol. 18, 1950, pp. 449.
- [27] Buff, F. P., “The spherical interface. I. Thermodynamics,” *The Journal of Chemical Physics*, Vol. 19, 1951, pp. 1591.

- [28] Tolman, R. C., “Consideration of the Gibbs theory of surface tension,” *The Journal of Chemical Physics*, Vol. 16, 1948, pp. 758.
- [29] Mukerjee, P. and Cardinal, J. R., “Benzene derivatives and naphthalene solubilized in micelles. Polarity of microenvironment, location and distribution in micelles, and correlation with surface activity in hydrocarbon-water systems,” *The Journal of Physical Chemistry*, Vol. 82, 1978, pp. 1620–1627.
- [30] van Gunsteren, W. F., *Computer Simulation of Biomolecular Systems: Theoretical and Experimental Applications*, Escom Science, 1989.
- [31] Straatsma, T. P., Zacharias, M., and McCammon, J. A., “Holonomic constraint contributions to free energy differences from thermodynamic integration molecular dynamics simulations,” *Chemical Physics Letters*, Vol. 196, 1992, pp. 297–302.
- [32] van der Spoel, D., Lindahl, E., Hess, B., van Buuren, A., Apol, E., Meulenhoff, P., Tieleman, D., Sijbers, A., Feenstra, K., van Drunen, R., and Berendsen, H., *Gromacs User Manual version 3.2*, www.gromacs.org, 2004.
- [33] Mobley, D., 2006, unpublished.
- [34] Shirts, M. R., Pitera, J. W., Swope, W. C., and Pande, V. S., “Extremely precise free energy calculations of amino acid side chain analogs: Comparison of common molecular mechanics force fields for proteins,” *The Journal of Chemical Physics*, Vol. 119, 2003, pp. 5740–5760.
- [35] Shirts, M. R. and Pande, V. S., “Solvation free energies of amino acid side chain analogs for common molecular mechanics water models,” *The Journal of Chemical Physics*, Vol. 122, 2005, pp. 134508.
- [36] Shirts, M., *Calculating Precise and Accurate Free Energies in Biomolecular Systems*, Ph.D. thesis, Stanford, 2005, and references cited therein.

- [37] Pearlman, D. A. and Rao, B. G., *Free Energy Calculations: Methods and Applications*, John Wiley & Sons, Ltd., New York, 1998.
- [38] Dejaegere, A. and Karplus, M., “Analysis of coupling schemes in free energy simulations: A unified description nonbonded contributions to solvation free energies,” *The Journal of Physical Chemistry*, Vol. 100, 1996, pp. 11148–11164.
- [39] Aqvist, J., Medina, C., and Samuelsson, J. E., “A new method for predicting binding affinity in computer-aided drug design,” *Protein Engineering*, Vol. 7, 1994, pp. 385–391.
- [40] King, G. and Barford, R., “Calculation of electrostatic free energy differences with a time-saving approximate method,” *The Journal of Physical Chemistry*, Vol. 97, 1993, pp. 8798–8802.
- [41] Yu, H. A., Roux, B., and Karplus, M., “Solvation thermodynamics: An approach from analytic temperature derivatives,” *The Journal of Chemical Physics*, Vol. 92, 1990, pp. 5020–5032.
- [42] Pettitt, B. M., Karplus, M., and Rossky, P. J., “Integral equation model for aqueous solvation of polyatomic solutes: Application to the determination of the free energy surface for the internal motion of biomolecules,” *The Journal of Physical Chemistry*, Vol. 90, 1986, pp. 6335–6345.
- [43] Chandler, D. and Andersen, H. C., “Optimized cluster expansions for classical fluids. II. Theory of molecular liquids,” *The Journal of Chemical Physics*, Vol. 57, 1972, pp. 1930–1937.
- [44] Honig, B., Sharp, K. A., and Yang, A. S., “Macroscopic models of aqueous solutions: Biological and chemical applications,” *The Journal of Physical Chemistry*, Vol. 97, 1993, pp. 1101–1109.

- [45] Gilson, M., Sharp, K. A., and Honig, B., “Calculating the electrostatic potential of molecules in solution: Method and error assessment,” *Journal of Computational Chemistry*, Vol. 9, 1988, pp. 327–335.
- [46] Gao, J. L. and Xia, X. F., “A priori evaluation of aqueous polarization effects through Monte Carlo QM-MM simulations,” *Science*, Vol. 258, 1992, pp. 631–635.
- [47] Schaefer III, H. F., editor, *Modern Theoretical Chemistry. Vol. 3: Method of Electronic Structure Theory*, Plenum, 1977.
- [48] Schaefer III, H. F., editor, *Modern Theoretical Chemistry. Vol. 4: Method of Electronic Structure Theory*, Plenum, 1977.
- [49] Segal, G., editor, *Modern Theoretical Chemistry. Vols. 7-8: Semiempirical Methods of Electronic Structure Calculation*, Plenum, 1977.
- [50] Field, M. J., Bash, P. A., and Karplus, M., “A combined quantum mechanical and molecular mechanical potential for molecular dynamics simulations,” *Journal of Computational Chemistry*, Vol. 11, 1990, pp. 700–733.
- [51] Pool, R. and Bolhuis, P. G., “Accurate free energies of micelle formation,” *The Journal of Physical Chemistry B*, Vol. 109, 2005, pp. 6650–6657.
- [52] Kolthoff, I. M. and Stricks, “Solubilization of dimethylaminoazobenzene in solutions of detergents,” *Journal of Physical Colloid Chemistry*, Vol. 52, 1948, pp. 915–943.
- [53] Klevens, H. B., “Solubilization,” *Chemical Reviews*, Vol. 47, 1950, pp. 1–78.
- [54] Lazaridis, T., Mallink, B., and Chen, Y., “Implicit solvent simulations of DPC micelle formation,” *The Journal of Physical Chemistry B*, Vol. 109, 2005, pp. 15098–15106.

- [55] Morisada, S., Shinto, H., and Higashitani, K., “Revised implicit solvent model for the simulation of surfactants in aqueous solutions,” *The Journal of Physical Chemistry B*, Vol. 109, 2005, pp. 11762–11769.
- [56] Shinto, H., Morisada, S., Miyahara, M., and Higashitani, K., “Langevin dynamics simulations of cationic surfactants in aqueous solutions using potentials of mean force,” *Langmuir*, Vol. 20, 2004, pp. 2017–2025.
- [57] Yamamoto, S., Maruyama, Y., and Hyodo, S., “Dissipative particle dynamics study of spontaneous vesicle formation of amphiphilic molecules,” *The Journal of Chemical Physics*, Vol. 116, 2002, pp. 5843–5849.
- [58] Bourov, G. K. and Bhattacharya, A., “Brownian dynamics simulation study of self-assembly of amphiphiles with large hydrophilic heads,” *The Journal of Chemical Physics*, Vol. 122, 2005, pp. 1–6.